Restore Lagoon Inflow Research (Phase 1)
Project Summary






PREPARED FOR

Florida Department of Education
325 W Gaines Street
Tallahassee, FL 32399

PREPARED BY

Matthew Shelton and Marcy Frick
Tetra Tech, Inc.
11 Riverside Drive, Suite 204
Cocoa, Florida 32922

For:
Florida Institute of Technology
150 West University Boulevard
Melbourne, FL 32901

September 2020

Table of Contents

List of Tables

List of Figures

Acknowledgements

The Restore Lagoon Inflow research team thanks Governor Ron DeSantis; the Florida legislature especially Representative Randy Fine, Representative Thad Altman and Senator Debbie Mayfield; and the Florida Department of Education for their roles in advancing Florida's water health and research. We would also like to thank the people and organizations in Brevard and Indian River counties concerned about the lagoon's recovery who continue to advocate for one of Florida's most precious resources. A special acknowledgement of Dr. John Windsor's contributions to the coordination of this report and his career long efforts toward improving the health of the Indian River Lagoon. In addition, we thank Dr. T. Dwayne McCay, Mr. Frank Kinney, and Mr. Robert Salonen for supporting Restore Lagoon Inflow Research project communications with all stakeholders.

The views, statements, findings, conclusions, and recommendations expressed herein are those of the authors and do not necessarily reflect the views of the State of Florida or any of its sub-agencies.

The photographs on the cover were provided by the Florida Tech Principal Investigators on this project.

List of Acronyms

ADCIRC	Advanced Circulation
ADCP	Acoustic Doppler Current Profiler
BRL	Banana River Lagoon
C	Centigrade
cm	Centimeters
COI	Cytochrome Oxidase Subunit I
DIN	Dissolved Inorganic Nitrogen
DNA	Deoxyribonucleic Acid
DO	Dissolved Oxygen
DON	Dissolved Organic Nitrogen
DOP	Dissolved Organic Phosphorus
eDNA	Environmental Deoxyribonucleic Acid
EFDC	Environmental Fluid Dynamics Code
FDEP	Florida Department of Environmental Protection
Florida Tech	Florida Institute of Technology
ft^3/s	Cubic Feet Per Second
FWRI-FIM	Fish and Wildlife Research Institute's Fisheries Independent Monitoring
HYCOM	Hybrid Coordinate Ocean Model
IRL	Indian River Lagoon
kg/m^3	Kilograms Per Cubic Meter
km	Kilometer
L	Liter
m	Meter
m^3/s	Cubic Meters Per Second
mg/L	Milligrams Per Liter
mL	Milliliter
N	Nitrogen
NASA	National Aeronautics and Space Administration
ng/µl	Nanograms Per Microliter

NH_4	Ammonium
NOx	Nitrate + Nitrite
P	Phosphorus
PAFB	Patrick Air Force Base
PCR	Polymerase Chain Reaction
PO_4	Ortho-phosphate
ppt	Parts Per Thousand
PSU	Practical Salinity Unit
SCUBA	Self-Contained Underwater Breathing Apparatus
SESC	Species of Environmental Shift Concern
SIC	Species Introduction Concern
SiO_2	Silica
SOD	Sediment Oxygen Demand
SJRWMD	St. Johns River Water Management District
SRP	Soluble Reactive Phosphorus
SWAN	Simulating Waves Nearshore
TDN	Total Dissolved Nitrogen
TDP	Total Dissolved Phosphorus
µm	Micrometer
µM	Micromoles Per Liter
µmoles/m^2/hr	Micromoles Per Square Meter Per Hour

Executive Summary

The Indian River Lagoon (IRL) is not a river, it is a lagoon. A lagoon is a special type of estuary that is oriented parallel to the coast and characterized by shallow coastal waters with restricted, but free, exchange with the adjacent open ocean. It is this exchange of fresh and saltwater that makes estuaries the most productive and fragile coastal ecosystems in the world. The IRL is a microtidal system that has limited exchange with the ocean through five engineered and stabilized inlets (Ponce de Leon, Sebastian, Fort Pierce, St. Lucie, and Jupiter).

With funding of $800,000 from the Florida Legislature, the Florida Institute of Technology (Florida Tech) completed Phase 1 of a multi-phase project to explore customized solutions for improving water quality within the IRL by restoring periodic historical ocean inflows. The project is working towards installing a temporary inflow pilot system to gather information on the feasibility of a potential full-scale, permanent system. The purpose of this first phase of the study was to gather baseline data and modeling on existing water quality, biological parameters, and hydrologic conditions at potential locations for a future permitted, temporary inflow pilot system, which may then lead to a full-scale, permanent system. The modeling and engineering proceeded in parallel with biological and water quality monitoring in advance of the temporary inflow pilot system study. This ecosystem monitoring was crucial to understanding the baseline status of the lagoon in the vicinity of the proposed inflow, so that the changes resulting from the proposed temporary inflow pilot system can continue to be monitored and evaluated.

A multi-disciplined team of research professionals, who were supported by university staff and students, was assembled to provide expertise in each area of study:

- Modeling and Engineering – Dr. Gary Zarillo, Dr. Robert Weaver, and Dr. Ashok Pandit
- Biological Monitoring – Dr. Kevin Johnson, Dr. Ralph Turingan, Dr. Jeffrey Eble, Dr. Johnathan Shenker, and Dr. Jesse Blanchard
- Geochemical Baseline – Dr. Austin Fox

Three potential inflow locations were selected for study: Port Canaveral and south Cocoa Beach in Brevard County and Bethel Creek in Indian River County.

Modeling and Engineering

The modeling and engineering objectives were aimed at testing the hypothesis that controlled water exchanges between the ocean and IRL can be engineered to provide improved flushing and water quality within local IRL compartments without the negative impacts on littoral sediment budgets linked to permeant stabilized inlets.

The modeling approach combined the Advanced Circulation (ADCIRC), Hybrid Coordinate Ocean Model (HYCOM), and Environmental Fluid Dynamics Code (EFDC) models in a nested system.

This approach focused on modeling a potential full-scale, permanent system to evaluate the movement of water on a basin-wide scale and the proposed design's effects on tides, water quality, sediment transport, and flushing rates. The modeling supported the concept of re-establishing ocean inflow to circulate the water in the IRL system, moving stagnant lagoon water and replacing it with ocean water. The inflow system would create very slow water movement toward the inlets, facilitating enhanced exchange and mixing with the larger IRL system. Localized changes in salinity are predicted near the outfalls, along with minimal changes in temperature.

Model results in the Banana River Lagoon (BRL) varied according to the location and magnitude of water inflows. The pump station option near Patrick Air Force Base reduced model simulation tracer concentrations by 65% to 75%, during the 365-day model period, in the BRL south compartment compared to a tracer reduction of about 40% under the base case. The pump station option pumping 10 cubic meters per second (m^3/s) into the BRL just north of Port Canaveral provided greater flushing due to its location. The model simulation tracer concentration in most BRL compartments was reduced by 60% to 75% under this option. The weir structure option located within Port Canaveral was predicted to have the greatest potential for exchanging water out of the BRL over a shorter period of time compared to the two pump options. The model simulation tracer concentration in the BRL central to north central compartments was 70% to 85% lower compared to the base case. In addition, an option for a 5 m^3/s pump station in Bethel Creek was modeled. This option flushed the IRL Bethel Creek compartment in days with minimal impacts on salinity and temperature. However, this pump station had minimal benefits on the surrounding IRL compartments.

Draft designs were also provided for three structure options: pipe with no pump, pump and pipe, and weir. The temporary inflow pilot system flow rate was set to a minimum of 5 m^3/s and the potential full-scale, permanent system flow rate was set to a minimum of 20 m^3/s. Each concept was focused on controlled inflow of ocean water into the BRL. For the temporary inflow pilot system, the engineering supported either an overland temporary pipe and pump or a weir in the northern BRL with a flow of 5 m^3/s. The engineering also identified two options for a full-scale, permanent system: pipe and pump or weir. The weir is most cost-effective approach that provides the greatest flexibility for flow at the lowest cost but is the most restrictive with location. The pipe and pump option is the most restrictive approach in cost as well as flow rates, but the most flexible with location. A final temporary pilot inflow system, and potential full-scale, permanent system, may be modified from the design and volume options included here based on further scientific, regulatory agency, and logistical requirements.

Biological Monitoring

Students conducting transect and quadrat sampling of shoal grass.

The biological monitoring objectives were to document the biological characteristics of the IRL and coastal ocean near the proposed inflow locations and assess the likely biological response to an inflow system. This approach assessed seagrass and drift algae near the proposed inflow sites and evaluated the percent cover, density, and canopy height. Sediment samples collected on the lagoon and ocean sides of the proposed inflow sites evaluated the abundance, diversity, and richness of fauna as well as environmental parameters in the sediment. Larval fish and invertebrates were collected and analyzed, and environmental parameters were used to see how fish species respond to changes in the lagoon and ocean

environments near the proposed inflow sites. The relationships between fish community structure and key water parameters were described using Florida Fish and Wildlife Conservation Commission's Fisheries Independent Monitoring database, which is the most extensive IRL fish database. Environmental deoxyribonucleic acid (eDNA) characterization was also used to identify the presence of key fish and invertebrate species.

Extensive data on species densities and distributions, and environmental and community associations, were collected as part of this baseline study. These data were used to evaluate the changes in the biological resources.

Many estuarine animals tolerate fluctuations in temperatures, salinities, turbidity, nutrients, and pollutants. By comparison, coastal ocean conditions are relatively constant and fall well within the ranges of estuarine organism tolerances. However, data are lacking on several key species of concern, such as the spawning populations of sportfish in the BRL. Indirect impacts on the estuarine community due to biotic factors, such as predation by, or competition with, organisms from the coastal ecosystem, are difficult to predict. Coastal organisms may be directly introduced via enhanced inflow, or migration into the estuary could be encouraged following a shift towards coastal-like conditions. However, the Port Canaveral shipping locks already provide a limited hydrodynamic connection and migration opportunity and the northern IRL estuary was historically connected to the coastal ocean via inlets. Reliable evaluation of the biological impacts of restored inflow would be best accomplished through a temporary inflow pilot system where biological responses are carefully monitored. This would allow a more confident projection of the likely effects of a full-scale, permanent inflow restoration.

Geochemical Baseline

The geochemical baseline objective was to identify a suite of geochemical parameters to make a comparison between the baseline and enhanced inflow conditions. These parameters are important indicators used to calibrate the models and provide predictors and causation for ecological shifts from the geochemical cycling of nutrients and other parameters. This approach deployed an array of sensors to continuously monitor bottom water conditions, including temperature, dissolved oxygen, and salinity (selected sites), near possible inflow locations. In addition, discrete nutrient samples were collected to vertically profile the areas adjacent to the potential inflow locations. Sediment samples were collected to evaluate variables that correlated with geochemical nutrient cycling. Benthic chambers equipped with sensors were deployed to evaluate geochemical changes in the sediments. These approaches were implemented at each inflow location on the ocean and lagoon side.

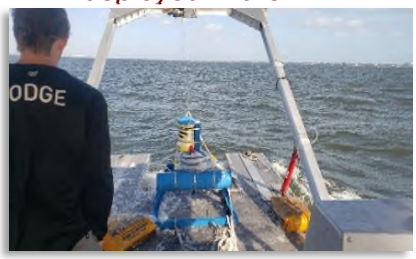

Ekman Grab Sampler (above) and ADCP (below) deployed in the IRL

An inflow to the IRL would result in corresponding outflows of lagoon water into the coastal ocean. These modest exchanges of water plus dissolved and particulate materials would lead to changes in water quality within the lagoon. These modest exchanges would have both direct impacts, such as conservative mixing of temperature and salinity, and indirect impacts, such as changes to geochemical nutrient cycling in response to changes to water quality. Changes to temperature and salinity would likely be small; however, the potential for stratification and the potential formation of a dense layer of seawater within the lagoon could be of significance at certain

locations. If inflow were to occur via pumping at 5 m^3/s, direct exchanges of water would yield a net removal of about 50 tons of nitrogen and 6 to 10 tons of phosphorus per year from the lagoon. Laboratory experiments carried out to estimate the potential impacts of a temporary inflow pilot system on geochemical nutrient cycling showed that lower lagoon temperature and higher lagoon salinity led to significant decreases in benthic fluxes for some nutrients. Laboratory experiments showed, under anaerobic conditions, ortho-phosphate fluxes were directed out of sediments whereas under aerobic conditions, sediments often were a sink for ortho-phosphate. Based on these data, enhanced circulation and increased bottom water dissolved oxygen would likely contribute to decreasing ortho-phosphate concentrations in lagoon water.

Recommendations and Next Steps

The multi-phased full research project scope is envisioned to include the baseline monitoring, design, permitting, implementation, and monitoring of a system providing temporary ocean inflow to the IRL. The results of the full Restore Lagoon Inflow Research project will provide information and analysis to the lead agency and appropriate decision-makers to help determine the viability of a full-scale, permanent ocean inflow system; identify factors that should be considered should a natural breach occur; or if further evaluation is necessary.

This report represents the foundational data collected during Phase 1 baseline monitoring and is an essential part of the project. The project team carefully evaluated the parameters required to assess the effectiveness, environmental effects, and limitations of an inflow system. These data will be invaluable not only for the inflow project but also for researchers requiring similar data for other applications in the IRL and nearshore Atlantic Ocean.

This Phase 1 monitoring represents three seasons of population dynamics in seagrasses, benthic infauna, phytoplankton, ichthyoplankton, fishes, and eDNA surveys, as well as geochemical data, but it is important to obtain at least one more year of these measurements to identify seasonal variation. Continuation of monitoring, site selection, preliminary design of the temporary inflow pilot system, and pre-application permitting meetings with regulators are planned for Phase 2. Regulatory and agency feedback will help inform analysis and data collection priorities in Phase 2 and subsequent phases of the research project.

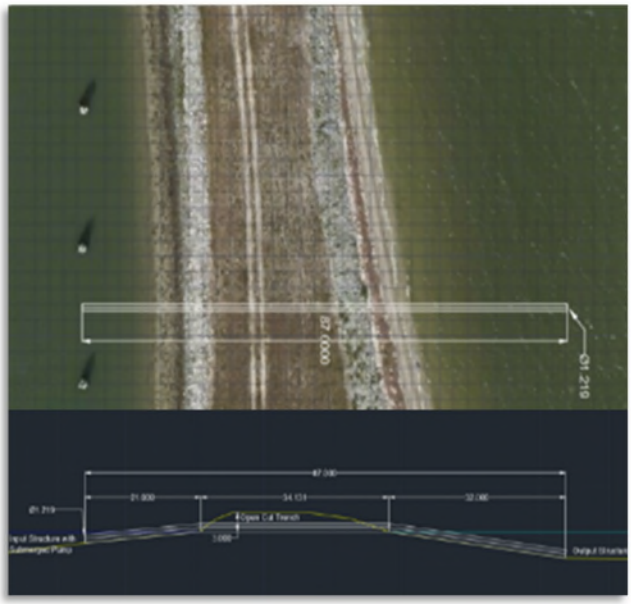

Potential pipe and pump pilot study location and conceptual design

For Phase 2, the temporary inflow pilot site location for establishing an exchange with the coastal ocean will be determined using the biological and geochemical data and modeling from this Phase 1 study and considering practicality (i.e., land ownership, utilities, distance, public roadways, zoning, noise impact, and agency permitting probability), existing exchange conditions, and how pilot flow impacts can meaningfully be extrapolated to other sites. Subsequent phases of the Restore Lagoon Inflow Research project are anticipated to involve permitting, implementation of the temporary inflow pilot system, continued monitoring, and analysis of the effects of the temporary inflow of seawater into the lagoon.

1 Introduction and Study Background

1.1 Introduction

The Indian River Lagoon (IRL) is a shallow (less than 5 meters [m]) bar-built, lagoon type estuary that extends approximately 250 kilometers (km) along the central east coast of subtropical Florida and ranges in width from less than 1 to approximately 9 km (Sigua et al. 2000). The IRL is connected to the ocean by six inlets (from north to south): Ponce de Leon, Port Canaveral, Sebastian, Fort Pierce, St. Lucie, and Jupiter (Figure 1-1). The inlets are directly connected to the ocean except for the Port Canaveral Inlet, which is separated from the lagoon by a lock system. Saltwater influx to the IRL comes from five widely spaced inlets, which classifies the IRL as a restricted lagoon (Kjerfve 1986, Smith 1990). A distance of approximately 145 km separates the two northernmost inlets, Ponce de Leon and Sebastian. With shallow water depths and narrow connections between the sub-basins in the northern IRL, there is little tidal exchange (Saberi and Weaver 2016a, Zarillo 2015).

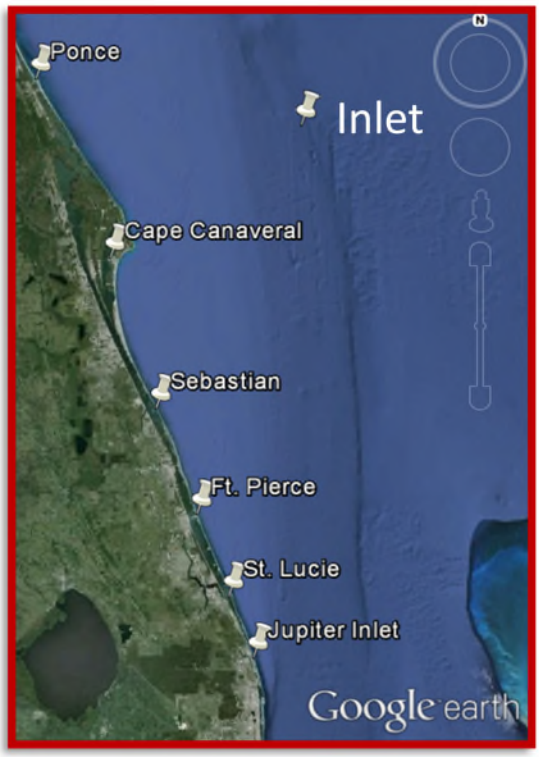

Figure 1-1: Location of the five IRL inlets

The Banana River Lagoon (BRL) is a sub-basin of the IRL that lies between Cape Canaveral and Merritt Island and extends from the National Aeronautics and Space Administration (NASA) Kennedy Space Center to Dragon Point. The BRL is poorly flushed with no direct connection to the ocean, which leads to some of the longest residence times in the IRL system. According to the Florida Department of Environmental Protection (FDEP), it takes approximately 2 years for the water to flush in the BRL (FDEP 2013). The northern section of BRL was historically connected to the IRL by a series of natural channels. Prior to the development of the barrier island, each sub-basin of the IRL was subjected to episodic over washing and breaching of the barrier island by storms as evidenced by the numerous relict tidal inlet shoals and expansive wash over sediment

fans. This historical inflow would bring ocean water into regions of the IRL and enhance the circulation in the estuary.

1.2 Restore Lagoon Inflow Research Background

In the past decade, IRL water quality has declined with more severe and frequent harmful algal blooms (Marine Resource Council 2018; Tetra Tech 2020). The purpose of the Restore Lagoon Inflow Research study is to evaluate the possible impacts of restoring lagoon inflow and enhancing circulation at three primary locations: (1) near Port Canaveral, (2) near Cocoa Beach, and (3) near Bethel Creek (Figure 1-2).

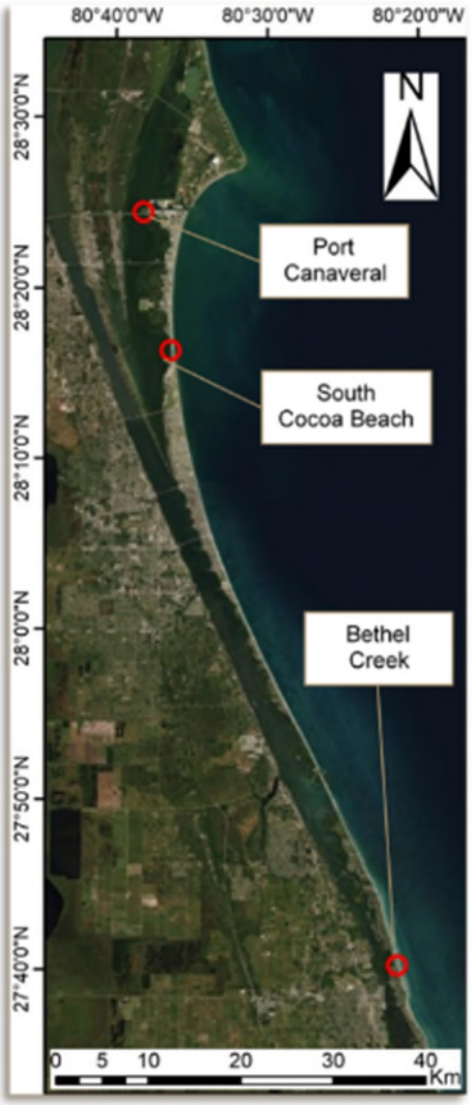

Figure 1-2: Map of the three proposed locations to restore lagoon inflow

The purpose of this first phase of the study is to gather baseline data and modeling on existing water quality, biological parameters, and hydrological conditions at potential locations for a temporary inflow pilot system. The modeling and engineering proceeded in parallel with biological and water quality monitoring in advance of a temporary inflow pilot system, which is part of a future project phase. This ecosystem monitoring is crucial to understanding the baseline status of the

lagoon near the proposed inflow, as a comparison to monitoring results from implementation of the temporary inflow pilot system project. The results of the full Restore Lagoon Inflow Research project will provide information and analysis to the lead agency and appropriate decision-makers to help determine the viability of a full-scale, permanent ocean inflow system, identify factors that should be considered should a natural breach occur, or if further evaluation is necessary.

Phase 1 of the study included three tasks:

1. **Modeling and Engineering** – Targeted numerical modeling was used to evaluate the effect of different inflow scenarios on the physical parameters of the IRL. A global circulation model was used to provide boundary conditions to an environmental fluids model that was used to predict the changes in water level, flow, salinity, and temperature that can be expected for each scenario. The model was calibrated and validated with measured data. Designs were also developed for flow structures that could be used for a temporary pilot study and a potential, future temporary system to create inflow from the ocean to the lagoon.
2. **Biological Monitoring** – Monitoring was conducted to document baseline biological characteristics of the IRL and coastal ocean in the vicinity of the proposed inflow locations. The monitoring data were also used to begin assessing the likely biological responses to an inflow system at the proposed locations.
3. **Geochemical Baseline** – Data were collected and evaluated to calculate the impacts of an inflow system on nutrient concentrations in the lagoon and the quantity of nutrients that could be discharged into the coastal ocean. Data from existing water quality sensors were extrapolated to determine conditions in bottom water near proposed inflow locations. In addition, changes to temperature, salinity, and dissolved oxygen (DO) that could result from various inflows were evaluated to determine the influence on the geochemical cycling of nitrogen (N), phosphorus (P), and oxygen in the lagoon.

Additional details about the data used, approach, and conclusions from each study task are included in Section 2. The recommendations from the Phase 1 tasks and next steps for Phase 2 are included in Section 3. The detailed reports for each task are attached in appendices.

2 Key Findings

The key findings in this section are a summary of the reports prepared by the Principal Investigators. The Task 1 Modeling and Engineering report, outlined below as Tasks 1a and 1b, respectively, was prepared by Dr. Gary Zarillo and Dr. Robert Weaver, and the full report is provided as Appendix A. The Task 2 Biological Monitoring report was prepared by Dr. Kevin Johnson, Dr. Ralph Turingan, Dr. Jeffrey Eble, Dr. Johnathan Shenker, and Dr. Jesse Blanchard, and the full report is provided as Appendix B. The Task 3 Geochemical Baseline report was prepared by Dr. Austin Fox, and the full report is provided as Appendix C.

2.1 Modeling (Task 1a)

With targeted numerical modeling, this study evaluates the effect of different inflow scenarios on IRL physical parameters. Using a global circulation model to provide boundary conditions, an environmental fluids model was used to predict the changes in water level, flow, salinity, and temperature for each temporary pilot inflow system and potential full-scale, permanent system scenarios. The model results were supported by in-situ measurements taken at locations in the BRL: where the water exchanges with the IRL proper, at Dragon Point, and the Barge Canal (Figure 2-1). Measured data were used to calibrate and validate the model performance. The model predictions were shared with project partners working on Tasks 2 and 3, the Biological Monitoring and Geochemical Baseline, respectively.

2.1.1 Approach

The model approach accounts for the forces of wind, current, and water elevation. Baseline data were collected from existing monitoring locations and supplemented by three Acoustic Doppler Current Profilers (ADCPs). These ADCPs were deployed strategically to capture current velocity and water level data at each of the entry points to the BRL (Figure 2-1). Wind input was obtained from the National Oceanic and Atmospheric Administration North American Mesoscale database. These data were used to calibrate and validate the model approach.

The numerical modeling scheme applied for flushing and transport (salt and heat) experiments was modified to accept forcing conditions from the open coastal ocean. This modification included extending the model grid though Ponce Inlet, Sebastian Inlet, and Fort Pierce Inlet into the coastal ocean. Water level, salinity, and water temperature time series were applied from output from the Advanced Circulation (ADCIRC) model and Hybrid Coordinate Ocean Model (HYCOM).

ADCIRC can be dynamically coupled with the Simulating Waves Nearshore (SWAN) model (Booij et al. 1999). In ADCIRC+SWAN, the ADCIRC model passes water level, current velocities, wind velocities, and friction roughness lengths to the SWAN model. SWAN then computes wave spectra. Wave characteristics are passed back to ADCIRC where the radiation stress gradients are evaluated at each vertex and used to compute the water level and current velocity at the next time step (Dietrich et al. 2011, 2012). Passing data back-and-forth in this manner represents true two-way coupling, producing results that consider the relevant coastal physics and changing water levels. Final output files from the model included global water elevations, global depth-averaged velocities, water elevations and depth-averaged velocities at specified stations, and meteorological output at specified stations.

Figure 2-1: Locations of ADCP deployments indicated in red

The model applied to meet the project objectives is the United States Environmental Protection Agency-supported Environmental Fluid Dynamics Code (EFDC) model (Tetra Tech 2007). The model includes features and capabilities that make it applicable to shallow estuarine environments. The project areas extend from the Mosquito Lagoon into the IRL compartments extending to the Fort Pierce Inlet. A coupled EFDC/Three-Dimensional Hydrodynamic-Eutrophication Model was developed and refined at the Virginia Institute of Marine Science (Hamrick 1992). This multi-parameter finite difference model represents estuarine flow and material transport in three dimensions and has been extensively applied to shallow estuarine environments in Florida and other coastal states.

Figure 2-2 shows the overall extent of the IRL model grid that extends from Ponce Inlet on the north to just south of the Fort Pierce Inlet. The model grid includes 10,094 active computational cells in the horizontal dimension and 5 layers in the vertical dimension.

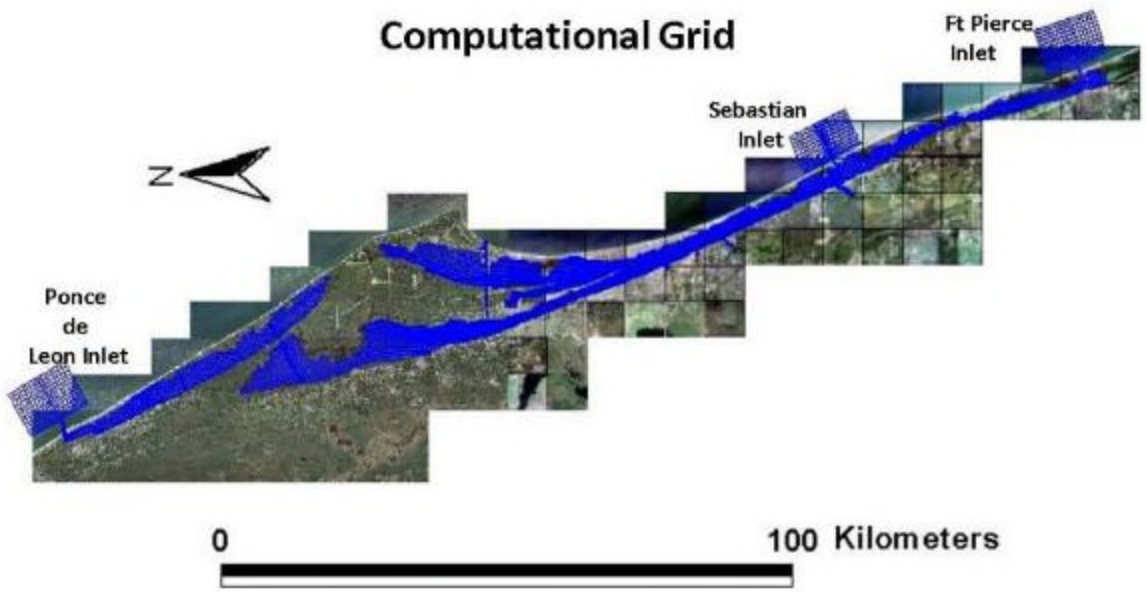

Figure 2-2. IRL model computational grid from Ponce de Leon Inlet to Fort Pierce Inlet

Model cases to examine the potential impact of enhanced inflows to the IRL from the coastal ocean were based on assumed pumping rates of ocean water into the system at selected locations. An additional case included a weir structure located in the west basin of Port Canaveral. Table 2-1 lists the hypothetical model cases evaluated in this project.

Model results, presented in terms numerical tracer concentrations, were used to evaluate the ability of inflows to promote exchanges of water out of particular IRL compartments. The use of estuarine water tagged with 100 parts per thousand (ppt) of a numerical tracer allowed the evaluation of the degree to which a particular IRL compartment can be flushed over a period of time. The model runs applied in this project were 365-day periods from January 2016 to January 2017. Each run had an approximate 10-day period of equilibration to boundary conditions at the beginning. Figure 2-3 shows the locations of the numerical monitoring stations in the BRL.

Table 2-1. Model test cases for enhanced flow

Case	Location	Rate of Enhanced Inflow
Base	No enhanced inflow	Zero
Pump Station 1	BRL near Patrick Air Force Base (PAFB)	10 cubic meters per second (m^3/s)
Pump Station 2	BRL North of Port Canaveral	10 m^3/s
Weir Structure	West Port Canaveral Basin	Variable
Pump Station 3	Bethel Creek IRL	5 m^3/s

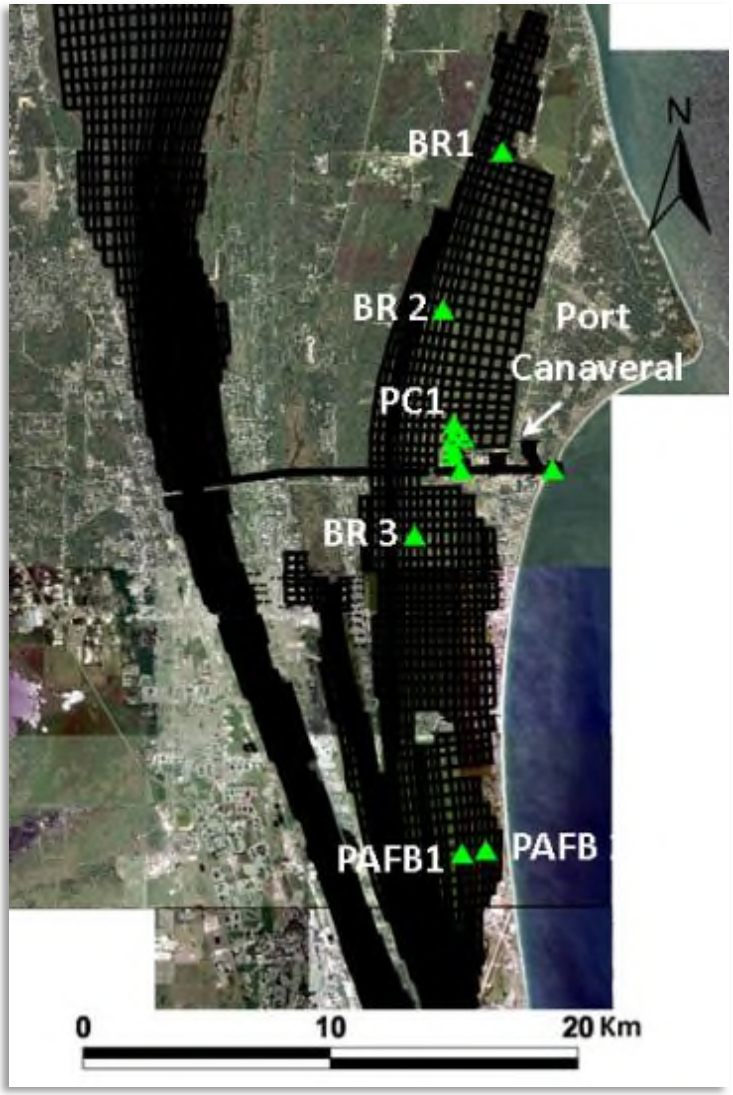

Figure 2-3. Location of numerical monitoring stations in the BRL

2.1.2 Data

EFDC model runs were completed in each of the potential inflow locations with the assumed flows outlined in Table 2-1. Results for the predicted tracer concentration in the base case were compared to each flow scenario: Pump Station 1 (PAFB), Pump Station 2 (north of Port Canaveral), and the Weir (Port Canaveral Locks) for 100 days (Figure 2-4) and 365 days of simulation (Figure 2-5). Pump Station 3 (Bethel Creek) was compared to the base case after 3 days (Figure 2-6) and 20 days of simulation (Figure 2-7).

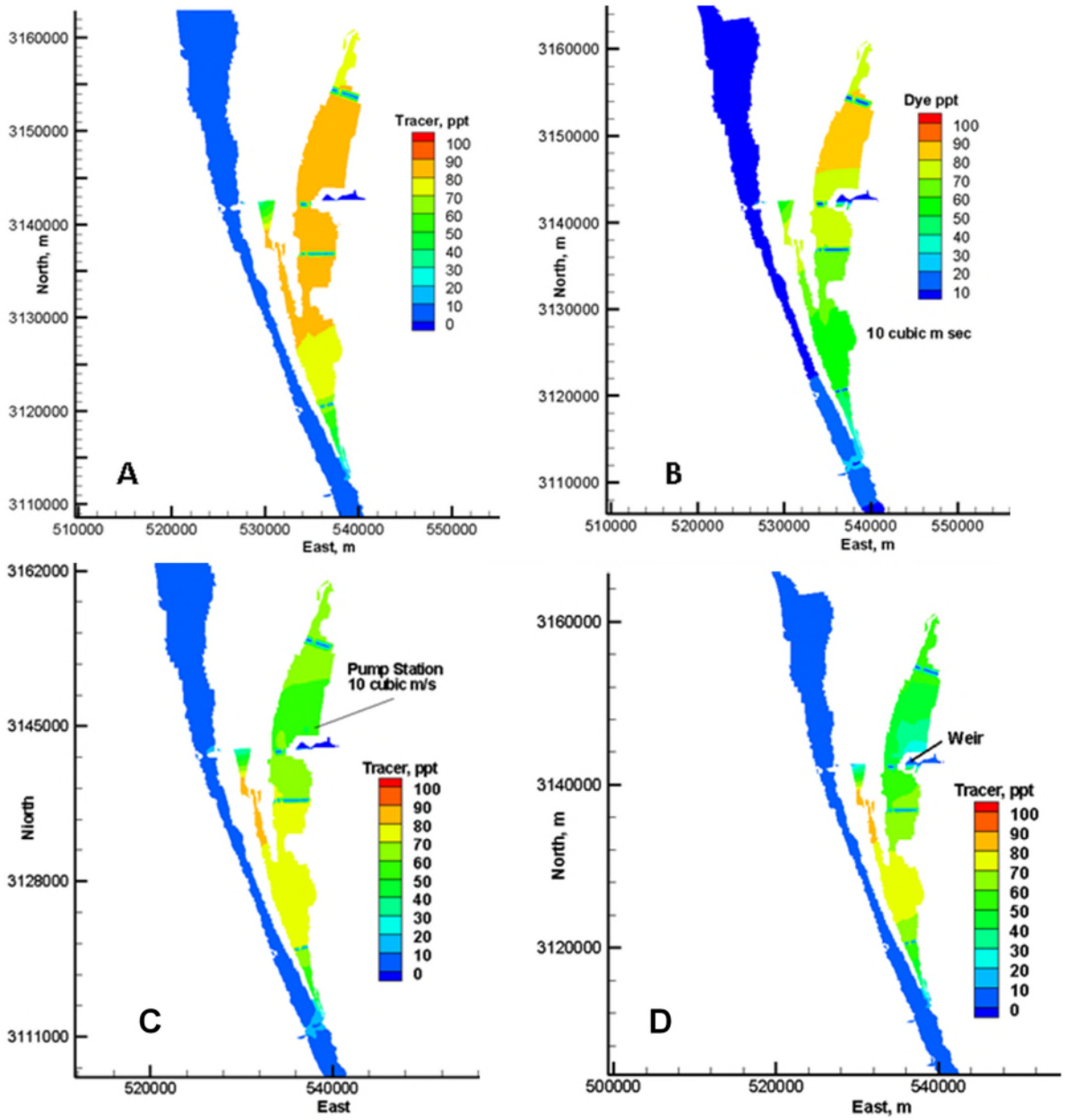

Figure 2-4. Predicted tracer concentration in the model surface layer after 100 days of simulation for the base case (A), Pump Station 1 (B), Pump Station 2 (C), and Weir (D)

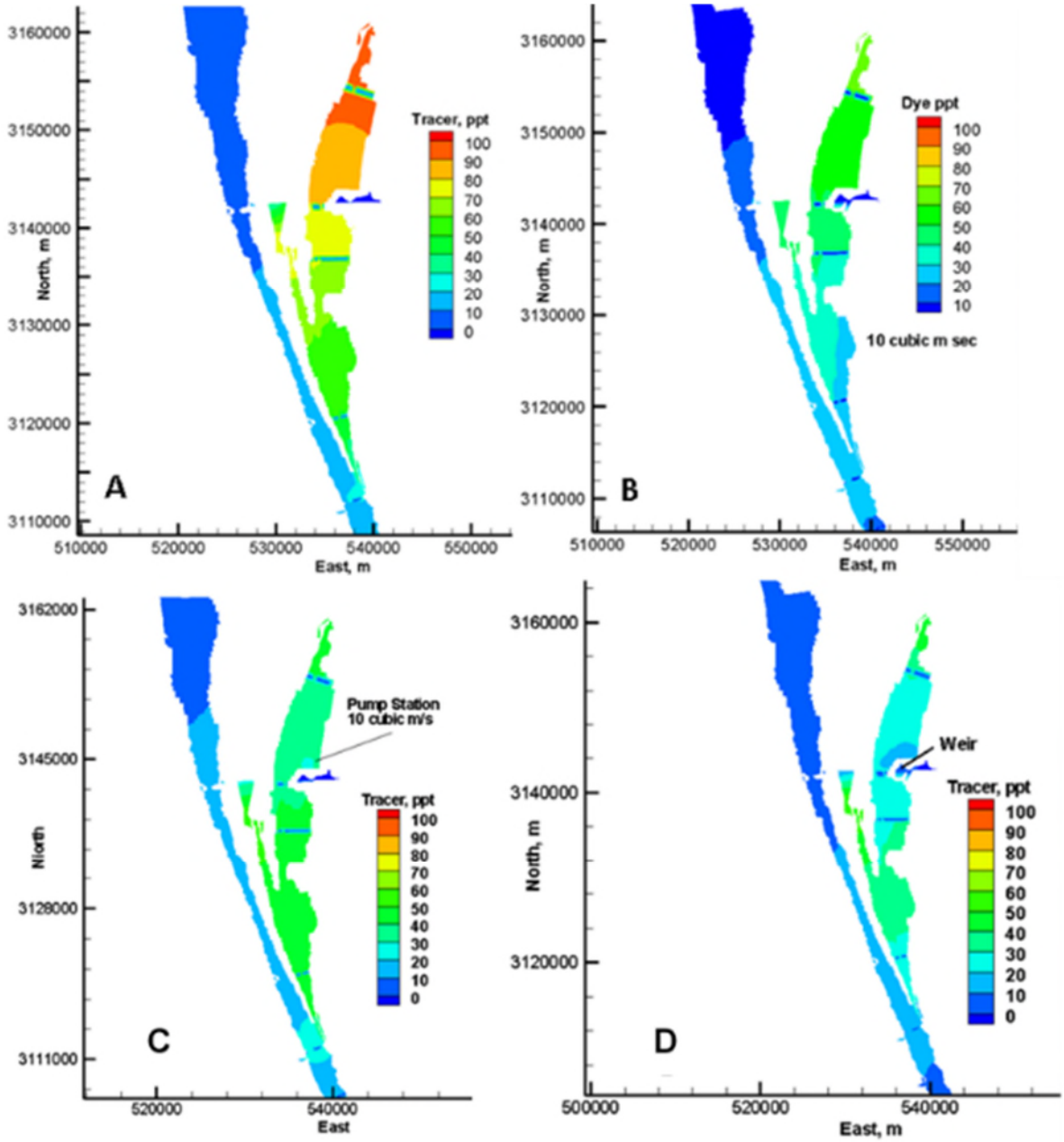

Figure 2-5. Predicted tracer concentrations in the BRL after 365 days of simulation for the base case (A), Pump Station (B), Pump Station 2 (C), and Weir (D)

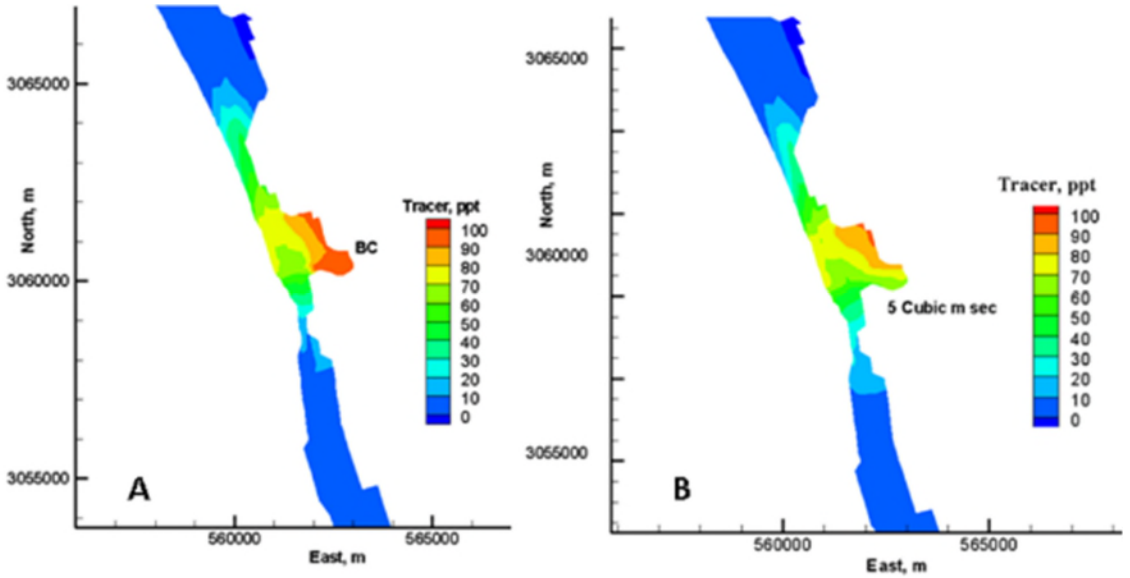

Figure 2-6. Predicted tracer concentration in the model surface layer at station BC2 after 3 days of simulation for the base case (A) and Pump 3 (B)

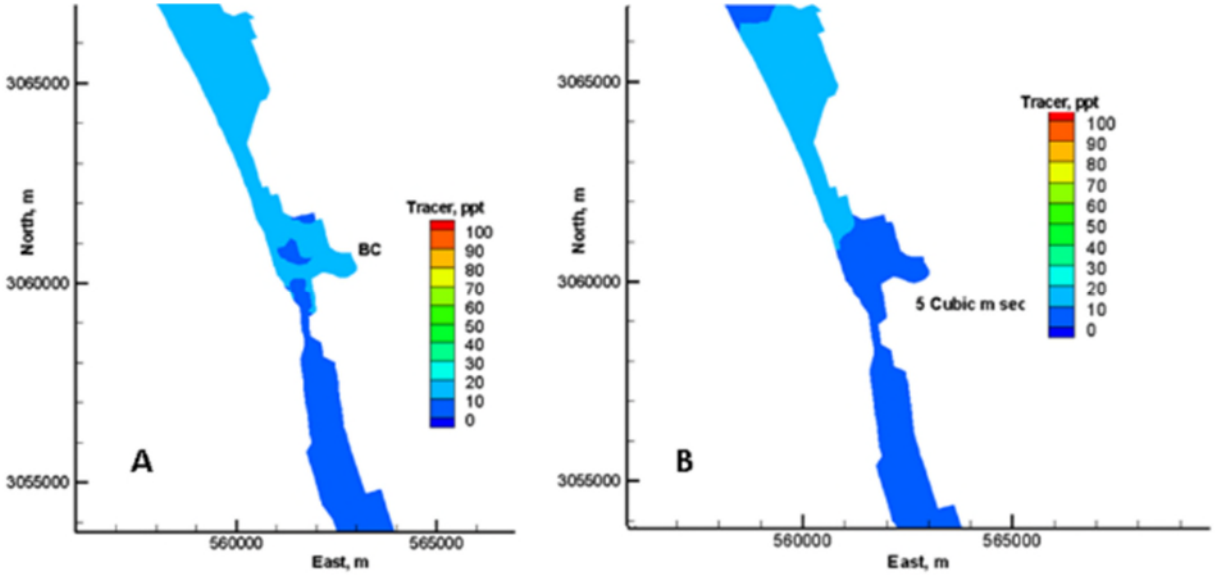

Figure 2-7. Predicted tracer concentration in the model surface layer at station BC2 after 20 days of simulation for the base case (A) and Pump 3 (B)

Predicted water temperature under each flow scenario was fractionally lower compared to the base case. The water temperature in the summer months was not subject to as extreme temperature fluctuations under the Pump 2 and Weir scenarios, due to the water temperature boundary condition applied to Pump 3, which was derived from HYCOM (Figure 2-11).

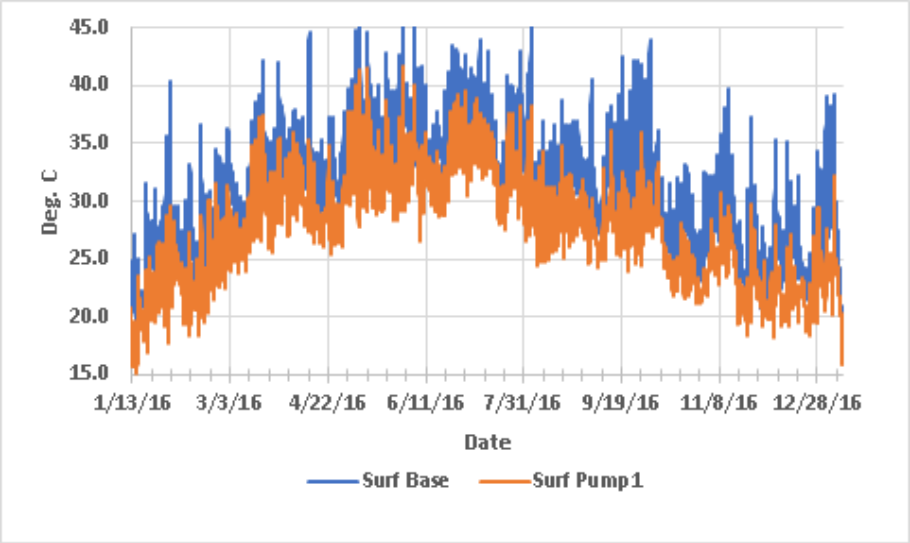

Figure 2-8. Predicted water temperature in the model surface layer at PAFB 1 for the base case and the Pump 1 case

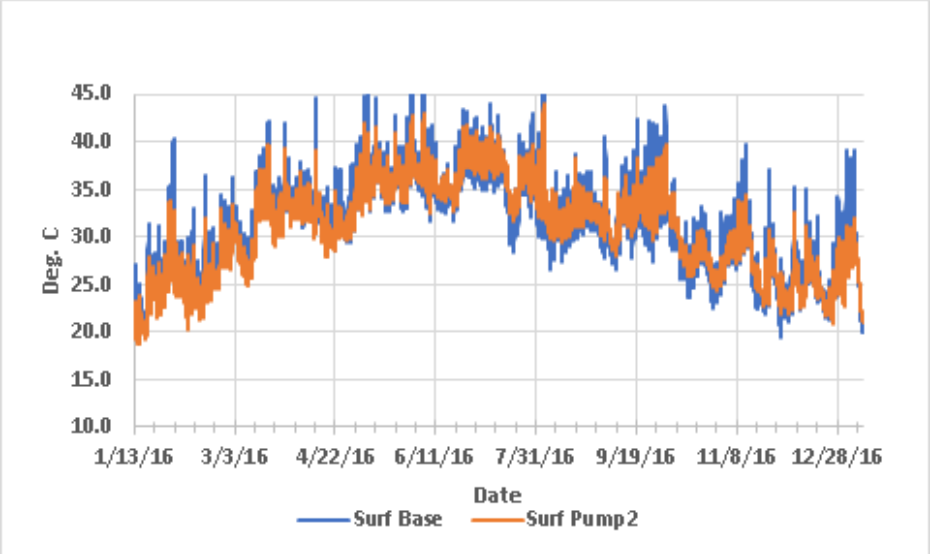

Figure 2-9. Predicted water temperature in the model surface layer at station PC1 for the base case and the Pump 2 case

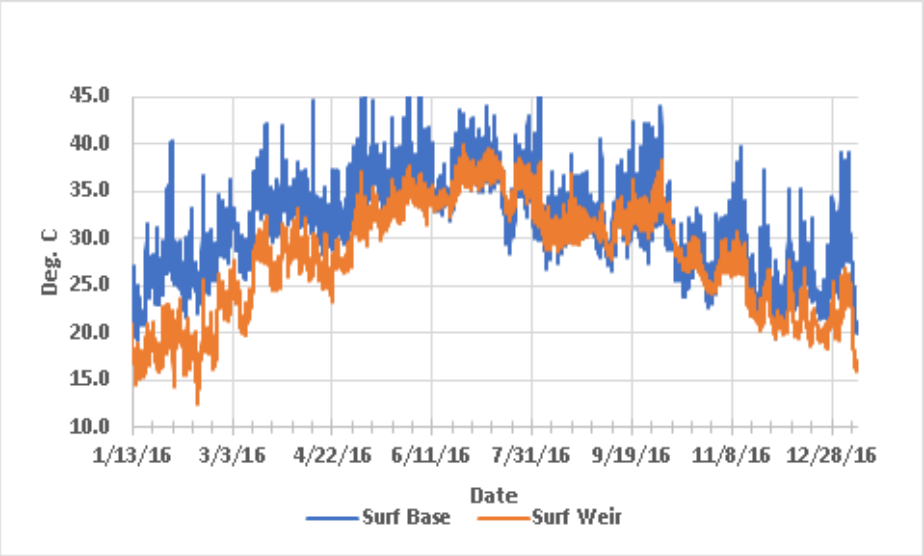

Figure 2-10. Predicted water temperature in the model surface layer at station PC1, adjacent to the inflows for the base case and the Weir case

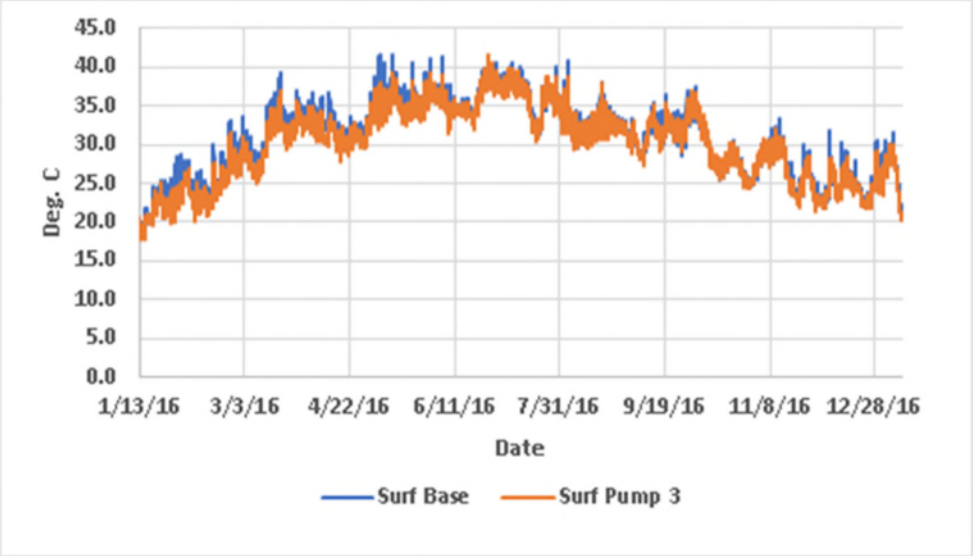

Figure 2-11. Predicted water temperature in the model surface layer at station BC1 in Bethel Creek for the base case and the Pump 3 case

Salinity under the Pump 1 and Pump 3 cases was higher at the pumping source with increasing salinity over time, but little to no change was identified in the modeling stations farther from the pumping source (Figure 2-12 and Figure 2-15, respectively). For the Pump 2 and Weir cases, the predicted increase in salinity was at or near 5 practical salinity units (PSU) within the first two months of pumping, and the locations farther from the pumping locations approached 5 PSU after 11 months of pumping (Figure 2-13 and Figure 2-14).

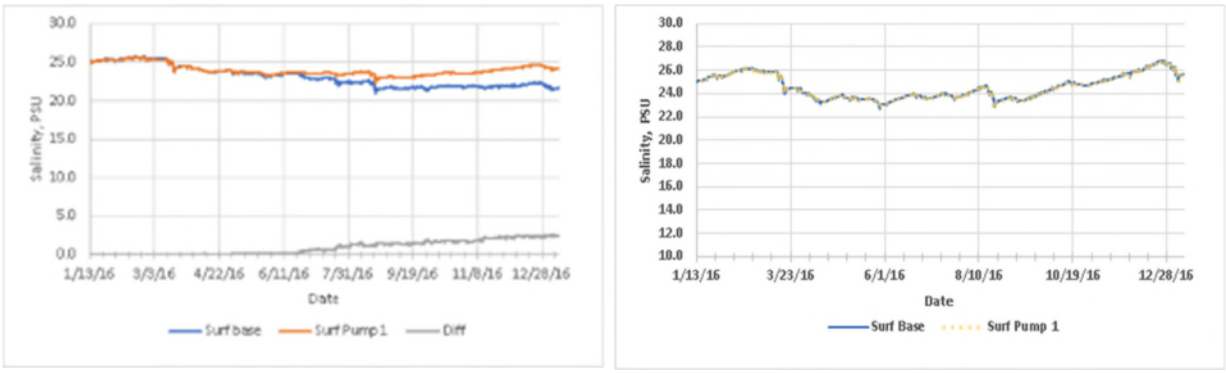

Figure 2-12. Predicted salinity in the surface model layer at PAFB 2 (left) and at BR 2 (right) for the Pump 1 case and the base case

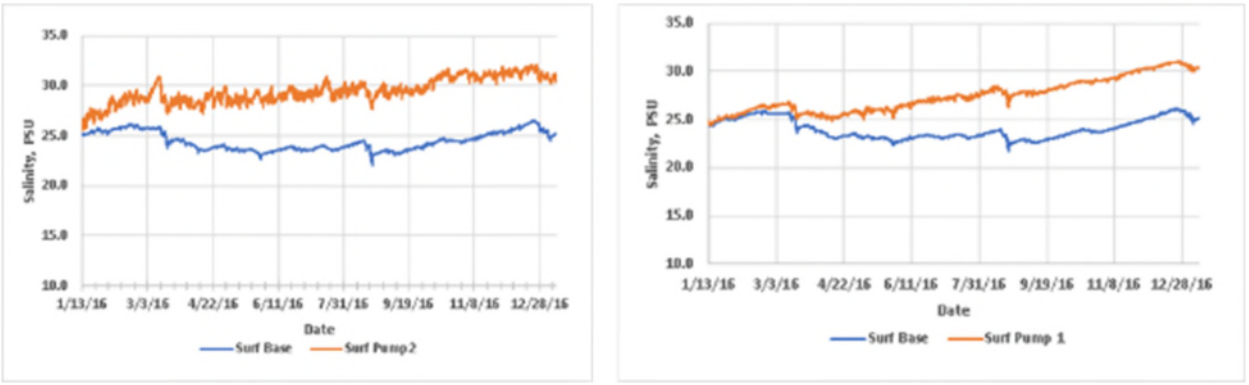

Figure 2-13. Predicted salinity in the surface model layer at PC2 (left) and BR1 (right) for the Pump 2 case and the base case

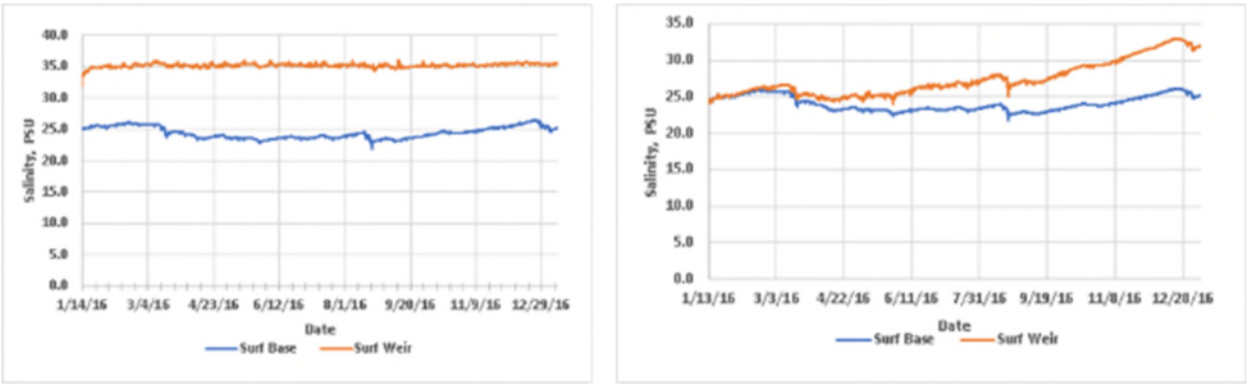

Figure 2-14. Predicted salinity in the surface model layer at station PC1 (left) and BR1 (right) for the Weir case and base case

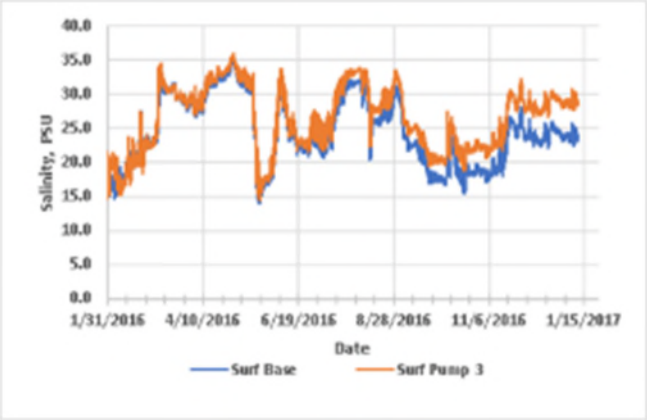

Figure 2-15. Predicted salinity in the surface model layer at station BC2 for the Pump 3 case and the base case

2.1.3 Conclusions

The ADCIRC model calibrated well to the ADCP data, although the models were very sensitive to the meteorological forcing inside the estuary (Weaver et al. 2016a and Weaver et al. 2016b). Outside the estuary, the models agreed with the available measured data from the Trident Pier station. The EFDC model calibrated well with measured data within the IRL and can be applied to evaluation of a temporary inflow pilot system with confidence.

Model tracer study results indicated that the BRL flushes to 50% or less of initial tracer concentration based on a 10 m^3/s pump station north of PAFB. This flushing was dependent on the location within the BRL. The south compartment flushed within 50 days, main compartment within 120 days, and entire BRL within 200 days. Under the base case, flushing times were more than 200 days.

Flushing time results improved for the pump station located just north of Port Canaveral. The potential for flushing of tracer out of a large portion of the BRL was much greater with the pumping located further north. Results indicated that siting an inflow structure as far north as possible will have the greatest impact on BRL tracer concentrations and flushing.

A weir at Port Canaveral provided flushing of north BRL compartments within 30 days, and the entire BRL within 80 days. The weir within Port Canaveral produced the greatest potential for exchanging water out of the BRL over a shorter time period compared to the two pump scenarios.

For each scenario, predicted changes in salinity ranged up to 5–10 PSU with the largest potential increase generated by the weir inflows. Predicted impacts on salinity were reduced with distance from the inflow structure. Changes in temperature were less pronounced amounting to a fractional decrease in temperature as the cooler ocean water mixed with the lagoon water near the structure.

Due to its location in the basin, Bethel Creek exchanged effectively with the adjacent IRL. The addition of a 5 m^3/s pump station flushed this IRL compartment in days with minimal impacts on salinity and temperature.

The modeling supported the concept of using ocean inflow to circulate BRL water, moving stagnant lagoon water and replacing it with ocean water. The temporary pilot inflow or a potential full-scale, permanent system will create a slow current that will circulate the water toward the inlets and facilitate enhanced exchange and mixing into the larger IRL system. Localized salinity changes are predicted with minimal temperature changes.

2.2 Engineering (Task 1b)

Designs were developed for flow structures for a temporary inflow pilot system and a potential full-scale, permanent system to create inflow from the ocean to the lagoon. Although the study site selection represented locations where structures may be most effective and feasible, no final siting determination has been made.

2.2.1 Approach

Designs of three potential structures were drafted: pipe with no pump, pipe and pump, and weir. The designs were formulated around the flow parameters selected earlier in the project. The temporary inflow pilot system flow rate was set to a minimum of 5 m^3/s and the potential full-scale, permanent system flow rate was set to a minimum of 20 m^3/s. Each concept was focused on controlled inflow of ocean water into the BRL. By only allowing one-way flow of water into the IRL, a hydraulic head is formed, thus creating a net transport in the BRL and IRL toward the inlets, where the water exits the IRL having mixed with the tidal prism. The structures must be manageable, consisting of pumps and/or gates to restrict the exchange of water, should there be indication of poor water quality in the coastal ocean (e.g. harmful algal blooms, chemical spill, low DO, etc.). Additionally, there are times of the year, from late September through mid-December, when the water levels along the Florida Shelf are elevated due to the intra-annual fluctuations and inflow could be restricted using a gated structure or flow control pumps.

The flow calculations for each option were based on a head value of 0.5 m (1.64 feet), representing the difference between the BRL and the Atlantic Ocean water levels. On the ocean side, the average maximum surface elevation from the closest National Oceanic and Atmospheric Administration tide gauge, Trident Pier station, is approximately 0.80 m (2.62 feet). In the BRL, long-term water level gauges measured a seasonal average high water elevation of approximately 0.3 m (0.98 feet). The 0.5 m (1.64 feet) value used for the calculations is a conservative estimate for the average maximum head.

2.2.1.1 Pipe No Pump Option

For the pipe no pump option, located at the north end of PAFB, the pipe would need to be drilled a total of 2,400 m (7,874 feet) horizontally underground before surfacing at each side. The pipe would be met with an intake structure in the Atlantic Ocean and an outfall structure in the BRL.

For a temporary inflow pilot system to reach a flow of 5 m^3/s (177 cubic feet per second [ft^3/s]), the inner diameter of one pipe would need to be 2.92 m (9.58 feet). If two pipes were drilled next to each other, each pipe would need an inner diameter of 2.20 m (7.22 feet). An aerial view of the design for the temporary inflow pilot system including two pipes is provided in Figure 2-16. For a potential full-scale, permanent system design to reach a flow of 20 m^3/s (706 ft^3/s), the inner diameter of one pipe would need to be 5.12 m (16.80 feet). If two pipes were drilled next to each other, each pipe would need to have an inner diameter of 3.86 m (12.66 feet). Due to the large diameter of pipe needed to achieve the desired flow rates, it was determined that the pipe no pump option would not be feasible.

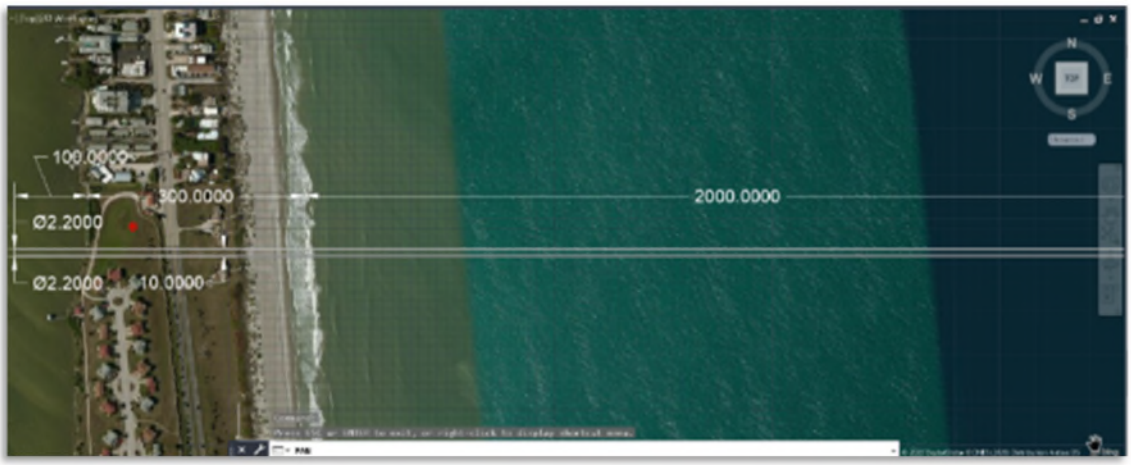

Figure 2-16: Temporary inflow pilot system with two pipes no pump located at the north end of PAFB (Google Earth 2019)

2.2.1.2 Pipe and Pump Option

For the pipe and pump option, located at the north end of PAFB, the pipe would need to be drilled 2,400 m (7,874 feet) horizontally underground; however, it would surface on the land portion to connect each side to a pump house. The pipe would be met with an intake structure in the Atlantic Ocean and an outfall structure in the BRL.

For a temporary inflow pilot system to reach a flow of 5 m^3/s (177 ft^3/s), the inner diameter of one pipe would need to be 1.86 meters (6.10 feet) when using a 200-horsepower pump. If two pipes were drilled next to each other and two 200-horsepower pumps were used, each pipe would need to have an inner diameter of 1.24 m (4.07 feet). A side view design for the Cocoa Beach (Pump 1 case) temporary inflow pilot system, including one pipe is provided in Figure 2-17.

For a temporary inflow pilot system located at the locks at Canaveral Port Authority to reach a flow of 5 m^3/s (177 ft^3/s), the inner diameter of the pipe would need to be 1.09 m (3.58 feet) when using a 200-horsepower pump. When rounding this diameter to standard pipe dimensions, the diameter would need to be 48 inches (1.219 m). The approximate location and pipe dimensions are shown in Figure 2-18 and Figure 2-19.

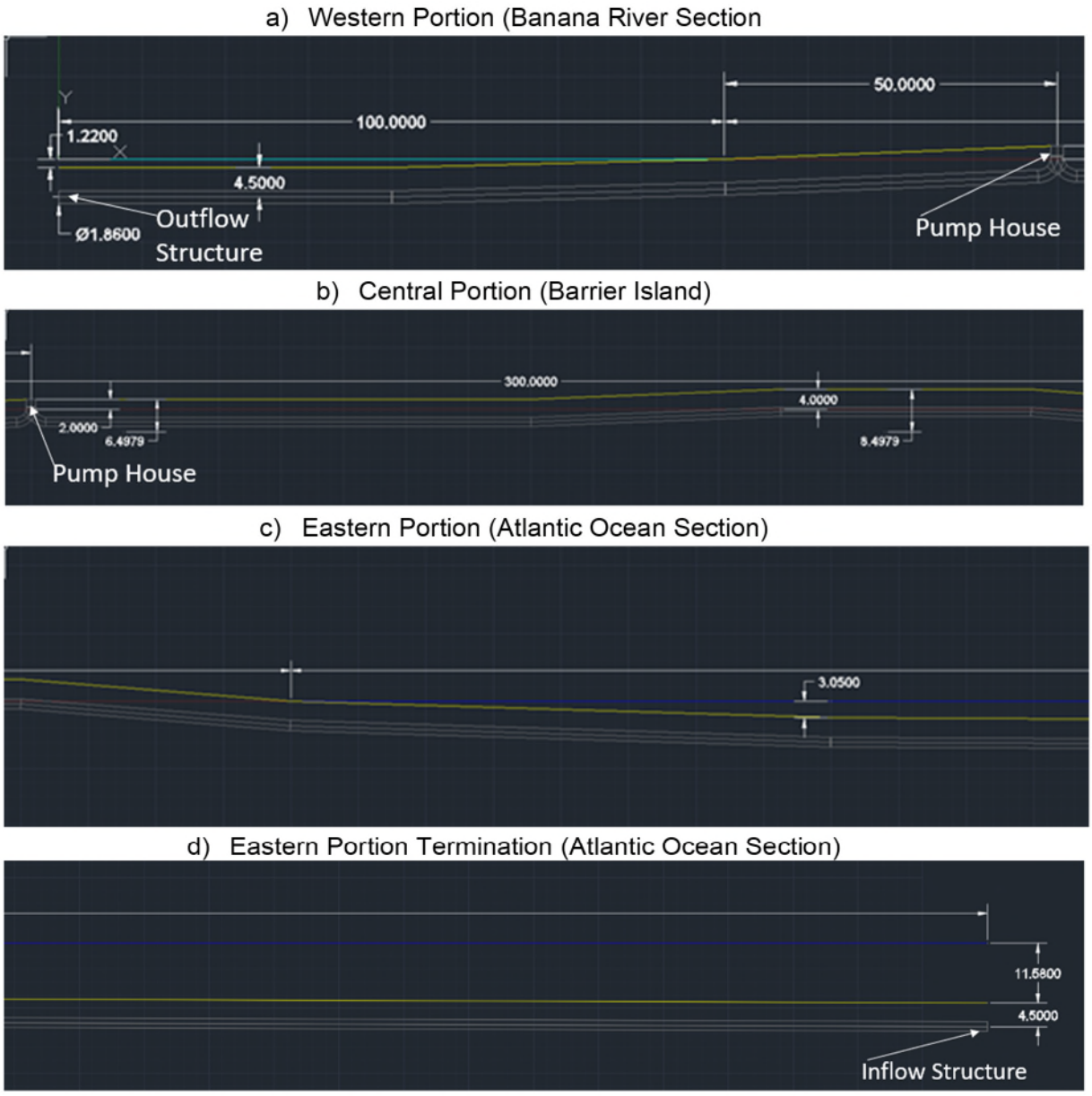

Figure 2-17: Temporary inflow pilot system side view with pump split into sections: a) western, b) central, c) eastern, and d) termination

Figure 2-18: Above ground pipeline location (Google Earth 2019)

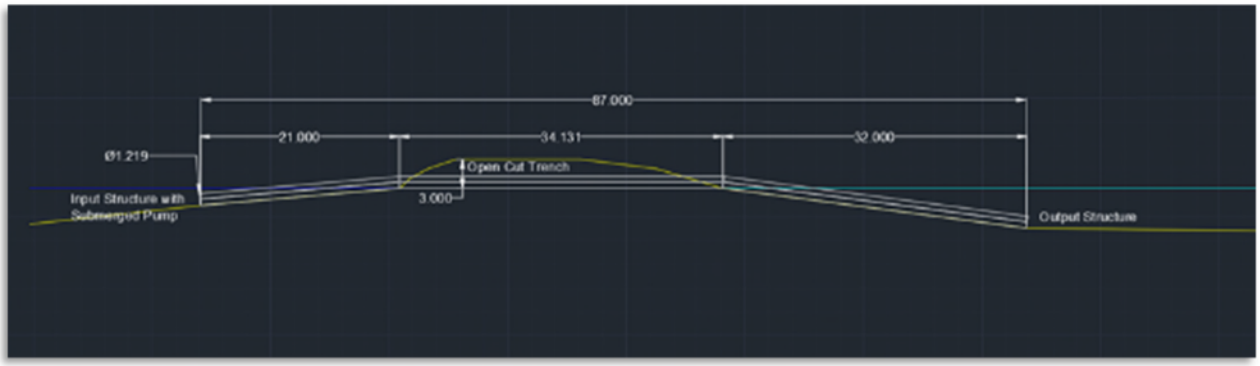

Figure 2-19: Above ground pipeline side view

2.2.1.3 Weir Option

A weir is a structure that governs the flow of water between two bodies of water. For this option, located at Port Canaveral, a rectangular weir was selected to maximize the flow rate. The geometry consists of a blunt front section and an angled aft slope (Figure 2-20 and Figure 2-21).

A sharp- crested weir geometry was chosen due to the project location specifications. Based on long-term water level data in the BRL, the weir height was determined to be 0.30 m (0.98 feet) above mean sea level. This elevation takes into consideration the intra-annual water level fluctuations in the BRL and is designed to not produce a backflow into the port. The weir head was determined using surface water elevation changes due to tides. The average maximum sea surface elevation was 0.80 m (2.62 feet) with the weir head calculated to be 0.50 m (1.64 feet).

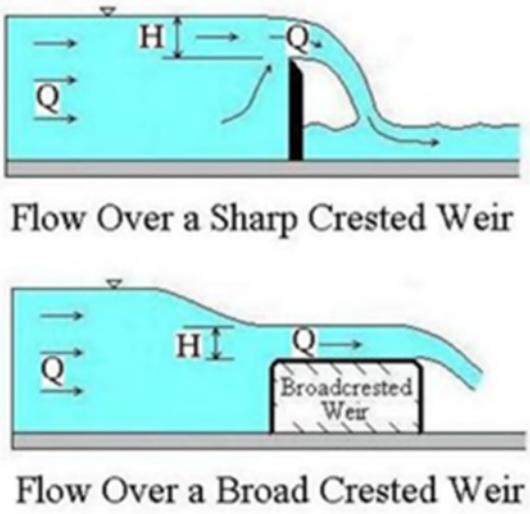

Figure 2-20: Sharp-crested versus broad-crested weirs (Bengtson 2018)

Figure 2-21: Example weir gate system (Pxfuel 2020)

2.2.2 Data

Costs and flow rates were considered for each approach, including a temporary inflow pilot system and potential full-scale, permanent system assessment.

2.2.2.1 Design Flows

Flow rates for the pipe and pump system are controlled by the pump. Design flow rates for the temporary inflow pilot system are 5 m^3/s, and flow rates for the potential full-scale, permanent system are 20 m^3/s. For the weir, the flow rate would be dictated by the width of the weir, as shown

in Table 2-2. Using a weir length of 200 m and weir head of 0.957 m (the maximum weir head predicted from March 16, 2019 to March 15, 2020), the flow rate would be 470.373 m^3/s.

Table 2-2: Average yearly flowrate

Weir Length (m)	50	100	150	200
Average Yearly Flowrate (m^3/s)	7.608	15.216	22.823	30.432
Average Yearly Flowrate per meter ($m^3/s/m$)	0.152	0.152	0.152	0.152
Maximum Hourly Flowrate (m^3/s)	117.593	235.189	352.780	470.373

2.2.2.2 System Costs

A high-level cost estimate was obtained from Laney Directional Drilling for the temporary inflow pilot system flowrate of 5 m^3/s with a single pipe (Table 2-3) and a double pipe (Table 2-4). Micro-tunneling would be used for the ocean and river outfalls. The pipe diameters were rounded to the nearest standard pipe dimension. Due to the costs of large diameter micro-tunneling, the single pipe cost estimate is approximately 30% higher than the double pipe option.

Table 2-3: Single pipe and pump temporary inflow pilot system cost estimate (5 m^3/s)

Item	Details	Quantity	Units	Per Unit Cost	Total Cost
Ocean Outfall Portion	Diameter = 1.86 meters (74"), Length = 2,000 meters (6,562 feet)	1	Each	$50,000,000.00	$50,000,000.00
River Outfall Portion	Specs: Diameter = 1.86 meters (74"), Length = 400 meters (1,312 feet)	1	Each	$8,000,000.00	$8,000,000.00
Pump	SJP 48PO-1	1	Each	$1,250,000.00	$1,250,000.00
Total +/-50%	**-**	**-**	**-**	**-**	**$59,250,000.00**

Table 2-4: Double pipe and pump temporary inflow pilot system cost estimate (5 m^3/s)

Item	Details	Quantity	Units	Per Unit Cost	Total Cost
Ocean Outfall Portion	Diameter = 1.24 meters (48"), Length = 2,000 meters (6,562 feet)	1	Each	$35,000,000.00	$35,000,000.00
River Outfall Portion	Diameter = 1.24 meters (48"), Length = 400 meters (1,312 feet)	1	Each	$6,000,000.00	$6,000,000.00
Pump	SJP 48PO-1	2	Each	$1,250,000.00	$2,500,000.00
Total +/-50%	**-**	**-**	**-**	**-**	**$43,500,000.00**

Again, a high-level cost estimate was obtained from Laney Directional Drilling for the full-scale, permanent system flowrate of 20 m^3/s with a single pipe (Table 2-5). Micro-tunneling would be used for both the ocean and river outfalls. The pipe diameters were rounded to the nearest standard pipe dimension.

Table 2-5: Single pipe and pump full-scale, permanent system cost estimate (20 m^3/s)*

Item	Details	Quantity	Units	Per Unit Cost	Total Cost
Ocean Outfall and River Outfall	Diameter = 3.26 meters (128"), Length = 2,400 meters (7,874 feet)	1	Each	$100,000,000.00	$100,000,000.00
Pump	-	1	Each	$1,250,000.00	$1,250,000.00
Total +/-50%	**-**	**-**	**-**	**-**	**$101,250,000.00**

*Note the estimate for the full-scale, permanent system was given as more than $100 million without an exact value.

Two design options, a weir and temporary pipe and pump system, are available if the Canaveral Port Authority site is selected. These represent the lowest cost alternative options (Table 2-6).

Table 2-6: Locks at Canaveral Port Authority above ground pipeline temporary inflow pilot system cost estimate (5 m^3/s with one pipe and pump)

Item	Quantity	Units	Per Unit Cost	Total Cost
Polymer coated pipe - D= 48"	285.5	feet	$64.47	$18,406.19
Pump: SJP 48PO-1 2.5m^3/s at 440 rotations per minute	2	Each	$1,250,000.00	$2,500,000.00
Input and Output structure	1	Each	$200,000.00	$200,000.00
Open Cut Trench	111.5	feet	$223.10	$24,875.65
Miscellaneous Site Work	1	Each	$160,000.00	$160,000.00
Subtotal	-	-	-	$2,903,281.84
Contractor Mobilization and Overhead (30%)	-	-	-	$870,984.55
Contingency (40%)	-	-	-	$1,161,312.73
Total +/- 50%	**-**	**-**	**-**	***$4,935,579.12***

Based on the annual average flow rate data in Table 2-7, the flow conditions for a flow rate up to the potential full-scale, permanent system flow of 20 m^3/s could be met with a 150 m weir at a cost of approximately $6.6 million.

Table 2-7: Total cost analysis for weir at different lengths

Weir length	Total Cost +/- 50%
50	$3,955,036.40
100	$5,266,572.80
150	$6,578,109.20
200	$7,889,645.60

2.2.3 Conclusions

To test the potential of a temporary inflow pilot system, the system would need to bring in a flow of 5 m^3/s. There are two options for a temporary inflow pilot system. One option is to construct the weir and control the flow over the weir by limiting the gate opening. When the temporary inflow pilot system testing is complete, the gates could be closed to leave the structure in place for potential future inflow, or the structure could be removed. The second option is a temporary structure. This study developed the design concept for an above ground pipe and pump option to deliver the temporary inflow pilot system flow. Most of the cost is in the hardware but portable pumping systems or a more fixed system can be used. When the temporary inflow pilot system testing is complete, the pumps and pipe can be removed and the open cut backfilled, leaving the site in the pre-study condition.

From the engineering perspective, there are two options for a full-scale, permanent system: pipe and pump or weir. The weir is the most cost-effective approach that provides the greatest flexibility for flow at the lowest cost but is the most restrictive with location. The pipe and pump option is the most restrictive approach in cost as well as flow rates, but the most flexible with location.

A final temporary pilot inflow system, and potential full-scale, permanent system, may be modified from the design and volume options included here based on further scientific, regulatory agency, and logistical requirements.

2.3 Biological Monitoring (Task 2)

The biological monitoring task had two objectives:

1. Document baseline biological characteristics of the IRL and coastal ocean in the vicinity of the proposed inflow locations.
2. Begin to assess the likely biological responses to an inflow system at the proposed locations.

The monitoring goal was to start gaining an understanding of the current biology at the proposed inflow sites, including natural seasonal or other fluctuations. Categories of biological characteristics monitored included:

1. Seagrasses and drift algae
2. Benthic fauna
3. Phytoplankton/harmful algae
4. Ichthyoplankton
5. Fishes
6. Environmental deoxyribonucleic acid (eDNA)

Extensive data on species densities and distributions, and environmental and community associations, were collected as part of this study and are summarized in the sections below. The full biological monitoring report is attached as Appendix B.

2.3.1 Approach

2.3.1.1 Seagrasses, Rooted Algae, and Drift Algae

At selected locations (Figure 2-22), transects 100-m long were surveyed perpendicular to the shoreline to document the presence of seagrasses and drift algae. Measurements included seagrass visual estimate percent cover (estimated coverage upon imagining the seagrass crowded into corner of quadrat at a high density), seagrass percent coverage or occurrence (proportion of 100 quadrat sub-squares having at least 1 blade of seagrass), seagrass density (number of shoots per area), seagrass canopy height (length of blade from sediment to tip), drift algae percent occurrence (proportion of 100 quadrat sub-squares having any drift algae), drift algae biomass estimate (estimated coverage upon imagining drift algae crowded into corner of quadrat), and drift algae canopy height (Virnstein and Morris 1996; Morris et al. 2001). This sampling strategy was repeated quarterly for all sites.

2.3.1.2 Benthic Fauna

Sediment grabs for infaunal analysis were collected at the 50-m mark along all seagrass transects (Figure 2-22) via petite Ponar grab. In addition, three stations were selected strategically from the BRL or IRL near proposed inflow sites, and three stations were selected from the ocean side of each proposed site. Triplicate samples were collected at each station. This sampling strategy was repeated quarterly for all sites. Sampling and identification of infauna were conducted consistent with the methods of benthic studies of the IRL (Mason 1998, Cooksey 2007) and were be tested for correlations with sediment parameters, including percent organic content (dry weight), percent water content by weight, and percent silt/clay content (dry weight), as well as environmental parameters.

As part of the baseline biological evaluation, surveys compared species and communities in the IRL and coastal ocean and documented environmental differences. When a species is present in both the IRL and the coastal ocean, then introduction to the IRL is less of a concern as the coastal population demonstrates the ability to withstand shifting environmental conditions as coastal

waters flow into the IRL ("Non-Concern Scenario Type II"). When species are present in the IRL but not in the coastal ocean, it is considered a potential Species of Environmental Shift Concern (SESC) and is monitored in the lagoon to determine the impacts of restored inflow. When species are present in the coastal ocean but absent in the IRL, this represents a Species Introduction Concern (SIC), which is evaluated to determine whether that species might be introduced to the lagoon with the inflow, whether it is likely to become established, and what the impacts would be to the IRL ecosystem. These species categories are summarized in Table 2-8. Species absences must be considered cautiously, as species can occur in the region but be uncommon enough to be missed in the sampling despite the spatially robust regimen.

Table 2-8. Categories of concern for scenarios of species presence and absence in the IRL versus the coastal ocean

	IRL Species Absent	IRL Species Present
Coastal Ocean Species Absent	Non-Concern Scenario, Type I	Environmental Shift Concern
Coastal Ocean Species Present	Species Introduction Concern	Non-Concern Scenario, Type II

2.3.1.3 Phytoplankton/Harmful Algae

Phytoplankton were sampled via plankton tows for cell identification and whole water samples for flow cytometer analysis. Samples were collected in conjunction with the infauna sampling schedule and locations shown in Figure 2-22. Four plankton tows were conducted quarterly at each proposed inflow site (four outside and four inside). Tows used a 20-micrometer (µm) mesh plankton net towed for approximately 2 minutes. Flow rate and submersion time were recorded and used to estimate volume processed for each plankton sample. Samples were preserved to await enumeration and identification via microscopy. Whole water samples for flow cytometry were collected at every station using a bottle to collect unfiltered water approximately 0.5 m below the water surface. These samples were set on ice and processed in the flow cytometer immediately upon returning from the field. This sampling strategy was repeated quarterly for all sites.

2.3.1.4 Ichthyoplankton

Some water flow between the IRL and coastal ocean occurs through the Port Canaveral Lock, which opens during daylight hours to allow vessels to move into or out of the IRL and also provides a pathway for larval fish to move between the habitats. Ichthyoplankton samples were collected by plankton light traps on the IRL and Port Canaveral sides of the lock (Figure 2-23) to examine internal IRL production of fish larvae and potential immigration of fish spawned in offshore waters. The light traps were cylinders of plankton netting (500 µm mesh), 0.75 m deep by 0.3 m diameter, with 4 funnels leading into the trap. An underwater dive light was suspended inside each trap, serving as an attractor for fish larvae. Light traps were deployed before sunset and retrieved the following morning. After retrieval, samples were preserved in 10% formalin for 48–96 hours, then switched to 70% ethanol and stored for analysis. Taxonomic analysis of larvae was performed using identification criteria provided by Smith (1989) and Richards (2005).

Light traps were deployed on three nights in late December 2019 from the bulkheads extending east and west of the lock. The lock was closed for maintenance on January 1, 2020, and access to the site could not be provided. Therefore, the sampling approach was switched to ichthyoplankton tows (1 m diameter net, 500 µm mesh) with the plankton surveys. Initial analysis of the samples collected in January and February 2020 showed that few larvae were collected, presumably due to the daytime net avoidance capabilities of larvae. In March, efforts shifted back to light traps at a marina within Port Canaveral and alongside a platform used by the Florida Tech

Biofouling Research Program. Samples were collected in mid-March and mid-May at the platform. The final samples were collected from the IRL and Port Canaveral sides of the lock in late May.

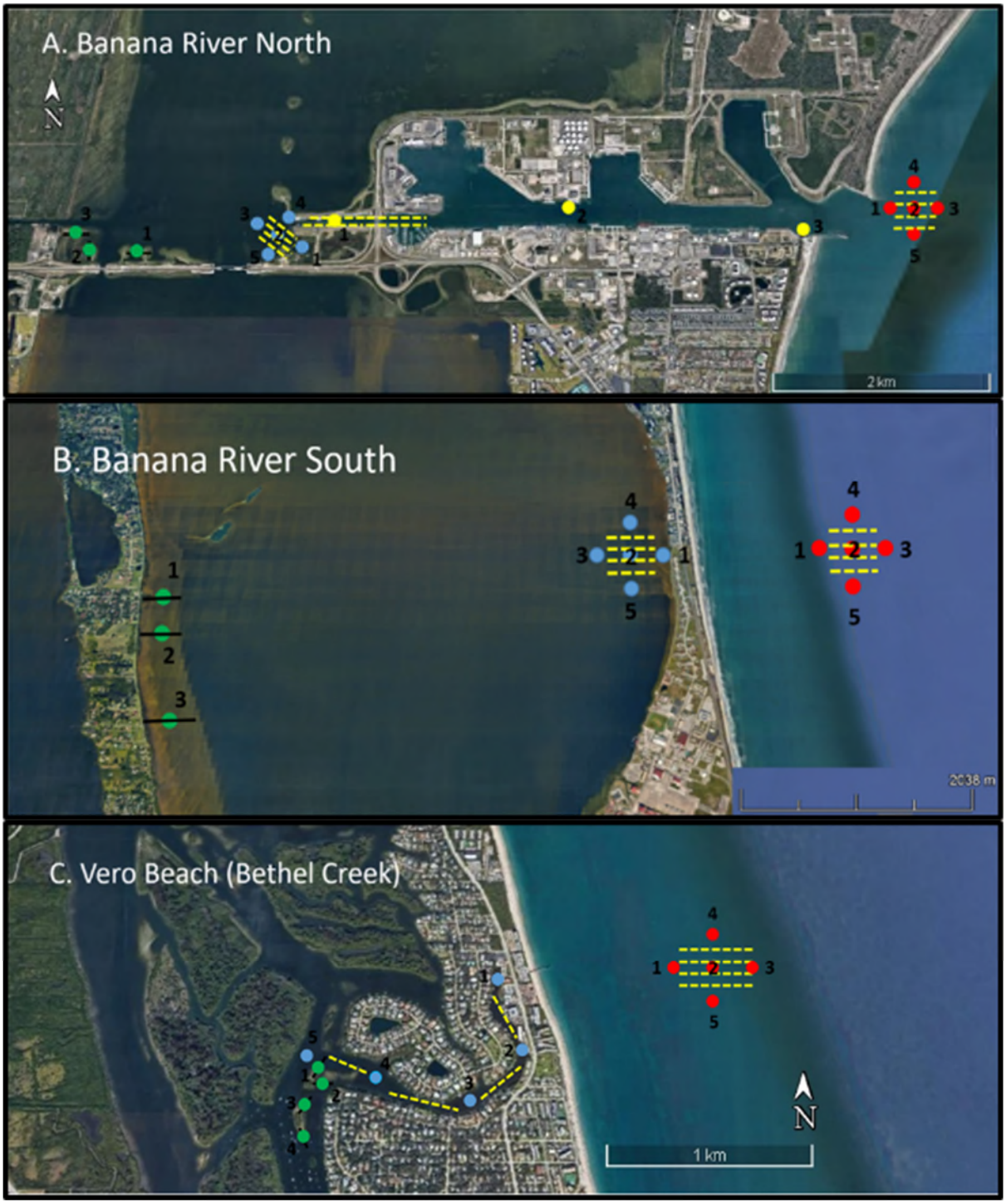

Note: Blue dots=infauna sampling stations in the IRL. Red dots=infauna sampling stations on the coastal ocean. Green dots=seagrass transect and associated stations. Yellow dashed line=plankton tow location.

Figure 2-22. Samples collected and station locations for three proposed inflow sites

Figure 2-23. Light trap sampling locations at the east and west sides of the Port Canaveral Lock and at the biofouling research platform

2.3.1.5 Fish Analysis

Fish and environmental data collection was conducted by the Florida Fish and Wildlife Conservation Commission's Fish and Wildlife Research Institute's (FWRI) Fisheries Independent Monitoring (FIM) program in the upper IRL (FWRI 2009). In this program, data have been collected monthly since 1996. In this study, all available data from 1996 to 2018 were used. Four gear types were used to make sure most, if not all, fishes were adequately sampled (Figure 2-24). Environmental data were collected concurrently with fish samples. Statistical analyses were used to determine the relative importance of key abiotic factors that influence fish health: salinity, temperature, DO, pH, conductivity, and depth. The key determinants of fish community structure, as revealed in the partial redundancy analyses, were subjected to a series of non-metric multidimensional scaling analyses to determine how community diversity varied under different conditions (low, moderate, and high) based on the observed ranges of each variable. These analyses were followed by similarity of percentages and analysis of similarities to determine which species was most affected by variations in abiotic factors (Santos et al. 2016). Statistical analyses were performed using the Vegan package (Oksanen et al. 2019) in R (R Core 2012).

Figure 2-24. The four gear types used in the FWRI-FIM program (adapted from Rubec et al. 2018)

2.3.1.6 eDNA

Advances in next-generation DNA sequencing were leveraged to assess and track biodiversity across taxonomic groups using eDNA (Eble et al. 2020). Three replicate 1,000 milliliter water samples were collected at each site (Figure 2-25) using bleach sterilized Nalgene bottles. To limit DNA degradation, samples were held on ice and filtered within 6 hours of collection using 0.45 µm pore size mixed cellulose ester filters. Filter membranes containing eDNA were then stored at -20° centigrade (C) in Longmire's buffer solution for later DNA extraction.

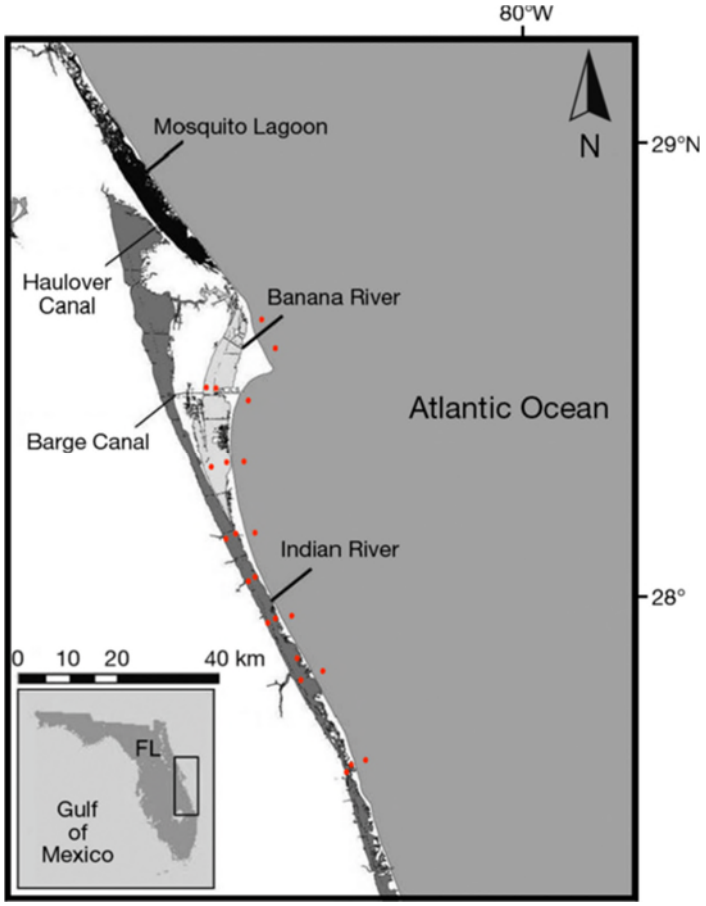

Figure 2-25. BRL, central IRL, Bethel Creek, and coastal Atlantic Ocean eDNA sampling locations (n = 23)

2.3.2 Data

2.3.2.1 Seagrasses, Rooted Algae, and Drift Algae

Seagrasses are present in the IRL and an attempt was made to sample the beds nearest to proposed inflow sites. On the coastal side of the barrier island, no seagrasses were detected via random benthic grab samples. Within the IRL, seagrasses were patchy and, when present, varied from sparse to abundant at the selected locations. The primary seagrass species observed at all locations was *Halodule wrightii* (Figure 2-26).

Figure 2-26. Transect and quadrat sampling of the shoal grass *Halodule wrightii*

Seagrass percent cover was greatest in the spring and ranged from 0–3%, 0–6%, and 0–17% at BRL North, BRL South, and Vero Beach, respectively (Figure 2-27). The *H. wrightii* canopy heights reached a maximum of 9 centimeters in spring at the Vero Beach seagrass transects. Shoot counts were always sparse and only exceeded a fractional count in a couple of quadrats in BRL North (winter) and Vero Beach (spring). Epiphytes growing on shoal grass blades showed different seasonal patterns based on site, and were most abundant at BRL North in the winter, BRL South in the fall, and Vero Beach in the spring. Rooted alga of the genus *Caulerpa* came on strong in the winter at BRL North, and were most abundant at BRL South in the spring, with percent cover from 3–70% (Figure 2-28). Rooted algae were largely absent from the Vero Beach transects. Drift algae made a strong appearance in the winter at BRL North and BRL South, with higher coverages ranging from 22–43% (Figure 2-29).

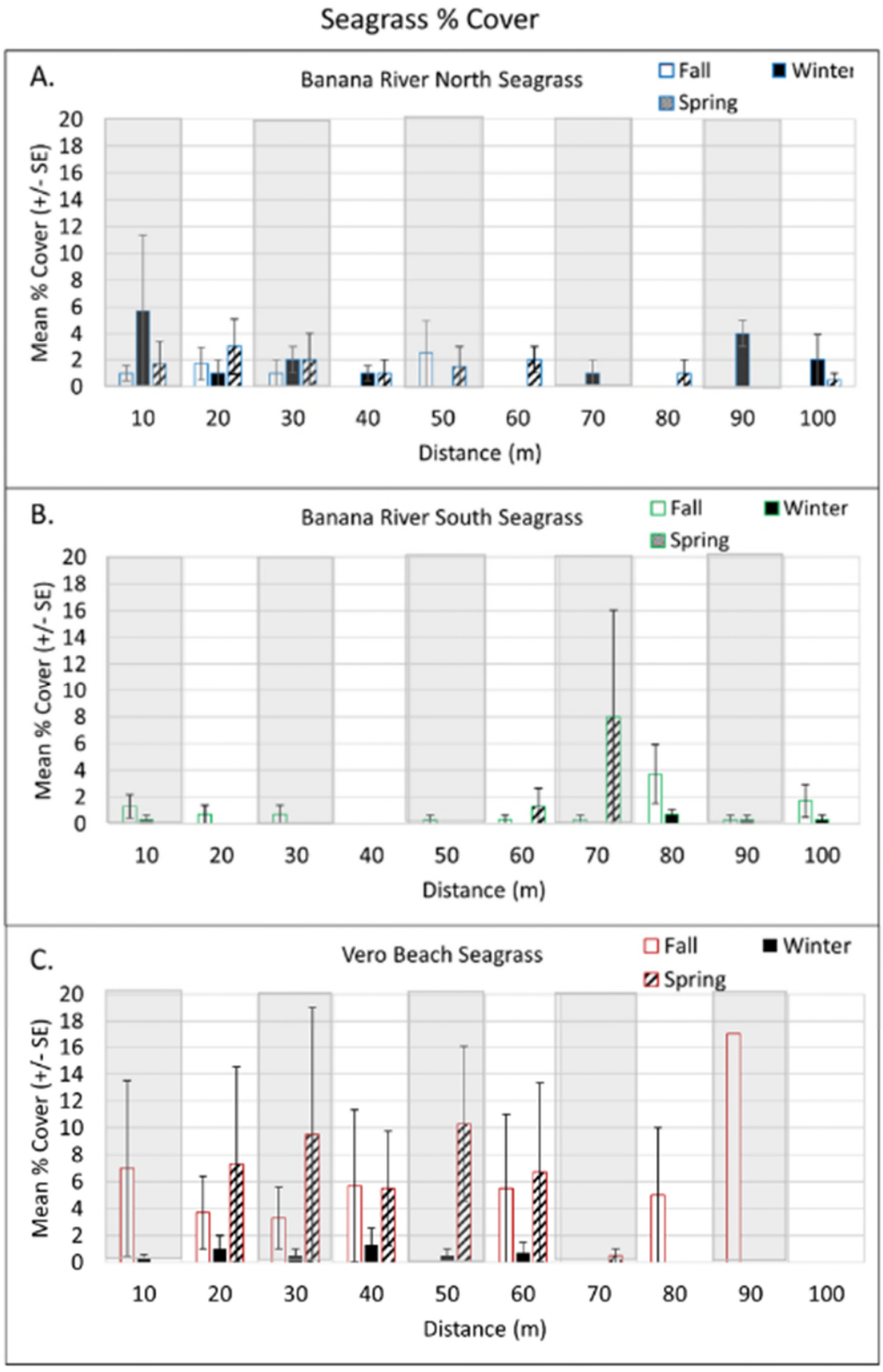

Note: Hollow bars = fall season, solid bars = winter season, diagonal stripe bars = spring season.

Figure 2-27. Seagrass mean percent cover for transects associated with the three proposed inflow sites

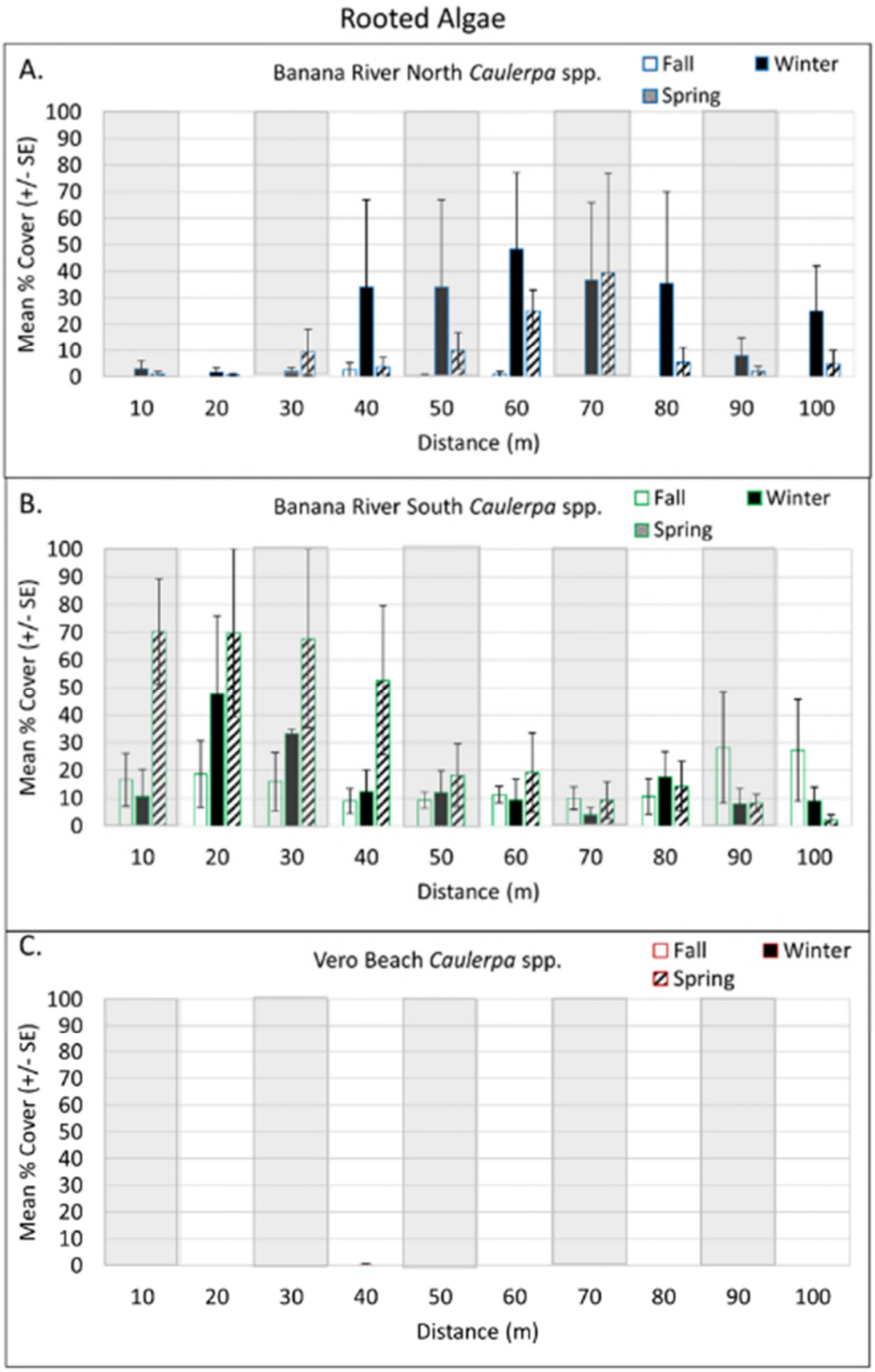

Note: Hollow bars = fall season, solid bars = winter season, diagonal stripe bars = spring season.

Figure 2-28. Rooted algae mean percent cover for transects associated with the three proposed inflow sites

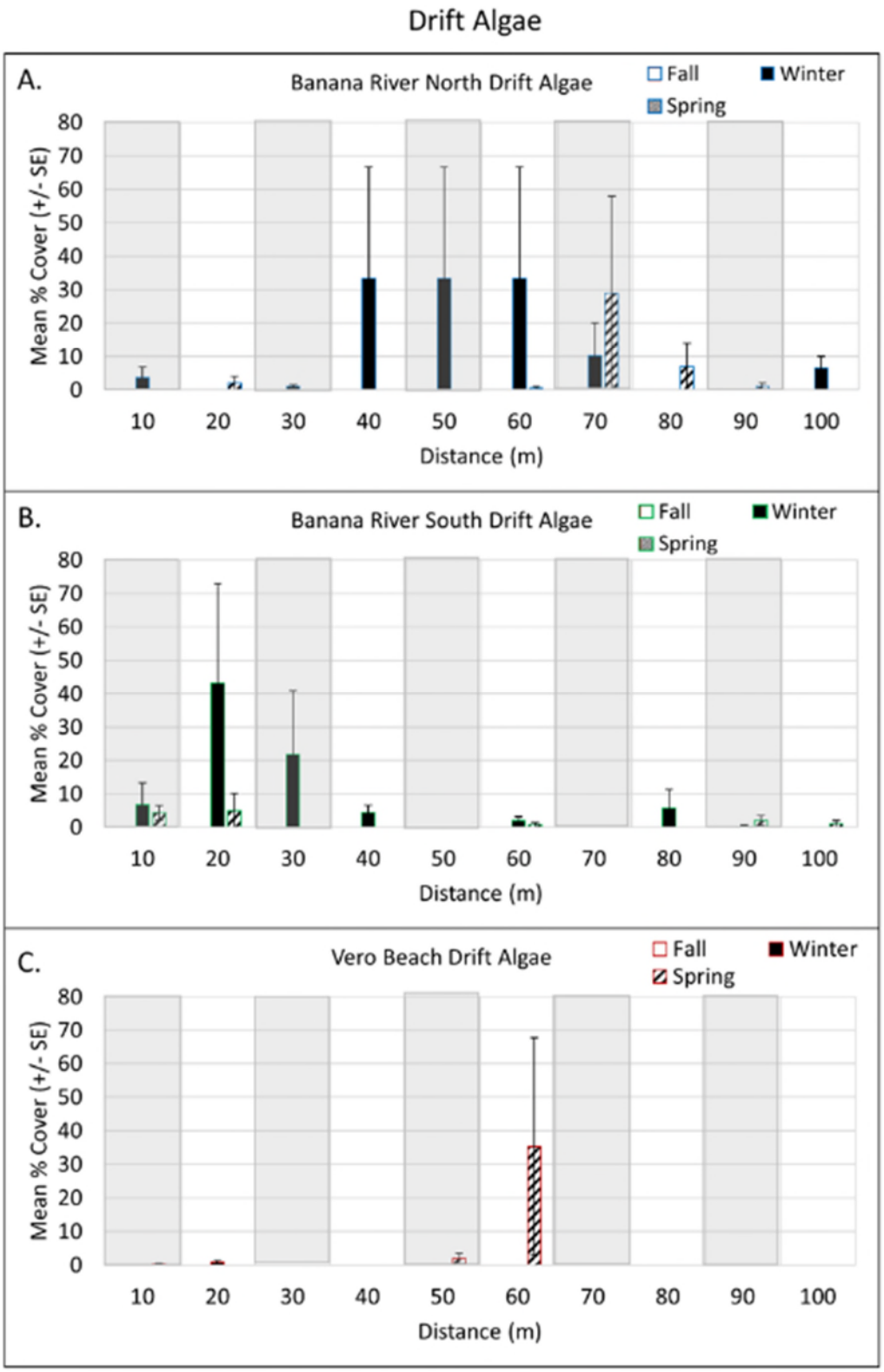

Note: Hollow bars = fall season, solid bars = winter season, diagonal stripe bars = spring season.

Figure 2-29. Drift algae mean percent cover for transects associated with the three proposed inflow sites

2.3.2.2 Benthic Fauna

The IRL and corresponding coast stations share many infaunal species in common, but some are unique to one environmental or the other.

List 1: Benthic Fauna Species of Non-Concern (Type II Scenario): Benthic fauna species found in both estuarine and coastal ocean sites included the following:

- The gammarid amphipods *Ampelisca abdita* and *Grandidierella bonnieroides*.
- All three cumacean species documented in this study, including *Oxyurostylis smithi*, an unidentified nannastacid cumacean ("Nannastacidae A"), and unidentified "Cumacean B."
- The caridean shrimp *Palaemonetes vulgaris.*
- The ostracod crustacean *Peratocytheridea setipunctata*.
- Both tanaid crustaceans documented in this study, *Hargeria rapax* and *Leptochelia dubia*.
- All polychaete annelids documented in this study, including *Alitta succinea*, *Ctenodrilus serratus*, *Glycera americana*, *Paradiopatra hispanica*, *Pectinaria gouldii*, *Armandia maculate,* and *Ophryorocha permanae*.
- The gastropods *Astyris lunata, Japonactaeon punctostriatus,* and *Phrontis vibex.*
- The bivalves *Angulus versicolor*, *Anomalocardia cuneimeris*, *Mulinia lateralis*, *Macoma carlottensis,* and *Amygdalum papyrium.*
- The brittle star *Ophiophragmus filograneus.*
- The foraminiferan protozoan *Ammonia parkinsoniana.*

List 2: Benthic Fauna Species of Potential Introduction Concern: Species found in the coastal ocean, but not observed in the IRL estuary in the surveys included the gastropod *Ecrobia truncata* (this species was rare even in coastal waters, and never observed in the IRL estuary).

A subcategory of SIC found ubiquitously in the coastal ocean but only in the IRL estuary at the BRL North inside sites, close to the locks, with regular propagule supply and water quality maintained by the ocean connection through Port Canaveral, included the gammarid amphipod *Americhelidium americanum*.

List 3: Benthic Fauna SESC: Species found in the IRL estuary, but not observed in the coastal ocean in the surveys included:

- The gammarid amphipods *Cerapus tubularis*, *Cymadusa compta*, and *Gammarus mucronatus*.
- The crustacean ostracod *Eusarsiella zostericola*.
- The bivalve mollusc *Parastarte triquetra*.
- The gastropod molluscs *Acteocina canaliculata* and *Haminoea elegans* (rare).

The mean abundances of total infauna (all taxonomic groups) were higher in the BRL sites when compared to the outer coast sites (Figure 2-30). The Vero Beach sites had dramatically fewer infauna within the lagoon, which corresponded with more organic sediments. Abundances and richness on the outer coast were on par with other coastal locations. The net effect is Vero Beach is the only site where abundances and diversity are greater on the outer coast than within the lagoon (Figure 2-30 and Figure 2-31). Vero Beach inside estuarine sediment organic content is greater than BRL North inside and BRL South inside sediments.

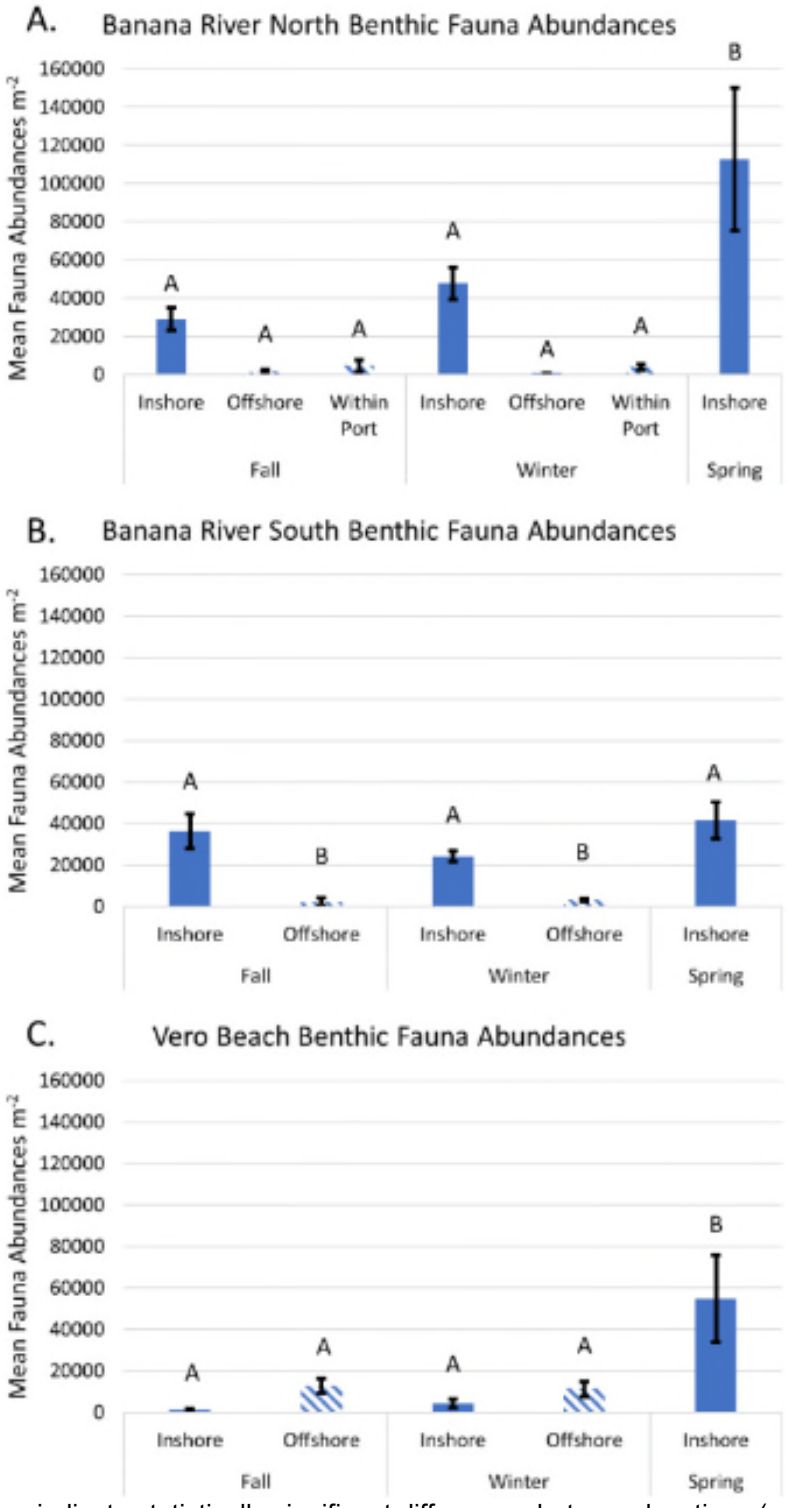

Note: Disparate letters indicate statistically significant differences between locations (α=0.05). Seasons are fall 2019, winter 2020, and spring 2020. “Inshore” is within the estuary. “Offshore” is coastal.

Figure 2-30. Benthic fauna densities for the proposed inflow sites

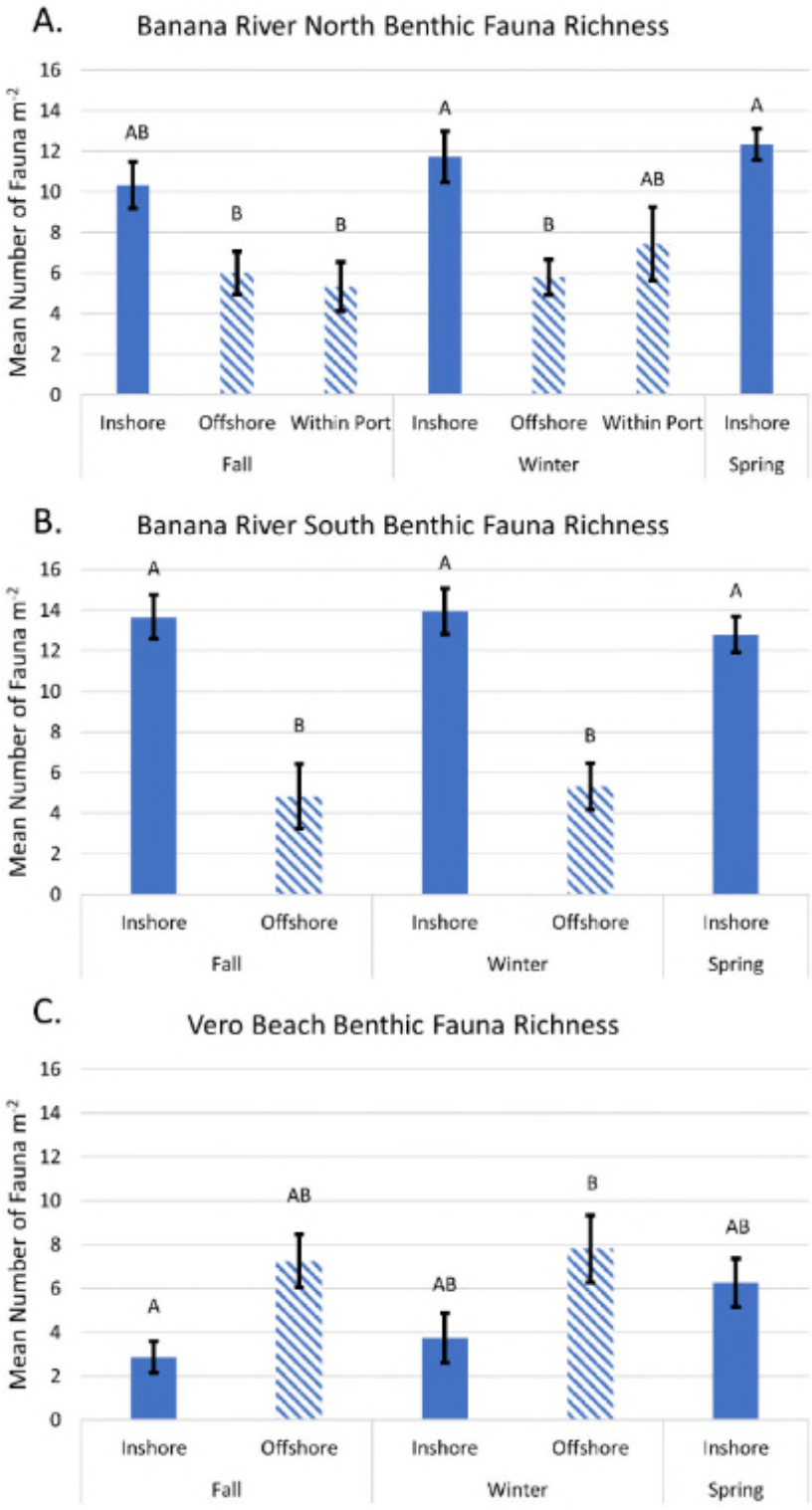

Note: Disparate letters indicate statistically significant differences between locations (α=0.05). Seasons are fall 2019, winter 2020, and spring 2020. “Inshore” is within the estuary. “Offshore” is coastal.

Figure 2-31. Benthic fauna species richness for the proposed inflow sites

2.3.2.3 Phytoplankton/Harmful Algae

The IRL and the corresponding outer coast stations share many phytoplankton species in common, but some are unique to one environmental or the other.

List 4: Phytoplankton Species of Non-Concern (Type II scenario): Phytoplankton and tintinnid ciliate species found in both estuarine and coastal ocean sites included the following. Species or groups known to be harmful despite lack of toxicity (e.g., those with gill spikes or reputed to form anoxic blooms) are annotated with an asterisk (*). Species or groups with known or suspected toxicity are annotated with two asterisks (**):

- The diatoms: *Actinoptychus senarius*, *Asterionellopsis glacialis*, *Amphiprora* sp., *Amphora* sp.**, *Bacillaria paxillifera*, Chaetoceros spp., *Coscinodiscus* spp. *Cyclotella* sp., *Cylindrotheca closterium*, *Diploneis* sp., *Dactyliosolen fragilissimus**, *Grammatophora* spp., *Leptocylindrus danicus*, *Licmophora* sp., *Lithodesmium undulatum, Navicula* spp., *Nitzschia longissimi***, *Nitzschia* spp.**, *Odontella* spp., *Paralia sulcate, Pleurosigma* spp., *Pseudo-nitzschia* spp.**, *Rhizosolenia* spp.**, *Skeletonema costatum***, *Surirella* sp., *Thalassionema frauenfeldii, Thalassionema nitzschoides, Thalassiosira* sp.
- The dinoflagellates *Ceratium* spp.**, *Dinophysis* sp.**, *Oxytoxum* sp., *Peridinium* sp.**, *Prorocentrum* sp.**, *Protoperidinium* spp.**, *Pyrodinium bahamense***.
- The blue-green alga *Anabaena* sp.**.
- The tintinnids *Helicostomella sp.* and *Tintinnopsis sp.*
- The silicoflagellate *Dictyocha fibula**.
- An unidentified raphidophycean*.
- Tylostyle sponge spicules.

List 5: Phytoplankton Species of Potential Introduction Concern: Phytoplankton and other planktonic species found in the coastal ocean, but not observed in the IRL estuary in the surveys included the following. Species or groups known to be harmful despite lack of toxicity (e.g., those with gill spikes or reputed to form anoxic blooms) are annotated with an asterisk (*). Species or groups with known or suspected toxicity are annotated with two asterisks (**):

- The diatoms *Actinoptychus splendens, Amphitetras* sp., *Bacteriastrum* spp., *Bellerochea horologicalis, Bellerochea malleus, Biddulphia alternans, Biddulphia rhombus, Biddulphia* sp., *Climacodium frauenfeldianum, Corethron* spp., *Cymatosira belgica, Delphineis surirella, Detonula pumila, Eucampia* sp.*, *Grammatophora marina, Guinardia flaccida*, Guinardia striata*, Gyrosigma fasciola, Haslea wawrickae, Hemiaulus hauckii, Hemiaulus membranaceus, Hemiaulus sinensis, Hemiaulus* spp., *Lioloma pacificum, Melosira moniliformis, Meuniera membranacea, Stephanopyxis* sp., *Triceratium brightwellii, Triceratium* sp., *Trigonium* sp., and an unidentified raphid diatom.
- The dinoflagellates *Ceratocorys armata*, *Oxyphysis* sp., *Podolampas* sp.
- An episodically abundant, unidentified protiste.
- The blue-green algae *Lyngbya* sp.** and *Oscillatoria* sp.**

List 6: Phytoplankton SESC: Phytoplankton and tintinnid ciliate species found in the IRL, but not observed in the coastal ocean in the surveys, included the following. Species or groups known to be harmful despite lack of toxicity (e.g., those with gill spikes or reputed to form anoxic blooms) are annotated with an asterisk (*). Species or groups with known or suspected toxicity are annotated with two asterisks (**):

- The diatoms: *Amphora proteoides*, *Eunotogramma* sp., and *Pseudofalcula hyaline*.

- The dinoflagellates: *Actiniscus pentasterias*, *Dinophysis argus*, *Gonyaulax* spp.**, *Gymnodinium* spp.**, *Pyrocystis fusiformis*, *Pyrocystis lanceolate*, and an unidentified *Peridinium*-like dinoflagellate.
- The tintinnids *Amphorellopsis* sp. and *Eutintinnus* sp.
- An unidentified cryptophycean.

Larger phytoplankton (greater than 25-µm due to tow net mesh size) were mostly diatoms and dinoflagellates. The greatest abundance was $4.5x10^3$ cells per liter $(L)^{-1}$ in the estuary at BRL South (Figure 2-32). Patterns of greatest abundance for phytoplankton greater than 25-µm are variable and may occur in the estuary or coastal waters at different sites and at different times of year (Figure 2-32).

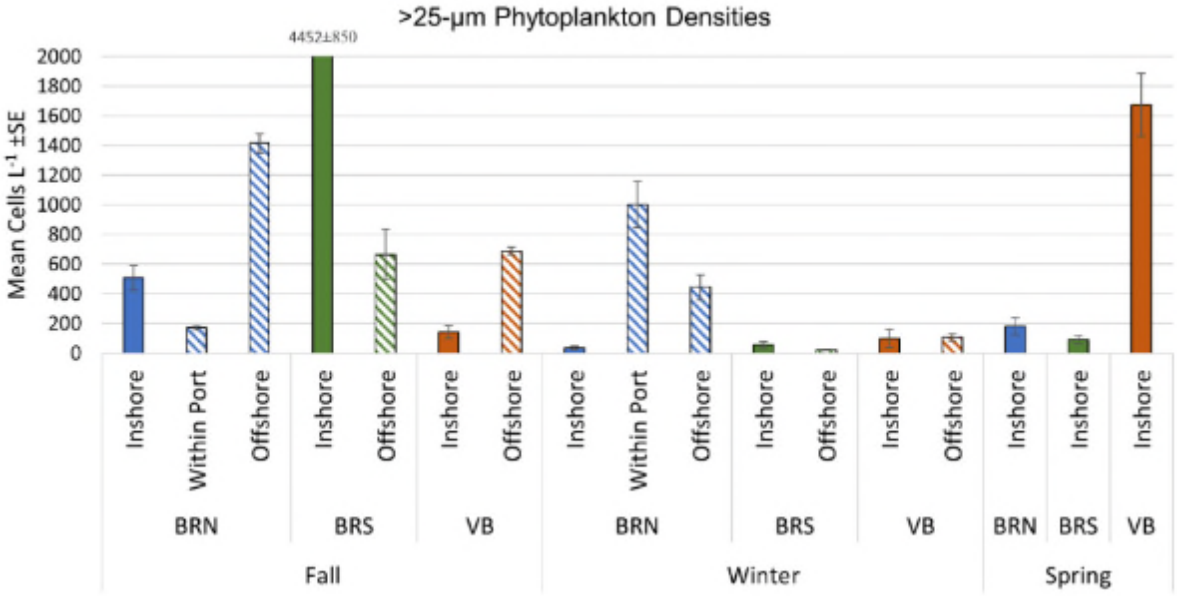

Note: "Inshore" is within the estuary. "Offshore" is coastal.

Figure 2-32. Greater than 25- µm phytoplankton mean densities inside and outside of potential inflow sites in fall 2019, winter 2020, and spring 2020

The most abundant phytoplankton were non-cyanobacterial cells less than 40-µm, which were more abundant in the estuary than the coastal water column, except for BRL North during the winter. The highest observed cell density was $6.1x10^7$ cells L^{-1} in the estuary at Vero Beach. The next most abundant group was the cyanobacteria identified by the presence of phycoerythrin pigments, which were more abundant in coastal compared to estuarine waters, with densities ranging from $1.1x10^7$ to $3.5x10^7$ cells L^{-1} (Figure 2-33).

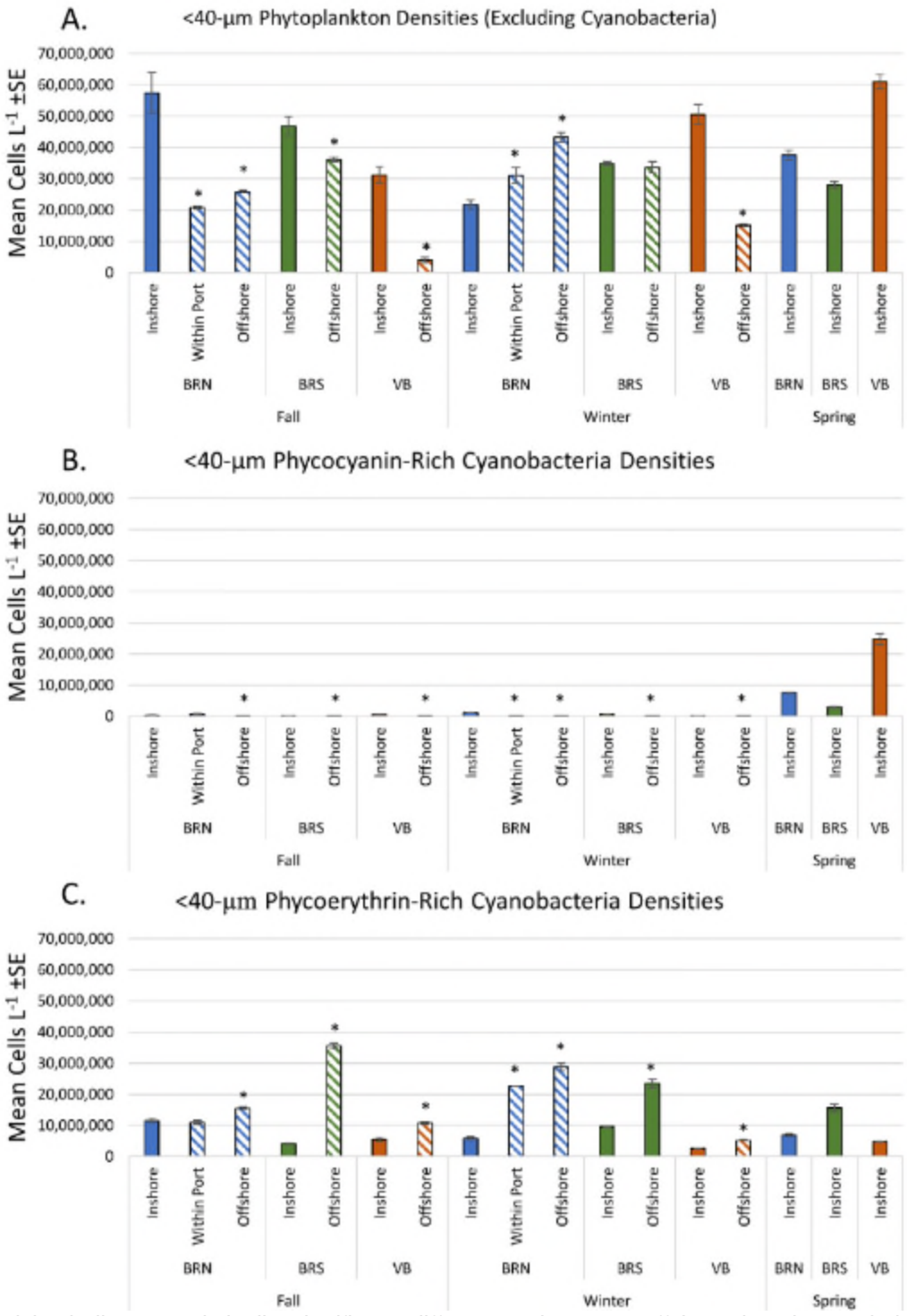

Note: Asterisks indicate statistically significant differences between offshore locations relative to their corresponding estuary site during a given season. "Inshore" is within the estuary. "Offshore" is coastal.

Figure 2-33. Less than 40-µm phytoplankton densities for non-cyanobacteria (A), cyanobacteria as indicated by phycocyanin presence (B), and cyanobacteria as indicated by phycoerythrin presence (C)

Phytoplankton biodiversity, species richness, and evenness were calculated for tow plankton less than 25-µm (Figure 2-34) and tended to be significantly greater in coastal waters.

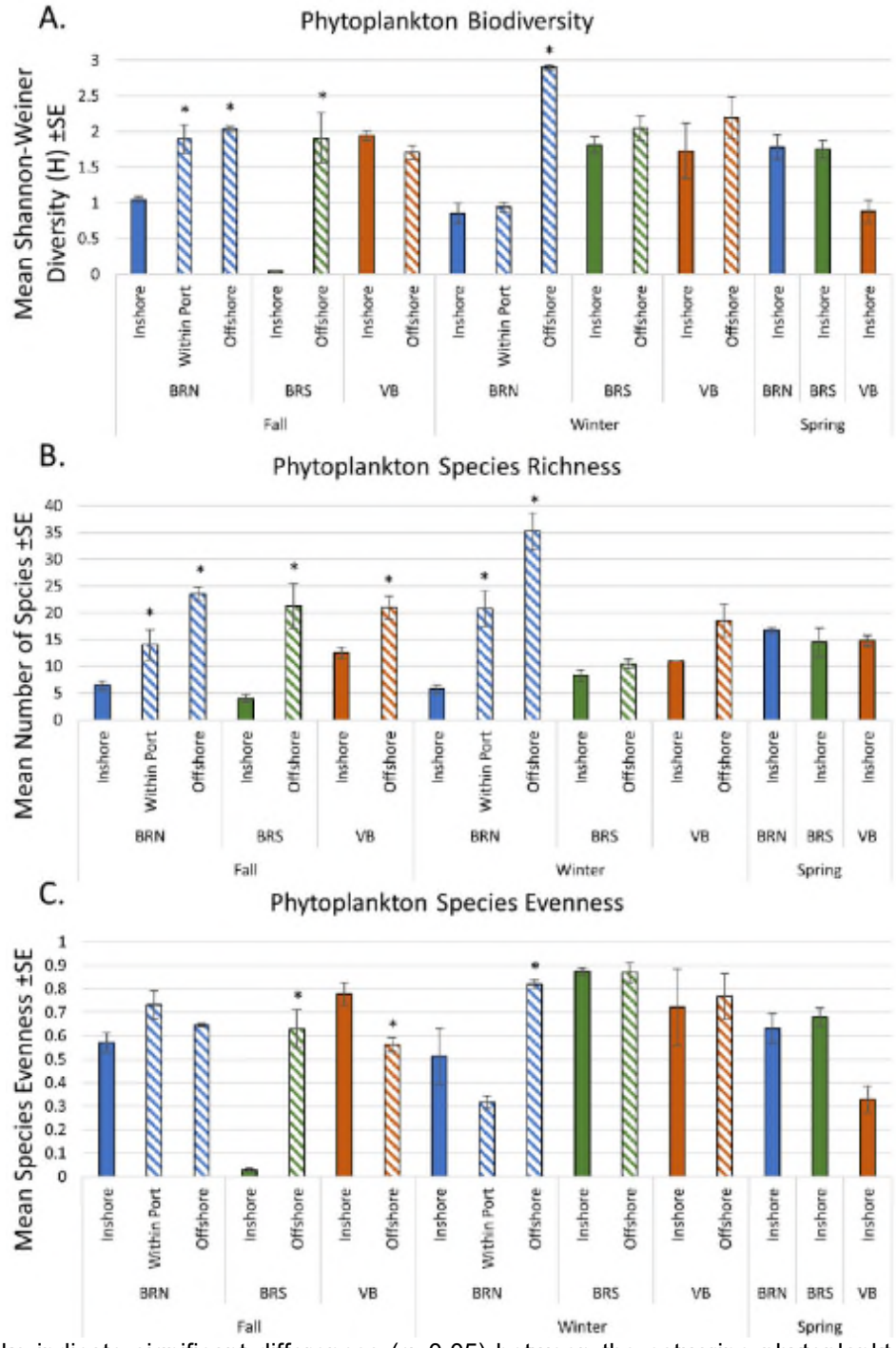

Note: Asterisks indicate significant differences (α=0.05) between the estuarine phytoplankton community relative to the coastal ocean at the same site. “Inshore” is within the estuary. “Offshore” is coastal.

Figure 2-34. Phytoplankton mean Shannon-Weiner Diversity Index (A), mean species richness (B), and mean community evenness (C) comparisons at the potential inflow sites

Phytoplankton species and groups documented in coastal waters, but not in the estuary, included 31 diatoms, three dinoflagellates, one unidentified protist, and two cyanobacteria. These included five harmful or toxic species. Due to the fluid connection between the coastal zone and the estuary through the Port Canaveral Lock and Sebastian Inlet, these microalgae likely had opportunities to be advected into the estuary. Their absence in the IRL may be due to inability to survive under variable estuarine conditions, or they may be present but undetectable during sampling (low numbers or in sediments). Two phytoplankton genera with known toxicity were present in the estuary, but not observed in coastal ocean plankton (SESC). Representatives of the genus *Gonyaulax* were somewhat present in the fall, absent in winter, and most consistently present in spring. However, even in spring, densities ranged from 1-18 cells L^{-1}, far below bloom densities. Representatives of the genus *Gymnodinium* were absent in the fall and somewhat present in winter and spring (8 and 9 cells L^{-1}, respectively, when present).

2.3.2.4 Ichthyoplankton

A total of 2,824 larval fishes from 23 taxa were collected in 52 light trap samples made on 11 nights at the Port Canaveral Lock and the Biofouling Research Platform. The ichthyoplankton samples taken in Port Canaveral and adjacent IRL illustrate seasonal patterns in reproduction in various species, and the role of the Port Canaveral Lock as a means of limited larval recruitment into the IRL. Only 12 larvae were taken in the towed ichthyoplankton samples (0–4 larvae/tow). Four species dominated the light trap samples, with Atlantic menhaden (*Brevoortia tyrannus*) comprising 35.2% of the total catch, bay anchovies (*Anchoa mitchilli*; 27.8%), scaled sardine (*Harengula jaguana*; 27.1%) and threadfin herring (*Opisthonema oglinum*; 6.2%). These species are pelagic schooling planktivores that are important prey for piscivorous fishes within the IRL. With the exception of the estuarine-spawning anchovies, the other species spawn in offshore waters and have larvae that migrate into estuarine nursery habitats.

The initial light trap samples, taken in December 2019 (Table 2-9), clearly demonstrated the larval distribution and movement patterns of menhaden and anchovies. During the first night of sampling, 130 anchovies were collected in light traps on the IRL side of the Port Canaveral Lock, while all 248 menhaden were in traps on the ocean side of the lock. The two other nights sampled in December showed a similar pattern, with 88% of anchovies collected on the IRL side, and 97% of menhaden larvae taken on the eastern side. Being estuarine spawners and inhabitants, the anchovies could spawn within Port Canaveral and the IRL and move through the lock when it opens during ebb or flood tides. Conversely, oceanic menhaden larvae appeared to accumulate at the eastern lock gate, move into the IRL when the lock opens, then disperse into the open IRL.

The only other species taken in light traps in December in significant numbers was ladyfish (*Elops saurus*). This offshore-spawning species produces larvae that migrate through inlets such as Sebastian Inlet (Wheeler 2000) to reach their estuarine nurseries along the southeast coast of the United States. As with offshore-spawning menhaden, the catch of ladyfish larvae was concentrated in traps on the Port Canaveral side of the lock, with the low catch on the IRL side, reflecting their dispersal into the IRL.

Light traps deployed in March at the Biofouling Research Platform showed that menhaden larvae were still recruiting into the system, even if they were not able to access the IRL nursery habitat. Large numbers of menhaden dominated the March samples, along with bay anchovies that presumably resulted from spawning within Port Canaveral waters (Table 2-10). Low numbers of other estuarine and offshore-spawning taxa were also collected by the light traps in March. Additional light trap sampling was conducted in mid-May, first at the Biofouling Research Platform and then at the lock. By May, the spawning season for menhaden had ceased, but large numbers of offshore-spawned larval scaled sardines (*Harengula jaguana*) and threadfin herrings

(*Opisthonema oglinum*) in the samples taken at both sites within the Port indicated the seasonal occurrence of their spawning activity (Table 2-9 and Table 2-10). Much lower numbers of these larvae were taken in the light traps on the IRL side of the lock, suggesting their rapid dispersal after movement into the IRL. As with menhaden, the planktivorous schooling scaled sardines and threadfin herrings use estuarine nursery habitats and play a major role as prey for many IRL fishes.

Two larval tarpon (*Megalops atlanticus*) were also collected in late May on the east side of the lock. These larvae represent the initial spawning efforts of a valuable species that spawns in offshore waters from May through September. Juveniles tarpon are often abundant in marsh and mosquito control impoundment nursery habitats in the northernmost areas of the IRL, around Mims and Scottsmoor (Zugelter 2019, personal observations). Although tarpon larvae recruit through Sebastian Inlet (Shenker et al. 2002), the inlet is more than 100 km from those nursery habitats, while Port Canaveral is only 45 km away. The lock may thus provide a pathway for larvae of this valuable fishery species to reach the northern IRL marsh habitats.

Examination of the total catch showed that 1,178 larvae from 13 offshore-spawning species and 485 larvae from 6 estuarine-spawning species were collected on the east and west sides of the lock in December and May. Nearly 78% of larvae were captured on the Port Canaveral side.

2.3.2.5 Fish Analysis

There are 258 species of fish in the IRL, including mostly forage fish and economically important species. Of these, 94 were noted in Site 1, 85 in Site 2, and 159 in Site 3. The rank order of abundance of the top 20 species in each location is presented in Table 2-11. The IRL is dominated by forage fish (also known as “lower trophic level species”), especially bay anchovies (*Anchoa mitchilli)*, striped mullet (*Mugil cephalus),* and pinfish (*Lagodon rhomboides)*. The rank order of abundance of these species, except for bay anchovies, which remained the most abundant fish in all sites, varied among the three sites of interest. Among the economically important species of fish, the spotted sea trout (*Cynoscion nebulosus)*, red drum (*Sciaenops ocellatus)*, and ladyfish (*Elops saurus)* occurred in at least two of the sites.

Table 2-9. Larval fish catches in light traps deployed overnight on the east and west sides of the Port Canaveral Lock

Note: n=number of light traps. % E=proportion of total catch of each taxon on the Port Canaveral (east) side of the lock. Spawning habitat: O=Ocean, E=Estuarine.

Species	Common Name	Spawn Habitat	12/20/19 E (n=2)	12/20/19 W (n=2)	12/23/19 E (n=2)	12/23/19 W (n=2)	12/31/19 E (n=2)	12/31/19 W (n=2)	5/27/20 E (n=3)	5/27/20 W (n=3)	5/28/20 E (n=2)	5/28/20 W (n=3)	5/29/20 E (n=3)	5/29/20 W (n=3)	Total (n=29)	% E
Harengula jaguana	Scaled sardine	O	0	0	0	0	0	0	38	1	18	1	551	5	614	98.9
Anchoa mitchilli	Bay anchovy	E	0	130	0	90	32	44	28	41	10	25	61	13	474	27.6
Brevoortia tyrannus	Atlantic menhaden	O	248	0	9	1	88	11	0	0	0	0	0	0	357	96.6
Opisthonema oglinum	Threadfin herring	O	0	0	0	0	0	0	4	0	8	0	164	0	176	100.0
Elops saurus	Ladyfish	O	0	0	0	0	12	2	0	0	1	0	2	0	17	88.2
Gobiosoma bosc	Naked goby	E	0	0	0	0	0	0	0	0	0	1	2	2	5	40.0
Eucinostomus sp.	Mojarras	O	0	0	0	0	0	0	1	0	1	1	1	0	4	75.0
Megalops atlanticus	Tarpon	O	0	0	0	0	0	0	0	0	0	1	2	0	3	66.7
Chasmodes sp.	Combtooth blenny	E	0	0	0	0	0	0	0	1	0	1	0	0	2	0.0
Lagodon rhomboides	Pinfish	O	1	0	0	0	0	0	0	0	0	0	0	0	1	100.0
Microgobius gulosus	Clown goby	E	0	0	0	0	0	0	1	0	1	0	0	0	2	100.0
Archosargus rhomboidalis	Sea bream	O	0	0	0	0	1	0	0	0	0	0	0	0	1	100.0
Caranx hippos	Jack crevalle	O	0	0	0	0	0	0	0	0	0	0	0	1	1	0.0
Gobiosoma ginsburgi	Seaboard goby	E	0	0	0	0	0	0	0	0	0	0	1	0	1	100.0
Micropogonias undulatus	Atlantic croaker	O	0	0	0	0	1	0	0	0	0	0	0	0	1	100.0
Stephanolepis hispidus	Planehead filefish	O	0	0	0	0	0	0	1	0	0	0	0	0	1	100.0
Syngnathus sp.	Pipefish	E	0	0	0	0	0	0	0	0	0	1	0	0	1	0.0
Trachinotus falcatus	Pompano	O	0	0	0	0	0	0	0	0	0	0	1	0	1	100.0
Leiostomus xanthurus	Spot	O	0	0	0	0	1	0	0	0	0	0	0	0	1	100.0
Unidentified	-	-	0	0	0	0	0	0	0	0	0	1	0	0	1	0.0
Total	***Total***	***-***	***249***	***130***	***9***	***91***	***135***	***57***	***73***	***43***	***39***	***32***	***785***	***21***	***1,664***	***77.5***

Table 2-10. Larval fish catches in light traps deployed overnight at the Biofouling Research Platform

Note: n=number of light traps. Spawning habitat: O=Oceanic, E=Estuarine.

Species	Common Name	Spawning Habitat	3/23/2020 (n=5)	3/24/2020 (n=5)	5/18/2020 (n=5)	5/19/2020 (n=4)	5/20/2020 (n=4)	Total (n=23)
Brevoortia tyrannus	Atlantic menhaden	O	444	190	0	0	2	636
Anchoa mitchilli	Bay anchovy	E	82	36	114	66	12	310
Harengula jaguana	Scaled sardine	O	0	0	120	23	7	150
Eucinostomus sp.	Mojarras	O	3	4	16	3	4	30
Gobiosoma bosc	Naked goby	E	0	0	8	1	0	9
Lagodon rhomboides	Pinfish	O	2	5	1	0	0	8
Microgobius gulosus	Clown goby	E	1	3	3	1	0	8
Haemulon sp.	Grunts	O	2	2	0	0	0	4
Blenniidae	Blennies	E	1	0	0	0	2	3
Sparidae	Porgies	O	1	0	0	0	0	1
Gobiidae	Gobies	E	1	0	0	0	0	1
Total Fishes	***Total***	**-**	***537***	***240***	***262***	***94***	***27***	***1,160***

Table 2-11. Top 20 most abundant fish species in the IRL and at each of the three inflow sites

Note: #Fish is presented as the highest annual total number of fish caught during the sampling period 1996 to 2018. Note the variation in the rank-order of the top 20 species in each location.

Top 20 Species in the IRL	#Fish	Top 20 Species in Site 1	#Fish	Top 20 Species in Site 2	#Fish	Top 20 Species in Site 3	#Fish
Anchoa mitchilli	231,704	*Anchoa mitchilli*	34,562	*Anchoa mitchilli*	33,327	*Anchoa mitchilli*	53,796
Lucania parva	23,040	*Micropogonias undulatus*	7,168	*Mugil cephalus*	1,924	*Micropogonias undulatus*	7,252
Leiostomus xanthurus	13,888	*Lucania parva*	6,880	*Lucania parva*	1,744	*Lagodon rhomboides*	4,748
Mugil cephalus	11,010	*Lagodon rhomboides*	6,618	*Bairdiella chrysoura*	1,722	*Harengula jaguana*	4,666
Lagodon rhomboides	9,798	*Opisthonema oglinum*	3,504	*Diapterus auratus*	1,581	*Orthopristis chrysoptera*	3,570
Bairdiella chrysoura	9,297	*Bairdiella chrysoura*	3,294	*Leiostomus xanthurus*	1,557	*Mugil curema*	3,006
Harengula jaguana	7,490	*Mugil cephalus*	1,998	*Lagodon rhomboides*	1,488	*Leiostomus xanthurus*	2,784
Diapterus auratus	7,398	*Poecilia latipinna*	1,728	*Eucinostomus harengulus*	1,035	*Mugil cephalus*	2,257
Micropogonias undulatus	7,252	*Mugil curema*	1,587	*Ariopsis felis*	940	*Diapterus auratus*	1,995
Mugil curema	4,780	*Leiostomus xanthurus*	1,424	*Microgobius gulosus*	768	*Bairdiella chrysoura*	1,728
Elops saurus	4,707	*Floridichthys carpio*	1,344	*Cynoscion nebulosus*	482	*Ariopsis felis*	1,461
Anchoa hepsetus	4,528	*Eucinostomus harengulus*	1,224	*Harengula jaguana*	452	*Anchoa hepsetus*	1,280
Eucinostomus gula	4,480	*Diapterus auratus*	1,179	*Eucinostomus gula*	432	*Lucania parva*	1,144
Eucinostomus harengulus	4,390	*Cynoscion complex*	776	*Mugil curema*	416	*Eucinostomus harengulus*	982
Opisthonema oglinum	4,143	*Microgobius gulosus*	716	*Gobiosoma robustum*	304	*Opisthonema oglinum*	957
Floridichthys carpio	3,904	*Cyprinodon variegatus*	688	*Oligoplites saurus*	282	*Archosargus rhomboidalis*	772
Orthopristis chrysoptera	3,570	*Ariopsis felis*	616	*Floridichthys carpio*	280	*Eucinostomus gula*	756
Ariopsis felis	2,637	*Sphoeroides nephelus*	588	*Menticirrhus americanus*	278	*Sciaenops ocellatus*	594
Anchoa cubana	2,636	*Gobiosoma robustum*	580	*Micropogonias undulatus*	234	*Microgobius gulosus*	432
Sciaenops ocellatus	2,466	*Membras martinica*	398	*Dasyatis sabina*	222	*Elops saurus*	423

The pattern of variation in average annual DO, salinity, pH, and temperature was similar among the three sites (Figure 2-35) during the sampling period 1996–2018. The average (median) and range of these water quality parameters are presented in Table 2-12. Salinity and temperature are the most variable as indicated by the first and third quartile range values in Table 2-12.

Table 2-12. Average pH, temperature, DO, and salinity in the IRL and the three inflow sites

Site	Statistics	pH	Temperature (°C)	DO (mg/L)	Salinity (PSU)
IRL	Median	8.10	25.50	7.20	26.25
IRL	1st Quartile	7.90	21.45	6.00	20.6
IRL	3rd Quartile	8.30	29.10	8.44	31.68
IRL	Range	3.95-9.60	6.15-40.00	0.20-18.60	0.20-48.40
1	Median	8.20	25.25	7.40	24.50
1	1st Quartile	8.07	20.80	6.20	19.60
1	3rd Quartile	8.40	29.30	8.65	29.50
1	Range	5.63-9.20	8.47-35.0	1.25-16.20	10.90-40.95
2	Median	8.13	25.20	7.35	22.40
2	1st Quartile	8.00	21.09	6.20	18.25
2	3rd Quartile	8.30	29.10	8.75	27.41
2	Range	7.20-9.15	10.63-33.50	1.66-13.20	11.70-35.75
3	Median	8.00	25.90	7.00	29.40
3	1st Quartile	7.90	21.84	5.95	24.70
3	3rd Quartile	8.20	29.50	8.10	32.88
3	Range	3.95-9.00	7.80-37.40	1.80-17.50	0.20-40.00

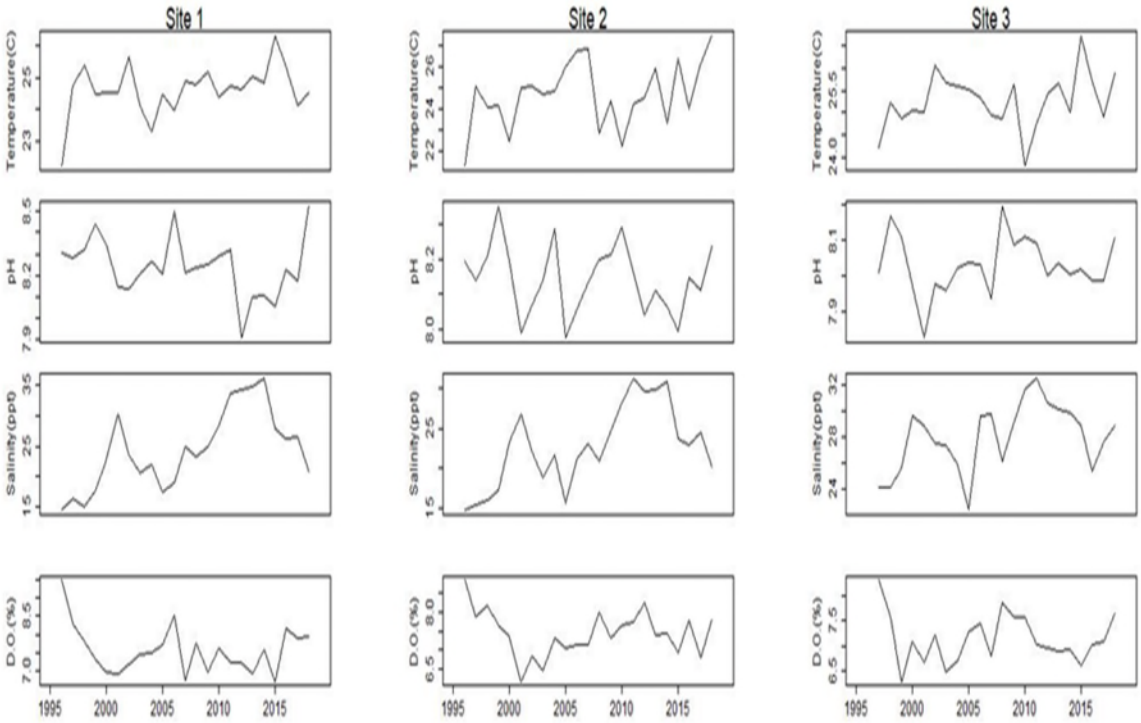

Figure 2-35. Annual variation in DO, salinity, pH, and temperature in Sites 1–3 during the period 1996–2018

The pattern of community fish structure in the IRL and in each of the three sites was driven by complex interactions among biotic and abiotic environmental factors that likely shape the IRL community fish structure. To determine which of the abiotic environmental parameters likely drive the pattern of variation in community structure of fishes, a series of partial redundancy analyses were conducted on the DO, temperature, salinity, pH, depth, and conductivity data collected along with fish abundance during the 1996–2018 sampling period. Although a mix of statistically significant and non-significant results were revealed (Table 2-12), DO and salinity were consistently the key determinants of fish community structure in the IRL and the three sites.

Multivariate analyses at the IRL-wide scale identified weak, but significant, effects of salinity and DO on the changes in the fish community structure. Analyses using non-metric multidimensional scaling indicated that variation in DO and salinity was associated with variation in fish diversity within the IRL and the three sites. The highest community diversity was found in areas of moderate salinity and low DO. These relationships were especially evident in the abundance changes in the lower trophic levels including bay anchovies (*Anchoa mitchilli)*, Jenny mojarra (*Eucinostomus gula)*, pinfish (*Lagodon rhomboides)*, and Irish pompano (*Diapterus auratus)*.

2.3.2.6 eDNA

A total of 135 surface water eDNA samples were collected during fall and winter sampling of the IRL and offshore coastal waters. To investigate the utility of alternative eDNA substrates and habitat sampling, eDNA was also sampled at three sites in the Sebastian River; six in central IRL sediment cores; and six tissue samples from filter feeding tunicates, barnacles, and sponges. Total DNA yield was highly variable between samples, with IRL samples yielding the highest concentration of DNA (31 $\pm$ 4.8 nanograms per microliter [ng/µl]) and coastal samples having the lowest yield (6.4 $\pm$ 1.9 ng/µl). In initial tests, polymerase chain reaction (PCR) inhibition was observed in 8 of 10 IRL and 2 of 10 coastal samples. To minimize false negatives, samples were filtered to remove inhibitors and diluted 1:2 prior to qPCR. Following inhibitor removal and dilution, 37 of 672 qPCR reactions failed to yield detectable amplification. Cycle quantification values for the remaining reactions were generally consistent (24.02 $\pm$ 3.72), although DNA retention following PCR clean-up varied (18.0 $\pm$ 2.9 ng/µl). DNA yield following the second PCR and PCR clean-up was higher for cytochrome oxidase subunit I (COI) (16.0 $\pm$ 7.59 ng/µl) than 16S (14.6 $\pm$ 3.79 ng/µl). After size selection and purification, DNA yield was 1.77 ng/µl and 0.849 ng/µl for RNA 16S gene and COI, respectively. Nano sequencing was completed in August 2020. Final results are pending ongoing sequence quality control and analysis. Sequences will be filtered, trimmed, and error checked prior to taxonomic assignment.

2.3.3 Conclusions

Many estuarine animals tolerate fluctuations in temperatures, salinities, turbidity, nutrients, and pollutants. By comparison, coastal ocean conditions are relatively constant and fall well within the ranges of estuarine organism tolerances. Given this, it could be expected that estuarine animals would respond more favorably to any shifts in the abiotic environment resulting from enhanced inflow; however, data are lacking on several key species of concern and aspects of the recipient community. Of particular note are the spawning populations of several key sportfish in the BRL. Similarly, indirect impacts on the estuarine community due to biotic factors, such as predation by, or competition with, organisms from the coastal ecosystem, are harder to predict. Coastal organisms may be directly introduced via enhanced inflow, or migration into the estuary could be encouraged following a shift towards coastal-like conditions.

Some evidences suggest that SESC (those found only in the estuary) may have minimal direct impacts from an influx of coastal water. First, species present in estuaries are frequently

euryhaline and eurythermal, meaning they can withstand fluctuations in salinity and temperature compared to ocean species. For instance, fish are among the most motile of estuarine populations, yet, even if they have tidal migration, an enhanced ability to osmoregulate in changing conditions is required (Allen et al. 2006). The pattern of estuarine species having wider ranges of tolerances for abiotic environmental conditions is found throughout disparate taxonomic groups. Estuarine phytoplankton have a wider salinity tolerance than oceanic phytoplankton, and coastal phytoplankton are intermediate in their tolerance (Brand 1984).

Reliable evaluation of the biological impacts of restored inflow would be best accomplished through a temporary inflow pilot system where biological responses are carefully monitored. This would allow a more confident projection of the likely effects of a full-scale, permanent inflow system.

2.4 Geochemical Baseline (Task 3)

The objectives of this geochemical evaluation were to:

- Calculate impacts of inflow, based on direct dilution by seawater, on nutrient concentrations in the lagoon, and calculate the quantity of nutrients that could be discharged into the coastal ocean.
- Determine if data from few existing water quality sensors (approximately 0.5–1.0 m) can be extrapolated to determine conditions in bottom water near proposed inflow locations.
- Determine how changes to temperature, salinity, and DO that could result from various levels of inflow would influence the geochemical cycling of N, P, and oxygen, plus sulfate and sulfide in the lagoon.

2.4.1 Approach

2.4.1.1 Field Sampling

Continuous vertical profiles for salinity, temperature, pH, oxidation reduction potential, and DO were obtained using a YSI ProDSS (Yellow Springs Instruments). The sonde was calibrated prior to each sampling event following the manufacturer's guidelines. Discrete water samples were collected using a 1.7 L horizontal Niskin water sampler (General Oceanics) that was tripped at targeted depths using a weighted messenger. Water samples were filtered immediately after collection using Whatman 0.45 µm polypropylene syringe filters. Additional unfiltered samples were collected for processing in the laboratory. All water samples were transported to the laboratory in a cooler on ice in the dark.

Sediment samples were obtained using a 0.1 square meter Ekman Grab that was lowered from an anchored boat until it hit the bottom. This process was observed by Self-Contained Underwater Breathing Apparatus (SCUBA) to verify collection of 10–15 centimeters (cm) of stratified sediment and overlying water (Figure 2-36). Any standing water was siphoned off prior to sample collection. An approximately 3 cm layer of surface sediments was subsampled from the grab using a clean spoon and placed in a 55 milliliter (mL) polycarbonate vial that was sealed with parafilm.

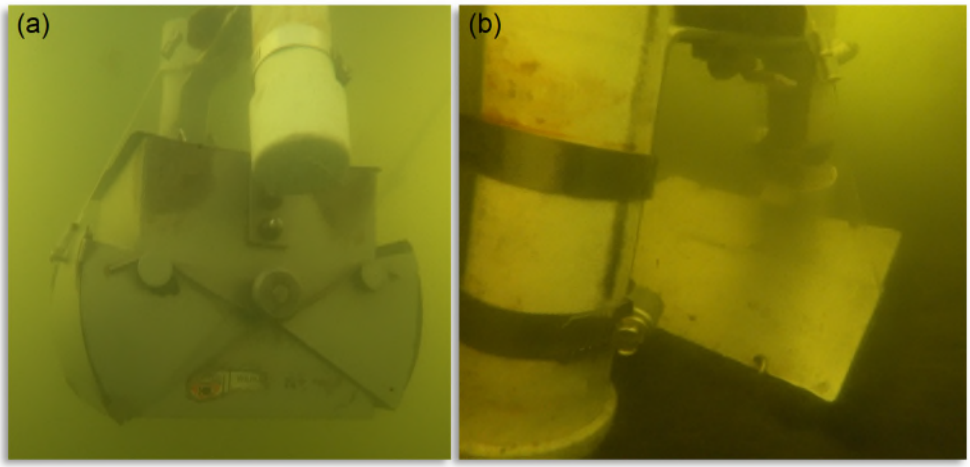

Figure 2-36. Ekman Grab (a) descending through the water column and (b) settled in sediments with no visible disturbance to the sample

Darkened, benthic (sediment) and "blank" chambers were used to determine sediment oxygen demand (SOD) fluxes and nutrients from sediments and suspended particles (water column respiration). Methods used in this study were developed following guidelines in a synthesis of techniques by Boynton et al. (2018). Blank chambers containing HOBO U26 DO data loggers and mechanical stirrers were rinsed and then completely filled with bottom water (Figure 2-37). Water samples were obtained and immediately filtered through Whatman 0.45 µm polypropylene syringe filters and stored on ice until returned to the laboratory. The volume of water removed for samples was replaced with bottom water and chambers containing no air were sealed and incubated for 1.5 to 2 hours. Chambers were kept in the shade at a constant in-situ temperature for the duration of the incubation. Following the incubation period, chambers were opened, and a final water sample was extracted and immediately filtered and placed on ice for transport to the laboratory.

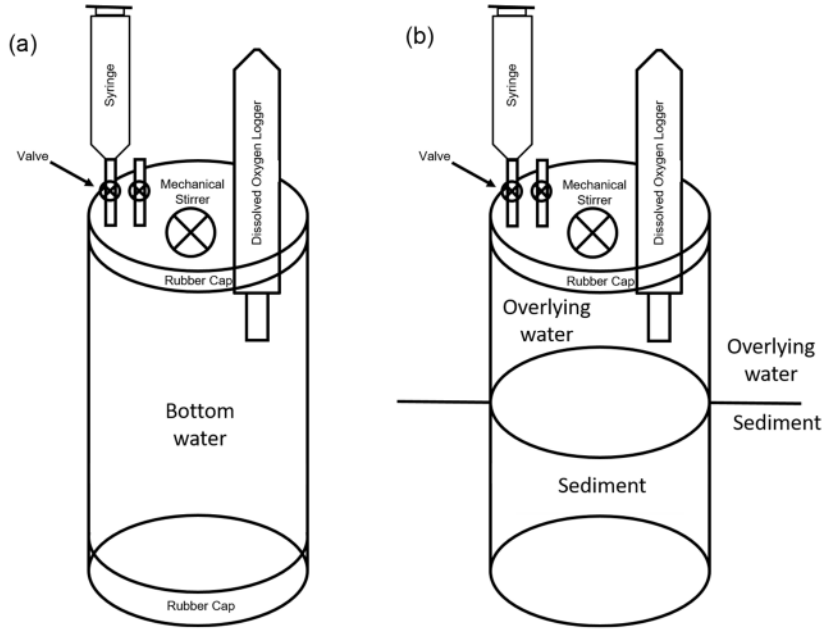

Figure 2-37. Schematic diagram of the (a) blank and (b) benthic chambers used to determine water column respiration, SOD, and nutrient fluxes

Benthic chambers were pushed vertically into sediments without side-to-side movement to avoid creating channels that would allow water exchanges. Chambers were pushed at least 10 cm into the sediments to prevent burrowing organisms from creating channels that would allow water exchange with the outside environment. The chamber height was recorded to calculate the total water volume in each chamber (e.g., Boynton et al. 2018). Once inserted, chambers were left open to the water column for 2–5 minutes to allow particles and sediments to settle and water to be exchanged with undisturbed bottom water. Before sealing each chamber, water samples were obtained from inside the chamber and immediately filtered using Whatman 0.45 µm polypropylene syringe filters. Chambers were then sealed with lids containing mechanical stirrers to keep the water well-mixed and prevent buildup of a concentration gradient in a boundary layer at the sediment-water interface. Stirrers were designed and deployed to mix the overlying water without causing sediment resuspension. HOBO U26 DO data loggers were mounted through an airtight seal in the lid of each chamber (Figure 2-37). The rate of DO decline within the chamber was measured over a 1.5- to 2-hour period for sand and for 20 to 45 minutes for mud. At the end of each deployment, a syringe was attached to a valve on the top of the chamber and a 60 mL water sample for nutrient analysis was extracted and immediately filtered and stored on ice. At the end of each deployment, a sediment sample was obtained from inside the sediment chamber and placed in a polycarbonate vial (about 55 mL) for sediment analysis. At least 2 L of unfiltered bottom water was also collected for determination of turbidity and chlorophyll *a*.

Sediment cores for laboratory incubation experiments were obtained by carefully pushing core barrels vertically into the sediments to avoid creating channels or resuspending sediments. Cores were capped to create a vacuum, extracted from the sediment, and a synthetic rubber stopper was immediately placed in the bottom of the core (Figure 2-38). Still underwater, caps were removed to prevent buildup of pressure as the synthetic rubber stopper was inserted fully. In addition to synthetic rubber stoppers, expansion plugs were inserted and expanded to prevent leaks. Caps were then replaced and the entire core, with no air, was placed in a cooler and transported to the laboratory. If any disturbance was noted throughout the collection process, the core was discarded and a new core obtained. Large (at least 2 L) unfiltered water samples were collected for replacement of the overlying water at the beginning of laboratory incubation experiments.

Figure 2-38. A student collects a sandy sediment core from shallow water (left), and Dr. Austin Fox returns a sediment core from deeper water using SCUBA (right)

In March 2020, benthic chambers were retrofitted with collapsible external bladders to measure groundwater seepage into the IRL (Martin et al. 2007). Bladders from the mini-seepage meters were completely empty at the start of each deployment. At the end of each deployment, bladders were recovered, and the water volume was recorded. Seepage was calculated by dividing the water volume in the bladder by the sediment surface area in the chamber by the length of deployment to yield seepage in cm/day, consistent with literature values (e.g., Martin et al. 2007, Pandit et al. 2017).

2.4.1.2 Laboratory Analyses

Concentrations of ammonium (NH_4), nitrate + nitrite (NOx), total dissolved nitrogen (TDN), ortho-phosphate (PO_4), total dissolved phosphorus (TDP), and silica (SiO_2) were determined using a SEAL AA3 HR Continuous Segmented Flow Autoanalyzer following manufacturer's methods. pH was determined using Hach Sension1 pH meter and an Oakton field probe. Turbidity was determined on unfiltered samples using a Hach 2100 turbidimeter. The turbidimeter was calibrated prior to each use and checked periodically throughout the analyses. Chlorophyll *a* concentrations were determined by vacuum filtering approximately 50 mL of homogenized water through pre-combusted Whatman 0.7 µm pore size glass fiber filters. Chlorophyll *a* was extracted from filters by placing them in a 90% acetone solution at 4°C in the dark for at least 24 hours. Extracted chlorophyll *a* was analyzed using a Turner Designs 10-AU fluorometer (Turner Designs, San Jose, California) following methods by Welschmeyer (1994). Concentrations of chloride, sulfate, and alkalinity were determined using a SEAL AQ400 discrete auto analyzer following manufacturer's methods.

Laboratory incubations were carried out in a manner consistent with previous studies (e.g., Cowan et al. 1996, Hammond et al. 2004, Boynton et al. 2018). Intact sediment cores were placed in temperature-controlled recirculating water baths set to approximate in-situ conditions (Figure 2-39). Incubations were set up by removing caps used to transport cores and siphoning off overlying water, leaving about 1 cm of overlying water to prevent disturbance of the sediment-water interface. Bottom water collected from the field site was then slowly pumped into the chamber using a floating diffuser to prevent disturbance of the sediment-water interface.

At the beginning of each incubation, water samples were collected from each core. Water samples were immediately filtered using Whatman 0.45 µm polypropylene syringe filters and stored in a refrigerator until analysis. The volume of water removed for the initial sample was displaced by the HOBO U26 DO data logger and mechanical stirrer attached to the lid. For laboratory incubations where salinity or temperature were manipulated, valves on each lid were open when the incubation cap was placed on the chamber to allow air and excess water to leave the chamber. Chambers containing no air were sealed and incubated for 1.5 to 2 hours. For experiments where DO was manipulated, mixed gases, air, and N were bubbled into each chamber to maintain constant DO concentrations and valves in each lid were left open to allow gases to escape. Following each incubation, chambers were opened, and a final water sample was extracted, immediately filtered, and stored in the refrigerator at 4˚C until analysis.

All sediment samples were weighed, freeze dried using a Labconco FreeZone 6 system, and reweighed to determine water content. Freeze dried samples were powdered using a SPEX Model 8000 Mixer/Mill. Loss on ignition at 550˚C was used to estimate the fraction of organic matter in the sample.

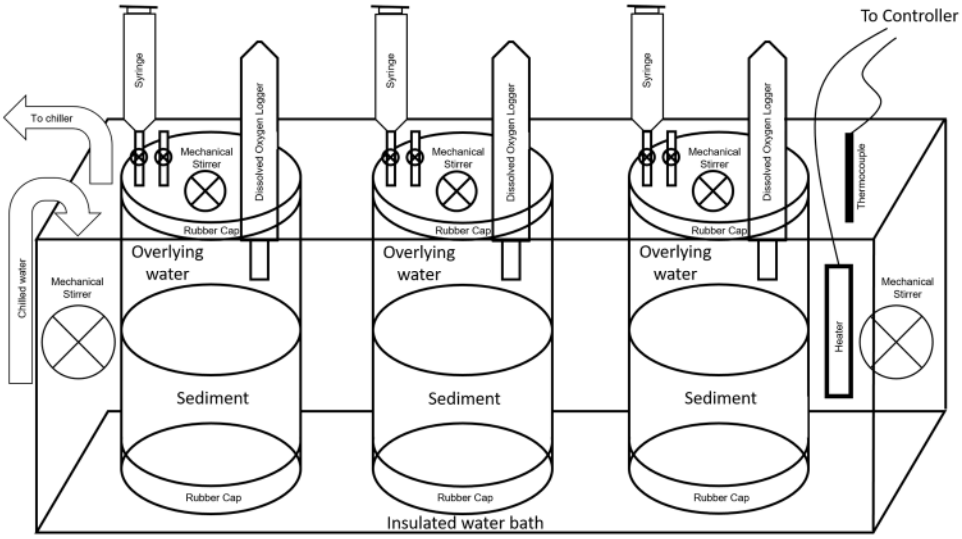

Figure 2-39. Schematic diagram of triplicate laboratory incubation chambers in an insulated, recirculating, temperature-controlled water bath

2.4.1.3 Data and Statistical Analyses

Data and graphical analyses were carried out using Systat 12, SigmaPlot 10 (Systat Software, Inc.), Excel 2016 (Microsoft), ArcGIS (Version 10.2.2.3552, Esri, Redlands, California) and HOBOware Pro 3.7.17. An alpha value to define statistical significance was set at 0.05 for statistical tests and regressions. Least squares linear regressions were calculated to determine relationships between individual pairs of parameters.

SOD was determined by subtracting the water column respiration values for "blank" chambers from values obtained from benthic chambers. The rate of oxygen use by sediments, accounting for the volume in the benthic chamber, was divided by the surface area of sediment to yield values for SOD. SOD values are reported in micromoles per square meter per hour (µmoles/m^2/hr).

Benthic nutrient fluxes were determined from benthic and blank chambers by subtracting initial nutrient concentrations (micromoles per liter [µM]) from final concentrations for both benthic and blank chambers. The changes in concentrations were then divided by the elapsed time of each incubation. The rate of nutrient production/utilization in blank chambers was subtracted from the rate calculated for benthic chambers to determine the production/utilization by sediments and particles independently. The rate for the benthic chamber was then multiplied by the chamber volume, calculated using the chamber height above the sediments, to yield the amount of nutrients produced/used by sediments in the chamber per hour. This value was divided by the sediment surface area in the chamber to yield a flux in µmoles/m^2/hr consistent with literature (e.g., Boynton et al. 2018). A similar approach was used to determine nutrient fluxes from laboratory incubations. Nutrient fluxes were evaluated against the oxygen utilization rate to ensure that linear nutrient production/utilization could be assumed. If the chamber went anaerobic during the deployment or oxygen use was non-linear, nutrient fluxes were flagged and not included in data interpretation.

2.4.2 Data

2.4.2.1 Temperature, Salinity, and Density

Long-term datasets for lagoon and seawater temperature and salinity were used to complement discrete data obtained during this study. Overall, lagoon temperatures followed seasonal patterns with a range of about 17°C from a minimum of approximately 15°C typically reported during February to maximum of approximately 32°C typically reported during August and September. Overall, average annual temperatures were close to 25°C with small, yet significant differences among stations (Figure 2-40). Seawater temperature followed similar seasonal patterns; however, minimum temperatures during winter were higher and maximum temperatures during summer were lower for a smaller annual temperature range with a minimum of about 16˚C typically reported during February to a maximum of approximately 31˚C typically reported during August and September (Figure 2-40). In addition to a smaller annual temperature range, temperatures were more uniform across the study area from offshore at Vero Beach to Port Canaveral.

Overall, salinity was lower in the BRL compared to Vero Beach near Bethel Creek (Figure 2-41). For example, during 2019, salinity in BRL ranged from 19.2–23.3 PSU relative to a range of 21.8–33.0 PSU in Vero Beach. As expected, these values were lower than the range of salinities obtained for the coastal Atlantic Ocean (33–35 PSU). Relative to samples collected offshore, seawater in Port Canaveral had lower salinity in surface water (31–32 PSU) increasing with depth to values consistent with values found offshore (33–35 PSU). These data are consistent with a source of lower salinity water, possibly related to the locks in Port Canaveral.

Using data for temperature and salinity, the density of each water mass was calculated as an indication of the likelihood of mixing or the degree of stratification that could occur if seawater were pumped into the system. Consistent with lower salinity, density was lower at the northern site in BRL with an average during 2019 of 1,012 kilograms per cubic meter (kg/m^3) relative to 1,018 kg/m^3 at the Bethel Creek site. These values were 1.3% and 1.7% less dense than typical seawater at 1,025 kg/m^3. This small difference in density is sufficient to maintain discrete stratified layers and is greater than differences in density identified among existing layers observed during this study. Stratified water columns within the IRL often result in lower bottom water DO concentrations that influence geochemical nutrient cycling. Regardless of the degree of mixing, inflow of seawater would stabilize temperature and salinity in the lagoon, producing cooler lagoon water during summer months and potentially warmer water during winter months. Salinity would likely increase in the area of inflow, but the increase would likely be small.

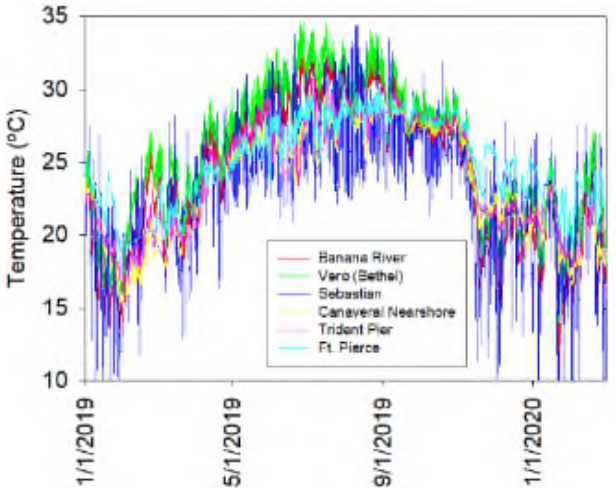

Figure 2-40. Temperature over time in BRL and Vero Beach near Bethel Creek

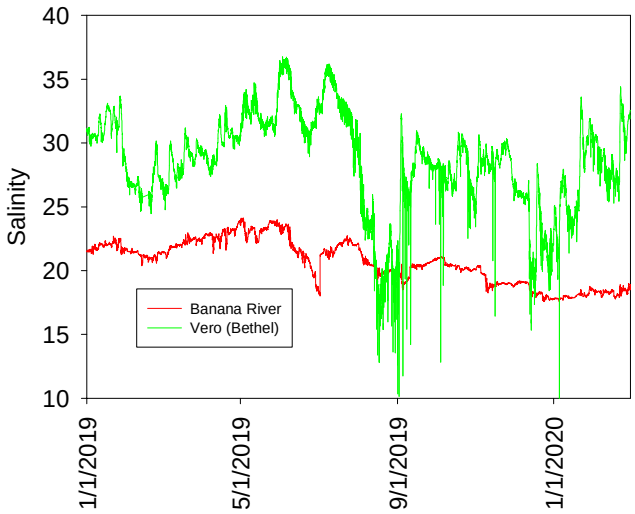

Figure 2-41. Salinity over time in BRL and Vero Beach near Bethel Creek

2.4.2.2 Dissolved Nutrients

Pumping water from offshore would bring cool seawater from below the thermocline into the lagoon versus a potential weir at the northern site that would supply warmer and less saline surface seawater from Port Canaveral. This subtle difference in seawater source would influence both direct nutrient exchanges and potential geochemical changes associated with different temperature, salinity, and DO.

Seawater samples were collected from three areas: (1) at 10-m isobaths located 1–2 km offshore, (2) in the surf zone (when weather prevented offshore sampling), and (3) in Port Canaveral. Overall, the lowest nutrient concentrations were obtained from offshore sites with average concentrations of 8.0 ± 2.4 µM TDN, 0.15 ± 0.05 µM TDP, and 3.3 ± 0.7 µM SiO_2, and no significant vertical trends were observed for TDN, TDP, SiO_2, or speciation. Offshore samples were also the most uniform spatially and temporally.

Nutrient concentrations in the lagoon were more variable. Large differences were observed among samples from the open lagoon (northern and central sites) and in Bethel Creek (southern site). Overall, concentrations at lagoon sites averaged 62.8 ± 24.3 µM TDN, 1.41 ± 0.72 µM TDP, and 51 ± 28 µM SiO_2, which are 7.9-fold, 9.4-fold, and 15.5-fold higher, respectively, than values for seawater. During this study, samples from the open lagoon averaged 72.1 ± 23.3 µM TDN, 1.38 ± 0.52 µM TDP, and 40 ± 13 µM SiO_2 versus 44.1 ± 12.7 µM TDN, 1.45 ± 0.91 µM TDP, and 71 ± 37 µM SiO_2 for samples from Bethel Creek.

Although total nutrient concentrations are frequently used as an indicator of the eutrophic state of an estuary, speciation and relative abundance of bioavailable species have consistently been shown to contribute to algal community. These data show higher N:P ratios at northern sites in the IRL and Lapointe et al. (2020) showed a similar pattern for the N:P ratio in seagrasses *S. filiforme* suggesting that some photosynthesizes adapt to varying abundances of N and P. Nevertheless, these seagrasses fit in a relatively narrow range of N:P and large differences in N:P have been shown to drive change in species composition of photosynthesizes. Based on global trends plus data from this study and long-term datasets, potential shift in N:P ratios should be considered a major component of overall water quality.

To use the most robust dataset available, 5-year averages for nutrient concentrations at sites near each inlet were used to calculate expected discharges (metric tons/year) based on various pumping levels (Table 2-13 and Table 2-14). Annual nutrient discharges through inlets to the coastal Atlantic Ocean associated with possible pumping of 5 m^3/s are calculated at approximately 70 metric tons of N and 6.7 to 11 metric tons of P per year (Table 2-13 and Table 2-14). Overall, the TDN discharged from any inlet would be about the same (70 tons/year); however, the speciation of the discharged N would differ. These data suggest that more readily bioavailable dissolved inorganic nitrogen (DIN) (NH_4^+ and NO_x) would be preferentially discharged at the southern location. Estimated annual discharges of TDP were about 60% greater at Fort Pierce (11 tons/year) versus Sebastian Inlet (6.7 tons/year), and the relative abundance of PO_4 to organic P was higher at 50:50 relative to 30:70 at Sebastian Inlet. Like N, discharges from the southern station would favor discharges of more readily bioavailable PO_4.

Table 2-13. Tons of N and P that would be discharged to the coastal ocean per year from Sebastian Inlet

Pumping Rate	L/day	L/year	NH_4 (tons/yr)	NOx (tons/yr)	DIN (tons/yr)	Org-N (tons/yr)	TDN (tons/yr)	PO_4 (tons/yr)	TDP (tons/yr)	DOP (tons/yr)
2.5 m^3/s	$2.2*10^8$	$7.9*10^{10}$	1.5	0.63	2.2	31	34	1.0	3.3	2.2
5 m^3/s	$4.3*10^8$	$1.6*10^{11}$	3.0	1.3	4.5	64	68	2.1	6.7	4.5
10 m^3/s	$8.6*10^8$	$3.2*10^{11}$	6.1	2.6	9.0	130	140	4.2	13	9.0
15 m^3/s	$1.3*10^9$	$4.7*10^{11}$	8.9	3.8	13	190	200	6.1	20	13
20 m^3/s	$1.7*10^9$	$6.3*10^{11}$	12	5.0	18	250	270	8.2	27	18

Table 2-14. Tons of N and P that would be discharged to the coastal ocean per year from Fort Pierce Inlet

Pumping Rate	L/day	L/year	NH_4 (tons/yr)	NOx (tons/yr)	DIN (tons/yr)	Org-N (tons/yr)	TDN (tons/yr)	PO_4 (tons/yr)	TDP (tons/yr)	DOP (tons/yr)
2.5 m^3/s	$2.2*10^8$	$7.9*10^{10}$	2.9	1.7	4.7	29	33	2.7	5.3	2.6
5 m^3/s	$4.3*10^8$	$1.6*10^{11}$	5.9	3.5	9.4	58	68	5.4	11	5.3
10 m^3/s	$8.6*10^8$	$3.2*10^{11}$	11.8	7.0	19	120	140	11	21	11
15 m^3/s	$1.3*10^9$	$4.7*10^{11}$	17.4	10	28	170	200	16	32	16
20 m^3/s	$1.7*10^9$	$6.3*10^{11}$	23.3	14	37	230	270	21	42	21

Based on this preliminary dataset, incoming seawater pumped at 5 m^3/s from offshore would bring approximately 18 metric tons of N and 0.7 metric tons of P into the lagoon per year (Table 2-15). The net change in nutrients associated with pumping water from offshore (5 m^3/s) into the lagoon was calculated at (out-in) about 50 tons/year of N and between 6 and 10 metric tons/year of P.

A weir at the northern site would have a higher exchange rate for water with estimates ranging from an average of about 7 m^3/s for a 50-m wide weir to about 20 m^3/s for a 150-m wide weir. Approximately 95 to 270 metric tons of N and about 9 to 27 metric tons of P were calculated to be discharged from inlets per year depending on the size of the weir (Table 2-13 and Table 2-14). Based on data obtained during this preliminary investigation, seawater overflowing a weir at 7 to 20 m^3/s from Port Canaveral would bring 76 to 216 tons of N per year and 1.8 to 4.9 tons of P per year into the IRL from Port Canaveral (Table 2-16). These calculations are likely overestimates because as water entered the lagoon from Port Canaveral, water would be replaced from offshore leading to improved water quality over time. Nevertheless, the net change to nutrients in the lagoon is an annual removal of 19 to 54 tons of N and 7 to 22 tons of P.

Table 2-15. Tons of N and P that would be pumped into the lagoon associated with pumping seawater from offshore

Pumping Rate	L/day	L/year	NH_4 (tons/yr)	NOx (tons/yr)	DIN (tons/yr)	Org-N (tons/yr)	TDN (tons/yr)	PO_4 (tons/yr)	TDP (tons/yr)	DOP (tons/yr)
2.5 m^3/s	$2.2*10^8$	$7.9*10^{10}$	1.0	0.3	1.3	5	9	0.1	0.4	0.2
5 m^3/s	$4.3*10^8$	$1.6*10^{11}$	2.1	0.6	2.7	11	18	0.3	0.7	0.4
10 m^3/s	$8.6*10^8$	$3.2*10^{11}$	4.2	1.2	5.4	21	36	0.6	1.4	0.9
15 m^3/s	$1.3*10^9$	$4.7*10^{11}$	6.2	1.7	7.9	31	52	0.8	2.1	1.3
20 m^3/s	$1.7*10^9$	$6.3*10^{11}$	8.3	2.3	10.6	42	70	1.1	2.8	1.8

Table 2-16. Tons of N and P that would flow into the lagoon from Port Canaveral associated with a weir

Pumping Rate	L/day	L/year	NH_4 (tons/yr)	NOx (tons/yr)	DIN (tons/yr)	Org-N (tons/yr)	TDN (tons/yr)	PO_4 (tons/yr)	TDP (tons/yr)	DOP (tons/yr)
2.5 m^3/s	$2.2*10^8$	$7.9*10^{10}$	6.0	1.1	7.0	20	27	0.5	0.6	0.1
5 m^3/s	$4.3*10^8$	$1.6*10^{11}$	12	2.2	14	41	55	1.1	1.3	0.2
10 m^3/s	$8.6*10^8$	$3.2*10^{11}$	24	4.3	28	81	110	2.1	2.5	0.4
15 m^3/s	$1.3*10^9$	$4.7*10^{11}$	35	6.3	42	119	161	3.1	3.7	0.6
20 m^3/s	$1.7*10^9$	$6.3*10^{11}$	48	8.5	56	160	216	4.2	4.9	0.8

Benthic fluxes of N and P from muck are estimated to contribute more than 40% of the annual N and P loading to the IRL (Tetra Tech 2020, Fox and Trefry 2018). These estimates are based only on fluxes from fine-grained, organic-rich sediments locally referred to as "muck." To evaluate the importance of these geochemical processes towards regulating nutrient concentrations in lagoon water, residence times for nutrients were calculated based on nutrient fluxes, long-term average nutrient concentrations in the lagoon water, and an average lagoon depth of 1.5 meters.

No significant trends for benthic nutrient fluxes versus the composition of sandy sediments (e.g., sediment organic matter content) have been identified in the IRL. This deviates from an established pattern where sediment water and organic matter content are strongly correlated with benthic fluxes from fine-grained, organic-rich sediments throughout the IRL (Fox and Trefry 2018). The absence of a trend for sandy sediments is likely partially due to groundwater seepage into the lagoon through water-permeable sandy sediments. Based on data from simple mini-seepage meters deployed during this study, it is likely most benthic chambers were influenced to some extent by groundwater seepage with rates ranging from less than 1 to about 30 cm/day (Bethel Creek) from sites within about 10 m of the shoreline. Where groundwater seepage occurs, fluxes were more likely the result of advective versus diffusive processes. Nevertheless, fluxes reported represent either inputs (positive values) or removal (negative values) of nutrients or oxygen from the lagoon system. Preliminary results show significant correlations between nutrient fluxes and latitude (Figure 2-42).

Median SOD (oxygen flux into sediments) for sandy sediments was -3,200 ± 900 µmoles $O_2/m^2/hr$. SOD of muddy sediments was higher at -4,300 ± 2,500 µmoles $O_2/m^2/hr$; however, muddy sediments were investigated during November through February (cooler months) and fluxes from muddy sediments almost certainly underestimate annual average values.

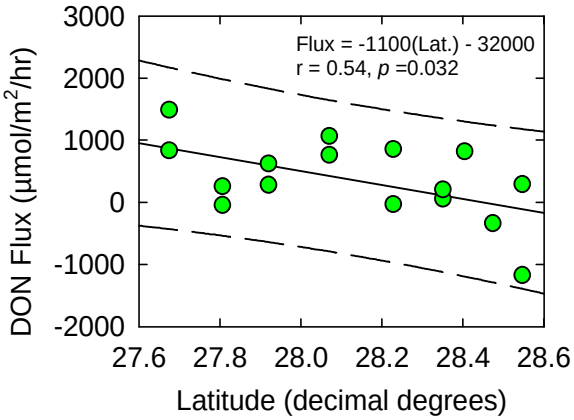

Figure 2-42. Benthic flux of dissolved organic nitrogen (DON) versus latitude

Overall, median N fluxes varied among areas with sandy versus muddy sediments. At sandy sites, DIN was released from sediments (median 32 tons/km^2/year) primarily as NOx (63% of DIN, 20 tons N/km^2/year), and NH_4 accounted for 37% of the DIN efflux at 11 tons N/km^2/year. At many sites, NH_4 fluxes were directed into sediments, possibly due to nitrification in aerobic surface sediments. Fluxes of DON were highly variable with median DON fluxes directed out of sediments for a median TDN flux from sandy sites at 35 tons N/km^2/year. At muddy sites (muck), fluxes of NOx were directed from the water into sediments (-22 tons N/km^2/year), consistent with the use of nitrate as an oxidizing agent for the decomposition of organic matter in suboxic/anaerobic sediments. Releases of DIN from muddy sediments were 100% NH_4 at a median of 71 tons N/km^2/year, 2.2-fold higher than DIN fluxes from sandy sediments. Fluxes of DON were highly variable, and no consistent trend was identified.

At sandy sites, the median PO_4 flux was 1.1 ton/km^2/year. This wide range of values was not unexpected because P fluxes vary as a result of bacterial decomposition and concentration gradients, but also due to changing redox conditions in sediments and overlying water. The net TDP flux was directed into sandy sediments from overlying water at -0.2 tons/km^2/year. At muddy sites, the median P flux was 9.3 tons/km^2/year. Fluxes of DOP were also directed out of sediments at 3.6 tons/km^2/year. Overall TDP fluxes were directed out of muddy sediments and the net flux of P was large and positive (Table 2-17).

Table 2-17. Median for benthic fluxes from sandy and muddy sediments in µmoles/m^2/hour (2019–2020)

Sediment	Oxygen	NH_4	NOx	DIN	PO_4	TDP	DOP
Sand	-3200 ± 900	90 ± 60	150 ± 150	260 ± 170	4.1 ± 8.1	-0.6	-4.7 ± 4.9
Muck (winter)	-4300 ± 2500	580 ± 460	-180 ± 200	400	34 ± 18	47	13 ± 26

Benthic nutrient and oxygen fluxes plus existing nutrient concentrations in the IRL were used to estimate residence (turnover) times for nutrients in the IRL. In sandy sediments, the residence time for NH_4 ranged from 22–43 hours based on 5-year average concentrations at Sebastian Inlet and Vero Beach. Nitrate fluxes from sandy sediments were higher and concentrations in lagoon water were lower, for turnover times ranging from 6–15 hours. Together, DIN fluxes could replace all DO in the water column in 190 hours or about 8 days. Turnover times for NH_4 and NOx from muck were 4–7 hours and 5–13 hours, respectively. Because nitrate fluxes into sediments are balanced by increased NH_4 fluxes from sediments, NH_4 flux accounts for nitrate fluxes with regards to turnover of N in the water column. NH_4 could replace all the dissolved N in the water column overlying muck in approximately 80 hours.

Turnover times for PO_4 from sandy sediments varied from 160–410 hours days compared to 18–48 hours for areas with muck sediments. To cycle the complete pool of dissolved P, it would take 500–800 hours for sandy sediments and 59–95 hours for muck sediment.

Due to the large temporal and spatial variability in DO throughout the lagoon, turnover times for oxygen were highly variable. If the 5-year average DO concentration in the lagoon is used, turnover times based on SOD ranged from 110 hours for sandy sites to 80 hours for mucky sites. When water column respiration and SOD are considered together, turnover times based on a 1.5-m deep water column were 25–28 hours. SOD accounted for 25% and 31% of the total oxygen demand for areas containing sand and muck, respectively. These short turnover times are relatively consistent with observed nighttime (dark) decreases in DO throughout the lagoon.

Table 2-18. Turnover times in hours calculated using benthic fluxes, nutrient concentration in the water column and an average depth of 1.5 m.

Sediment	Oxygen (hours)	NH_4 (hours)	NOx (hours)	DIN to replace TDN (hours)	PO_4 (hours)
Sand	110	22 to 43	6 to 15	190	160 to 410
Muck (winter)	80	4 to 7	5 to 13	80	18 to 48

2.4.2.3 Laboratory Experiments (Sandy Sediments)

Despite the importance of benthic-pelagic coupling and short residence times for nutrients in shallow coastal systems, improved water quality that could result from the proposed inflow would likely modify geochemical processes, increasing or decreasing benthic fluxes into overlying water and changing residence times for nutrients. To address some of these potential changes, laboratory incubation experiments were carried out to investigate how changes to temperature, salinity, and DO might influence nutrients in the lagoon.

Temperature was adjusted between 13˚C and 32˚C using microcontroller controlled recirculating water baths to simulate the maximum annual range of lagoon temperatures. Sediments cores from the IRL were slowly adjusted to the desired temperature within 1 hour of collection. After reaching the desired temperature, cores were allowed to equilibrate for at least 1 hour before overlying water was drained and replaced with new water from the collection site. Once temperature was stable for about 30 minutes, start samples were collected and cores were sealed with DO loggers and mechanical stirrers. Stirrers were selected for their ability to prevent the buildup of concentration gradients at the sediment-water interface without causing resuspension. Overall, the lowest SODs were identified at 13˚C and 15˚C and the highest fluxes were identified at 22˚C. Above 22˚C, SOD decreased as temperature increased towards 32˚C.

Nutrient fluxes responded to changes in temperature in different ways. No consistent temperature related trends were identified for fluxes of any N species from sandy sediments when temperatures ranged from 13˚C to 32˚C. NH_4 fluxes followed patterns for SOD; however, NH_4 accounted for a small fraction of the DIN and in many cases fluxes were directed into sediments. Fluxes of NOx were variable and positive in all but one core. These data suggest that some degree of nitrification occurred in sediments across the entire temperature range.

Fluxes of dissolved PO_4 from sandy sediments were positively correlated with temperature and increased from near 0 µmoles/m^2/hr at 13˚C to 5 to 10 µmoles/m^2/hr at 32˚C. No consistent trends were identified for DOP or TDP. No significant correlation was identified for SiO_2 fluxes versus sediment temperature; however, a general trend for increasing SiO_2 with increasing sediment temperature was observed with a slope of 5.4 µmoles/m^2/hr per ˚C.

Based on the significant positive correlation between sediment temperature and PO_4 flux, any decrease in water temperature associated with inflow would likely decrease PO_4 fluxes into the lagoon. A 1˚C decrease in lagoon temperature would decrease PO_4 fluxes from sandy sediments by about 0.16 tons/km^2/year (0.58 µmoles/m^2/hr per ˚C) or about 15% from the current median at 4.1 µmoles/m^2/hr (1.1 ton/km^2/year). Applied to the complete surface area of the lagoon, this potential decrease in P flux could be of more significance to PO_4 concentrations in the lagoon than decreases due to dilution by seawater.

Laboratory experiments were carried out to evaluate potential uptake or releases of nutrients and oxygen consumption associated with changes to salinity in overlying water. These experiments were conducted in water baths at 22˚C. Overall, no significant correlation was identified between SOD and the salinity of overlying water. Despite the absence of a trend, SOD decreased with salinity for samples using a mixture of site water and deionized water. This decrease in SOD is not the result of lower water column respiration due to dilution of site water and water column processes were not likely the main driver of this trend.

All N species showed lower fluxes at higher salinities. Significant correlations were identified for NOx with a decrease in NOx flux of 4.7 µmoles/m^2/hr per PSU or about 3% per PSU from the median of 150 µmoles/m^2/hr for sandy sites throughout the lagoon.

Fluxes of P and SiO_2 followed patterns observed for N with a general trend of lower fluxes at higher salinities; however, once salinity increased beyond about 20 PSU, fluxes of PO_4 increased, consistent with observations for oxygen. The absence of statistically significant trends is likely related to the relatively small sample size obtained during the first year of sampling. Both DIN and soluble reactive phosphorus (SRP) fluxes decreased with increasing salinity, and based on these preliminary data, no shift in the ratio of DIN:SRP fluxes is currently expected base on a potential shift in lagoon salinity.

Although DO is not a conservative property of seawater, it is one of the water quality variables likely to change if seawater were to flow into the lagoon by way of pumping or a weir. Changes to DO would likely result from (1) a change in solubility due to changing temperature and salinity, plus (2) inflow of lower turbidity seawater with lower respiration, and (3) higher density seawater and enhanced circulation that could disrupt areas currently subject to stagnation and low DO. To manipulate DO concentrations in the laboratory, cores were place in temperature stable water baths and continuously bubbled using mixed gases (air and N) to maintain DO concentrations between 0% (0 mg/L) and 100% saturation (7–8 mg/L). Because oxygen was controlled, no data for respiration or SOD were obtained for these experiments.

N fluxes were relatively low. Nevertheless, a significant positive correlation was identified between NH_4 fluxes and bottom water DO. No significant correlations were identified for other N species. The significant trend for NH_4 fluxes versus DO was likely due to enhanced bacterial metabolism under aerobic versus anaerobic conditions. No significant correlations were identified for P fluxes versus bottom water DO; nevertheless, in anaerobic (0% DO) experiments PO_4 fluxes were always directed out of sediments (positive flux), consistent with the release of sorbed P from dissolution of iron oxy-hydroxides (Boynton et al. 2018, Foster and Fulweiler 2019). These data reinforce the recurring observation that releases of P relative to N are enhanced under low oxygen conditions and can support low molar N:P ratios in anaerobic environments (Boynton et al. 2018). A significant negative correlation was identified between SiO_2 and bottom water DO.

To assist modeling efforts, long-term datasets for DO concentrations from the IRL and BRL were obtained for surface water from the St. Johns River Water Management District (SJRWMD).

Existing sensors record DO near the surface or at fixed depths and can miss events that are restricted to the near bottom. Data for DO in surface water showed an annual trend that is relatively consistent with variations in DO solubility. For example, at a salinity of 25, a reasonable average for the IRL, DO solubility increased from 6.4 mg/L at 32°C to 8.7 mg/L at 15°C, an annual range of 2.3 mg/L (Figure 2-43). In addition to this range in DO, values are often below saturation during summer with some instances of hypoxia (less than 2 mg/L) recorded in the surface water.

Temporal and spatial differences in bottom water DO can cause sediments to alternate between sinks and sources of nutrients. Changes to DO in bottom water lead to changes in concentrations and the relative abundance of bioavailable N and P with implications to algal community composition and density. Overall, DO in bottom water at sandy sites tracked values for surface water (Figure 2-44). In some cases, DO was much lower in bottom water, possibly related to fouling of the sensor by mud or smothering by drift algae. To minimize the impacts of fouling and provide adequate quality assurance and quality control for these data, two sensors were assigned to each station with one deployed and one returned for cleaning and calibration before redeployment on 2-week cycles. Although the trend may be partially due to the presence of drift algae that restricted circulation with overlying water, DO in bottom water was close to values for surface water during cooler winter months. During April, a difference in DO began to develop between surface and bottom water, which continued into summer months (Figure 2-44). Even if this trend is partially the result of a layer of drift algae, it still represents the conditions experienced in bottom water near the sediment-water interface that influence sediment processes. These data begin to establish a baseline for monitoring conditions near the sediment-water interface to better understand the relationship between DO in the water column and sedimentary processes.

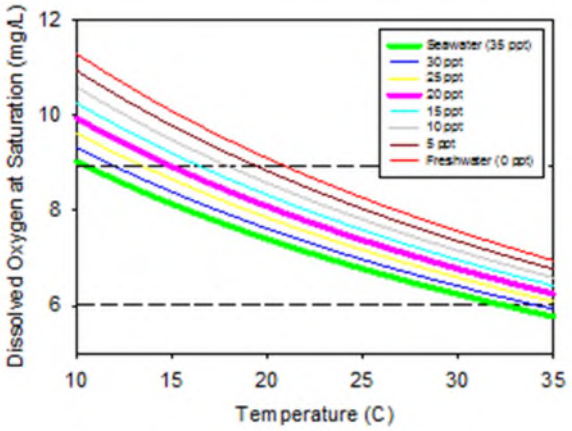

Figure 2-43. DO at saturation versus temperature for seawater at 35 PSU, freshwater at 0 PSU, and at 5 PSU intervals

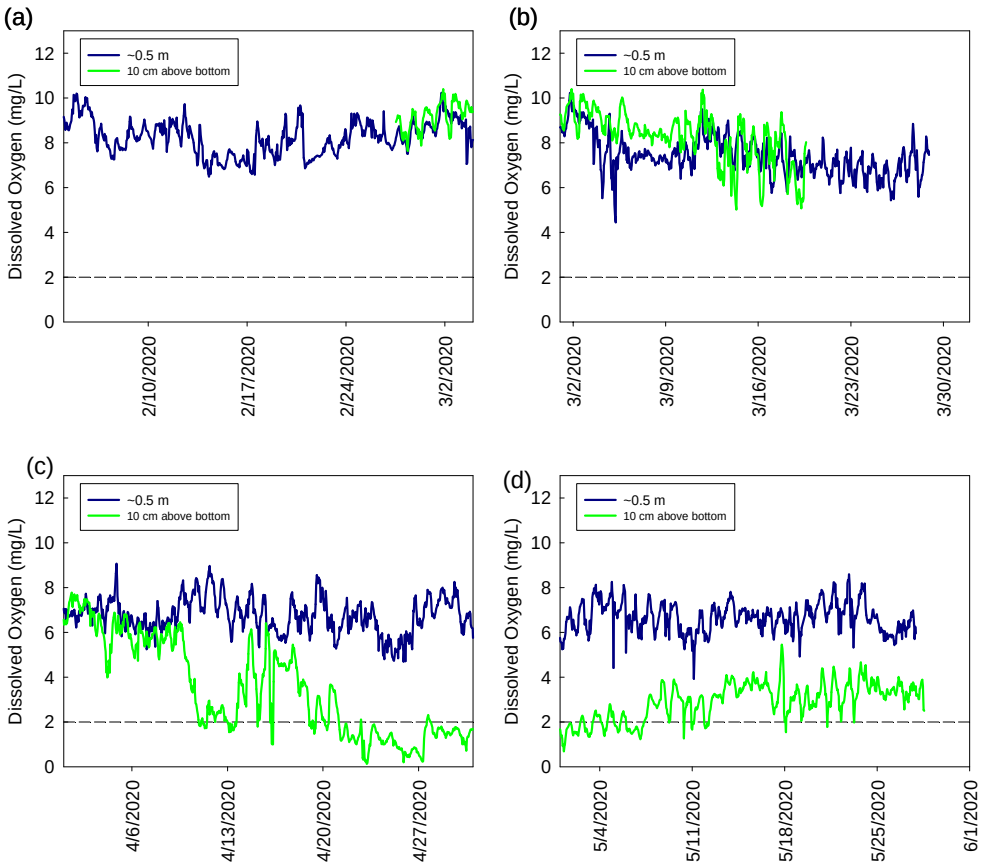

Figure 2-44. DO concentrations in bottom water (green line) and near the surface (blue line) in the IRL during (a) February, (b) March 2020, (c) April, and (d) May 2020

Sensors deployed in BRL, near the potential central BRL pump location, show stark differences for bottom water overlying muck versus sand even though the sensors are only about 200 m apart (Figure 2-45). These data are consistent with differences in SOD among substrates and are consistent with the existence of a stratified water column at deeper sites where fine-grained sediments are more likely to accumulate. DO concentrations were more variable with larger diurnal fluctuations in DO. These fluctuations were likely responsible for the large diurnal variability in DO overlying sandy sites adjacent to muck deposits (green line in Figure 2-45 versus green line in Figure 2-44). Bottom water in deeper areas overlying muddy deposits also experienced several extended periods of anoxia (Figure 2-45).

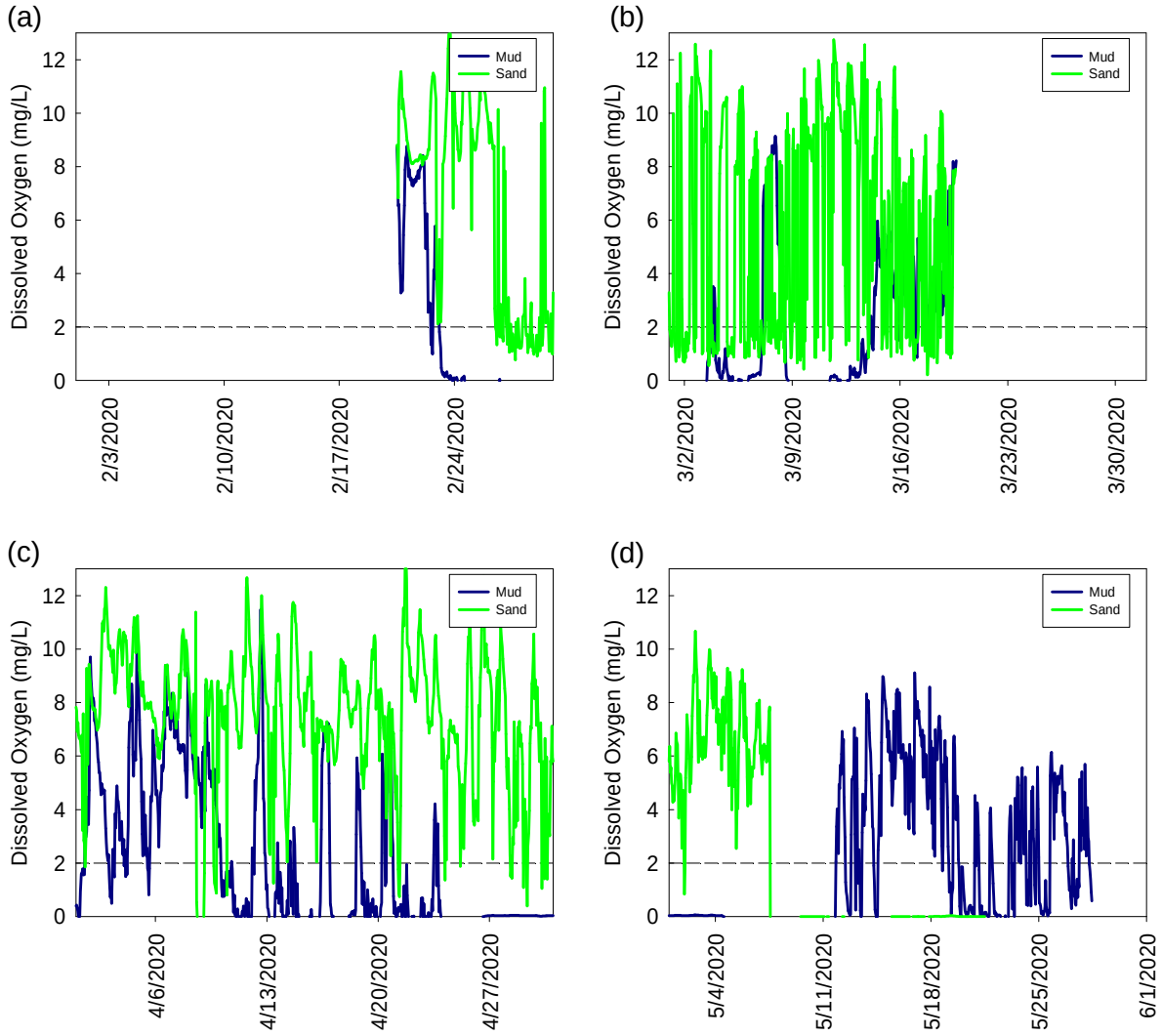

Figure 2-45. DO concentration in bottom water (less than 30 cm above the bottom) near the central BRL location for an area with sandy sediments (green line) and muddy sediments (blue line) during (a) February, (b) March 2020, (c) April and, (d) May 2020

2.4.3 Conclusions

Enhanced inflow of seawater to the IRL system would drive corresponding discharges of lagoon water into the coastal ocean. These exchanges of water plus dissolved and particulate materials would lead to changes in water quality within the lagoon. These exchanges would have both direct impacts, such as conservative mixing of temperature and salinity, and indirect impacts, such as changes to geochemical nutrient cycling in response to changes to water quality. Based on a combination of data from this study plus long-term datasets, the coastal Atlantic Ocean is cooler than the lagoon by about 1°C during summer months and warmer than the lagoon during the winter. This subtle difference and potential buffering of temperature by inflow could mitigate extreme nutrient fluxes during hot summer months; but it may also lead to small increases in flux during winter. Changes to both temperature and salinity would likely be small; however, the potential for stratification and the potential formation of a dense layer of seawater within the lagoon could be of significance at certain locations.

If inflow were to occur via pumping at 5 m^3/s, direct water exchanges would yield a net removal of about 50 tons of N and 6 to 10 tons of P per year from the lagoon. If inflow were to occur via a weir at 7–20 m^3/s, water exchanges would yield a net removal of 19 to 54 tons of N and 7 to 22 tons of P per year from the lagoon.

Benthic nutrient fluxes from sandy sediments were higher than would be expected by extrapolating trends previously identified for muddy sediments in the IRL. These relatively high fluxes from sandy sediments located within 10 m of the shoreline in the IRL were likely related to groundwater seepage driving advective rather than diffusive fluxes. Benthic fluxes would cycle nutrients in the lagoon in a matter of hours to days. Short residence times for nutrients versus water indicate that geochemical processes help to regulate concentrations of nutrients in the IRL and can buffer against changes that might result from external sources.

Laboratory experiments conducted to estimate the potential impacts of inflow on geochemical nutrient cycling showed that lower lagoon temperature and higher lagoon salinity led to significant decreases in benthic fluxes for some nutrients, although this trend was not significant (likely due to the relatively small dataset obtained to date for other nutrients) for most nutrients in the lagoon. These observations suggest that geochemical responses to potential inflow would likely contribute to further decreasing IRL nutrient concentrations. Even small changes to benthic fluxes are large when applied to the entire sediment surface area within the lagoon. Using changes to fluxes from this study, a small decrease in lagoon temperature (less than 1 ˚C) would likely prevent tons of PO_4 from entering the lagoon from sandy sediments each year.

DO concentrations in bottom water followed patterns observed for surface water but often at lower concentrations. In some cases, lower concentrations near the bottom were likely related to the accumulation of drift algae that restricted circulation of water. Nevertheless, DO near the sediments is most important for geochemical cycling within the sediments. DO in bottom water overlying muck was lower than DO in bottom water overlying sand and, in several cases, DO in water overlying muck remained anoxic for several days. Laboratory experiments showed that under anaerobic conditions PO_4 fluxes were directed out of sediments whereas under aerobic conditions sediments often were a sink for PO_4. Enhanced circulation and increased bottom water DO would likely contribute to decreasing PO_4 concentrations in lagoon water.

3 Recommendations and Next Steps

The multi-phased, full research project scope is envisioned to include the baseline monitoring, design, permitting, implementation, and monitoring of a system providing temporary ocean inflow to the IRL. The results of the full Restore Lagoon Inflow Research project will provide information and analysis to the lead agency and appropriate decision-makers to help determine the viability of a full-scale, permanent ocean inflow structure; identify factors that should be considered should a natural breach occur; or if further evaluation is necessary.

3.1 Recommendations

This report represents the foundational data collected during Phase 1 baseline monitoring and is an essential part of the project. The project team has carefully evaluated the parameters required to assess the effectiveness, environmental effects, and limitations of an inflow system. These data will be invaluable not only for the inflow project but for researchers requiring similar data for applications within the IRL and nearshore Atlantic Ocean.

The modeling and engineering tasks laid the groundwork for the design of a temporary inflow pilot system, which will ultimately help to inform a potential full-scale, permanent inflow system, if necessary in the future. The biological data gathered on estuarine and coastal populations, and their ecosystems, is the start of an essential baseline for successful project monitoring. This monitoring represents three seasons of population dynamics in seagrasses, benthic infauna, phytoplankton, ichthyoplankton, fishes, and eDNA surveys, but it is important to obtain at least one more year of these measurements before a temporary inflow pilot system starts to identify seasonal variation. Then it may be possible to identify major responses of the temporary inflow pilot system without confusion over seasonal changes. The geochemical data collection and analyses also provide important baseline conditions. The data collection should continue to inform changes within the lagoon system as part of a temporary inflow pilot system. The data collected as part of this phase from all tasks will help to evaluate shifts in water quality, geochemical cycling, and biological populations and to determine if those shifts are natural or related in part to the temporary pilot inflow system.

3.2 Next Steps

In 2020, the Florida Legislature awarded a $800,000 grant to Florida Tech for Phase 2 of the Restore Lagoon Inflow Research. This second phase will provide continued monitoring, recommendation of a temporary inflow pilot system site, design of a temporary inflow system, and pre-application permitting for the temporary pilot inflow system research site.

Continuation of monitoring, site selection, preliminary design of the temporary inflow pilot system, and pre-application permitting meetings with regulators are planned for Phase 2. Regulatory and agency feedback will help inform analysis and data collection priorities in Phase 2 and subsequent phases of the research project. For Phase 2, the temporary inflow pilot system site location for establishing an exchange with the coastal ocean will be determined using data and modeling from this Phase 1 study and considering practicality (i.e., land ownership, utilities, distance, public roadways, zoning, noise impact, and agency permitting probability), existing exchange conditions, and how pilot flow impacts can meaningfully be extrapolated to other sites.

Subsequent phases of the full Restore Lagoon Inflow Research project are anticipated to involve permitting, implementation of the temporary inflow pilot system, continued monitoring, and observations/analysis of the effects of the temporary inflow of seawater into the lagoon.

4 References

Allen, L., Lokyavich, M., Cailliet, G. and M. Horn. 2006. Ch.5 Bays and Estuaries, In: The Ecology of Marine Fishes: California and Adjacent Waters (editors: Allen, L., Pondella, D., and Horn, M.). University of California Press, Berkeley. 659 pp.

Bengtson, Harlan. Measuring Open Channel Flow Rates with a Weir or a Flume. 2018. Bright Hub Engineering, 12 Nov. 2018, www.brighthubengineering.com/hydraulics-civil-engineering/51435-introduction-to-the-weir-and-flume/.

Berman, D. 2019. Canaveral Lock at Port Canaveral to close to boaters for four months for repairs. Florida Today, 30 July 2019. https://www.floridatoday.com/story/news/2019/07/30/canaveral-lock-port-canaveral-close-four-months-repairs/1864684001/.

Berry, T. E., Osterrieder, S. K., Murray, D. C., Coghlan, M. L., Richardson, A. J., Grealy, A. K., Stat, M., Bejder, L., and Bunce, M. 2017. DNA metabarcoding for diet analysis and biodiversity: A case study using the endangered Australian sea lion (Neophoca cinerea). Ecology and Evolution, 7(14), 5435-5453.

Booij, N., Ris, R.C., and Holthuijsen, L.H., 1999. A third-generation wave model for coastal regions: 1. Model description and validation. Journal of Geophysical Research: Oceans 104 (C4), 7649e7666. http://swanmodel.sourceforge.net/references/references.htm.

Boynton, W.R., Ceballos, M.A.C., Bailey, E.M., Hodgkins, C.L.S., Humphrey, J.L., and Testa, J.M. 2018. Oxygen and nutrient exchanges at the sediment-water interface: a global synthesis and critique of estuarine and coastal data. Estuaries and Coasts 41:301-333.

Brand, L. 1984. The salinity tolerance of forty-six marine phytoplankton isolates. Estuarine, Coastal and Shelf Science, 1984, Volume 18, Issue 5.

Cooksey, C. and Hyland, J. 2007. Sediment quality of the Lower St. Johns River, Florida: An integrative assessment of benthic fauna and general characteristics. Marine Pollution Bulletin 54:9–21.

Cowan, J.L.W., Pennock, J.R., and Boynton, W.R. 1996. Seasonal and interannual patterns of sediment-water nutrient and oxygen fluxes in Mobile Bay, Alabama (USA): regulating factors and ecological significance. Marine Ecology Progress Series 141:229-245.

DiBattista, J.D., Stat, M., Huggett, M.J., Bernasconi, R., Berry, T.E., Newman, S.J., and Bunce, M. 2017. Ecosystem biomonitoring with eDNA: metabarcoding across the tree of life in a tropical marine environment. Scientific Reports 7, 12240.

Dietrich, J.C., Tanaka, S., Westerink, J.J., Dawson, C.N., Luettich Jr., R.A., Zijlema, M., Holthuijsen, L.H., Smith, J.M., Westerink, L.G., and Westerink, H.J. 2012. Performance of the unstructured-mesh, SWAN+ADCIRC model in computing hurricane waves and surge. Journal of Scientific Computing. http://dx.doi.org/10.1007/s10915-011-9555-6.

Dietrich, J.C., Zijlema, M., Westerink, J.J., Holthuijsen, L.H., Dawson, C., Luettich, R.A., Jensen, R., Smith, J.M., Stelling, G.S., and Stone, G.W. 2011. Modeling hurricane waves and storm surge using integrally-coupled, scalable computations. Coastal Engineering 58, 45e65.

Eble, J. A., Daly-Engel, T. S., DiBattista, J. D., Koziol, A., and Gaither, M. R. 2020. Marine Environmental DNA: Approaches, Applications, and Opportunities. Advances in marine biology, 86(1), 141-169.

FDEP. 2013. Basin Management Action Plan for the Implementation of Total Maximum Daily Loads for Nutrients Adopted by the Florida Department of Environmental Protection in the Indian River Lagoon Basin: Banana River Lagoon. http://www.dep.state.fl.us/water/watersheds/docs/bmap/banana-river-lagoon-bmap.pdf.

Foster, S.Q. and Fulweiler, R.W. 2019. Estuarine sediments exhibit dynamic and variable biogeochemical responses to hypoxia. Journal of Geophysical Research: Biogeosciences 124:737-758.

Fox, A.L., and Trefry, J.H. 2018. Environmental dredging to remove fine-grained, organic-rich sediments and reduce inputs of nitrogen and phosphorus to a subtropical estuary. Marine Technology Society 52: 42-57.

FWRI. 2009. Fisheries-Independent Monitoring Program Procedure Manual.

Gianuca, A. T., Declerck, S. A. J., Cadotte, M. W., Souffreau, C., De Bie, T., and De Meester, L. 2016. Integrating trait and phylogenetic distances to assess scale-dependent community assembly processes. Ecography: 1–11.

Hammond, D.E., Cummins, K.M., McManus, J., Berelson, W.M., Smith, G., and Spagnoli, F. 2004. Methods for measuring benthic nutrient flux on the California margin: comparing shipboard core incubations to in situ lander results. Limnology and Oceanography 2:146.

Hamrick, J.M. 1992. A Three-Dimensional Environmental Fluid Dynamics Code: Theoretical and Computational aspects. Special Report 317 in Applied Marine Science and Ocean Engineering, Virginia Institute of Marine Science, Gloucester Point, VA 23062.

Kjerfve, B. 1986. Comparative Oceanography of Coastal Lagoons. Estuarine Variability, (December 1986), 63–81. https://doi.org/10.1016/b978-0-12-761890-6.50009-5.

Kumar, G., Eble, J. E., and Gaither, M. R. 2020. A practical guide to sample preservation and pre-PCR processing of aquatic environmental DNA. Molecular Ecology Resources, 20(1), 29-39.

Lapointe, B.E., Herren, L.W., Brewton, R.A., and Alderman, P.K. 2020. Nutrient over-enrichment and light limitation of seagrass communities in the Indian River Lagoon, an urbanized subtropical estuary. Science of the Total Environment 699:134068.

Leray, M., Yang, J. Y., Meyer, C. P., Mills, S. C., Agudelo, N., Ranwez, V., Boehm, J.T., and Machida, R. J. 2013. A new versatile primer set targeting a short fragment of the mitochondrial COI region for metabarcoding metazoan diversity: application for characterizing coral reef fish gut contents. Frontiers in Zoology, 10(1), 34.

Marine Resources Council. 2018. Indian River Lagoon Health Update.

Martin, J.B., Cable, J.E., Smith, C., Roy, M., and Cherrier, J. 2007. Magnitudes of submarine groundwater discharge from marine and terrestrial sources: Indian River Lagoon, Florida. Water Resources Research 43:1-15.

Mason, W.T., Jr. 1998. Macrobenthic monitoring in the lower St. Johns River, Florida. Environmental Monitoring and Assessment 50:101-130.

Morris, L.J., Hall, L.M., and Virnstein, R.W. 2001. Field guide for fixed seagrass transect monitoring in the Indian River Lagoon. St. Johns River Water Management District, Palatka, Florida.

Oksanen, J., Blanchet, F.G., Friendly, M., Kindt, R., Legendre, P., McGlinn, D., Minchin, P.R., O'Hara, R.B., Simpson, G.L., Solymos, P., Steven, M.H.H., Szoecs, E., and Wagnerr, H. 2019. Vegan: Community Ecology Package. https://CRAN.R-project.org/package=vegan.

Pandit, A., Heck, H.H., Berber, A., Al-Taliby, W., and Mamoua, K. 2017. Sediment Survey and Fluxes of Nutrients from Sediments and Groundwater in the Northern Indian River Lagoon, Florida (Part III). Annual report submitted to SJRWMD for Contract # 27815.

Pxfuel. 2020. Landscape, Building, Concrete, River, Weir, the Floodgates, Water, Blue, Squares, Architecture. www.pxfuel.com/en/free-photo-xsrpx.

R Core, T. 2012. R: A language and environment for statistical computing. R Foundation for Statistical Computing, Vienna, Austria.

Richards, W.J. 2005. Early Stages of Atlantic Fishes: An Identification Guide for the Western Central North Atlantic. Boca Raton, FL: CRC Taylor & Francis.

Rubec, P.J., Santi, C., Ghile, Y., and Chen, Z. 2018. Modeling to Assess Spatial Distributions and Population Numbers of Estuarine Species for Baseline and Minimum Flows in Lower Peace River Shell Creek and Charlotte Harbor, Florida. https://doi.org/10.13140/RG.2.2.29417.39524.

Saberi, A. and Weaver, R. 2016. Simulating Tidal Flushing Response to the Construction of a Low-Crested Weir Connecting Port Canaveral to the Banana River, Florida. Journal of Waterway, Port, Coastal, and Ocean Engineering 10.1061/(ASCE)WW.1943-5460.0000337, 05016002.

Santos, R.O., Rehage, J.S., Boucek, R., and Osborne, J. 2016. Shift in recreational fishing catches as a function of an extreme cold event. Ecosphere 7:1–16.

Shenker, J.M, Crabtree, R., Cowie, E., Patterson, H., Stevens, C., and Yakubik, K. 2002. Recruitment of tarpon (*Megalops atlanticus*) leptocephali into the Indian River Lagoon, Florida. Contributions in Marine Science 35:55-69.

Sigua, G.C., Steward, J.S., and Tweedale, W.A. 2000. Water-Quality Monitoring and Biological Integrity Assessment in the Indian River Lagoon, Florida: Status, Trends, and Loadings (1988-1994). Environmental Management 25:199-209.

Smith, D.G. 1989. Fishes of the Western North Atlantic. Part 9. Leptocephali. Sears Foundation for Marine Research.

Smith, N. P. 1990. Computer simulation of tide-induced residual transport in a coastal lagoon. Journal of Geophysical Research, vol. 95, no. 10, 1990, pp. 18205-18211.

Sweat, L.H., Swain, G., Hunsucker, K., and Johnson, K.B. 2017. Transported biofilms and their influence on subsequent macrofouling colonization. Biofouling 33(5):433-449.

Tetra Tech. 2007. The Environmental Fluid Dynamics Code Theory and Computation Volume 1: Hydrodynamics and Mass Transport. 61p.

Tetra Tech, Inc. and Closewaters LLC. 2020. Save Our Indian River Lagoon Project Plan 2020 Update for Brevard County, Florida.

Virnstein, R.W. and Morris, L.J. 1996. Seagrass preservation and restoration: A diagnostic plan for the Indian River Lagoon. SJRWMD, Technical Memorandum No. 14, Palatka, Florida.

Weaver, R.J., Johnson, J.E., and Ridler, M. 2016a. Wind-driven circulation in a shallow microtidal estuary: the Indian River Lagoon. Journal of Coastal Research. 322, 1333–1343. https://doi.org/10.2112/JCOASTRES-D-15-00046.1.

Weaver, R.J., Taeb, P., Lazarus, S., Splitt, M., Holman, B.P., and Colvin, J. 2016b. Sensitivity of modeled estuarine circulation to spatial and temporal resolution of input meteorological forcing of a cold frontal passage. Estuarine, Coastal and Shelf Science 183, 28–40. https://doi.org/10.1016/j.ecss.2016.10.014.

Welschmeyer, N.A. 1994. Fluorometric analysis of chlorophyll a in the presence of chlorophyll b and phaeopigments. Limnology and Oceanography 39:1985-1992.

Wheeler, E.P. and Shenker, J.M. 2000. Age and developmental stage at recruitment of ladyfish, Elops saurus. M.S. Thesis, Florida Institute of Technology, Melbourne. 42 p.

Ye, J., Coulouris, G., Zaretskaya, I., Cutcutache, I., Rozen, S., and Madden, T. 2012. Primer-BLAST: A tool to design target-specific primers for polymerase chain reaction. BMC Bioinformatics. 13:134.

Zarillo, G.A. 2015. Indian River Lagoon Numerical Model Flushing Experiments. SJRWMD, Final Report, Palatka, Florida.

Zugelter, A. 2019. Nursery Habitat Characteristics of Juvenile Tarpon, Megalops atlanticus, in the northern Indian River Lagoon, FL. M.S. Thesis, Florida Institute of Technology.

Appendix A Task 1 – Modeling and Engineering Report

Restore Lagoon Inflow Research (Phase 1)
Task 1 - Modeling and Engineering

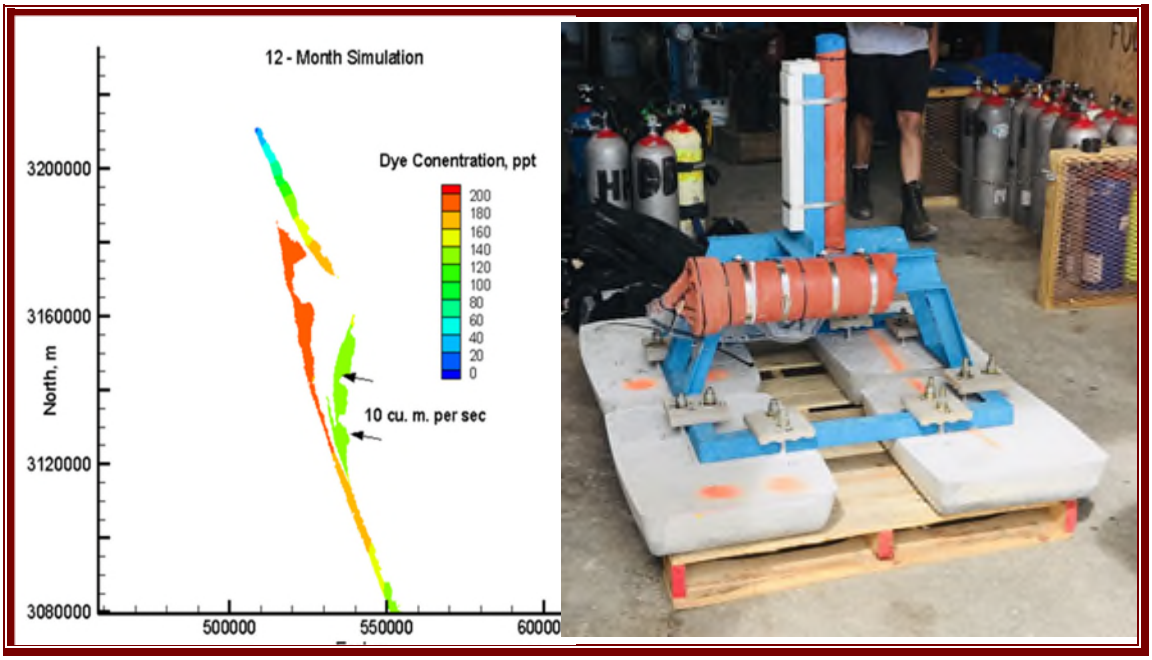

PREPARED FOR

Florida Department of Education
325 W Gaines Street
Tallahassee, FL 32399

PREPARED BY

Robert J. Weaver , Gary A. Zarillo
Florida Institute of Technology
150 West University Boulevard
Melbourne, FL 32901

September 2020

Table of Contents

List of Tables

List of Figures

Acknowledgements

We would like to thank our representatives in the Legislature and the public for overwhelming support of lagoon science. We thank Robert Salonen and Frank Kinney for their efforts that made this research at Florida Tech possible. We would also like to thank John Windsor for his tireless leadership and guidance, and the other Principle Investigators on this project for their collaboration and support. Additionally, the Undergraduate and Graduate students who worked tirelessly to perform the duties that enabled this project to finish on time: Marc Di Ciccio who helped with the deployment and servicing of the Acoustical Doppler Current Profilers (ADCPs), Nicole McClain who worked on the engineering design, Caleb Lodge who performed the Advanced Circulation (ADCIRC) modeling and assisted in the field, Samuel Boyd who helped with the modeling and in the field, and Richard Caserta who assisted with the deployment of the ADCPs. We would also like to thank the anonymous external reviewers for applying their expertise to reviewing this work.

Photographs on cover: Flushing results based on hypothetical pumping stations placed in Port Canaveral and South Patrick Shores, with model results shown at 125 days into the simulation (left). Example of a fully assembled ADCP deployment mooring (right).

List of Acronyms

2DDI	Two-dimensional Depth Integrated
ADCIRC	Advanced Circulation
ADCP	Acoustic Doppler Current Profiler
BMAP	Basin Management Action Plan
BRL	Banana River Lagoon
CBR	Central Banana River
cm	Centimeter
EFDC	Environmental Fluid Dynamics Code
FDEP	Florida Department of Environmental Protection
ft^3/s	Cubic Feet Per Second
GIS	Geographic Information System
HDD	Horizontal Directional Drilling
HEM3D	Three-Dimensional Hydrodynamic-Eutrophication Model
HYCOM	Hybrid Coordinate Model
IRL	Indian River Lagoon
Km	Kilometers
kN	Kilonewtons
LOBO	Land/Ocean Biogeochemical Observatory
m	Meter
m^3/s	Cubic Meters Per Second
NAM	North American Mesoscale
NASA	National Aeronautics and Space Administration
NAVD88	North American Vertical Datum of 1988
NBR	North Banana River
NLCD	National Land Cover Dataset
NOAA	National Oceanic and Atmospheric Administration
NODBC	National Ocean Data Buoy Center
ORCA	Ocean Research and Conservation Association
PAFB	Patrick Air Force Base

ppt	Parts Per Thousand
PSU	Practical Salinity Units
RMSE	Root Mean Square Error
RPM	Rotations Per Minute
SAS	South Alternate Site
SJRWMD	St. Johns River Water Management District
SWAN	Simulating Waves Nearshore
USGS	United States Geological Survey
WGS84	World Geodetic System 1984

Executive Summary

Task 1 of the Restore Lagoon Inflow Research Phase I – Modeling and Engineering is focused on determining the change in flow, salinity, and temperature that would be caused by bringing in ocean water into the Indian River Lagoon (IRL) and exploring the various structures and means of transporting ocean water into the IRL. The goal of Task 1 is to evaluate IRL inflow scenarios designed to create water exchanges with the coastal ocean that were historically produced by episodic over washing and breaching of the barrier island by storms as evidenced by the numerous relict tidal inlet shoals and expansive washover sediment fans.

Objectives of Task 1 are:

1) Selection of three locations (two in Banana River and one in Indian River County) where exchanges of coastal ocean water into the IRL system can be optimized with respect to practicality, effective water control structures, and eventual permitting;
2) Setup up a system of nested hydrodynamic and transport models that can be operated by accurately exchanging model boundary conditions from the coastal ocean into the IRL estuarine system;
3) Calibrate the modeling system with respect to historical process data;
4) Test the potential for improved circulation and flushing of based on controlled ocean inflows to IRL at three selected locations (two in Banana River and one in Indian River County); and
5) Produce a 20% percent design for water control structures at two locations that can produce the modeled inflows.

Although locations have been selected for the modeling and inflow structure design, model performance and structure design can be extrapolated to alternate locations should one be found to be more desirable. This study focuses on two locations in the Banana River, Port Canaveral between Canaveral Locks and the 401 Bridge, and the north end of Patrick Air Force Base, and one location in Indian River County, Bethel Creek.

The modeling of salinity and temperature provides a guide for what can be expected with an inflow system. In modeling the salinity, researchers must not only get the correct ocean boundary conditions, including tides and low frequency intra-annual water level fluctuations, but the freshwater inflows must also be included. Freshwater enters the IRL from natural rivers and streams, man-made drainage canals and surface water conduits, rainfall, and groundwater. Unlike previous studies, we include an estimate for groundwater inflow in our IRL modeling effort.

The Advanced Circulation (ADCIRC) model generated ocean water level boundary conditions and passed those on to the Environmental Fluid Dynamics Code (EFDC) circulation and transport model for prediction of numerical tracer transport and flushing times. Coastal Ocean water temperature and salinity values are assigned to EFDC ocean model boundaries from hindcasts of Hybrid Coordinate Model (HYCOM).

The IRL is modeled in its current configuration, and in a configuration that includes structures that will bring ocean water into the lagoon. The result is a series of numerical model experiments of controlled water exchanges between the IRL and the coastal ocean that simulate engineered pumping stations and weir-type water control structures. Our focus is on establishing the expected changes in flow, salinity, temperature and water elevations in the Banana River, which is known to have slow flushing rates and be a hotspot for harmful algal bloom inception. Numerical model studies compute water level, flow, salinity, and temperature for unmodified and modified

engineered conditions. Numerical modeling data are compared to available *in-situ* data for model validation.

Model output of salinity and temperature changes are provided to the Principle Investigators working on Task 2 and 3. The model data will provide critical information as those teams evaluate the potential impacts on Biology and Geochemistry.

The numerical modeling results support the concept of using ocean inflow to circulate the water in the IRL, moving stagnant lagoon water and replacing with ocean water. Model predictions simulating the dispersal of water tagged by a numerical tracer indicate reductions of tracer concentration of 60% to 85% in the Banana River as a result of enhanced inflows over a 365-day model period. The inflow will create a very slow current that will circulate the water toward the inlets and facilitate enhanced exchange and mixing into the larger IRL system. Localized changes in salinity of 5% for the pipe and pump inflow structures and up to 10% for the weir structure are predicted near the outfalls, along with minimal changes in water temperature.

The modeling effort is supported by the *in-situ* measurements of hydrodynamic properties of the basin at selected locations in the IRL and Banana River. Limited data are already available for model validation. We proposed to install new instrumentation that will measure current, water elevation, temperature, and salinity at three sites in the Banana River. Based on existing modeling studies, instruments were deployed near the mouth of the barge canal, entrance to Sykes Creek, and near Dragon Point just south of Mather's bridge.

Engineering designs of controlled flow structures (weir, directionally drilled pipeline, etc.) are developed for the site(s) deemed most appropriate for establishing exchanges with the coastal ocean.

Of the semi-permanent designs explored, the weir is most cost-effective approach that provides the greatest flexibility for flow at the lowest cost but is the most restrictive with regards to location. A 150 meter (m) weir will meet the potential permanent full-scale system flow criteria of a minimum of 20 cubic meters per second (m^3/s) on an annual average basis, and a 50 m structure will meet the temporary pilot scale flow criteria of a minimum of 5 m^3/s on an average annual basis. A smaller weir structure will meet the flow criteria during certain portions of the year. The pipe and pump structure is the most flexible with respect to location, but the most restrictive approach in cost as well as flow rates.

A temporary inflow pilot system with an overland pipe and submerged pump is investigated. The largest single cost is the pump. A section of the Northern Banana River north of the Locks at Port Canaveral can receive a modest 5 m^3/s inflow of ocean water for a pilot scale study of the impacts of ocean water on the IRL.

The design study supports either an overland temporary pipe and pump structure, or a weir structure for delivering the temporary pilot scale flow of 5 m^3/s be installed in the Northern Banana River.

A final temporary pilot inflow system, and potential permanent full-scale system, may be modified from the design and volume options included here based on further scientific, regulatory agency, and logistical requirements.

1 Introduction

The Indian River Lagoon (IRL) is a shallow (less than 5 meters [m]) bar-built, lagoon type estuary that extends approximately 250 kilometers (km) along the central east coast of subtropical Florida and ranges in width from less than 1 to approximately 9 km (Smith 1990), Figure 1-1). The IRL is connected to the ocean by six inlets: Ponce de Leon Inlet in the north, Port Canaveral Inlet in the center east of Banana River, Sebastian Inlet in the middle, Fort Pierce Inlet, St. Lucie Inlet, and Jupiter Inlet in the south. All the inlets are directly connected to the ocean except for the Port Canaveral Inlet, which is separated from the lagoon by a lock system. Saltwater influx to the IRL comes from five widely spaced inlets, which classifies the IRL as a restricted lagoon (Kjerfve 1986, Smith 1990). A distance of approximately 145 km separates the two northernmost inlets, Ponce and Sebastian. With shallow water depths and narrow connections between the sub-basins in the northern IRL, there is little tidal exchange (Saberi and Weaver 2016, Zarillo 2015). The Banana River is a poorly flushed subsystem of the IRL, Figure 1-1(b). The Banana River, with no direct connection to the ocean has some of the longest residence times. According to the Florida Department of Environmental Protection (FDEP), it takes approximately 2 years for the water to flush in the Banana River (FDEP 2013).

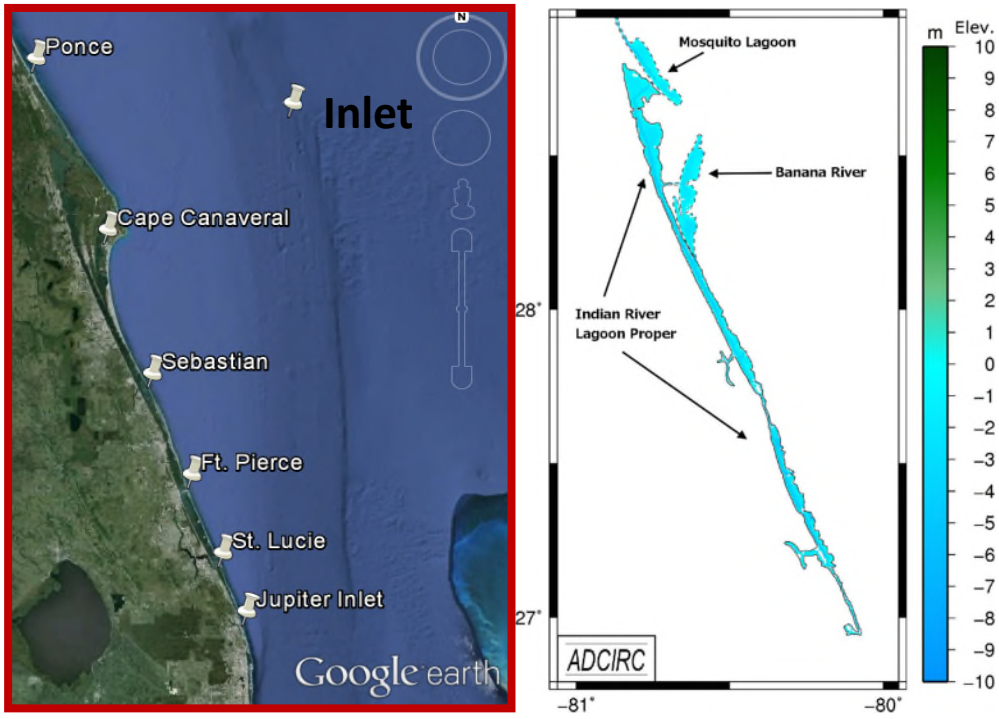

a) b)

Figure 1-1: Indian River Lagoon on Florida's east coast. a) Location of the 5 inlets, and Port Canaveral. b) Identification of the 3 sub-basins that make up the northern IRL between Ponce Inlet and Sebastian Inlet.

The Banana River is a sub-basin of the IRL that lies between Cape Canaveral and Merritt Island and extends from the National Aeronautics and Space Administration (NASA) Kennedy Space Center to Dragon Point. The Banana River is connected to the IRL proper by two narrow channels, the Barge Canal and Dragon Point. The Banana River is the only part of the IRL that does not have a direct connection to the ocean, except for a small amount of water exchange via lock system at Port Canaveral (Lasater 1970). The Banana River can be divided into a northern section

and a southern section. The northern section is the area north of Port Canaveral Locks and the Barge Canal, and the southern section extends below the locks to Dragon Point. The northern section of the Banana River was historically connected to the IRL by a series of natural channels. The main connection, Banana Creek, was closed when NASA built the crawler roadway connecting the Vehicle Assembly Building to Launch Complex 39. Prior to the development of the barrier island, each sub-basin of the IRL was subjected to episodic over washing and breaching of the barrier island by storms as evidenced by the numerous relict tidal inlet shoals and expansive washover sediment fans. This historic inflow would bring ocean water into regions of the IRL and enhance the circulation in the estuary.

In the past decade, water quality in the IRL has declined with more severe and more frequent harmful algal blooms (Marine Resource Council 2018; Tetra Tech 2020). This study is carried out to evaluate the possible impacts of restoring lagoon inflow and enhancing circulation at three primary locations: (1) the North Banana River (NBR) (centered near 28.4071, -80.6412), (2) the Central Banana River (CBR) (centered near 28.2722, -80.6104) and (3) near Bethel Creek, South Alternate Site (SAS) (Centered near 27.6656, -80.3702), Figure 1-2.

Figure 1-2: Map of the study area showing the three proposed pumping locations (from north to south: NBR, CBR and SAR). Red circles show a 1 km radius around the proposed pumping location.

With targeted numerical modeling, this study evaluates the effect of different inflow scenario on the physical parameters of the IRL. Using a global circulation model to provide boundary conditions an environmental fluids model will be used to predict the changes in water level, flow, salinity, and temperature that can be expected for each of the tested scenario. The model results are supported by *in-situ* measurements taken the locations in the Banana River where the water exchanges with the IRL proper at Dragon Point and the Barge Canal. Measured data will be used to calibrate and validate the model performance. The model predictions are shared with project partners working on Tasks 2 and 3, the Biology and Geochemical, respectively.

Finally, designs are developed for flow structures that could be used for a temporary inflow pilot system, creating inflow from the ocean to the lagoon. Though the site selections of the structures in this study represent the locations where structures may be most effective and feasible, no final determination of siting has been made.

2 Instrument Data Acquisition

One of the deliverables for Task 1 is data retrieval from the deployed Acoustic Doppler Current Profilers (ADCPs). The data are used to validate the Advanced Circulation (ADCIRC) and Environmental Fluid Dynamics Code (EFDC) numerical models. During the end of Quarter 2 and beginning of Quarter 3 instrumentation was deployed in the IRL. During Quarter 3, six trips were made to offload the data from the ADCPs. More than two months of data have been offloaded from the instruments. The instrument in Sykes Creek was pulled from the water for a memory upgrade and returned to field once field operations were resumed, following the statewide stay-at-home order. A Florida Tech built pontoon boat with lift capabilities was successfully used for deployment and retrieval of the instruments.

2.1 ADCPs

Three ADCPs have been deployed strategically in the Banana River. These three are located to capture the flow at each of the entry points to the Banana River (Figure 2-1, Table 2-1). The figure on the cover is an example of a quadripod mooring assembly.

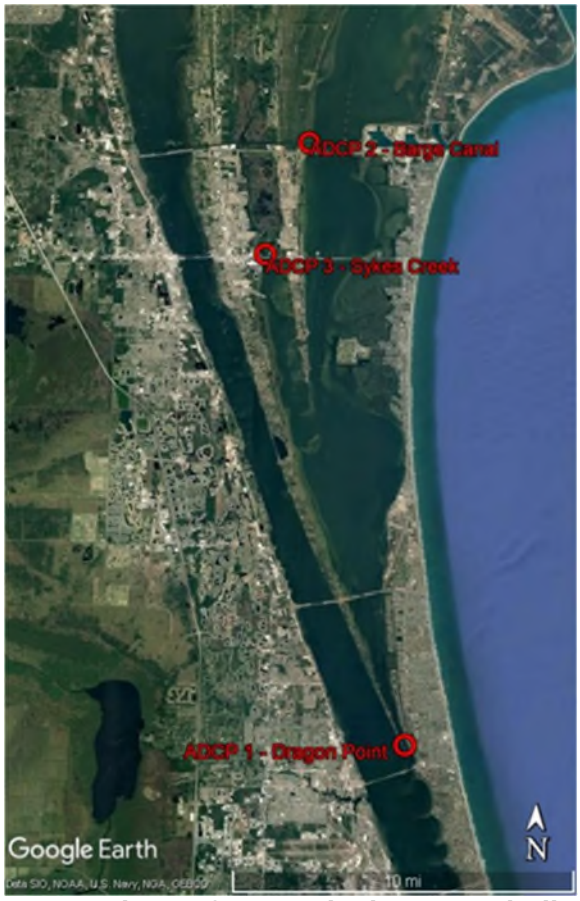

Figure 2-1: Locations of ADCP deployments indicated red.

Table 2-1: ADCP deployment

ADCP Manufacturer	Deployment Location
Sontek	Dragon Point (SBR)
Sontek	Entrance to Barge Canal (NBR)
Nortek	Sykes Creek (SAS)

2.1.1 *Data Acquisition*

The instruments record pressure and current velocity measurements, allowing for circulation model validation. In addition, each ADCP is waves capable, and collecting burst wave data. These wave data are used to validate the wave model that is run coupled to the circulation model.

As data were offloaded from the instruments, they were stored on a local computer for analysis. The data were compiled to produce a continuous time series from each station. The two ADCPs in Banana River at the entrance to the Barge Canal (NBR) (Figure 2-2), and Dragon Point (SBR) (Figure 2-3), have been in the water continuously since initial deployment. The ADCP in Sykes Creek (SAS) (Figure 2-4) was removed in late March for an upgrade and due to Covid-19 restrictions, was delayed in getting back into the water.

Future work will continue to collect and offload data from the ADCPs. Longer data sets allow for a more rigorous validation of the numerical models.

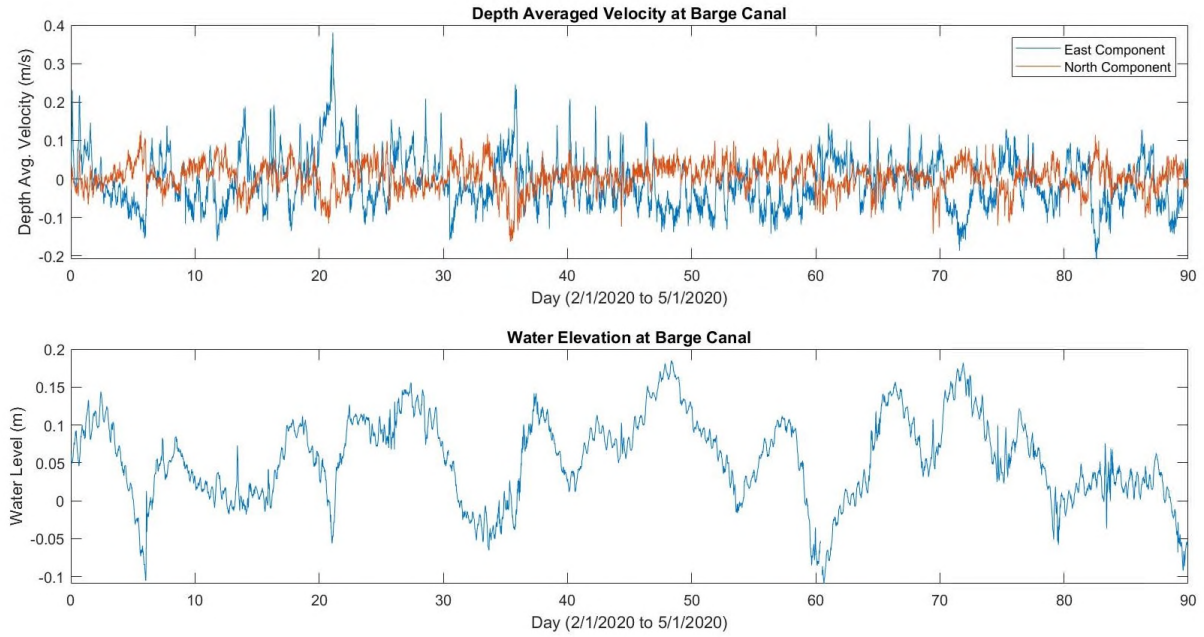

Figure 2-2: Barge Canal ADCP current (upper plot) and water level (lower plot) data for the date range February 1, 2020–May 1, 2020.

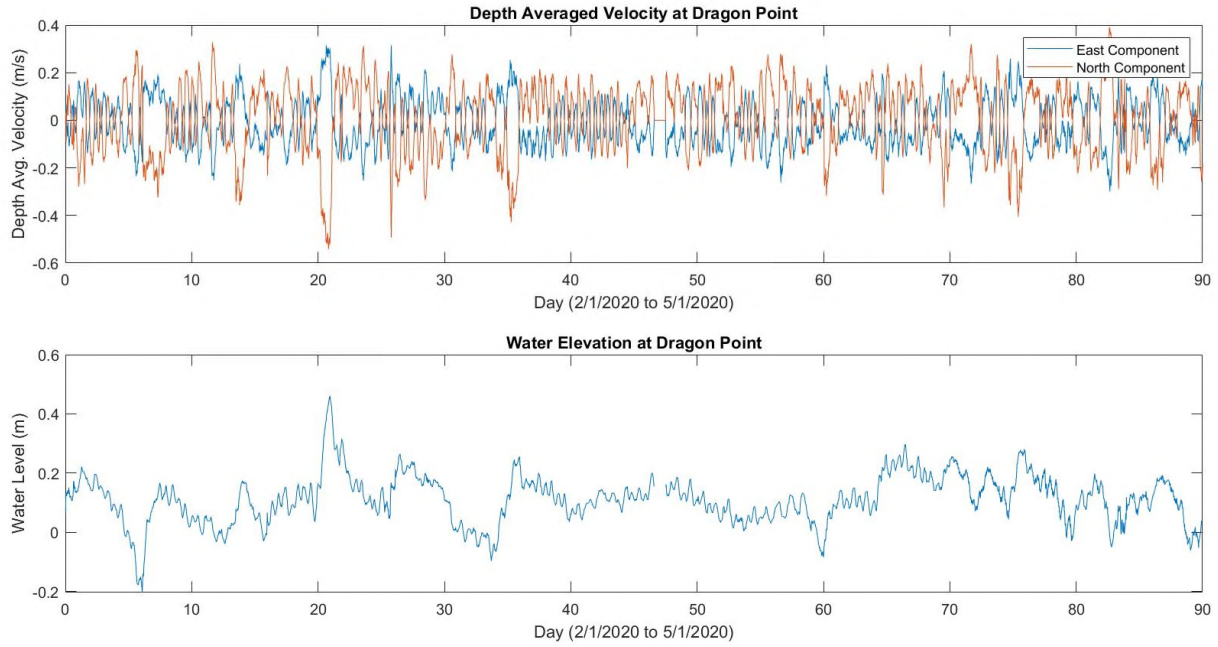

Figure 2-3: Dragon Point ADCP current (upper plot) and water level (lower plot) data for the date range February 1, 2020May 1, 2020.

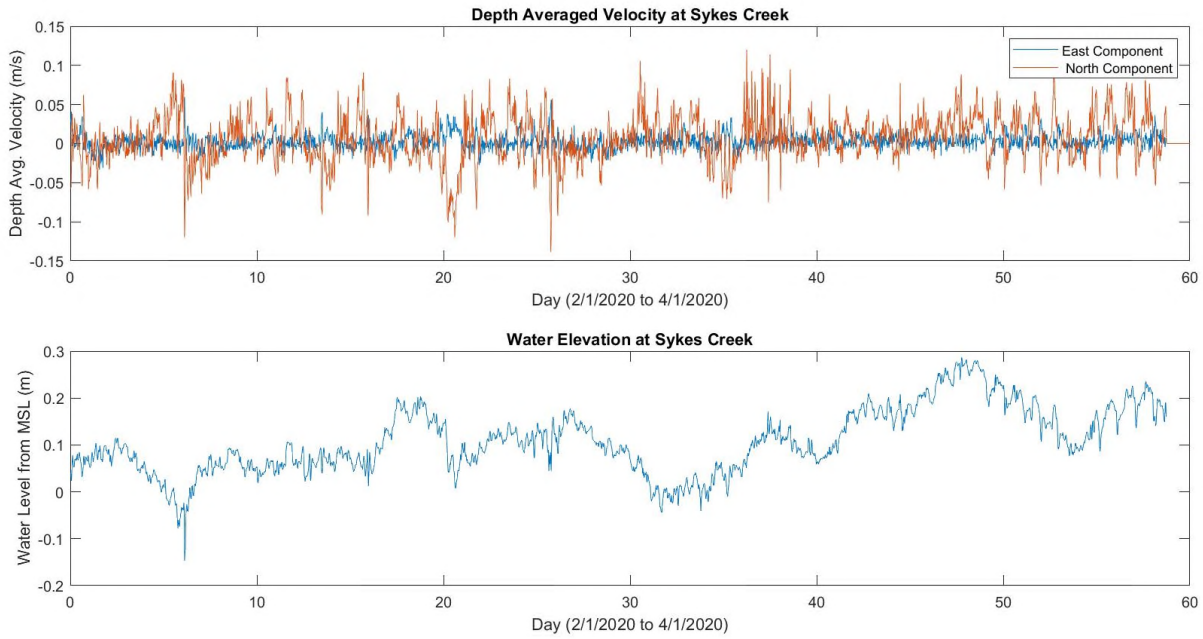

Figure 2-4: Sykes Creek ADCP current (upper plot) and water level (lower plot) data for the date range February 1, 2020–April 1, 2020.

3 ADCIRC Hydrodynamic Modeling

The application numerical modeling scheme being applied for flushing and transport (salt and heat) experiments is being modified to accept forcing conditions from the open coastal ocean. This modification includes extending the model grid structure though Ponce Inlet, Sebastian Inlet, and Fort Pierce Inlet into the coastal ocean. Here, water level, salinity, and water temperature time series will be applied from output from the ADCIRC and HYCOM basin scale models as described in the project proposal.

The ADCIRC (Luettich et al. 1992, Westerink et al. 1991, Luettich and Westerink 2004, 2006) utilizes the finite element method which provides the flexibility to resolve complex bathymetry and configuration of bayous and shallow bays along the Louisiana coast. The governing equations in ADCIRC consist of the continuity and momentum equations as follows:

$$\frac{\partial \delta}{\partial t} + \frac{\partial (UH)}{\partial x} + \frac{\partial (HV)}{\partial y} = 0 \qquad (1)$$

$$\frac{\partial U}{\partial t} + U\frac{\partial U}{\partial x} + V\frac{\partial U}{\partial y} - fV = -\frac{\partial}{\partial x}\left[\frac{P_s}{\rho_0} + g\delta\right] + \frac{\tau_{sx}}{\rho_0 H} - \frac{\tau_{bx}}{\rho_0 H} + M_x \qquad (2)$$

$$\frac{\partial V}{\partial t} + U\frac{\partial V}{\partial x} + V\frac{\partial V}{\partial y} + fU = -\frac{\partial}{\partial y}\left[\frac{P_s}{\rho_0} + g\delta\right] + \frac{\tau_{sy}}{\rho_0 H} - \frac{\tau_{by}}{\rho_0 H} + M_y \qquad (3)$$

Where t represents time; (x,y) are the Cartesian coordinates; (U,V) are the depth-averaged velocity components in the x and y directions; H is the total water depth; δ is the free surface elevation; f is the Coriolis parameter; g is the acceleration of gravity; p_s is the atmospheric pressure at the surface; ρ_0 is the reference density of water; (τ_{sx}, τ_{sy}) are the sea surface stresses; (τ_{bx}, τ_{by}) are the bottom shear stresses; and (M_x, M_y) are the horizontal momentum diffusion components.

These equations are differentiated and combined to get the Generalized Wave Continuity Equations (Luettich et al. 1992).

The input to the model includes the bathymetry and topography on an unstructured grid referenced to a common datum, spatial distribution of wind velocity and atmospheric pressure, bottom drag coefficients, as well as boundary conditions (tide and river discharges). The system computes sea surface elevations and currents.

ADCIRC can be dynamically coupled with the Simulating Waves Nearshore (SWAN) wave model (Booij et al. 1999; http://swanmodel.sourceforge.net/references/references.htm). In ADCIRC+SWAN, the ADCIRC model passes water level, current velocities, wind velocities, and friction roughness lengths to the SWAN model. SWAN then computes wave spectra. Wave characteristics are passed back to ADCIRC where the radiation stress gradients are evaluated at each vertex and used to compute the water level and current velocity at the next time step (Dietrich et al. 2011, 2012). Passing data back-and-forth in this manner represents true two-way coupling, producing results that take into account the relevant coastal physics and the changing water levels. ADCIRC is typically applied in a barotropic two-dimensional depth integrated (2DDI) mode.

3.1 Model Set-up

For this study we use a spatially varying depth dependent bottom friction coefficient (in water) based on a Manning's *n* type formula, with *n* = 0.02 while the surface roughness for flow over inundated land is determined from the National Land Cover Dataset (NLCD) (Arcement and Schneider, 1989; Fry et al., 2011; Luettich and Westerink, 2004). A minimum value for the drag coefficient is set, $C_{D_{min}} = 2.0 * 10^{-3}$. The ADCIRC+SWAN model configuration is the same for all simulations. The model domain is a 167,652 node unstructured mesh, with grid resolution varying from a minimum on the order of 25 m in the inlets, canals, and channels of the IRL, to over 10 km in the Atlantic Ocean (Figure 3-1). For each of the simulations, the fields are interpolated from the input meteorological grid to each node in the ADCIRC model domain without any adjustments. The focus of the analysis presented here is the central IRL, shown in the inset to Figure 3-1. The topography for the domain is interpolated from a 5-foot horizontal resolution Digital Elevation Model created for Brevard County based on 2007 Light Detection and Ranging data. The bathymetric data is adjusted based on National Oceanic and Atmospheric Administration (NOAA) nautical charts to include a representation of the Intracoastal Waterway, a 3,000-mile long intermittent inland waterway along the east and Gulf coasts of the United States of America. Model topography is referenced to vertical datum, North American Vertical Datum of 1988 (NAVD88).

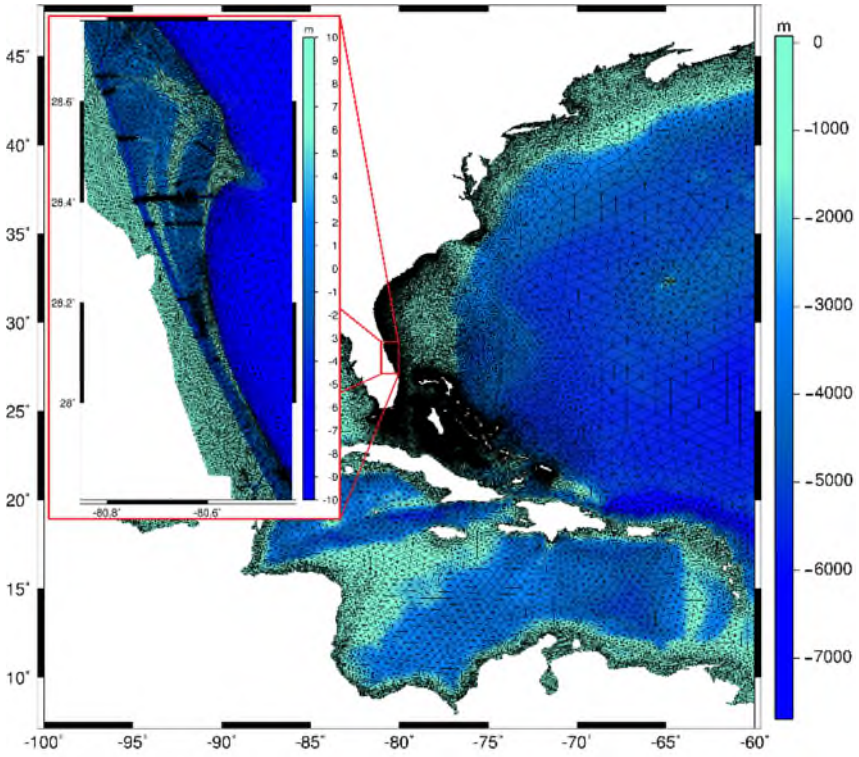

Figure 3-1: Computational domain for the ADCIRC model

3.2 Simulations

A hindcasted two-dimensional ADCIRC model has been prepared to generate an accurate and detailed depiction of water circulation in the IRL. For this project, the model is configured to provide simulated water elevation and flow velocity data at high-resolution throughout the IRL over the duration from January 1, 2016 through December 31, 2017. This two-year control model validates the method and verifies the parameters to be used in future simulations of the IRL under prospective flushing conditions.

Wind input is obtained from the NOAA North American Mesoscale (NAM) database. The NAM wind resolution is low, with grid spacing of 25-km. Pressure is in millibars, and the wind data are 10-minute averaged at a 10-m elevation. NOAA's NAM database contains files in grib format for all of 2016 and the first three months of 2017. Then, the files switch to grib2 format for the remainder of 2017. Due to the nature of the utility program, separate sets of input files had to be made for each format. As such, the full two-year control model was split into two parts: a 461-day run and a 270-day run. April 6, 2017 marks the switch from grib to grib2 NAM data and the beginning of the second part. The files are re-formatted from their original NAM wind and pressure data format into a suitable format for ADCIRC. The ADCIRC input files generated are a pressure field (fort.221), a wind velocity field (fort.222), and a wind control file (fort.22).

Governing variables and tidal potential constituents for the ADCIRC model were defined in the fort.15 control file. Most values, such as model type, continuity equation factors, and friction factors, were sourced from ADCIRC recommendations and previous IRL simulations. To ensure stability, a ramp function was included (10 days for part one and 5 days for part 2), advective terms were omitted, and the timestep was set to one second. Tidal potential constituents for the assigned time period were extracted using the tide_fac utility program.

3.3 Results

Final output files from the model include global water elevations (fort.63), global depth-averaged velocities (fort.64), water elevations and depth-averaged velocities at specified stations (fort.61/62), and meteorological output at specified stations (fort.71/72). Output was compared to data collected at NOAA Trident Pier station in Port Canaveral, and Sykes Creek ADCP station, both indicated in Figure 3-2.

3.3.1 *Water Level Validation*

Water elevations were processed in MATLAB. Stations were input into ADCIRC for specific water elevations, including NOAA buoys, pressure sensor locations, and coordinates inside relevant inlets (Sebastian, Ponce, and Fort Pierce). ADCIRC output the elevation at each of these stations every 30 minutes during the simulation.

One of the model recording stations corresponds with the location of NOAA's Trident Pier tidal station, which provides verified water levels used to compare to ADCIRC (Figure 3-3 and Figure 3-4). As demonstrated in the MATLAB plots above, the ADCIRC model was in phase with existing tides and produced a similar tidal amplitude. However, Trident Pier buoy data reveal the low frequency water levels that ADCIRC does not account for, which are attributed to seasonal variations in Gulf Stream flow rate. The low frequency displacement has a regular pattern, evident in offset between the verified station data and the model data in Figure 3-3. That low frequency intra-annual water level will be extracted from the Trident Pier data and applied to the ADCIRC output in post-processing. The total water levels, ADCIRC + low frequency signal from Trident Pier, are passed to EFDC as boundary conditions at the predefined boundary locations.

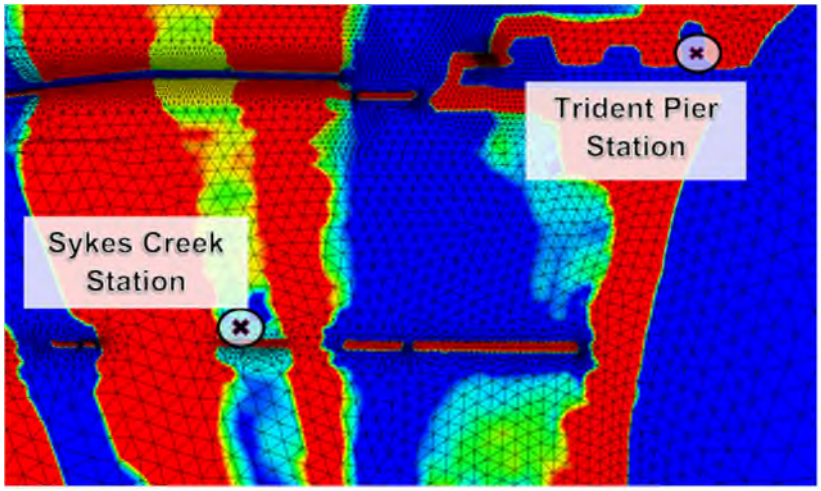

Figure 3-2: Data collection points on model grid

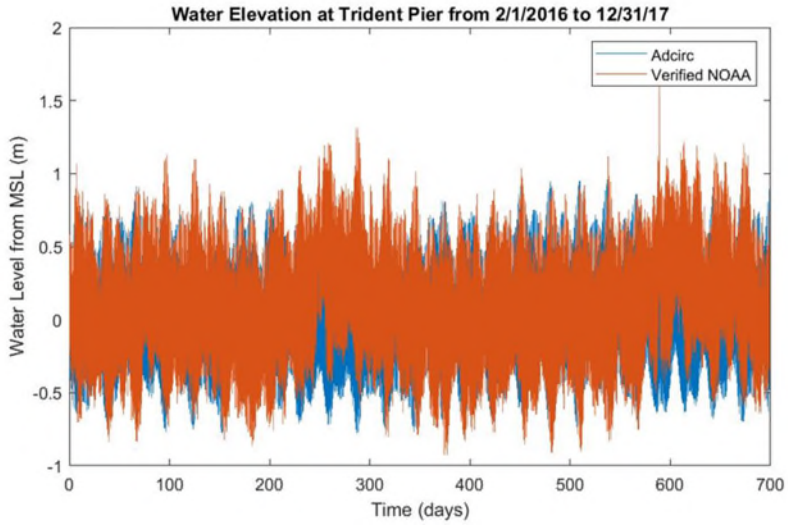

Figure 3-3: Plot comparing ADCIRC water elevations to NOAA data at Trident Pier

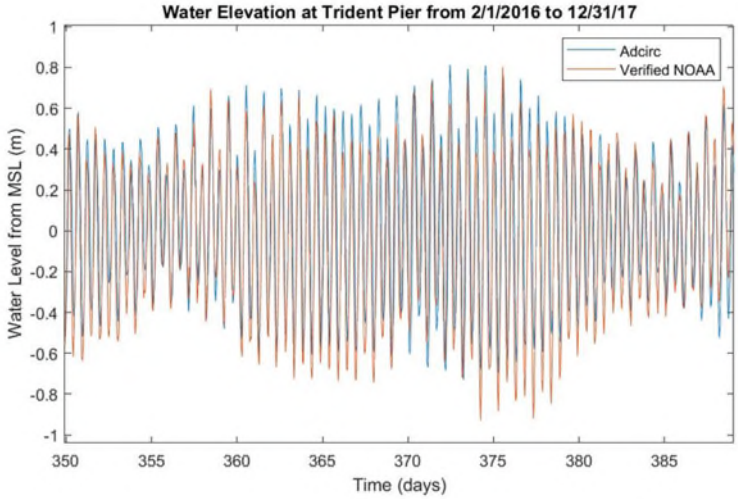

Figure 3-4: Magnification of Figure 3-3, where 350 days is equivalent to January 16, 2017

3.3.2 *Current Validation*

To validate depth-averaged velocity from the ADCIRC program, a separate model was set up to simulate conditions during the month of February 2020. Output was compared to data collected by a Nortek Aquadopp 2 MHz ADCP, deployed for that same duration in Sykes Creek. The raw data from the ADCP gave a velocity profile split into seven bins for the approximate 1.5 m column of water above it. MATLAB was used to calculate X and Y components of the depth-averaged velocity (+X being East and +Y being North), then plot the Y component against ADCIRC data for the closest node. As the creek spans north to south, the X component of depth-averaged velocity was negligible.

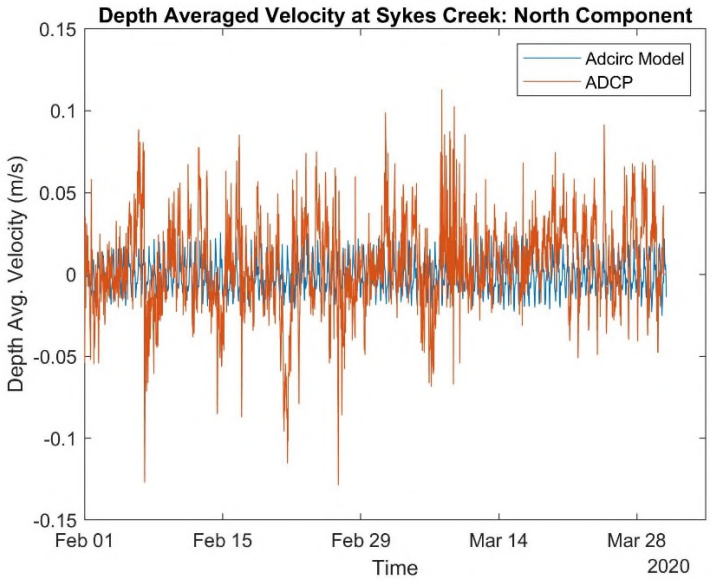

Figure 3-5: Plot comparing north-south component of depth-averaged velocities at Sykes Creek with ADCIRC model forcing from NAM winds and pressures.

Velocities are not expected to exactly coincide; as the ADCIRC model is run in two-dimensional mode and therefore computes the average velocity over the full water column while the ADCP only detects velocities in the upper 1 m of flow, where velocities are the highest, and does not capture the bottom flow that may be in the opposite direction. For the first ADCIRC simulation, the winds and pressures were downloaded from the NOAA NAM site and are forecast products (Figure 3-5). The ADCIRC model underpredicts the measured data, and misses the peaks and troughs measured by the ADCP. One reason for the poor agreement is that the NAM modeled wind products do not match the measured winds and pressures. True current velocity may also be influenced by variables such as boat traffic and wave orbital velocities. If outliers in the ADCP data are excluded, the trends in the signal begin to resemble ADCIRC model velocities. Future validation may include a targeted three-dimensional simulation in ADCIRC to compare to the ADCP data.

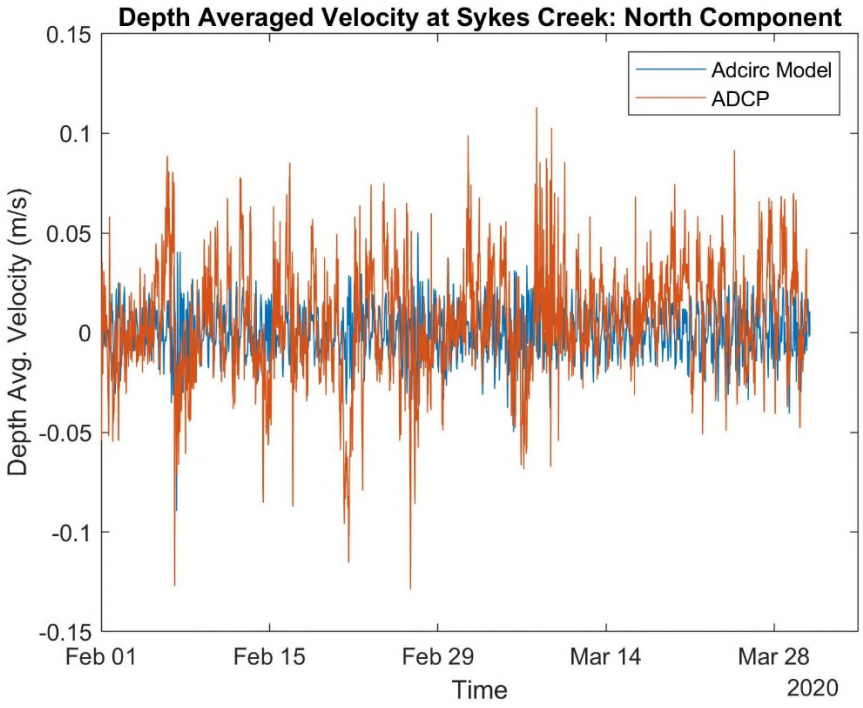

Figure 3-6: Plot comparing north-south component of depth-averaged velocities at Sykes Creek with ADCIRC model forcing from measured data at Trident Pier.

A second simulation was performed forcing the ADCIRC model with the measured wind and pressures from the Trident Pier station (Figure 3-6). For this simulation, ADCIRC picks up more of the peak events, and the model has a better match to the measured data. The measured data provided a valuable tool for understanding model behavior and validating circulation models in this restricted basin. Future work will continue to calibrate the ADCIRC model to the measured ADCP data, specifically looking at friction in the channels.

4 Enhanced Inflow Numerical Modeling

4.1 Model Overview

The model applied to meet the project objectives is the United States Environmental Protection Agency supported EFDC model (Tetra Tech 2007). The model includes features and capabilities that make it applicable to shallow estuarine environments. The project areas extend from the Mosquito Lagoon into the IRL compartments extending to Fort Pierce Inlet. EFDC/Three-Dimensional Hydrodynamic-Eutrophication Model (HEM3D) was developed and refined at the Virginia Institute of Marine Science over the time period of 1988–1995 (Hamrick 1992). This multi-parameter finite difference model represents estuarine flow and material transport in three dimensions and has been extensively applied to shallow estuarine environments in Florida and other coastal states. A few examples include the central IRL (Zarillo and Surak 1994, Zarillo and Yuk 1996), Lake Jesup, Florida (Zarillo 2001), Loxahatchee River Estuary in south Florida (Zarillo 2004), Lake Worth Lagoon, Florida (Zarillo 2003).

EFDC's hydrodynamic scheme solves the three-dimensional, vertically hydrostatic, free-surface, turbulent-averaged primitive equations of motion for a variable density fluid (Tetra Tech 2007). Also solved are the dynamically coupled transport equations for turbulent kinetic energy, turbulent length scale, salinity, and temperature. Figure 4-1 shows a flow diagram of the various components of the EFDC model. The Mellor-Yamada level 2.5 turbulence closure scheme as modified by Galperin and others (1988) is implemented for the two turbulence parameter equations used in the model. The time integration of the momentum and continuity equations uses a second-order, semi-implicit, three-time-level, leap frog-trapezoidal method, with an insertion of a two-time level trapezoidal step to suppress the mode generated by the three-level scheme. The barotropic and baroclinic modes are split with a method that is implicit in the horizontal for the barotropic, and in the vertical for the baroclinic. Thus, the solution is a finite difference scheme with an internal-external mode splitting procedure to separate the internal shear or baroclinic mode from the external free surface gravity wave or barotropic mode. The external mode solution is semi-implicit, and simultaneously computes the two-dimensional surface elevation field by a preconditioned conjugate gradient procedure. The external solution is completed by the calculation of the depth averaged barotropic velocities using the new surface elevation field. Advection is handled with an upwind difference technique described in Hamrick (Hamrick 1992 and 1994). The EFDC model can be used to drive a number of external water quality models using internal linkage processing procedures described by Tetra Tech (2007).

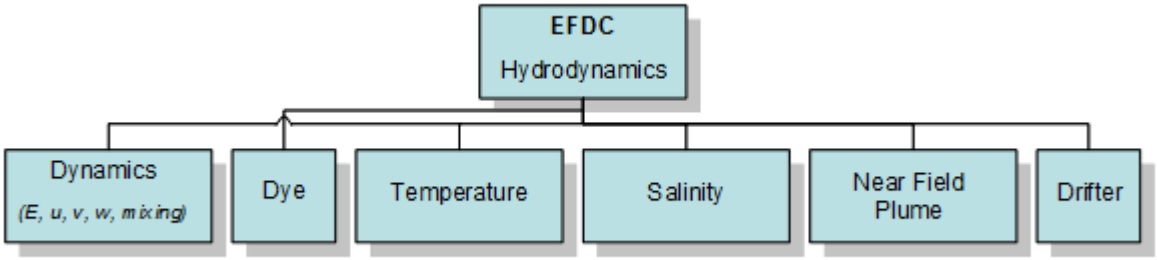

Figure 4-1: Flow diagram for the EFDC hydrodynamic and transport model

The application numerical modeling scheme being applied for flushing and transport (salt and heat) experiments was modified to accept forcing conditions from the open coastal ocean. This modification included extending the model grid structure though Ponce Inlet, Sebastian Inlet, and

Fort Pierce Inlet into the coastal ocean. Here, water level, salinity, and water temperature time series will be applied from output from the ADCIRC and HYCOM basin scale models as described in the project proposal.

4.2 EFDC Model Set-up

Application of the EFDC model to inflow studies in the IRL leverages the modeling platform built to assess the benefits of muck dredging in the IRL (Zarillo and Listopad 2020). Under this project, the model grid was initially developed along with external and internal model boundary conditions. These were updated and modified for the present inflow evaluation project. The following subsections of this report provide an overview of the model development and update to the inflow project.

4.2.1 *Model Computational Grid*

Figure 4-2 shows the overall extent of the IRL model grid that extends from Ponce Inlet on the north to just south the Fort Pierce Inlet at the south end. The model grid includes 10,094 active computational cells in the horizontal and 5 layers in the vertical dimension.

The model grid was designed as a layer in the ArcGIS software platform. A recent set of aerial images was used as a background over which a data layer was hand drawn to fit the model grid to shoreline boundaries and other morphologic features of the IRL system. Care was taken to include extensive marsh and mangrove areas as well as include the details of the numerous causeway-bridge combinations within the IRL system. The EFDC model software platform includes grid generating software. Once a boundary fitted curvilinear orthogonal grid is visualized as a Geographic Information System (GIS) layer. The grid generator uses a subscripted array of cell types and the x,y coordinates of the corner points of all water cells to produce model input files that numerically represent the model grid. A time-consuming step in the grid generation process can be to digitize the water cell corner points. To speed this process, Applied Ecology, Inc. developed a digitizing tool that operates under ESRI ArcGIS^{TM} 10.3. (Listopad 2017). The hand drawn grid layer is opened by the tool and the coordinates of the cell corner points are digitized in order, row by row from the southwest corner of the grid to the northeast corner of the grid. The grid tool assigns I (row) and J (column) indices to each set of cell coordinates. The subscripted list of cell coordinates, along with an or ordered two-dimensional array of cell types and depth value inputs are then used by the grid generator to calculate an ordered list of cell dimensions (file dxdy.out) and a file specifying horizontal cell center coordinates and cell orientations(file lxly.out). These files are restated as input files along with control and boundary forcing information.

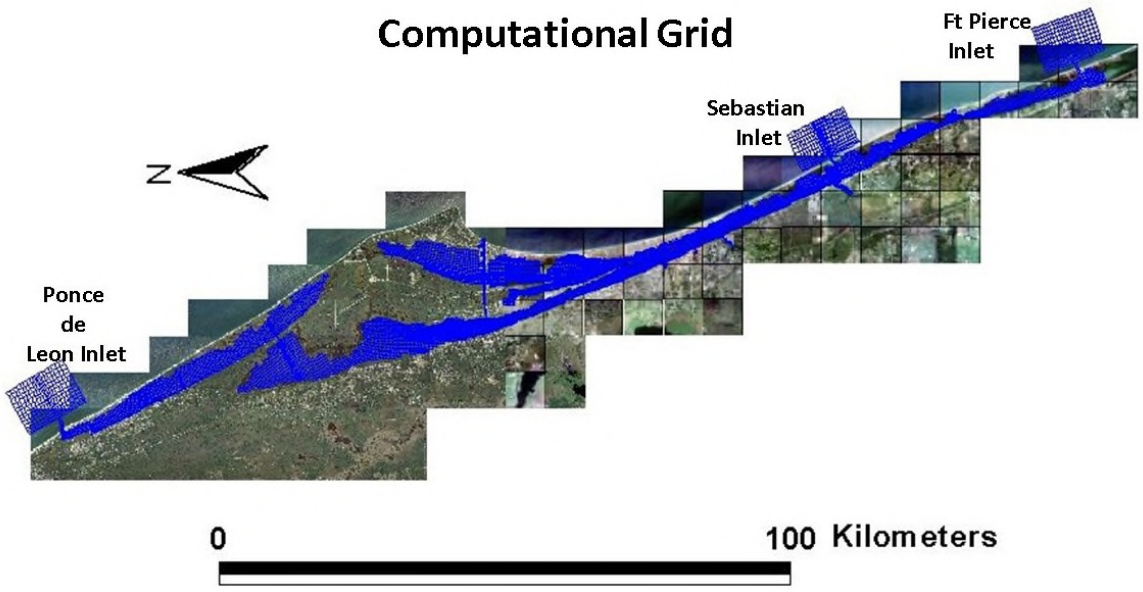

Figure 4-2. Model computational grid extending from Ponce de Leon Inlet to Fort Pierce Inlet, FL.

4.2.2 *EFDC boundary conditions and input files*

Data sets have been assembled from a wide range of sources and evaluated for use in the model. Among the most important data sets are those maintained by the St. Johns River Water Management District (SJRWMD), by the U.S. geological Survey (USGS) under sponsorship by the SJRWMD and, data collected by the Harbor Branch Land/Ocean Biogeochemical Observatory (LOBO). Data from these stations include time series of water level, salinity, temperature, discharge, and meteorological parameters. These data sources were used to either set internal model boundary conditions such as freshwater inflow or to check the calibration of the model for salinity and water temperatures. Another important source of data applied to the model was estimates of groundwater inflows into the lower layer of the EFDC model to simulate groundwater flux. At the time scale of this project the contribution of groundwater is secondary to the overall hydrologic balance of the system but can be of increasing importance at the longer time scales of a decade or longer in which the major balance is between evaporation and groundwater flux. Groundwater flows were provided by the work of Mamoua et al.(2019) under an ongoing IRL groundwater assessment project that includes both data collection and modeling. Data from meteorological stations maintained by the SJRWMD and the National Weather Service are used to setup air sea interaction boundary conditions for the hydrodynamic model.

The major model input files are listed in Table 4-1. For each of the of the model time series files listed in Table 4-1, the complete available data record is loaded in the model boundary input file. Although the available data sets are generally of high quality, having been quality controlled levelled to NAVD88 with respect to water level, they are limited in time span, especially for the model boundaries that extend into the coastal ocean at Ponce de Leon, Sebastian Inlet, and Fort Pierce Inlet.

Table 4-1 Major EFDC input files

Input File	Description
efdc.inp	Main control file
aser.inp	Atmospheric forcing time-series file.
cell.inp	Horizontal cell type identifier file.
dxdy.inp	File specifying horizontal grid spacing or metrics, depth, bottom elevation, bottom roughness and vegetation classes for either Cartesian or curvilinear orthogonal horizontal grids.
Dye.inp	Initial numerical tracer assigned to selected model cells
lxly.inp	File specifying horizontal cell center coordinates and cell orientations.
pser.inp	Water level time series
qser.inp	Volumetric source-sink time-series file. Including groundwater (inflow-outflow)
salt.inp	File with initial salinity distribution for cold start, salinity stratified flow simulations.
sser.inp	Salinity time-series file.
temp.inp	File with initial water temperature distribution for cold start, salinity stratified flow simulations.
tser.inp	Temperature time-series file
wser.inp	Wind speed and direction

To provide water level time series at model cells in the coastal ocean offshore of Ponce de Leon Inlet, Sebastian Inlet, and Fort Piece Inlet, predicted time series of water elevation were provided at these locations from the ADCIRC model as described in other sections. Since ADCIRC only provides water level time series in the tidal frequency band, it is important to add lower frequency components that include water level oscillations outside the frequency of the tides. This signal can include seas level shifts of up to 1 m at time scales of a few weeks to seasonal (Zarillo 2019). Figure **4-3** is an example of the water level time series applied offshore on Ponce de Leon Inlet.

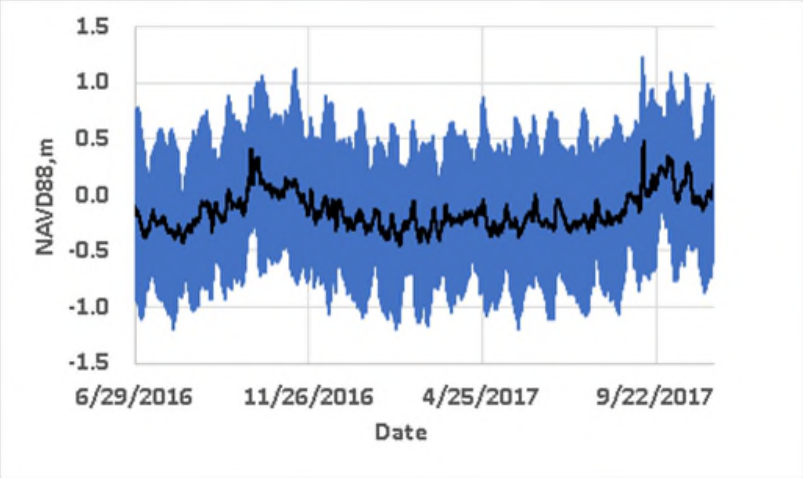

Figure 4-3**. Water level time series applied to model boundary cells offshore of Ponce de Leon Inlet showing the combined tidal and sea level signals. Black line shows the non-tidal sea level, whereas the blue line shows the combined series.**

Non-tidal water levels combined with the ADCIRC model data were derived by filtering measured data at NOAA Station 8721604 at the Trident Pier, Cape Canaveral Florida. Observations show that non-tidal sea levels are coherent at regional spatial scales, as seen in Figure 4-4, illustrating tidal and filtered non-tidal water level records from Trident Pier and from measured data at Sebastian Inlet 65 km to the south.

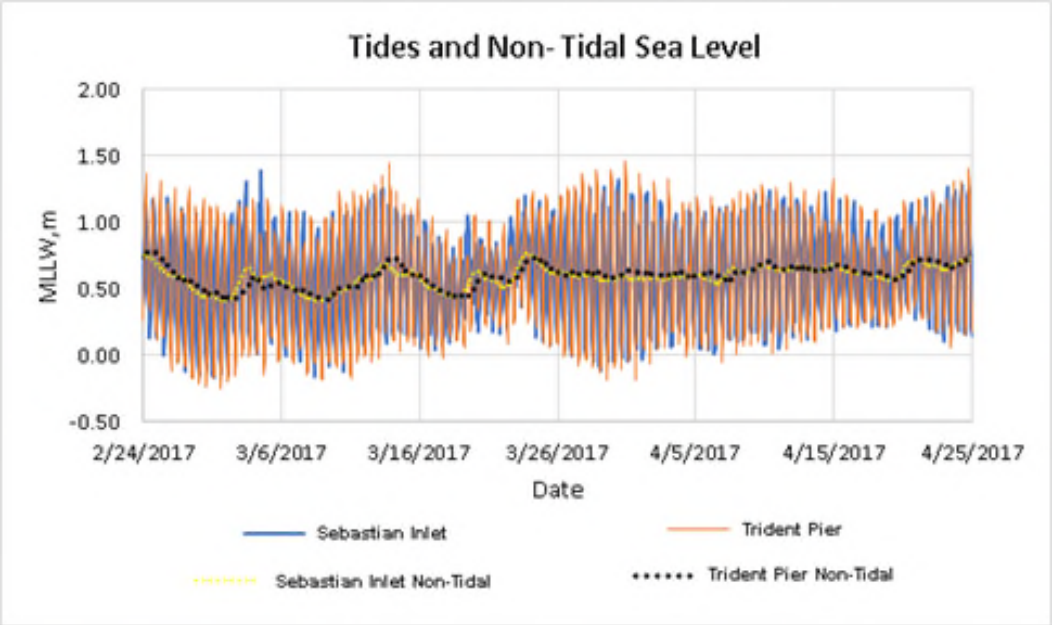

Figure 4-4. Measured tidal and non-tidal water level records from NOAA Station 8721604 (Trident Pier, Cape Canaveral FL) and Sebastian Inlet.

Salinity and water temperature time series were assigned to the coastal ocean model boundary cells offshore of Ponce de Leon Inlet, Sebastian Inlet, and Fort Pierce Inlet. These data were provided from the archive of model runs maintained by HYCOM Consortium (https://www.hycom.org/). Figure 4-5 is an example of salinity and water temperature data provided by HYCOM assigned to the surface layer of offshore model cells at Sebastian Inlet. Similar HYCOM time series of salinity and water temperature were assigned to model boundary cells offshore of Ponce de Leon Inlet and Fort Pierce Inlet.

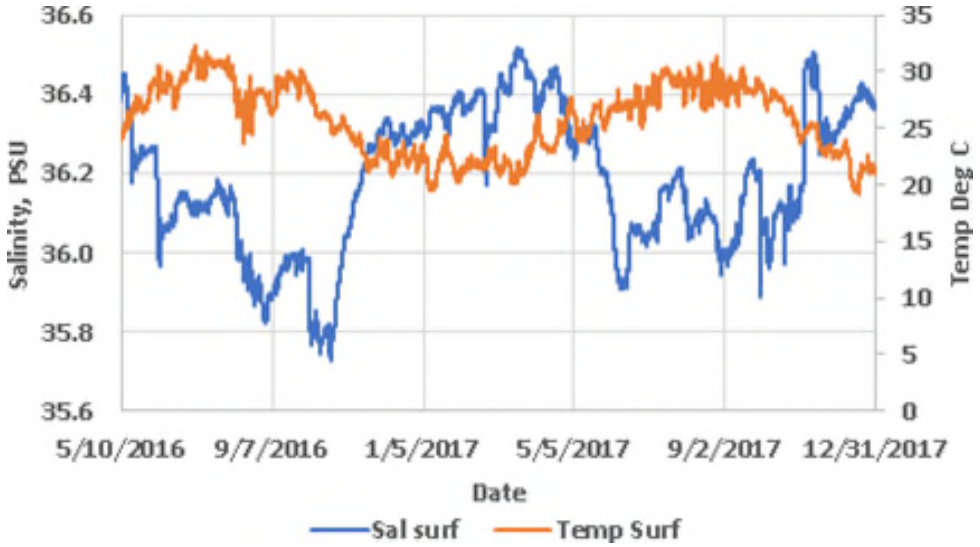

Figure 4-5. Example of salinity and water temperature data provided by HYCOM for offshore model cells at Sebastian Inlet.

4.3 EFDC Model Calibration and Verification

Model calibration and validation results for the IRL model developed at Florida Tech were described in an earlier project report (Zarillo and Listopad 2016). However, there was an update of model boundary conditions in the coastal ocean for this project, an additional check on model performance was conducted.

Figure 4-6 compares observed and model water levels at the Wabasso Bridge in north Indian River County, where a long-term water level sensor has been maintained by the USGS on behalf of the SJRWMD. The time period shown in Figure 4-6 corresponds to the overall time period in which the latest round of model predictions were made. The root mean square error (RMSE) of the comparison is 0.034 m (3.4 centimeters [cm]) and the ratio between RMSE and the range of observed values of water level is 0.037 representing an error of 3.7% In the original calibration and validation exercise, the observations to model companions were 7.7% and 9.4%, respectively (Zarillo and Listopad 2016).

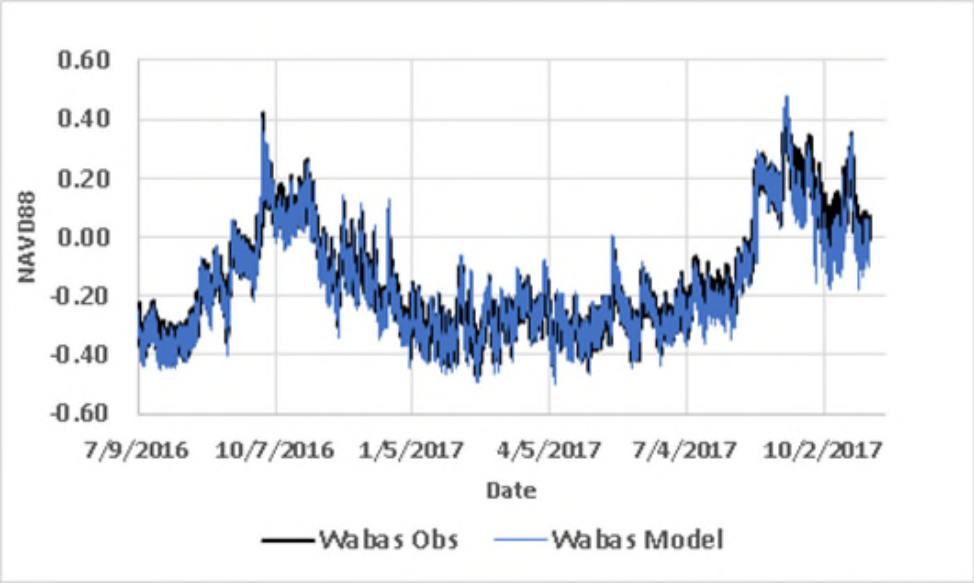

Figure 4-6. Observed and predicted water levels at Wabasso Bridge, north Indian River County, FL.

Calibration and validation of model salinity and water temperature data were provided (Zarillo and Listopad 2016). However, since the HYCOM time series are an update of outer model boundary conditions, a comparison of observed and model salinity data and water temperature data was made for the 2016 to 2017 data. Figure 4-7 compares model predicted salinity values with observed salinity data recorded by LOBO Station IRL-SB. This station is located in the Intracoastal Waterway to the west of Sebastian Inlet. The observation to model data comparison was made for the surface layer of the model, which represents the upper 20% of the water column. The RMSE for the comparison is about 2.1 practical salinity units (PSU) representing an error of about 11.5%, which is comparable to the calibration and validation error values reported earlier (Zarillo and Listopad 2016). Figure 4-8 compares water temperature observations with model data at LOBO Station IRL-SB. The RMSE for the comparison is 2.14 for a relative percentage error of about 8.2% when comparing the RMSE value to the range of observed values.

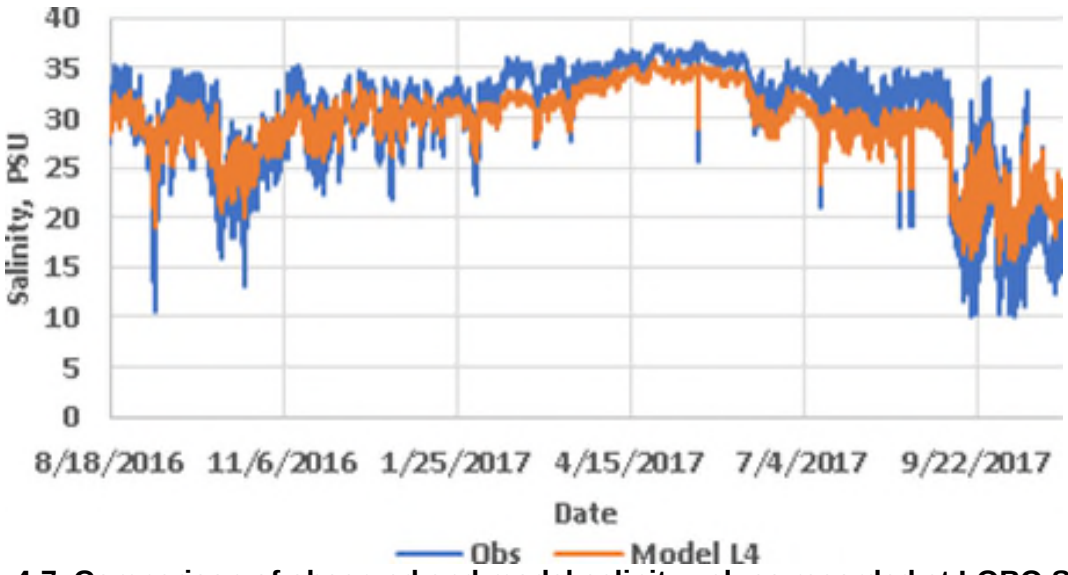

Figure 4-7. Comparison of observed and model salinity values recorded at LOBO Station IRL-SB.

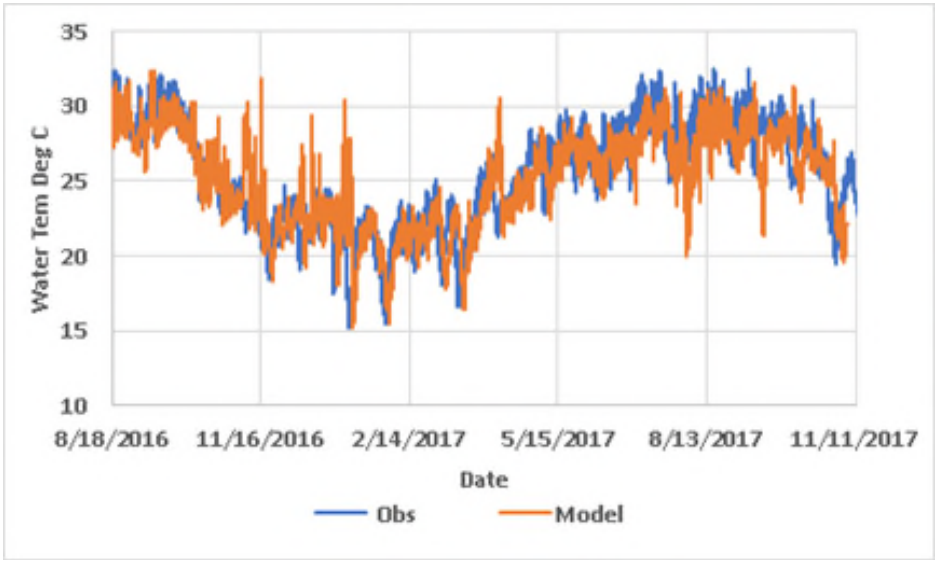

Figure 4-8. Comparison of observed and model water temperature values recorded at LOBO Station IRL-SB

4.4 EFDC Model Predictions

4.4.1 *Overview*

Model cases to examine the potential impact of enhanced inflows to the IRL system from the coastal ocean were based on assumed rates of pumping of ocean water into the system at selected locations. An additional case included a hypothetical weir structure located in the west basin of Port Canaveral. Table 4-2 lists the hypothetical model cases evaluated in this project. In the following sections each of these hypothetical cases is evaluated for the potential contribution to enhanced flushing of the estuarine compartments served by the enhanced flow. Comparisons are made between the base model test cased of no enhanced inflows to the IRL system and the model cases that provide for increased inflows. The location of the enhanced inflow is described in each of the sub-sections dedicated to the individual cases. The model results are presented as

comparisons of predicted tracer concentrations with and without inflow enhancement and a comparison of predicted salinity and water temperature.

Model results presented in terms numerical tracer concentrations are used to evaluate the ability to promote exchanges of water out of particular compartments served by the enhanced flow. The use of estuarine water tagged with 100 parts per thousand (ppt) of a numerical tracer allows the evaluation of the degree to which a particular sub-basin of the IRL system can be flushed over a period of time. The model runs applied in this project were 365 days period from January of 2016 to January of 2017. At the beginning of each run there is an approximate 10-day period of equilibration to boundary conditions.

Table 4-2. Model test cases for enhance flow.

Case	Location	Rate of Enhanced Inflow	Duration
Base	No enhanced inflow	zero	365 days
Pump Station 1	Banana River vicinity of Patrick Air Force Base (PAFB)	10 cubic meters per second (m^3/s)	365 days
Pump Station 2	Banana North of Port Canaveral	10 m^3/s	365 days
Weir Structure	West Port Canaveral Basin	variable	365 days
Pump Station 3	Bethel Creek Indian River Lagoon	5 m^3/s	365 days

4.4.2 *Model base case: Banana River*

Under the base model test case no additional sea water is introduced into the model domain during the test run. The following figures depict the changes in tracer concertation during this model test in the areas subjected to hypothetical inflows in model enhanced inflow cases. In addition, to instruct the model to map the predictions globally over the entire model domain, a series of numerical monitoring stations were set up the capture model predictions at key locations. Data from these stations are used to compare tracer concentrations, water levels, salinity concentrations and water temperature predictions among the model test cases. Figure 4-9 shows the locations of the numerical monitoring stations in the Banana River. The cluster of stations located within Port Canaveral are named later in this report under the section describing model results from the hypothetical weir structure.

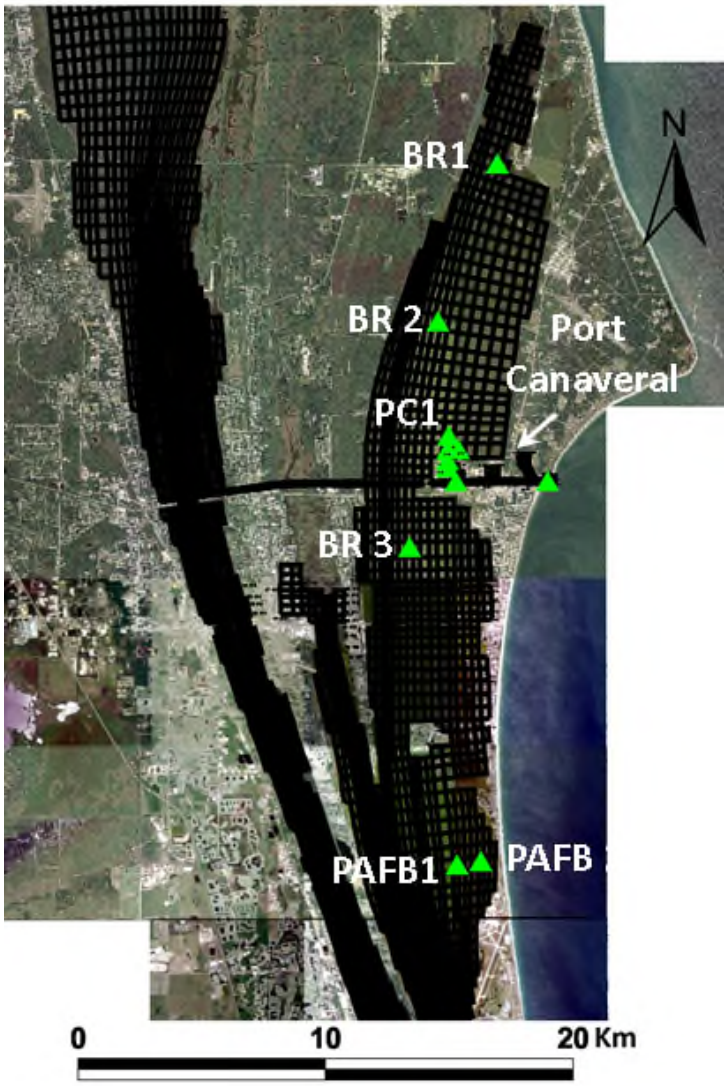

Figure 4-9. Location of numerical monitoring stations distributed in the Banana River.

The remainder of this report describes the changes in tracer concentration during this under base model test involving no enhanced inflow. Subsequent sections of this report compare this base case with model results of the enhanced inflow model tests listed in Table 4.2.

Figure 4-10 shows the predicted concentration of tracer in the surface layer of the model throughout the model domain at the end of 365-day model run. An initial tracer was confined to the Banana River at a concentration of 100 ppt. It can be seen in the figure that concentrations remain high in the Banana River, ranging from about 90 ppt in the north compartment of the Banana River to about 56 ppt near the convergence of the Banana River with the IRL. The lack of flushing on an annual time scale predicted by the EFDC model is consistent with previous model predictions using the U.S. Army Corps of Engineers Coastal Model System (Zarillo 2018).

Figure 4-11 compares predicted tracer concentrations in the Banana River at 1 day, 50 days, and 75 days into the model run for the base case (Table 2). Likewise, Figure 4-12 shows model surface layer tracer concentrations at 150 days, 200 days and at the end of the model run at 365 days.

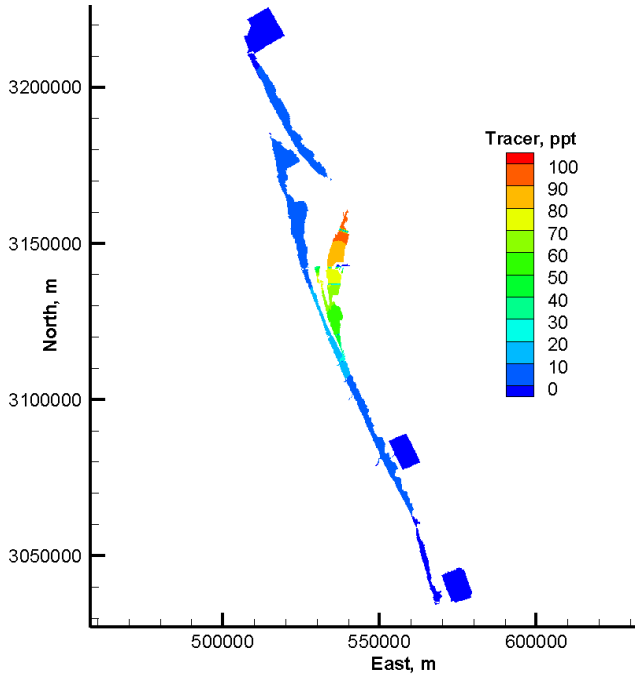

Figure 4-10. Predicted concentration of tracer dye in the surface layer of the model throughout the model domain at the end of 365- day base model run.

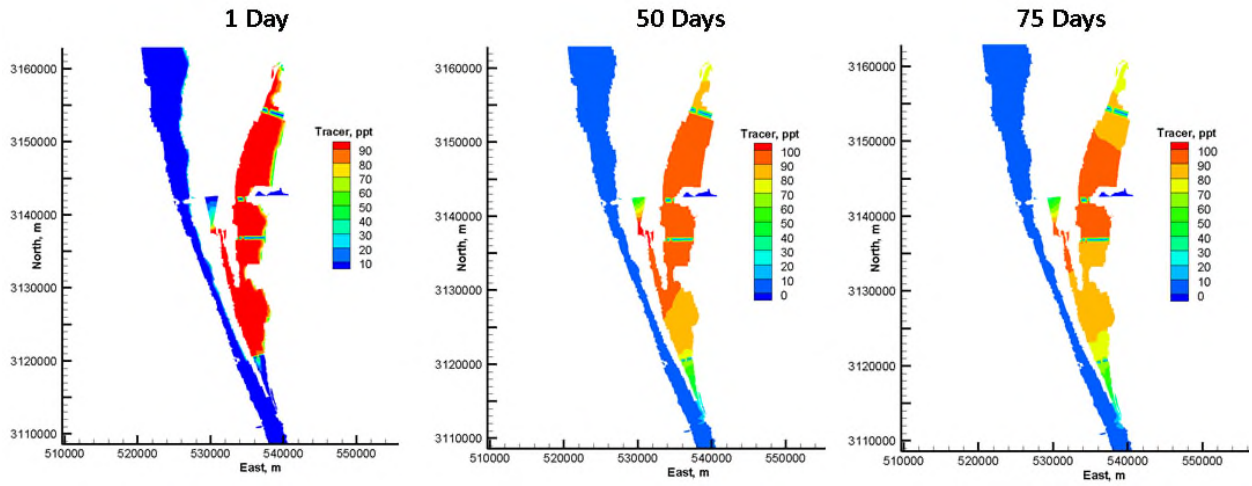

Figure 4-11. Predicted tracer concentrations in the Banana River at 5 days, 50 days, and 75 days into the model run for the base case

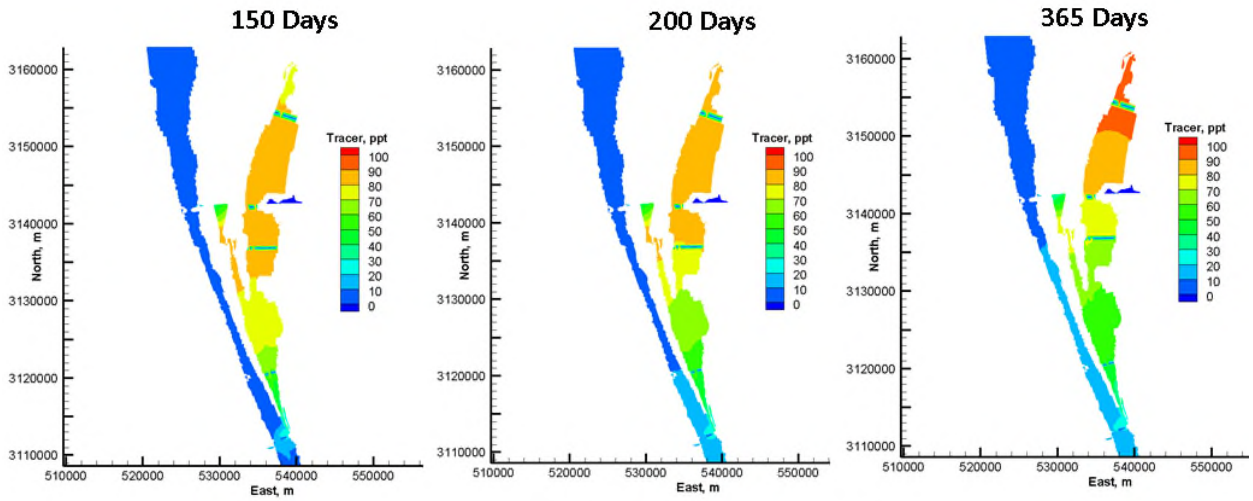

Figure 4-12. Predicted model surface layer tracer concentrations at 150 days, 200 days and at the end of the model run at 365 days.

Figure 4-13 combines the predicted tracer concentration in the surface layer of the model from six numerical monitoring stations in the Banana River. Surface tracer concentrations at stations PAFB 1 and PAFB 2 drop to about 56 ppt, whereas concentration levels remained above 70 ppt for all stations located further north in the Banana River basin. These tracer concentration records will be compared to predicted concentrations produced by the hypothetical introduction of coastal ocean water into the Banana River, according to the model cases listed in Table 2.

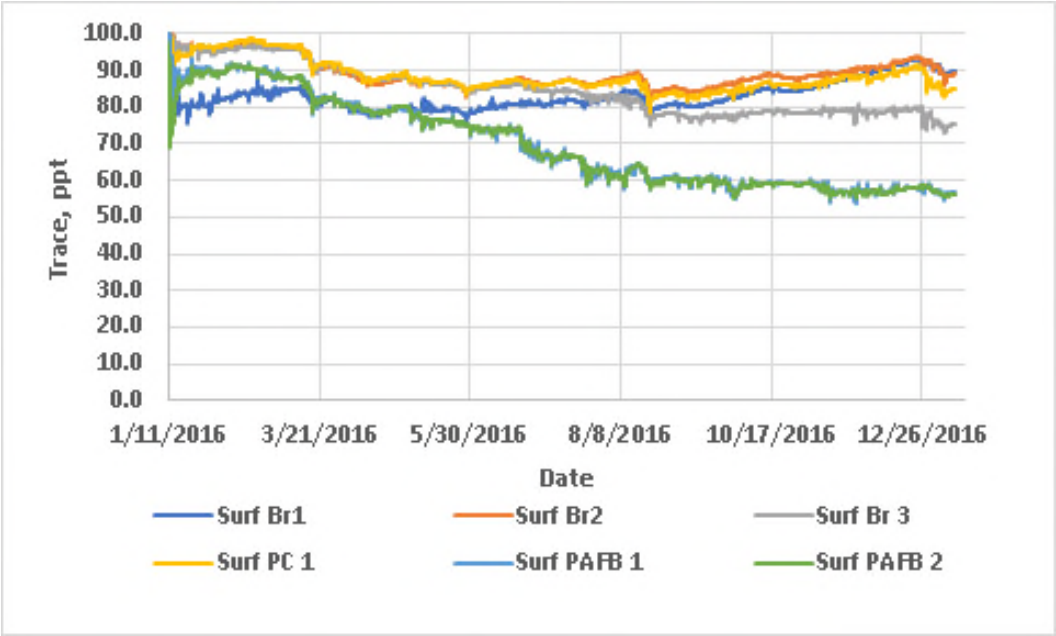

Figure 4-13. Predicted tracer concentration in the surface layer of the model from six numerical monitoring stations in the Banana River.

4.4.3 *Model Base Case: Bethel Creek*

Figure **4-14** shows the distribution of numerical monitoring stations within Bethel Creek in North Indian River County, Florida. Model predictions at these stations and within the adjacent IRL basin show that predicted tracer concentration levels drop to below 10 ppt within 20 days without enhanced inflows from the coastal ocean. Figure 4-15 presents a sequence of tracer concentration predictions at day 1, day 5, and day 20 of the base case model run. From this sequence the tracer can be seen to flush out of Bethel Creek and spread into the adjacent compartment of the IRL where tracer concentration increases from an initial value of zero to about 10 ppt.

Figure 4-16 shows the predicted tracer concentrations in all five layers of the model over the model run at numerical monitoring station BC 1, which is positioned well into the interior of Bethel Creek. Here, predicted concentrations drop to below 10 ppt within about 30 days. Figure 4-17 shows the predicted concentrations from monitoring station BC 1, BC 2, and BC 3 over the first three months of the model run. A similar rate of declined occurs at all three stations after an initial period of about five days. The patterns and rates of predicted tracer concertation declines in the Bethel Creek area under the base case will be compared with the enhanced flow case (Table 4-2) in which hypothetical pumping of coastal ocean water will be applied at a rate of 5 m^3/s for the duration of the model test.

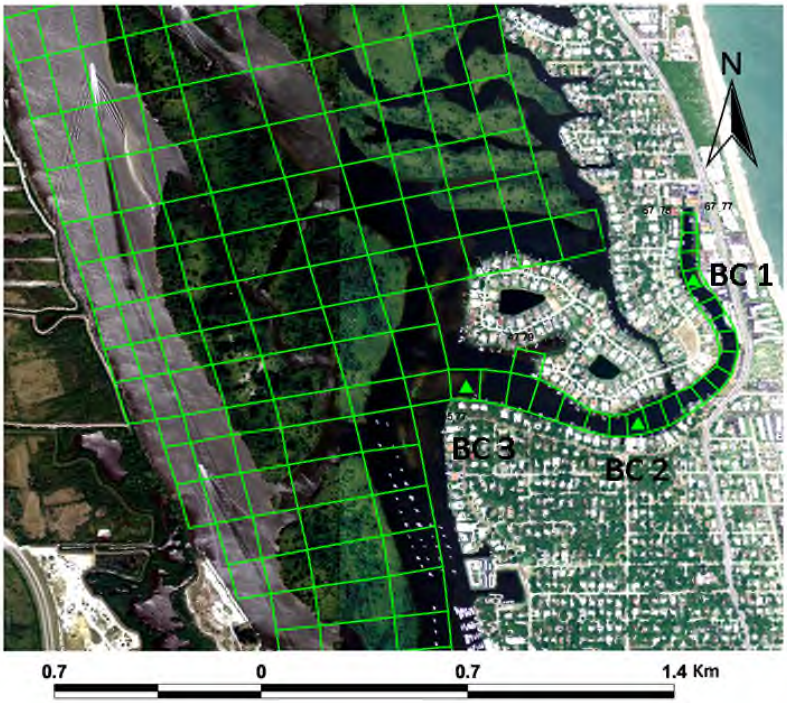

Figure 4-14**. Location of Bethel Creek in the IRL within Indian River County. Triangles show the location of numerical monitoring stations.**

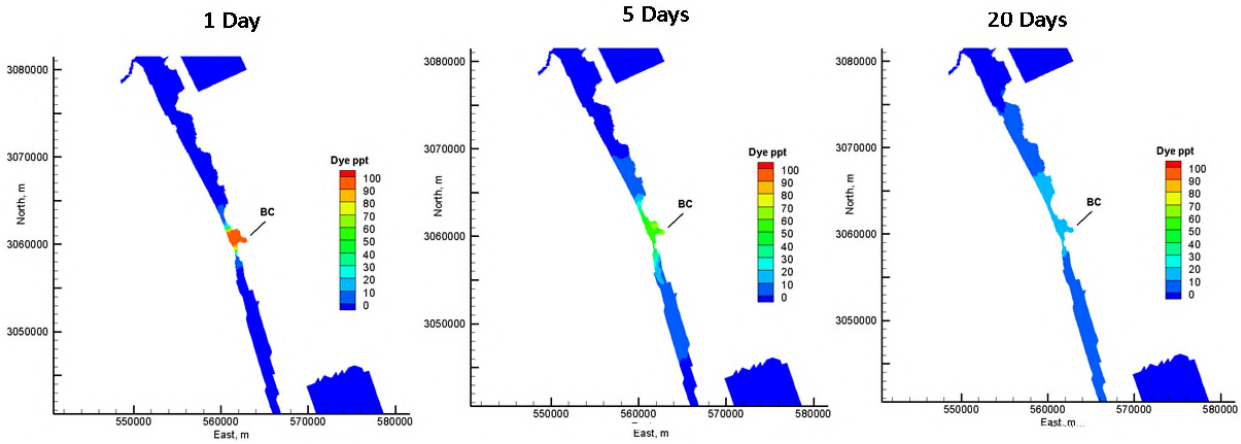

Figure 4-15. A 20-day sequence of predicted tracer concentrations in the vicinity of Bethel Creek.

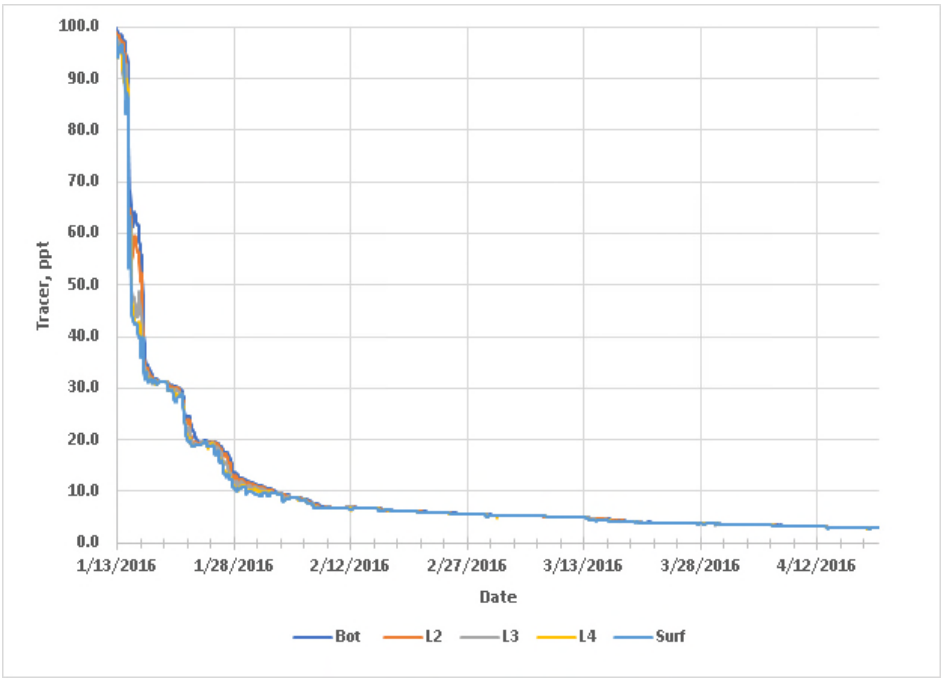

Figure 4-16. Predicted tracer concentrations for the base case at monitoring station BC1 over a 365-day period.

Figure 4-17. Comparison of tracer concentrations in the surface model layer for the base case at monitoring stations BC1, BC2, and BC3.

4.4.4 *Pump Station 1: Vicinity of PAFB*

This hypothetical case examines the impact of a pump station located in the vicinity of PAFB as shown in Figure 4-18. This location is somewhat generic since the exact location does not necessarily have to be located on military property. The pump station could be located anywhere along this narrow section of the barrier island. The pump rate was set at a nominal 10 m^3/s since this rate is likely to be achievable in the temporary inflow pilot system. However, the model input files can be readily modified to accommodate higher or lower pump rates or an alternating schedule involving period of pumping followed by periods of lower pump rate or cessation of the pumps.

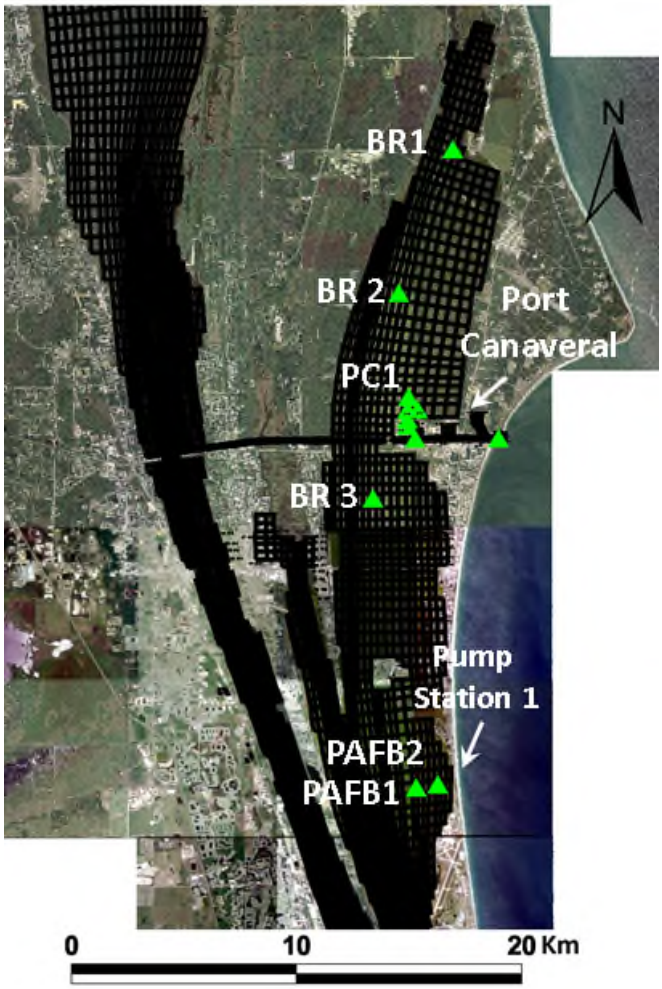

Figure 4-18. Location of Pump Station 1 adjacent to PAFB.

Figure 4-19 compares predicted tracer concentration in the surface model layer under the base model case with the Pump 1 case after 50 days of simulation. Likewise, Figure 4-20 and Figure 4-21 compares predicted tracer concentrations in the Banana River for the base and Pump 1 model runs at 100 and 200 days, respectively. Finally, Figure 4-22 shows the predicted tracer concentrations compared at day 365 of the model run. Tracer concentrations under the Banana River Pump 1 case are persistently lower compared to the base case depicting the existing condition without enhanced flow introduced at Pump Station 1.

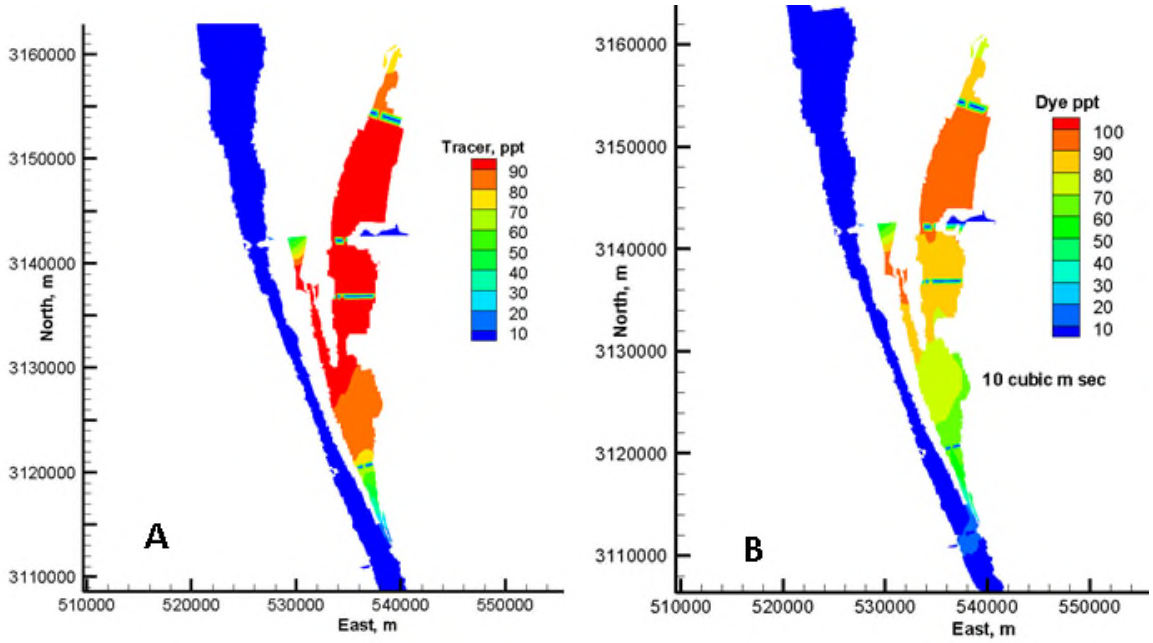

Figure 4-19. Predicted tracer concentration in the surface model layer under the base model case (A) and with the Pump 1 case (B) after 50 days of simulation.

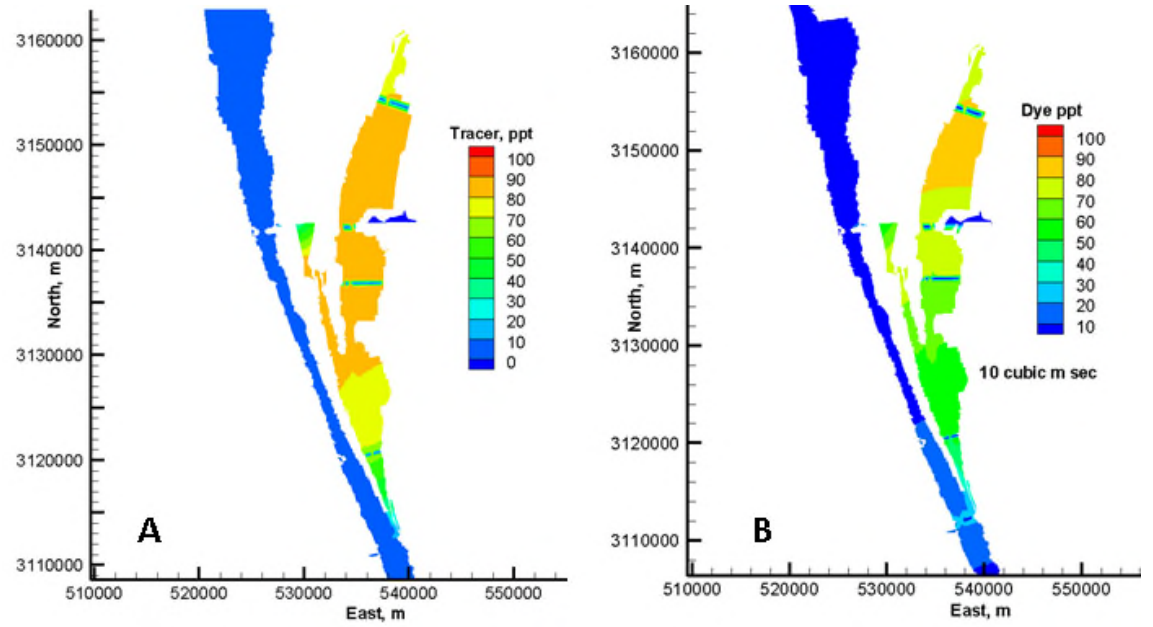

Figure 4-20. Predicted tracer concentration in the surface model layer under the base model case (A) and with the Pump 1 case (B) after 100 days of simulation.

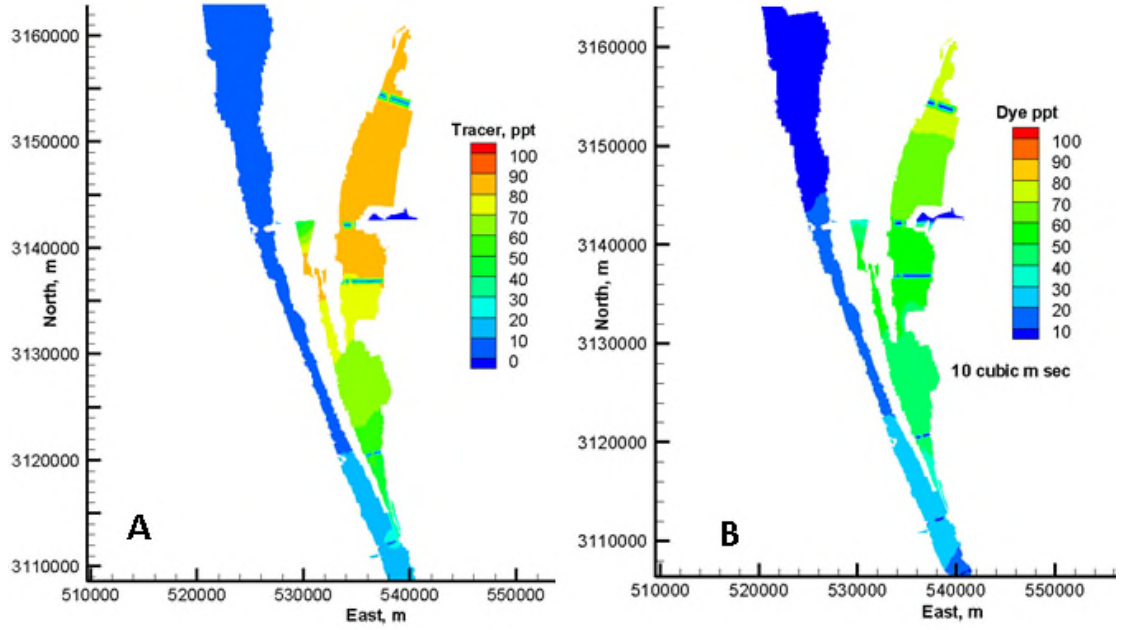

Figure 4-21. Predicted tracer concentrations in the Banana River for the base case (A) and Pump 1 model runs (B) at 200 days.

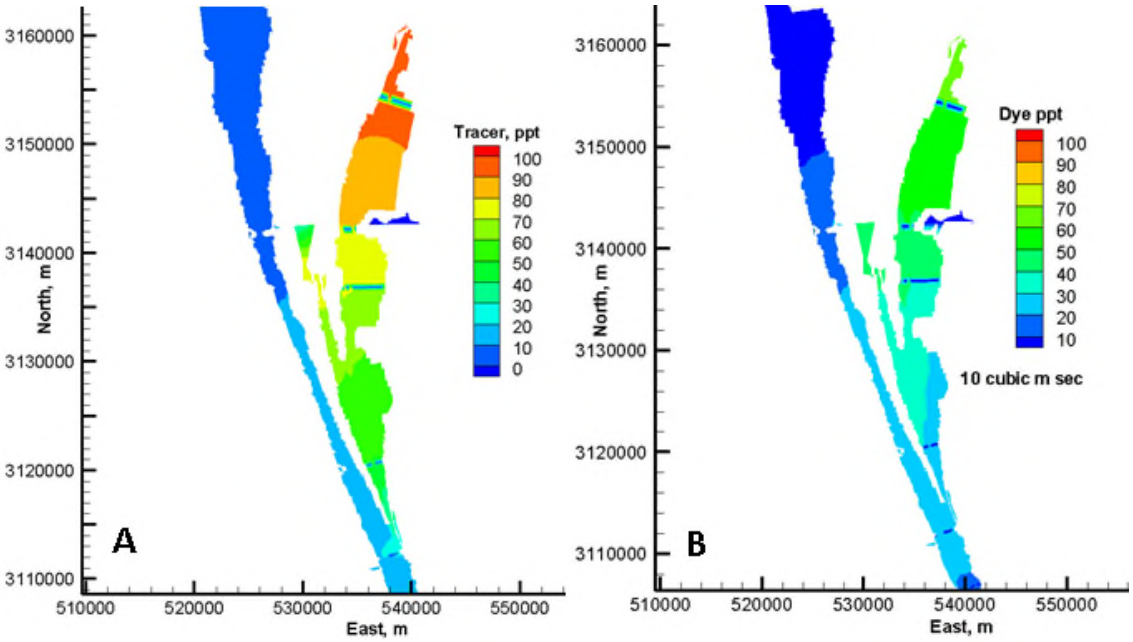

Figure 4-22. Predicted tracer concentrations in the Banana River for the base case (A) and Pump 1 model runs (B) compared at day 365 of the model run.

Observing the predicted tracer concentrations at Station PAFB 1 shows that there can be up to a 5 ppt difference between the predicted surface and bottom layer concentrations in the model as seen in Figure 4-23. Overall, by the end of the 365-day model run tracer concentrations at this station are reduced by 65 to 75%. This compared with a maximum reduction of about 45% predicted in the surface model layer under the base case as shown in Figure 4-24.

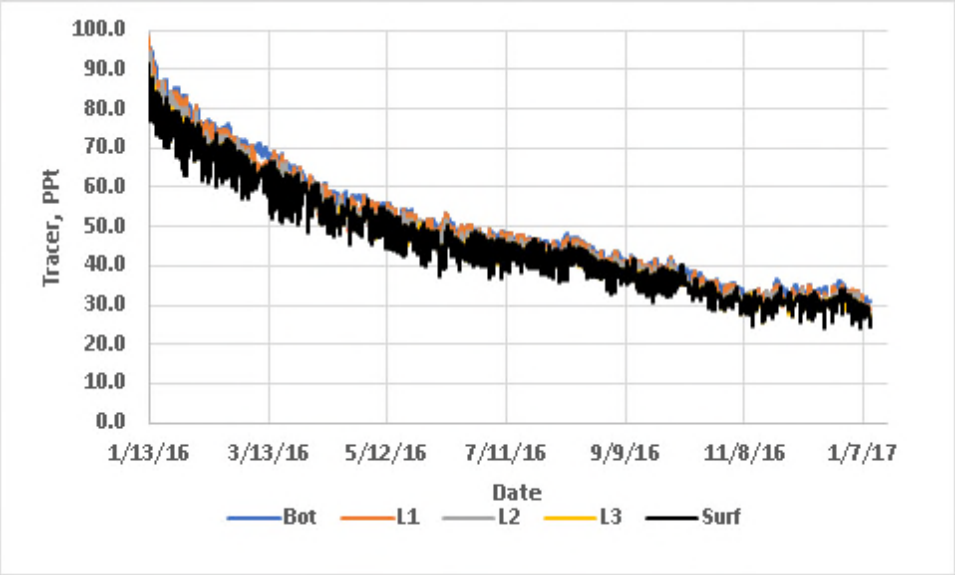

Figure 4-23 Predicted tracer concentrations at Station PAFB 1.

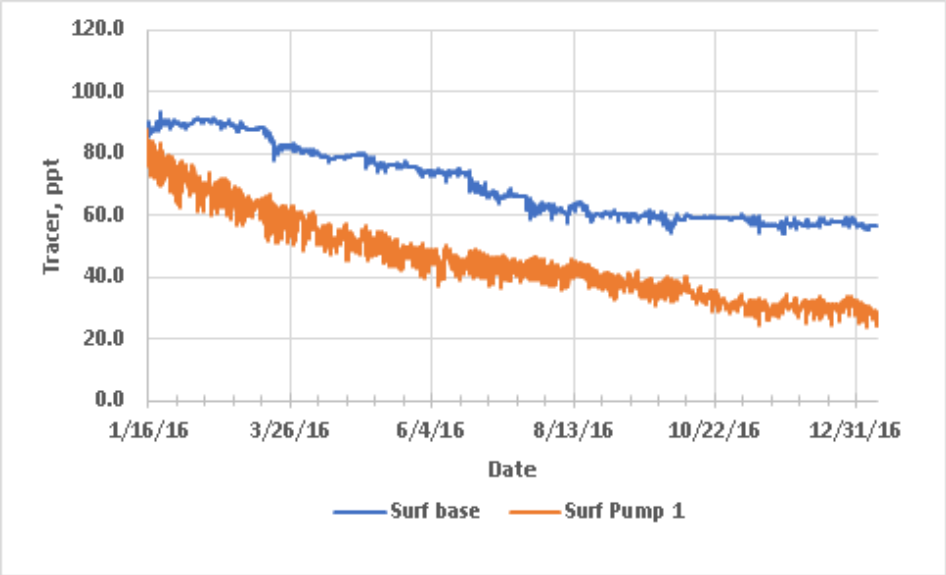

Figure 4-24. Predicted tracer concentrations at Station PAFB 1.

Figure 4-25 makes a similar comparison at numerical monitoring station BR3 in the north compartment of the Banana River. Here, the overall reduction in predicted tracer concentration is not as large as in the vicinity of the Pump1 station, but there is a clear distinction between the base case and the Pump 1 model results. In the north Banana River under existing conditions the reaction in predicted tracer concentration is on the order of 10 to 14%. Under the Pump 1 model test the predicted reduction in tracer concentration in the surface model layer reaches a maximum of about 45% by the end of the model run.

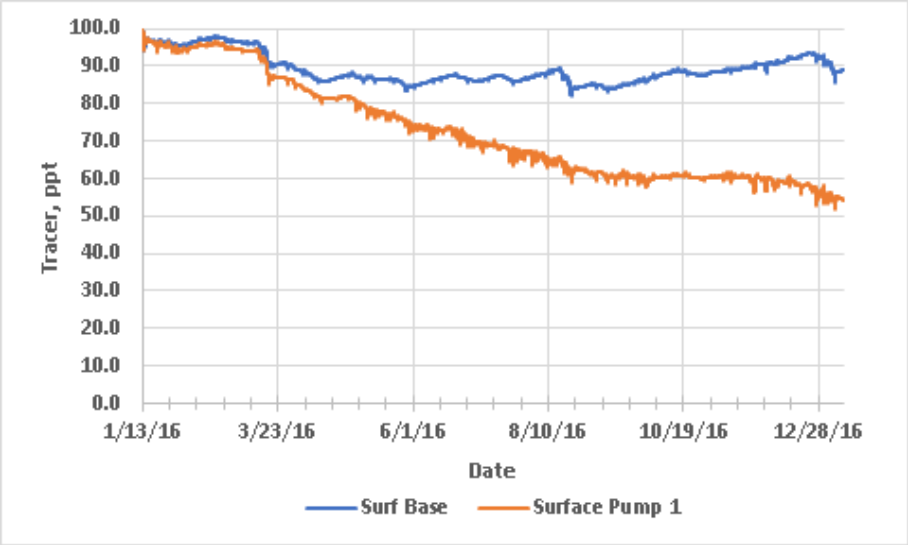

Figure 4-25 Predicted tracer concentration in the model surface layer at numerical monitoring station BR 2 under the base case (A) and the Pump 1 case (B).

Salinity predictions indicate a well-mixed water column under most conditions in the Banana River. Figure 4-26 shows nearly uniform predicted salinity in all model layers at station PAFB 2 under the Pump 1 model conditions. However, a comparison between the base model case and Pump 1 model predictions indicates that enhanced inflow of the sea water having full ocean salinity may slightly increase salinity (Figure 4-27). As shown in Figure 4-27 inflows from the coastal ocean were predicted to increase salinity at PAFB 2 by up to 2.5 PSU by the end of the 365-day model run. At a location more distal from the Pump 1 the predicted salinity at BR 2 was less than 0.1 PSU higher compared to the base case (Figure 4-28).

Figure 4-26. Predicted salinity in all model layers at station PAFB 2 under the Pump 1 model conditions.

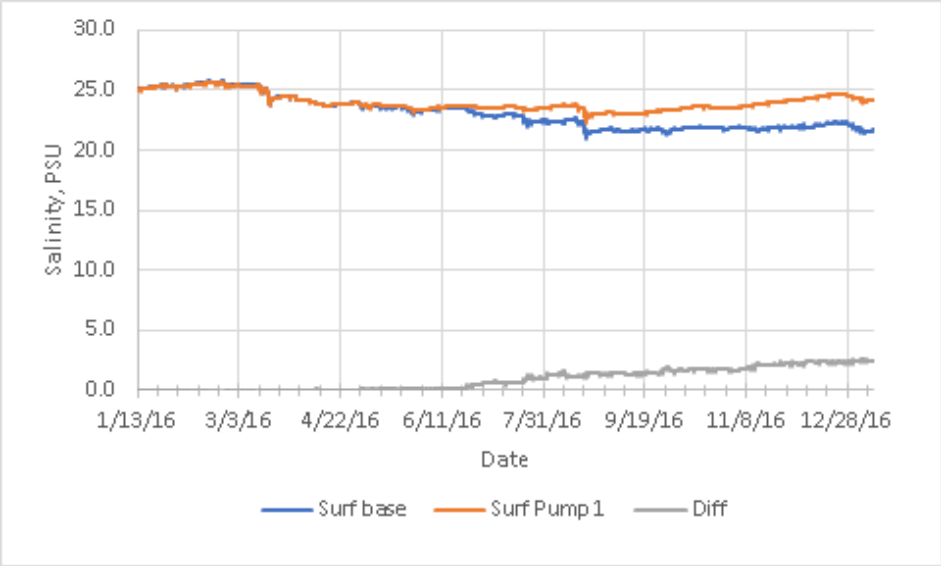

Figure 4-27. Predicted salinity at PAFB 2 in the surface model layer for the Pump 1 case and the base case.

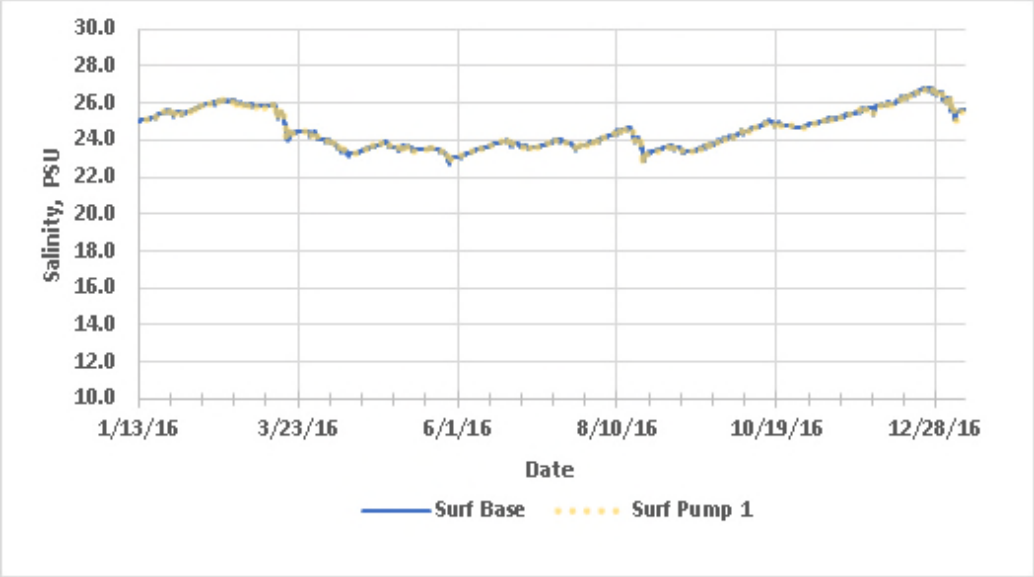

Figure 4-28. Predicted salinity in the surface model layer at BR 2 for the base case and the Pump 1 case.

Predicted temperatures proximal to the Pump 1 location were measurably altered compared to the base case. At station PAFB 2 surface water temperature was reduced by an average of 3 °C as a result of the Pump 1 model test (Figure 4-29). Predicted temperature differences were minimal at numerical monitoring station BR 2 in the north Banana River (Figure 4-30Figure 4-30. Predicted water temperature in the model surface layer at station BR 2 for the base case and the Pump 1 case. Here the predicted water temperature under the Pump 1 case was less than 0.1 degree cooler in the surface layer of the model. Predicted water temperature in the bottom layer of the model were cooler and less variable along with minimal difference between the two model cases (Figure 4-31).

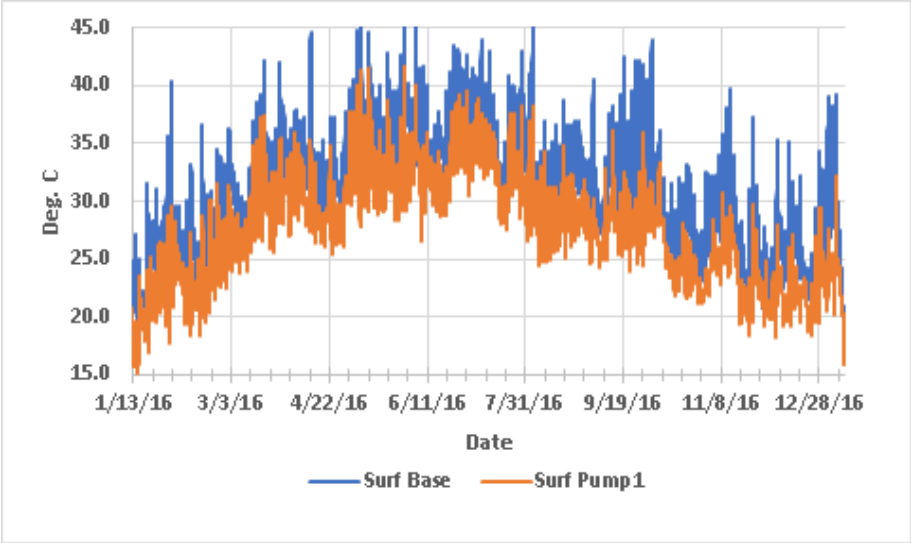

Figure 4-29. Predicted water temperature in the model surface layer at PAFB 1 for the base case and the Pump1 case.

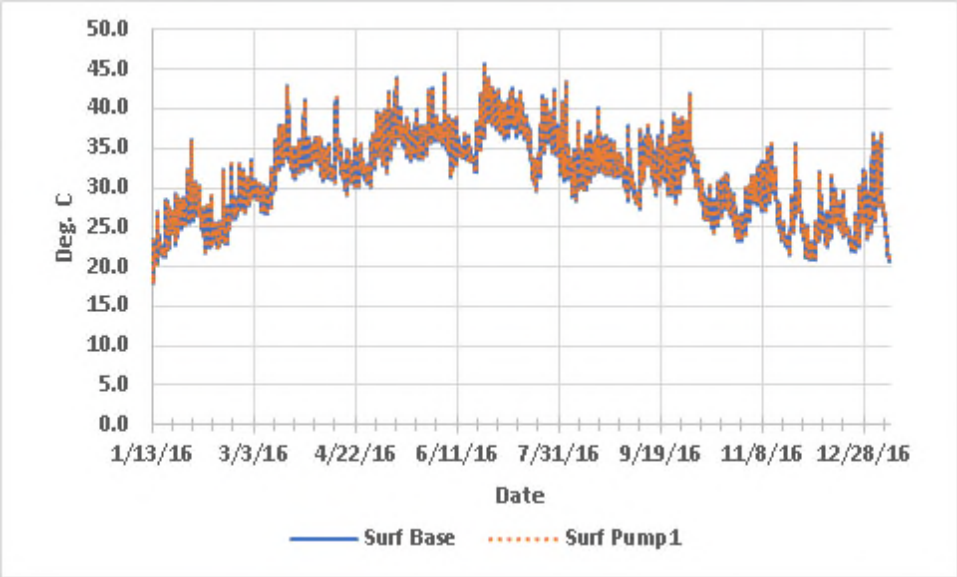

Figure 4-30. Predicted water temperature in the model surface layer at station BR 2 for the base case and the Pump 1 case.

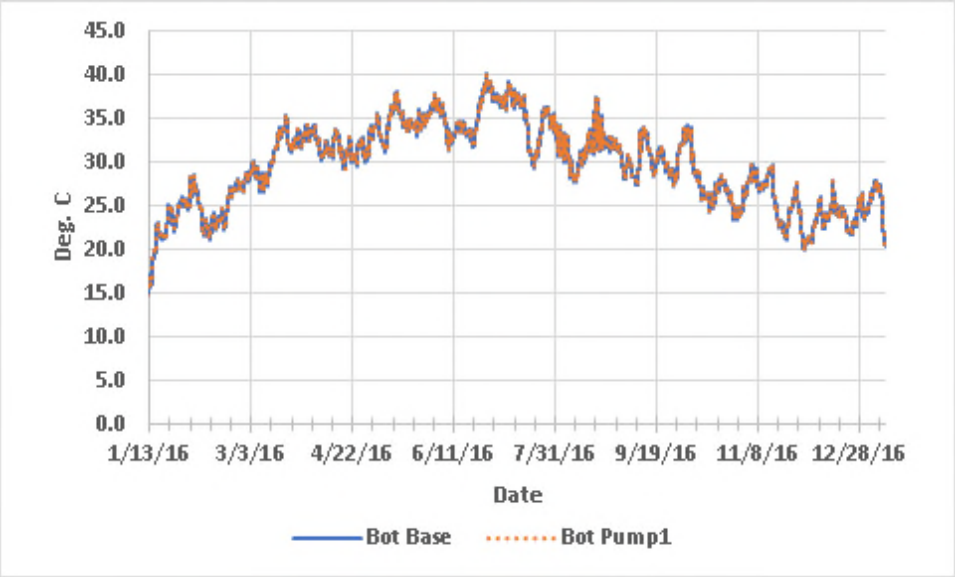

Figure 4-31. Predicted water temperature in the model bottom layer at station BR 2 for the base case and the Pump 1 case.

4.4.5 *Pump Station 2: North of Port Canaveral*

Hypothetical Pump Station 2 is located on the north side of Port Canaveral as shown in Figure 4-32. Here, the hypothetical pump station moved water across the south flank of Cape Canaveral into the north Banana River. This site was chosen for a location that could contribute enhanced flushing of the north Banana River compartments. North Banana River tracer concentrations were not as reduced under the Pump 1 case, which had a greater impact on the south Banana River compartments.

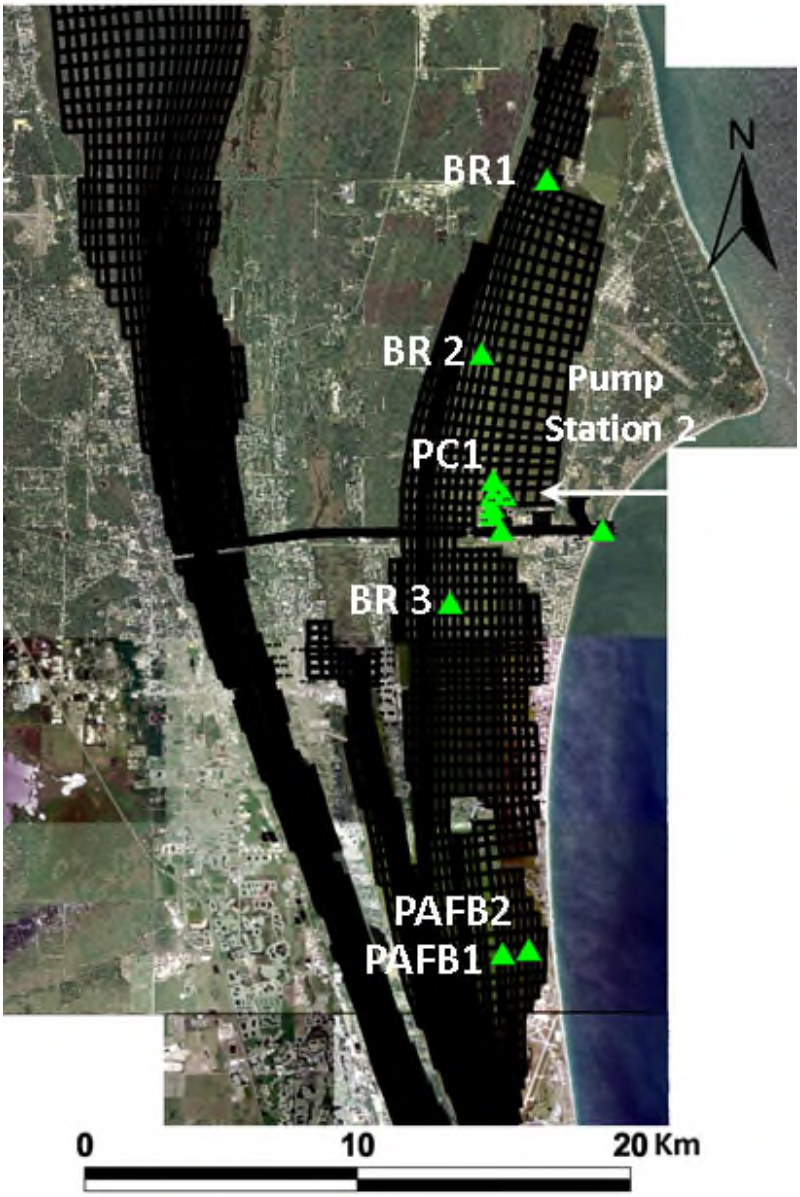

Figure 4-32. Location of Pump Station 2, north of Port Canaveral.

Figure 4-33 compares predicted tracer concentration in the surface model layer under the base case with the Pump 2 case after 50 days of simulation. Figure 4-34 and Figure 4-35 compare predicted tracer concentrations in the Banana River for the base case and Pump 2 model runs at 100 and 200 days, respectively. Finally, Figure 4-36 shows the model results compared at day 365 of the model run. Tracer concentrations under the Banana River Pump 2 case are persistently lower compared to the base case depicting the existing condition without enhanced flow introduced at Pump Station 1.

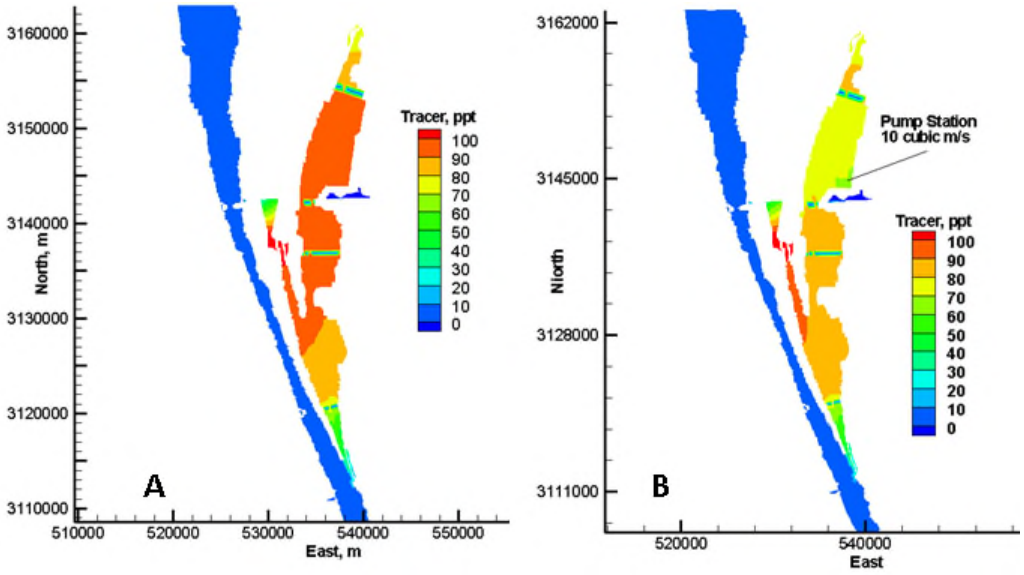

Figure 4-33. Comparison of predicted tracer concentration at day 50 under the base case (A) and the Pump 2 case (B).

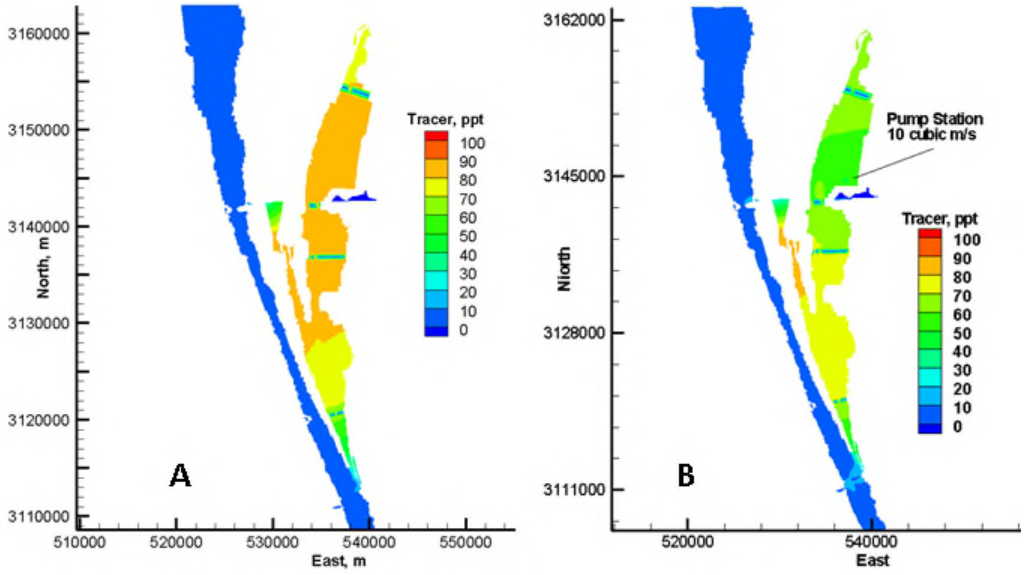

Figure 4-34. Comparison of predicted tracer concentration at day 100 under the base case (A) and the Pump 2 case (B).

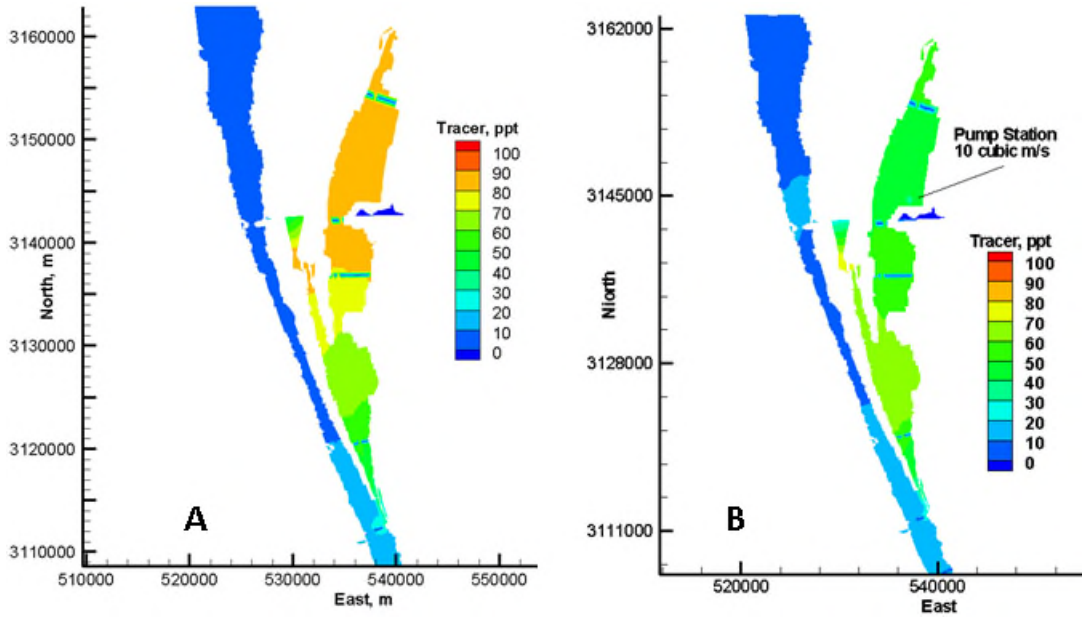

Figure 4-35. Comparison of predicted tracer concentration at day 200 under the base case (A) and the Pump 2 case (B).

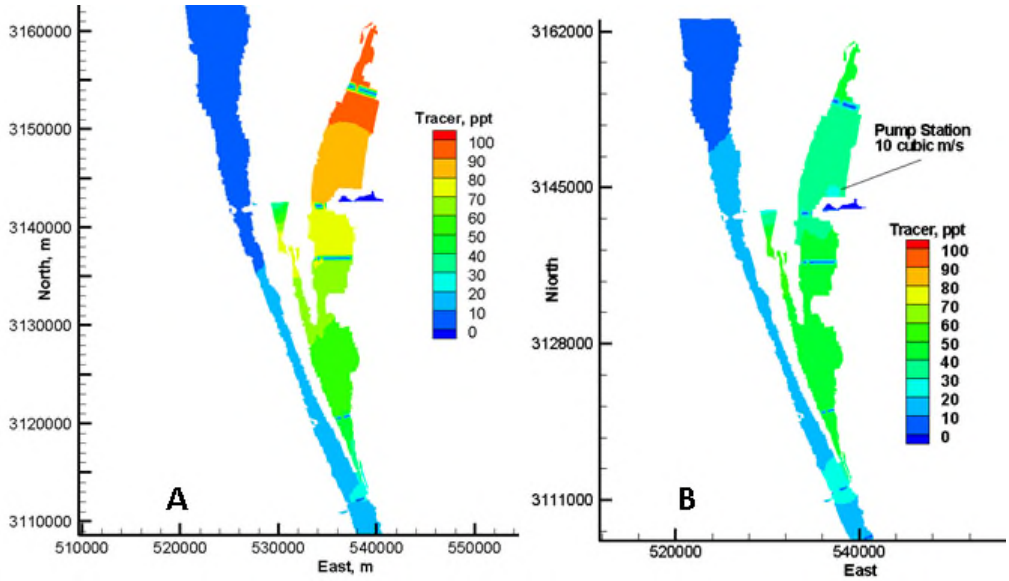

Figure 4-36. Comparison of predicted tracer concentration at day 365 under the base case (A) and the Pump 2 case (B).

Figure 4-37 compares predicted tracer concentration in all model layers at numerical monitoring station PC1, located to the west of the Pump Station 2 outfall in the Banana River. The enhanced inflow results in up to a 70% decline in tracer concentration by the end of the 365-day model run. Under the base condition predicted tracer concentration declines by 10 to 15% from the initial 100 ppt concentration.

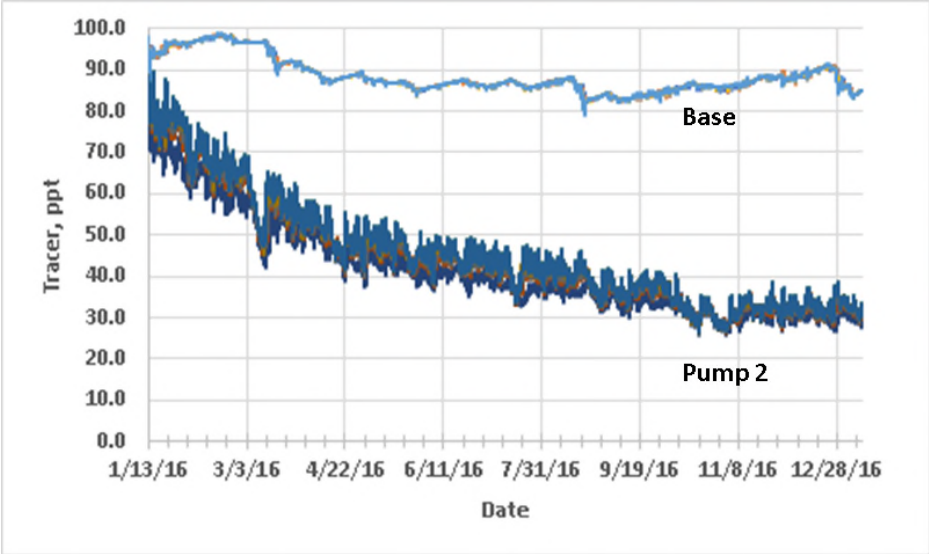

Figure 4-37. Comparison of predicted tracer concentration in all model layers at numerical monitoring station PC1.

In the northern most compartment of the Banana River, tracer concentrations at station BR 1 are predicted to sharply decline under the Pump 2 case (Figure 4-38). The Pump 2 case model results show tracer concentration reduced by 60% by the end of the model run. After an initial decline of about 20% tracer concentration rises to about 90 ppt during the final month of the base case model run. This is also reflected in the dark red color in the north section of the Banana River in Figure 4-36

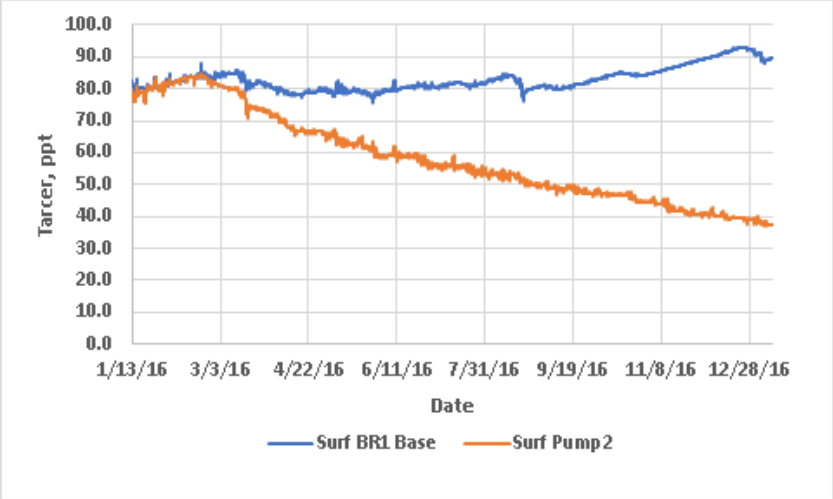

Figure 4-38. Comparison of predicted tracer concentration in the surface model layer at numerical monitoring station BR1.

Further south in the vicinity of the Pump 1 location tracer concentrations are also predicted to decline below those predicted for the base case, but not as sharply (Figure 4-39). This location, predicted tracer concentration declines to about 46 ppt under the Pump 2 case compared to about 56 ppt under the base case.

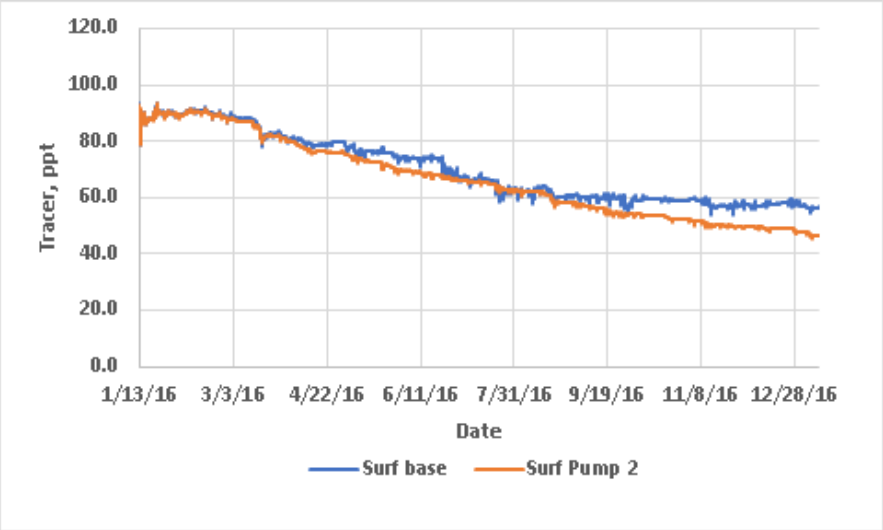

Figure 4-39. Comparison of predicted tracer concentrations in the surface model layer at numerical monitoring station BR3.

Salinity differences are also seen in the model results. In the vicinity of Pump Station 2, the predicted salinity resulting from the enhanced inflows tracks about 5 PSU above the predicted base case salinity (Figure **4-40**). Salinity difference remains on the order of 5 PSU by the end of the model run period at station BR1 in the north Banana River compartment (Figure 4-41). At a more distal location to the south in the vicinity of the Pump 1 station salinity differences are of the same magnitude although the overall salinity is lower due the distance from the pump station. Figure 4-42 shows predicted salinity in the model surface layer at station PAFB2, which is about 20 km south of the Pump 2 station.

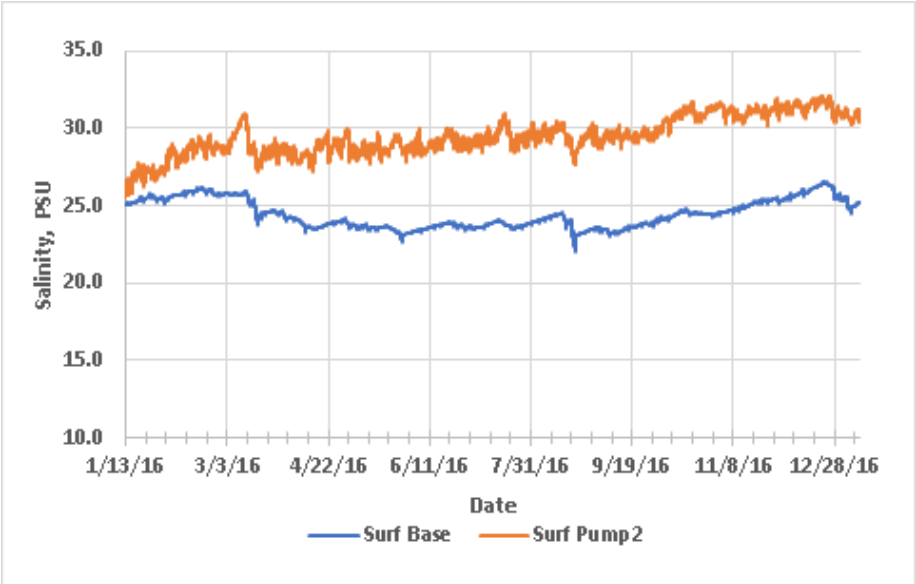

Figure 4-40**. Predicted salinity in the surface model layer at PC2 for the base case and the Pump 2 case.**

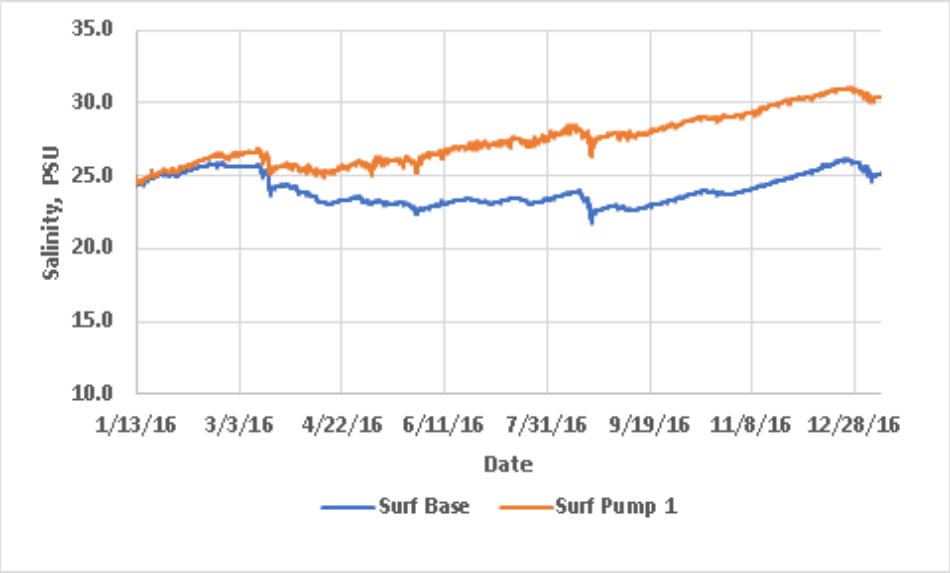

Figure 4-41. Predicted salinity in the surface model layer at station BR1 in the north Banana River compartment for the base case and the Pump 2 case.

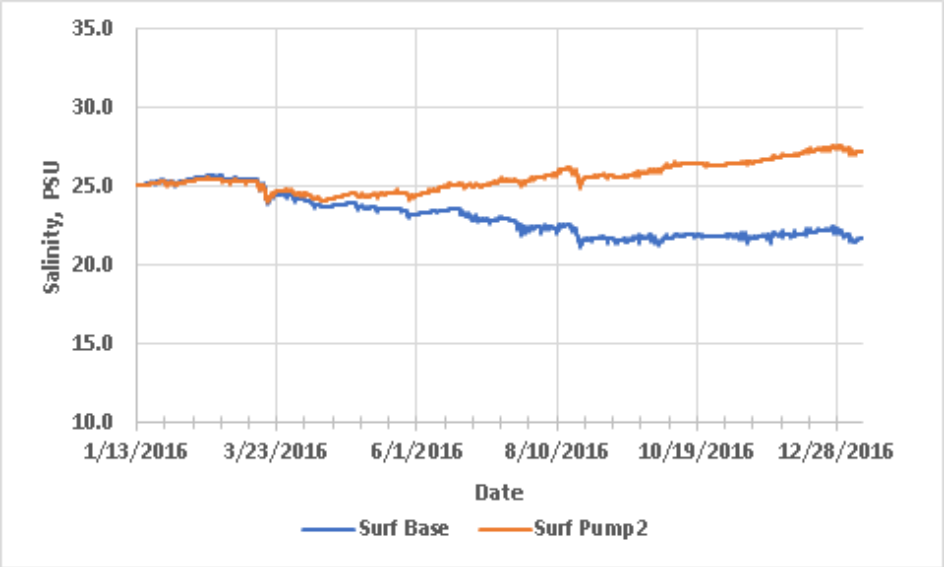

Figure 4-42. Predicted salinity in the surface model layer at station PAFB2 compartment for the base case and the Pump 2 case.

Predicted water temperature also includes the effects of hypothetical inflows at Pump 2. Predicted water temperatures show some vertical stratification but are predicted to be minimally lower as a result of pumping. Predicted water temperature values in the surface model layer at station PC1 directly are fractionally lower by 0.4 °C in the Pump 2 case (Figure 4-43). Approximately 10 km to the south at Station PAFB1 predicted water temperature in the surface model layer is on average 0.2 °C lower compared to the base case (Figure 4-44).

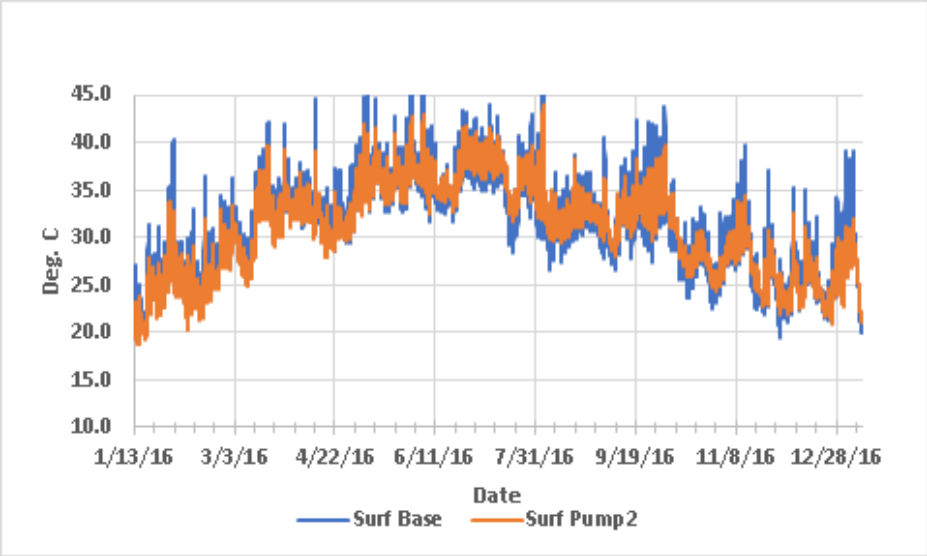

Figure 4-43. Predicted water temperature in the model surface layer at station PC1 for the base case and the Pump 2 case.

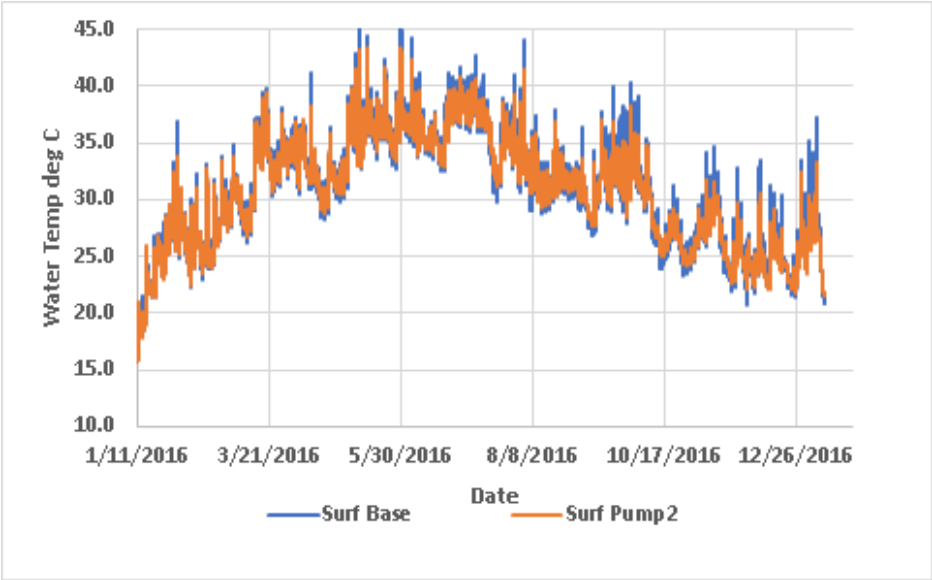

Figure 4-44. Predicted water temperature in the model surface layer at station PAFB2 for the base case and the Pump 2 case.

4.4.6 *Port Canaveral Weir Structure*

The location of the hypothetical weir is shown in Figure 4-45. Within the model setup the weir is specified as being 100 feet wide from east to west and controlled by an input file consisting of a series of specified one-way flows across the weir, with flow rates governed by the water level elevation above the weir crest. Flows rage from zero when the water elevation is at or below the crest of the weir to a maximum of 60 m^3/s when the water level is 0.5 m above the weir crest. At higher water levels the flows are specified to be reduced to zero. The weir control input file can be adjusted for alternative flow rates and weir sizes.

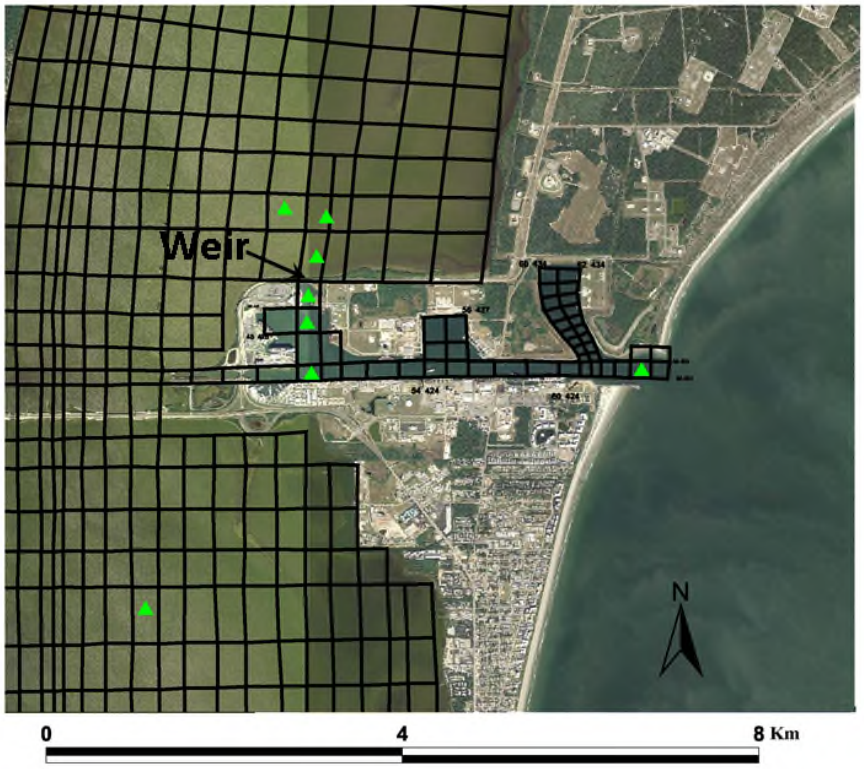

Figure 4-45. Weir location at Port Canaveral

A sequence of comparisons of tracer concentration in the surface layer of the model is shown in Figure 4-46 through Figure 4-49. At 50 days the tracer in the northern compartments of the Banana River are reduced by 35% to 55%, whereas in the south compartments, tracer concentrations are reduced by 10% to 20%. This compares with the base case in which tracer concentrations throughout most of the Banana River are above 90 ppt. After 100 days of simulation, predicted tracer concentrations in the north compartments are reduced by 50 to 60% and by 30 to 40% in the south compartments of the Banana River (Figure 4-47). Under the base case tracer concentrations are above 90 ppt over most of the Banana River. At 200 days into the Weir based model run, tracer concentrations in the Banana River were predicted to be reduced by 55% to 70%. Predicted tracer concentration under the base case remained above 80 ppt in the north compartments and above 50% in the south compartments (Figure 4-48). After 365 days of model simulation predicted tracer concentrations in the Banana River for the Weir case were reduced by 75% to 85% within the central compartments and by about 65 to 70% in the south compartments (Figure 4-49). In the northern most compartment predicted tracer concentrations were reduced by 60% or more.

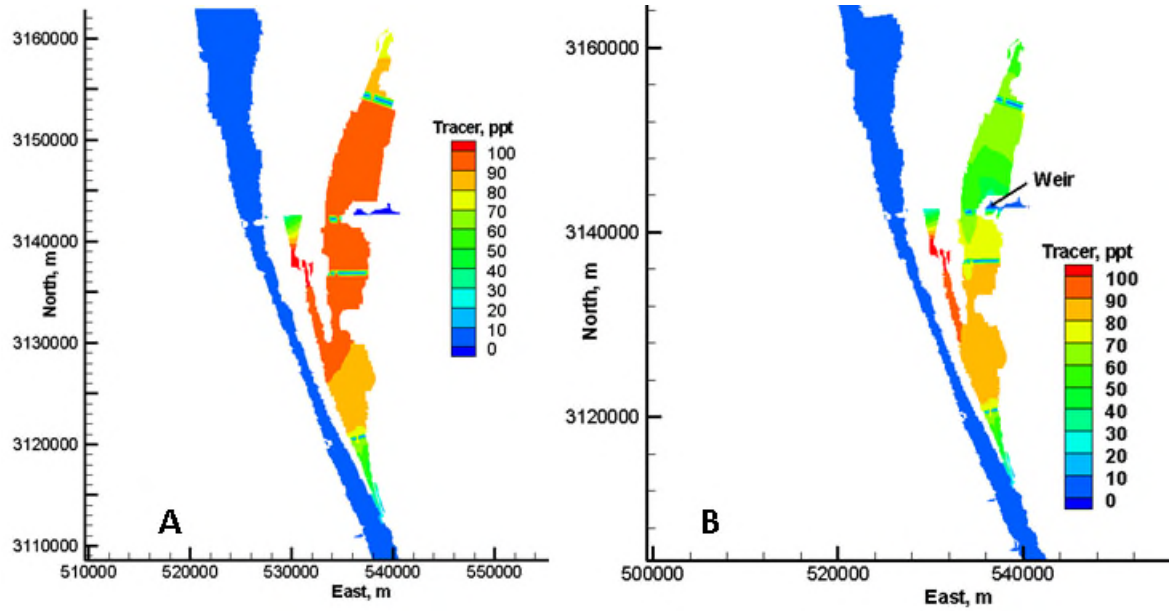

Figure 4-46. Predicted tracer concentration in the model surface layer after 50 days of simulation. The base case is shown in panel A and the Weir case is shown in panel B.

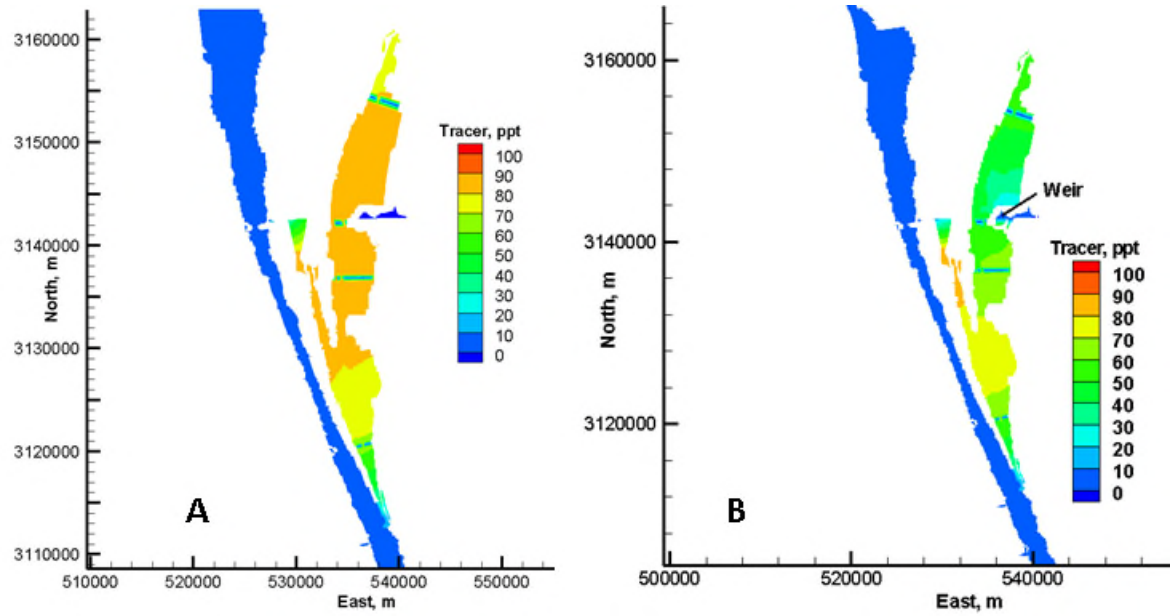

Figure 4-47. Predicted tracer concentration in the model surface layer after 100 days of simulation. The base case is shown in panel A and the Weir case is shown in panel B.

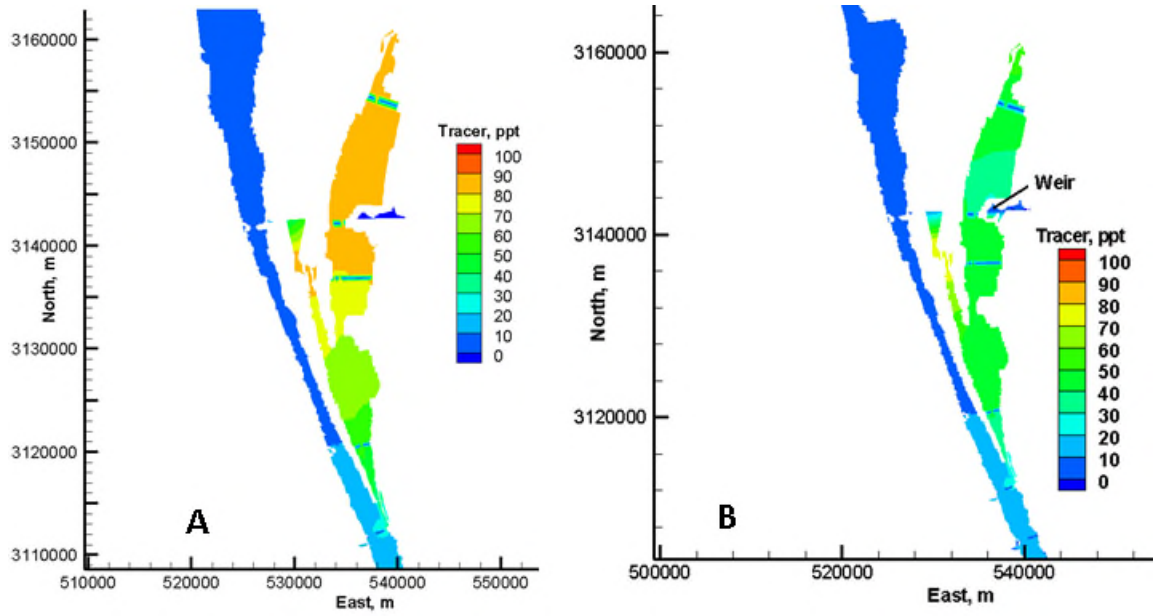

Figure 4-48. Predicted tracer concentration in the model surface layer after 200 days of simulation. The base case is shown in panel A and the Weir case is shown in panel B.

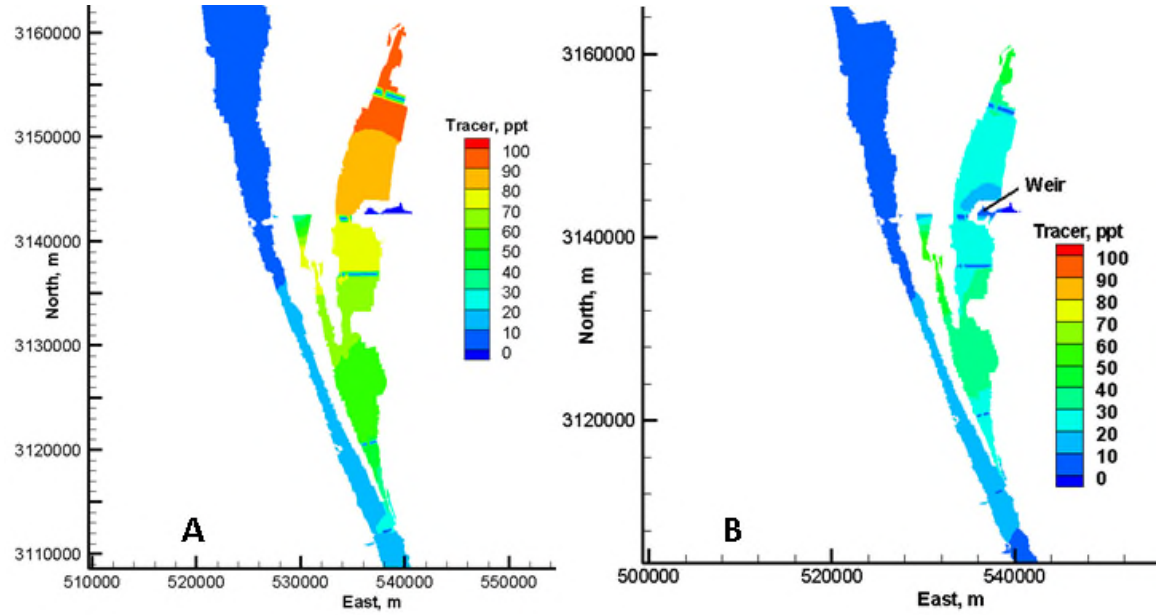

Figure 4-49. Predicted tracer concentration in the model surface layer after 365 days of simulation. The base case is shown in panel A and the Weir case is shown in panel B.

Predicted salinity values were also impacted by inflows specified by operation of the Weir. The model boundary condition for salinity that influences weir inflows was set by the HYCOM salinity data extracted closed to the outer entrance of Port Canaveral. At Station PC1, located just to the west of Port Canaveral, predicted salinity for the Weir case tracked about 10 PSU higher compared to the base case (Figure 4-50) and averaged about 35 PSU. At locations more distal from the immediate influence of Weir structure produced inflow the impact on salinity was lower. At station BR1, in the northernmost compartment of the Banana River, Weir influenced salinity

tracked about 5 to 7 PSU higher compared to the base case by the end of the 365 day simulation (Figure 4-51).

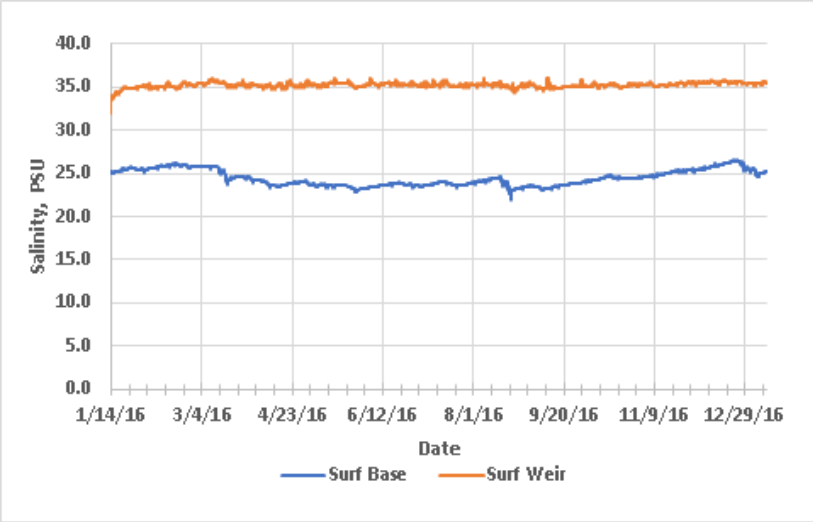

Figure 4-50. Predicted salinity in the surface model layer at station PC1 adjacent to Port Canaveral and Weir inflows for the base case and the Weir case.

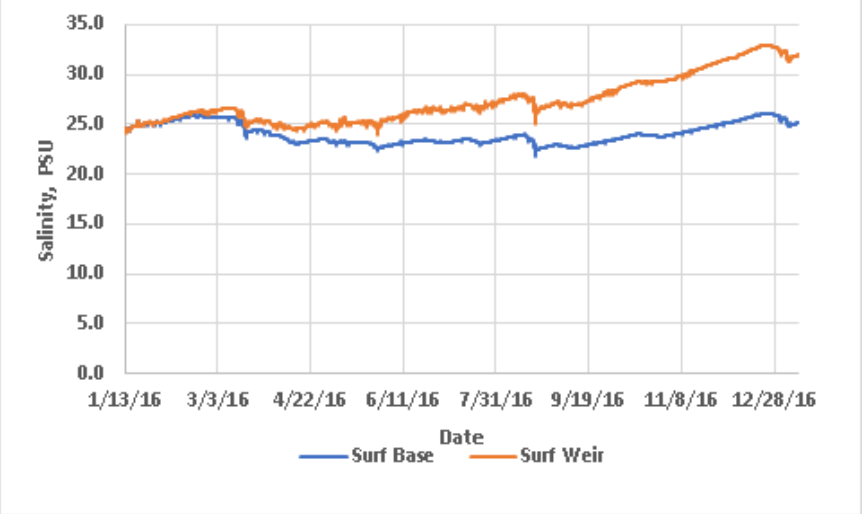

Figure 4-51. Predicted salinity in the surface model layer at BR1 for the base case and the Weir case.

Predicted water temperatures throughout the Banana River were more uniform and were predicted to be on the average lower by about 0.2 °C compared to water temperatures under the base case (Figure 4-52). However, similarly to the Pump 1 case the influence of the weir inflows is more apparent at station PC 1, where predicted water temperatures tracked lower by an average of about 3 °C under the Weir case (Figure 4-53).

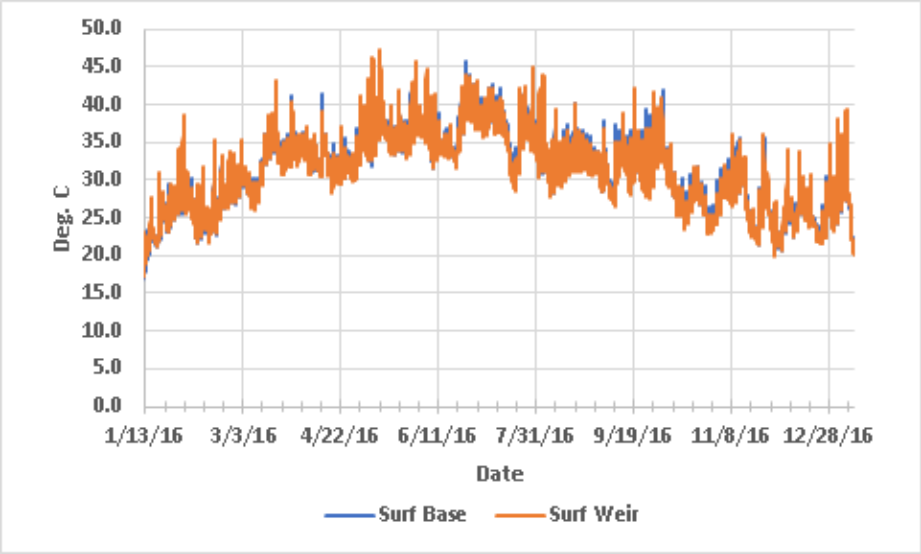

Figure 4-52. Predicted water temperature in the model surface layer at station BR1 in the north Banana River compartment for the base case and the Weir case.

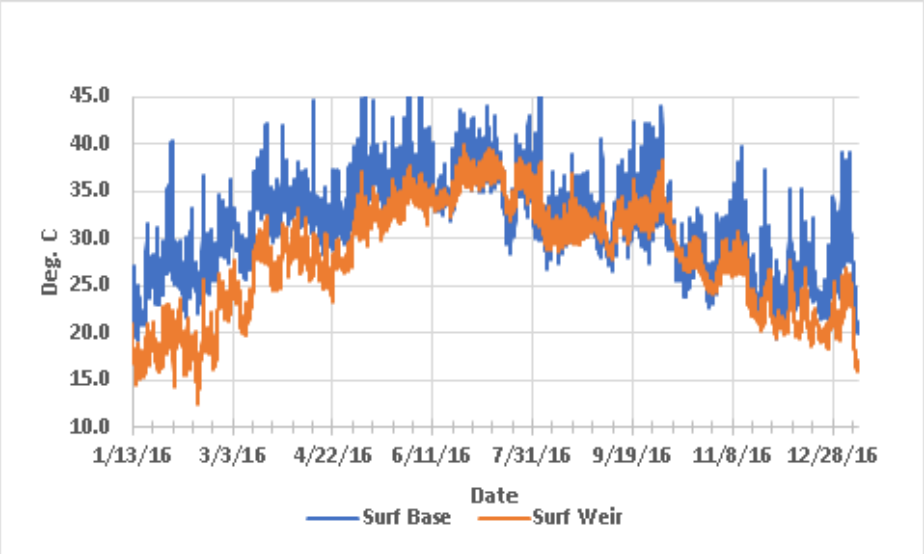

Figure 4-53. Predicted water temperature in the model surface layer at station PC1, adjacent to the Weir inflows for the base case and the Weir case.

4.4.7 *Pump Station 3: Bethel Creek*

The Bethel Creek area is shown in Figure 4-54 including the monitoring stations used to capture individual time series of data. An inflow rate of 5 m^3/s was specified at the Pump 3 location.

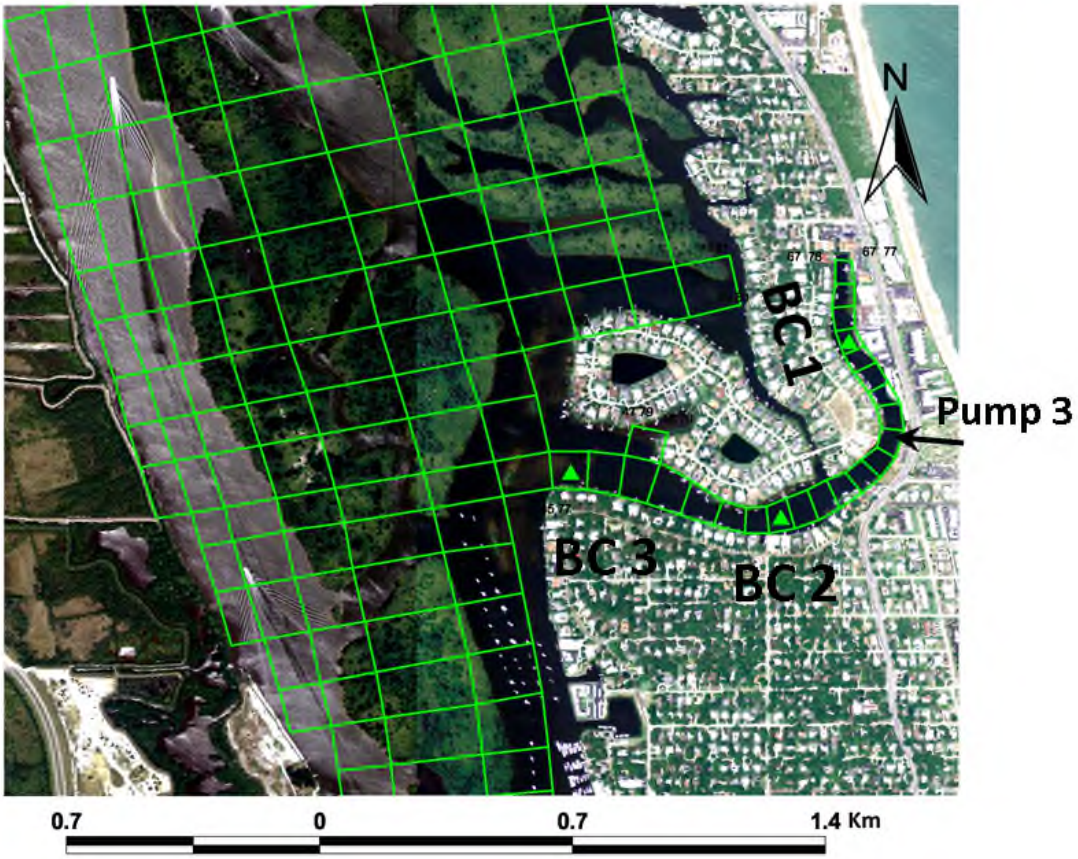

Figure 4-54. Location of Pump 3 in Bethel Creek along with three numerical monitoring stations.

Figure 4-55 through Figure 4-58 show a sequence of predicted tracer concentration in Bethel Creek and vicinity. The sequence extends out to 30 days and shows that tracer concentration in Bethel Creek rapidly declines under both the base case and the Pump 3 case. However, in the Pump 3 model test declines are more rapid, especially within the Creek. After 3 days of simulation, the tracer can be seen exiting the Creek and spreading both north and south along the main estuarine body of the IRL under both the base case and the Pump 3 case. Tracer concentration in Bethel Creek under the base case remained above 90 ppt but is reduced about 50% within Bethel Creek as result of pumping of sea water (Figure 4-55). After 10 days tracer concentration in Bethel Creek is at or below 30 ppt under the Pump 3 case compared to concentrations of about 50 ppt or greater for the base case (Figure 4-56). The tracer can be seen exiting and spreading in the adjacent IRL. After 20 days of model simulation tracer concentration in Bethel Creek is 10 ppt or less in the Pump 3 case , and under the base case tracer concentration in Bethel Creek is between 10 and 20 ppt (Figure 4-57). Finally, after 30 days on simulation the numerical tracer concentration in Bethel Creek is less than 10 ppt for both cases and extends into the IRL estuarine channel at low concentrations (Figure 4-58).

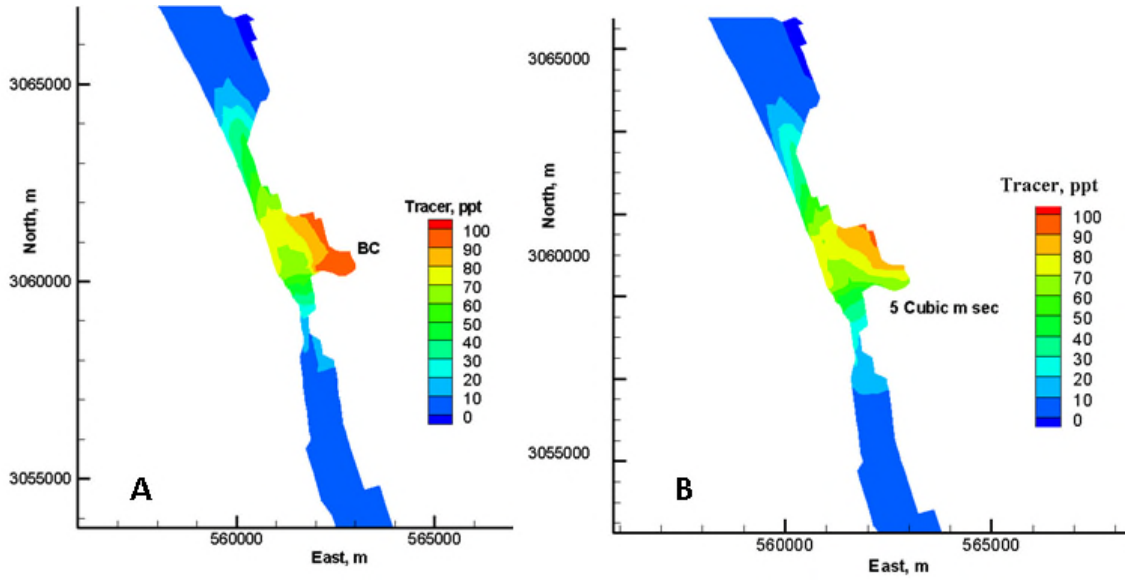

Figure 4-55. Predicted tracer concentration in the model surface layer at station BC2 after 3 days of simulation. The base case is shown in panel A and the Pump 3 case is shown in panel B.

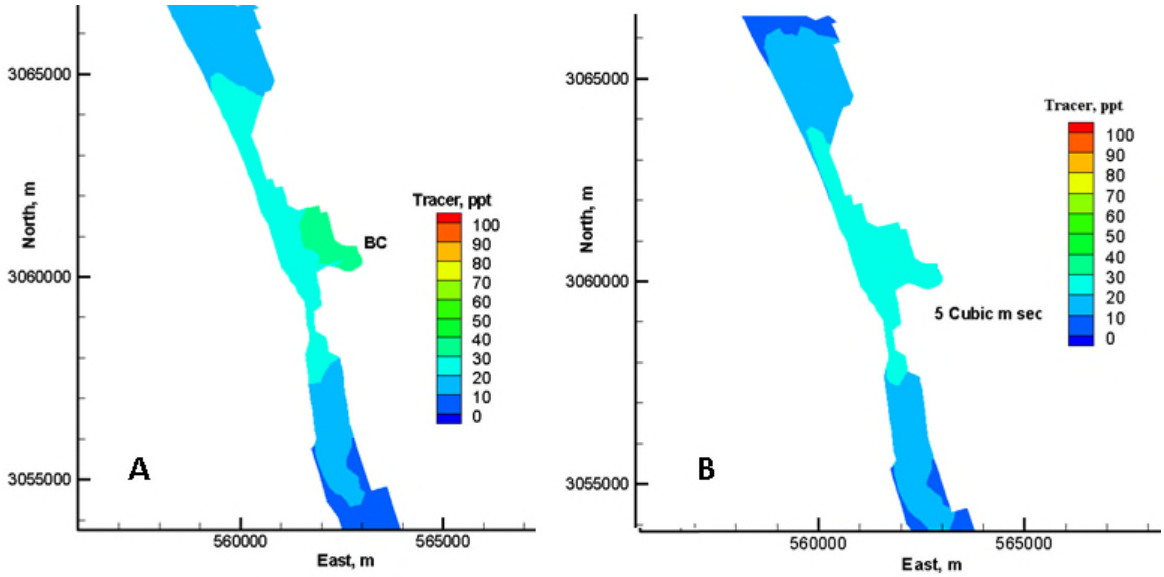

Figure 4-56. Predicted tracer concentration in the model surface layer at station BC2 after 10 days of simulation. The base case is shown in panel A and the Pump 3 case is shown in panel B.

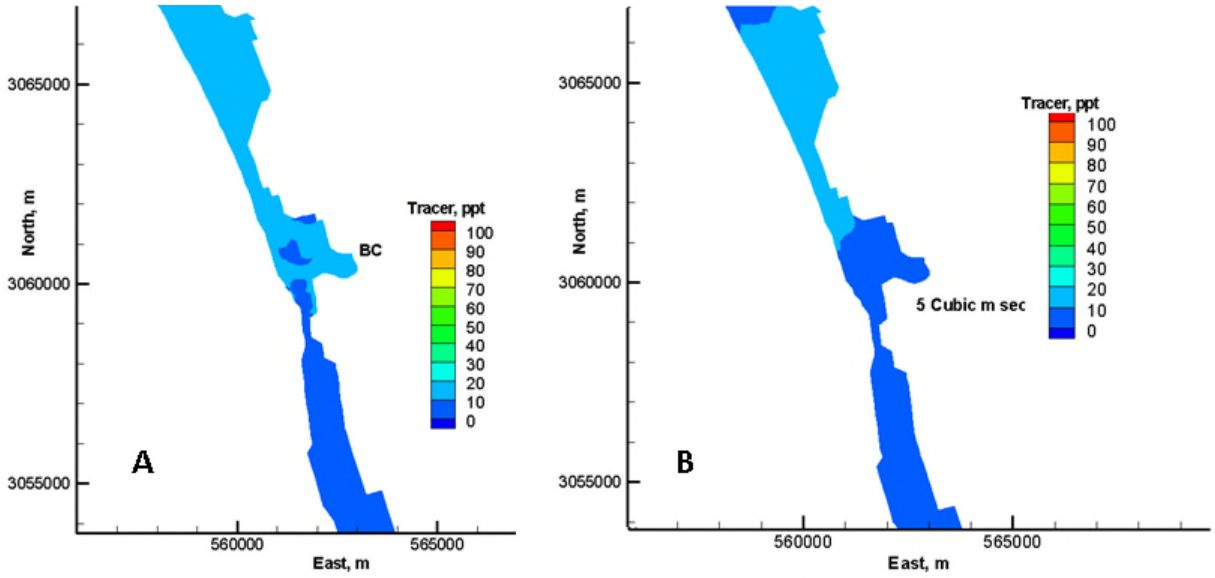

Figure 4-57. Predicted tracer concentration in the model surface layer at station BC2 after 20 days of simulation. The base case is shown in panel A and the Pump 3 case is shown in panel B.

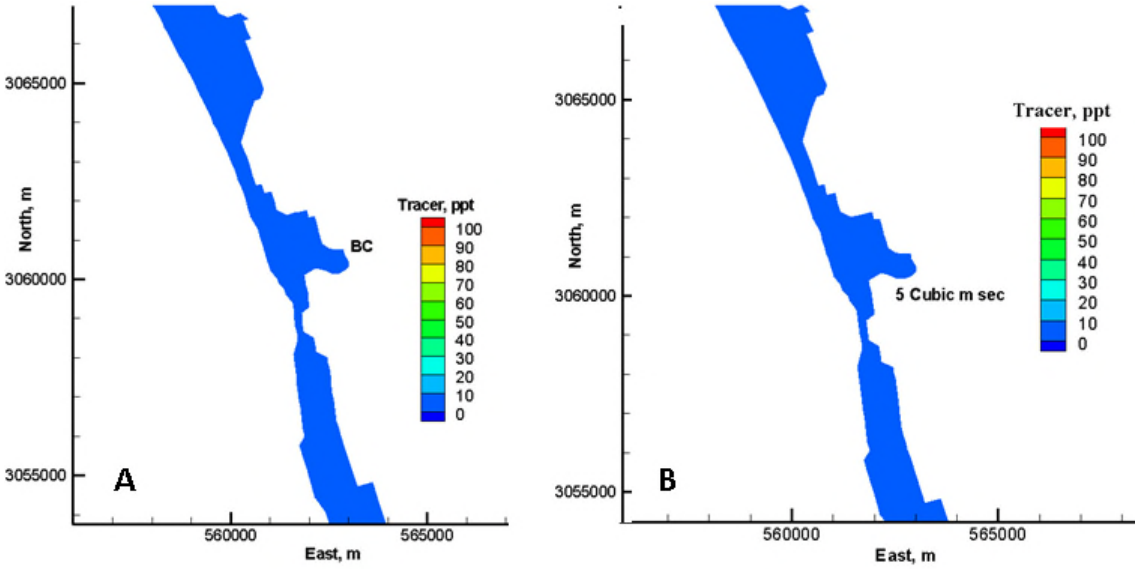

Figure 4-58. Predicted tracer concentration in the model surface layer at station BC2 after 30 days of simulation. The base case is shown in panel A and the Pump 3 case is shown in panel B.

Although tracer concentrations are low for both cases tested in Bethel Creek, it can be seen in Figure 4-59 that concentration under the Pump 3 case are about 2 ppt lower compared to the base case. The predicted salinity record at station BC2 shows that after a year of simulation, salinity under the Pump 3 case is about 3 to 4 PSU higher compared to the base case. This can be attributed to higher salinity in the coastal ocean that was represented by HYCOM salinity data, which was applied as a boundary condition for water moving though Pump 3 (Figure 4-60). Likewise, predicted water temperature under the Pump 3 case is fractionally lower compared to

the base case due to the water temperature boundary condition applied to Pump 3, which again is derived from HYCOM (Figure 4-61).

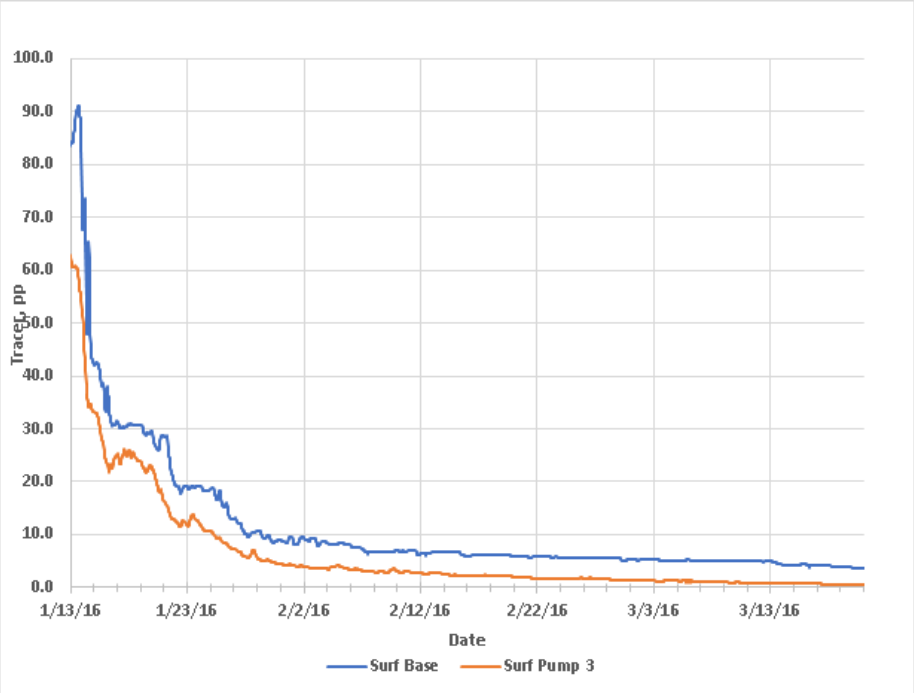

Figure 4-59. Predicted tracer concentration at station BC 2 during the first 60 days of the simulation where the base case is compared with the Pump 3 case.

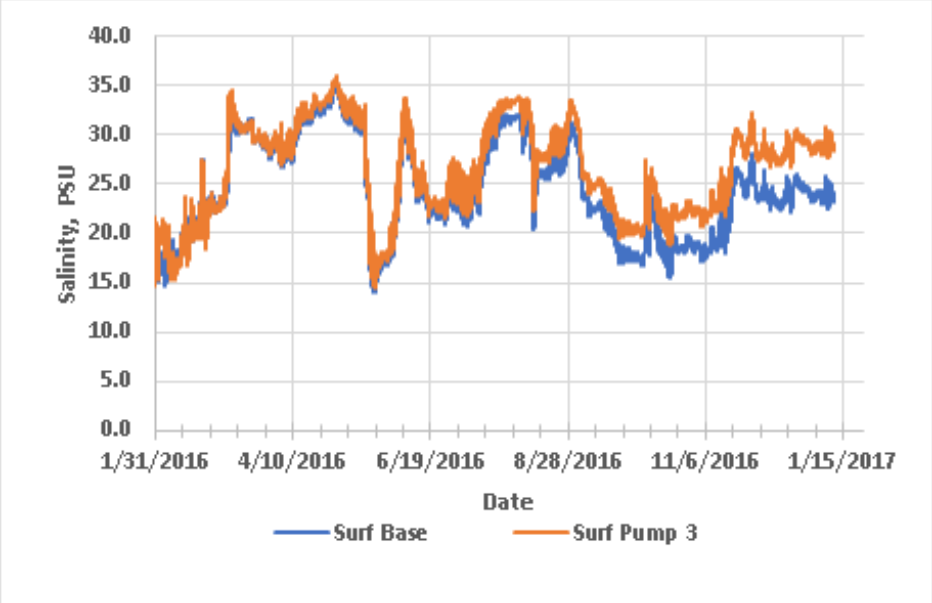

Figure 4-60. Predicted salinity in the model surface layer at station BC2 in Bethel Creek for the base case and the Pump 3 case.

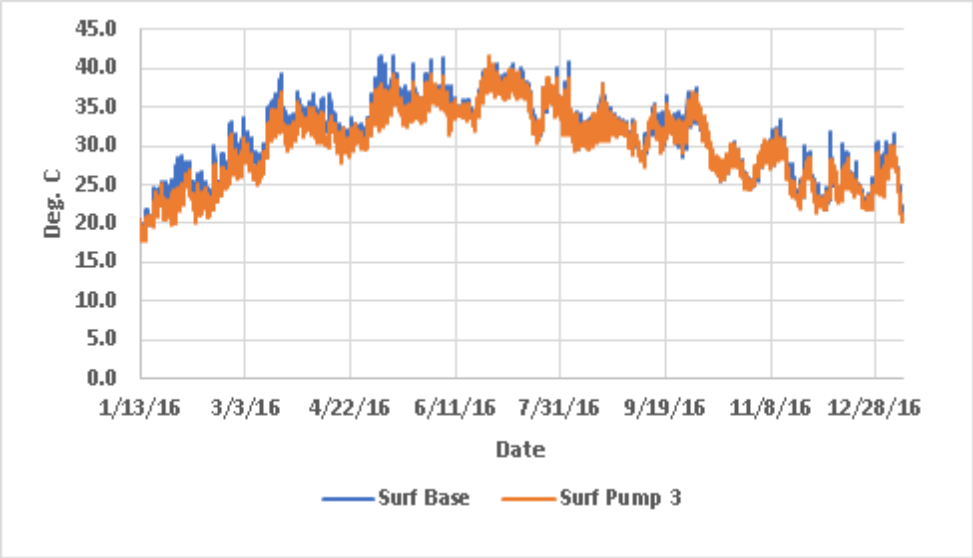

Figure 4-61. Predicted water temperature in the model surface layer at station BC1 in Bethel Creek for the base case and the Pump 3 case.

4.5 Conclusions: Numerical Modeling of Enhanced Flow

The potential impacts of enhanced inflow of coastal ocean water into selected portions of the Banana River, along with Bethel Creek in Indian River County were examined through the application of the EFDC model. Boundary conditions were derived from a variety of sources consisting of a combination of measured data and data from the ADCIRC and HYCOM ocean models. Inflow tests were set at three location in the Banana River to promote water exchanges with the larger IRL basin. In Bethel Creek, a single pump location was positioned to promote flushing.

Model results in the Banana River according to the location and magnitude of water inflows. The Pump 1 station, located in the vicinity of PAFB, produced a notable reduction in tracer concentration in the south compartment of the River where tracer concentrations were lower by 65% to 75% at the end the 365-day model run. This compares to a tracer reduction in the south compartment of the Banana River of about 40% under the base case. The ability of the Pump 1 case reduce tracer concentration and exchange water out of in the north compartments of the Banana River was less effective. Here, predicted tracer concentrations remained above 80 ppt until the close of the model simulation at 365 days.

The Pump 2 case assessed the potential result of pumping 10 $m^{3/}$s into the Banana River at a location just north of Port Canaveral. Due to the location of Pump 2 well north of Pump 1, the potential for flushing of tracer out of a large portion of the Banana River was much greater. By the end of the model simulation tracer concentration in most compartments of the Banana River were reduced by 60% to 75%.

The hypothetical weir structure located within Port Canaveral is predicted to have the greater potential for exchanging water out of the Banana River over shorter a period of time compared to the two pump scenarios. At the end of the model simulation tracer concentration in the central to north central compartment of the Banana River was 70% to 85% lower compared to tracer concentration not reduced by more than 20% under the base case. The adjoining Banana River

compartments to the north and south of the central section were characterized by predicted tracer concentrations of up to 65%.

Model predictions indicate some impact on the salinity regime from both the pump cases and the hypothetical weir. These impacts were characterized by local increases in salinity of up to 5 PSU proximal to the pumps and up to 10 PSU in areas proximal to the weir inflows. Predicted impacts on the salinity regime were reduced with distance from the inflow locations. Potential impact on estuarine water temperature are indicted to be low including only a fractional decline in salinity at most locations that are influenced by cooler ocean water.

The Bethel Creek model test shows that the rate of water exchange between the creek and the adjacent estuarine change of the IRL is relatively rapid, being completed in 30 days or less. However, hypothetical pumping of ocean water directly in the creek at a rate of 5 m^3/s was predicted to increase the rate of complete flush flushing by a few days. Potential impacts on local salinity and water temperature were to be minimal as a result of the pumping scenario at Bethel Creek.

5 Inflow Structure Design

The team has draft designs of three structures: two pipe and pump structures and a weir structure. The designs are formulated around the flow parameters selected earlier in the project. The pilot-scale flow rate is set to a minimum of 5 m^3/s and the potential permanent full-scale system flow rate is set to a minimum of 20 m^3/s Each concept is focused on controlled inflow of ocean water into the Banana River. By only allowing one-way flow of water into the IRL, a hydraulic head is formed, thus creating a net transport in the Banana River and IRL toward the inlets, where the water exits the IRL having mixed with the tidal prism. The structures must be manageable, consisting of pumps and/or gates to restrict the exchange of water, should there be indication of poor water quality in the coastal ocean (e.g. harmful algal blooms, chemical spill, low dissolved oxygen, etc.). Additionally, there are times of the year when the water levels along the Florida Shelf are elevated due to the intra-annual fluctuations. During these months, late September through mid-December, the inflow could be restricted. A gated structure or flow control pumps would allow for this level of control.

5.1 Draft Design 1: Temporary Inflow Pilot System and Permanent Full-Scale System Pipe and Pump Options

Design 1 is a pipe and pump structure drilled under the barrier island and beneath the coastal ocean. Such a structure is similar to the Destin Harbor project or the St. Lucie Power Plant coolant intakes. This design was selected because it can be implemented at a wide range of geographic locations. Burying the inflow pipe will cause minimal disturbance of critical infrastructure. The footprint on the surface is minimal, only needing a pump house where the ocean inflow pipe and lagoon outflow pipe are joined by the pump. This also gives a location for access and servicing of the pipe for periodic cleaning. Though we highlight a specific location for our proposed design, the design and cost estimates can readily be extrapolated to any alternate location.

5.1.1 *Site Location*

The primary site chosen for the pipe and pump structure for the IRL inflow project is north PAFB located in Brevard County. Situated at 28°16’16” N, 80°36’26” W, the north section of PAFB is a relatively thin stretch of land with minimal permanent structures. The Atlantic Ocean meets the land from the east while the Banana River borders the land on the west; the Banana River ultimately deposits water into the Indian River Lagoon. Figure 5-1 is an aerial view from PAFB to Cocoa Beach with an arrow pointing to the site location.

The maximum elevation seen in the proposed location is approximately 4 m near the dune, with the majority of the land elevation being 2 m (referenced to World Geodetic System 1984 [WGS84]). The distance over land from the lagoon to the ocean is approximately 300 m (984 feet), including the dune and the beach. A close-up of the chosen location is provided in Figure 5-2.

Highway A1A, a main travel route for citizens living on the island, runs parallel to the coastline almost in the center of the selected site.

Figure 5-1: PAFB to Cocoa Beach aerial map (Google Earth 2019)

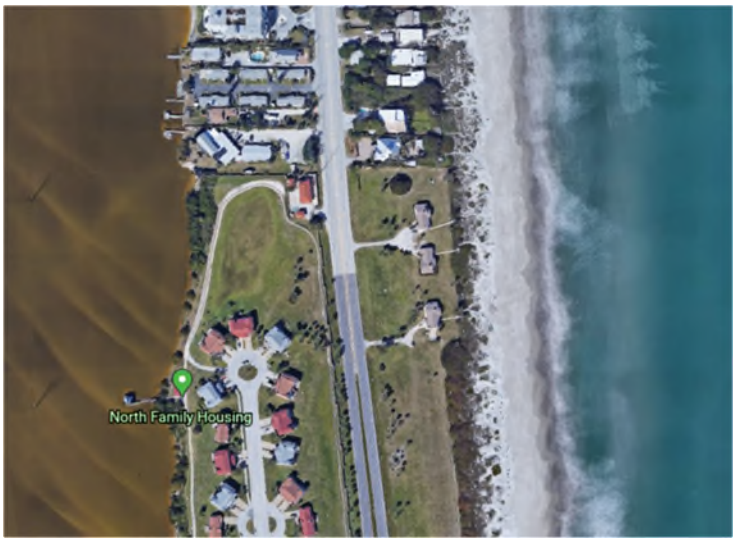

Figure 5-2: North PAFB aerial map (Google Earth 2019)

5.1.2 *Site Plots*

The bathymetry is needed when determining how far into the ocean the pipe needs to go so it does not disrupt sediment transport. Figure 5-3 shows the bathymetry plot of the Atlantic Ocean side near the design site. Soundings on the plot are in feet.

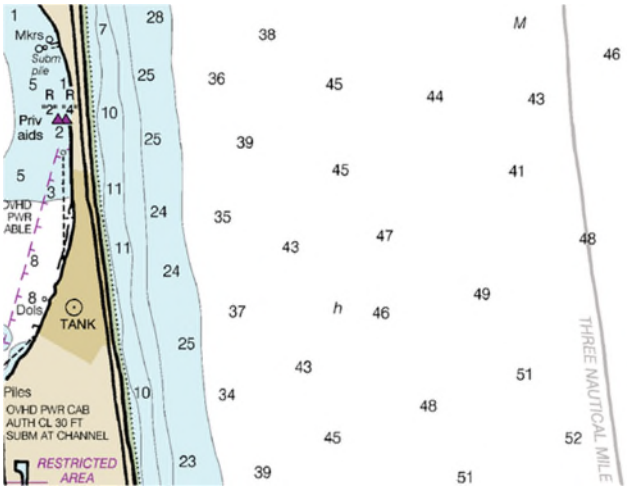

Figure 5-3: Bathymetry plot of Atlantic Ocean near PAFB (NOAA 2020)

It was determined that an appropriate depth for the intake portion of the pipe, located in the ocean, would be around 12 m (40 feet). This depth would allow the top of the riser to be low enough in the water column to reduce the forces during storm events; it also would prevent the coastline's natural processes from being disturbed. From the map, the ocean reaches a depth of 12 m at about 2,000 m (6,562 feet) offshore.

The bathymetry is also needed for the Banana River to determine where the pipe will be able to surface from underground to release water into the river. Figure 5-4 is a bathymetry plot of the Banana River near the design site.

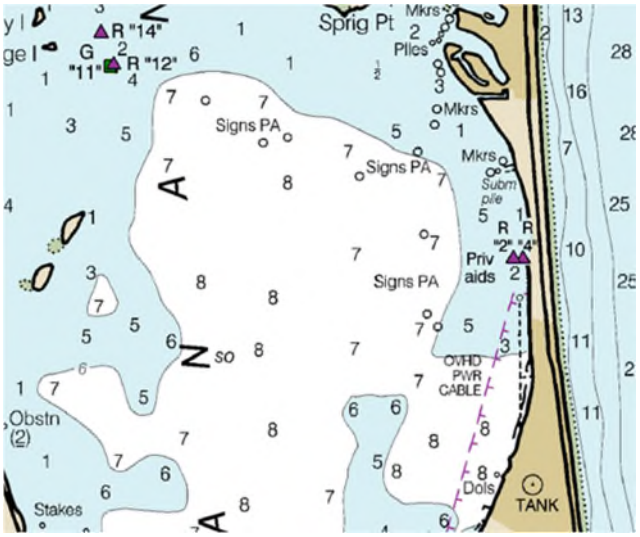

Figure 5-4: Bathymetry plot for Banana River near PAFB (NOAA 2020)

The depth of the Banana River is much shallower than the ocean, and it ranges from 0.3 m to 1.5 m (1 to 5 feet) along the coast. The pipe will extend into the river close to 100 m (328 feet) where the depth is 1.5 m (5 feet).

5.1.3 *Design Summary*

The design is proposed to be a pipeline that has an intake in the Atlantic Ocean and an outfall in the Banana River. There were two different design approaches taken during the design process, one utilizing only tidal energy and gravity to propel the water and the other utilizing a pump house with a pump to drive the water flow. In both designs, the pipe is to be drilled underneath the land so that there is no disturbance to Highway A1A or any existing infrastructure. The drilling distance from one side of the land to the other is 300 m (984 feet). The pipe will then continue to be drilled/ trenched into the Atlantic 2,000 m (6,562 feet) offshore and into the Banana River 100 m (328 feet) from the coast.

For the installation of the pipeline, a trenchless method is needed so that the structures already present on land are not disturbed, such as Highway A1A and houses. Initially, horizontal directional drilling (HDD) was looked at as the method of drilling; however, it was determined the diameter and length of the drill are too great for HDD machines. Micro-tunneling is a more feasible option because it is used for large diameter pipes and would be able to drill an outer diameter of up to 3.7 me (12 feet).

The flow calculations in this section are based on a head value of 0.5 m (1.64 feet), representing the difference between the Banana River and the Atlantic Ocean water levels. On the ocean side, the average maximum sea surface elevation from the closest NOAA tide gauge, Trident Pier station, is approximately 0.80 m (2.62 feet). In the Banana River, long-term water level gauges measured a seasonal average high-water elevation of approximately 0.3 m (0.98 feet). The 0.5 m (1.64 feet) value used for the calculations is a conservative estimate for the average maximum head.

5.1.3.1 No Pump Option

For the no pump option, the pipe would need to be drilled a total of 2,400 m (7,874 feet) horizontally underground before surfacing at each side. The pipe would be met with an intake structure in the Atlantic and an outfall structure in the Banana River.

For a temporary inflow pilot system, assuming a head of 0.5 m as indicated above, to reach a flow of 5 m^3/s (177 cubic feet per second [ft^3/s]), the inner diameter of one pipe would need to be 2.92 m (9.58 feet). If two pipes were drilled next to each other, each pipe would need to have an inner diameter of 2.20 m (7.22 feet) to reach the flow of 5 m^3/s. An aerial view of the design for the temporary inflow pilot system, including two pipes with inner diameters of 2.20 m, is provided in Figure 5-5.

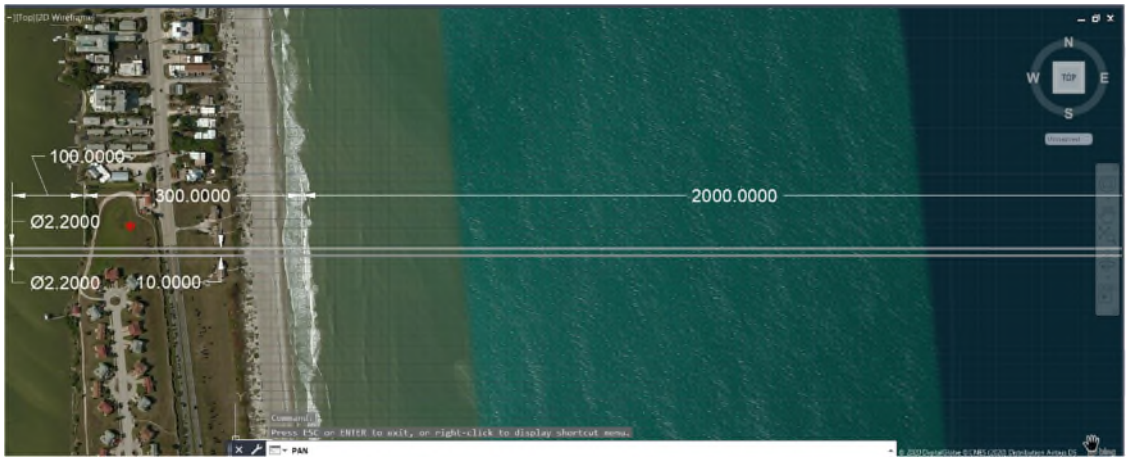

Figure 5-5: Temporary inflow pilot system two pipes no pump (Google Earth 2019)

For a permanent full-scale system design, assuming a head of 0.5 m as indicated above, to reach a flow of 20 m^3/s (706 ft^3/s), the inner diameter of one pipe would need to be 5.12 m (16.80 feet). If two pipes were drilled next to each other, each pipe would need to have an inner diameter of 3.86 m (12.66 feet) to reach the flow of 20 m^3/s. Figure 5-6 is an aerial view design for the permanent full-scale project, including two pipes with inner diameters of 3.86 m.

Figure 5-6: Potential permanent full-scale system two pipes no pump (Google Earth 2019)

Due to the extremely large diameter of pipeline needed to achieve the desired flow rates for the temporary inflow pilot system and full- scale design, it was determined that the no pump option would not be feasible.

5.1.3.2 Pump Option

For the pump option, the pipe would still need to be drilled a total of 2,400 m (7,874 feet) horizontally underground; however, it would surface on the land portion of the drill to connect each side of the pipe to a pump house. The pipe would be met with an intake structure in the Atlantic and an outfall structure in the Banana River.

For a temporary inflow pilot system, to reach a flow of 5 m^3/s (177 ft^3/s), the inner diameter of one pipe would need to be 1.86 meters (6.10 feet) when using a 200-horsepower pump. If two pipes were drilled next to each other and two 200-horsepower pumps were used, each pipe would need to have an inner diameter of 1.24 m (4.07 feet) to reach the flow of 5 m^3/s. A side view design for the temporary inflow pilot system, including one pipe with inner diameter of 1.86 meters is provided in Figure 5-7 (top to bottom: a) Banana River Section, b) Land Section, c) Ocean Section, and d) Ocean Section Termination.

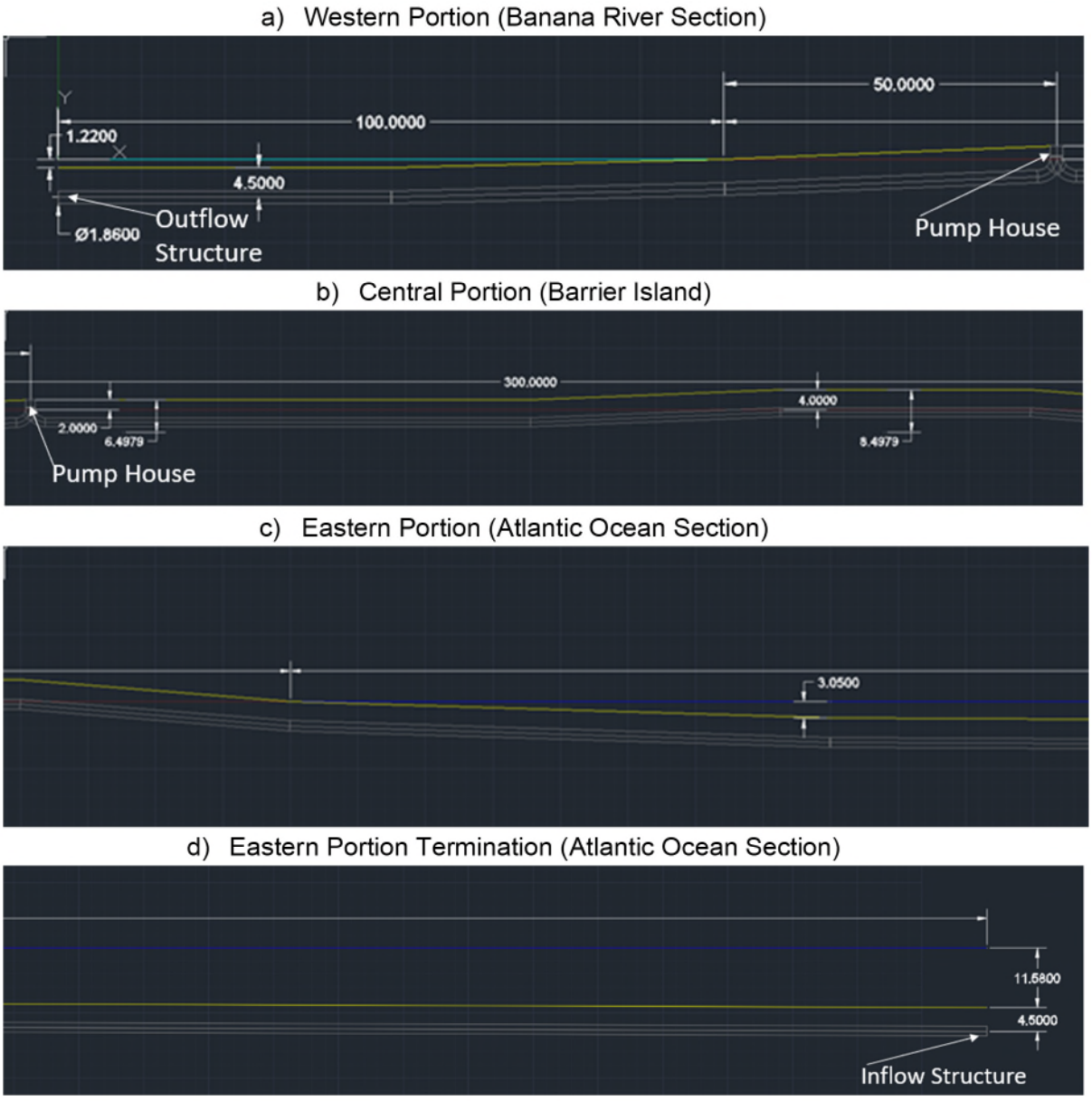

Figure 5-7: Temporary inflow pilot system side view with pump split into four sections: a) western, b) central, c) eastern, and d) eastern termination. Outflow, inflow, and pump house locations are indicated, but the structures are not shown.

For a potential permanent full-scale system, to reach a flow of 20 m^3/s (177 ft^3/s), the inner diameter of one pipe would need to be 3.26 m (10.70 feet) when using a 200-horsepower pump. If two pipes were drilled next to each other and two 200-horsepower pumps were used, each pipe would need to have an inner diameter of 2.18 m (7.15 feet) to reach the flow of 20 m^3/s.

5.1.4 *Cost Estimate*

Cost estimates for the temporary inflow pilot system and potential permanent full-scale system pipe and pump option are provided. For both designs, micro-tunneling will be the chosen method of installation for the pipeline. Costs are based on estimates provided by Laney Directional Drilling and are representative within +/- 50% depending on the geology, time of year, pipe composition, site restrictions, dewatering required, and available marine support. These costs do not include permitting or annual maintenance costs.

5.1.4.1 Pilot scale

A high-level cost estimate was obtained from Laney Directional Drilling for the temporary inflow pilot system flowrate of 5 m^3/s with a single pipe, Table 5-1, and a double pipe, Table 5-2, system. Micro-tunneling would be used for both the ocean outfall and river outfall portions. The pipe diameters were rounded to the nearest standard pipe dimension.

Table 5-1: Single pipe and pump temporary inflow pilot system cost estimate (5 m^3/s)

Item	Details	Quantity	Units	Per Unit Cost	Total Cost
Ocean Outfall Portion	Diameter = 1.86 meters (74"), Length = 2,000 meters (6,562 feet)	1	Each	$50,000,000.00	$50,000,000.00
River Outfall Portion	Specs: Diameter = 1.86 meters (74"), Length = 400 meters (1,312 feet)	1	Each	$8,000,000.00	$8,000,000.00
Pump	SJP 48PO-1	1	Each	$1,250,000.00	$1,250,000.00
Total +/-50%	**-**	**-**	**-**	**-**	**$59,250,000.00**

Table 5-2: Double pipe with double pump temporary inflow pilot system cost estimate (5 m^3/s)

Item	Details	Quantity	Units	Per Unit Cost	Total Cost
Ocean Outfall Portion	Diameter = 1.24 meters (48"), Length = 2,000 meters (6,562 feet)	1	Each	$35,000,000.00	$35,000,000.00
River Outfall Portion	Diameter = 1.24 meters (48"), Length = 400 meters (1,312 feet)	1	Each	$6,000,000.00	$6,000,000.00
Pump	SJP 48PO-1	2	Each	$1,250,000.00	$2,500,000.00
Total +/-50%	**-**	**-**	**-**	**-**	**$43,500,000.00**

Due to the high costs of large diameter micro-tunneling, the single pipe cost estimate is approximately 30% larger than the double pipe option.

5.1.4.2 Permanent Full-Scale System

Again, a high- level cost estimate was obtained from Laney Directional Drilling for the potential permanent full-scale system flowrate of 20 m^3/s with a single pipe system, Table 5-3. Micro-tunneling would be used for both the ocean outfall and river outfall portions. The pipe diameters were rounded to the nearest standard pipe dimension.

Table 5-3: Single pipe and pump permanent full-scale system cost estimate (20 m^3/s)*

Item	Details	Quantity	Units	Per Unit Cost	Total Cost
Ocean Outfall and River Outfall	Diameter = 3.26 meters (128"), Length = 2,400 meters (7,874 feet)	1	Each	$100,000,000.00	$100,000,000.00
Pump	-	1	Each	$1,250,000.00	$1,250,000.00
Total +/-50%	**-**	**-**	**-**	**-**	**$101,250,000.00**

5.2 Draft Design 2: Temporary Inflow Pilot System and Permanent Full-Scale Weir Options

The weir design is based on two studies (Saberi and Weaver 2015 and Zarillo 2018). The design is based on a gated, low-crested dam structure connecting the coastal ocean to the Banana River. Though this design option is the least expensive permanent full-scale structure with the most flexible flow rates, it is also the most restrictive geographically. Any structure constructed in the nearshore region will impact the littoral zone and affect the longshore sediment transport. For this reason, a new cut through the barrier island was not considered. Because the weir option needs to connect the coastal ocean and the lagoon directly, we sought a location where the coastal ocean and the lagoon are separated by a thin strip of land with minimal to no existing infrastructure. The impact on infrastructure and the effect on littoral transport guided our site selection.

A gated weir system would have a small footprint and versatile flow capabilities. Servicing and cleaning would not require divers and fouling is not as much of a concern as it is with the pipe and pump option.

5.2.1 *Site Location*

The primary site chosen for the IRL inflow project using a weir structure is inside of Port Canaveral near Canaveral Lock. Situated on the north side of the channel between the Lock and the 410 bridge, 28°24’33” N, 80°38’17” W, the proposed site does not contain any major roadways or interfere with existing infrastructure. The location also allows for a large range of influence since it would feed directly into the Banana River, enabling it to flush the Banana River and the IRL. Imagery of the chosen site location for the weir structure are provided in Figure 5-8 and Figure 5-9.

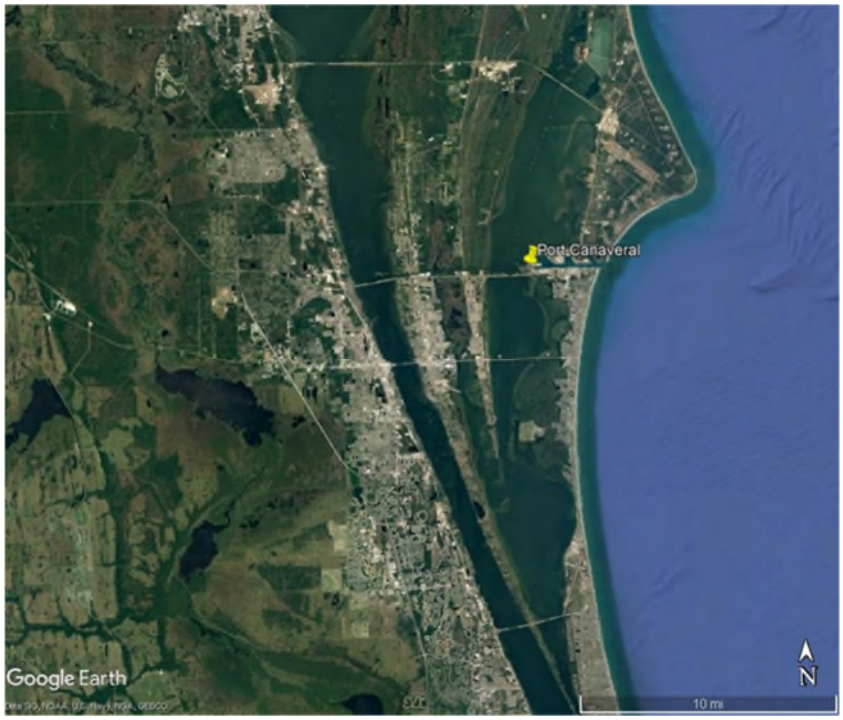

Figure 5-8: Port Canaveral aerial view (Google Earth 2019)

Figure 5-9: Canaveral Lock aerial view with proposed location for weir structure outlined in red (Google Earth 2019).

5.2.2 *Site Plots*

The depth near the structure on the port side and the Banana River side was determined using Navionics. The Port Canaveral Lock channel has an average depth of 12.5 feet in the center with a steep gradient towards the north and south banks. On the river side, the bottom slope is 0.03

with a gradual change in depth; the initial depth is 1 foot. On the north bank of the Port Canaveral Lock channel, dolphin structures, which are used as mooring devices, are present. Figure 5-10 is an image of the bathymetry for the proposed project location.

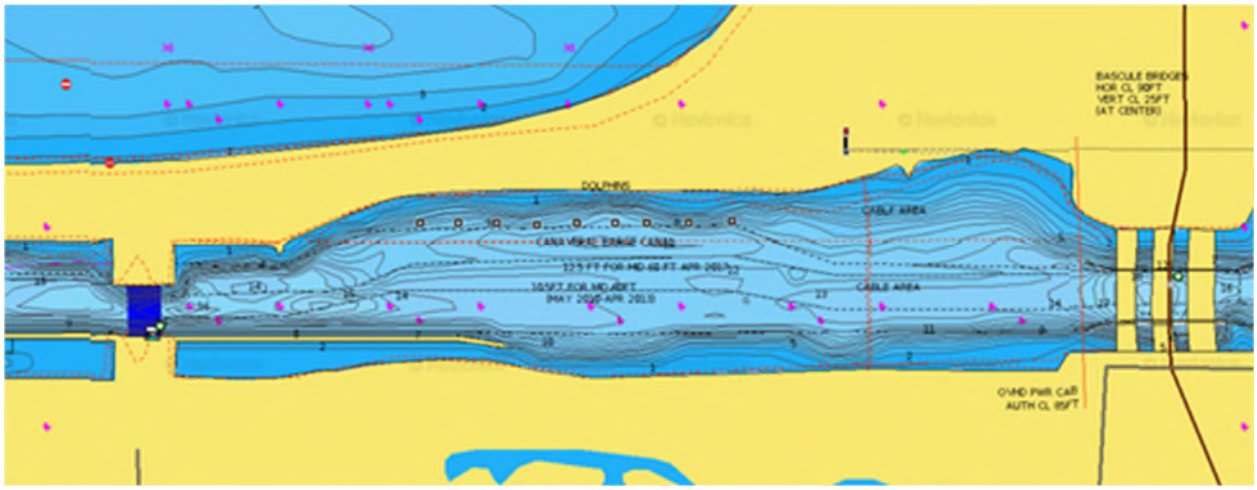

Figure 5-10: Bathymetry plot of Port Canaveral Lock (Garmin 2020)

5.2.3 *Design Concept*

A weir is a structure that governs the flow of water between two bodies of water. For this design, a rectangular passage was selected in order to maximize the flow rate. The geometry consists of a blunt front section and an angled aft slope.

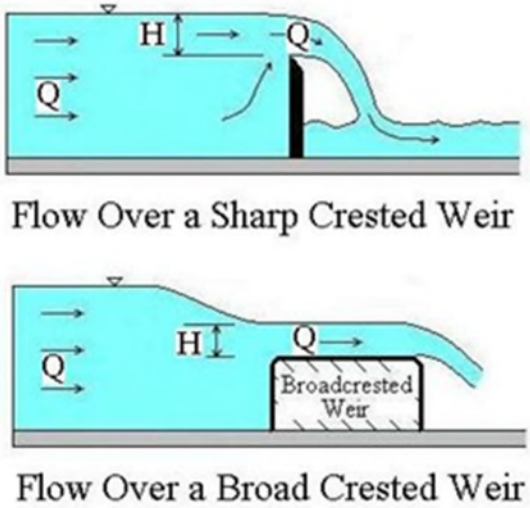

Figure 5-11: Sharp- crested vs. broad- crested weirs (Bengtson 2018)

A sharp- crested weir geometry, **Error! Reference source not found.**, was chosen due to the project location specifications. Based on long-term water level data in the Banana River, the weir height (w) was determined to be 0.30 m (0.98 feet) above mean sea level. This elevation takes into consideration the intra-annual water level fluctuations in the Banana River and is designed such that there is limited chance of the water level in the Banana River being higher than the crest of the weir, so the structure does not produce a backflow into the port. The weir head (h) was determined to change as the surface water elevation changes with the tides and can be found by

subtracting the weir height from the expected sea surface elevation above mean sea level in the port. The surface elevation plot at Trident Pier, Port Canaveral, Florida can be seen in Figure 5-12, taken from NOAA Tides and Currents. For calculation purposes, the average maximum sea surface elevation used was 0.80 m (2.62 feet) with the weir head calculated to be 0.50 m (1.64 feet).

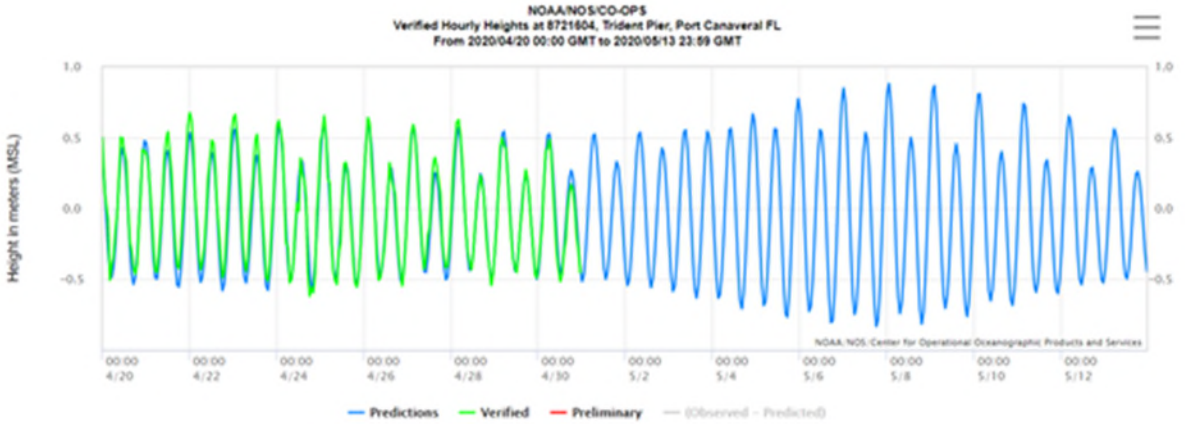

Figure 5-12: Trident Pier surface elevation plot (tidesandcurrents.noaa.gov)

The flow rate of a sharp- crested rectangular weir system is a function of the length of the weir, the head above the weir structure, and the discharge coefficient, given in the equation:

$$Q = \frac{2}{3} C_d b h \sqrt{2gh}$$

For h/w greater than or equal to 5, the discharge coefficient can be calculated using the equation:

$$C_d = 0.611 + 0.075 \frac{h}{w}$$

Since the h/w value was calculated to be 1.667, the discharge coefficient using this equation was found to be 0.736. Flow rates were calculated for several different weir lengths (b), and the results are displayed in Table 5-4. When dividing the flow rate of the weir by the weir length, an overall flow rate per meter length was calculated as 0.768 $m^3/s/m$.

Table 5-4: Flow rate for different weir widths

b, weir length (m)	Q_{weir} (m^3/s)
50	38.420
100	76.841
150	115.261
200	153.681
250	192.102
300	230.522
350	268.942
400	307.363

It was determined that a length of 250 m and greater (Table 5-4) would not be practical given the available length of the land where the weir would be placed. Additionally, the flow rates for the longer weir lengths are in excess of the flow rates desired for the potential permanent full-scale system. The remainder of the study will focus on weir lengths from 50 m to 250 m. When dividing the flow rate of the weir by the weir length, an overall flow rate per meter length was calculated as 0.768 $m^3/s/m$.

A weir rating curve, shown in Figure 5-13, was produced for each weir length with a weir crest height of 0.30 meters; the curve compares the flow rate of the weir at different water surface elevations.

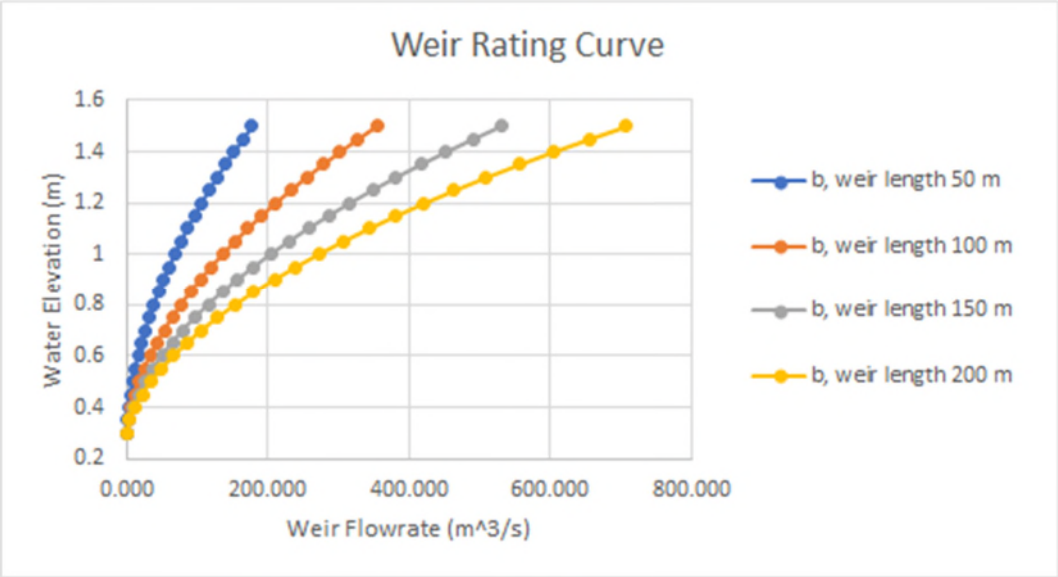

Figure 5-13 Weir flow rate vs. water elevation

Using the equations shown in Table 5-5 for each weir length, the water surface elevation can be entered as x and the equation would return the flow rate at that surface elevation.

Table 5-5: Weir flow rating equations

b, weir length (m)	Equation to return flowrate
50	$y = 99.95x^2 - 32.13x + 0.05$
100	$y = 199.91x^2 - 64.26x + 0.10$
150	$y = 299.86x^2 - 96.391x + 0.15$
200	$y = 399.81x^2 - 128.52x + 0.20$

Tidal elevation data from March 16, 2019 to March 15, 2020 were used to obtain an average yearly flow for each weir length. The verified elevation listed hourly was plugged into the equations in Table 5-5 to return the hourly flowrate; the hourly flowrate was then averaged for a yearly average flowrate and average flowrate per meter. The yearly average flowrate values and the maximum flowrate value are provided in Table 5-6.

Table 5-6: Average yearly flowrate

Weir Length (m)	50	100	150	200
Average Yearly Flowrate (m^3/s)	7.608	15.216	22.823	30.432
Average Yearly Flowrate per meter (m^3/s /m)	0.152	0.152	0.152	0.152
Maximum Hourly Flowrate (m^3/s)	117.593	235.189	352.780	470.373

Using a weir length of 200 m and weir head of 0.957 m (the maximum weir head predicted in the year range from March 16, 2019 to March 15, 2020) for the remainder of the calculations, the flow rate of water would be approximately 470.373 m^3/s.

The total pressure on the weir would be 104,647.022 Pa (15.177 psi) and was found by adding the static and dynamic pressure. The static and dynamic pressure equations are:

$$P_{static} = \rho g H + P_{atm}$$

$$P_{dynamic} = \frac{1}{2}\rho V^2$$

$$P_{tot} = P_{static} + P_{dynamic}$$

The total force on the weir due to the water must also be calculated and compared to the frictional force between the weir and the ground to ensure the weir will not move and fail. The total force was found to 6,446.004 kilonewtons (kN) (724.531 tons force) using the equation:

$$F_{tot} = P_{tot} b w$$

The crest width, used when calculating the mass of the structure, is adjusted so that the frictional force is greater than the total force. The minimum crest width for the weir was found to be 7.541 m, so a crest width of 7.750 m was used for the frictional force calculation. The frictional force was found using the equation:

$$F_f = N \mu_s$$

The resistance coefficient used was 0.6 and the normal force was calculated by multiplying the mass of the structure by gravity. The frictional force was calculated to be 6,568.776 kN (738.330 tons force), which is greater than the total force.

The weir would also be built with a flood gate system to ensure control over the flow; if the flow needed to be stopped at any time due to an emergency or maintenance, the gates would lower down into the water to seal the openings. Images of a similar gate system that would be used, Figure 5-14, are provided for reference. A front and side view of the proposed weir structure are shown in Figures Figure 5-15, Figure 5-16, and Figure 5-17. Actual gate dimensions would be determined during the final design phase.

Figure 5-14: Example weir gate system (Pxfuel 2020)

Figure 5-15: Weir structure front view

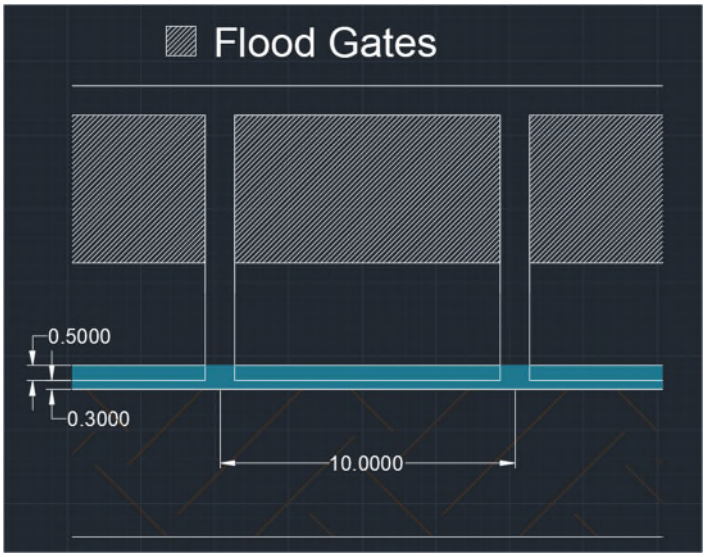

Figure 5-16: Weir structure close up

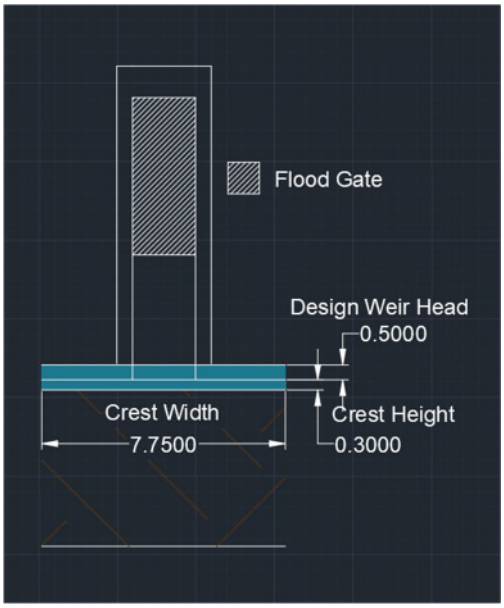

Figure 5-17: Weir structure side view

5.2.4 *Cost Estimate*

A study performed at Delft University analyzed eight existing structures and the associated cost of construction based on structure width, height, and head, (van der Toorn 2010). An average cost estimate was given as $55,600 (€30,000) per cubic meter; this price includes the basic weir structure. The cubic meter dimension is calculated by multiplying together the weir width, the weir height, and the weir head. Table 5-7 is a list of cost estimates for the weir structure with increasing weir lengths.

Table 5-7: Weir cost with varying lengths

b, weir length (m)	h, weir head (m)	w, weir height (m)	b*h*w (m^3)	cost/ m^3	cost
50	0.5	0.3	7.5	$55,600.00	$417,000.00
100	0.5	0.3	15	$55,600.00	$834,000.00
150	0.5	0.3	22.5	$55,600.00	$1,251,000.00
200	0.5	0.3	30	$55,600.00	$1,668,000.00

The total cost of the weir project must also include the cost of the gates, the land that would need to be excavated, contractor mobilization and overhead and a 40% contingency. Based on a weir length of 200 m, a weir head of 0.28 m, a weir height of 0.42 m, and a crest width of 7.5 m, the total project cost of the weir structure is $7,889,645.60, Table 5-8.

Table 5-8: Total cost analysis for weir (length = 200 m, weir head 0.50 m, weir height 0.30 m, crest width 7.75 m)

Item	Quantity	Units	Per Unit Cost	Total Cost
Weir Structure	200	m	$8,340.00	$1,668,000.00
Excavated Land	2,746.8	yd^3	$200.00	$549,360.00
Flood gates (length = 10 m)	20	gates	$43,430.40	$868,608.00
Cofferdam	3,000	m^2	$470.00	$1,410,000.00
Landscaping/reinstatement	1	unit	$100,000.00	$100,000.00
Control Building	1	unit	$45,000.00	$45,000.00
Subtotal	-	-	-	$4,640,968.00
Contractor Mobilization and Overhead (30%)	-	-	-	$1,392,290.40
Contingency (40%)	-	-	-	$1,856,387.20
Total +/- 50%	**-**	**-**		***$7,889,645.60***

The cost breakdown of the entire project for a weir length of 50 m 100 m, 150 m, and 200 m using the same cost analysis used in Table 5-8 is provided in Table 5-9.

Table 5-9: Total cost analysis for weir at different lengths

Weir length (m)	Total Cost +/- 50%
50	$3,955,036.40
100	$5,266,572.80
150	$6,578,109.20
200	$7,889,645.60

Based on the annual average flow rate data in Table 5-6, the flow conditions for any desired flow rate up to the permanent full-scale 20 m^3/s structure could be met with a 150 m length weir at a cost of approx. $6.6 million.

5.3 Draft Design 3: Temporary above Ground Pipe and Pump

As an additional third design, we evaluated a temporary over ground pipe and pump option for a pilot scale test case. Such an option will allow for the *in-situ* study of the physical, chemical, and biological impacts that ocean inflow would have on a localized mesocosm of the Banana River. It is recommended that any temporary over ground pilot study be conducted at or near the same location as a potential permanent full-scale structure. The above ground pumping option may also be extrapolated to alternate locations, if it is possible to make use of existing stormwater infrastructure.

This design is similar to a design developed by CDM Smith for SJRWMD (CDM 2017). The selected site for this concept eliminates the need to tunnel underneath a road and would not endanger critical infrastructure.

5.3.1 *Site Location*

The primary site chosen for the above ground pipe and pump temporary structure for the IRL inflow project is inside of Port Canaveral near Canaveral Lock. Situated on the north side of the channel between the lock and the 410 bridge, 28°24’33” N, 80°38’17” W, the proposed site does not contain any major roadways or interfere with existing infrastructure. The location also allows

for a large range of influence, since it would feed directly into the northern compartment of the Banana River, enabling it to flush the Banana River and portions of IRL as water circulates toward the inlets. The chosen site location is the same location as the weir, Figure 5-18 and Figure 5-19.

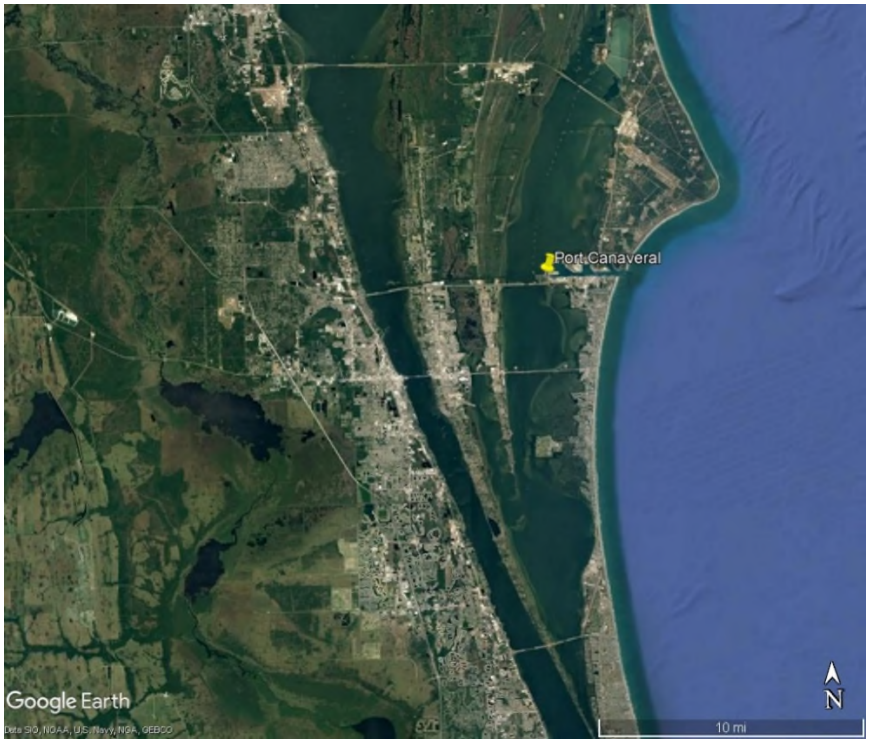

Figure 5-18: Port Canaveral aerial view (Google Earth 2019)

Figure 5-19: Port Canaveral Lock aerial view (Google Earth 2019)

The proposed project site of the above ground pipeline on the north side of the Port Canaveral Lock, is approximately 250 m (820 feet) and the average width of the land is 32 m (105 feet).

5.3.2 *Site Plots*

The depth near the structure on the port side and the Banana River side was determined using Navionics charts. The Port Canaveral Lock channel has an average depth of 3.81 m (12.5 feet) in the center with a steep gradient towards the north and south banks; the bottom slope was determined to be 0.2083. On the Banana River side, the bottom slope is 0.0308 with a gradual change in depth; the initial depth is 0.30 m (1 foot). On the north bank of the Port Canaveral Lock

channel, dolphin structures, which are used as mooring devices, are present. In Figure 5-20, the bathymetry for the proposed project location is provided.

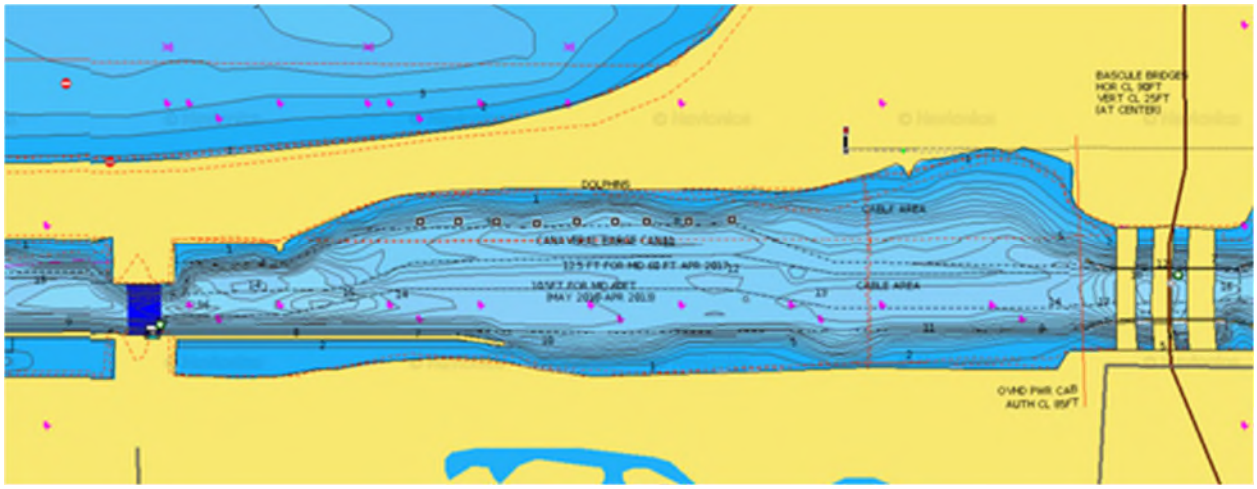

Figure 5-20: Bathymetry plot of Port Canaveral Lock (Garmin 2020)

5.3.3 *Design Summary*

The design is proposed to be a temporary above ground pipeline that has an intake inside Port Canaveral near the Port Canaveral Lock and an output in the Banana River. The design approach taken during the design process utilizes a submerged pump to drive the water flow. The pipe will run above ground to make it a temporary structure that can be used as a temporary inflow pilot system. The total distance of pipe needed for the proposed location is 87 m (285.5 feet).

For a temporary inflow pilot system, to reach a flow of 5 m^3/s (177 ft^3/s), the inner diameter of the pipe would need to be 1.09 m (3.58 feet) when using a 200-horsepower pump. When rounding this diameter to standard pipe dimensions, the diameter of the pipe would need to be 48 inches (1.219 m). The approximate location of where the pipe would be placed along with its dimensions is shown in Figure 5-21.

An open cut trench would be used to ensure the land is level where the pipe would be placed. The open cut trench would be a total length of about 34 m (111.5 feet) across the land; the elevation for this stretch of land ranges from positive 3 to positive 6 m (9.84 feet to 19.69 feet) above sea level, so the open cut trench would be dug to positive 3 m of elevation. The pipe would be met with an intake structure and submerged pump in Port Canaveral and an output structure in the Banana River. A side view of the proposed above ground pipe and pump system is provided in Figure 5-22.

Figure 5-21: Above ground pipeline location (Google Earth 2019)

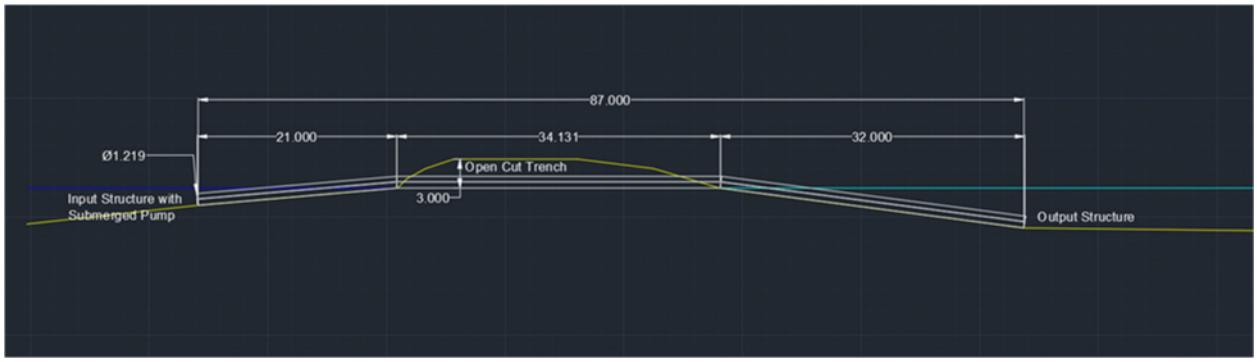

Figure 5-22: Above ground pipeline side view

5.3.4 *Cost Estimate*

A cost estimate was prepared for the temporary inflow pilot system above ground temporary pipeline using standard engineering unit costs. These costs do not include permitting or annual maintenance costs. The pipe diameters were rounded up to match standard pipe dimensions. A 30% contractor mobilization and overhead cost was added to the final project price; a contingency

of 30% was also added for uncertainties. A cost estimate for the pilot study at 5 m^3/s is provided in Table 5-10.

Table 5-10: Above ground pipeline temporary inflow pilot system cost estimate (5 m^3/s with one pipe and pump)

Item	Quantity	Units	Per Unit Cost	Total Cost
Polymer coated pipe - D= 48"	285.5	feet	$64.47	$18,406.19
Pump: SJP 48PO-1 2.5 m^3/s @ 440 rotations per minute (RPM)	2	Each	$1,250,000.00	$2,500,000.00
Input and Output structure	1	Each	$200,000.00	$200,000.00
Open Cut Trench	111.5	feet	$223.10	$24,875.65
Miscellaneous Site Work	1	Each	$160,000.00	$160,000.00
Subtotal	-	-	-	$2,903,281.84
Contractor Mobilization and Overhead (30%)	-	-	-	$870,984.55
Contingency (40%)	-	-	-	$1,161,312.73
Total +/- 50%	**-**	**-**	**-**	***$4,935,579.12***

The bulk of the cost is in the purchase of two new high flow rate pumps. Pump prices are based on an estimate from HydraService, Inc. for the Sulzer SJP 48PO-1 2.5 m^3/s @ 440 RPM Pump. The cost not including the purchase of two new pumps is approximately $700,000.00. During the final design phase, it is recommended that an alternative source for pumps be investigated, including pump rental or partnership with an agency with access to pumps (e.g. SJRWMD, U.S. Army Corps of Engineers, etc.).

5.4 Inflow Structure Design Summary

After review of the designs presented in this study, the weir is most cost-effective approach that provides the greatest flexibility for flow at the lowest cost but is the most restrictive with regards to location. A 150-m weir will meet the permanent full-scale flow criteria of a minimum of 20 m^3/s on an annual average basis. A smaller weir structure will meet the flow criteria during certain portions of the year. The pipe and pump is the most restrictive approach in cost as well as flow rates, but the most flexible with respect to location.

6 Conclusions

The potential impacts of enhanced inflow of coastal ocean water into selected portions of the Banana River, along with Bethel Creek in Indian River County were examined through the application of the EFDC model. Boundary conditions were derived from a variety of sources consisting of a combination of measured data and data from the ADCIRC and HYCOM ocean models. Inflow tests were set at three location in the Banana River to promote water exchanges with the larger IRL basin. In Bethel Creek, a single pump location was positioned to promote flushing.

The numerical models are a robust predictor of estuarine flow and mixing. Both the general circulation model, ADCIRC, and the estuary environmental model, EFDC, calibrate well for water level. The EFDC also calibrates well for salinity and temperature. This validated model response provides confidence in the modified estuary simulations results. The results from testing are able to predict what the flows would be from the addition of an ocean inflow structure.

6.1 Modeling

The ADCIRC model calibrates well to the ADCP data, although inside the estuary the models are very sensitive to the meteorological forcing (Weaver et al. 2016a and Weaver et al. 2016b). Outside the estuary, the models agree with the available measured data from the Trident Pier station. The EFDC model calibrates well with measured data within the IRL and can be applied to evaluation of enhanced inflow scenarios with confidence.

Model tracer study results indicate that the Banana River flushes to 50% or less of initial tracer concentration based on a 10 m^3/s pump station located north of PAFB. This flushing is dependent on the location within the Banana River basin. The south compartment flushes within 50 days, the main compartment within 120 days, and the entire Banana River within 200 days. Currently flushing times are over 200 days.

Flushing time results improved for the pump station located just north of Port Canaveral. The potential for flushing of tracer out of a large portion of the Banana River was much greater with the pumping located further north in the basin. Results indicate that siting an inflow structure as far north as possible will have the greatest impact on tracer concentrations and flushing of the Banana River

A weir structure located at Port Canaveral provides flushing of north Banana River compartments within 30 days, and the entire Banana River flushes within 80 days. The weir structure located within Port Canaveral produced the greater potential for exchanging water out of the Banana River over shorter a period of time compared to the two pump scenarios.

For each scenario, predicted changes in salinity ranged up to 5-10 PSU with the larger potential increase generated by the weir inflows. Predicted impacts on salinity were reduced with distance from the inflow structure. Changes in temperature were less pronounced amounting to only a fractional decrease in temperature as the cooler ocean water mixed with the lagoon water in the vicinity of the structure.

Due to its location in the basin, Bethel Creek exchanges effectively with the adjacent IRL. The addition of a 5 m^3/s pump station flushes IRL compartment in days with minimal impacts on salinity and temperature.

The modeling supports the concept of using ocean inflow to circulate the water in the IRL, moving stagnant lagoon water and replacing with ocean water. The inflow will create a very slow current that will circulate the water toward the inlets and facilitate enhanced exchange and mixing into the larger IRL system localized changes in salinity are predicted along with and minimal changes in temperature.

6.2 Structure Design

From the engineering perspective, there are two clear options for a potential permanent full-scale system: either a pipe and pump or a weir structure. The weir is most cost-effective approach that provides the greatest flexibility for flow at the lowest cost but is the most restrictive with regards to location. Due to the potential to impact coastal sediment transport, as well as infrastructure, the placement of a weir structure is limited. One potential location with minimal impact on infrastructure and limited impact on coastal sediment transport is adjacent to the Port Canaveral Locks. By relying on the tidal fluctuations to move water into the Banana River, there is not additional costs for operating a pump system. There will be annual maintenance costs and costs associated with operating the gates during an emergency when the gates may need to be closed.

The pipe and pump option is the most restrictive approach in cost as well as flow rates, but the most flexible with respect to location. Due to construction, techniques of HDD and micro-tunneling, pipes can be constructed beneath infrastructure with minimal impact. A pipe and pump structure could potentially be located at any location with a minimal footprint above ground. To get the desired flowrates, the pipes would need to have a large diameter, which drives up the costs. The conceptual cost of a pipe and pump structure is greater than 10 times the cost of a weir structure, and then the flow rates are constrained. Additional costs of full time operation of the pump would add significantly to the annual maintenance of a pipe and pump option. Maintenance costs would also need to include servicing and cleaning of the fouling that will build up in the pipe and at the inflow and outfall structures.

To test the potential of an inflow system a temporary structure would need to be built to bring in the pilot scale flow of 5 m^3/s. There are two options for a temporary inflow pilot system. One option is to construct the weir and control the flow over the weir by limiting the gate opening. This would require constructing the structure and at the end of the temporary test closing the gates and leaving the structure in place for potential future inflow, or complete removal post pilot study.

The second option is a strictly temporary structure. This study developed the design concept for an open cut (above ground) pipe and pump option for delivering the pilot scale flow. The majority of the cost for such a system is in the hardware. Pumps capable of 2.5 m^3/s flow rates can range in cost from $400,000 to $1.25 million, and a temporary inflow pilot system would require two pumps. Pump cost aside this option is similar to a conceptual design put forward by CDM Smith (2017). This option can make use of portable pumping systems or a more fixed system to deliver the desired flow rates. At the end of the temporary pilot study the pumps and pipe can be removed, and the open cut backfilled, leaving the site in the pre-study condition. The estimated cost of a temporary inflow pilot system weir that can also be implemented at permanent full-scale system ranges from 2-3 times that of a pipe and pump overland solution depending on the cost of the pumps.

A final temporary pilot inflow system, and potential permanent full-scale system, may be modified from the design and volume options included here based on further scientific, regulatory agency, and logistical requirements.

7 References

Arcement, G.J., Schneider, V.R., 1989. Guide for Selecting Manning's Roughness Coefficients for Natural Channels and Flood Plains. U.S. Geological Survey Water- Supply Paper; 2339, 38p.

Bengtson, Harlan. “Measuring Open Channel Flow Rates with a Weir or a Flume.” Bright Hub Engineering, 12 Nov. 2018, www.brighthubengineering.com/hydraulics-civil-engineering/51435-introduction-to-the-weir-and-flume/.

Booij, N., Ris, R.C., Holthuijsen, L.H., 1999. A third-generation wave model for coastal regions: 1. Model description and validation. J. Geophys. Res. Oceans 104 (C4), 7649e7666.

CDM Smith and Taylor Engineering. 2017. Conceptual Design for Artificial Flushing Projects in the Indian River Lagoon Conceptual Design and Conceptual Cost Estimates for Pilot Testing, Draft Report, PW.PL1.9247.220078.03.02.IRL Conceptual Design Report August 2017_v2.docx.

Dietrich, J.C., Tanaka, S., Westerink, J.J., Dawson, C.N., Luettich Jr., R.A., Zijlema, M., Holthuijsen, L.H., Smith, J.M. ,Westerink, L.G., Westerink, H.J., 2012. Performance of the unstructured-mesh, SWAN+ADCIRC model in computing hurricane waves and surge. J. Sci. Comput. http://dx.doi.org/10.1007/s10915-011-9555-6.

Dietrich, J.C., Zijlema, M., Westerink, J.J., Holthuijsen, L.H., Dawson, C., Luettich, R.A., Jensen, R., Smith, J.M., Stelling, G.S., Stone, G.W., 2011. Modeling hurricane waves and storm surge using integrally-coupled, scalable computations. Coast. Eng. 58, 45e65.

FDEP, 2013. Basin Management Action Plan (2013). “Indian River Lagoon Basin Banana River Lagoon.” http://www.dep.state.fl.us/water/watersheds/docs/bmap/banana-river-lagoon-bmap.pdf.

Fry, J., Xian, G., Jin, S., Dewitz, J., Homer, C., Yang, L., Barnes, C., Herold, N., Wickham, J., 2011. Completion of the 2006 National Land Cover Database for the Conterminous United States. PE&RS 77 (9), 858e864.

Galperin, B., L. H. Kantha, S. Hassid, and A. Rosati, 1988: A quasi-equilibrium turbulent energy model for geophysical flows. J. Atmos. Sci., 45, 55-62.

Garmin. “Navionics ChartViewer.” Navionics, 2020, webapp.navionics.com/?lang=en#boating@undefined&key=gyklDpc%60kN.

Google Earth 7.3.2.5776 (2019). Patrick Air Force Base 28°16’16” N, 80°36’26” W. 3D map, viewed 3 April 2020. http://www.google.com/earth/index.html.

Google Earth 7.3.2.5776 (2019). Port Canaveral 28°24’33” N, 80°38’17” W. 3D map, viewed 26 April 2020. http://www.google.com/earth/index.html.

Hamrick, J. M., 1994a: Linking hydrodynamic and biogeochemical transport models for estuarine and coastal waters. Estuarine and Coastal Modeling, Proceedings of the 3rd International Conference, M. L. Spaulding et al, Eds., American Society of Civil Engineers, New York, 591-608.

Hamrick, J.M. 1992. A Three-Dimensional Environmental Fluid Dynamics Code: Theoretical and Computational aspects. Special Report 317 in Applied Marine Science and Ocean Engineering, Virginia Institute of Marine Science, Gloucester Point, VA 2302.

Kjerfve, B. (1986). Comparative Oceanography of Coastal Lagoons. *Estuarine Variability*, (December 1986), 63–81. https://doi.org/10.1016/b978-0-12-761890-6.50009-5.

Lasater, J. A. (1970). "Indian/Banana river-Indian river lagoon project." Air and Water Pollution Control Dept. of the State of Florida. http: //engineerradcc.library.link/portal/Summary-report-on-the-IndianBanana -River-Indian/TqLndOnRF7w/.

Luettich, R. A., Westerink, J. J., and Scheffner, N.W. (1992). "ADCIRC: An advanced three dimensional circulation model for shelves, coasts and estuaries, report 1: Theory and methodology of ADCIRC-2DDI and ADCIRC-3DL." Dredging Research Program Technical Rep. DRP-92-6, U.S. Army Engineers Waterways Experiment Station, Vicksburg, MS.

Luettich, R.A., Westerink, J.J., 2004. In: Luettich, R. (Ed.), Formulation and Numerical Implementation of the 2D/3D ADCIRC Finite Element Model Version 44.XX. http://www.unc.edu/ims/adcirc/adcirc_theory_2004_12_08.pdf, 74pp.

Luettich, R.A., Westerink, J.J., 2006. ADCIRC: a parallel advanced circulation model for oceanic, coastal and estuarine waters. http://www.adcirc.org.

Marine Resources Council. Indian River Lagoon Health Update. 2018.

Mamoua, K., Pandit, A., and Heck, H. 2019. "Nutrient Loading in the Indian River Lagoon from Groundwater at the River Walk Transect" EWRI World Environmental & Water Resources Congress, May 20-23, Pittsburgh, PA, USA.

NOAA. "NOAA Chart 11476." NOAA, 2020, charts.noaa.gov/PDFs/11476.pdf.

NOAA. "Water Levels - NOAA Tides & Currents." Tides & Currents, 2020, tidesandcurrents.noaa.gov/waterlevels.html?id=8721604&units=metric&bdate=20200401&edate=20200428&timezone=GMT&datum=MSL&interval=h&action=.

Pxfuel. "Landscape, Building, Concrete, River, Weir, the Floodgates, Water, Blue, Squares, Architecture." Pxfuel, 2020, www.pxfuel.com/en/free-photo-xsrpx.

Saberi, A. and Weaver, R. (2016). Simulating Tidal Flushing Response to the Construction of a Low-Crested Weir Connecting Port Canaveral to the Banana River, Florida. *J. Waterway, Port, Coastal, Ocean Eng.*10.1061/(ASCE)WW.1943-5460.0000337, 05016002.

Smith, N. P. "Computer simulation of tide-induced residual transport in a coastal lagoon." Journal of Geophysical Research, vol. 95, no. 10, 1990, pp. 18205-18211.

Smith, N. P. "Tidal and non-tidal flushing of Florida's Indian River Lagoon." Estuaries, vol. 16, no. 4, 1993, pp. 739–746.

Tetra Tech. 2007. The Environmental Fluid Dynamics Code Theory and Computation Volume1: Hydrodynamics and Mass Transport. 61p.

Tetra Tech Inc., and CloseWaters LLC. Save Our Lagoon Project Plan for Brevard County, Florida. 2020.

Van der Toorn, Ad. “Cost Estimation for a Canalized River Rhine.” *Delft University of Technology*, 25 Nov. 2010, edepot.wur.nl/326448.

Weaver, R.J., Johnson, J.E., Ridler, M., 2016a. Wind-driven circulation in a shallow microtidal estuary: the Indian River lagoon. J. Coast Res. 322, 1333–1343. https:// doi.org/10.2112/JCOASTRES-D-15-00046.1.

Weaver, R.J., Taeb, P., Lazarus, S., Splitt, M., Holman, B.P., Colvin, J., 2016b. Sensitivity of modeled estuarine circulation to spatial and temporal resolution of input meteorological forcing of a cold frontal passage. Estuary. Coast Shelf Sci. 183, 28–40. https://doi.org/10.1016/j.ecss.2016.10.014.

Westerink, J. J., and Luettich, R. A. 1991. “Tide and storm surge prediction in the Gulf of Mexico using model ADCIRC-2D.” U.S. Army Engineer Waterways Experiment Station (http://adcirc.org/home /documentation/adcirc-related-publications/).

Zarillo, Gary A., 2015. Indian River Lagoon Numerical Model Flushing Experiments. SJRWMD, Final Report, Palatka, Florida, 25p.

Zarillo, G.A. 2003. Salinity Distribution and Flow Management Studies: A Three Dimensional Model of the Lake Worth Lagoon, FL, South Florida Water Management District, 70p.

Zarillo, G.A., 2006. Calibration of the Environmental Fluid Dynamics Code for Sebastian Inlet and Vicinity. Prepared for the Sebastian Inlet Tax District., 22p.

Zarillo, G.A. 2004. Final Report: EFDC/HEM3D Hydrodynamic and Water Quality Model of the Loxahatchee River and Estuary. Prepared For: Tetra Tech, Inc., Tallahassee, FL.

Zarillo, G.A., 2001. Lake Jesup Hydrodynamic Model. Phase II. St. Johns River Water Management District. 55p.

Zarillo, G.A. and Yuk, S-s., 1996. Indian River lagoon/Sebastian River Hydrodynamic and Salinity Model. St. Johns River Water Management District. 47p.

Zarillo, G.A. and Surak, C.R. 1994. Indian River Lagoon/Turkey Creek Hydrodynamics and Salinity Model. Final Report to the St. Johns River Water Management District. 145pp.

Appendix B Task 2 – Biological Monitoring Report

Restore Lagoon Inflow Research Project (Phase 1) Modeling and Engineering

Task 2, Biological Monitoring

PREPARED FOR

Florida Department of Education
325 W Gaines Street
Tallahassee, FL 32399

PREPARED BY

Kevin B. Johnson, Ralph Turingan, Jeff Eble, Jon Shenker, and Jesse Blanchard
Florida Institute of Technology
150 West University Boulevard
Melbourne, FL 32901

FLORIDA TECH

September 2020

Table of Contents

List of Tables

List of Figures

Acknowledgments

We would like to thank our representatives in the Legislature and the public for support of lagoon science. We thank Robert Salonen and Frank Kinney for their efforts that made this research at Florida Tech possible. We would also like to thank John Windsor for his tireless leadership and guidance. Thanks to Drs. Nicole Phillips (University of Southern Mississippi), Paul Wills (Harbor Branch Oceanographic Institute), Michelle Gaither (University of Central Florida), and Toby Daly-Engel (Florida Tech) for their contributions. Danielle Juzwick, Connor Wong, Sean Crowley, and Rachael Stark helped with collection and analysis of seagrass, infauna, and plankton. We would also like to thank the anonymous external reviewers for applying their expertise to reviewing this work. In addition, we would like to express our profound gratitude to the Florida Fish and Wildlife Conservation Commission Fish and Wildlife Research Institute (FWRI) for giving us access to the IRL database. We especially thank Richard Paperno and Douglas Adams of the FWRI laboratory in Melbourne for their sustained support and advice in this project.

List of Acronyms

ANOSIM	Analysis of Similarities
ANOVA	Analysis of Variance
BRN	Banana River North
BRNI	Banana River North Inside
BRNO	Banana River North Outside
BRS	Banana River South
BRSI	Banana River South Inside
BRSO	Banana River South Outside
CO	Coastal Ocean
COI	Cytochrome Oxidase Subunit I
DO	Dissolved Oxygen
eDNA	Environmental Deoxyribonucleic Acid
FWRI-FIM	Fish and Wildlife Research Institute's Fisheries Independent Monitoring
HAB	Harmful Algal Bloom
IRL	Indian River Lagoon
km	Kilometers
m	Meters
ng/µl	nanogram per microliter
NMDS	Non-Metric Multidimensional Scaling
NOAA	National Oceanic and Atmospheric Administration is an American
PCR	Polymerase Chain Reaction
ppt	Parts Per Thousand
psu	Practical Salinity Unit
qPCR	Quantitative Polymerase Chain Reaction
RDA	Redundancy Analysis

SE	Standard Error
SESC	Species of Environmental Shift Concern
SIC	Species of Introduction Concern
µm	Micrometer
VB	Vero Beach
VBI	Vero Beach Inside
VBO	Vero Beach Outside

Executive Summary

Herein are reported biological population abundance and distribution data, and associated environmental and community information, for species and taxonomic groups within the Indian River Lagoon (IRL) estuary and nearby coastal environment. Data were collected for the northern Banana River (near Port Canaveral), southern Banana River (near Patrick Air Force Base), and Vero Beach (near Bethel Creek), when possible from both sides of the barrier island (Fisheries Independent Monitoring data are regional and lagoon-specific). These three locations are candidates to be a coastal water crossover site for a potential inflow restoration project. These data constitute the first stage of baseline data collection in anticipation of a temporary pilot inflow system, where the goal would be to measure ecological responses to restored inflow. Species, taxonomic groups, and environmental data being monitored include seagrasses, rooted algae, drift algae, benthic fauna, phytoplankton, ichthyoplankton, fishes, and environmental deoxyribonucleic acid (eDNA). This report discusses whether changing estuarine conditions will directly impact a species or group, or whether indirect effects through predators or competitors might be in play, provided sufficient data is available in the scientific literature to warrant predictions about responses. The Task 2 Biological Monitoring project has two explicit objectives, which are:

Objective 1: To document baseline biological characteristics of the IRL and coastal ocean in the vicinity of the proposed inflow locations.

Objective 2: To assess the likely biological responses to a temporary pilot inflow system at proposed locations.

The main biological concerns when restoring inflow are species which occur on only one side of the barrier island, and the environmental factors (biotic and abiotic) which may impact their responses to inflow. When a species or group is found only on the coastal side, they are a potential Species of Introduction Concern and the focus of discussion will be on the niche characteristics of that species, inasmuch as that species might displace those already in the estuary through competition, predation, or indirect effects. In contrast, when a species or group is found only on the estuary side, they are a Species of Environmental Shift Concern, where the potential concern is how introduced seawater may impact the estuarine species.

An ongoing project developed in tandem with this one (Task 1 Modeling and Engineering) has generated model projections of salinity changes in the area of influence of up to 5 parts per thousand (ppt). The area of impact is limited as the plans for a temporary inflow pilot system are modest, and this will afford an opportunity to monitor ecosystem responses in the lagoon in a finite area immediately surrounding the point of inflow (see Task 1 Modeling and Engineering).

Seagrasses: The main seagrass in the northern IRL, and the only seagrass detected in this study, is the shoal grass *Halodule wrightii*. Shoal grass is considered a weed-like pioneer species. It is eurythermal and euryhaline (tolerates broad ranges of temperature and salinity). *H. wrightii* is also flexible with regard to nutrient and organic sediment levels. Shoal grass can be found in sediments ranging from organic mud to cleaner sand. With these impressive ranges of tolerances, and with the knowledge that *H. wrightii* occurs in slightly deeper coastal ocean water in the tropics where water clarity is better, it seems unlikely that *H. wrightii* would be directly harmed by the abiotic environmental changes that will come with restored lagoon inflow. If water clarity improves, *H. wrightii* may even be able to recruit into deeper parts of the IRL previously inaccessible due to depth and photosynthesis limitations. If the water column becomes less eutrophic, or if sediments have less silt and organic material, shoal grass could benefit from a less polluted and stressful environment. On the other hand, shoal grass is considered a tolerant pioneer species and if there

is dramatic water quality and sediment improvement, they could experience competition for space with other seagrass species which are absent or rare under current conditions. There is currently a lack of sufficient information to predict how *H. wrightii* might be impacted by changes in herbivory or competition due to a shifting ecosystem driven by restored inflow. If a temporary inflow pilot system project is undertaken, continued ecosystem and biological monitoring will allow comparisons with the data reported herein, and it should be possible to more fully describe the impacts of restored inflow on *H. wrightii* via complex ecosystem dynamics.

Rooted Algae and Drift Algae: Data on these macroalgae are collected simultaneously with that of seagrasses via the transect-and-quadrat method, and results are reported in the same section as seagrasses. Data collected on these groups provides the beginning of a baseline and will be used for comparison with macroalgae data collection during and after a temporary inflow pilot system project. This is especially useful when data are collected side-by-side with seagrasses, which are often considered competitors with drift algae.

Benthic Fauna: It is recommended that monitoring of benthic fauna be ongoing before, during, and after the implementation of a temporary inflow pilot system project. Another year of monitoring ahead of a temporary inflow pilot system is advisable from the perspective of having a solid understanding of the biology and ecology of the system, including a nominal perception of seasonal impacts. Species which occur both in the estuary and in outer coast sediments are of lesser concern than those which are present on only one side or the other.

- Species/groups found only in coastal sediments constitute a possible introduction concern.
- Species/groups found only in estuarine sediments constitute an environmental shift concern.
- Many estuarine benthic animals are relatively sessile, eurythermal, and euryhaline.
- Eurythermal and euryhaline species are unlikely to be directly harmed by the addition of coastal water to the estuary.
- Indirect impacts due to inflow introductions or responses of other species are harder to predict and will require continued monitoring before, during, and after any temporary inflow pilot system study.
- Continued monitoring is required to document establishment of coastal species in the IRL or responses of those already in the estuary.
- Recommendation for careful monitoring of benthic fauna responses to a temporary inflow pilot system project.

Phytoplankton: These drifting microscopic photosynthesizers create turbidity and attenuate light. This has caused the disappearance of tens-of-thousands of acres of seagrasses in the IRL. Such dense blooms of algae are considered harmful algal blooms (HABs) because they kill seagrasses and fish and can harm other lagoon life. HABs may also be a result of toxicity, which is present in some species. HABs are largely responsible for public alarm concerning the state of the lagoon.

- Species/groups found only in coastal plankton constitute a possible introduction concern.
- Species/groups found only in estuarine plankton constitute an environmental shift concern.
- Many estuarine phytoplankton are eurythermal and euryhaline.
- Two toxic dinoflagellate groups were observed in only coastal plankton and may constitute a potential introduction concern.
- The IRL already has numerous species of potentially harmful algae (harmful either through dense blooming or toxicity) regularly present throughout the estuary.
- If restored inflow is successful in improving water quality via the pumping of less eutrophic coastal ocean water, HABs will likely be reduced in frequency and/or severity.

- Recommendation for careful monitoring of phytoplankton responses to a temporary inflow pilot system project.

Ichthyoplankton: The drifting life stages of fish are called "ichthyoplankton", and many fish species have this type of life cycle. Ichthyoplankton drift with currents, and they could potentially be transported by a restored inflow project.

- The northern IRL has a lower fish species diversity than the central IRL, that is at least partly due to limitations on entry of offshore-spawned larvae into the northern IRL.
- The northern IRL supports valuable recreational fisheries for spotted sea trout, red drum, black drum, and other species. These populations appear to be driven by larvae produced within the estuary.
- Some marine-spawned larvae can enter the northern IRL through the Port Canaveral Lock. During winter 2019/spring 2020, those larvae were dominated by pelagic schooling species such as Atlantic menhaden, scaled sardines and threadfin herring. These species are valuable prey for many fishes in the upper IRL. Species spawning during other seasons, including snappers, snook, jacks and other fishes, presumably can enter the IRL through the lock as well.
- Lock inflow is sporadic and of limited volume, compared to a temporary inflow pilot system and potential permanent inflow system. Marine larval influence in the northern IRL is thus minimal at present.
- Measurement of densities of marine-spawned larvae across seasons and years inside Port Canaveral will provide an assessment of the potential change in larval supply into the northern IRL. This assessment, coupled with evaluations of inflow impacts on seagrass and other nursery habitats, will help determine if changes in larval supply can alter the fish communities in the northern IRL habitats.

Fish Community Structure: Fish are important members of the ecosystem, often at the top of the food chain, grazing on seagrasses or macroalgae, filtering phytoplankton, or foraging on benthic fauna. Changes to the fish community in the IRL would have impacts on other habitats and taxonomic groups.

- The IRL is an essential habitat for a very rich assemblage of ecologically and economically important fish species.
- Multivariate analyses reveal that the community structure of these fishes is partly determined by a complex interaction of biophysical factors that have become critical components of this ecosystem.
- Among the key physical factors that are known to shape community structure of fishes in estuarine ecosystems, dissolved oxygen (DO) and salinity, with temperature as a covariate, stand out as key drivers of the structuring of fish communities within the IRL.
- The covariation between water quality parameters and fish community structure varies among the three sites of interest in this study; highest fish diversity is associated with moderate levels of DO and salinity.
- The contribution of biological factors, such as trophic relationships, to the structuring, variation, and sustainability of the fish communities in the IRL need to be further explored, considering the substantial amount of residual variation unexplained by the variation in the physical factors examined in this study.
- A critical area of inquiry for a temporary inflow pilot system is the investigation of the direct effects of changes in water quality, especially salinity, DO, pH, and temperature to the behavior and physiology of fish.

It is critically important that impacts on the ecosystem and numerous key species be documented through a temporary inflow pilot system project before implementing anything larger. However, extensive ecosystem and biological measurements during and after a temporary inflow pilot system project will reveal little without baseline data for comparison. The data presented herein on estuarine and coastal populations, and their ecosystems, is the start of the essential baseline for successful project monitoring. This monitoring report represents three seasons of population dynamics in seagrasses, rooted algae, drift algae, benthic infauna, phytoplankton, ichthyoplankton, fishes, and eDNA surveys, but another year of these measurements are recommended before a temporary inflow pilot system study starts in order to identify seasonal variation. Then it may be possible to identify major responses of a temporary inflow pilot system without confusion over seasonal effects. Natural changes due to seasonal or annual shifts in water quality (unrelated to restored inflow), geochemical cycling, reproductive cycles, and other sources of variability can be accounted for in evaluating project impacts if baseline ecosystem monitoring is sufficiently robust.

Inflow initiation or restoration projects for mitigating impaired estuaries have been carried out in other locations, and some have been successful from the perspective of enhanced fisheries or reduced HABs. The Maketu Estuary of New Zealand was restored to a century-old riparian flow pattern in 2019 to restore collapsing fisheries for indigenous Māori tribes. This restoration is ongoing but showing success in clearing sediments and increasing fishery populations (Johnson *unpublished*). A restored tidal exchange in western Australia reduced eutrophication and drift algae and increased larger pelagic fish (Potter et al. 2016). Multiple projects have had success in reducing HABs in estuaries through hydrological ecosystem engineering (summarized in Elliott et al. 2016). In other cases, storms may create accidental inlets with positive water quality impacts, and such was the outcome with Hurricane Sandy, where clam growth showed improvement after a breach at Fire Island (Long Beach Barrier Island, New York) (Gobler et al. 2019).

COVID-19 Pandemic Impacts

The COVID-19 pandemic impacted the biological monitoring work in the following ways: boat work, other field work, and laboratory processing were delayed and sometimes required revised approaches for successful completion. Boat work was especially challenging under pandemic restrictions. For a time, boat sampling was disallowed. Later, there was a limitation of two personnel per boat to maintain social distancing. Many field activities are most efficiently carried out by 3–4 personnel. The necessity to use fewer personnel resulted in days being added to field work to collect the contracted data.

1 Introduction and Objectives

1.1 Background

"Ecosystem monitoring is critical to ecosystem health and answers important questions about the effectiveness of programs to maintain ecosystem health."

- U.S. Geological Survey
https://www.usgs.gov/centers/oki-water/science/ecological-monitoring?qt-science_center_objects=0#qt-science_center_objects

This USGS statement on ecological monitoring is even more relevant when the strategy for maintaining ecosystem health is a dramatic intervention intended to reverse the decline of a degraded system. A large-scale engineering project intended to mitigate poor water quality and improve habitats, such as the proposed enhancement of circulation of the Indian River Lagoon (IRL), requires an accurate understanding of the current status of water quality and biological resources to determine impacts and assess project success. In the IRL system, possible changes or improvements are best measured by their impacts on water quality (e.g., salinity, temperature and nutrients) and biological responses (plankton, fishes, seagrasses and benthic fauna).

For monitoring to authoritatively demonstrate an after-effect, it is necessary to have baseline measurements "before" for comparison. It is especially important to monitor well in advance of anticipated changes to a system to provide an understanding of expected population fluctuations unrelated to the mitigation effort. Natural changes due to seasonal or annual shifts in water quality, geochemical cycling, reproductive cycles, and other sources of variability can be accounted for in evaluating project impacts if baseline ecosystem monitoring is sufficiently robust.

There are some historical and publicly available records for seagrasses and fishes in the IRL that can inform on the status and trends of these communities. However, the sites of historical data collection are not tailored to the sites being considered as possible ocean pumping locations. It is critical that pumping and ecological sampling sites be tightly aligned to reliably investigate the extent of pumped water impacts, both in severity and area influenced. This is particularly true for benthic sessile organisms that will be unable to flee the region of greatest impact and will therefore be subjected to the most extreme environmental changes.

1.1.1 Study Area

The IRL is a shallow (less than 5 meters (m)) bar-built, lagoon type estuary that extends 250 km along the central east coast of subtropical Florida and ranges in width from less than 1 to approximately 9 kilometers (km) (Note: Red circles show a 1 km radius around the proposed pumping location. Figure 1-1). In the past decade, water quality in the IRL has declined with more severe and more frequent harmful algal blooms (HABs) (IRL coalition; Tetra Tech 2016). The IRL is poorly flushed with 140 km between the Sebastian and Ponce de Leon inlets. The northern portion of the IRL is "micro-tidal" and tides have only a minor (negligible) influence on flushing of the estuary (Smith 1993). Based on rainfall and low-frequency coastal water level variations, the 50% renewal time for water in the northern and central IRL sections ranges from approximately 100–300 days (Smith 1993).

Note: Red circles show a 1 km radius around the proposed pumping location.

Figure 1-1. Map of the study area showing the three proposed pumping locations (north to south: Banana River North, Banana River South, and Vero Beach near Bethel Creek).

1.1.2 Objectives

Objective 1: To document baseline biological characteristics of the IRL and coastal ocean in the vicinity of the proposed inflow locations. Proposed locations were provided by the engineering team working in tandem with this project (see Task 1 Modeling and Engineering). The goal is to understand the current biology of proposed sites, including natural seasonal or other fluctuations, as much as is feasible in 8 months of sampling. Categories of biological characteristics to be monitored include:

1. Seagrasses and drift algae
2. Benthic fauna

3. Phytoplankton/harmful algae
4. Ichthyoplankton
5. Fishes
6. eDNA

This objective will be met by making comparisons over space and time, including abundances, species richness, community associations and critical abiotic environmental variables. Where appropriate, statistical analyses were conducted, including Analyses of Variance (ANOVAs), T-tests, and Non-Metric Multidimensional Dimensional Scaling (NMDS). Abundances are presented in the way most appropriate for the particular taxonomic group and data collection technique.

Extensive data on species densities and distributions, and environmental and community associations, was collected as part of the baseline study. This baseline biological data will become even more valuable in phases II and III. In Phase II, comparisons will be made through another cycle of seasons to identify seasonal trends. Beyond Phase II, post-inflow restoration data will be compared to earlier baselines to reveal the impacts of the project.

Objective 2: To assess the likely biological responses to a temporary inflow pilot system project at proposed locations. Selected IRL organisms were examined via environmental tolerances published in the literature to evaluate the likely impact of restored lagoon inflow on those species. Published biological information, including environmental tolerances, was used alongside the information collected for the first objective to make predictions of likely responses of key selected species.

2 Methods

2.1 Seagrasses, Rooted Algae, and Drift Algae Methods

At selected locations (Figure 2-1), transects 100-m long were surveyed perpendicular to the shoreline with the goal of documenting the presence of seagrasses and drift algae. Quadrats were laid down every 10-m along the transect lines, and seagrasses and drift algae were scored according to standard methods (Virnstein and Morris 1996; Morris et al. 2001). Measurements included seagrass visual estimate percent cover (estimated coverage upon imagining the seagrass crowded into corner of quadrat at a high density), seagrass percent coverage or occurrence (proportion of 100 quadrat sub-squares having at least 1 blade of seagrass), seagrass density (number of shoots per area), seagrass canopy height (the length of blade from sediment to tip), drift algae percent occurrence (the proportion of 100 quadrat sub-squares having any drift algae), drift algae biomass estimate (estimated coverage upon imagining drift algae crowded into corner of quadrat), and drift algae canopy height (Virnstein & Morris 1996; Morris et al. 2001). This sampling strategy was repeated quarterly for all sites.

2.2 Benthic Fauna Methods

Sediment grabs for infaunal analysis were collected at the 50-m mark along all seagrass transects described above (Figure 2-1) via petite Ponar grab (n=3 per transect). In addition, three stations were selected strategically from the Banana River Lagoon or IRL near proposed inflow sites, and three stations were selected from the ocean side of each proposed site. Triplicate samples were collected at each station. This sampling strategy was repeated quarterly for all sites. Sampling and identification of infauna were conducted consistent with the methods of benthic studies of the IRL (Mason 1998, Cooksey 2007) and were be tested for correlations with sediment parameters, including percent organic content (dry weight), percent water content by weight, and percent silt/clay content (dry weight), and also environmental parameters. Where appropriate, statistical analyses included ANOVAs for spatial comparisons on a given day, ANOVAs for temporal comparisons for a given site, and NMDS community analyses with post hoc Analyses of Similarity (ANOSIMs).

As part of the baseline biological evaluation, surveys compared species and communities in the IRL and coastal ocean, while also documenting environmental differences. Special consideration is given to species present only in one or the other of the coastal ocean or IRL. When a species is present in both the IRL and the coastal ocean, then introduction to the IRL is less of a concern as the coastal population demonstrates the ability of the species to withstand shifting environmental conditions as coastal waters flow into the IRL (“Non-Concern Scenario Type II”, Table 2-1).

Table 2-1. Categories of concern for scenarios of species presence and absence in the IRL vs. coastal ocean, assuming movement of coastal ocean water into the IRL.

	IRL Species Absent	IRL Species Present
Coastal Ocean Species Absent	Non-Concern Scenario, Type I	Environmental Shift Concern
Coastal Ocean Species Present	Species Introduction Concern	Non-Concern Scenario, Type II

When species are present in the IRL, but not observed in the corresponding coastal ocean, it is considered a potential Environmental Shift Concern (ESC), meaning that it is being considered and monitored in the lagoon to project the impacts of restored inflow. Conversely, when species

are present in the coastal ocean but absent in the IRL (Species Introduction Concern [SIC]), it is considered whether that species might be introduced to the lagoon with the inflow, is likely to become established, and what would be the impacts to the local IRL ecosystem. Note that species absences must be considered cautiously, as species can certainly occur in the region, yet be uncommon enough to be missed entirely despite the spatially robust sampling regimen.

2.3 Phytoplankton/Harmful Algae Methods

Phytoplankton were sampled via plankton tows for cell identification, and via whole water samples for flow cytometer analysis. Both types of samples were collected in conjunction with the infauna sampling schedule and locations shown in Figure 2-1 and discussed above. Regarding plankton tows, four were conducted quarterly at each proposed inflow site (n=4 outside and n=4 inside). Tows utilized a 20-micrometer (µm) mesh plankton net towed for approximately 2 minutes. Flow rate and submersion time were recorded and used to estimate volume processed for each plankton sample. Samples were preserved in 4% buffered formaldehyde to await enumeration and identification via microscopy. Whole water samples for flow cytometry were collected at every station (n=5) using a bottle to collect unfiltered water approximately 0.5 m below the surface of the water. These samples were set on ice and processed in the flow cytometer immediately upon returning from the field. This sampling strategy was repeated quarterly for all sites.

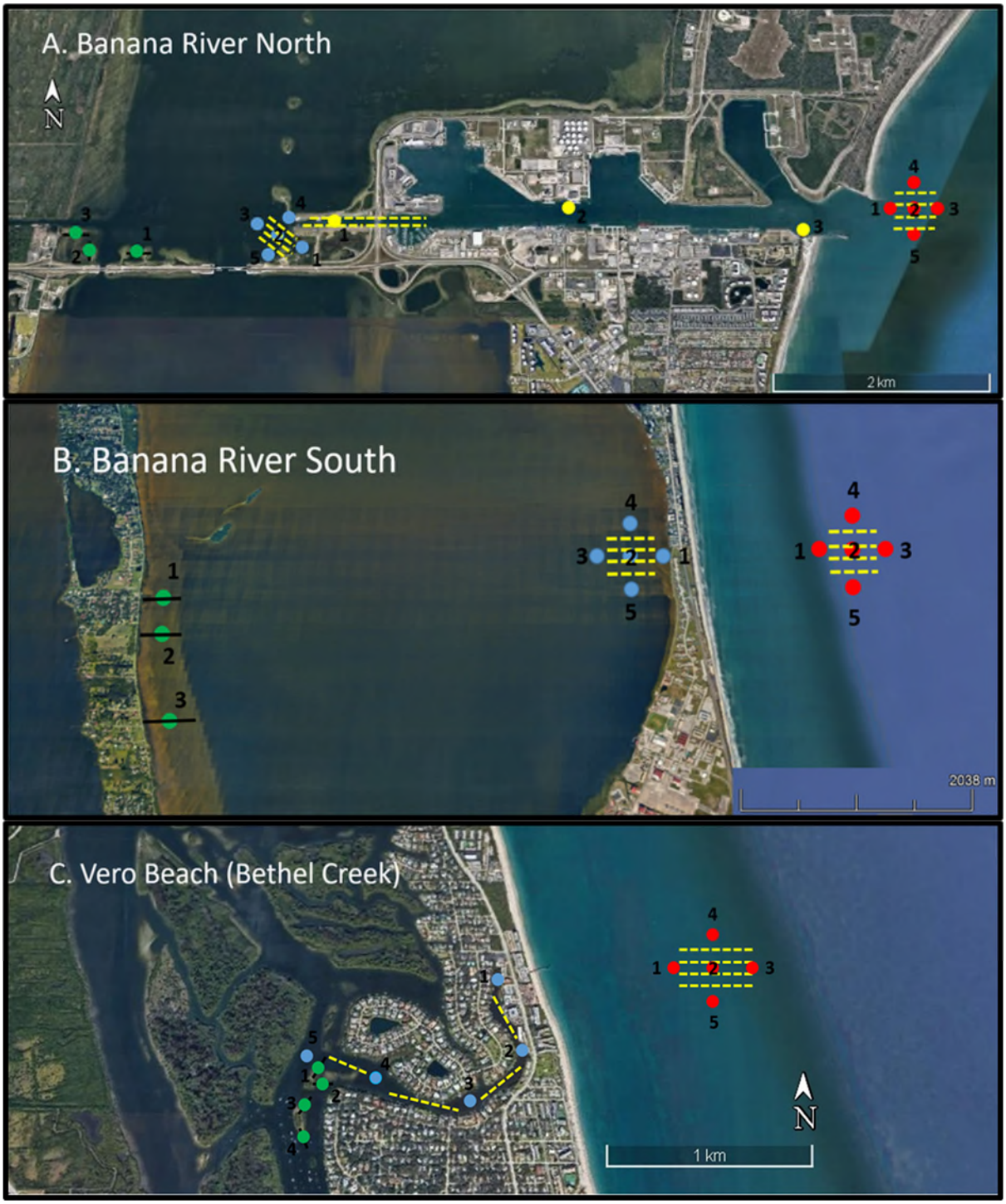

Note; Blue dots = infauna sampling stations inside the IRL. Red dots = infauna sampling stations on the outer coast. Green dots = seagrass transect and associated infauna stations. All dots, infauna sample n=3. Yellow dashed line = plankton tow location. Whole water flow cytometer samples were collected at all infauna sampling stations (blue, red, and green dots), with n=4 per station.

Figure 2-1. Samples collected and station locations for three proposed inflow sites for restoring inflow: A. Banana River North near Port Canaveral, B. Banana River South near Patrick Airforce Base, and C. Vero Beach at Bethel Creek.

2.4 Ichthyoplankton Methods

Fish spawning and recruitment of larvae into nursery habitats is an extremely important factor controlling fish community structure and abundance. Fishes within the IRL can be generated from spawning within the lagoon itself, or from offshore spawning and larval movement through inlets into the estuarine habitats. Reyier and Shenker (2007) and Reyier et al. (2008) showed that larval fishes in the northern IRL were almost completely dominated by spawning occurring within the lagoon, with very little influence from marine-spawning spawning species. Conversely, very large numbers of marine-spawned larvae moved through Sebastian Inlet into estuarine nursery habitats around the inlet (Smith 1995, Ferrell 1999, Wheeler 2000, Shenker et al. 2002), contributing to a more marine-oriented fish community than found further north in the IRL. These patterns of larval recruitment and the resulting structure of fish communities significantly influence the focus of recreational fishing activities in different sections of the lagoon.

The proposed project to introduce coastal water into the northern IRL raises concerns about the potential impacts of introducing more marine-spawned larvae into the habitat and altering fish community structure. Some water flow between IRL and coastal habitats currently occurs through the Port Canaveral Lock, which was built in 1965 and is managed by the U.S. Army Corps of Engineers. The lock opens as needed during daylight hours to permit vessel traffic to move into or out of the IRL, and thus provides a pathway for larval fish to move between the habitats. Although flow rates through the lock is limited by the infrequent and short open periods, evaluation of this larval movement can serve as a model for the role of a larger water inflow project on larval recruitment and its potential impact on northern IRL fish communities.

Ichthyoplankton samples were collected by plankton light traps (Figure 2-2) on the IRL and Port Canaveral sides of the Port Canaveral Lock to examine internal IRL production of fish larvae and potential immigration of fish spawned in offshore waters. The light traps were cylinders of plankton netting (500 µm mesh), 0.75 m deep x 0.3 m diameter, with 4 funnels leading into the trap. An underwater dive light was suspended inside each trap, serving as an attractor for fish larvae, just as moths are attracted to artificial lights at night. They are most effective in low current velocity environments (Anderson et al. 2002), such as at the Port Canaveral Lock which does not open at night. Light traps were deployed before sunset and retrieved the following morning. After retrieval, samples were preserved in 10% formalin for 48–96 hours, then switched to 70% ethanol and stored for analysis. Taxonomic analysis of larvae was performed using identification criteria provided by Smith (1989) and Richards (2005).

Upon receipt of a permit from the U.S. Army Corps of Engineers, light traps were deployed on three nights in late December 2019 from the bulkheads extending east and west of the lock, into Port Canaveral and the IRL, respectively (Figure 2-3). The lock was closed for maintenance on January 1, 2020, and access to the active construction site could not be provided. Because deploying an array of highly visible and unattended traps overnight in an area with high human activity was considered to be unwise, the sampling approach was switched to conducting ichthytoplankton tows (1 m diameter net, 500 µm mesh) in association with the plankton surveys described in Section 2.3. Initial analysis of the samples collected in January and February 2020 showed that very few larvae were being collected, presumably due to the daytime net avoidance capabilities of fish larvae.

In March, efforts shifted back to light traps being deployed at a marina within Port Canaveral, alongside a platform containing materials being tested by a Florida Institute of Technology Biofouling Research Program. Samples were collected in mid-March, and then in mid-May at the biofouling platform. Upon receipt of a renewed U.S. Army Corps of Engineering permit to resume

collections at the newly re-opened Port Canaveral Lock, the final samples were collected from the IRL and Port Canaveral sides of the Lock in late May.

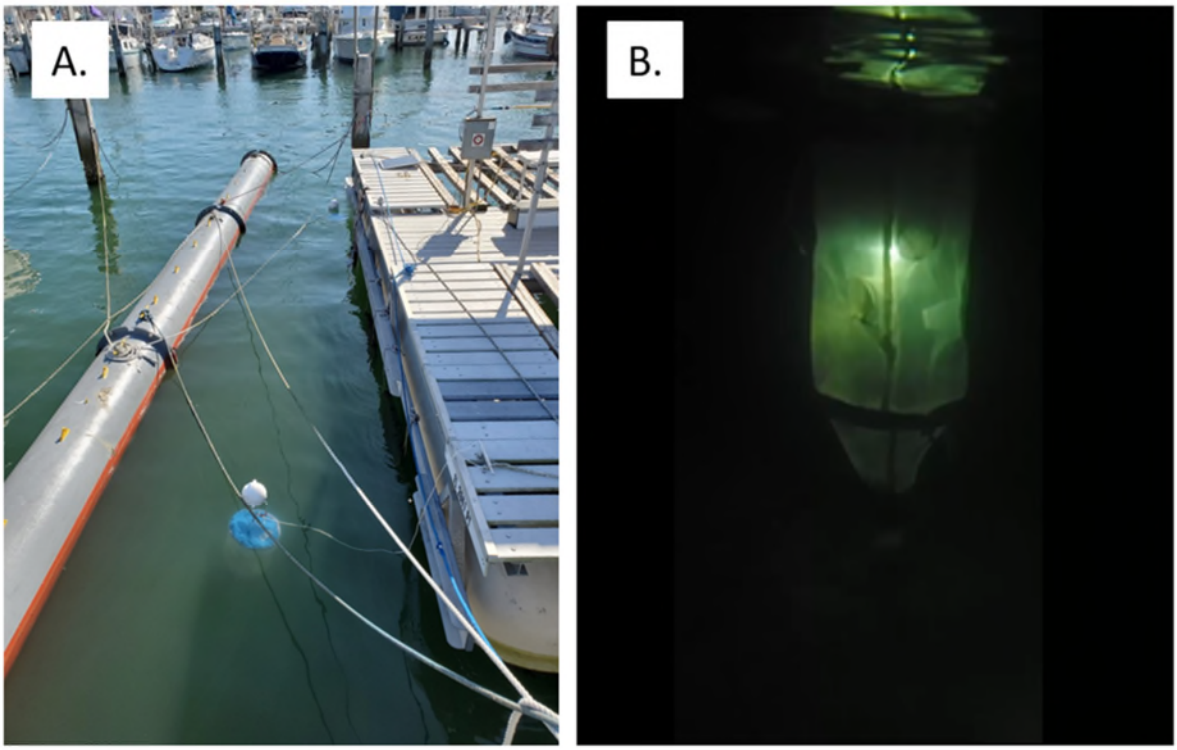

Figure 2-2. Subsurface floating light trap in Port Canaveral at the Biofouling Research Platform (A) and light trap at night (B).

Figure 2-3. Light trap sampling locations in Port Canaveral at the east and west sides of the Port Canaveral Lock, and at the Biofouling Research Platform.

2.5 Fish Analysis Methods

Data collection was conducted in collaboration with the Florida Fish and Wildlife Conservation Commission's Fish and Wildlife Research Institute's Fisheries Independent Monitoring (FWRI-FIM) program in the upper IRL. The FWRI-FIM program conducts the most comprehensive monitoring work in the IRL (FWRI, 2009). In this study, data collected in 1996–2018 were used. Four gear types were used to make sure most, if not all, fishes were adequately sampled (Figure 2-4). Environmental data (dissolved oxygen [DO], salinity, temperature, pH, conductivity, and depth) were collected concurrently with fish samples.

Figure 2-4. The four gear types used in FWRI-FIM program (adapted from Rubec et al., 2018)

The statistical analyses focused on four spatial scales: the entire IRL, Site 1 = Banana River North (BRN), Site 2 = Banana River South (BRS), and Site 3 = Vero Beach (VB) (Bethel Creek) (see Figure 1-1).

A series of statistical analyses using partial Redundancy Analysis (RDA) on Hellinger-transformed fish- (Legendre and Gallagher, 2001) and center-scaled abiotic data were used to determine the relative importance of key abiotic factors (Loughnan and Gilbert 2017, Mehner et al. 2014) that influence fish health: salinity, temperature, DO, pH, conductivity and depth. The key determinants of fish community structure as revealed in the partial RDAs were subjected to a series of NMDS analyses to determine how community diversity vary under different conditions: Low, Moderate, and High based on the observed ranges of each variable. For DO, these conditions were Low <6.33%, 6.33% ≤Moderate <12.46% and High ≥12.46%. For salinity, these conditions were Low < 16.26 parts per thousand (ppt), 16.26 ppt ≤ Moderate < 32.33 ppt, and High ≥ 32.33 ppt. These analyses were followed by similarity of percentages and ANOSIM to determine which species was most affected by variation in abiotic factors (Santos et al. 2016). All statistical analyses were performed using the Vegan package (Oksanen et al. 2019) in R (R Core 2012).

2.6 Environmental Deoxyribonucleic Acid (eDNA) Sampling and Detection

To investigate potential impacts of ocean water pumping, advances in next-generation DNA sequencing were leveraged to assess and track biodiversity across taxonomic groups using eDNA (Eble et al. 2020). Three replicate water samples each of 1,000 milliliters were collected at each site (Figure 2-5) using bleach sterilized Nalgene bottles. Bottles were sterilized between uses by soaking for 10 minutes in 50% bleach followed by immersion in deionized water. To limit DNA degradation, samples were held on ice and filtered within 6 hours of collection using 0.45 µm pore size mixed cellulose ester filters (Figure 2-6). Filter membranes containing eDNA were then stored at -20° C in Longmire's buffer solution for later DNA extraction. DNA will be extracted from filters using the DNeasy Blood and Tissue commercial extraction kits (Qiagen Inc., Germantown,

Maryland), which has been used with great success in marine eDNA metabarcoding (DiBattista et al. 2017; Djurhuus et al. 2017; Kumar et al. 2019), followed by the OneStep Polymerase Chain Reaction (PCR) Inhibitor Removal kit (Zymo Research, Inc., Irvine, California). To reduce the likelihood of sample cross-contamination, all extractions were conducted in a ultraviolet sterilized workstation.

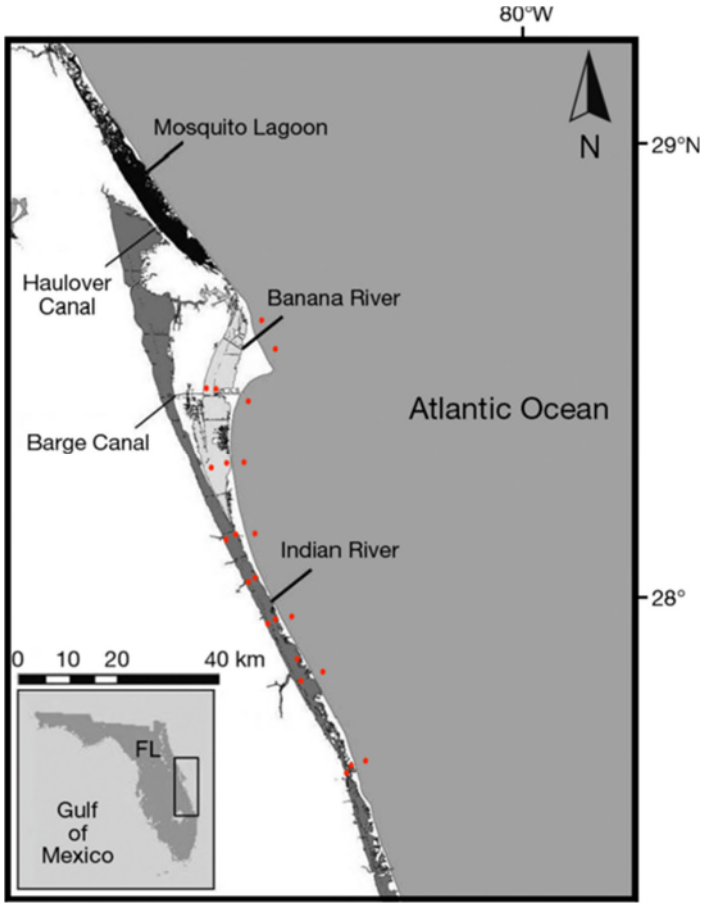

Figure 2-5. Banana River, central IRL, Bethel Creek, and coastal Atlantic eDNA sampling locations (n = 23).

Figure 2-6. Twelve sample eDNA filtering array.

Five primer sets previously used for analysis of metazoan eDNA were selected for in silico testing to characterize primer specificity, efficiency, and sequencing compatibility. Primer-BLAST (Ye et al. 2012) was used to screen candidate primer sets against target and non-target taxa sequence

databases maintained by the National Center for Biotechnology Information. To assess primer specificity and potential for non-specific eDNA amplification, primers were screened independently and in pairs against vertebrate classes and subclasses 'Mammalia,' 'Actinopterygii,' and 'elasmobranches;' invertebrate phyla 'Gastropoda' and 'Porifera;' and the arthropod subphylum 'Crustacea' Primers were also screened against the heterokont alga *Aureoumbra lagunensis* to reduce chances of unintended amplification of this abundant IRL alga. Product size and primer annealing temperature were estimated to determine primer-sequencing compatibility. From this, one primer set targeting the mitochondrial DNA cytochrome oxidase subunit I (COI) gene was selected for characterization of metazoan biodiversity (mlCOIintf/jgHCO2198; Leray et al. 2013) and one primer set targeting ribosomal ribonucleic acid 16s gene was selected to provide more detailed information on fishes (16SF/16S2R; Berry et al. 2017, Deagle et al. 2007).

Amplicon libraries were prepared for sequencing on the Miseq system (Illumina, San Diego, California) by amplifying extracted eDNA using the two selected primers sets. Aliquots and reactions were prepared in a ultraviolet sterilized hood to avoid cross contamination. For each primer set, a two-step PCR was used to generate amplicon libraries (Cruaud et al. 2017). In the first quantitative PCR (qPCR) reaction, the target gene fragment is amplified using taxa specific primers flanked by a linker sequence. The linker sequence allows for a second PCR reaction to add Illumina adaptor sequences and sample specific indexes. To allow sample assignment and reduce index hopping each sample library was developed with a unique dual index (Kozich et al. 2013). To avoid false negatives duplicate qPCR reactions were run and replicate reactions were pooled.

Amplicon libraries were quantified using a Qubit 4 Fluorometer (Life Technologies, Carlsbad, California), purified with the E.Z.N.A. Cycle-Pure Kit (Omega Bio-Tek Inc., Norcross, Georgia) and pooled in equimolar amounts. Pooled PCR products were size-selected, purified, and bi-directionally sequenced on an Illumina MiSeq using 300-cyle V2 Nano and 600-cycle V3 reagent kits. Sequences will be filtered and trimmed in Geneious Pro (Drummond et al. 2009) and using the DADA2 bioinformatics package (Callahan et al. 2016) in the R software environment following the bioinformatics pipeline of DiBattista et al. (2017). Pooled reads that pass quality filtering will be queried against a custom reference DNA sequence database that combines publicly available sequences from the National Center for Biotechnology Information and Barcode of Life Data System. Results of the database query will be imported into MetaGenome Analyzer (Huson and Weber 2013) and taxonomic identities will be assigned to the lowest taxonomic designation based on thresholds of 95% match for genus level designations and 98% for species-level. Rarefaction curves will be produced to estimate species richness as a function of sequencing depth. To identify biodiversity patterns, species richness and taxonomic distinctness are included (Clarke and Warwick 2001) to provide complimentary measures of alpha and beta diversity for each site.

3 Results

3.1 Seagrasses, Rooted Algae, and Drift Algae Results

Seagrasses are present in the IRL and an attempt was made to seek out the nearest beds to proposed crossover sites. At this same latitude on the coastal side of the barrier island no seagrasses were detected via random benthic grab samples. Within the IRL, seagrasses are patchy and, when present, vary from sparse to abundant at the selected seagrass locations examined for this study. The primary species of seagrass observed at all locations has been the seagrass *Halodule wrightii* (Figure 3-1).

Figure 3-1. Transect and quadrat sampling of the shoal grass *Halodule wrightii*, the dominant seagrass in the northern IRL and the only seagrass sampled in the IRL estuary at sites being evaluated for potential restored inflow.

Abundances of seagrass in terms of percent cover are presented in Figure 3-2. Seagrass percent cover was greatest in the spring and ranged from 0–3%, 0–6 %, and 0–17% at BRN, BRS, and VB, respectively. The *H. wrightii* canopy heights reached a maximum of 9 centimeters in spring at the VB seagrass transects (Figure 3-3). Shoot counts were always sparse and only exceeded a fractional count in a couple of quadrats in BRN (winter) and VB (spring) (Figure 3-4). Epiphytes growing on shoal grass blades showed different seasonal patterns based on site, and were most abundant at BRN in the winter, BRS in the fall, and VB in the spring (Figure 3-5). Rooted alga of the genus *Caulerpa* came on strong in the winter at BRN, and were most abundant at BRS in the spring, with percent cover from 3–70% (Figure 3-6). Rooted algae were largely absent from the VB transects. Drift algae made a strong appearance in the winter at BRN and BRS, with some of the higher coverages ranging from 22–43% (Figure 3-7).

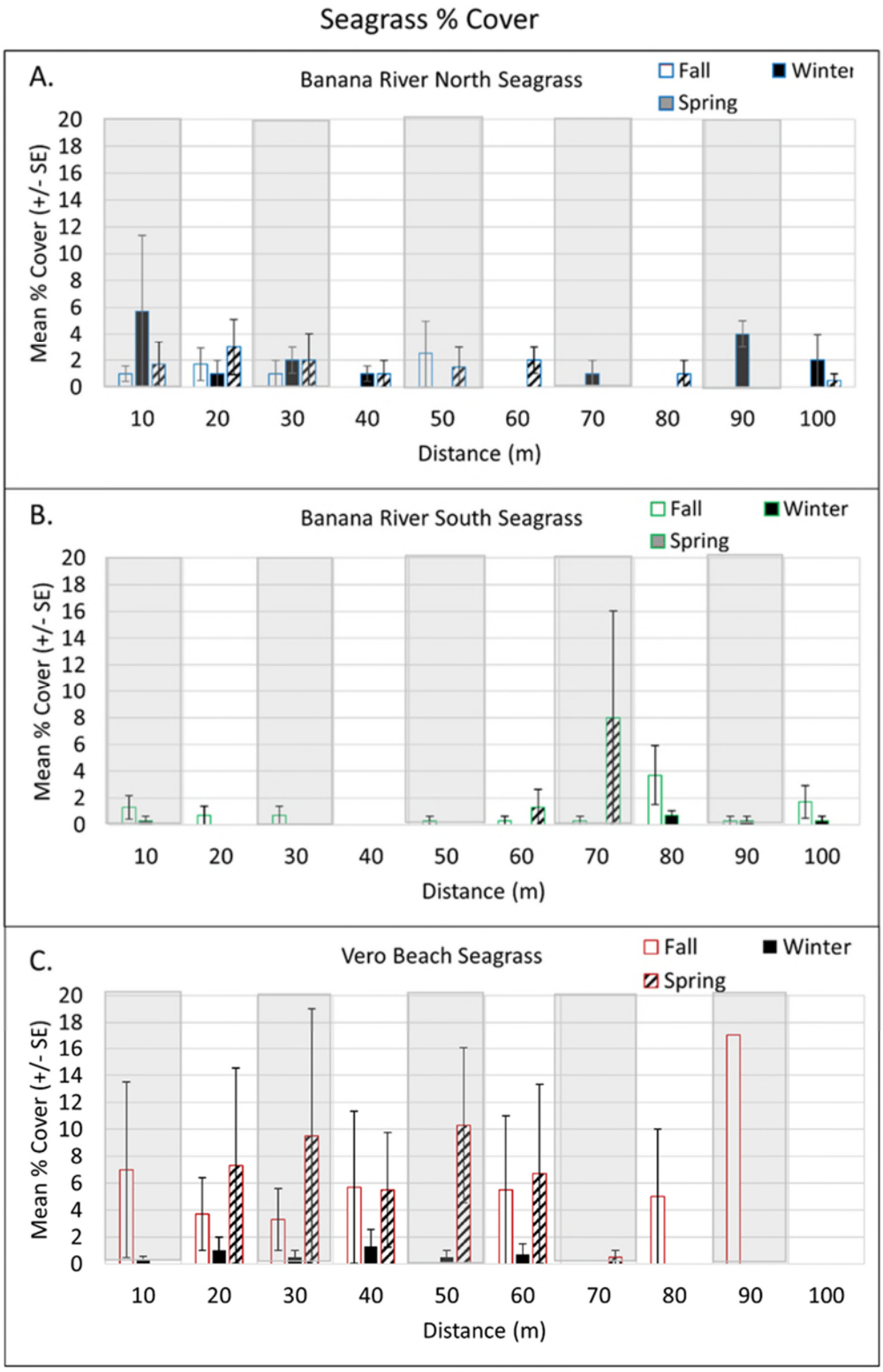

Note: Hollow bars = fall season, solid bars = winter season, diagonal stripe bars = spring season.

Figure 3-2. Seagrass mean percent cover for transects associated with the three proposed inflow crossover points: A. BRN, B. BRS, and C. VB.

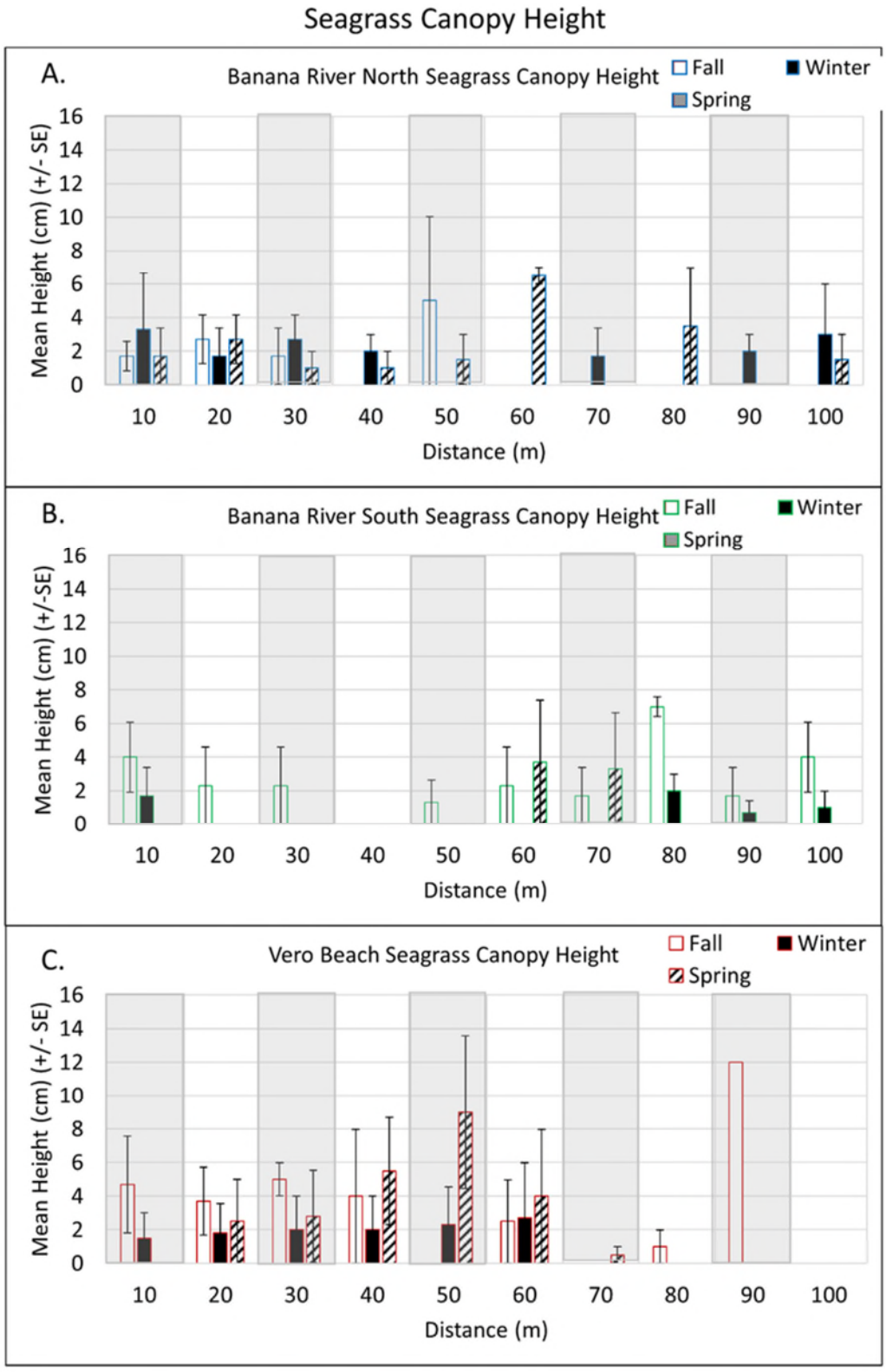

Note: Hollow bars = fall season, solid bars = winter season, diagonal stripe bars = spring season.

Figure 3-3. Seagrass mean canopy height for transects associated with the three proposed inflow crossover points: A. BRN, B. BRS, and C. VB.

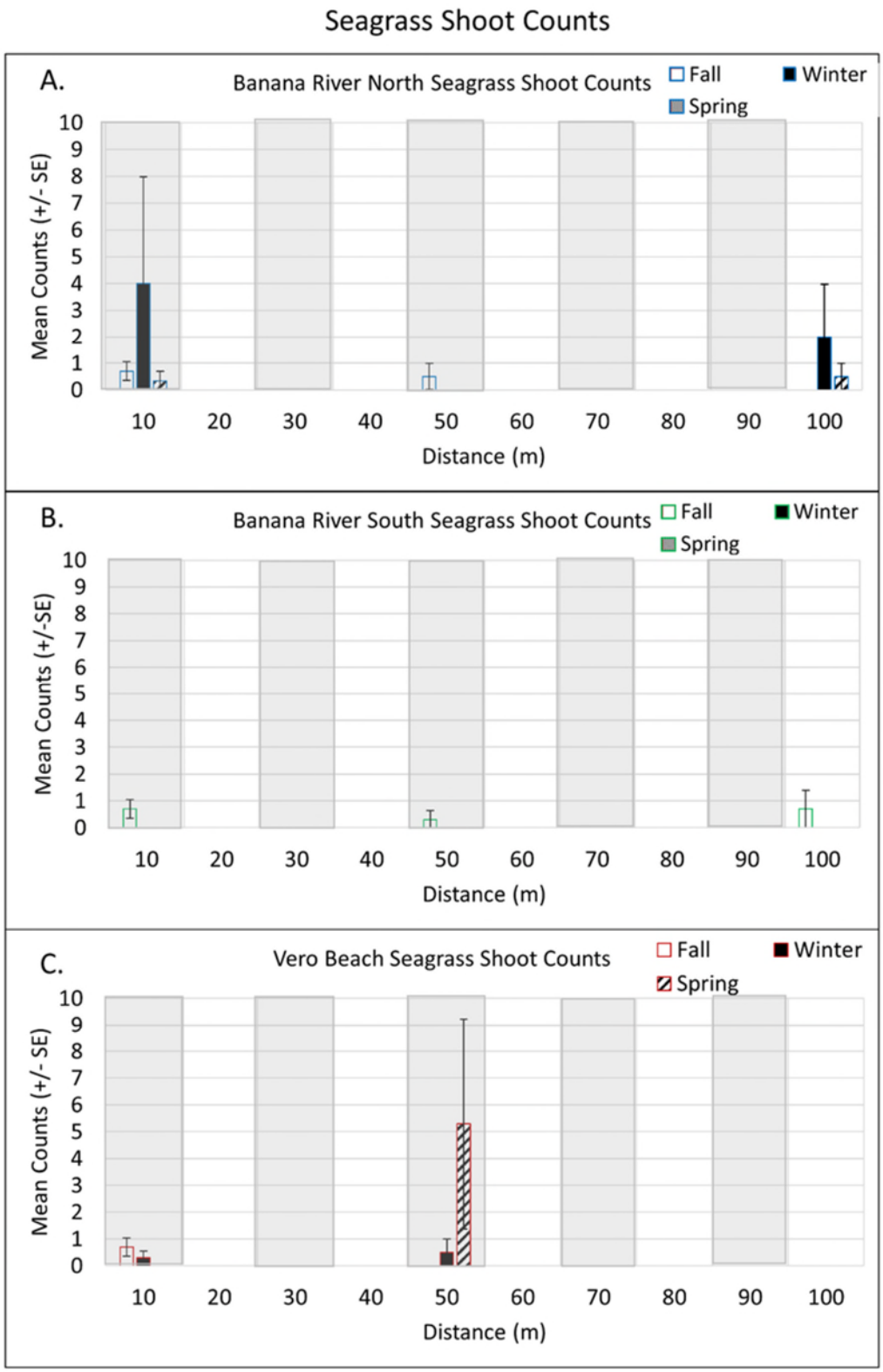

Note: Hollow bars = fall season, solid bars = winter season, diagonal stripe bars = spring season.

Figure 3-4. Seagrass mean shoot count for transects associated with the three proposed inflow crossover points: A. BRN, B. BRS, and C. VB.

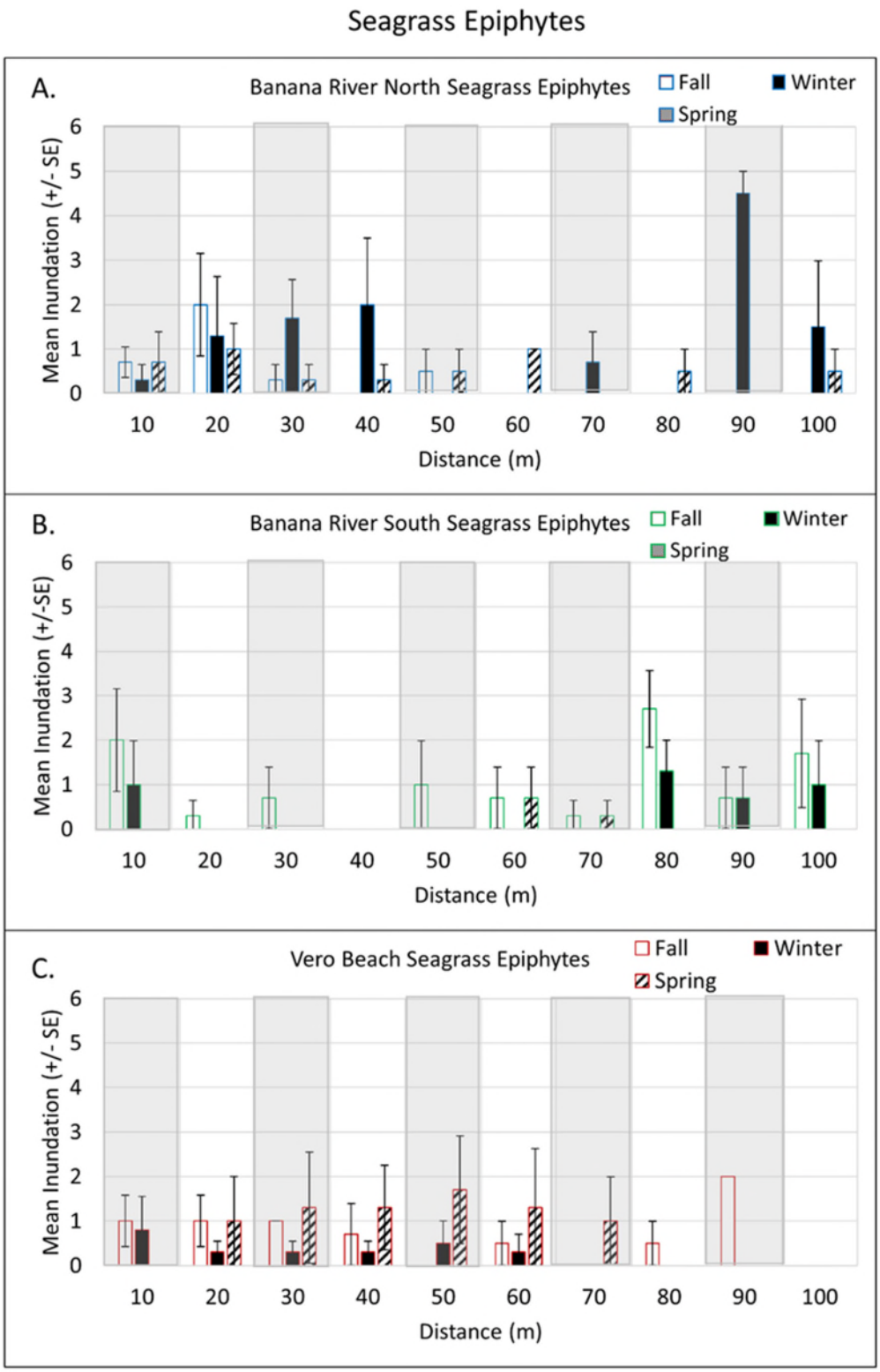

Note: "Inundation" is a subjective determination of the relative abundance of epiphytes on a scale of 0–5. Hollow bars = fall season, solid bars = winter season, diagonal stripe bars = spring season.

Figure 3-5. Epiphyte mean inundation for transects associated with the three proposed inflow crossover points: A. BRN, B. BRS, and C. VB.

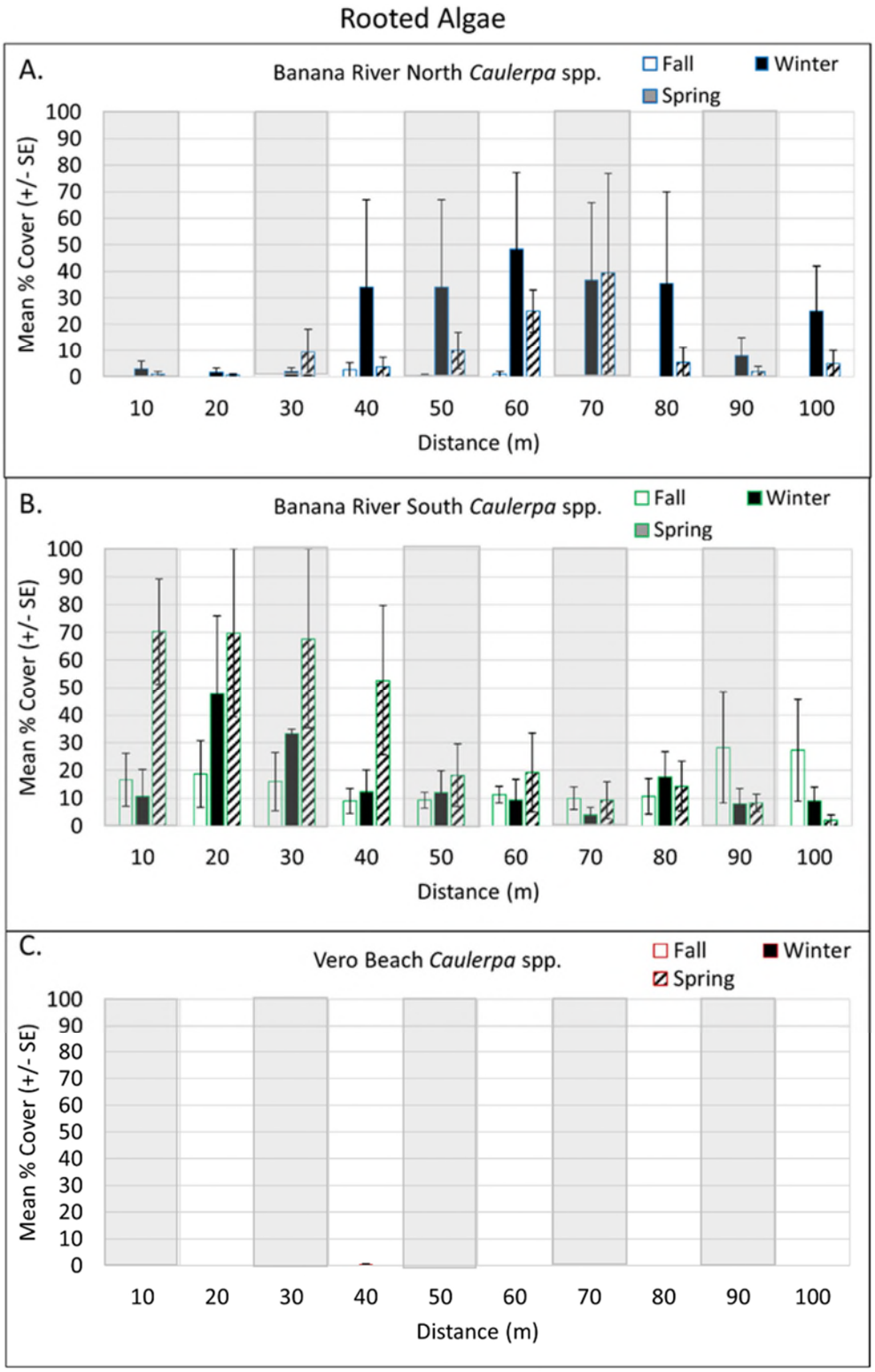

Note: Hollow bars = fall season, solid bars = winter season, diagonal stripe bars = spring season.

Figure 3-6. Rooted algae mean percent cover for transects associated with the three proposed inflow crossover points: A. BRN, B. BRS, and C. VB.

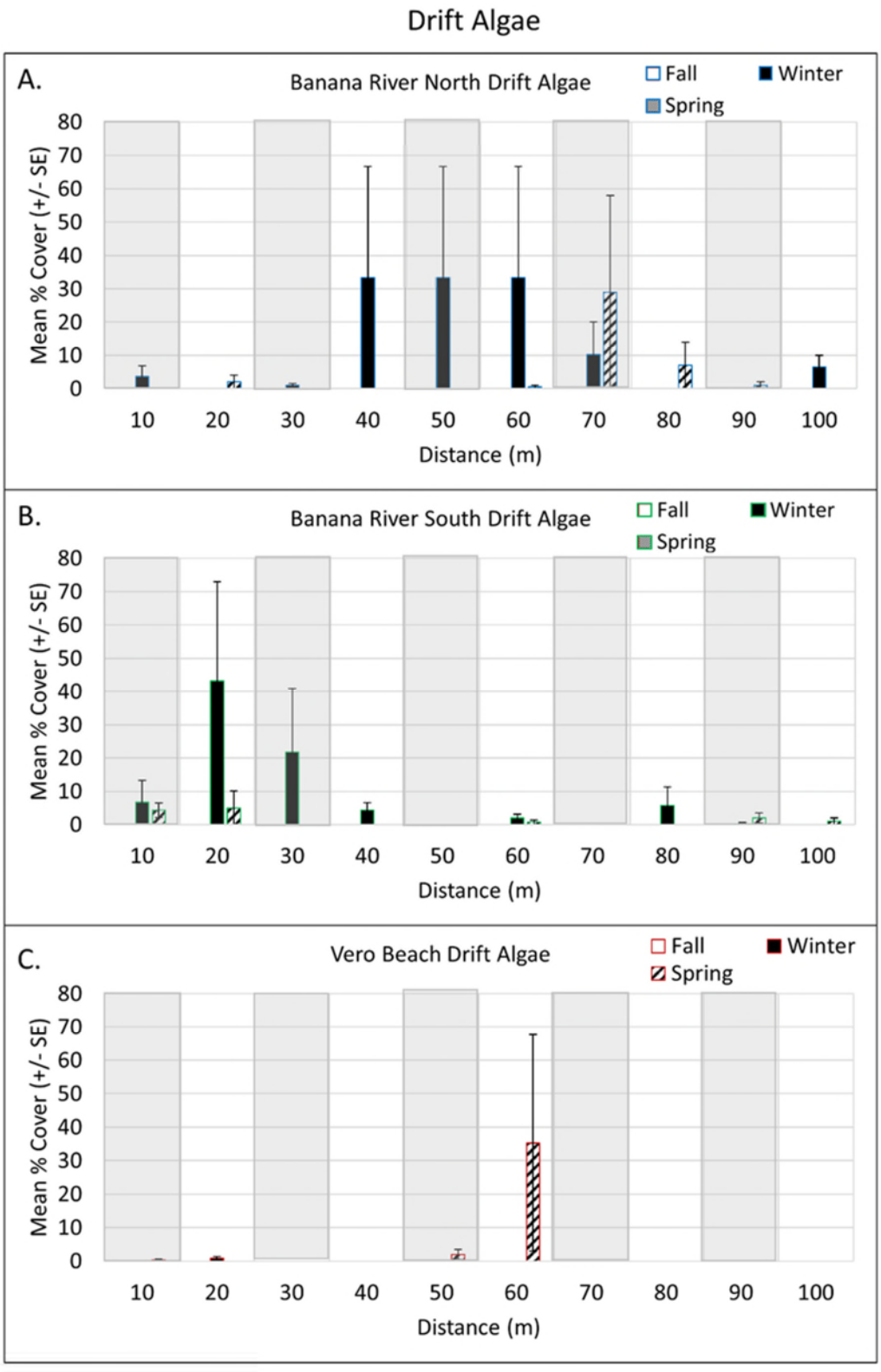

Note: Hollow bars = fall season, solid bars = winter season, diagonal stripe bars = spring season.

Figure 3-7. Drift algae mean percent cover for transects associated with the three proposed inflow crossover points: A. BRN, B. BRS, and C. VB.

3.2 Benthic Fauna Results

The IRL and the corresponding outer coast stations share many infaunal species in common, but some are unique to one environmental or the other.

List 1: Benthic Fauna Species of Non-Concern (Type II Scenario): Benthic fauna species found in both estuarine and coastal ocean sites include the following (from Table 3-1):

- The gammarid amphipods *Ampelisca abdita* and *Grandidierella bonnieroides*.
- All three cumacean species documented in this study, including *Oxyurostylis smithi*, an unidentified nannastacid cumacean ("Nannastacidae A"), and unidentified "Cumacean B."
- The caridean shrimp *Palaemonetes vulgaris.*
- The ostracod crustacean *Peratocytheridea setipunctata*.
- Both tanaid crustaceans documented in this study, *Hargeria rapax* and *Leptochelia dubia*.
- All polychaete annelids documented in this study, including *Alitta succinea*, *Ctenodrilus serratus*, *Glycera americana*, *Paradiopatra hispanica*, *Pectinaria gouldii*, *Armandia maculate,* and *Ophryorocha permanae*.
- The gastropods *Astyris lunata, Japonactaeon punctostriatus,* and *Phrontis vibex.*
- The bivalves *Angulus versicolor*, *Anomalocardia cuneimeris*, *Mulinia lateralis*, *Macoma carlottensis,* and *Amygdalum papyrium.*
- The brittle star *Ophiophragmus filograneus.*
- The foraminiferan protozoan *Ammonia parkinsoniana.*

List 2: Benthic Fauna Species of Potential Introduction Concern: Species found in the coastal ocean, but not observed in the IRL estuary in the surveys (from Table 3-1):

- The gastropod *Ecrobia truncata* (note this species was rare even in coastal waters, and never observed in the IRL estuary).

A subcategory of species of potential SIC: species found ubiquitously in the coastal ocean but found only in the IRL estuary at the Banana River North Inside (BRNI) sites, close to the locks, with regular propagule supply and water quality maintained by the ocean connection through Port Canaveral:

- The gammarid amphipod *Americhelidium americanum*.

List 3: Benthic Fauna Species of Environmental Shift Concern (SESC): species found in the IRL estuary, but not observed in the coastal ocean in the surveys (from Table 3-1):

- The gammarid amphipods *Cerapus tubularis*, *Cymadusa compta*, and *Gammarus mucronatus*.
- The crustacean ostracod *Eusarsiella zostericola*.
- The bivalve mollusc *Parastarte triquetra*.
- The gastropod molluscs *Acteocina canaliculata* and *Haminoea elegans* (rare)

Table 3-1. Occurrence of benthic species at potential restored lagoon inflow sites (Banana River North, Banana River South, and Vero Beach).

Note: Species present (letters present), absent (blank), and broad categories of relative abundances (L, M, and H for low, medium, and high abundances, respectively) are indicated. "L" means represented in a single replicate of one station at the site. "M" is representation in 2–4 stations. "H" is representation in 5 stations. Data are reported for the IRL and corresponding coastal ocean (CO) sites.

	Banana River North					Banana River South					Vero Beach				
	Fall		Winter		Spring	Fall		Winter		Spring	Fall		Winter		Spring
	IRL	CO	IRL	CO	IRL	IRL	CO	IRL	CO	IRL	IRL	CO	IRL	CO	IRL
Foraminifera (Protozoa)															
Ammonia parkinsoniana	M	M	H		H	M	M	H		H	M	H	M	M	H
Amphipods (Crustacea)															
Cerapus tubularis	M		M		L	M		M		M					
Cymadusa compta	L				M	M		M		L			L		
Ampelisca abdita	H	L	H		H	M		M		H	L		L		
Grandidierella bonnieroides	M		H	L	H	H		M		H	L		L		M
Gammarus mucronatus			L		M	M		M		H	L				L
Americhelidium americanum		H	L	M			M		M			L		L	
Cumaceans (Crustacea)															
Oxyurostylis smithi	M	M	M	M		H	M	M	M	M					
Nannastacidae A			M	L	M	H				M			L		
Cumacean B				L				L	L				L	H	L
Ostracods (Crustacea)															
Eusarsiella zostericola	H		H		M	M		L		L			L		L
Peratocytheridea setipunctata	M		M	L	H	M		M	M	L			M		M
Caridean Shrimp (Crustacea)															
Palaemonetes vulgaris		H	M	L	M	M	M			L	M	L		M	
Tanaids (Crustacea)															
Hargeria rapax	M	L	M		M	M		M		M					
Leptochelia dubia	M		M	L	H	H		M		H					
Polychaetes (Annelida)															
Alitta succinea	H		M	M	M	H		H	L	M		M	M	M	M
Ctenodrilus serratus	H		M	L	H	H	M	H	M	H	M	M	M	M	M
Glycera americana	M	M	M	L	L	M		H	L	M			L		M
Paradiopatra hispanica	M	M	L	M	L	M	M	M		M				L	
Pectinaria gouldii	H		H	M	M	H	M	M		M	L		L		
Armandia maculate		H	L	M			H		M			M	M		
Ophryorocha permanae		M		M			M		L		L	M		M	
Ophiuroids (Echinodermata)															
Ophiophragmus filograneus	L	L		L											L
Bivalves (Mollusca)															
Amygdalum papyrium	M		H		M	M		M	L	M					
Angulus versicolor		M	L	H			H		M		M				
Anomalocardia cuneimeris			M	L	M	H		M	M	M	L				L
Mulinia lateralis	H	L	H	L	H	H		M		H	L	L	M		L
Parastarte triquetra	M		H		M	M		H		M	L		L		L
Macoma carlottensis			L	M					M						L
Gastropods (Mollusca)															
Acteocina canaliculata	M		M		M	M		M		M	M				L
Astyris lunata	L	L						L				L			
Haminoea elegans	L		L												
Phrontis vibex		M	L	M		H		M		M					
Ecrobia truncata									L						
Japonactaeon punctostriatus											M		M	L	L

The mean abundances of total infauna (all taxonomic groups) was higher in Banana River sites when compared to their correlated outer coast sites (Figure 3-8 panels A and B). The VB sites, in contrast, had dramatically fewer infauna within the lagoon, which corresponded with more organic sediments. Abundances and richness on the outer coast were on par with other coastal locations. The net effect is VB is the only site where abundances and diversity are greater on the outer coast compared to that same latitude within the lagoon (Figure 3-8 and Figure 3-9). Vero Beach Inside (VBI) estuarine sediment organic content is greater than BRNI and Banana River South Inside (BRSI) sediments.

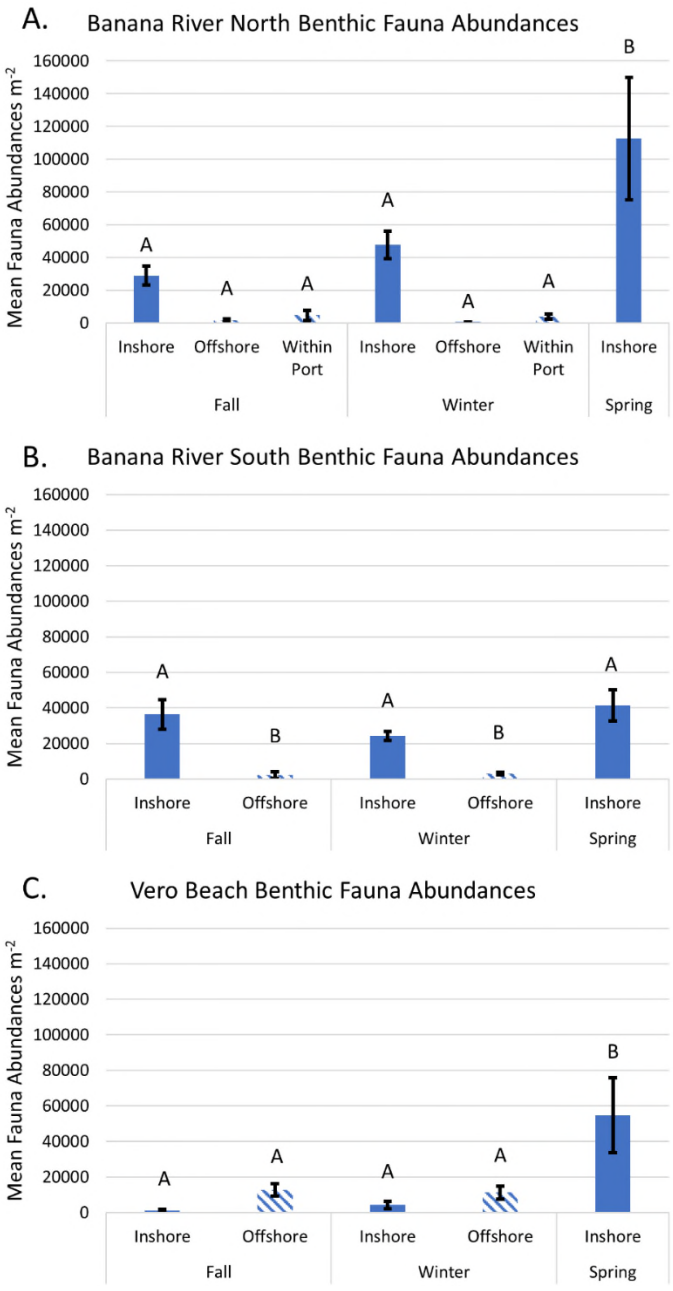

Note: Disparate letters indicate statistically significant differences between locations (α=0.05). Seasons are fall 2019, winter 2020 and spring 2020. “Inshore” is within the estuary. “Offshore” is coastal.

Figure 3-8. Benthic fauna densities for A. BRN, B. BRS, and C. VB proposed inflow sites.

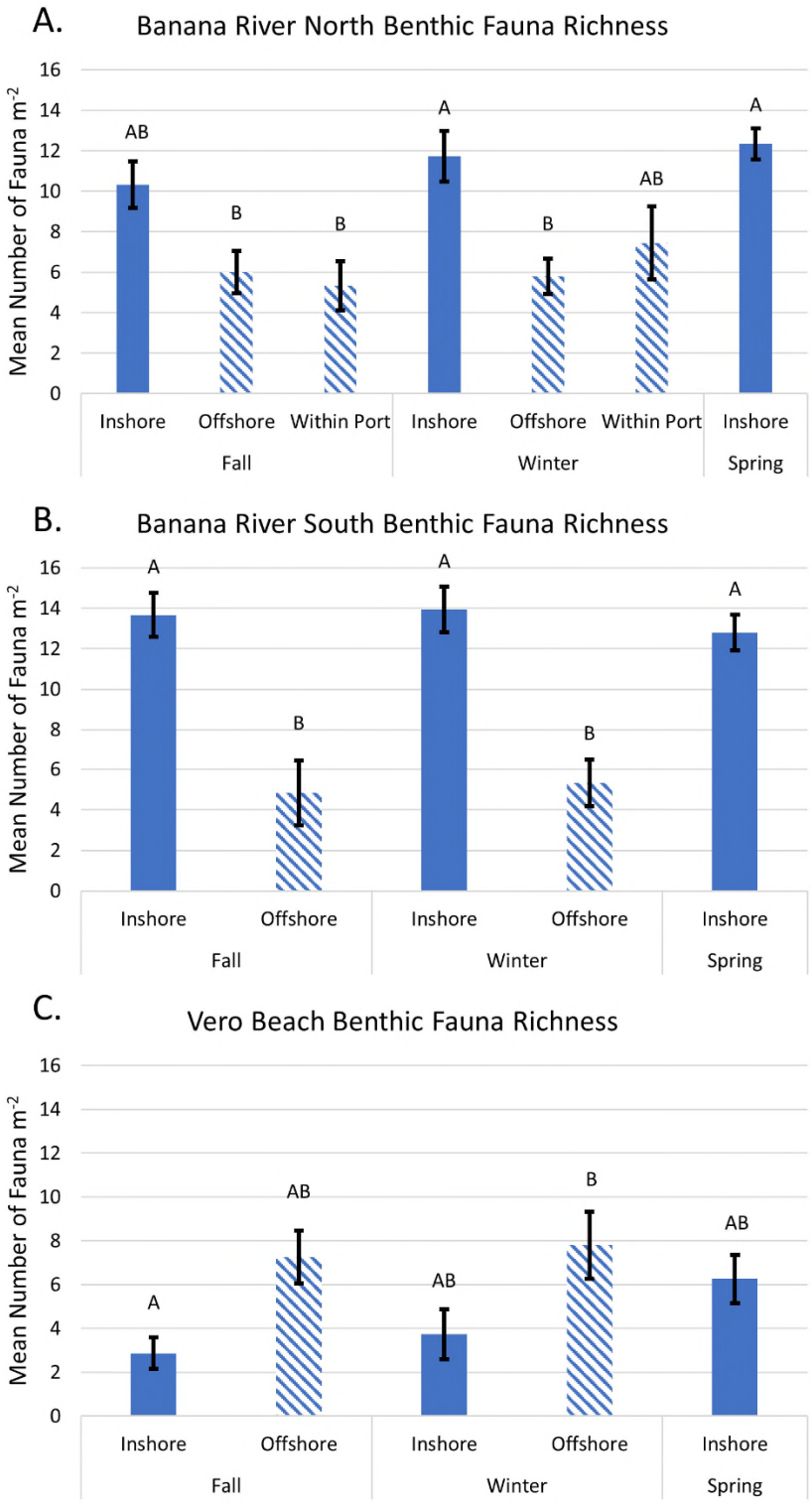

Note: Disparate letters indicate statistically significant differences between locations (α=0.05). Seasons are fall 2019, winter 2020 and spring 2020. "Inshore" is within the estuary. "Offshore" is coastal.

Figure 3-9. Benthic fauna species richness for A. BRN, B. BRS, and C. VB proposed inflow sites.

Coastal benthic fauna communities (Figure 3-10, blue ellipses), are most similar to one another, but still have considerable overlap with estuarine bare sediment (Figure 3-10, brown ellipses) and estuarine seagrass bed sediment (Figure 3-10, green ellipses). There is not a strong pattern of community separation based on estuarine vs. coastal comparisons via ANOSIM (R=0.49–0.60, stress 0.16–0 .24) and Permutational Multivariate ANOVA (R^2=0.30–0.33).

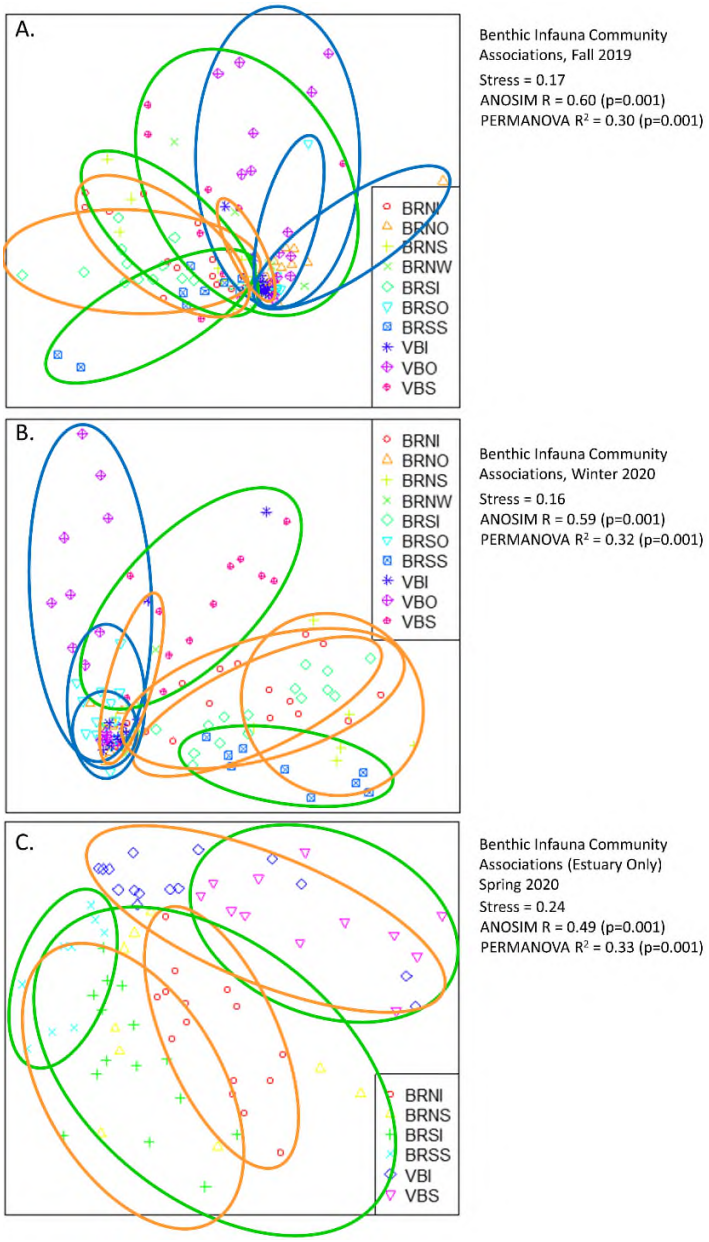

Note: Groupings compare the following habitats: estuarine bare sediments (brown ellipses), estuarine seagrass beds (green ellipses), and outer coastal bare sand (blue ellipses). Sites are BRN, BRS, and VB, with the additional notation of “O”, “I”, or “S” to indicate outer coast, inside the estuary, and within seagrass beds, respectively.

Figure 3-10. NMDS associations of infaunal communities based on species and abundances in fall 2019, winter 2020, and spring 2020, respectively.

Three species absent from estuary samples, but present in the coastal ocean (SIC) were selected based on their abundances and reputation as being ecologically important (Note: "0" indicates cases of zero mean and variance.
Figure 3-11 and Figure 3-12). Propagules of these species could potentially be transported with restored inflow into the estuary, and the likelihood of survival and establishment will be considered in the discussion.

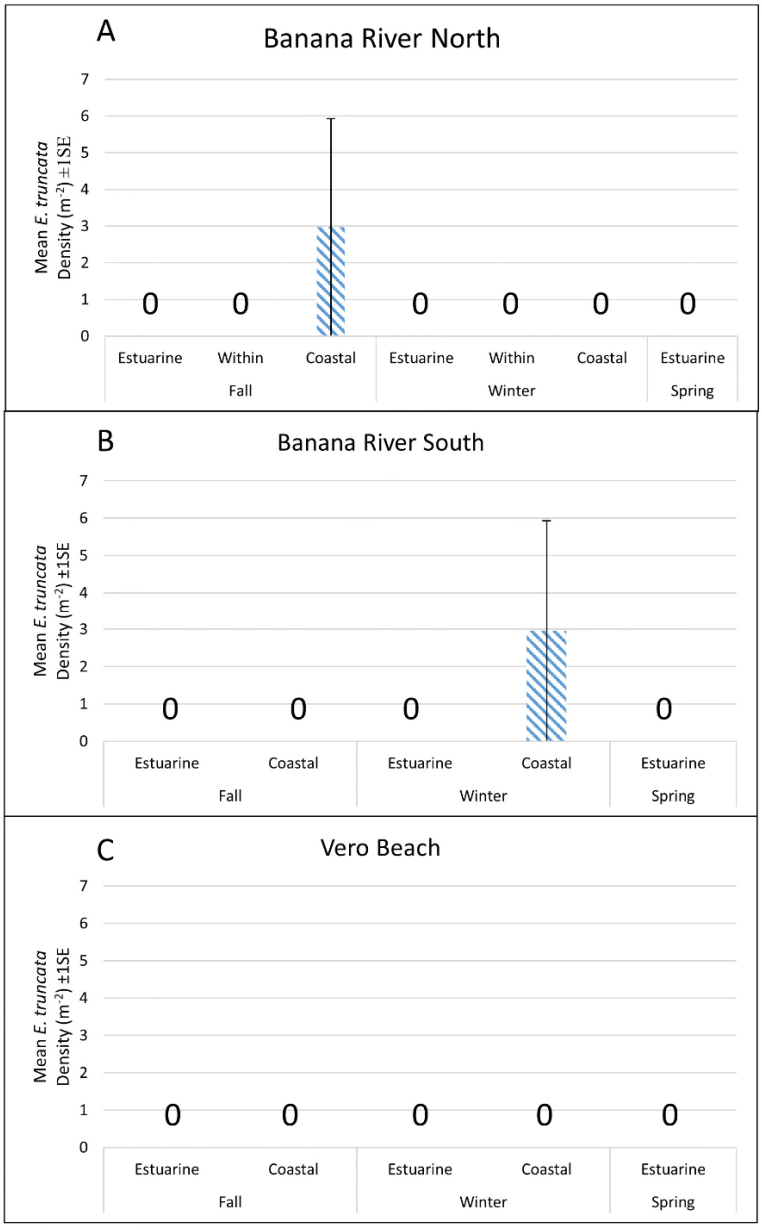

Note: "0" indicates cases of zero mean and variance.

Figure 3-11. Seasonal mean densities (number of individuals m-2) ±1 standard error (SE) of the gastropod *Ecrobia truncata* (SIC), in coastal sediments at two different proposed inflow sites (Banana River North Outside [BRNO] and Banana River South Outside [BRSO] – panels A and B, respectively).

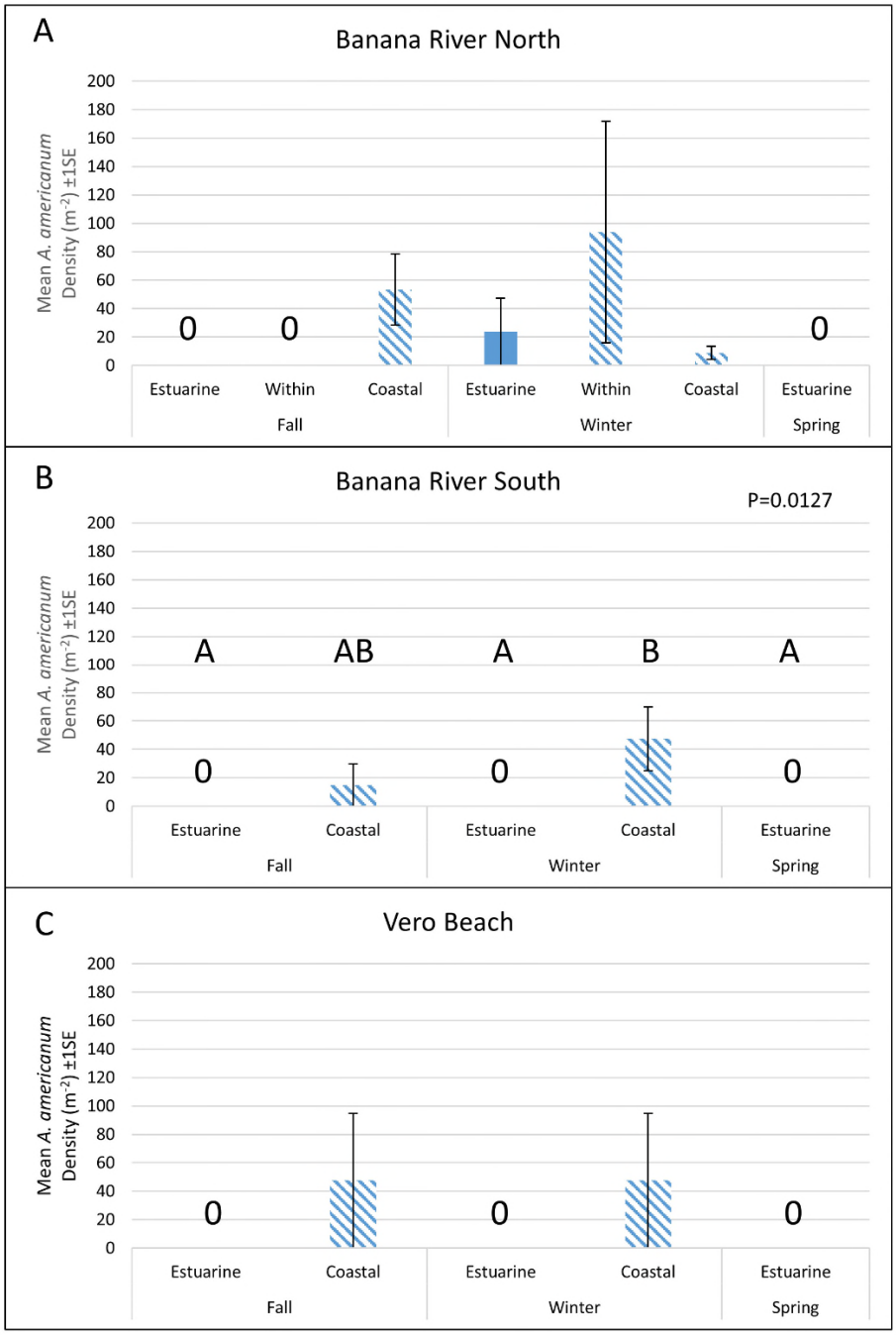

Note: “0” indicates cases of zero mean and variance. Statistically significantly different treatments based on ANOVA are indicated with disparate letters over the columns (α=0.05).

Figure 3-12. Seasonal mean densities (number of individuals m-2) ±1SE of the gammarid amphipod *Americhelidium americanum* (SIC), in coastal sediments at the three proposed inflow sites (BRNO, BRSO, and Vero Beach Outside [VBO] – panels A, B, and C, respectively). Limited abundance in estuary near lock at BRNI only.

Seven benthic infauna species were present in the estuary, but not observed in the coastal ocean (SESC). One species, the gastropod *Haminoea elegans*, was rare and found in just one replicate

sample in BRNI in each of fall and winter. Because of its scarcity, its abundance was not graphed here, but focus on the six other species which were absent from coastal samples, but present in the lagoon. They were three gammarid amphipods, one ostracod crustacean, one bivalve mollusc, and one gastropod mollusc (Figure 3-13 through Figure 3-18, respectively).

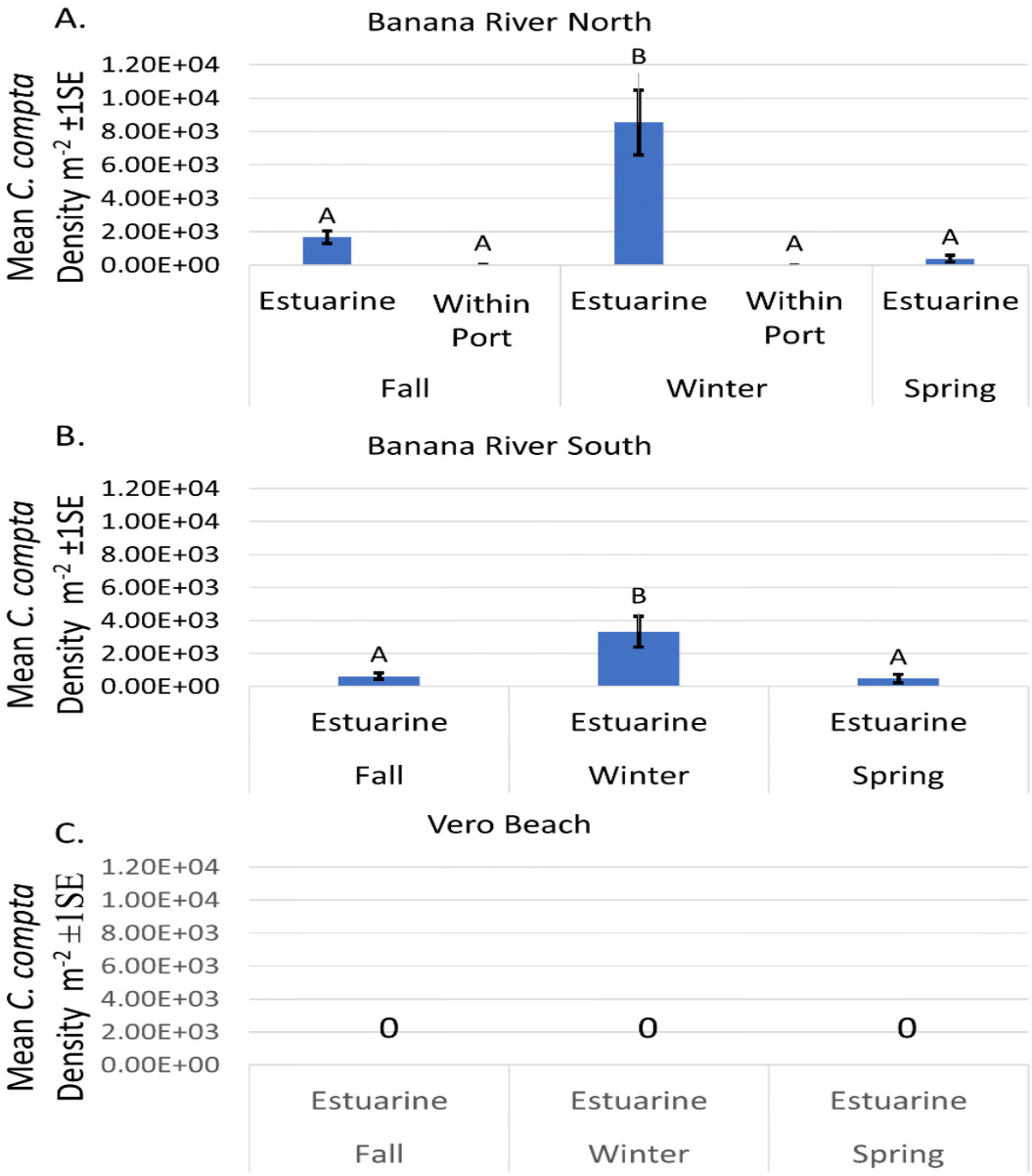

Note: "0" indicates zero mean and variance. Statistically significantly different treatments based on ANOVA are indicated with disparate letters (α=0.05). There were no *Cymadusa compta* in coastal sediments.

Figure 3-13. Seasonal mean densities (number of individuals m-2) ±1SE of the gammarid amphipod *Cymadusa compta* (SESC), in the IRL at three different proposed inflow sites (BRN, BRS, and VB – panels A, B, and C, respectively).

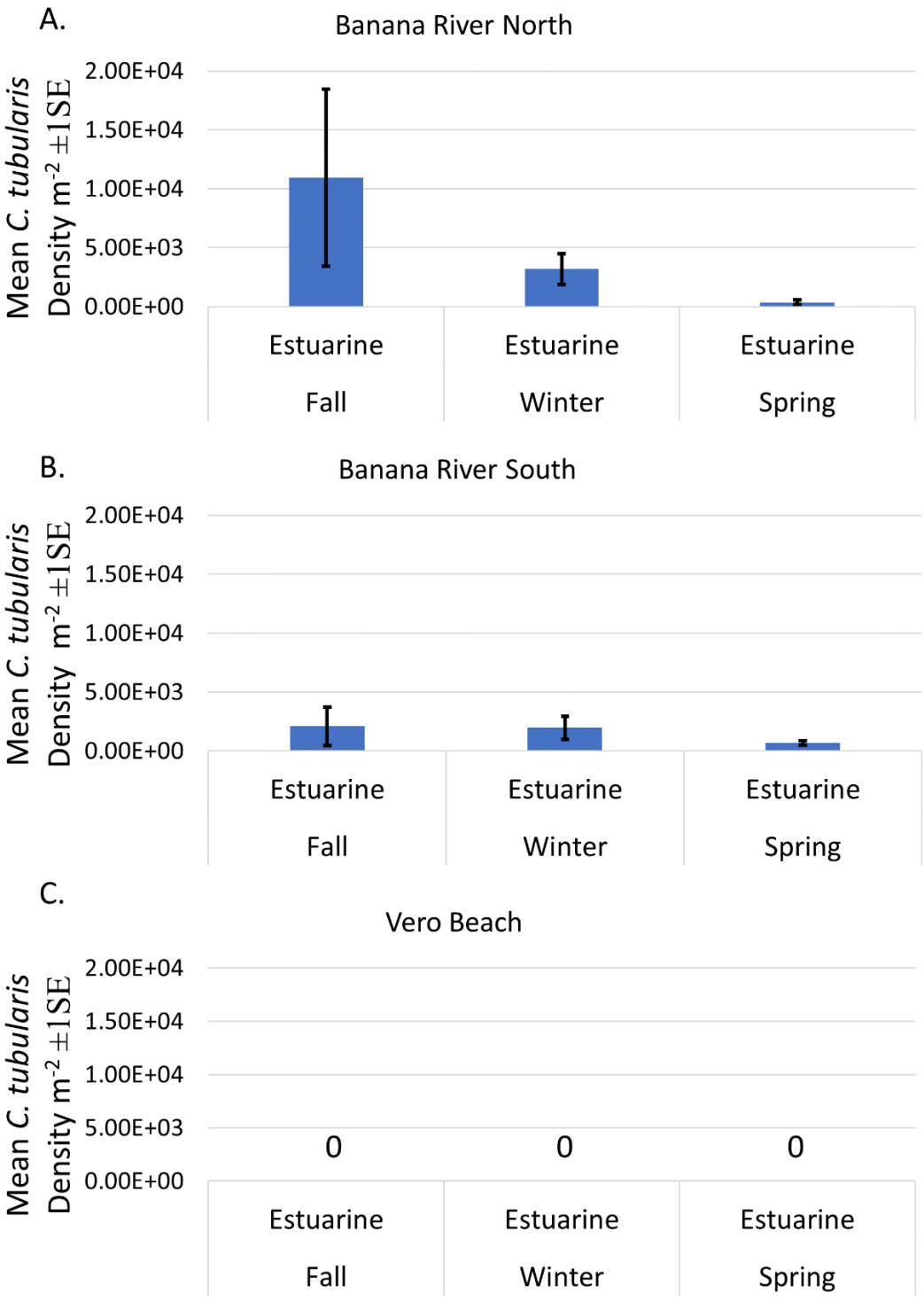

Note: "0" indicates cases of zero mean and variance. There were no *Cerapus tubularis* in coastal sediments.

Figure 3-14. Seasonal mean densities (number of individuals m-2) ±1SE of the gammarid amphipod *Cerapus tubularis* (SESC), in the IRL estuary at three different proposed inflow sites (BRN, BRS, and VB – panels A, B, and C, respectively).

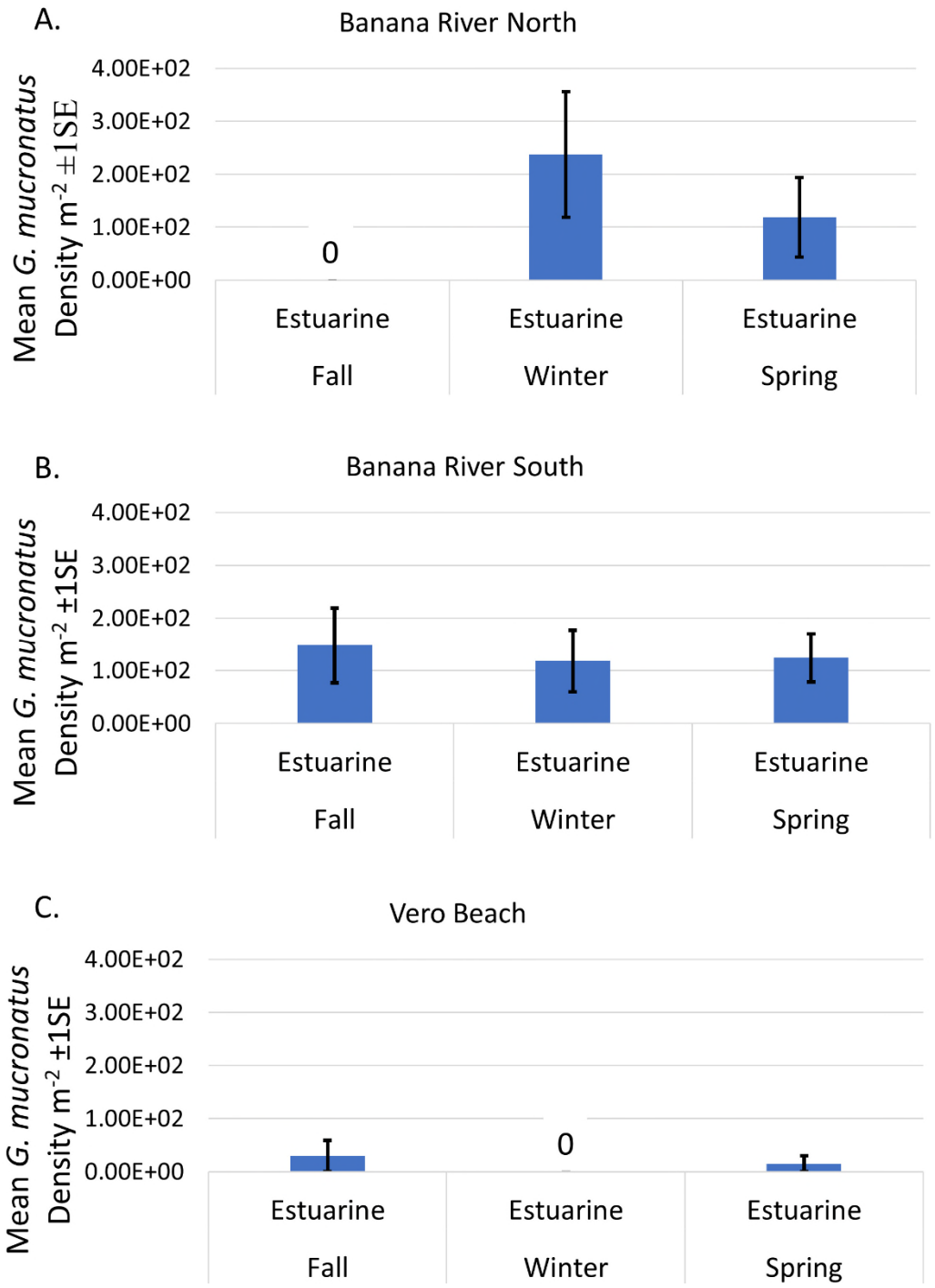

Note: "0" indicates cases of zero mean and variance. There were no *Gammarus mucronatus* in coastal sediments.

Figure 3-15. Seasonal mean densities (number of individuals m-2) ±1SE of the gammarid amphipod *Gammarus mucronatus* (SESC), in the IRL estuary at three different proposed inflow sites (BRN, BRS, and VB, panels – A, B, and C, respectively).

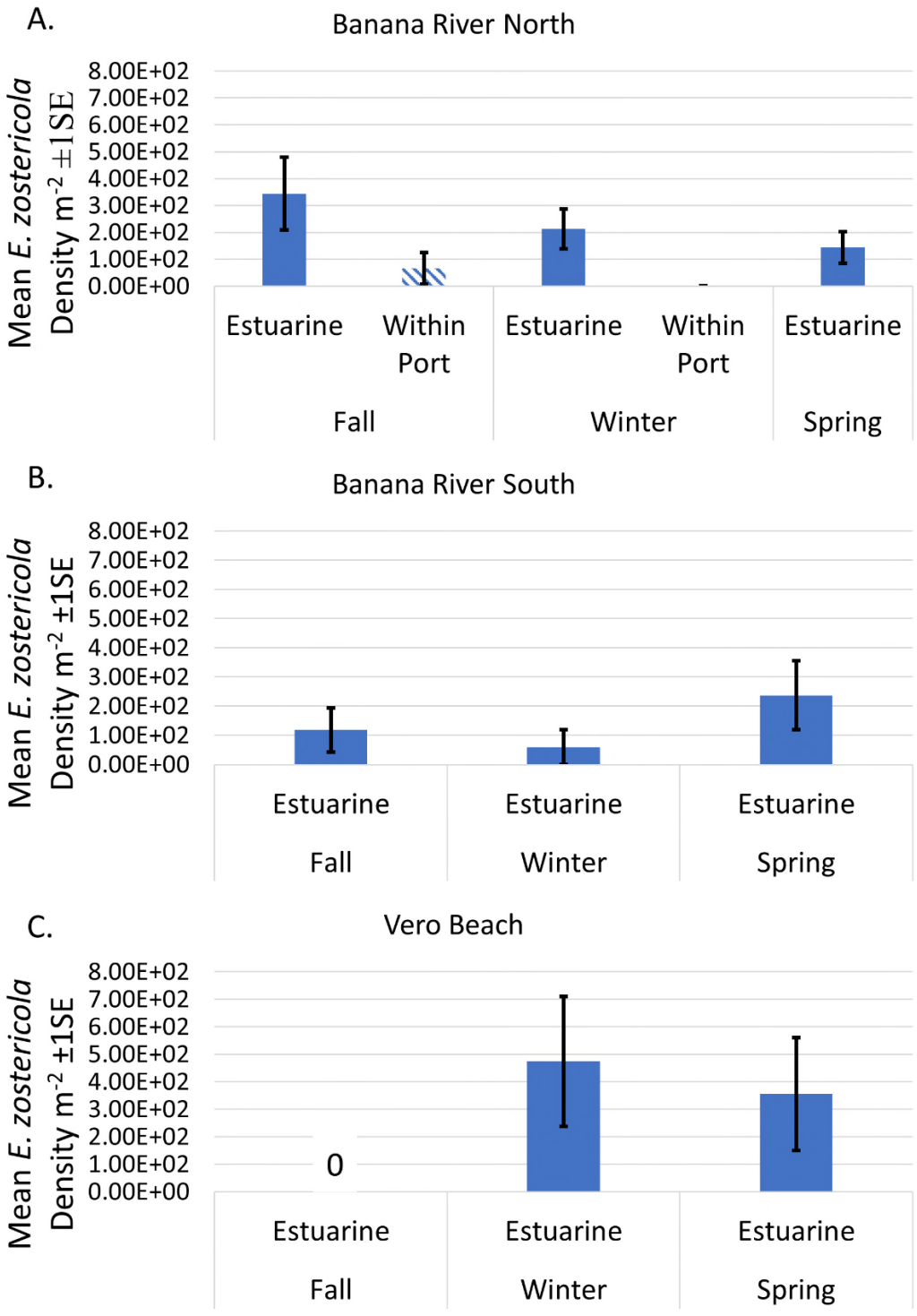

Note: "0" indicates cases of zero mean and variance. There were no *Eusarsiella zostericola* in coastal sediments.

Figure 3-16. Seasonal mean densities (number of individuals m^{-2}) ±1SE of the ostracod crustacean *Eusarsiella zostericola* (SESC), in the IRL estuary at three different proposed inflow sites (BRN, BRS, and VB – panels A, B, and C, respectively).

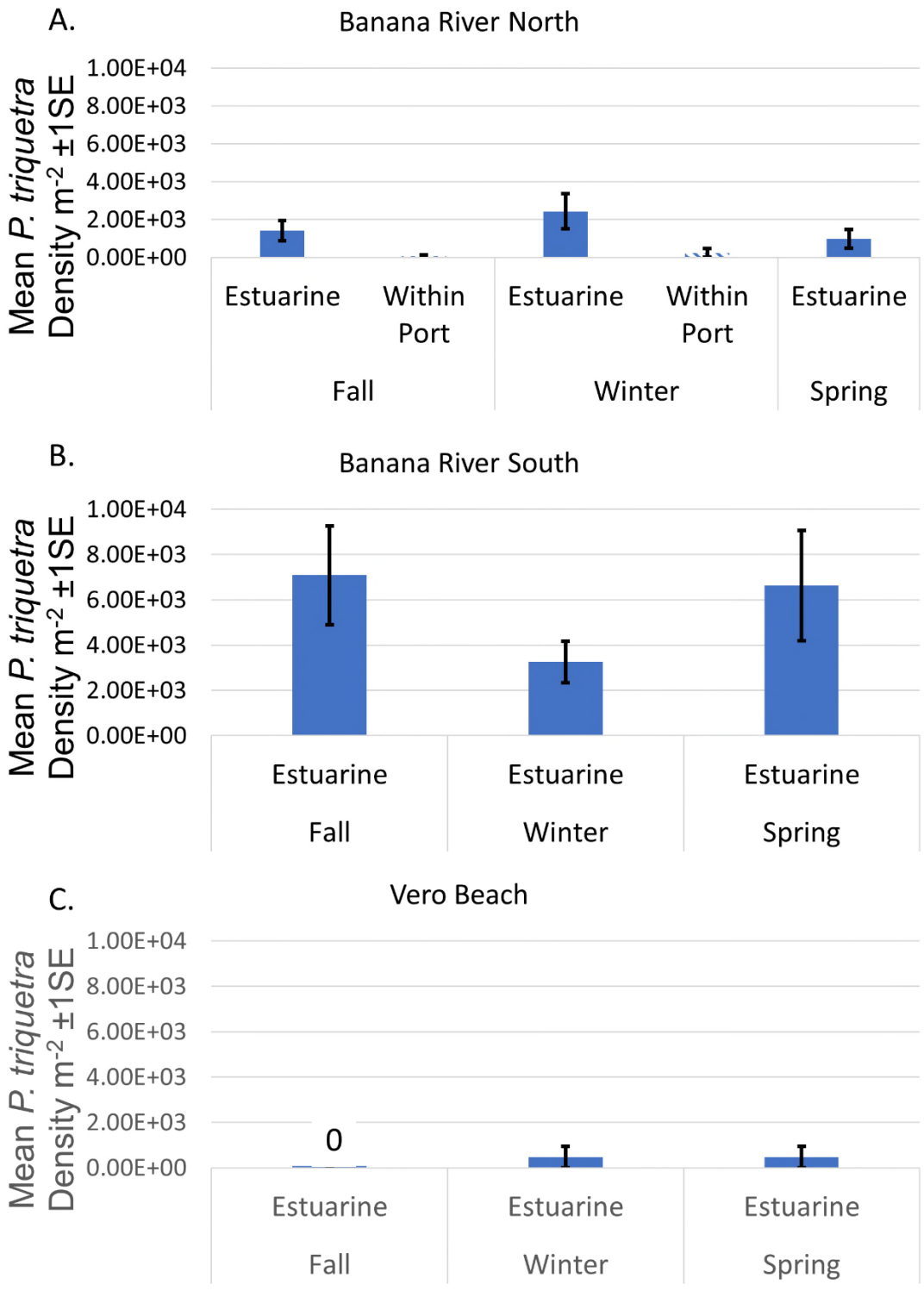

Note: "0" indicates cases of zero mean and variance. There were no *Parastarte triquetra* in coastal sediments.

Figure 3-17. Seasonal mean densities (number of individuals m^{-2}) ±1SE of the bivalve mollusc *Parastarte triquetra* (SESC), in the IRL estuary at three different proposed inflow sites (BRN, BRS, and VB – panels A, B, and C, respectively).

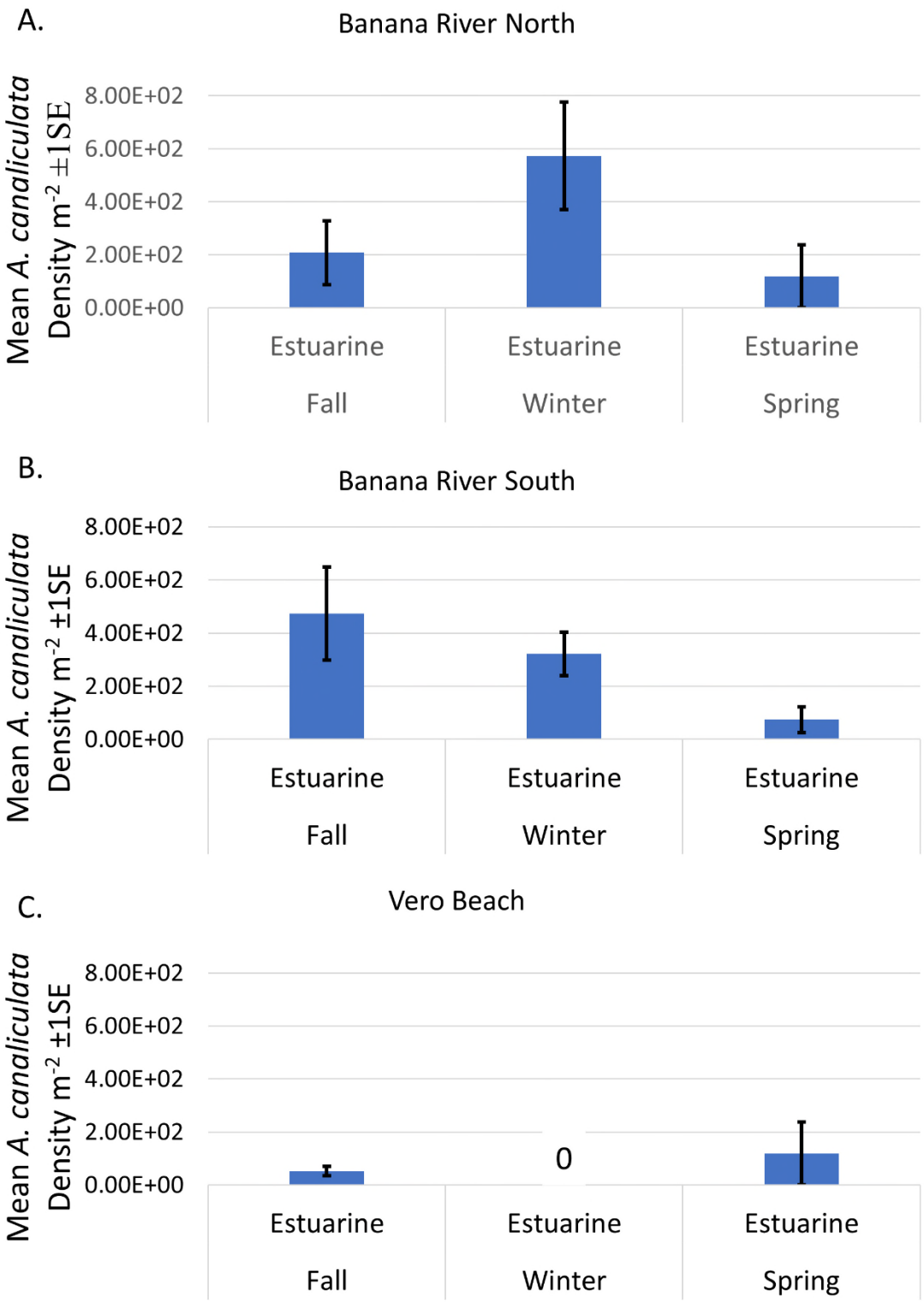

"0" indicates cases of zero mean and variance. There were no *Acteocina canaliculata* in coastal sediments.

Figure 3-18. Seasonal mean densities (number of individuals m^{-2}) ±1SE of the gastropod mollusc *Acteocina canaliculata* (SESC), in the IRL estuary at three different proposed inflow sites (BRN, BRS, and VB – panels A, B, and C, respectively).

3.3 Phytoplankton/Harmful Algae Results

The IRL and the corresponding outer coast stations share many phytoplankton species in common, but some are unique to one environmental or the other. For a list of the distributions and relative abundances of diatoms, see Table 3-2; for a similar list of dinoflagellates and other plankton, see Table 3-3.

List 4: Phytoplankton Species of Non-Concern (Type II scenario): Phytoplankton and tintinnid ciliate species found in both estuarine and coastal ocean sites include the following (from Table 3-2 and Table 3-3). Species or groups known to be harmful despite lack of toxicity (e.g., those with gill spikes or reputed to form anoxic blooms) are annotated with an asterisk (*). Species or groups with known or suspected toxicity are annotated with two asterisks (**):

- The diatoms: *Actinoptychus senarius*, *Asterionellopsis glacialis*, *Amphiprora* sp., *Amphora* sp.**, *Bacillaria paxillifera*, Chaetoceros spp., *Coscinodiscus* spp. *Cyclotella* sp., *Cylindrotheca closterium*, *Diploneis* sp., *Dactyliosolen fragilissimus*, *Grammatophora* spp., *Leptocylindrus danicus*, *Licmophora* sp., *Lithodesmium undulatum, Navicula* spp., *Nitzschia longissimi***, *Nitzschia* spp.**, *Odontella* spp., *Paralia sulcate, Pleurosigma* spp., *Pseudo-nitzschia* spp.**, *Rhizosolenia* spp.**, *Skeletonema costatum***, *Surirella* sp., *Thalassionema frauenfeldii, Thalassionema nitzschoides, Thalassiosira* sp.
- The dinoflagellates *Ceratium* spp.**, *Dinophysis* sp.**, *Oxytoxum* sp., *Peridinium* sp.**, *Prorocentrum* sp.**, *Protoperidinium* spp.**, *Pyrodinium bahamense***.
- The blue-green alga *Anabaena* sp.**.
- The tintinnids *Helicostomella sp.* and *Tintinnopsis sp.*
- The silicoflagellate *Dictyocha fibula**.
- An unidentified raphidophycean*.
- Tylostyle sponge spicules.

List 5: Phytoplankton Species of Potential Introduction Concern: Phytoplankton and other planktonic species found in the coastal ocean, but not observed in the IRL estuary in the surveys include the following (from Table 3-2 and Table 3-3). Species or groups known to be harmful despite lack of toxicity (e.g., those with gill spikes or reputed to form anoxic blooms) are annotated with an asterisk (*). Species or groups with known or suspected toxicity are annotated with two asterisks (**):

- The diatoms *Actinoptychus splendens, Amphitetras* sp., *Bacteriastrum* spp., *Bellerochea horologicalis, Bellerochea malleus, Biddulphia alternans, Biddulphia rhombus, Biddulphia* sp., *Climacodium frauenfeldianum, Corethron* spp., *Cymatosira belgica, Delphineis surirella, Detonula pumila, Eucampia* sp.*, *Grammatophora marina, Guinardia flaccida*, Guinardia striata*, Gyrosigma fasciola, Haslea wawrickae, Hemiaulus hauckii, Hemiaulus membranaceus, Hemiaulus sinensis, Hemiaulus* spp., *Lioloma pacificum, Melosira moniliformis, Meuniera membranacea, Stephanopyxis* sp., *Triceratium brightwellii, Triceratium* sp., *Trigonium* sp., and an unidentified raphid diatom.
- The dinoflagellates *Ceratocorys armata*, *Oxyphysis* sp., *Podolampas* sp.
- An episodically abundant, unidentified protiste.
- The blue-green algae *Lyngbya* sp.** and *Oscillatoria* sp.**

List 6: Phytoplankton SESC: Phytoplankton and tintinnid ciliate species found in the IRL estuary, but not observed in the coastal ocean in the surveys (from Table 3-2 and Table 3-3). Species or groups known to be harmful despite lack of toxicity (e.g., those with gill spikes or reputed to form

anoxic blooms) are annotated with an asterisk (*). Species or groups with known or suspected toxicity are annotated with two asterisks (**):

- The diatoms: *Amphora proteoides*, *Eunotogramma* sp., and *Pseudofalcula hyaline*.
- The dinoflagellates: *Actiniscus pentasterias*, *Dinophysis argus*, *Gonyaulax* spp.**, *Gymnodinium* spp.**, *Pyrocystis fusiformis*, *Pyrocystis lanceolate*, and an unidentified *Peridinium*-like dinoflagellate.
- The tintinnids *Amphorellopsis* sp. and *Eutintinnus* sp.
- An unidentified cryptophycean.

Table 3-2. Seasonal presence/absence of planktonic diatoms at proposed inflow sites, inside the estuary (IRL) and in the coastal ocean (CO).

Note: Species present (L, M, or H), absent (blank), and relative abundances (L, M, and H for low, medium, and high) are indicated. "L" is present in 1 station, "M" is 2–3, and "H" is 4. Known harmful algae (anoxia) are indicated with at least one asterisk (*), while known or suspected toxin producers have two asterisks (**).

	Banana River North							Banana River South					Vero Beach				
	Fall			Winter			Spring	Fall		Winter		Spring	Fall		Winter		Spring
Diatoms	IRL	WP	CO	IRL	W	CO	IRL	IRL	CO	IRL	CO	IRL	IRL	CO	IRL	CO	IRL
Actinoptychus senarius			L			L	L		L			M			L		
Actinoptychus splendens									L								
Asterionellopsis glacialis		H	H		M	M			H					L	L	M	
Amphiprora sp.						M	L				L			M	L	M	
Amphitetras sp.									L								
Amphora proteoides													L				
Amphora sp. **			M	M	H	L	L			L	L	L	L	L	M	M	M
Bacillaria paxillifera			M		L	L			L				H		L	L	
Bacteriastrum spp.			M			H			M		L			H		M	
Bellerochea horologicalis			L														
Bellerochea malleus		L							M								
Biddulphia alternans					H	M											
Biddulphia rhombus						M			L								
Biddulphia sp.					L											L	
Chaetoceros spp.	H	H	H	H	H	H	H	H	H	M	H	M	H	H	L	M	H
Climacodium																L	
Corethron spp.		L	M		L	H			M					L			
Coscinodiscus spp.	M	H	H	L	H	H	H	M	H		L	M	M	M	M	M	L
Cyclotella sp.	L		L		L	L	M					L					
Cylindrotheca closterium *		H	H	M	M	M			H	L	M		H	M	L	H	M
Cymatosira belgica		L	H		M	H			M					L		M	
Delphineis surirella		L															
Diploneis sp.									L								L
Dactyliosolen fragilissimus *					M	L	H			M						M	
Detonula pumila					L												
Eucampia sp. *					M	H										M	
Eunotogramma sp.				L			L								L		L
Grammatophora marina			L														
Grammatophora spp.		L					L						M				L
Guinardia flaccida *		M	M			M			M					H			
Guinardia striata *			M		L	M			M		M			M		M	
Gyrosigma fasciola					L												
Haslea wawrickae			L													L	
Hemiaulus hauckii		M	M			H								M			
Hemiaulus membranaceus						H			M					M			
Hemiaulus sinensis					L	L											
Hemiaulus spp.			L			L			M					M		L	
Leptocylindrus danicus	H	H	L	L	L	M	H	H		M	M		M	H		L	
Licmophora sp.						H							L	L		L	L
Lioloma pacificum						L											
Lithodesmium undulatum									L				M		M		
Melosira moniliformis					L												
Meuniera membranacea									L								
Navicula spp. **			H	H	M	H			M	L	M	L	M	M	M	M	M
Nitzschia longissima **			L		L		L						L				
Nitzschia spp.		M	M	L	H	H	M	L	M		H	L	H	M	H	M	M
Odontella spp.		M	H		H	H			M	M		M		M		M	
Paralia sulcata		M	H	L	H	H			H	L			M	M	H	L	M
Pleurosigma spp.		M	H	M	H	H	M		M	M	L	M	M	M	L	H	H
Pseudofalcula hyalina															M		
Pseudo-nitzschia spp. **		M	H		L	M			M		L			H	H	H	M
Rhizoselenia spp. **	H	M	H			H	H	L	H	H	H	L	H	H	M	H	H
Skeletonema costatum **		L	H		L	H			H		L		H			M	H
Stephanopyxis sp. *		H	M		L	M								M			
Surirella sp.					M							L					L
Thalassionema frauenfeldii		M	H			L			H		L		L	H		H	
Thalassionema nitzschoides		H	H	L	H	H			H	L	M		M	H	L	H	
Thalassiosira sp.					L	M	L										
Triceratium brightwellii					M	H											
Triceratium sp.		L	L		L	M			M								
Trigonium sp.						L											
Unidentified Raphid Diatom			L														

Table 3-3. Seasonal presence/absence of dinoflagellates and other plankton at proposed inflow sites, inside the estuary (IRL) and in the coastal ocean (CO).

Note: Species present (L, M, or H), absent (blank), and relative abundances (L, M, and H for low, medium, and high, respectively) are indicated. "L" is present in 1 station, "M" is 2–3 , and "H" is 4. Known harmful algae (e.g., those reputed to form blooms causing anoxia) are indicated with at least one asterisk (*), while known or suspected toxin producers have two asterisks (**).

	Banana River North							Banana River South						Vero Beach				
	Fall			Winter			Spring	Fall		Winter		Spring		Fall		Winter		Spring
Dinoflagellates	IRL	WP	CO	IRL	W	CO	IRL	IRL	CO	IRL	CO	IRL		IRL	CO	IRL	CO	IRL
Actiniscus pentasterias																L		
Ceratium spp. **	L	L	H			M	H	L	M		H	H		L	H		M	H
Ceratocorys armata											L							
Dinophysis argus							L					L						
Dinophysis sp. **						M												L
Gonyaulax spp. **	M						H					H						M
Gymnodinium spp. **										H		L						M
Oxyphysis sp.						L												
Oxytoxum sp.												M					L	
Peridinium sp. **						M	M				M	H						H
Peridinium-like sp.	L																	
Podolampas sp.						L					M							
Prorocentrum sp. **					L	M	H		M	L		H						M
Protoperidinium spp. **	L						M			L		L		L	M			
Pyrocystis fusiformis												L						
Pyrocystis lanceolata																		L
Pyrodinium bahamense **		L					L					L						
Blue-Green Algae																		
Anabaena sp. **						L										L		
Lyngbya sp. **																	L	
Oscillatoria sp. **					L												M	
Tintinnids:																		
Amphorellopsis sp.												L						
Eutintinnus sp.							H					M						H
Helicostomella sp.	H					H	L								H			
Tintinnopsis sp.						M						L				M		M
Silicoflagellates:																		
Dictyocha fibula *			M		M	M	H		M						M			
Other:																		
Cryptophycean												L						
Raphidophycean *	L						H	L	M	M		H						L
Sponge Spicules				L	M		L	L		L		M			L	H	L	
Unidentified Protist					H	M												

The most abundant phytoplankton were non-cyanobacterial cells less than 40-µm, and these tended to be more abundant in the estuary than the coastal water column, except for BRN during the winter. The highest observed cell density was 6.1×10^7 cells L^{-1} in the estuary at Vero Beach (Figure 3-19 panel A). The next most abundant group of phytoplankton were the cyanobacteria identified by the presence of phycoerythrin pigments, and these tended to be more abundant in coastal compared to estuarine waters, with densities ranging from 1.1×10^7 to 3.5×10^7 cells L^{-1} (Figure 3-19 panel C).

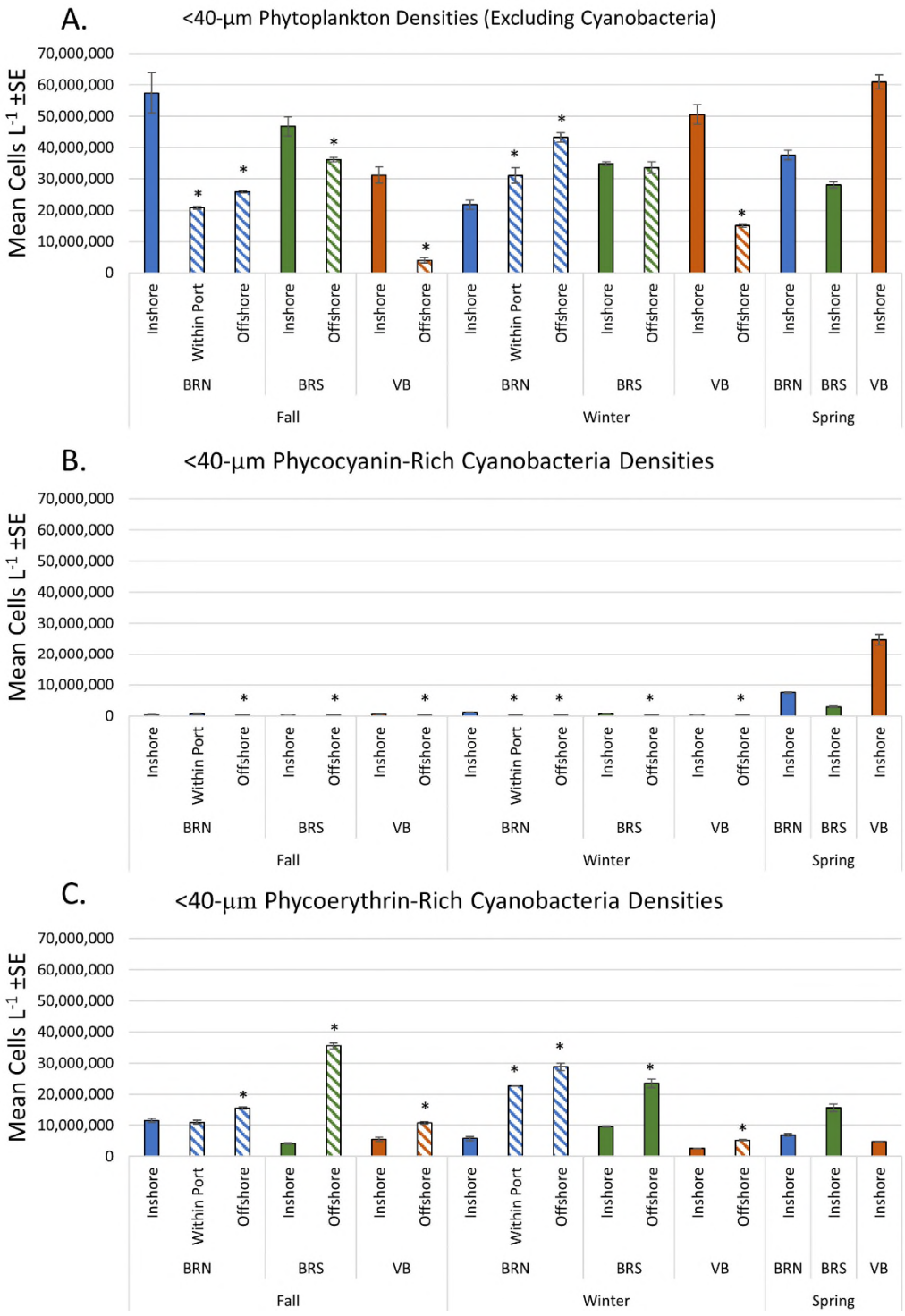

Note: Asterisks indicate statistically significant differences between offshore locations relative to their corresponding estuary site during a given season. "Inshore" is within the estuary. "Offshore" is coastal.

Figure 3-19. Less than 40-µm phytoplankton densities for A. non-cyanobacteria, B. cyanobacteria as indicated by phycocyanin presence, and C. cyanobacteria as indicated by phycoerythrin presence.

Larger phytoplankton (greater than 25-µm due to tow net mesh size) were mostly diatoms and dinoflagellates (Table 3-2 and Table 3-3). The greatest abundance of greater than 25-µm cells was $4.5x10^3$ cells L^{-1} in the estuary at BRS (Figure 3-20). Patterns of greatest abundance for phytoplankton greater than 25-µm are variable and may occur in the estuary or coastal waters at different sites and at different times of year (Figure 3-20).

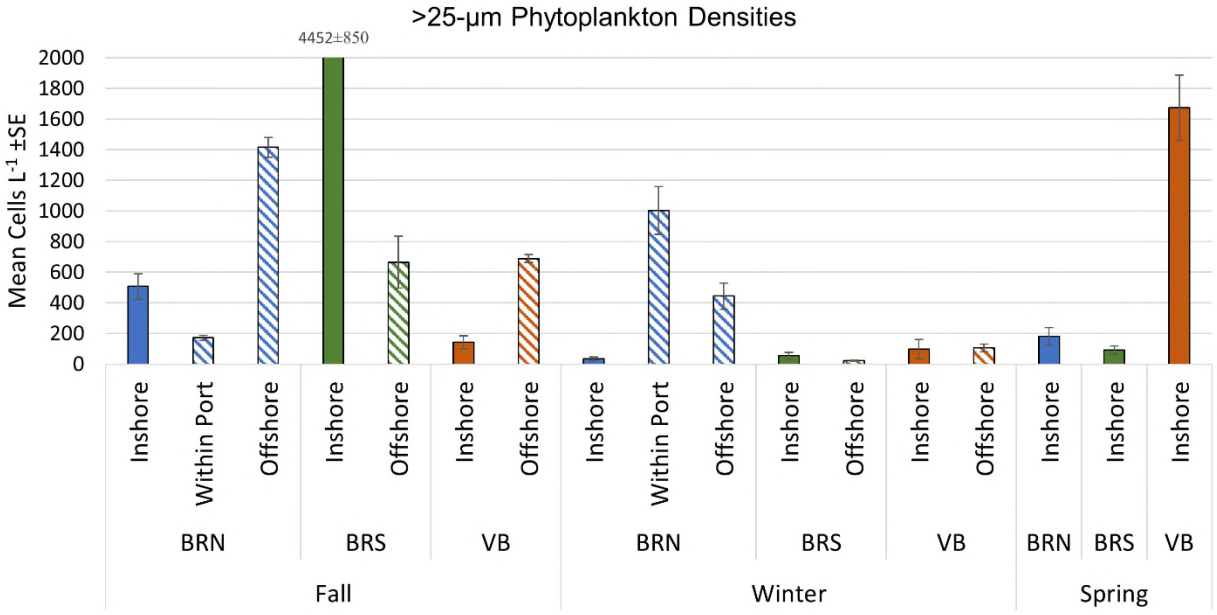

Note: "Inshore" is within the estuary. "Offshore" is coastal.

Figure 3-20. Greater than 25-µm phytoplankton mean densities inside and outside of potential inflow sites in fall 2019, winter 2020, and spring 2020.

Phytoplankton biodiversity, species richness, and evenness were calculated for tow plankton less than 25-µm (Figure 3-21). Diversity, richness, and evenness tended to be significantly greater in coastal waters.

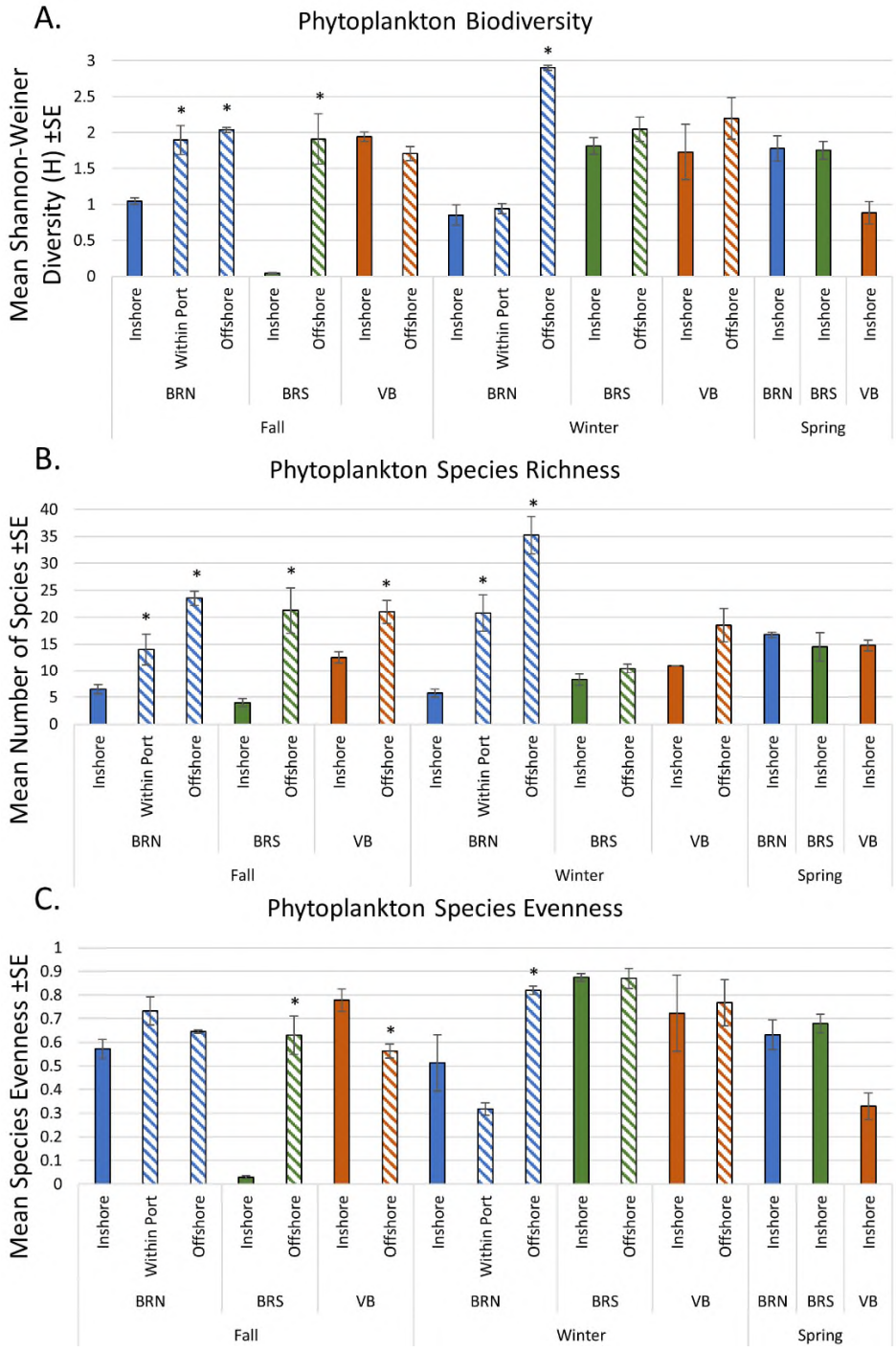

Note: Asterisks indicate significant differences (α=0.05) between the estuarine phytoplankton community relative to the coastal ocean at the same site. "Inshore" is within the estuary. "Offshore" is coastal.

Figure 3-21. Phytoplankton mean Shannon-Weiner Diversity Index (A), mean species richness (B), and mean community evenness (C). Comparisons are made between the estuary (BRNI, BRSI, and VBI, respectively) and the same latitude in the coastal ocean at each of the potential inflow sites (BRNO, BRSO and VBO, respectively).

Using NMDS plots to group communities based on relative species abundances shows communities fall out based on season and location (Figure 3-22, stress 0.11–0.19, ANOSIM

R=0.93– 0.96, p<0.05). Estuarine plankton communities were more distinct from one another based on the three sites within the estuary. Coastal community groupings from different sites were closer together and came very close to overlapping.

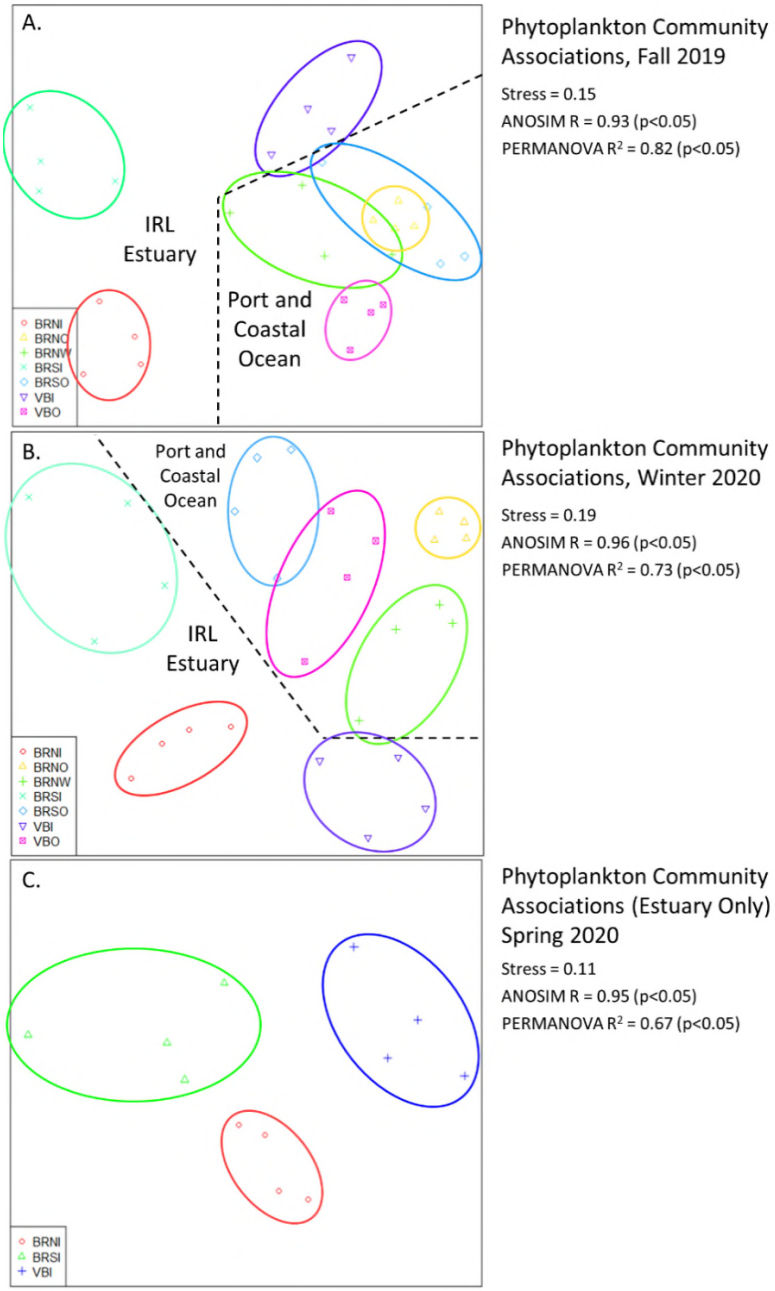

Note: See legends for site key for color/shape symbols. Symbols represent Banana River North (BRNI, BRN Within-Port, and BRNO), Banana River South (BRSI and BRSO), and Vero Beach (VBI and VBO).

Figure 3-22. NMDS associations of less than 25-µm phytoplankton communities based on species and abundances, comparing within the estuary vs. the outer coast for fall 2019, winter 2020, and spring 2020 (panels A, B and C, respectively).

Phytoplankton species and groups documented in coastal waters, but unobserved in the estuary, included 31 diatoms, three dinoflagellates, one unidentified protist, and two cyanobacteria (see Table 3-2 and Table 3-3, and the lists presented at the beginning of this section). These included

five harmful or toxic species. Due to the fluid connection between the coastal zone and the estuary through the Port Canaveral locks and Sebastian Inlet, these microalgae have likely had opportunities to be advected into the estuary. Their absence in the IRL may be due to inability to survive under variable estuarine conditions, or they may be present but undetectable during sampling (low numbers or encysted in sediments).

Two phytoplankton genera with known toxicity were present in the estuary, but not observed in coastal ocean plankton (SESC). Representatives of the genus *Gonyaulax* were somewhat present in the fall, absent in winter, and most consistently present in spring (Figure 3-23). However, even in spring, densities ranged from 1-18 cells L^{-1}, far below bloom densities. Representatives of the genus *Gymnodinium* were absent in the fall and somewhat present in winter and spring (8 and 9 cells L-1, respectively, when present; Figure 3-23).

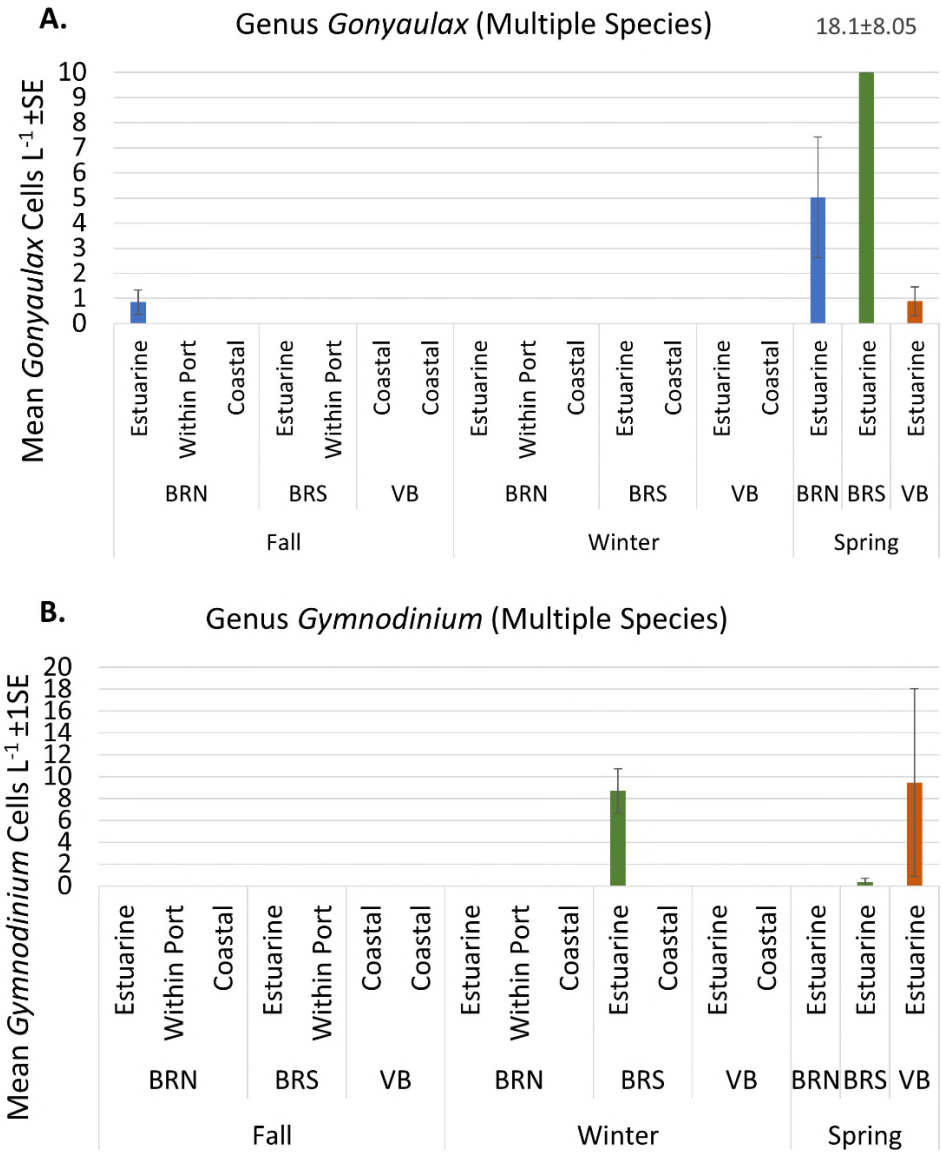

Figure 3-23. Mean densities (number of individuals m^{-3}) ±1SE of phytoplankton species D (SESC), comparing in the estuary vs. the outer coast at three different potential sites of restored lagoon inflow.

3.4 Ichthyoplankton Results

A total of 2,824 larval fishes from 23 taxa were collected in 52 light trap samples made on 11 nights at the Port Canaveral Lock and the Biofouling Research Platform. The ichthyoplankton samples taken in Port Canaveral and the adjacent IRL illustrate seasonal patterns in reproduction in various species, and the role of the Port Canaveral Lock as a means of limited larval recruitment into the IRL. Only 12 larvae were taken in the towed ichthyoplankton samples (0–4 larvae/tow). Four species dominated the light trap samples, with Atlantic menhaden (*Brevoortia tyrannus*) comprising 35.2% of the total catch, bay anchovies (*Anchoa mitchilli*; 27.8%), scaled sardine (*Harengula jaguana*; 27.1%) and threadfin herring (*Opisthonema oglinum*; 6.2%). These species are pelagic schooling planktivores that are important prey for piscivorous fishes within the IRL. With the exception of the estuarine-spawning anchovies, the other species spawn in offshore waters and have larvae that migrate into estuarine nursery habitats.

The initial sets of light trap samples, taken in December 2019 (Table 3-4) clearly demonstrate the larval distribution and movement patterns of menhaden and anchovies. Although both species are pelagic schooling fishes, anchovies spawn within the estuary, while menhaden spawn in offshore waters near the western edge of the Gulf Stream along the Atlantic seaboard, with larvae then migrating into estuarine nursery habitats (Checkley et al. 1981; Warlen and Burke 1990). During the first night of sampling, all 130 anchovies collected were taken in light traps on the IRL side of the Port Canaveral Lock, while all 248 menhaden were in traps on the ocean side of the lock. The two other nights sampled in December showed a similar pattern, with 88% of all anchovies collected on the IRL side, and 97% of menhaden larvae taken on the eastern side. Being estuarine spawners and inhabitants, the anchovies could spawn within Port Canaveral as well as the IRL and move through the lock when it opens during ebb or flood tides. Conversely, oceanic menhaden larvae appear to accumulate at the eastern lock gate, move into the IRL when the lock opens, then disperse into the open IRL.

The only other species taken in light traps in December in significant numbers was ladyfish (*Elops saurus*). This offshore-spawning species produces larvae that migrate through inlets such as Sebastian Inlet (Wheeler 2005) to reach their estuarine nurseries along the southeast coast of the United States. As with offshore-spawning menhaden, the catch of ladyfish larvae was concentrated in traps on the Port Canaveral side of the lock, with the low catch on the IRL side of the lock reflecting their dispersal into the IRL.

Although the lock maintenance shutdown precluded light trap sampling in early 2020, and the daytime plankton tows in January and February were not successful at catching fish larvae, light traps deployed in March at the Biofouling Research Platform in Port Canaveral showed that menhaden larvae were still recruiting into the system, even if they were not able to access the IRL nursery habitat. Large numbers of menhaden dominated the March samples, along with bay anchovies that presumably resulted from spawning within Port Canaveral waters (Table 3-5). Low numbers of other estuarine and offshore-spawning taxa were also collected by the light traps in March. Additional light trap sampling was conducted in mid-May, first at the Biofouling Research Platform and then at the lock. By May, the spawning season for menhaden had ceased, but large numbers of offshore-spawned larval scaled sardines (*Harengula jaguana*) and threadfin herrings (*Opisthonema oglinum*) in the samples taken at both sites within the Port indicated the seasonal occurrence of their spawning activity (Table 3-4 and Table 3-5). Much lower numbers of these larvae were taken in the light traps on the IRL side of the lock, suggesting their rapid dispersal after movement into the IRL. As with menhaden, the planktivorous schooling scaled sardines and threadfin herrings use estuarine nursery habitats and play a major role as prey for many IRL fishes.

Table 3-4. Total catches of larval fishes taken in light traps deployed overnight on the East side and West side of the Port Canaveral Lock.

Note: n = number of light traps. % E = proportion of total catch of each taxon on the Port Canaveral (east) side of the lock. Spawning habitat: O = Ocean, E = Estuarine.

Species	Common Name	Spawn Habitat	12/20/19 E (n=2)	12/20/19 W (n=2)	12/23/19 E (n=2)	12/23/19 W (n=2)	12/31/19 E (n=2)	12/31/19 W (n=2)	5/27/20 E (n=3)	5/27/20 W (n=3)	5/28/20 E (n=2)	5/28/20 W (n=3)	5/29/20 E (n=3)	5/29/20 W (n=3)	Total (n=29)	% E
Harengula jaguana	Scaled sardine	O	0	0	0	0	0	0	38	1	18	1	551	5	614	98.9
Anchoa mitchilli	Bay anchovy	E	0	130	0	90	32	44	28	41	10	25	61	13	474	27.6
Brevoortia tyrannus	Atlantic menhaden	O	248	0	9	1	88	11	0	0	0	0	0	0	357	96.6
Opisthonema oglinum	Threadfin herring	O	0	0	0	0	0	0	4	0	8	0	164	0	176	100.0
Elops saurus	Ladyfish	O	0	0	0	0	12	2	0	0	1	0	2	0	17	88.2
Gobiosoma bosc	Naked goby	E	0	0	0	0	0	0	0	0	0	1	2	2	5	40.0
Eucinostomus sp.	Mojarras	O	0	0	0	0	0	0	1	0	1	1	1	0	4	75.0
Megalops atlanticus	Tarpon	O	0	0	0	0	0	0	0	0	0	1	2	0	3	66.7
Chasmodes sp.	Combtooth blenny	E	0	0	0	0	0	0	0	1	0	1	0	0	2	0.0
Lagodon rhomboides	Pinfish	O	1	0	0	0	0	0	0	0	0	0	0	0	1	100.0
Microgobius gulosus	Clown goby	E	0	0	0	0	0	0	1	0	1	0	0	0	2	100.0
Archosargus rhomboidalis	Sea bream	O	0	0	0	0	1	0	0	0	0	0	0	0	1	100.0
Caranx hippos	Jack crevalle	O	0	0	0	0	0	0	0	0	0	0	0	1	1	0.0
Gobiosoma ginsburgi	Seaboard goby	E	0	0	0	0	0	0	0	0	0	0	1	0	1	100.0
Micropogonias undulatus	Atlantic croaker	O	0	0	0	0	1	0	0	0	0	0	0	0	1	100.0
Stephanolepis hispidus	Planehead filefish	O	0	0	0	0	0	0	1	0	0	0	0	0	1	100.0
Syngnathus sp.	Pipefish	E	0	0	0	0	0	0	0	0	0	1	0	0	1	0.0
Trachinotus falcatus	Pompano	O	0	0	0	0	0	0	0	0	0	0	1	0	1	100.0
Leiostomus xanthurus	Spot	O	0	0	0	0	1	0	0	0	0	0	0	0	1	100.0
Unidentified	-	-	0	0	0	0	0	0	0	0	0	1	0	0	1	0.0
Total	***Total***	***-***	***249***	***130***	***9***	***91***	***135***	***57***	***73***	***43***	***39***	***32***	***785***	***21***	***1,664***	***77.5***

Table 3-5. Total catch of larval fishes in light traps deployed overnight at the Biofouling Research Platform in Port Canaveral.

Note: n = number of light traps. Spawning habitat: O = Oceanic, E = Estuarine.

Species	Common Name	Spawning Habitat	3/23/2020 (n=5)	3/24/2020 (n=5)	5/18/2020 (n=5)	5/19/2020 (n=4)	5/20/2020 (n=4)	Total (n=23)
Brevoortia tyrannus	Atlantic menhaden	O	444	190	0	0	2	636
Anchoa mitchilli	Bay anchovy	E	82	36	114	66	12	310
Harengula jaguana	Scaled sardine	O	0	0	120	23	7	150
Eucinostomus sp.	Mojarras	O	3	4	16	3	4	30
Gobiosoma bosc	Naked goby	E	0	0	8	1	0	9
Lagodon rhomboides	Pinfish	O	2	5	1	0	0	8
Microgobius gulosus	Clown goby	E	1	3	3	1	0	8
Haemulon sp.	Grunts	O	2	2	0	0	0	4
Blenniidae	Blennies	E	1	0	0	0	2	3
Sparidae	Porgies	O	1	0	0	0	0	1
Gobiidae	Gobies	E	1	0	0	0	0	1
Total Fishes	***Total***	***-***	***537***	***240***	***262***	***94***	***27***	***1,160***

Two larval tarpon (*Megalops atlanticus*) larvae were also collected in late May on the east side of the lock. These larvae represent the initial spawning efforts of a valuable species that spawn in offshore waters from May through September. Juveniles tarpon are often abundant in marsh and mosquito control impoundment nursery habitats in the northernmost areas of the IRL, around Mims and Scottsmoor (Zugelter 2019; personal observations). Although tarpon larvae recruit through Sebastian Inlet (Shenker et al. 2002), the inlet is over 100 km from those nursery habitats, while Port Canaveral is only 45 km away. The lock may thus provide a pathway for larvae of this valuable fishery species to reach the northern IRL marsh habitats.

Examination of the total catch showed that 1,178 larvae from 13 offshore-spawning species and 485 larvae from 6 estuarine-spawning species were collected on the east and west sides of the lock in December and May. Nearly 78% of all larvae were captured on the Port Canaveral side of the lock.

3.5 Fish Analysis Results

There are 258 species of fish in the IRL including mostly forage fish and economically important species (Appendix 1). Of this total number of fish species, 94 were noted in Site 1, 85 in Site 2, and 159 in Site 3. The rank order of abundance of the top 20 species in each location is presented in Table 3-6. The IRL is dominated by forage fish (also known as “lower trophic level species”), especially bay anchovies, *Anchoa mitchilli*, striped mullet, *Mugil cephalus* and pinfish, *Lagodon rhomboides*. The rank order of abundance of these dominant species, except for bay anchovies, which remains the most abundant fish in all sites, varies among the three sites of interest. Among the economically important species of fish, the spotted sea trout, *Cynoscion nebulosus*, red drum, *Sciaenops ocellatus*, and ladyfish, *Elops saurus* occur in at least two of the sites of interest.

Table 3-6. Top 20 most abundant fish species in the IRL and in each of the three sites of interest.

Note: #Fish is presented as the highest annual total number of fish caught during the sampling period 1996 to 2018. Note the variation in the rank-order of the top 20 species in each location.

Top 20 Species in the IRL	#Fish	Top 20 Species in Site 1	#Fish	Top 20 Species in Site 2	#Fish	Top 20 Species in Site 3	#Fish
Anchoa mitchilli	231,704	*Anchoa mitchilli*	34,562	*Anchoa mitchilli*	33,327	*Anchoa mitchilli*	53,796
Lucania parva	23,040	*Micropogonias undulatus*	7,168	*Mugil cephalus*	1,924	*Micropogonias undulatus*	7,252
Leiostomus xanthurus	13,888	*Lucania parva*	6,880	*Lucania parva*	1,744	*Lagodon rhomboides*	4,748
Mugil cephalus	11,010	*Lagodon rhomboides*	6,618	*Bairdiella chrysoura*	1,722	*Harengula jaguana*	4,666
Lagodon rhomboides	9,798	*Opisthonema oglinum*	3,504	*Diapterus auratus*	1,581	*Orthopristis chrysoptera*	3,570
Bairdiella chrysoura	9,297	*Bairdiella chrysoura*	3,294	*Leiostomus xanthurus*	1,557	*Mugil curema*	3,006
Harengula jaguana	7,490	*Mugil cephalus*	1,998	*Lagodon rhomboides*	1,488	*Leiostomus xanthurus*	2,784
Diapterus auratus	7,398	*Poecilia latipinna*	1,728	*Eucinostomus harengulus*	1,035	*Mugil cephalus*	2,257
Micropogonias undulatus	7,252	*Mugil curema*	1,587	*Ariopsis felis*	940	*Diapterus auratus*	1,995
Mugil curema	4,780	*Leiostomus xanthurus*	1,424	*Microgobius gulosus*	768	*Bairdiella chrysoura*	1,728
Elops saurus	4,707	*Floridichthys carpio*	1,344	*Cynoscion nebulosus*	482	*Ariopsis felis*	1,461
Anchoa hepsetus	4,528	*Eucinostomus harengulus*	1,224	*Harengula jaguana*	452	*Anchoa hepsetus*	1,280
Eucinostomus gula	4,480	*Diapterus auratus*	1,179	*Eucinostomus gula*	432	*Lucania parva*	1,144
Eucinostomus harengulus	4,390	*Cynoscion complex*	776	*Mugil curema*	416	*Eucinostomus harengulus*	982
Opisthonema oglinum	4,143	*Microgobius gulosus*	716	*Gobiosoma robustum*	304	*Opisthonema oglinum*	957
Floridichthys carpio	3,904	*Cyprinodon variegatus*	688	*Oligoplites saurus*	282	*Archosargus rhomboidalis*	772
Orthopristis chrysoptera	3,570	*Ariopsis felis*	616	*Floridichthys carpio*	280	*Eucinostomus gula*	756
Ariopsis felis	2,637	*Sphoeroides nephelus*	588	*Menticirrhus americanus*	278	*Sciaenops ocellatus*	594
Anchoa cubana	2,636	*Gobiosoma robustum*	580	*Micropogonias undulatus*	234	*Microgobius gulosus*	432
Sciaenops ocellatus	2,466	*Membras martinica*	398	*Dasyatis sabina*	222	*Elops saurus*	423

The pattern of variation in average annual DO, salinity, pH, and temperature is similar among the three sites of interest (Figure 3-24) during the sampling period 1996–2018. The average (median) and range of these water quality parameters are presented in Table 3-7. Among these parameters, salinity and temperature are the most variable as indicated by the first and third quartile range values in Table 3-7.

Table 3-7. Average (median) pH, temperature, DO, and salinity in the IRL and the three sites of interest.

Site	Statistics	pH	Temperature (°C)	DO (mg/L)	Salinity (psu)
IRL	Median	8.10	25.50	7.20	26.25
IRL	1st Quartile	7.90	21.45	6.00	20.6
IRL	3rd Quartile	8.30	29.10	8.44	31.68
IRL	Range	3.95-9.60	6.15-40.00	0.20-18.60	0.20-48.40
1	Median	8.20	25.25	7.40	24.50
1	1st Quartile	8.07	20.80	6.20	19.60
1	3rd Quartile	8.40	29.30	8.65	29.50
1	Range	5.63-9.20	8.47-35.0	1.25-16.20	10.90-40.95
2	Median	8.13	25.20	7.35	22.40
2	1st Quartile	8.00	21.09	6.20	18.25
2	3rd Quartile	8.30	29.10	8.75	27.41
2	Range	7.20-9.15	10.63-33.50	1.66-13.20	11.70-35.75
3	Median	8.00	25.90	7.00	29.40
3	1st Quartile	7.90	21.84	5.95	24.70
3	3rd Quartile	8.20	29.50	8.10	32.88
3	Range	3.95-9.00	7.80-37.40	1.80-17.50	0.20-40.00

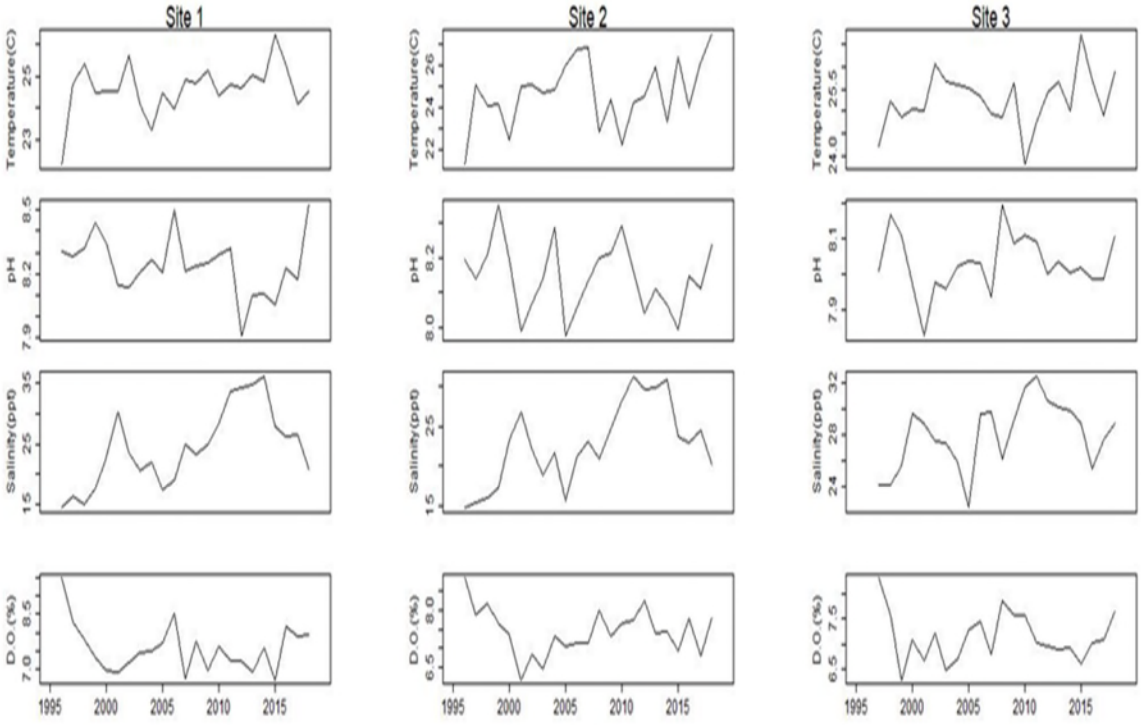

Figure 3-24. Annual variation in DO, salinity, pH, and temperature in Sites 1–3 during the period 1996–2018.

The pattern of community structure of fishes in the IRL and in each of the three sites of interest in this study is driven by complex interactions among biotic and abiotic environmental factors that likely shape the community structure of fishes in the IRL. In an attempt to determine which of the abiotic environmental parameters likely drive the pattern of variation in community structure of fishes, a series of partial RDA were conducted on all abiotic data (DO, temperature, salinity, pH, depth, conductivity) collected along with fish abundance during the 1996–2018 sampling period. Although a mix of statistically significant and non-significant results were revealed in these analyses (see Appendix 1, Table 3-7), DO and salinity consistently stand out as the key determinants of fish community structure in the IRL and in each of the three sites of interest, as described in Section 2 (Figure 3-25).

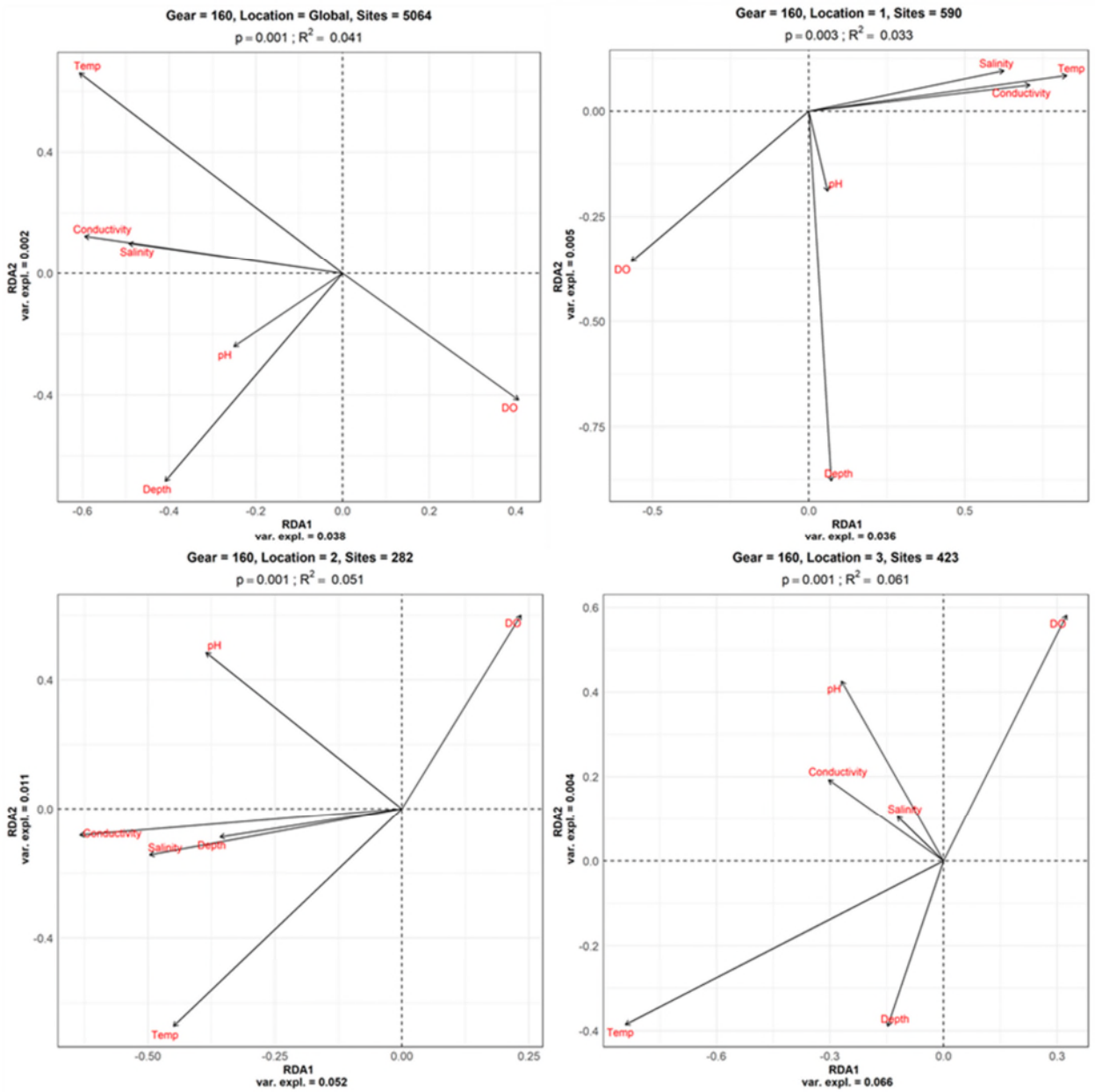

Figure 3-25. Representative biplot from the partial RDAs showing the association among the key water-quality determinants of community structure of fishes in the IRL (global), and in each of the three sites of interest.

Multivariate analyses at the IRL-wide scale have identified weak, but significant effects of salinity and DO on the changes in the fish community structure. In general, analyses using NMDS indicate that variation in DO and salinity is associated with variation in the diversity of fishes within the IRL and within each of the three sites of interest in this study. It is interesting to note that highest community diversity is found in areas of moderate salinity and low DO (Figure 3-26). These relationships were especially evident in the changes in abundance of fish in the lower trophic levels including bay anchovies, *Anchoa mitchilli*, Jenny mojarra, *Eucinostomus gula*, pinfish, *Lagodon rhomboides*, and Irish pompano, *Diapterus auratus* (see Appendix 1).

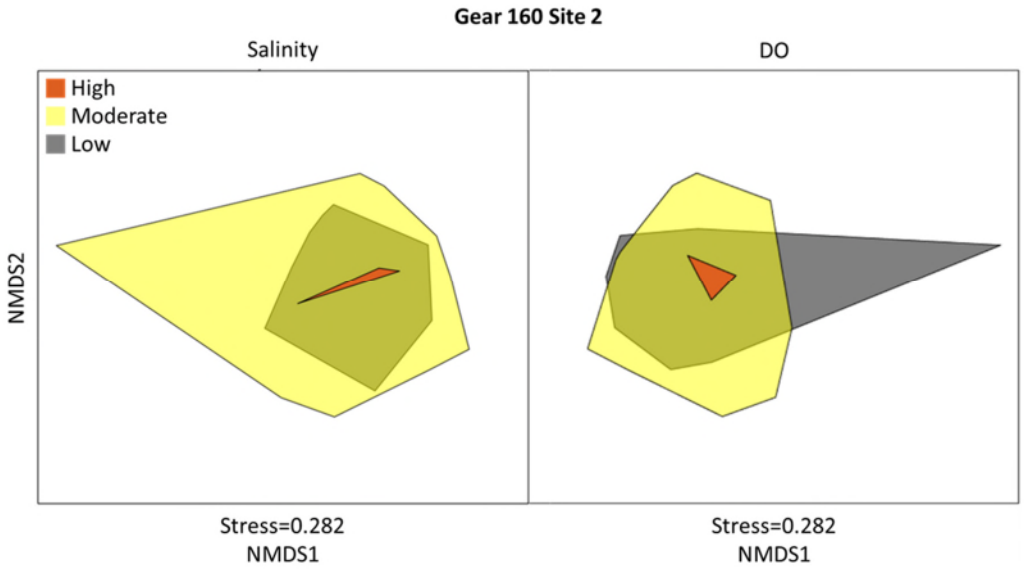

Figure 3-26. Representative biplot from the NMDS analyses showing the association between variation in community structure and variation in the key water quality parameters in each of the three sites of interest.

Approximately 60 light trap and ichthyoplankton net samples have been collected and these represent the larval supply for adult fish communities. Sample sorting began by switching samples from formalin to ethanol 48–96 hours after preservation, followed by sorting larval fishes and macroinvertebrates from the other zooplankton in the samples. Once larval identifications have been made, data will be interpreted in the context of IRL ichthyoplankton community dynamics presented in surveys such as Ferrell 1999, Shenker et al. 2002, Reyier and Shenker 2007, Reyier et al. 2008, and in the context of fish community structure as determined in this project.

3.6 eDNA Sampling and Detection Results

A total of 135 surface water eDNA samples were collected during fall and winter sampling of the IRL and offshore coastal waters. To investigate the utility of alternative eDNA substrates and habitat sampling eDNA was also sampled at 3 sites in the Sebastian River and in 6 central IRL sediment cores and 6 tissue samples collected from filter feeding tunicates, barnacles, and sponges. Total DNA yield was highly variable between samples, with IRL samples yielding the highest concentration of DNA (31 $\pm$ 4.8 nanogram per microliter [ng/µl]) and coastal samples having the lowest yield (6.4 $\pm$ 1.9 ng/ul). In initial tests, PCR inhibition was observed in 8 of 10 IRL samples and 2 of 10 coastal samples. To minimize false negatives, all samples were filtered to remove inhibitors and diluted 1:2 prior to qPCR. Following inhibitor removal and dilution 37 of 672 qPCR reactions failed to yield detectable amplification. Cycle quantification values for the remaining reactions were generally consistent (24.02 $\pm$ 3.72), though DNA retention following PCR clean-up varied (18.0 $\pm$ 2.9 ng/µl). DNA yield following the second PCR and PCR clean-up was higher for COI (16.0 $\pm$ 7.59 ng/µl) than 16S (14.6 $\pm$ 3.79 ng/µl). After size selection and purification, DNA yield was 1.77 ng/µl and 0.849 ng/µl respectively for 16S and COI. DNA was diluted 3:4 for both the V2 Nano and V3 rerun, improving cluster PF to 86.2% and 65.5% respectively. Nano sequencing was completed in August 2020. Final results are pending ongoing sequence quality control and analysis. Sequences will be filtered, trimmed, and error checked prior to taxonomic assignment. Rarefaction curves will be generated to estimate sequencing depth and species richness, and taxonomic distinctness will be used to estimate site and region alpha and beta diversity.

4 Discussion

This report describes the spatial and temporal variation in species occurrence within estuarine and coastal environments over three seasons starting in fall 2019. These data constitute the first stage of baseline data collection in anticipation of a temporary inflow pilot system project by the state of Florida, with the goal being the improvement of estuarine water quality via the addition of coastal ocean water to same. Included herein, when the scientific literature provides sufficient data, are discussions of whether changing estuarine conditions will directly impact a species or group, or whether indirect effects through predators or competitors might be in play.

Objective 1: To document baseline biological characteristics of the IRL and coastal ocean in the vicinity of the proposed inflow locations. Abundance and distribution data presented herein form the foundation of a baseline dataset collected within estuarine and coastal environments near three proposed inflow sites. Fish population and eDNA data were collected in the general region of these sites, while seagrass, infauna, and plankton data were collected from both sides of the barrier island in the immediate vicinity of those locations. Should a restoration of inflow be initiated at, or near, any of the sites, these data can be used to track and evaluate the condition of the system and identify ecological risk, with a focus on determining responses in seagrasses, benthic fauna, phytoplankton, ichthyoplankton, and fishes.

It should be noted that the first year of baseline sampling did not include summer sampling. Summer is an active spawning period for many populations and summer data are also needed to better predict and detect the effects of restored inflow on the system.

Objective 2: To assess the likely biological responses to a temporary inflow pilot system project at proposed locations. Estuaries are semi-enclosed coastal bodies where interaction between freshwater from rivers and streams, and tidally forced salt water from the sea, produce a highly dynamic system subject to changes occurring over short spatial and temporal scales. Estuarine species are therefore commonly euryhaline and eurythermal, meaning they can withstand relatively large fluctuations in salinity and temperature, while organisms found in offshore coastal environments are typically restricted to a narrow range of salinities and temperatures.

The moderate salinity and temperature ranges maintained within a few kilometers of ocean inlets (e.g. Sebastian Inlet) allow many offshore species to use estuaries for foraging and nursery habitat. Upstream of inlets, environmental conditions vary considerably, favoring species with broad physiological tolerances. The pattern of estuarine species having wider ranges of tolerances for abiotic environmental conditions is found throughout disparate taxonomic groups. While IRL estuarine species may be adapted to withstand a predicted maximum increase of 5 psu salinity above non-inflow levels these species have evolved under the added constraints of competition and predation. Most species are under intense competitive and predatory pressure during one or more life stages and any change in ecological interactions due to increased migration and larval transport (Johnson and Soltis 2017) between coastal and lagoon environments could unbalance the ecosystem with unforeseen consequences.

The main biological concerns when restoring inflow are species which occur on only one side of the barrier island, and the environmental factors (biotic and abiotic) which may impact their responses to inflow. When a species or group is found only on the coastal side (SIC), the focus of discussion will be on the niche characteristics of that species, inasmuch as that species might displace those already in the estuary through competition, predation, or indirect effects. In

contrast, when a species or group is found only on the estuary side (SESC), the potential concern is how introduced seawater may impact the estuarine species.

4.1 Seagrass, Rooted Algae, and Drift Algae Discussion

Seagrasses provide habitat for other organisms, and a protective nursery environmental for vulnerable developmental stages. They are a food source for numerous animals, and serve to stabilize sediments (Zieman 1982, Dawes et al. 1995).

There are seven species of seagrasses known to occur in various parts of the IRL estuary. However, in the northern IRL, the shoal grass *Halodule wrightii* dominates and was the only seagrass species documented in the surveys conducted for this study. *H. wrightii* has a wide range of habitats and lives in salt marshes, estuaries and, under some circumstances, coastal areas. It occurs both intertidally and in shallow subtidal habitats. In the northern IRL, *H. wrightii* is thought to occur no deeper than about 2 m, and optimally less than 1 m (Phillips 1960), due to turbidity and lack of water clarity severely limiting light penetration. However, in the clearer water of the Florida Keys and the Caribbean, it can be found as deep as 12 m (Bulthuis 1987). Coastal surveys in this study were too deep (greater than 10 m) to conduct via snorkeling, but hundreds of sediment grab samples have not yielded incidental seagrass capture. Additionally, anecdotal video evidence by tethered remotely operated vehicle shows no *H. wrightii* on the coastal side of proposed inflow locations. Further south in coastal waters, however, there are almost certainly beds of *H. wrightii* living subtidally at depths not possible in the turbid northern IRL. Propagules or vegetative fragments would be carried northward by longshore currents. *H. wrightii* would likely inhabit the coastal sites in this study were it not for unhospitable depths and water clarity.

The environmental tolerances of *H. wrightii* are broad. Shoal grass is considered a weed-like pioneer species. It is eurythermal and euryhaline, with likely optimal temperature tolerance range of 20–30°C (MacMillan 1982) and reported in Florida to withstand salinities of at least 12–38.5 ppt (Phillips 1960). *H. wrightii* is also flexible with regard to nutrient and organic sediment levels and can be found in sediments ranging from silty mud to sand with limited organic material (Phillips 1960). With these impressive ranges of tolerances, and with the knowledge that *H. wrightii* occurs in deeper coastal ocean water in the tropics where water clarity is better, it seems unlikely that *H. wrightii* would be directly harmed by the abiotic environmental changes that will come with restored lagoon inflow. If water clarity improves, *H. wrightii* may even be able to recruit into deeper parts of the IRL previously inaccessible due to depth and photosynthesis limitations. If the water column becomes less eutrophic, or if sediments have less silt and organic material, shoal grass could benefit from a less polluted and stressful environment. On the other hand, shoal grass is considered a tolerant pioneer species (Gutierrez 2010); if there is dramatic water quality and sediment improvement, shoal grasses could experience competition for space with other seagrass species which are not present under current conditions. It should be noted that there is currently a lack of sufficient information to predict how *H. wrightii* might be impacted by changes in herbivory or competition due to a shifting ecosystem driven by restored inflow. If a temporary inflow pilot system study is undertaken, continued ecosystem and biological monitoring will allow comparisons with the data reported herein, and it should be possible to say something about the impacts, or lack thereof, of complex ecosystem dynamics due to restored inflow.

Notorious herbivorous fish known to graze on *H. wrightii* include pinfish (*Lagodon rhomboides*), surgeonfish (*Acanthurus bahianus* and *A. coeruleus*), and parrotfish (*Scarus taeniopterus*, *S. iseri* and *Sparisoma aurofrenatum*). Increases in these fish in the IRL due to restored inflow would likely increase grazing pressure on *H. wrightii*. The West Indian Manatee is a voracious grazer on *H. wrightii*, but it is not anticipated that restored inflow will greatly change manatee presence

directly due to water quality conditions, since they are found regularly both in the estuary and on the outer coast. Monitoring of seagrasses and these grazers during a temporary inflow pilot system study would provide data on how inflow impacts seagrasses through water quality changes and, possibly, a shifting guild of grazers.

4.2 Benthic Fauna Discussion

"Benthic infauna are increasingly employed as a bioindicator of environmental quality"
- *Kuk-Dzul et al. 2012*

Benthic fauna are key indicators of local environmental conditions due to their unique life histories and, therefore, an important component of monitoring. Their benthic and sessile nature (relative to fishes, for example) renders them unable to easily escape when sediment or water column conditions shift. For this reason, discussion here will focus on a number of key benthic infauna species, their life history, environmental tolerances, and ecological niches, to better understand how they may respond to restored lagoon inflow and how that may impact the ecosystem as a whole.

Species of Introduction Concern: These two benthic infauna species were the only infauna found in the coastal ocean, but not the estuary.

The gastropod *Ecrobia truncata* was observed in only one sample, from coastal sediments in winter at BRSO. This species was never present in estuarine samples. While it is possible that, with restored inflow this species could be introduced or more strongly established, it seems unlikely given its rarity in the coastal environment. Additionally, the modeling team (Task 1) does not predict large dramatic changes in the salinities and correlated factors due to inflow, at least not at the flow rates proposed for the temporary inflow pilot system, and there is already a connection between the ocean and Banana River through the Port Canaveral lock. However, this species is not abundant, possibly not present, in the IRL. The literature indicates that *Ecrobia truncata* is known as a brackish water species, frequenting near-shore estuarine seagrasses and saltmarsh grasses (Vandendorpe et al. 2019), so it seems unlikely that ocean water inflow is going to render estuarine water conditions more hospitable to this species.

The gammarid amphipod *Americhelidium americanum* is found consistently in coastal sediments, and in medium to high occurrence in fall and winter. It is found in low numbers inside the northern IRL (BNRI) in winter, but otherwise coastal only. The proximity of BRNI to the Port Canaveral Lock, which opens and average of 48 times daily for the passage of vessels between the IRL and Port (Berman 2019), likely is responsible for bringing this amphipod from the ocean/port into the estuary. However, it is apparent they have not spread to benthic habitats further away from the lock. They are primarily found in coastal shelf sediments (Camp et al. 1998) and they may, therefore, require regular propagule replenishment through the lock to maintain the IRL population. If estuarine waters were to become more coastal-like, it could facilitate the persistence and spread of this species. However, the hydrographic model (Task 1) indicates that salinities may only increase by 5 psu, and this may not reach a state to support *A. americanum*.

SESC: these six benthic fauna are all those observed to occur in the IRL estuary, but not in coastal sediments (with the exception of the gastropod *Haminoea elegans*, which was rarely found in fall and winter at BRNI only).

The gammarid amphipod *Cymadusa compta* is a ubiquitous amphipod found throughout the IRL in almost all benthic habitats (Zimmerman 1971, Stoner 1983). Its latitudinal distribution ranges from the coast of Maine and southward to Florida and the Gulf of Mexico (Bousfield 1973, Morgan and Kitting 1984, Hauxwell et al. 1998), and is therefore considered eurythermal. It has been collected at salinities ranging from 5-44 psu (Boesch and Diaz 1974, National Oceanic and Atmospheric Administration is an American [NOAA] National Benthic Inventory). *C. compta* feeds on drift algae, epiphytes, and phyto-detritus (Zimmerman et al. 1979, Luczkovich et al. 2002). These food sources are abundantly available in the IRL estuary, and this may explain why *C. compta* tends to be found there, but not on the outer coast. Temperature and salinity changes in the IRL due to inflow are unlikely to directly force the displacement of *C. compta* given its broad physical and chemical tolerances, although if water quality changes were to successfully reduce drift algae, epiphytes and detritus, *C. compta* might be impacted by reduced food availability. Live healthy seagrasses are not a primary food source for *C. compta* (Kelly et al. 1990). Pinfish and other benthic foraging fish are important predators on *C. compta* (Stoner 1979 and 1983, Nelson 1995), and environmental shifts that impact those fish populations could well have an indirect impact on benthic prey like *C. compta*.

The gammarid amphipod *Cerapus tubularis'* distribution, tolerances, and life history are not well-described in the literature, especially for Florida and the IRL (NOAA National Benthic Inventory, Felder and Camp 2009). However, it is consistently present in the IRL estuary in medium abundances. Because it is absent from coastal samples, this is a species that should be monitored for impacts due to inflow if a temporary inflow pilot system project is undertaken. As many gammarid amphipods, this species may be an important food source for benthic foraging fish (Stoner 1979), and there is the potential for indirect trophic web impacts if inflow changes the guild or ratio of predators.

The gammarid amphipod *Gammarus mucronatus* is thought to occur in both brackish estuaries and out coastal sediments from the Gulf of St. Lawrence (Nova Scotia) to Florida and the Gulf of Mexico (Bousfield 1969 and 1973). *G. mucronatus* were not observed in outside coastal sediments, but they are likely there based on published preferred habitats and regional distributions (Watling and Maurer 1972, Bousfield 1973, van Maren 1978, Nelson 1980). *G. mucronatus* is recognized as strongly eurythermal (Fredette and Diaz 1986) and euryhaline (Bousfield 1973), and those in the estuary are not likely to be displaced directly by seawater influx. They are, like the gammarids above, an important part of the diet of benthic foraging fish, such as the pinfish *Lagodon rhomboids* (Nelson 1979 and 1980), surgeonfish, and parrotfish. Seawater impact on those fish populations may indirectly impact gammarid amphipods, including *G. mucronatus*.

The ostracod crustacean *Eusarsiella zostericola* is eurythermal, occurring from Maine to the Gulf of Mexico, and can tolerate salinities from 22–36 ppt (Kornicker 1967 and 1986). *E. zostericola* was observed within the IRL estuary at all inside sites (BRNI, BRSI, and VBI) in low, medium, and high abundances in all seasons. In contrast, they were not observed in coastal sediments. Given their persistence in the IRL through fall, winter, and spring, it seems likely they can withstand salinities below 22 ppt. *E. zostericola* has been an invasive species in some parts of the world, but is has not been documented to displace species, nor does it have recognizable trophic impacts through grazing on prey or serving as food for predators (Ruiz et al. 2011).

The bivalve mollusc *Parastarte triquetra* is subtropical to tropical, found from Florida through most of the Caribbean (Abbott and Morris 1995), and is considered a characteristic

species of the IRL, where it can occur in densities exceeding $2x10^4$ m^{-2} (Mikkelsen et al. 1995). *P. triquetra* was found within the IRL estuary at all inside sites (BRNI, BRSI, and VBI) in low, medium, and high abundances in all seasons. In contrast, they were not observed in coastal sediments in this study, though they are known from Florida Bay, more tropical (warmer) water that is coastal. Relatively little is known about the detailed tolerances, life history, and ecological interactions of this bivalve, and it should be monitored before, during, and after any inflow project is undertaken.

The gastropod mollusc *Acteocina canaliculata* is eurythermal, occurring in Maine, the mid-Atlantic, Florida, throughout the Caribbean, and at least as far south as Suriname (Brunel et al. 1998, Rosenberg et al. 2009). Found in sediments with less than 38% silt-clay content (Kennish et al. 2004, Flanagan et al. 2018). In the IRL, this level of silt-clay tends to accompany polluted organic sediments. Coastal sediments rarely have this level of silt-clay, and this may explain why *A. canaliculata* is not found at BRNO, BRSO, and VBO. Franz (1971) collected individuals for spawning that were in water that varied 28-31 in salinity, but their occurrence throughout the IRL makes it almost certain they can withstand much lower salinities.

Benthic fauna of economic or ecological significance. The benthic fauna sampling approach employed for this study, a Petite Ponar grab sampler, was not designed for special examination of the following economically and ecologically important benthic invertebrate species. These species occur in the IRL (Anderson et al. 2019, Arnold et al. 1996, Hines et al. 2003, Ehlinger and Tankersley 2007, respectively) and could occur in inflow areas, although they were neither sampled, nor even observed anecdotally, at the project sites. Still, consideration should be given to possible inflow effects on these populations and it is recommended that nearby populations be identified and monitored closely during a temporary inflow pilot system study.

The oyster *Crassostrea virginica* is an historically important shellfishery in the IRL and (Arnold and Berrigan 2002). Sponges *Cliona* spp. are known parasites of *C. virginica* and thrive in more saline water (Hopkins 1962, Turner 1985). Full ocean salinity may favor boring sponges *Cliona* spp. Oysters were never captured or observed while sampling around the proposed inflow sites. Also, even with increased salinity, levels may periodically dip low enough to discourage prolific establishment of *Cliona* spp. To examine this potential problem, *C. virginica* populations nearest the inflow should be identified, and populations and water quality monitored closely throughout the temporary inflow pilot system activities.

The hard clam *Mercenaria mercenaria* is also an historically important shellfish in the IRL. It is not as susceptible to boring sponges and thrives in nearly full coastal salinity (Arnold et al. 1991). It is still recommended, however, to monitor the nearest *M. mercenaria* populations to proposed inflow sites, including their population dynamics and water quality.

The blue crab *Callinectes sapidus* is notoriously an extremely euryhaline species (Milliken and Williams 1984, Cadman and Weinstein 1988) and is known to be found in abundance both in the IRL and coastal ocean.

The horseshoe crab *Limulus polyphemus* is held by many to be a keystone species (Martinez 2012). *L. polyphemus* spawns annually in the northern IRL (Ehlinger and Tankersley 2007) and their massive spawns serve as food for migrating seabirds (Takahashi 2016). *L. polyphemus* is somewhat euryhaline (Shuster 1982), but growth rates decrease at extreme salinities, including salinities of 40 ppt (Jegla and Costlow 1982). It is not clear whether the

increases in salinity projected for inflow will cause this type of problem, and monitoring of horseshoe crabs is recommended.

It is recommended that monitoring of benthic fauna be ongoing before, during, and after the implementation of a temporary inflow pilot system project. Another year of monitoring ahead of pilot inflow is advisable from the perspective of having a better understanding of the biology and ecology of the system. Biological populations are notoriously variable, and that variation increases with seasonal changes. With only one year of monitoring, it is difficult or impossible to differentiate differences due to treatments (estuarine, coastal, or pumping conditions) vs. differences due to seasonal fluctuations (Giovannoni and Vergin 2012, Kroodsma et al. 2018). With more than one year, the contribution of season to variability becomes more apparent and treatment impacts more certain.

4.3 Phytoplankton/Harmful Algae Discussion

*"*Algal blooms are indicators of marine ecosystem health; thus, their monitoring is a key component of effective management of coastal and oceanic resources*."*

- Blondeau-Patissier et al. 2014

Phytoplankton are drifting microalgae of various taxa (e.g., dinoflagellates, diatoms, nanoflagellates), and can sometimes be responsible for harmful or toxic algal blooms. Phytoplankton, by definition, drift with currents, and will travel wherever the flow directs. Monitoring their distributions is challenging, because they are extremely variable and patchy in time and space (e.g., Bengfort et al. 2006, Trudnowsky et al. 2016, Breier et al. 2018). Phytoplankton data were collected using two different methods for this evaluation. Larger phytoplankton (greater than 25-µm) were collected via plankton net tow, and visually identified and counted via light microscopy. Smaller phytoplankton (less than 40-µm) are difficult, often impossible, to identify the taxon visually. These small cells were counted via whole water samples using a flow cell cytometer. The cytometer cannot differentiate species. It does, however, reveal different size groups of the small cells, which have a greater chance of being a coherent bloom. The cytometer also analyzes the photosynthetic pigments, which reveals to which major phytoplankton groups the small cells likely belong.

Species of Introduction Concern: There are 31 species or groups of diatoms, 3 dinoflagellates, 2 cyanobacteria, and an unidentified flagellate found only in coastal plankton via plankton tow monitoring (cells less than 25-µm). If these species indeed do not occur in the estuary, they could present a potential introduction concern if water conditions in the estuary change sufficiently due to inflow. However, because they drift with currents and are patchy, estuary and ocean differences must be considered carefully. Planktonic species and groups found only in the coastal environment can easily be transported through inlets and the Port Canaveral lock. There are two likely possibilities for their fate once they enter the estuary. If they cannot tolerate estuarine conditions, they may die rapidly after being advected into the estuary. On the other hand, some of these species may be undetected-but-present in the estuary, only blooming and detectable under a specific combination of complex environmental conditions not met while sampling was occurring. In the first scenario, a species might enter the estuary with inflow and bloom in the immediate vicinity, provided inflow changes conditions sufficiently for that species. In the second circumstance, they could potentially bloom in the estuary due to conditions unrelated to restored inflow. Vigorous monitoring of phytoplankton on both sides of the barrier island will reveal a better picture of coastal phytoplankton distributions and tolerances, and their potential for impacting the estuarine ecosystem.

SESC: There are 3 species or groups of diatoms, 7 dinoflagellates, 2 tintinnids, and 1 cryptophyte observed to occur in the IRL estuary, but not in coastal plankton based upon plankton tow monitoring (cells >25-μm). These species play a role in the planktonic ecosystem within the IRL, and they could be directly or indirectly impacted by changes in estuarine water quality. Plankton monitoring in the estuary should continue in order to describe responses in these species or groups. Due to the important ecosystem role played by toxic and HABs (Hallegraeff 2003), this discussion focuses on possibilities presented by the two prominent groups of toxic dinoflagellates in the SESC group: *Gonyaulax* spp. and *Gymnodinium* spp.

The dinoflagellate genus *Gonyaulax* has shown salinity tolerance in the range of 15–33 ppt (Brand 1984). The IRL estuary is usually in this range, meaning *Gonyaulax* spp. can bloom in most of the estuary with regards to salinity. Dinoflagellates in this genus are known for producing saxitoxins, a neurotoxin which, when concentrated through the phytoplankton-shellfish food chain, can cause Paralytic Shellfish Poisoning in humans (Bates et al. 1978). They may also produce other types of toxins with similar implications for consumers of seafood (Kirkpatrick et al. 2004). The genus *Gonyaulax* is closely related to the genus *Alexandrium*, which produces similar toxins (Faust and Gulledge 2002). The occurrence of *Gonyaulax* spp. within the estuary was medium to high, especially in the Spring, and at all potential inflow sites on the estuarine side. When present, the densities recorded for *Gonyaulax* spp. in the monitoring have been between 1 and 18 cells L^{-1}, which are relatively low concentrations and would not create turbidity or discoloring of water in what one would call a "bloom." Additionally, toxins are unlikely to be concentrated through the food chain when densities are this low. For instance, a related species delivered saxitoxin in amounts impacting human health when cells were at a concentration of 750,000 L^{-1}. Because problems from HABs are among the primary justifications for a project restoring inflow to the IRL, phytoplankton, and especially HAB species, should be monitored carefully before, during and after an inflow restoration project is implemented. It is expected that, if restoring inflow reduces eutrophic nutrients in the IRL water column, HABs will decrease, and this potential outcome is a main motivation of this project.

The dinoflagellate genus *Gymnodinium* has shown salinity tolerance in the range of 15–45 ppt (Brand 1984). They are possibly more tolerance of wide-ranging salinities than *Gonyaulax* spp. and can likely persist and bloom under most IRL salinity conditions. Like *Gonyaulax*, *Gymnodinium* produces saxitoxins (Albinsson et al. 2014), a neurotoxin which, when concentrated through the phytoplankton-shellfish food chain, can cause Paralytic Shellfish Poisoning in humans (Bates et al. 1978). The occurrence of *Gymnodinium* spp. within the estuary was highest in winter at BRSI, and this may be a form temporal partitioning of niche in two related toxic dinoflagellates. When present, the densities recorded for *Gymnodinium* spp. in the monitoring have been between 0.2 and 9 cells L^{-1}, less than half of the already low concentrations observed for *Gonyaulax* spp. As with *Gonyaulax*, toxins are unlikely to be concentrated through the food chain when densities are this low. Because problems from HABs are among the primary justifications for a project restoring inflow to the IRL, phytoplankton, and especially HAB species, should be monitored carefully before, during and after an inflow restoration project is implemented. It is expected that, if restoring inflow reduces eutrophic nutrients in the IRL water column, HABs will decrease, and this potential outcome is a main motivation of this project.

HABs caused by phytoplankton create turbidity and attenuate light and have caused the death of tens-of-thousands-of-acres of seagrasses in the IRL (Tetra Tech 2016), and HABs are largely responsible for public alarm concerning the state of the lagoon. Should an inflow project be implemented, one of the most positive potential outcomes would be a reduction in frequency and

severity of IRL HABs. For the toxic and otherwise harmful dinoflagellates, diatoms, and larger cyanobacteria, there are now baseline lists and concentrations at inflow sites to compare if an inflow restoration project is undertaken by the state. It will be critical to follow these populations to document the successes and shortcomings of the project. It is recommended to monitor phytoplankton, including HAB species, before, during, and after inflow restoration. Another year of monitoring ahead of pilot inflow is advisable from the perspective of having a better understanding of the biology and ecology of the system. Biological populations, especially phytoplankton, are notoriously variable. Seasonal fluctuations contribute to that variability. At least one more year of baseline (pre-pumping) monitoring is recommended to help differentiate seasonal fluctuations from pumping responses (Giovannoni and Vergin 2012, Kroodsma et al. 2018). With more than one year of baseline data, seasonal impacts are more apparent and treatment impacts more certain.

Most of the HABs in the IRL over the last decade have been in a size range termed nanoplankton (2-20 μm) (e.g., Kang et al. 2015, Tetra Tech 2016). Therefore, for some species or groups of critical concern, the primary data are flow cytometer cell sizes, counts, and photosynthetic pigmentation. This is a powerful dataset, but certain identification of HAB nanophytoplankton is challenging. Larger SIC and SESC HAB cells are discussed in the paragraphs above, while concentrations of different types of nanoplankton-sized cells are reported in Figure 3-19.

4.4 Ichthyoplankton Discussion

The fish fauna within the long, narrow IRL shows longitudinal variation in species richness that has been attributed to physiological and ecological associations with variable environmental parameters, as presented in this report, to spawning patterns of fishes within the IRL, and to limitations in the ability of many species of offshore-spawned larvae to disperse widely through the lagoon from the few narrow and widely spaced inlets (Gilmore 1988; Kupschus and Tremain 2001).

Reyier and Shenker (2007) conducted the only major larval fish survey that evaluates larval production within eight estuarine sub-regions, from the open IRL near the Sebastian Inlet to the northern IRL, the Banana River and the Mosquito Lagoon. The results of the survey indicate that fish larvae within these regions are dominated by anchovies and gobies (74% and 17% of all larvae, respectively). Habitats around the northern IRL and Banana River Lagoon yielded large catches of newly-hatched spotted seatrout (*Cynoscion nebulosus*), southern kingfish (*Menticirrhus americanus*) and red drum (*Sciaenops ocellatus*), indicating localized estuarine spawning of those valuable sportfishery species. Closer to inlets, red drum spawn on ebbing tides, allowing larvae to undergo their initial development in coastal waters, with subsequent recruitment back into the estuary (Peters and McMichael 1987; Rooker 2008). Marine-spawned larvae comprised less than 0.2% of all the larvae in the IRL ichthyoplankton survey, reflecting lack of marine larvae in many areas away from inlets, the older age and larger size that marine larvae reach by the time they enter an estuary, and the competence of many marine larvae to settle and assume a demersal existence upon estuarine entry.

The importance of the northern IRL to fishery species such as red drum, spotted sea trout, and black drum (*Pogonias cromis*) is illustrated by the many world-record sized fish taken in the region. Based on International Game Fishing Association data, 44% of all spotted sea trout world records from 1939 to 2007 (based on catches made in different fishing line weight classes) occurred in the northern IRL, along with 55% of the red drum world records and 67% of the black drum world records (Bohnsack 2011). While many of these records were made after establishment of the *de facto* Marine Protected Area around the Kennedy Space Center in 1962, the number of records

made in the northern IRL far exceed the number of record-sized fish taken in the protected Everglades habitat. Conversely, the Everglades has produced far more world records for snook (*Centropomus undecimalis*) than has the northern IRL. The northern IRL habitat is thus an excellent spawning and nursery habitat for these valuable fishery species and for the production of large and abundant adult fish.

Will the introduction of additional oceanic water into the northern IRL have a significant impact on these and other estuarine fisheries? Based on the limited sampling conducted in the winter and early spring of 2019–2020, the light trap surveys in Port Canaveral show that limited influx of marine fish larvae does occur indeed through the Canaveral Lock. Lock operations are very limited, however, so the overall volume of water entering the lagoon and larval entrainment, would be small relative to a potential permanent system for inflow (Zarillo, *personal communication*).

Most of the marine fish entering the IRL from the coastal ocean during the winter and spring were pelagic schooling species such as menhaden, scaled sardines and threadfin herring. These highly mobile fishes, along with bay anchovies, are important prey for piscivorous species throughout the estuarine habitat. Given their mobility, it would be reasonable to hypothesize that larvae entering through other IRL inlets could disperse throughout the entire lagoon ecosystem. Allowing increased entry into the northern IRL would appear to increase the prey base for predatory fishes. Conversely, increased consumption of zooplankton could potentially reduce zooplankton grazing of phytoplankton in the lagoon, with impacts on water turbidity and production of algal blooms.

Large numbers of other offshore-spawning fishes are anticipated to occur in the winter-spring Port Canaveral samples. A few larval pinfish (*Lagodon rhomboides*), Atlantic croaker (*Micropogonias undulatus*) and mojarras (*Eucinostomus* spp.) were captured, but these species recruit in large numbers into estuarine habitats all along the southeast coast of the United States (Shenker and Dean 1979, Warlen and Burke 1990, Paperno 2002). No white mullet (*M. curema*) or striped mullet (*M. cephalus*) were captured, despite being known to spawn offshore and recruit into estuaries in the winter and spring (Collins and Stender 1989). Speckled worm eel (*Myrophis punctatus*) is often one of the most abundant taxa recruiting into the coastal estuaries (Shenker and Dean 1979, Abel et al. 2011) but was also completely absent from the light trap samples. Light traps are routinely used in reef and tropical habitats (Anderson et al. 2002) but have not yet been adopted for use in estuarine environments. Larvae that were expected to be present, but did not appear in the light trap samples, may not have strong nocturnal phototactic responses (Hickford and Schiel 1999), or the turbidity in the estuary reduced the effectiveness of the light lure.

The sampling also occurred during the non-spawning season for many species. As Reyier and Shenker (2007) and Reyier et al. (2008) showed spotted sea trout, red drum, southern kingfish, and many other species within the IRL, spawn during the summer or early fall. In addition, many coastal species spawn and move into the IRL during those seasons. Larval/juvenile fish sampling in Sebastian Inlet and adjacent nursery habitats during the summer and fall months collected 69 taxa within 40 families of fish entering the IRL (Smith 1995, Wieher 1995, Ferrell 1999; Poulakis et al. 2002). Samples were dominated by mojarras, 5 species of snappers (Lutjanidae), 6 species of jacks (Carangidae), snook (*Centropomus undecimalis*), and red drum. Unlike the spawning observed within the northern IRL, red drum close to inlets spawn just offshore on ebbing tides, allowing larvae to undergo their initial development in coastal waters, with subsequent recruitment back into the estuary (Peters and McMichael 1987; Rooker 2008). Larvae of some species, such as bay anchovy and spotted sea trout were also collected in the inlet on flood time samples, but it is likely that these estuary-spawned larvae were moving out and in of the estuary with the tides.

The potential impact of increasing the recruitment of larvae of these offshore-spawning fishes into the estuarine fish community in the northern IRL could depend on the volume of water brought into the IRL through a temporary inflow pilot system project and subsequent potential permanent system, the configuration of the water intake structure, the densities of larvae entrained into the IRL and their subsequent survival and ecological interactions within the estuary. Engineering and hydrographic considerations would dictate the structure and magnitude of a temporary inflow pilot system and potential permanent system. Generating estimates of larval inflow will require quantitative ichthyoplankton monitoring in Port Canaveral, with sampling throughout the year to assess species spawning during different seasons. Collections should be made using large plankton nets at night to minimize net avoidance by the larvae, and to provide estimates of larval density. These larval estimates, coupled with ecological evaluations of the impacts of inflow on sea grass and other fish nursery habitats, could be used to begin an assessment of potential changes in fish community structure in the region. If changes appear likely, it will be important to engage in discussions with the recreational anglers, fishing guides and associated businesses to determine public reactions about whether changes would be considered beneficial or negative to the fishing community.

4.5 Fish Analysis and eDNA Sampling and Detection Discussion

The data and analyses on fish species and eDNA contribute to the robust baseline characterizations of the ecosystems being considered for restored inflow. Both the fish analysis and the eDNA sampling bring a broader regional perspective to the sampling coverage, which compliments the more site-specific local sampling for seagrasses, benthic fauna, and phytoplankton. This fish and eDNA data baseline will enable comparisons with data collected during and after a temporary inflow pilot system project.

5 Conclusions and Recommendations

Most estuarine animals tolerate fluctuations and relative extremes in temperatures, salinities, turbidity, nutrients, and pollutants. By comparison, coastal ocean conditions are relatively constant and fall well within the ranges of estuarine organism tolerances. Given this, it could be expected that estuarine animals would respond more favorably to any shifts in the abiotic environment resulting from enhanced inflow; however, data are still lacking on several key species of concern and aspects of the recipient community. Of particular note are the spawning populations of several key sportfish in the Banana River. Similarly, indirect impacts on the estuarine community due to biotic factors, such as predation by, or competition with, organisms from the coastal ecosystem, are harder to predict. Coastal organisms may be directly introduced via enhanced inflow, or migration into the estuary could be encouraged following a shift towards coastal-like conditions Projecting ecosystem changes that may accompany restored inflow is limited to some cautious generalizations, punctuated by better predictions for a few species for which the scientific literature provides ample information. Reliable evaluation of the biological impacts of restored inflow would be best accomplished through a temporary inflow pilot system project where biological responses are carefully monitored. This would be an ecologically risky undertaking if the two ecosystems (the IRL estuary and the coastal ocean) were isolated hydrodynamically and migration between populations on either side of the barrier island was not possible. However, given that (1) the northern IRL estuary has been connected to the coastal ocean via inlets in the past, and (2) the Port Canaveral shipping locks already provide a limited hydrodynamic connection and migration opportunity, it would seem a reasonable proposition to conduct a temporary inflow pilot system project to document small-scale ecosystem changes. This would allow a more confident projection of the likely effects of a permanent inflow system. Certainly, a permanent system should be preceded by a temporary inflow pilot system, where biological and ecosystem responses are carefully evaluated before approval of the larger project.

Inflow initiation or restoration projects for mitigating impaired estuaries have been carried out in other locations, and some have been successful from the perspective of enhanced fisheries or reduced HABs. The Maketu Estuary of New Zealand was restored to a century-old riparian flow pattern in 2019 to restore collapsing fisheries for indigenous Māori tribes. This restoration is ongoing but is showing success in clearing sediments and increasing fishery populations (K.B. Johnson, *unpublished*). A restored tidal exchange in western Australia reduced eutrophication and drift algae and increased larger pelagic fish (Potter et al. 2016). Multiple projects have had success in reducing HABs in estuaries through hydrological ecosystem engineering (summarized in Elliott et al. 2016). In other cases, storms may create accidental inlets with positive water quality impacts, and such was the outcome with Hurricane Sandy, where clam growth showed improvement after the breach (Gobler et al. 2019).

Some evidences suggest that SESC (those found only in the estuary) may have minimal direct impacts form an influx of coastal water. First, species present in estuaries are frequently euryhaline and eurythermal, meaning they can withstand relatively large fluctuations in salinity and temperature compared to ocean species. For instance, fish are among the most motile of estuarine populations, yet, even if they have tidal migration, an enhanced ability to osmoregulate in changing conditions is required (Allen et al. 2006). The pattern of estuarine species having wider ranges of tolerances for abiotic environmental conditions is found throughout disparate taxonomic groups. Additional examples include estuarine molluscs, which must be adapted to extreme fluctuations of salinity and pollutants (Levinton et al. 2011). Estuarine phytoplankton have a wider salinity tolerance than oceanic phytoplankton, and, as one might predict, coastal phytoplankton are intermediate in their tolerance (Brand, 1984). Additional information easing some concerns about inflow impacts on estuarine species includes the already existing ocean

connection through the Port Canaveral Lock and the subtlety of projected changes due to restoring IRL inflow (based on Dr. Gary Zarillo's hydrodynamic model, Task 1 Modeling and Engineering). The lock, located in the northern Banana River, opens to vessel passage an average of 48 times daily, and water levels can change by 3–4 feet as water moves from the ocean to the estuary (Berman 2019). Thus, there is already some degree of coastal influence in the northern Banana River. With the open lock comes the opportunity for migration, larval transport, and gene flow between coastal and estuarine populations. Diatoms may be transported with water, or on the boats themselves (Sweat et al. 2017). The hydrodynamic model suggests that, with restored inflow of 10 m^3 s^{-1}, after 50 days water conditions will reach equilibrium with Banana River Lagoon salinity rising approximately 5 psu above non-inflow levels (Task 1, Modeling and Engineering). This is unlikely to impact adults of euryhaline species, many of which can withstand much greater fluctuations, including species tolerating the full spectrum of salinity from freshwater to oceanic (Ahmad and Hellebust 1984, Henry et al. 2002, Sampaio and Bianchini 2002, Schmidt et al. 2015). However, reproduction-related impacts and indirect impacts due to shifting environmental conditions, such as the possibility of new predators and competitors being introduced into the system, or a shift in existing community balance, are harder to predict and ongoing monitoring will help reveal those interactions.

It is critically important that impacts on the ecosystem and numerous key species be documented through a temporary inflow pilot system project before implementing anything larger. However, extensive ecosystem and biological measurements during and after a pilot project will reveal little without baseline data for comparison. The data presented herein on estuarine and coastal populations, and their ecosystems, is the start of the essential baseline for successful project monitoring. This monitoring reported represents three seasons of population dynamics in seagrasses, benthic infauna, phytoplankton, ichthyoplankton, fishes, and eDNA surveys, but it is important to get at least one more year of these measurements before a temporary inflow pilot system study starts to identify seasonal variation. Then it may be possible to identify major responses of temporary pilot inflow without confusion over seasonal changes. Natural changes due to seasonal or annual shifts in water quality (unrelated to restored inflow), geochemical cycling, reproductive cycles, and other sources of variability can be accounted for in evaluating project impacts if baseline ecosystem monitoring is sufficiently robust and continues for more than one year.

6 References

Abbott, R.T. & Morris, P.A. A Field Guide to Shells: Atlantic and Gulf Coasts and the West Indies. New York: Houghton Mifflin, 1995. 73.

Able, KW, DM Allen, G. Bath-Martin, JA. Hare, DE Hoss, KE Marancik, PM Powles, DE Richardson, JD Taylor, HJ Walsh, SM Warlen, C Wenner 2011. Life history and habitat use of the speckled worm eel, Myrophis punctatus, along the east coast of the United States. Environmental Biology of Fishes 92: 237-259.

Ahmad, I., & Hellebust, J. A. (1984). Osmoregulation in the extremely euryhaline marine micro-alga *Chlorella autotrophica*. Plant physiology, 74(4), 1010-1015.

Albinsson, Maria E., Andrew P. Negri, Susan I. Blackburn, and Christopher JS Bolch. "Bacterial community affects toxin production by Gymnodinium catenatum." Plos one 9, no. 8 (2014): e104623.

Allen, L., Lokyavich, M., Cailliet, G. and M. Horn. 2006. Ch.5 Bays and Estuaries, In: The Ecolog of Marine Fishes: California and Adjacent Waters (eds: Allen, L, Pondella, D., and M. Horn). University of California Press, Berkeley. 659 pp.

Anderson, TW, CT Bartels, MA Hixon, E. Bartels, MH Carr, JM Shenker. 2002. Current velocity and catch efficiency in sampling settlement-stage larvae of coral-reef fishes. US Fishery Bulletin 100: 404-413.

Anderson, L., Sacks, P., Donnelly, M., Barker, V., Anderson, S., Walters, L. 2019. Oyster reef enhancement utilizing gardened oysters in a subtropical estuary. Restoration Ecology Vol. 27, Iss. 5: 966-973.

Arnold, W.S., Marelli, D., Bert, T.S., Jones, D.S., Quitmyer, I.R. 1991. Habitat-specific growth of hard clams *Mercenaria mercenaria* (L.) from the Indian River, Florida. J Exp Mar Biol Ecol 147:245-265.

Arnold, W.S. and Berrigan, M.E. 2002. A summary of the oyster (*Crassostrea virgini*a) fishery in Florida. A Report to the Division of Marine Fisheries, Florida Fish and Wildlife Commission, St. Petersburg, Florida, USA.

Arnold, W.S., Bert, T.M., Marelli, D.C., Cruz-Lopez, H., and Gill, P.A. 1996. Genotype-specific growth of hard clams (genus *Mercenaria*) in a hybrid zone: variation among habitats. Marine Biology 125, no. 1: 129-139.

Bates, Hans A., Richard Kostriken, and Henry Rapoport. "The occurrence of saxitoxin and other toxins in various dinoflagellates." Toxicon 16, no. 6 (1978): 595-601.

Bengfort, Michael, Ulrike Feudel, Frank M. Hilker, and Horst Malchow. "Plankton blooms and patchiness generated by heterogeneous physical environments." Ecological complexity 20 (2014): 185-194.

Berman, D. 2019. Canaveral Lock at Port Canaveral to close to boaters for four months for repairs. Florida Today, 30 July 2019. https://www.floridatoday.com/story/news/2019/07/30/canaveral-lock-port-canaveral-close-four-months-repairs/1864684001/.

Berry, T. E., Osterrieder, S. K., Murray, D. C., Coghlan, M. L., Richardson, A. J., Grealy, A. K., ... & Bunce, M. 2017. DNA metabarcoding for diet analysis and biodiversity: A case study using the endangered Australian sea lion (Neophoca cinerea). Ecology and Evolution, 7(14), 5435-5453.

Blondeau-Patissier, David, James FR Gower, Arnold G. Dekker, Stuart R. Phinn, and Vittorio E. Brando. "A review of ocean color remote sensing methods and statistical techniques for the detection, mapping and analysis of phytoplankton blooms in coastal and open oceans." Progress in oceanography 123 (2014): 123-144.

Boesch DF and RJ Diaz. 1974. New records of peracarid crustaceans from oligohaline waters of the Chesapeake Bay. Chesapeake Science 15:56-59.

Bohnsack, JA. 2011. Impacts of Florida coastal protected areas on recreational world records for spotted sea trout, red drum, black drum, and common snook. Bulletin of Marine Science 87:939-970.

Brand, L. 1984. The salinity tolerance of forty-six marine phytoplankton isolates. Estuarine, Coastal and Shelf Science, 1984, Volume 18, Issue 5.

Bousfield EL. 1969. New records of Gammarus (Crustacea: Amphipoda) from the Middle Atlantic Region. Chesapeake Science 10:1-17.

Bousfield EL. 1973. Shallow-water gammaridean Amphipoda of New England. Cornell University Press, Ithaca, New York. 312p.

Boussarie, G., Bakker, J., Wangensteen, O.S., Mariani, S., Bonnin, L., Juhel, J.B., Vigliola, L., 2018. Environmental DNA illuminates the dark diversity of sharks. Sci. Adv. 4, eaap9661.

Breier, Rebekka E., Cristian C. Lalescu, Devin Waas, Michael Wilczek, and Marco G. Mazza. "Emergence of phytoplankton patchiness at small scales in mild turbulence." Proceedings of the national academy of sciences 115, no. 48 (2018): 12112-12117.

Brunel, P.; Bosse, L.; Lamarche, G. (1998). Catalogue of the marine invertebrates of the estuary and Gulf of St. Lawrence. Canadian Special Publication of Fisheries and Aquatic Sciences, 126. 405 p.

Bulthuis, D. 1987. Effects of temperature on photosynthesis and growth of seagrasses. Aquatic Botany. 27: 27–40. doi:10.1016/0304-3770(87)90084-2.

Cadman, L.R., Weinstein, M.P. 1988. Effects of temperature and salinity on the growth of laboratory-reared juvenile blue crabs *Callinectes sapidus* Rathbun. Journal of Experimental Marine Biology and Ecology 121: 193-207.

Callahan, B. J., McMurdie, P. J., Rosen, M. J., Han, A. W., Johnson, A. J. A., & Holmes, S. P. 2016. DADA2: high-resolution sample inference from Illumina amplicon data. Nature methods, 13(7), 581-583.

Camp, David K. "Checklist of shallow-water marine malacostracan Crustacea of Florida." Checklists of selected shallow-water marine invertebrates of Florida. Florida Marine Research Institute Technical Report TR-3 (1998): 123-189.

Checkley, DM, S Raman, GL Maillet, KM Mason 1988. Winter storm effects on the spawning and larval drift of a pelagic fish. Nature. 335:346-348.

Clarke, K. R., & Warwick, R. M. 2001. A further biodiversity index applicable to species lists: variation in taxonomic distinctness. Marine ecology Progress series, 216, 265-278.

Collins, M.R., B.W. Stender. 1989. Larval striped mullet (Mugil cephalus) and white mullet (Mugil curema) off the southeastern United States. Bulletin of Marine Science 45:580-5.

Cooksey, C., Hyland, J. 2007. Sediment quality of the Lower St. Johns River, Florida: An integrative assessment of benthic fauna and general characteristics. Marine Pollution Bulletin 54:9–21.

Cox, A., Hope, D., Zamora-Duran, MA., Johnson, KB. 2018. Environmental factors influencing benthic polychaete distributions in a subtropical lagoon. Marine Technology Society Journal 52:58-74.

Cruaud, P., Rasplus, J. Y., Rodriguez, L. J., & Cruaud, A. 2017. High-throughput sequencing of multiple amplicons for barcoding and integrative taxonomy. Scientific reports, 7, 41948.

Dawes CJ, Hanisak D, Kenworthy JW. 1995. Seagrass biodiversity in the Indian River Lagoon. Bull Mar Sci 57: 59-66.

Deagle, B. E., Gales, N. J., Evans, K., Jarman, S. N., Robinson, S., Trebilco, R., & Hindell, M. A. 2007. Studying seabird diet through genetic analysis of faeces: a case study on macaroni penguins (Eudyptes chrysolophus). PLoS One, 2(9), e831.

Djurhuus, A., Port, J., Closek, C. J., Yamahara, K. M., Romero-Maraccini, O., Walz, K. R., ... & Chavez, F. P. 2017. Evaluation of filtration and DNA extraction methods for environmental DNA biodiversity assessments across multiple trophic levels. Frontiers in Marine Science, 4, 314.

Drummond, A. J., Newcomb, R. D., Buckley, T. R., Xie, D., Dopheide, A., Potter, B. C., ... & Park, D. 2015. Evaluating a multigene environmental DNA approach for biodiversity assessment. GigaScience, 4(1), s13742-015.

Eble, J. A., Daly-Engel, T. S., DiBattista, J. D., Koziol, A., & Gaither, M. R. 2020. Marine Environmental DNA: Approaches, Applications, and Opportunities. Advances in marine biology, 86(1), 141-169.

Ehlinger, G.S. and Tankersley, R.A. 2007. Reproductive ecology of the American horseshoe crab *Limulus polyphemus* in the Indian River Lagoon. Florida Scientist; Orlando Vol. 70, Iss. 4, (Autumn 2007): 449-463.

Elliott, M., Mander, L., Mazik, K., Simenstad, C., Valesini, F., Whitfield, A., & Wolanski, E. (2016). Ecoengineering with ecohydrology: successes and failures in estuarine restoration. Estuarine, Coastal and Shelf Science, 176, 12-35.

Faust, M.A. and R.A. Gulledge. 2002. Identifying Harmful Marine Dinoflagellates. Contributions from the United States National Herbarium , 2002, Vol. 42 (2002), pp. 1-144.

Felder, Darryl L., and David K. Camp, eds. *Gulf of Mexico origin, waters, and biota: Biodiversity*. Texas A&M University Press, 2009.

Ferrell, H. E. 1999. Storms and the recruitment of larval and juvenile fishes through Sebastian Inlet, Florida. MS Thesis, Florida Institute of Technology, Melbourne. 106 p.

Flanagan, Alison M; Flood, Roger D; Frisk, Michael G; Garza, Corey D; Lopez, Glenn R; et al. 2018. The relationship between observational scale and explained variance in benthic communities. PLoS One; San Francisco Vol. 13, Iss. 1, (Jan 2018): e0189313. DOI:10.1371/journal.pone.0189313.

Franz, David R. "Development and metamorphosis of the gastropod Acteocina canaliculata (Say)." Transactions of the American Microscopical Society (1971): 174-182.

Fredette TJ and RJ Diaz. 1986. Life history of Gammarus mucronatus Say (Amphipoda: Gammaridae) in warm temperate estuarine habitats, York River, Virginia. Journal of Crustacean Biology 6:57-78.

FWRI, 2009. Fisheries-Independent Monitoring Program Procedure Manual. Gianuca, A. T., S. A. J. Declerck, M. W. Cadotte, C. Souffreau, T. De Bie, and L. De Meester. 2016. Integrating trait and phylogenetic distances to assess scale-dependent community assembly processes. Ecography:1–11.

Gianuca, A. T., S. A. J. Declerck, M. W. Cadotte, C. Souffreau, T. De Bie, and L. De Meester. 2016. Integrating trait and phylogenetic distances to assess scale-dependent community assembly processes. Ecography:1–11.

Gilmore, RG Jr. 1995. Environmental and biogeographic factors influencing ichthyofaunal diversity in the Indian River Lagoon. Bulletin of Marine Science 57: 153–170.

Giovannoni, Stephen J., and Kevin L. Vergin. "Seasonality in ocean microbial communities." Science 335, no. 6069 (2012): 671-676.

Gobler, J.C et al. 2019. Accidental ecosystem restoration? Assessing the estuary-wide impacts of a new ocean inlet created by Hurricane Sandy. Estuarine, Coastal and Shelf Science. Volume 221, 31 May 2019, Pages 132-146.

Gutierrez, M. A., Cardona, A. A., & Smee, D. L. (2010). Growth patterns of shoal grass Halodule wrightii and manatee grass Syringodium filiforme in the western Gulf of Mexico. Gulf and Caribbean Research, 22(1), 71-75.

Hallegraeff, G. M. "Harmful algal blooms: a global overview." Manual on harmful marine microalgae 33 (2003): 1-22.

Hauxwell J, McClelland J, Behr PJ, and I Valiela. 1998. Relative importance of grazing and nutrient controls of macroalgal biomass in three temperate shallow estuaries. Estuaries 21:347-360.

Henry, R. P., Garrelts, E. E., McCarty, M. M., & Towle, D. W. (2002). Differential induction of branchial carbonic anhydrase and Na+/K+ ATPase activity in the euryhaline crab, Car*cinus maenas*, in response to low salinity exposure. Journal of Experimental Zoology, 292(7), 595-603.

Hickford, M.J.H, D.R. Scheil. Evaluation of the performance of light traps for sampling inshore fish larvae in inshore temperate waters. Marine Ecology – Progress Series 186:293-302.

Hines, A.H., Jivoff, P.R., Bushmann, P.J., van Montfrans, J., Reed, S.A., Wolcott, D.L., and Wolcott, T.G. 2003. Evidence for sperm limitation in the blue crab, *Callinectes sapidus*. Bulletin of Marine Science, 72(2), 287-310.

Hopkins, S.H. Distribution of species of *Cliona* (boring sponge) on the Eastern Shore of Virginia in relation to salinity. *Chesapeake Science* 3, 121–124 (1962). https://doi.org/10.2307/1351224.

Huson, D. H., & Weber, N. 2013. Microbial community analysis using MEGAN. In Methods in enzymology (Vol. 531, pp. 465-485). Academic Press.

Jegla T.C. and Costlow, J.D. 1982. Temperature and salinity effects on developmental and early posthatch stages of Limulus. Prog Clinic Biol Res 81: 103-113.

Johnson, KB, and K Soltis. 2017. Larval supply and recruitment of the ivory barnacle Balanus eburneus on oyster cultch used in oyster-reef restoration. The Journal of Crustacean Biology 37(3), 243–248.

Kennish, Michael J; Haag, Scott M; Sakowicz, Gregg P; Durand, James B. 2004. Benthic Macrofaunal Community Structure along a Well-Defined Salinity Gradient in the Mullica River-Great Bay Estuary. Journal of Coastal Research, suppl. Special Issue; Fort Lauderdale Vol. SI, Iss. 45: 209-226.

Kelly JR, Levine SN, Buttel LA, Carr KA, Rudnick DT, and RD Morton. 1990. The effects of tributyltin within a Thalassia seagrass ecosystem. Estuaries 13:301-310.

Kirkpatrick, Barbara; Fleming, Lora E.; Squicciarini, Dominick; Backer, Lorrie C.; Clark, Richard; Abraham, William; Benson, Janet; Cheng, Yung Sung; Johnson, David (2004). "Literature review of Florida red tide: implications for human health effects". Harmful Algae. 3 (2): 99–115. doi:10.1016/j.hal.2003.08.005.

Kornicker LS (1967) A study of three species of Sarsiella (Ostracoda: Myodocopina). Proceedings of the United States National Museum 122(3594): 1–46, 4 pls.

Kornicker LS (1986) Sarsiellidae of the Western Atlantic and Northern Gulf of Mexico, and revision of the Sarsiellinae (Ostracoda: Myodocopina).

Kozich, J. J., Westcott, S. L., Baxter, N. T., Highlander, S. K., & Schloss, P. D. 2013. Development of a dual-index sequencing strategy and curation pipeline for analyzing amplicon sequence data on the MiSeq Illumina sequencing platform. Applied and environmental microbiology, 79(17), 5112-5120.

Kroodsma, David A., Juan Mayorga, Timothy Hochberg, Nathan A. Miller, Kristina Boerder, Francesco Ferretti, Alex Wilson et al. "Tracking the global footprint of fisheries." Science 359, no. 6378 (2018): 904-908.

Kruskal, J. B., and M. Wish. 1978. Multidimensional scaling. Vol 11. Sage.

Kuk-Dzul, J. Gabriel, G. Gold-Bouchot, and P-L. Ardisson. "Benthic infauna variability in relation to environmental factors and organic pollutants in tropical coastal lagoons from the northern Yucatan Peninsula." Marine Pollution Bulletin 64, no. 12 (2012): 2725-2733.

Kumar, G., Eble, J. E., & Gaither, M. R. (2020). A practical guide to sample preservation and pre-PCR processing of aquatic environmental DNA. Molecular Ecology Resources, 20(1), 29-39.

Kupschus, S, D. Tremain. 2001. Associations between fish assemblages and environmental factors in nearshore habitats of a subtropical estuary. Journal of Fish Biology 58: 1383–1403.

Legendre, P., and E. Gallagher. 2001. Ecologically meaningful transformations for ordination of species data. Oecologia 129:271–280.

Leray, M., Yang, J. Y., Meyer, C. P., Mills, S. C., Agudelo, N., Ranwez, V., ... & Machida, R. J. 2013. A new versatile primer set targeting a short fragment of the mitochondrial COI region for metabarcoding metazoan diversity: application for characterizing coral reef fish gut contents. Frontiers in zoology, 10(1), 34.

Levinton, M. Doall, D. Ralston, A. Starke, B. Allam. 2011. Climate change, precipitation and impacts on an estuarine refuge from disease. PLoS One, 6 (2011), p. e18849.

Luczkovich JJ, Ward GP, Johnson JC, Christian RR, Baird D, Neckles H, and WM Rizzo. 2002. Determining the trophic guilds of fishes and macroinvertebrates in a seagrass food web. Estuaries 25:1143-1163.

Madeira, D., Narciso, L., Cabral, H.N. and Vinagre, C., 2012. Thermal tolerance and potential impacts of climate change on coastal and estuarine organisms. Journal of Sea Research, 70, pp.32-41.

McMillan C. 1982. Reproductive physiology of tropical seagrasses. Aquat Bot 14: 245-258.

Martinez, S.E. 2012. Spatial ecology of American horseshoe crab (*Limulus polyphemus*) in Chatham, Cape Cod, MA: Implications for conservation and management. Master's Thesis, Wildlife and Fisheries Conservation, University of Massachusetts Amherst.

Mason, W.T., Jr. 1998. Macrobenthic monitoring in the lower St. Johns River, Florida. Environmental Monitoring and Assessment 50:101-130.

Morgan MD and CL Kitting. 1984. Productivity and utilization of the seagrass Halodule wrightii and its attached epiphytes. Limnology 29:1066-1076.

Mikkelsen, Paula M., Paul S. Mikkelsen, and David J. Karlen. "Molluscan biodiversity in the Indian River lagoon, Florida." Bulletin of Marine Science 57, no. 1 (1995): 94-127.

Milliken, M. and Williams, A. 1984. Synopsis of biological data on the blue crab, *Callinectes sapidus* Rathbun. NOAA National Marine Fisheries Service Tech Memo. U.S. Department of Commerce 1: 1-39.

Miya, M., Sato, Y., Fukunaga, T., Sado, T., Poulsen, J.Y., Sato, K., Kondoh, M., 2015. MiFish, a set of universal PCR primers for metabarcoding environmental DNA from fishes: detection of more than 230 subtropical marine species. R. Soc. Open Sci. 2, 150088.

Morris, L.J., Hall, L.M., Virnstein, R.W. 2001. Field guide for fixed seagrass transect monitoring in the Indian River Lagoon. St. Johns River Water Management District, Palatka, Florida.

Nelson WG. 1979. Experimental studies of selective predation on amphipods: Consequences for amphipod distribution and abundance. Journal of Experimental Marine Biology and Ecology 38:225-245.

Nelson WG. 1980. The biology of eelgrass (Zostera marina L.) amphipods. Crustaceana 39:59-89.

Nelson WG. 1995. Amphipod crustaceans of the Indian River Lagoon: current status and threats to biodiversity. Bulletin of Marine Science 57:143-152.

NOAA National Benthic Inventory: https://products.coastalscience.noaa.gov/nbi/.

Paperno, R. 2002. Age-0 Spot (Leiostomus xanthurus) from Two Estuaries Along Central Florida's East Coast: Comparisons of the Timing of Recruitment, Seasonal Changes in Abundance, and Rates of Growth and Mortality. Florida Scientist 65:85–99.

Paperno, R., and R. B. Brodie. 2004. Effects of environmental variables upon the spatial and temporal structure of a fish community in a small, freshwater tributary of the Indian River Lagoon, Florida. Estuarine, Coastal and Shelf Science 61:229–241.

Paperno, R., D. M. Tremain, D. H. Adams, A. P. Sebastian, J. T. Sauer, and J. Dutka-Gianelli. 2006. The Disruption and Recovery of Fish Communities in the Indian River Lagoon, Florida, Following Two Hurricanes in 2004. Estuaries and Coasts 29:1004–1010.

Peters, KM, RH McMichael. 1987. Early life history of the red drum, Sciaenops ocellatus (Pisces: Sciaenidae), in Tampa Bay, Florida. Estuaries 10:92-107.

Phillips RC. 1960. Observations on the ecology and distribution of the Florida seagrasses. Professional Paper Series No. 2. Florida State Board Conserv Mar Lab, St. Petersburg, FL.

Potter, Ian & Veale, Lauren & Tweedley, James & Clarke, K. (2016). Decadal changes in the ichthyofauna of a eutrophic estuary following a remedial engineering modification and subsequent environmental shifts. Estuarine, Coastal and Shelf Science. 181. 10.1016/j.ecss.2016.08.023.

Poulakis, GR, JM Shenker, DS Taylor. 2002. Habitat use by fishes after tidal reconnection of an impounded estuarine wetland in the Indian River Lagoon, Florida (USA). Wetlands Ecology and Management 10:51-69.

R Core, T., 2012. R: A language and environment for statistical computing. R Foundation for Statistical Computing, Vienna, Austria.

Reyier, E. and J.M. Shenker. 2007. Ichthyoplankton community structure in a shallow subtropical estuary of the Florida Atlantic coast. Bull. Mar. Sci. 80:267-293.

Reyier, E.A., J.M. Shenker and D. Christian. 2008. Role of an estuarine fisheries reserve in the production and export of ichthyoplankton. Mar. Ecol. Prog. Ser. 359:249-260.

Richards, WJ, ed. 2005. Early Stages of Atlantic Fishes: An Identification Guide for the Western Central North Atlantic. Boca Raton, FL: CRC Taylor & Francis.

Rosenberg, G.; Moretzsohn, F.; García, E. F. (2009). Gastropoda (Mollusca) of the Gulf of Mexico, Pp. 579–699 in: Felder, D.L. and D.K. Camp (eds.), Gulf of Mexico–Origins, Waters, and Biota. Texas A&M Press, College Station, Texas.

Rubec, P.J., Santi, C., Ghile, Y., Chen, Z., 2018. Modeling to Assess Spatial Distributions and Population Numbers of Estuarine Species for Baseline and Minimum Flows in Lower Peace River Shell Creek and Charlotte Harbor , Florida. https://doi.org/10.13140/RG.2.2.29417.39524.

Ruiz, Gregory, Paul Fofonoff, Brian Steves, and Alisha Dahlstrom. "Marine crustacean invasions in North America: a synthesis of historical records and documented impacts." In in the Wrong Place-Alien Marine Crustaceans: Distribution, Biology and Impacts, pp. 215-250. Springer, Dordrecht, 2011.

Sampaio, L. and A. Bianchini. 2002. Salinity effects on osmoregulation and growth of the euryhaline flounder *Paralichthys orbignyanus*. Journal of Experimental Marine Biology and Ecology. Volume 269, Issue 2, 29 March 2002, Pages 187-196.

Santos, R. O., J. S. Rehage, R. Boucek, and J. Osborne. 2016. Shift in recreational fishing catches as a function of an extreme cold event. Ecosphere 7:1–16.

Schmidt, Victor T., Katherine F. Smith, Donald W. Melvin, and Linda A. Amaral-Zettler. "Community assembly of a euryhaline fish microbiome during salinity acclimation." Molecular ecology 24, no. 10 (2015): 2537-2550.

Shenker, JM, JM Dean. 1979. The utilization of an intertidal salt marsh creek by larval and juvenile fishes: Abundance, diversity and temporal variation. Estuaries 2:154-163.

Shenker, J.M, R. Crabtree, E. Cowie, H. Patterson, C. Stevens, K. Yakubik. 2002. Recruitment of tarpon (*Megalops atlanticus*) leptocephali into the Indian River Lagoon, Florida. Contrib. Mar. Sci. 35:55-69.

Shuster Jr., C.N. 1982. A pictorial review of the natural history and ecology of the horseshoe crab Limulus polyphemus, with reference to other Limulidae. Prog Clinic Biol Res 81: 1-52.

Smith, DG. 1989. Fishes of the Western North Atlantic. Part 9. Leptocephali. Sears Foundation for Marine Research.

Smith, N.P., 1993. Tidal and non-tidal flushing of Florida's IRL. *Estuaries* 16.4, 739-746.

Smith, SL. 1995. Recruitment of larval snappers (Family Lutjanidae) through Sebastian Inlet, Florida. MS Thesis, Florida Institute of Technology, Melbourne. 48 p.

Stat, M., Huggett, M.J., Bernasconi, R., DiBattista, J.D., Berry, T.E., Newman, S.J., Bunce, M., 2017. Ecosystem biomonitoring with eDNA: metabarcoding across the tree of life in a tropical marine environment. Sci. Rep. 7, 12240.

Stoner AW. 1979. Species-specific predation on amphipod Crustacea by the pinfish Lagodon rhomboides: Mediation by macrophyte standing crop. Marine Biology 55:201-207.

Stoner AW. 1983. Distributional ecology of amphipods and tanaidaceans associated with three sea grass species. Journal of Crustacean Biology 3:505-518.

Sweat, LH, G Swain, K Hunsucker, and KB Johnson. 2017. Transported biofilms and their influence on subsequent macrofouling colonization. Biofouling 33(5):433-449.

Takahashi, F. 2016. Shorebird utilization of horseshoe crab (*Limulus polyphemus*) eggs at Cape Romain National Wildlife Refuge, South Carolina. Master's Thesis, Clemson University, 84 pp.

Tetra Tech. 2016. Save Our Lagoon Project Plan for Brevard County, Florida. Contract #: 260070-14-009. Prepared by Tetra Tech, Inc. and Closewaters, LLC. 82 pp.

Trudnowska, Emilia, Marta Gluchowska, Agnieszka Beszczynska-Möller, Katarzyna Blachowiak-Samolyk, and Slawomir Kwasniewski. "Plankton patchiness in the Polar Front region of the West Spitsbergen Shelf." Marine Ecology Progress Series 560 (2016): 1-18.

Tunberg, B.G., Jones, S., Reed, S., Stephens, M.C. 2008. Pre and post dredge benthic environmental monitoring in Sebastian River. First Phase Final Report to St. Johns River Water Management District (November 2008). 44 pp. (Smithsonian Project No. 786081).

Turner, H.M. 1985. Parasites of eastern oysters from subtidal reefs in a Louisiana estuary with a note on their use as indicators of water quality. Estuaries 8, 323. https://doi.org/10.2307/1351493.

van Maren MJ. 1978. Distribution and ecology of Gammarus tigrinus Sexton, 1939 and some other amphipod Crustacea near Beaufort (NC, USA). Bijdragen tot de Dierkunde 48:46-56.

Vandendorpe, Justine, Christiaan GC van Baak, Björn Stelbrink, Diana Delicado, Christian Albrecht, and Thomas Wilke. "Historical faunal exchange between the Pontocaspian Basin and North America." Ecology and Evolution 9, no. 18 (2019): 10816-10827.

Virnstein, R.W., Morris, L.J. 1996. Seagrass preservation and restoration: A diagnostic plan for the Indian River Lagoon. SJRWMD, Tech. Memorandum No. 14, Palatka, Florida.

Warlen, SM, JS Burke. 1990. Immigration of larvae of fall/winter spawning marine fishes into a North Carolina estuary. Estuaries 13:453-461.

Watling L, and D Maurer. 1972. Marine shallow water amphipods of the Delaware Bay area, USA. Crustaceana, Suppl. 3:251-266.

Wheeler, EP, JM Shenker. 2000.Age and developmental stage at recruitment of ladyfish, Elops saurus. MS Thesis, Florida Institute of Technology, Melbourne. 42 p.

Wieher, CR. 1995. The movement of juvenile fishes between the Indian River Lagoon and mosquito impoundments north of Sebastian inlet, Florida. M.S. Thesis, Florida Inst. of Tech.

Ye J., Coulouris G., Zaretskaya I., Cutcutache I., Rozen S., Madden T., 2012. Primer-BLAST: A tool to design target-specific primers for polymerase chain reaction. BMC Bioinformatics. 13:134.

Zieman JC. 1982. Ecology of the seagrasses of south Florida: a community profile. No. FWS/OBS-82/25. Virginia Univ: Charlottesville, VA (USA). Dept Environ Sci.

Zimmerman R, Gibson R, and J Harrington. 1979. Herbivory among gammaridean amphipods from a Florida seagrass community. Marine Biology 54:41-47.

Zugelter, A. 2019. Nursery Habitat Characteristics of Juvenile Tarpon, Megalops atlanticus, in the northern Indian River Lagoon, FL. M.S. Thesis, Florida Institute of Technology.

Appendix 1. Fish Analysis Supporting Information

Table 1-1. Relative abundance of fishes in the IRL and in each of the three sites of interest.

Species	IRL	Site 1	Site 2	Site 3
Abudefduf saxatilis	2	0	0	0
Acanthostracion quadricornis	6	2	0	3
Acanthurus chirurgus	3	0	0	0
Achiridae spp.	9	0	0	0
Achirus lineatus	81	44	26	24
Aetobatus narinari	3	0	0	3
Agonostomus monticola	8	2	0	0
Albula vulpes	54	10	36	54
Aluterus monoceros	2	0	0	0
Aluterus schoepfii	9	0	0	6
Ameiurus catus	16	0	0	0
Ameiurus nebulosus	4	0	0	0
Anchoa cubana	2636	0	0	252
Anchoa hepsetus	4528	4	18	1280
Anchoa lamprotaenia	28	0	0	28
Anchoa lyolepis	1882	0	0	408
Anchoa mitchilli	231704	34562	33327	53796
Ancylopsetta quadrocellata	3	0	0	0
Anguilla rostrata	3	0	0	0
Anisotremus surinamensis	8	0	0	0
Anisotremus virginicus	15	0	0	2
Apalone ferox	4	0	0	0
Archosargus probatocephalus	456	204	140	208
Archosargus rhomboidalis	1764	3	20	772
Ariopsis felis	2637	616	940	1461
Astroscopus y graecum	3	0	0	0
Bagre marinus	66	15	66	24
Bairdiella chrysoura	9297	3294	1722	1728
Bairdiella spp.	4	0	0	0
Balistes capriscus	4	0	0	0
Bathygobius soporator	10	0	0	8
Bathygobius spp.	2	0	0	2
Bothus robinsi	2	0	0	2
Calamus arctifrons	3	0	0	2
Calamus bajonado	2	0	0	0
Calamus penna	3	0	0	0
Canthidermis maculata	2	0	0	0
Caranx bartholomaei	3	0	0	0
Caranx crysos	6	0	0	3
Caranx hippos	1077	266	45	315
Caranx latus	129	4	0	15
Carcharhinus brevipinna	2	0	0	0
Carcharhinus leucas	3	0	0	2
Caretta	3	0	0	0
Centropomus parallelus	4	0	0	0
Centropomus pectinatus	4	0	0	2
Centropomus undecimalis	224	48	26	92

Species	IRL	Site 1	Site 2	Site 3
Centropristis philadelphica	1.20E+01	0	0	0
Centropristis striata	25	0	0	0
Chaetodipterus faber	207	93	40	54
Chasmodes bosquianus	2	1	0	1
Chasmodes saburrae	118	81	8	27
Chelonia mydas	6	6	0	6
Chilomycterus schoepfii	160	57	160	40
Chloroscombrus chrysurus	354	44	63	276
Chriodorus atherinoides	1.00E+00	0	0	0
Cichlasoma urophthalmus	4	0	0	0
Citharichthys macrops	4	0	0	2
Citharichthys spilopterus	82	12	2	82
Corvula sanctaeluciae	128	0	0	124
Coryphaena hippurus	2	0	0	0
Ctenogobius boleosoma	242	0	6	242
Ctenogobius shufeldti	30	0	0	8
Ctenogobius smaragdus	30	0	0	15
Ctenogobius stigmaticus	10	0	0	0
Ctenogobius stigmaturus	4	0	0	0
Cynoscion complex	776	776	54	57
Cynoscion nebulosus	884	90	482	156
Cynoscion nothus	4	0	0	0
Cynoscion spp.	3	0	0	0
Cyprinodon variegatus	896	688	78	17
Dasyatis americana	3	0	0	0
Dasyatis sabina	516	242	222	196
Dasyatis say	66	33	46	15
Dasyatis spp.	3	0	0	0
Diapterus auratus	7398	1179	1581	1995
Diapterus rhombeus	22	0	0	6
Diodon holocanthus	2	0	0	2
Diplectrum bivittatum	2	0	0	0
Diplodus holbrookii	62	0	0	62
Dormitator maculatus	6	0	0	3
Dorosoma cepedianum	114	2	3	9
Dorosoma petenense	20	0	0	4
Dorosoma spp.	2	0	0	0
Echeneis naucrates	3	3	3	0
Echeneis neucratoides	3	2	0	0
Echeneis spp.	3	0	3	0
Elacatinus macrodon	3	0	0	0
Elops saurus	4707	158	168	423
Elops smithi	15	1	0	2
Engraulis eurystole	2	0	0	0
Epinephelus itajara	3	0	0	2
Epinephelus morio	3	0	0	0
Erotelis smaragdus	3	0	0	3
Esox niger	2	0	0	0
Etropus crossotus	42	0	0	4
Eucinostomus argenteus	382	0	0	16
Eucinostomus gula	4480	240	432	756
Eucinostomus harengulus	4390	1224	1035	982

Species	IRL	Site 1	Site 2	Site 3
Eucinostomus jonesii	138	3	0	114
Eucinostomus lefroyi	34	0	0	34
Eucinostomus melanopterus	18	3	0	0
Eugerres plumieri	246	28	36	98
Evorthodus lyricus	16	2	0	6
Floridichthys carpio	3904	1344	280	109
Fundulus chrysotus	2	0	0	0
Fundulus confluentus	2	1	0	0
Fundulus grandis	385	44	2	54
Fundulus heteroclitus	2	0	0	0
Fundulus majalis	21	0	2	0
Fundulus seminolis	6	0	0	0
Fundulus similis	14	10	0	0
Gambusia holbrooki	1056	192	0	5
Gerres cinereus	90	18	3	48
Gobiesox strumosus	9	6	2	2
Gobioides broussonetii	3	0	0	0
Gobiomorus dormitor	3	0	0	3
Gobionellus oceanicus	156	4	0	16
Gobiosoma bosc	32	2	4	20
Gobiosoma ginsburgi	4	0	0	0
Gobiosoma robustum	968	580	304	384
Gymnura micrura	39	4	33	32
Haemulon aurolineatum	4	0	0	0
Haemulon flavolineatum	2	0	0	2
Haemulon parra	444	0	0	146
Haemulon plumierii	54	0	0	6
Haemulon sciurus	6	0	0	4
Halichoeres radiatus	24	0	0	0
Harengula humeralis	46	0	0	0
Harengula jaguana	7490	357	452	4666
Hippocampus erectus	32	16	10	14
Hippocampus zosterae	108	33	2	3
Histrio histrio	2	0	0	0
Hoplosternum littorale	2	0	0	0
Hypleurochilus geminatus	3	0	0	0
Hyporhamphus meeki	68	26	4	68
Hyporhamphus unifasciatus	6	2	0	0
Hypsoblennius hentz	3	0	0	0
Ictalurus punctatus	24	0	0	0
Kyphosus incisor	2	0	0	0
Kyphosus sectatrix	2	0	0	0
Labridae spp. parrotfishes	2	0	0	0
Labrisomus nuchipinnis	4	0	0	1
Lachnolaimus maximus	6	0	0	6
Lactophrys spp.	3	0	0	0
Lactophrys trigonus	9	2	0	9
Lactophrys triqueter	3	0	0	3
Lagodon rhomboides	9798	6618	1488	4748
Leiostomus xanthurus	13888	1424	1557	2784
Lepisosteus osseus	4	0	0	0
Lepisosteus platyrhincus	2	0	0	0

Species	IRL	Site 1	Site 2	Site 3
Lepomis macrochirus	8	0	0	0
Lepomis microlophus	3	0	0	0
Lepomis spp.	3	0	0	0
Lobotes surinamensis	8	2	3	4
Lophogobius cyprinoides	18	0	0	2
Lucania parva	23040	6880	1744	1144
Lupinoblennius nicholsi	3	0	0	0
Lutjanus analis	76	0	0	30
Lutjanus apodus	4	0	0	2
Lutjanus cyanopterus	2	0	0	0
Lutjanus griseus	132	27	24	132
Lutjanus jocu	3	0	0	2
Lutjanus synagris	152	0	3	40
Megalops atlanticus	24	3	20	2
Membras martinica	1482	398	74	78
Menticirrhus americanus	298	153	278	194
Menticirrhus littoralis	2	0	0	0
Menticirrhus saxatilis	6	0	0	0
Microgobius gulosus	1412	716	768	432
Microgobius microlepis	80	0	0	80
Microgobius thalassinus	68	8	8	50
Microphis brachyurus	1.00E+00	0	0	0
Micropogonias undulatus	7252	7168	234	7252
Micropterus salmoides	4	0	0	0
Monacanthus ciliatus	8	0	0	4
Monacanthus spp.	2	0	0	0
Mugil cephalus	11010	1998	1924	2257
Mugil curema	4780	1587	416	3006
Mugil rubrioculus	48	10	16	33
Mugil trichodon	10	0	0	2
Mycteroperca bonaci	6	0	0	4
Mycteroperca microlepis	48	0	0	48
Myliobatis freminvillii	3	0	0	0
Myrophis punctatus	16	0	0	4
Negaprion brevirostris	2	0	0	0
Nicholsina usta	56	0	0	2
Notropis maculatus	3	0	0	0
Ocyurus chrysurus	9	0	0	4
Ogcocephalus cubifrons	2	0	0	0
Oligoplites saurus	512	60	282	84
Opisthonema oglinum	4143	3504	117	957
Opistognathus robinsi	3	0	0	0
Opsanus beta	2	0	0	0
Opsanus tau	24	9	12	16
Oreochromis spp.	3	0	0	0
Orthopristis chrysoptera	3570	33	93	3570
Ostraciidae spp.	6	0	0	3
Parablennius marmoreus	2	0	0	2
Paraclinus fasciatus	3	0	0	0
Paraclinus marmoratus	2	0	0	0
Paralichthys albigutta	148	0	3	148
Paralichthys lethostigma	28	3	0	20

Species	IRL	Site 1	Site 2	Site 3
Poecilia latipinna	1728	1728	1	20
Pogonias cromis	666	130	69	36
Pomatomus saltatrix	24	3	12	24
Prionotus rubio	3	0	0	0
Prionotus scitulus	45	30	30	6
Prionotus tribulus	10	0	0	8
Pseudupeneus maculatus	3	0	0	0
Pterygoplichthys spp.	2	0	0	0
Rachycentron canadum	3	0	0	0
Rhinoptera bonasus	63	0	36	4
Sardinella aurita	774	0	0	30
Sarotherodon spp.	35	32	0	9
Sarotherodon melanotheron	98	44	38	18
Sciaenops ocellatus	2466	158	40	594
Scomberomorus cavalla	2	0	0	0
Scomberomorus maculatus	28	0	4	10
Scomberomorus regalis	21	0	0	21
Scorpaena brasiliensis	3	0	0	1
Scorpaena grandicornis	6	0	0	6
Scorpaena plumieri	6	0	0	3
Selar crumenophthalmus	8	0	0	0
Selene setapinnis	3	0	0	0
Selene vomer	906	6	42	120
Seriola fasciata	1.00E+00	0	0	0
Seriola rivoliana	2	0	0	0
Sparidae spp.	3	0	0	0
Sparisoma radians	26	0	0	1
Sparisoma rubripinne	3	0	0	3
Sphoeroides nephelus	588	588	138	159
Sphoeroides spengleri	46	0	3	14
Sphoeroides testudineus	250	2	3	82
Sphyraena barracuda	33	4	12	16
Sphyraena borealis	12	0	0	6
Sphyraena guachancho	3	0	0	2
Sphyrna tiburo	10	0	0	4
Stephanolepis hispidus	78	0	3	27
Stephanolepis setifer	2	0	0	2
Strongylura marina	96	60	21	96
Strongylura notata	274	108	124	44
Strongylura timucu	16	16	3	16
Syacium spp.	3	0	0	0
Symphurus civitatium	3	0	0	2
Symphurus plagiusa	36	0	0	10
Syngnathus fuscus	1.00E+00	0	0	0
Syngnathus louisianae	34	27	8	21
Syngnathus scovelli	339	177	130	339
Synodus foetens	40	3	3	15
Tetraodontidae spp.	2	0	0	0
Trachinotus carolinus	87	6	6	6
Trachinotus falcatus	416	88	18	146
Trichiurus lepturus	5	0	0	0
Trinectes maculatus	588	2	0	3

Species	IRL	Site 1	Site 2	Site 3
Tylosurus acus	1.00E+00	0	0	1
Tylosurus crocodilus	12	0	6	4
Urophycis floridana	4	0	0	0
Species Richness (# Species)	***258***	***94***	***85***	***159***

Table 1-2. Summary statistical results of the Partial RDA for the IRL site.

Gear	Factor	RDA1	RDA2
20	**Eigenvalue**	2.47E+05	2.72E+03
20	**Depth**	0.44	0.49
20	**Temperature**	0.63	-0.57
20	**Conductivity**	-0.33	-0.01
20	**pH**	-0.38	-0.66
20	**Salinity**	-0.41	0.06
20	**DO**	-0.63	-0.02
160	**Eigenvalue**	1.89E+04	1.24E+03
160	**Depth**	-0.41	-0.68
160	**Temperature**	-0.61	0.66
160	**Conductivity**	-0.60	0.12
160	**pH**	-0.25	-0.24
160	**Salinity**	-0.49	0.10
160	**DO**	0.41	-0.42
300	**Eigenvalue**	3.07E+05	2.21E+03
300	**Depth**	-0.89	0.26
300	**Temperature**	-0.17	-0.75
300	**Conductivity**	-0.05	-0.05
300	**pH**	0.47	0.53
300	**Salinity**	-0.05	-0.03
300	**DO**	0.03	0.81
301	**Eigenvalue**	3.51E+03	5.33E+02
301	**Depth**	0.37	-0.23
301	**Temperature**	0.01	-0.89
301	**Conductivity**	0.69	0.04
301	**pH**	-0.51	0.11
301	**Salinity**	0.70	0.16
301	**DO**	-0.34	0.49

Table 1-3. Summary statistical results of the Partial RDA for Site 1.

Gear	Factor	RDA1	RDA2
20	**Eigenvalue**	2.61E+04	4.66E+03
20	**Depth**	-0.59	0.14
20	**Temperature**	-0.39	0.64
20	**Conductivity**	-0.16	0.10
20	**pH**	0.68	0.38
20	**Salinity**	-0.15	-0.07
20	**DO**	0.61	0.07
160	**Eigenvalue**	1.40E+04	1.80E+03
160	**Depth**	0.07	-0.88
160	**Temperature**	0.83	0.08
160	**Conductivity**	0.71	0.06
160	**pH**	0.06	-0.19
160	**Salinity**	0.62	0.10
160	**DO**	-0.57	-0.36
300	**Eigenvalue**	1674000.00	1374.00
300	**Depth**	-0.89	0.36
300	**Temperature**	0.29	-0.01
300	**Conductivity**	-0.75	-0.21
300	**pH**	0.50	0.32
300	**Salinity**	-0.78	-0.27
300	**DO**	-0.18	0.17
301	**Eigenvalue**	ID	ID
301	**Depth**	ID	ID
301	**Temperature**	ID	ID
301	**Conductivity**	ID	ID
301	**pH**	ID	ID
301	**Salinity**	ID	ID
301	**DO**	ID	ID

Table 1-4. Summary statistical results of the Partial RDA for Site 2.

Gear	Factor	RDA1	RDA2
20	**Eigenvalue**	7.99E+05	1.89E+03
20	**Depth**	-0.84	0.27
20	**Temperature**	-0.42	-0.68
20	**Conductivity**	-0.26	0.48
20	**pH**	0.17	-0.19
20	**Salinity**	-0.16	0.57
20	**DO**	0.21	0.25
160	**Eigenvalue**	7.86E+03	1.60E+03
160	**Depth**	-0.36	-0.09
160	**Temperature**	-0.45	-0.67
160	**Conductivity**	-0.63	-0.08
160	**pH**	-0.39	0.49
160	**Salinity**	-0.50	-0.14
160	**DO**	0.23	0.60
300	**Eigenvalue**	1.19E+03	6.65E+02
300	**Depth**	0.48	-0.07
300	**Temperature**	0.09	-0.35
300	**Conductivity**	-0.32	0.29
300	**pH**	-0.27	0.19
300	**Salinity**	-0.06	0.58
300	**DO**	-0.19	0.60
301	**Eigenvalue**	ID	ID
301	**Depth**	ID	ID
301	**Temperature**	ID	ID
301	**Conductivity**	ID	ID
301	**pH**	ID	ID
301	**Salinity**	ID	ID
301	**DO**	ID	ID

Table 1-4. Summary statistical results of the Partial RDA for Site 3.

Gear	Factor	RDA1	RDA2
20	**Eigenvalue**	1.85E+05	1.82E+03
20	**Depth**	0.26	-0.19
20	**Temperature**	0.42	-0.08
20	**Conductivity**	-0.59	-0.60
20	**pH**	-0.22	-0.38
20	**Salinity**	-0.68	-0.54
20	**DO**	-0.59	0.19
160	**Eigenvalue**	3.21E+04	2.17E+03
160	**Depth**	-0.15	-0.39
160	**Temperature**	-0.84	-0.39
160	**Conductivity**	-0.30	0.19
160	**pH**	-0.27	0.43
160	**Salinity**	-0.12	0.11
160	**DO**	0.32	0.58
300	**Eigenvalue**	6.21E+03	4.29E+02
300	**Depth**	0.30	0.41
300	**Temperature**	-0.13	0.12
300	**Conductivity**	0.33	0.33
300	**pH**	0.54	-0.66
300	**Salinity**	0.40	0.41
300	**DO**	0.67	-0.26
301	**Eigenvalue**	4.64E+03	1.32E+03
301	**Depth**	-0.24	0.09
301	**Temperature**	-0.29	0.55
301	**Conductivity**	-0.58	-0.39
301	**pH**	0.01	0.55
301	**Salinity**	-0.63	-0.44
301	**DO**	-0.18	-0.13

Table 1-5. Summary of statistical results of the Similarity of Percentages and Analysis of Similarities for salinity at Site 2 using gear 20.

Note: Mean and standard deviation refer to the difference between the three scenarios of the abiotic factor being investigated. The species-specific P value, Spp. P., represents the significance of these differences. The Global P = 0.139 and R_2 = 0.049, which refer to the strength of the model.

Species	Mean	St. Dev.	Cum. Var. Exp.	Spp. P
Anchoa mitchilli	0.422	0.357	0.474	0.901
Lucania parva	0.106	0.208	0.593	0.04
Microgobius gulosus	0.09	0.153	0.694	0.762
Leiostomus xanthurus	0.037	0.131	0.736	0.089
Gobiosoma robustum	0.024	0.058	0.763	0.218
Bairdiella chrysoura	0.024	0.08	0.79	0.753
Cynoscion nebulosus	0.02	0.048	0.812	0.149
Floridichthys carpio	0.017	0.065	0.831	0.654
Mugil cephalus	0.015	0.082	0.847	0.119
Lagodon rhomboides	0.014	0.056	0.863	0.257
Syngnathus scovelli	0.014	0.029	0.879	0.386
Membras martinica	0.013	0.064	0.893	0.356
Strongylura notata	0.011	0.043	0.905	0.525
Diapterus auratus	0.01	0.043	0.917	0.188
Eucinostomus harengulus	0.01	0.051	0.927	0.683
Oligoplites saurus	0.008	0.026	0.936	0.327
Orthopristis chrysoptera	0.007	0.037	0.944	0.168
Achirus lineatus	0.004	0.025	0.949	0.465
Eucinostomus gula	0.004	0.015	0.954	0.158
Mugil curema	0.004	0.024	0.958	0.861

Table 1-6. Summary of statistical results of the Similarity of Percentages and Analysis of Similarities for salinity at Site 3 using gear 20.

Note: Mean and standard deviation refer to the difference between the three scenarios of the abiotic factor being investigated. The species-specific P value, Spp. P., represents the significance of these differences. The Global P = 0.139 and R_2 = 0.017, which refer to the strength of the model.

Species	Mean	St. Dev.	Cum. Var. Exp.	Spp. P
Anchoa mitchilli	0.375	0.345	0.414	0.01
Lagodon rhomboides	0.053	0.13	0.473	1
Leiostomus xanthurus	0.046	0.133	0.524	0.525
Diapterus auratus	0.041	0.108	0.569	0.119
Harengula jaguana	0.04	0.136	0.613	0.228
Micropogonias undulatus	0.036	0.114	0.653	0.564
Microgobius gulosus	0.034	0.074	0.725	0.02
Eucinostomus gula	0.032	0.076	0.759	0.822
Sciaenops ocellatus	0.03	0.071	0.79	0.01
Gobiosoma robustum	0.029	0.068	0.819	0.059
Mugil cephalus	0.026	0.09	0.845	0.05
Eucinostomus harengulus	0.024	0.066	0.863	0.951
Bairdiella chrysoura	0.016	0.061	0.879	0.931
Lucania parva	0.015	0.06	0.893	0.654
Anchoa hepsetus	0.013	0.067	0.905	0.743
Orthopristis chrysoptera	0.011	0.053	0.916	1
Syngnathus scovelli	0.01	0.027	0.925	0.257
Cynoscion nebulosus	0.008	0.022	0.932	0.208
Opisthonema oglinum	0.006	0.031	0.938	0.753
Mugil curema	0.006	0.036	0.942	0.594

Table 1-7. Summary of statistical results of the Similarity of Percentages and Analysis of Similarities for salinity at Site 2 using gear 160.

Note: Mean and standard deviation refer to the difference between the three scenarios of the abiotic factor being investigated. The species-specific P value, Spp. P., represents the significance of these differences. The Global P = 0.356 and R_2 = 0.015, which refer to the strength of the model.

Species	Mean	St. Dev.	Cum. Var. Exp.	Spp. P
Lagodon rhomboides	0.16	0.216	0.188	0.931
Mugil curema	0.158	0.189	0.375	0.01
Ariopsis felis	0.07	0.113	0.458	0.743
Diapterus auratus	0.067	0.145	0.536	0.772
Bairdiella chrysoura	0.055	0.14	0.601	0.753
Eucinostomus harengulus	0.043	0.097	0.652	0.376
Mugil cephalus	0.042	0.074	0.701	0.139
Dasyatis sabina	0.04	0.061	0.747	0.257
Sphoeroides nephelus	0.035	0.066	0.789	0.455
Leiostomus xanthurus	0.026	0.092	0.82	0.743
Elops saurus	0.026	0.068	0.851	0.04
Archosargus probatocephalus	0.014	0.036	0.867	0.267
Sciaenops ocellatus	0.013	0.029	0.882	0.149
Menticirrhus americanus	0.012	0.033	0.896	0.149
Oligoplites saurus	0.009	0.037	0.907	0.248
Eucinostomus gula	0.008	0.038	0.916	0.604
Chilomycterus schoepfii	0.008	0.029	0.926	0.168
Cynoscion nebulosus	0.008	0.019	0.935	0.416
Dasyatis say	0.007	0.02	0.944	0.455
Harengula jaguana	0.006	0.03	0.951	0.396

Table 1-8. Summary of statistical results of the Similarity of Percentages and Analysis of Similarities for salinity at Site 1 using gear 300.

Note: Mean and standard deviation refer to the difference between the three scenarios of the abiotic factor being investigated. The species-specific P value, Spp. P., represents the significance of these differences. The Global P = 0.48 and R_2 = 0.002, which refer to the strength of the model.

Species	Mean	St. Dev.	Cum. Var. Exp.	Spp. P
Gobiosoma robustum	0.184201	0.23459	0.209	0.1683
Anchoa mitchilli	0.102832	0.16041	0.326	0.1881
Micropogonias undulatus	0.100394	0.16532	0.44	0.9901
Menticirrhus americanus	0.098567	0.13737	0.553	0.0099
Syngnathus scovelli	0.07421	0.09114	0.637	0.1485
Bairdiella chrysoura	0.046274	0.0677	0.69	0.1386
Microgobius gulosus	0.041966	0.06457	0.737	0.4059
Achirus lineatus	0.03987	0.07271	0.783	0.4257
Sphoeroides nephelus	0.036227	0.08237	0.824	0.1683
Cynoscion nebulosus	0.0315	0.05765	0.86	0.2376
Chilomycterus schoepfii	0.022023	0.04119	0.885	0.297
Lagodon rhomboides	0.016741	0.05831	0.904	0.604
Lucania parva	0.016136	0.04718	0.922	0.2376
Syngnathus louisianae	0.012575	0.02148	0.936	0.1089
Chasmodes saburrae	0.007222	0.01397	0.945	0.5743
Cynoscion complex	0.007034	0.02074	0.952	0.1683
Microgobius thalassinus	0.006837	0.01405	0.96	0.1485
Ariopsis felis	0.005967	0.01431	0.967	0.3069
Gobiosoma bosc	0.00506	0.01167	0.973	0.6436

Table 1-8. Summary of statistical results of the Similarity of Percentages and Analysis of Similarities for salinity at Site 2 using gear 300.

Note: Mean and standard deviation refer to the difference between the three scenarios of the abiotic factor being investigated. The species-specific P value, Spp. P., represents the significance of these differences. The Global P = 0.9 and R_2 = 0.09, which refer to the strength of the model.

Species	Mean	St. Dev.	Cum. Var. Exp.	Spp. P
Syngnathus scovelli	0.19	0.18	0.24	0.51
Gobiosoma robustum	0.15	0.14	0.43	0.62
Anchoa mitchilli	0.12	0.24	0.58	0.33
Menticirrhus americanus	0.07	0.08	0.66	0.95
Cynoscion nebulosus	0.04	0.11	0.71	0.99
Chilomycterus schoepfii	0.04	0.06	0.76	0.74
Micropogonias undulatus	0.03	0.04	0.79	0.58
Dasyatis sabina	0.03	0.04	0.82	0.28
Achirus lineatus	0.02	0.03	0.85	0.49
Lucania parva	0.02	0.04	0.87	0.24
Orthopristis chrysoptera	0.02	0.05	0.9	0.13
Ariopsis felis	0.02	0.03	0.92	0.88
Bairdiella chrysoura	0.01	0.02	0.94	0.12
Microgobius gulosus	0.01	0.03	0.95	0.97
Sphoeroides nephelus	0.01	0.02	0.97	0.5
Microgobius thalassinus	0.01	0.02	0.97	0.72
Gobiosoma bosc	0.01	0.01	0.98	0.03
Lagodon rhomboides	0	0.02	0.99	0.87
Chasmodes saburrae	0	0.01	0.99	0.43
Syngnathus louisianae	0	0.01	0.99	0.82

Table 1-9. Summary of statistical results of the Similarity of Percentages and Analysis of Similarities for salinity at Site 3 using gear 300.

Note: Mean and standard deviation refer to the difference between the three scenarios of the abiotic factor being investigated. The species-specific P value, Spp. P., represents the significance of these differences. The Global P = 0.67 and R_2 = -0.02, which refer to the strength of the model.

Species	Mean	St. Dev.	Cum. Var. Exp.	Spp. P
Anchoa mitchilli	0.21	0.27	0.24	0.29
Eucinostomus gula	0.08	0.12	0.32	0.35
Orthopristis chrysoptera	0.06	0.09	0.4	0.13
Lagodon rhomboides	0.06	0.09	0.46	0.98
Cynoscion complex	0.05	0.07	0.51	0.01
Menticirrhus americanus	0.05	0.05	0.56	0.06
Micropogonias undulatus	0.04	0.09	0.61	0.28
Ariopsis felis	0.04	0.08	0.65	0.29
Bairdiella chrysoura	0.03	0.08	0.69	0.13
Syngnathus scovelli	0.03	0.07	0.73	0.93
Gobiosoma robustum	0.03	0.08	0.76	0.88
Chilomycterus schoepfii	0.02	0.03	0.78	0.43
Microgobius microlepis	0.02	0.04	0.8	0.17
Achirus lineatus	0.02	0.02	0.82	0.01
Diapterus auratus	0.01	0.03	0.84	0.55
Leiostomus xanthurus	0.01	0.06	0.85	0.82
Archosargus probatocephalus	0.01	0.04	0.86	0.48
Sphoeroides nephelus	0.01	0.03	0.88	0.27
Syngnathus louisianae	0.01	0.03	0.89	0.11
Cynoscion nebulosus	0.01	0.03	0.9	0.11

Table 1-9. Summary of statistical results of the Similarity of Percentages and Analysis of Similarities for salinity at Site 3 using gear 301.

Note: Mean and standard deviation refer to the difference between the three scenarios of the abiotic factor being investigated. The species-specific P value, Spp. P., represents the significance of these differences. The Global P = 0.15 and R_2 = 0.03, which refer to the strength of the model.

Species	Mean	St. Dev.	Cum. Var. Exp.	Spp. P
Anchoa mitchilli	0.21	0.29	0.24	0.26
Syngnathus scovelli	0.09	0.12	0.33	0.16
Lagodon rhomboides	0.07	0.16	0.41	0.96
Gobiosoma robustum	0.07	0.12	0.49	0.92
Diapterus auratus	0.07	0.14	0.56	0.03
Eucinostomus gula	0.06	0.11	0.62	0.68
Orthopristis chrysoptera	0.05	0.06	0.67	0.44
Bairdiella chrysoura	0.03	0.07	0.71	0.24
Chilomycterus schoepfii	0.03	0.05	0.74	0.65
Sphoeroides nephelus	0.02	0.06	0.76	0.02
Micropogonias undulatus	0.02	0.05	0.78	0.39
Menticirrhus americanus	0.02	0.05	0.81	0.02
Syngnathus louisianae	0.02	0.03	0.83	0.06
Ariopsis felis	0.02	0.06	0.84	0.62
Archosargus probatocephalus	0.01	0.02	0.86	0.33
Sphoeroides testudineus	0.01	0.03	0.87	0.06
Paralichthys albigutta	0.01	0.03	0.88	0.14
Leiostomus xanthurus	0.01	0.07	0.89	0.94
Anchoa hepsetus	0.01	0.03	0.9	0.12
Lutjanus griseus	0.01	0.02	0.91	0.69

Appendix C Task 3 – Geochemical Baseline Report

Restore Lagoon Inflow Research (Phase 1)
Task 3, Geochemical Baseline

PREPARED FOR

Florida Department of Education
325 W Gaines Street
Tallahassee, FL 32399

PREPARED BY

Austin Fox
Assistant Professor of Ocean Sciences
afox@fit.edu
Florida Institute of Technology
150 West University Boulevard
Melbourne, FL 32901

FLORIDA TECH

September 2020

Table of Contents

List of Tables

List of Figures

Acknowledgements

I would like to thank our representatives in the Legislature and the public for overwhelming support of lagoon science. I thank Robert Salonen, Frank Kinney for their efforts that made this research at Florida Tech possible. I would also like to thank John Windsor for his tireless leadership and guidance, and the other Principle Investigators on this project for their collaboration and support. I would also like to thank the anonymous external reviewers for applying their expertise to reviewing this work. Finally, I would like to thank the students and technicians helping to support this project. I would especially like to thank Abigail Gering, Maria Hernandez Garcia, Stacey Fox, Tyler Provoncha, and Iulia Bibire.

Photograph on cover: Austin Fox

List of Acronyms

BRL	Banana River Lagoon
cm	Centimeter
DIN	Dissolved Inorganic Nitrogen
DO	Dissolved Oxygen
DON	Dissolved Organic Nitrogen
DOP	Dissolved Organic Phosphorus
IRL	Indian River Lagoon
kg/m^3	Kilograms Per Cubic Meter
km^2	Square Kilometer
L	Liter
LOI	Loss on Ignition
m	Meter
m^2	Square Meter
m^3/sec	Cubic Meters Per Second
mg/L	Milligrams Per Liter
mL	Milliliter
N	Nitrogen
NH_4	Ammonium
NOx	Nitrate + Nitrite
O	Oxygen
OM	Organic Matter
ORP	Oxidation Reduction Potential
Org-N	Organic Nitrogen
Org-P	Organic Phosphorus
P	Phosphorus
PO_4	Phosphate
PSU	Practical Salinity Unit
SCUBA	Self-Contained Underwater Breathing Apparatus
SE	Standard Error

Si	Silicon
SiO_2	Silica
SJRWMD	St. Johns River Water Management District
SOD	Sediment Oxygen Demand
SRP	Soluble Reactive Phosphorus
TDN	Total Dissolved Nitrogen
TDP	Total Dissolved Phosphorus
µM	Micromoles Per Liter
µm	Micrometer
µmol/m^2/hr	Micromoles Per Square Meter per Hour
µmol O_2/m^2/hr	Micromoles of Oxygen Per Square Meter per Hour

Executive Summary

In recent decades, estuaries worldwide have been impacted by eutrophication; however, systems that are poorly flushed with long residence times for water, like the Indian River Lagoon (IRL) are less resilient to increased nutrient loading than well-flushed systems. Enhancing circulation and potentially increasing or stabilizing concentrations of dissolved oxygen (DO) in the IRL could lower nutrient concentrations that contribute to algal blooms and loss of ecosystem services. Enhanced circulation could also help to increase the lagoon's resilience to anoxia and fish kills. The goal of this geochemical evaluation of potential impacts of flushing was to: (1) examine impacts on water quality that could result from direct dilution by seawater, (2) evaluate existing conditions for to non-conservative variables such as DO, and (3) evaluate potential impacts of flushing on geochemical process (i.e., fluxes of nutrients and oxygen) that help to regulate nutrient concentrations in the lagoon.

Long-term datasets for temperature and salinity were used to compare values between the lagoon and seawater. Overall, average annual temperatures in the lagoon were close to 25°C and vertical profiles showed vertical temperature gradients where surface water was approximately 1˚C warmer compared to bottom water at an average depth of approximately1.5 meters (m). Temperatures in seawater displayed similar seasonal patterns, but with higher minimum temperatures during the winter and lower maximum temperatures during the summer. Vertical profiles for seawater displayed temperature stratification in the coastal ocean with distinct surface and bottom layers where surface water was on average approximately 1˚C warmer. Temperature in Port Canaveral displayed the largest vertical gradient of the three regions and surface water was on average approximately 2˚C warmer than bottom water (Figure ES-1). In general, salinity in Banana River Lagoon (BRL) was lower (19.2–23.3 practical salinity units [PSU] in 2019) compared to salinities in Vero Beach (21.9–33 PSU in 2019). Overall, salinities in the lagoon were, as expected, lower than the range of salinities identified during this study for the coastal Atlantic Ocean (33–35 PSU). Overall, no vertical trends were identified for salinity in the lagoon or in seawater; but like temperature, salinities showed vertical gradients in Port Canaveral (Figure ES-1). Density, calculated from data for temperature and salinity, was lowest at the northern site in BRL (average density=1,012 kilograms per cubic meter [kg/m^3]) compared to Bethel Creek (1,018 kg/m^3) and both sites were less dense than typical seawater (1,025 kg/m^3) (Figure ES-1). Small difference in density can maintain discrete stratified layers; therefore, seawater entering the lagoon via artificial inflow could create a discrete higher density layer that would flow along the bottom of the lagoon. If mixing were to occur upon inflow, any increases in salinity would be small (likely less than 1 PSU); however, if stratification were to occur sediments could experience salinities as high as 34–35 PSU and temperatures as much as a degree warmer or cooler (depending on seasonality and the degree of mixing). While temperature and salinity are conservative properties of seawater, other variables are less predictable. The impacts of changing temperature, salinity, and DO on benthic nutrient fluxes as well as nutrient loading from sandy and muddy sediments in the IRL/BRL were investigated. Overall, pumping may result in a small decrease in lagoon temperature, an increase in salinity, and more stable DO.

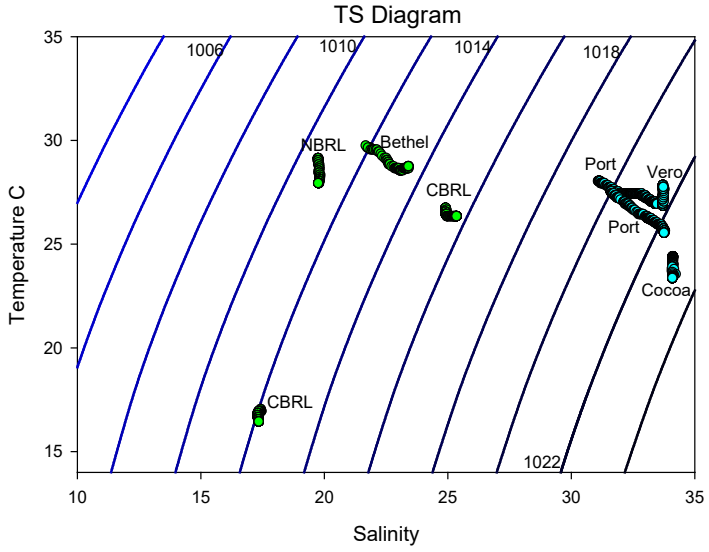

Figure ES-1. Temperature, salinity, and density for water samples obtained during this study.

Nutrient concentrations in the coastal Atlantic Ocean were relatively uniform both spatially and temporally with average concentrations of total dissolved nitrogen (TDN), total dissolved phosphorus (TDP) and silica (SiO_2) at 8.0 ± 2.4 micromoles per liter (µM), 0.15 ± 0.05 µM and 3.3 ± 0.7 µM, respectively. In Port Canaveral, nutrient concentrations averaged 24.4 ± 5.5 µM TDN, 0.44 ± 0.04 µM TDP, and 11 ± 2 µM SiO_2 and values varied between those identified for the coastal Atlantic Ocean and the IRL, consistent with trends identified for temperature and salinity. Nutrient concentrations in the lagoon were variable with large differences observed among samples from the open lagoon versus more restricted areas like Bethel Creek. Overall, lagoon samples averaged 62.8 ± 24.3 µM TDN, 1.41 ± 0.72 µM TDP, and 51 ± 28 µM SiO_2, 7.9-fold, 9.4-fold, and 15.5-fold higher than values for seawater. Samples from the open lagoon averaged 72.1 ± 23.3 µM TDN, 1.38 ± 0.52 µM TDP, and 40 ± 13 µM SiO_2, versus 44.1 ± 12.7 µM TDN, 1.45 ± 0.91 µM TDP, and 71 ± 37 µM SiO_2 for samples from Bethel Creek. Large differences in TDN and TDP among sampling locations were accompanied by variations in nutrient speciation. For example, phosphate (PO_4, soluble reactive phosphorus [SRP]) and dissolved organic phosphorus (DOP) accounted for 38% and 62% of the TDP at offshore sites, 54% and 46% in the open lagoon, 82% and 18% in Bethel Creek, and 85% and 15% in Port Canaveral (Figure ES-2). The difference in speciation influences bioavailability with implications to algal community composition. The speciation and relative abundance of bioavailable nitrogen (N):phosphorus (P):silicon (Si) can contribute to algal community composition and shifts in speciation and the relative abundance of N:P:Si can lead to shifts from less harmful photosynthesizers to harmful species or vice versa. Redfield's N:P ratio at 16:1 was used as a basis for evaluating N:P ratios; overall, dissolved inorganic nitrogen (DIN):SRP ratios varied among locations. At offshore sites, DIN:SRP averaged 20 which was 5-fold higher than the DIN:SRP ratio of the open lagoon (3.9) and 2.4-fold higher than the ratio in Bethel Creek (8.4). In both the ocean and lagoon, TDN:TDP ratios were greater than ratios of DIN:SRP and TDN:TDP ratios were above the Redfield value at 16. Overall the highest TDN:TDP ratios were identified at northern sites in the IRL, consistent data from previous investigations and with data showing that *Aureoumbra lagunensis*, one of the dominant bloom species found throughout the northern IRL and BRL, prefers high TDN:TDP.

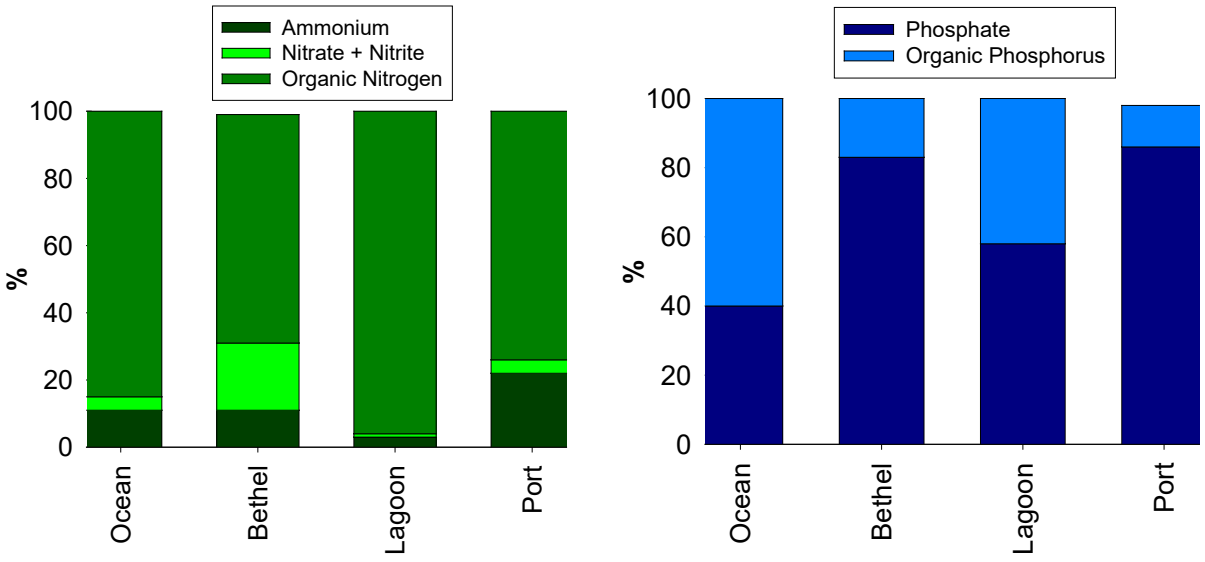

Figure ES-2. Stacked bar graphs showing (a) the percent ammonium, percent nitrate + nitrite, and percent organic nitrogen; and (b) the percent PO_4 and percent organic phosphorus in the water column.

Based on nutrient concentrations in the IRL, in the coastal Atlantic Ocean and in Port Canaveral, the quantity of nutrients that would be discharged from the lagoon and brought into the lagoon via inflow were calculated (Table ES-1 and Table ES-2). At a pumping rate of 5 cubic meters per second (m^3/sec) at the central or southern sites, it is expected that 1.6 x 10^{11} liters (L) of lagoon water would be discharged through inlets per year (Table ES-1 and Table ES-2). Using these data, annual discharges of nutrients through inlets to the coastal Atlantic Ocean associated with possible pumping (5 m^3/sec) were calculated at approximately 70 metric tons of N and 7 to 11 metric tons of P per year. At Sebastian Inlet, ammonium (NH_4), nitrate + nitrite (NO_x), and dissolved organic nitrogen (DON) would account for approximately 4%, 2%, and 94% of the TDN, compared to approximately 9%, 5%, and 86%, respectively, at Fort Pierce Inlet. Based on data collected during this study, molar ratios of DIN:SRP and TDN:TDP discharged from the lagoon would differ depending on where discharges occurred. If discharges occurred through Sebastian Inlet, DIN:SRP and TDN:TDP would be 4.8 and 22 relative to 3.8 and 14 if discharges were to occur through Vero Beach Inlet. Lower N:P values for discharged lagoon water compared to inflow water into the lagoon could promote a shift towards higher N:P ratios throughout the lagoon. Overall, the net change in nutrients quantities linked with pumping water from offshore (5 m^3/sec) into the lagoon and associated discharges were calculated at (out-in): approximately 50 tons N/year and between 6 and 10 metric tons P/year. If inflow were to occur via a weir structure at 7–20 m^3/sec, approximately 95 to 270 metric tons of N and approximately 9 to 27 metric tons of P would be discharged from inlets per year with net removal of 19 to 54 tons of N/year and 7 to 22 tons of P/year.

Table ES-1. Tons of N and P that would be discharged to the coastal ocean per year from Sebastian Inlet, associated with various levels of inflow.

Pumping Rate	L/day	L/year	NH_4 (tons/yr)	NOx (tons/yr)	DIN (tons/yr)	Organic N (Org-N (tons/yr)	TDN (tons/yr)	PO_4 (tons/yr)	TDP (tons/yr)	DOP (tons/yr)
2.5 m^3/sec	$2.2*10^8$	$7.9*10^{10}$	1.5	0.63	2.2	31	34	1.0	3.3	2.2
5 m^3/sec	$4.3*10^8$	$1.6*10^{11}$	3.0	1.3	4.5	64	68	2.1	6.7	4.5
10 m^3/sec	$8.6*10^8$	$3.2*10^{11}$	6.1	2.6	9.0	130	140	4.2	13	9.0
15 m^3/sec	$1.3*10^9$	$4.7*10^{11}$	8.9	3.8	13	190	200	6.1	20	13
20 m^3/sec	$1.7*10^9$	$6.3*10^{11}$	12	5.0	18	250	270	8.2	27	18

Table ES-2. Tons of N and P that would be discharged to the coastal ocean per year from Fort Pierce Inlet, associated with various levels of inflow.

Pumping Rate	L/day	L/year	NH_4 (tons/yr)	NOx (tons/yr)	DIN (tons/yr)	Org-N (tons/yr)	TDN (tons/yr)	PO_4 (tons/yr)	TDP (tons/yr)	DOP (tons/yr)
2.5 m^3/sec	$2.2*10^8$	$7.9*10^{10}$	2.9	1.7	4.7	29	33	2.7	5.3	2.6
5 m^3/sec	$4.3*10^8$	$1.6*10^{11}$	5.9	3.5	9.4	58	68	5.4	11	5.3
10 m^3/sec	$8.6*10^8$	$3.2*10^{11}$	11.8	7.0	19	120	140	11	21	11
15 m^3/sec	$1.3*10^9$	$4.7*10^{11}$	17.4	10	28	170	200	16	32	16
20 m^3/sec	$1.7*10^9$	$6.3*10^{11}$	23.3	14	37	230	270	21	42	21

No significant trends were identified for benthic nutrient fluxes versus the composition of sandy sediments (e.g., sediment water and organic matter [OM] content); this was likely at least partially due to groundwater seepage into the lagoon through sandy sediments. Based on data from this study, it is likely that most benthic chambers were influenced by groundwater seepage with estimated rates ranging from less than 1 up to about 30 cm/day for sites in this study that were within approximately 10 m of the shoreline. If this effort were to continue preliminary data showing north-south trends for nutrient fluxes would be pursued.

Median ± standard error (SE) sediment oxygen demands (SOD) for sandy sediments were -3,200 ± 900 micromoles of oxygen per square meter per hour (µmol O_2/m^2/hr), while SOD of muddy sediments was higher at -4,300 ± 2500 µmol O_2/m^2/hr (Table ES-3). At sandy sites, DIN was released from sediments primarily as NO_x while NH_4^+ accounted for approximately 40% of the DIN flux at 90 ± 60 µmol/m^2/hr (Table ES-3). Median TDN fluxes were 290 ± 430 µmol/m^2/hr at sandy sites. At muddy sites, fluxes of NO_x were directed from the water into sediments (-180 ± 200 µmol/m^2/hr; -22 tons/square kilometer (km^2)/year) and releases of DIN from muddy sediments were 100% NH_4^+ at a median of 580 ± 460 µmol/m^2/hr (Table ES-3). The median PO_4 flux from sandy sites was 4.1 ± 8.1 µmol/m^2/hr. The wide range of values was not unexpected because PO_4 fluxes vary as a result of bacterial decomposition and concentration gradients as well as fluctuating redox conditions experienced by surface sediments. Overall, DOP flux was directed into sandy sediments at -4.7 ± 4.9 µmol/m^2/hr with TDP fluxes directed into sandy sediments from overlying water at -0.6 µmol/m^2/hr (Table ES-3). In contrast, PO_4 fluxes from muddy sediments were 34 ± 18 µmol/m^2/hr and fluxes of DOP were directed out of sediments at 13 ± 26 µmol/m^2/hr (Table ES-3).

Table ES-3. Median ± SE for benthic fluxes from sandy and muddy sediments in µmoles/m^2/hour (2019–2020)

Sediment	Oxygen	NH_4	NOx	DIN	PO_4	TP	DOP
Sand	-3,200 ± 900	90 ± 60	150 ± 150	260 ± 170	4.1 ± 8.1	-0.6	-4.7 ± 4.9
Muck (winter)	-4,300 ± 2500	580 ± 460	-180 ± 200	400	34 ± 18	47	13 ± 26

Ratios of oxygen (O):N have been used in other studies to help describe processes occurring in the sediments. Median O:NH_4 for sandy sediments was 21.4 ± 34.2 versus 6.9 ± 6.8 for muddy sediments, suggesting that coupled nitrification-denitrification may occur in sandy sediment (Nixon 1981) and also that different oxidizing agents are likely being consumed in muddy sediments. These data are consistent with results from this study showing NOx fluxes directed into muddy sediments. In both mud and sand wide range of N:P flux ratios, were likely related to seasonal variations in temperature and DO with the lowest ratios identified for anaerobic muddy sediments.

The theoretical amount of time required for a nutrient in the water column to be either re-generated or consumed (turnover times) were estimated using benthic nutrient and O fluxes coupled with existing nutrient concentrations in the IRL. Based on benthic fluxes alone, residence times were calculated for an average lagoon depth of 1.5 m. In sandy sediments, the residence time for ammonium ranged from 22 to 43 hours based on 5-year average ammonium concentrations at Sebastian Inlet and Vero Beach (Table ES-4). NO_x fluxes from sandy sediments were higher than NH_4 fluxes and concentrations in lagoon water were lower yielding turnover times ranging from about 6 to 15 hours (Table ES-4). Together, DIN fluxes could replace all dissolved nitrogen in the water column (TDN) in 190 hours or approximately 8 days. In muddy sediments, the turnover time for NH_4^+ and NO_x from muck were 4–7 hours and 5–13 hours (NOx into sediments), respectively (Table ES-4). Based on data collected during this study, NH_4^+ fluxes could replace all the dissolved N in the water column overlying muck in approximately 80 hours or 3.3 days (Table ES-4). Residence times for PO_4 from sandy sediments varied from 160–410 hours compared to 18–48 hours for areas with muddy sediments (Table ES-4). In sandy sediments, it would take 500–800 hours for sediments to cycle the complete pool of dissolved phosphorus versus 59–95 hours for muddy sediments. Turnover times for DO were variable due to variations in solubility associated with the annual range of lagoon temperatures. Based on water at 20 PSU salinity and 25˚C, the solubility of DO is 7.4 milligrams per liter (mg/L). Based on this value, turnover times using SOD alone ranged from 110 hours for sandy sites to 80 hours for muddy sites (Table ES-4). If coupled with water column respiration, the turnover times were on the order of 30 hours; these short turnover times are relatively consistent with observed nighttime (dark) decrease in DO throughout the lagoon. Based on some simple calculations for the study, SOD accounted for 25% and a minimum of 31% of the total O demand for areas containing sand and muck, respectively. Such short residence times demonstrate the tight benthic-pelagic coupling in this system and suggest that sediments play in important role in sustaining nutrient concentrations in overlying water even when external loading varies, for example during the dry versus wet seasons.

Table ES-4. Turnover times in hours calculated using benthic fluxes, nutrient concentration in the water column, and an average depth of 1.5 m.

Sediment	Oxygen (hours)	NH_4 (hours)	NOx (hours)	DIN to replace TDN (hours)	PO_4 (hours)
Sand	110	22 to 43	6 to 15	190	160 to 410
Muck (winter)	80	4 to 7	5 to 13	80	18 to 48

To addresses potential changes to benthic fluxes that could result from proposed inflow, laboratory incubation experiments were carried out to simulate changes in lagoon temperature, salinity, and DO. These experiments investigated fluxes from sandy sediments at temperatures ranging from 13˚C–32˚C, salinities ranging from 0–34 PSU, and DO ranging from 0% (0 mg/L) to 100% (approximately 8 mg/L). Overall, the lowest SODs were at 13˚C and 15˚C and the highest fluxes were at 22˚C (Figure ES-3). Above 22˚C, SOD decreased as temperature increased

towards 32˚C. Based on this preliminary dataset, no consistent temperature-related trends were identified for nitrogen fluxes; however, as expected, NH_4^+ and other fluxes followed patterns for SOD.

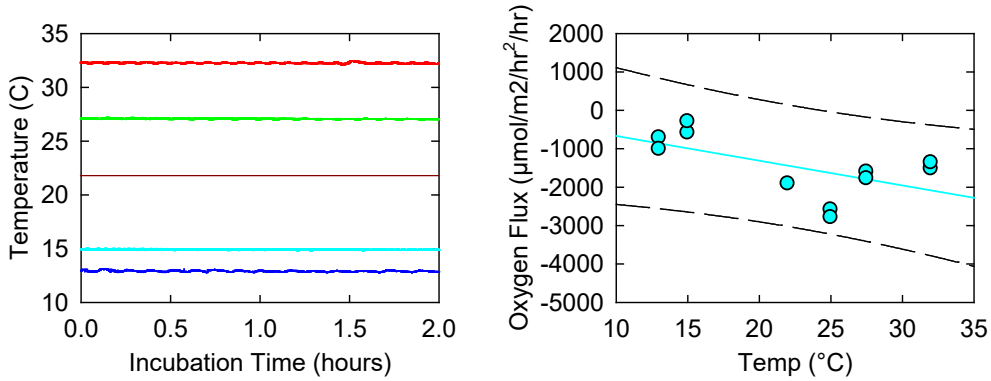

Figure ES-3. Data from laboratory experiments showing (a) laboratory-controlled sediment temperature over time and (b) oxygen flux (SOD) versus sediment temperature.

Fluxes of dissolved PO_4 were positively correlated with temperature (PO_4 flux [µmol/m^2/hr] = 0.58 * [˚C] – 7.6, p = 0.04, r = 0.63) and increased from near 0 µmol/m^2/hr at 13˚C to 5–10 µmol/m^2/hr at 32˚C. There was no significant correlation identified for DOP, TDP, and SiO_2 fluxes versus temperature. There was also no significant trend for the molar N:P ratio, but a positive correlation between PO_4 and temperature and no trend for N suggests that the N:P ratio may respond to changes in lagoon temperature. Based on these data, a 1˚C decrease in lagoon temperature would decrease PO_4 fluxes from sandy sediments by approximately 0.16 tons/km^2/year. When this small change in PO_4 flux is extrapolated to the entire surface area of sand in the IRL, this equates to 10s of tons per year less PO_4 entering the system as temperature decreases. Overall, there was no significant correlation identified between SOD and the salinity of overlying water. In contrast, all N species did show lower fluxes at higher salinities, with significant correlations identified for NO_x flux (µmol/m^2/hr) = -4.7 * [PSU] + 180) with a decrease in NO_x flux of 4.7 µmol/m^2/hr (~0.6 tons/km^2/hr) per PSU from a median of 150 µmol/m^2/hr (20 tons N/km^2/year) for sandy sites in the lagoon (Figure ES-4). There was no significant trend identified for fluxes of P and SiO_2, likely due to low sample size obtained during this first year of study. Nevertheless, P and Si fluxes followed patterns similar to N with a general trend of lower fluxes at higher salinities. With increasing salinity, both DIN and SRP fluxes decreased. In general, the observations from this study are likely the result of changes to diffusion coefficients and sorption, desorption reactions versus changes to bacterial metabolism (i.e., no correlations with SOD).

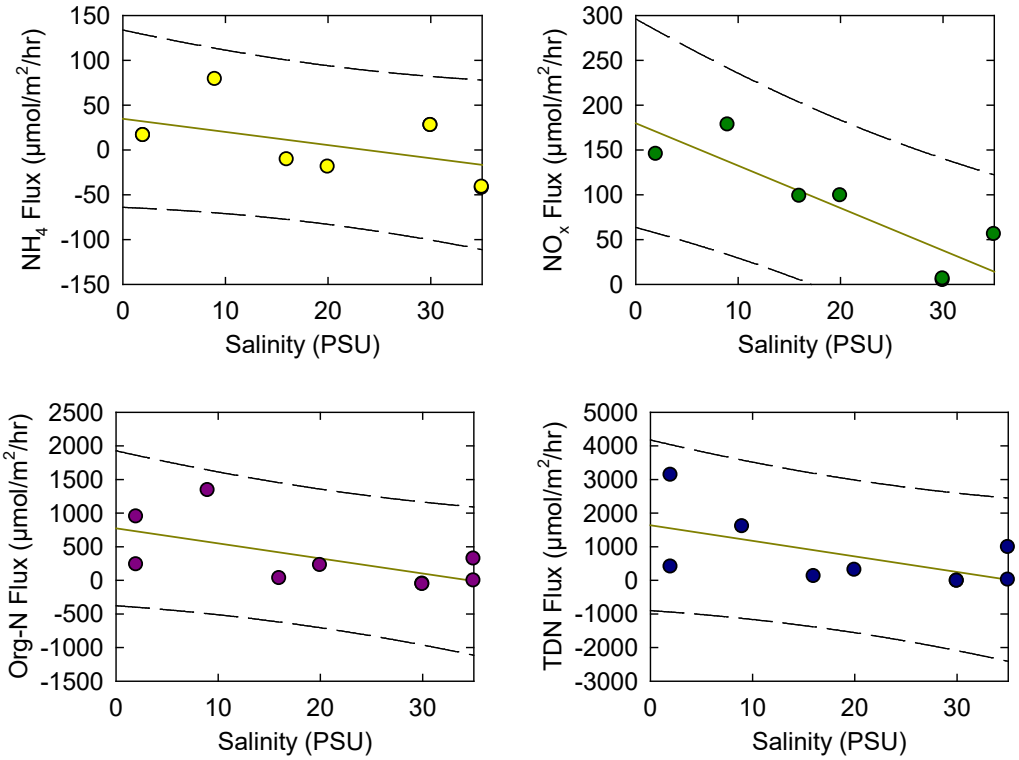

Figure ES-4. Results from laboratory incubation experiments showing fluxes in µmoles/m2/hour versus the salinity of overlying water for (a) NH4, (b) NOx, (c) Org-N and (d) TDN.

In the laboratory incubations where DO concentrations were manipulated, a significant positive correlation was identified between NH_4 fluxes and bottom water DO (NH_4 flux [µmol/m^2/hr] = 3.1 * DO [mg/L] + -0.22; p = 0.02, r = 0.64) but no significant correlations were observed for other N species. No significant correlations were identified for P fluxes versus bottom water DO, but in anaerobic (0% DO) conditions, PO_4 fluxes were always directed out of sediments. A significant negative correlation was identified between SiO_2 fluxes and bottom water DO (SiO_2 flux [µmol/m^2/hr] = -19 * DO [mg/L] + -27; p = 0.02, r = 0.65). It is difficult to extrapolate these data to approximate the potential impacts of inflow based on the complex biogeochemical responses to hypoxia.

DO concentrations in surface water from the IRL displayed annual trends consistent with variations in solubility. For instance, at a salinity of 25, DO solubility increases from 6.4 mg/L at 32°C to 8.7 mg/L at 15°C, an annual range of 2.3 mg/L. To complement this study, DO sensors were deployed in bottom water near existing sensors located between approximately 0.5 and 1.0 m. Overall, DO in bottom water at sandy sites tracked values for surface water but, in some cases, DO was much lower near the bottom within 30 cm of the sediment-water interface (Figure ES-5). Near the potential central BRL pumping location, distinct differences in DO were observed for bottom water overlying mud (muck) versus sand, consistent with differences in SOD among substrates (-3,200 µmol/m2/hr for sandy sites and -4,300 µmol/m^2/hr for muddy sites in winter months). Bottom water in deeper sites overlying muddy sediments also experiences extended periods of anoxia, likely due to poor water circulation in deep areas that develop in layers of high-density water that can becomes stagnant. Data obtained during this study begin to establish a

baseline for monitoring conditions near the sediment-water interface and will help modelers to better predict water quality throughout the lagoon.

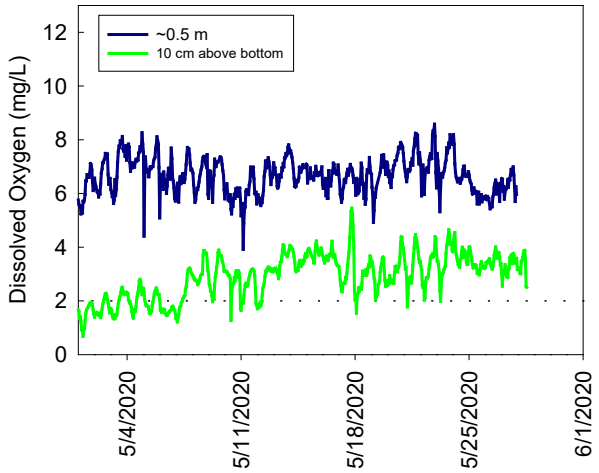

Figure ES-5. DO concentrations in bottom water (green line) and near the surface (blue line) in the IRL near the Eau Gallie Causeway during April 2020. Surface (~0.5 m) data obtained from SJRWMD.

Inflow of seawater to the IRL system would promote net discharges of nutrients to the coastal ocean. Based on calculations from this study, direct exchanges would likely remove (net = out-in) between 19 and 54 tons of N and between 6 and 22 tons of P per year from the lagoon. Inflow would likely lead to lower summertime lagoon temperatures and higher lagoon salinities. The extent to which temperature and salinity would be altered by enhanced inflow is discussed in the corresponding modeling effort of this final report. Preliminary data from this geochemical investigation show that lower temperatures and higher salinities would likely promote lower benthic fluxes for some nutrients into the IRL. If this study were to continue, more robust datasets are expected to provide better estimates and more powerful interpretations that will assist future modeling efforts. Nevertheless, data from this investigation suggest that geochemical responses to inflow would likely enhance any benefits from direct exchanges of water. Even small changes to benthic fluxes are of major significance when applied to the large surface area of the IRL, potentially decreasing nutrient inputs by tens of tons per year.

1 Introduction

1.1 Background

Globally, eutrophication of coastal marine ecosystems has become increasingly common due to enhanced nutrient loading from adjacent watersheds (Brady et al. 2013, Diaz and Rosenberg 2008). As the eutrophic state progresses, sediment mineralization becomes an increasingly important source of nutrients and can sustain eutrophication through the dry season as well as destabilize the trophic state of an estuary (Cowan and Boynton 1996, DiDonato et al. 2006, Seitzinger 1988, Kemp et al. 1990). Extended periods of eutrophication can lead to a shift from seagrass-dominated ecosystems to degraded, algae-dominated systems (DiDonato et al. 2006). During recent decades and associated with eutrophication, catastrophic losses of seagrass beds have been reported worldwide (Burkholder et al. 2007). Co-occurring with seagrass losses are more frequent harmful algal blooms and occurrences of hypoxia and anoxia (Tetra Tech 2020). Even short hypoxic or anoxic events can decrease macrofaunal abundance and promote loss of ecosystem services including bioturbation that helps to maintain oxic surface sediments. Loss of ecosystem services can lead to an increasingly anoxic sedimentary environment with implications to mineralization of organic matter and nutrients and geochemical nutrient cycling (Pelegri et al. 1994, Foster and Fulweiler 2019, Seitzinger 1991, Kemp et al. 2009). These changes not only influence nutrient concentrations, but also the relative abundance of nutrients that can promote a shift in algal community composition (Harris 1986).

Shifts in the relative abundances of nitrogen (N), phosphorus (P), and silica (SiO_2) are known to greatly influence phytoplankton communities and harmful algal blooms can be promoted under silicon (Si) and P limitation (Harris 1986). For example, the brown tide species *Aureoumbra lagunensis* responsible for the 2016 and 2018 harmful algal blooms and the toxin-producing *Pyrodinium bahamense* thrive at high N:P ratios (Liu et al. 2001, Azanza et al. 2004). Previous studies have demonstrated that as estuarine sediments become impaired, denitrification can be hindered due to low nitrate availability promoting a shift towards higher N:P ratios (e.g., Cowan and Boynton 1996).

A distinct difference in the ability to cope with eutrophication has been observed among estuaries with varying geomorphologies and residence times or flushing times for water (Twilley et al. 1999, Defne and Ganju 2015). Poorly flushed estuaries with long residence times, like the Indian River Lagoon (IRL), more readily retain nutrients to promote algal blooms, loss of seagrass beds, hypoxia, and loss of ecosystem services (Defne and Ganju 2015, Kemp et al. 1992; Twilley et al. 1999). Conversely, well-flushed estuaries with shorter residence times have greater resilience to the impacts of eutrophication (Defne and Ganju 2015). Historically, estuarine flushing has been controlled by fluvial discharge, tides, wind mixing, geomorphology of the estuary, as well as other forcing over longer timescales (Defne and Ganju 2015, Csanady 1978; Jassby and Van Nieuwenhuyse 2005).

The processes responsible for exchanges of water in estuaries can influence stratification with implications to nutrient cycling and ultimately the degree to which circulation can mitigate the impacts of eutrophication (Defne and Ganju 2015). For example, freshwater discharges can promote stratification that circulate water; however, geochemical processes occurring at the sediment-water interface can promote continued eutrophication and hypoxia or anoxia in a layer of bottom water (Jassby and Van Nieuwenhuyse 2005). In shallow estuaries, the impacts of stratification are often overcome by wave-induced circulation (Csanady 1978). Nevertheless, stratification that may result from additions of water can have important implications to nutrient cycling. In contrast to unidirectional fluvial discharges, bidirectional tidal forcing near inlets has

been shown to mix water throughout the water column; however, despite mixing, tidal exchanges are typically limited in spatial extent (Defne and Ganju 2015).

Enhanced circulation in the IRL may contribute towards lowering nutrient concentrations that support the onset and proliferation of algal blooms. Another potential benefit may be to increase the concentration of dissolved oxygen (DO) yielding enhanced resilience to anoxia and fish kills. The main benefits of decreased nutrient concentrations and possibly increased DO would likely result from changes to geochemical cycling, with spatially limited impacts from direct dilution by seawater. The objectives of this effort were to determine potential impacts to water quality that could result from: (1) direct dilution by seawater, plus changes to the residence time for water in the lagoon; and (2) changes in geochemical cycling that result from changes to temperature, salinity, and DO that could occur due to various levels of proposed pumping. Water quality sensors were used to determine the homogeneity of bottom water conditions both temporally and spatially over a variety of sediment types. In addition to contributing towards establishing a "baseline," this study will determine if data from existing water quality sensors can be extrapolated to determine bottom water conditions near proposed pumping locations. Data from this investigation will be available to modelers to better predict changes to nutrient and DO concentrations and ratios could changes under various pumping scenarios.

1.2 Study Area

The IRL is a shallow (less than 5 meter [m]) bar-built, lagoon-type estuary that extends 250 kilometers (km) along the central east coast of subtropical Florida and ranges in width from less than 1 to approximately 9 km (Sigua et al. 2000, Figure 1-1). In the past decade, water quality in the IRL has declined with more severe and more frequent harmful algal blooms (IRL coalition; Tetra Tech 2020). The IRL is poorly flushed with 140 km between the Sebastian and Ponce de Leon inlets. The northern portion of the IRL is microtidal and tidal flushing is negligible (Smith 1993) where tides are of only minor significance toward flushing (Smith 1993). Based on rainfall and low-frequency coastal water level variations, the 50% renewal time for water in the northern and central IRL sections ranges from approximately 100–300 days (Smith 1993).

This study was carried out to evaluate possible impacts of enhanced circulation in the IRL with an emphasis at three primary locations: (1) the North Banana River (centered near 28.4071, -80.6412), (2) the Central Banana River (centered near 28.2722, -80.6104), and (3) near Bethel Creek (centered near 27.6656, -80.3702) (Figure 1-1 and Figure 1-2). Sampling sites inside the IRL and Banana River Lagoon (BRL) were selected using a stratified, random approach to ensure that data are scientifically and statistically sound and can be extrapolated to a larger area (e.g., White et al. 1992). Sampling locations in the ocean are located along 10-m isobaths found approximately 1 to 2 km offshore from the mean water line. Additional seawater samples were also collected from within Port Canaveral.

Figure 1-1. Map of the study area showing the three potential pumping locations from north to south: North Banana River, Central Banana River, and Bethel Creek. Red circles show a 1 km radius around the proposed pumping location.

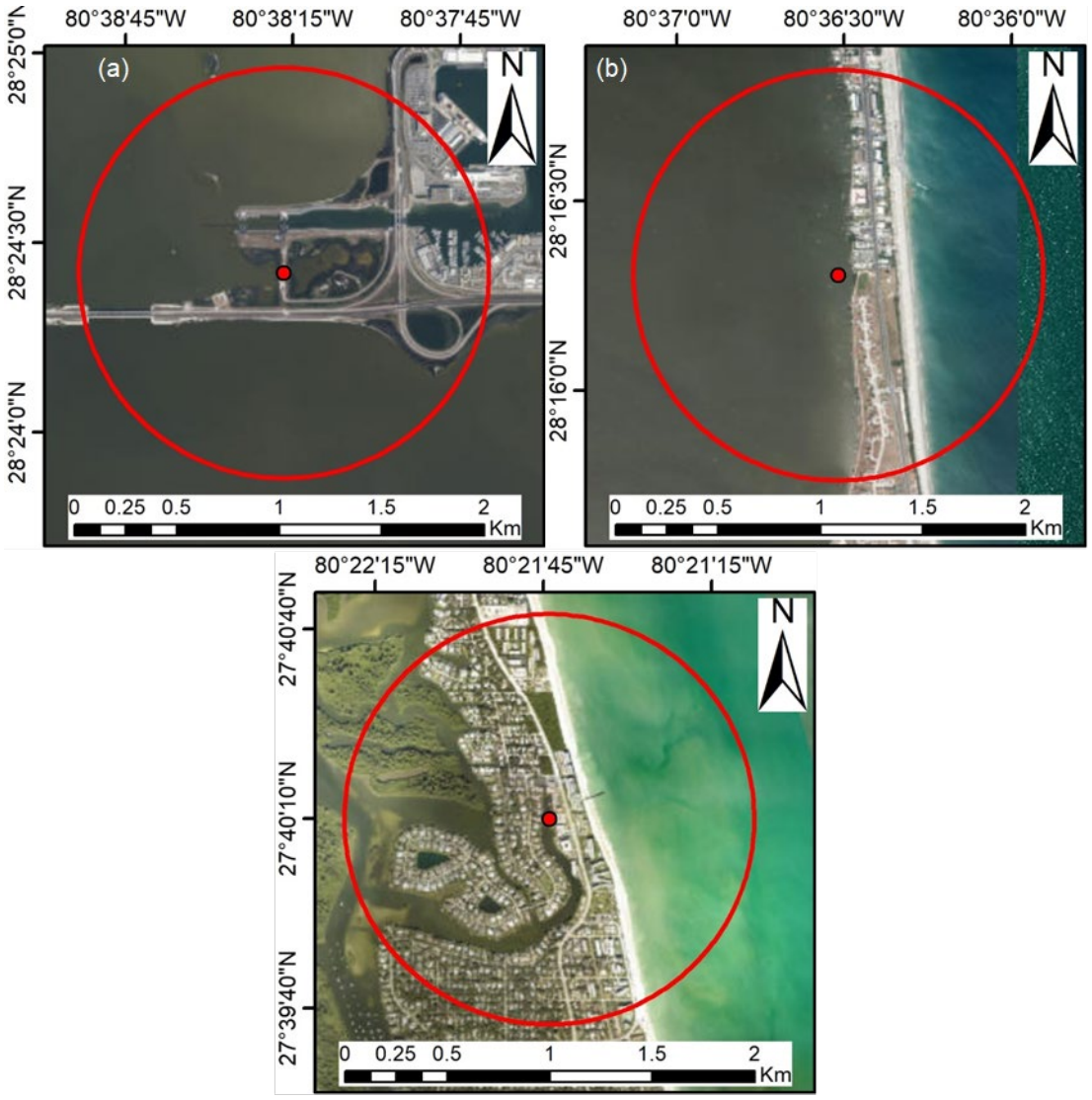

Figure 1-2. Inflow locations 1-3, (a) Central Banana River Lagoon, (b) North Banana River Lagoon, and (c) Bethel Creek. Red circles show a 1-km radius around each potential pumping location.

1.3 Objectives

The objectives of this geochemical evaluation were as follows:

- Calculate impacts of pumping, based on direct dilution by seawater, on concentrations of nutrients in the lagoon, plus calculate the quantity of nutrients that could be discharged into the coastal ocean.
- Determine if data from few existing water quality sensors (approximately 0.5–1.0 m) can be extrapolated to determine conditions in bottom water near proposed pumping locations.
- Determine how changes to temperature, salinity, and DO that could result from various levels of pumping would influence the geochemical cycling of N, P, oxygen (O), plus sulfate and sulfide in the lagoon.

2 Methods

2.1 Field Sampling

2.1.1 Water Sampling

Continuous vertical profiles for salinity, temperature, pH, oxidation reduction potential (ORP) and DO were obtained using a YSI ProDSS (Yellow Springs Instruments). The sonde was calibrated prior to each sampling event following the manufacturer's guidelines. Discrete water samples were collected using a 1.7 liter (L) horizontal Niskin water sampler (General Oceanics) that was tripped at targeted depths using a weighted messenger (Figure 2-1). Water samples were filtered immediately after collection using Whatman 0.45 micrometer (µm) polypropylene syringe filters. Additional unfiltered samples were collected for processing in the laboratory. All water samples were transported to the laboratory in a cooler on ice in the dark.

Figure 2-1. Dr. Fox (left) and a student collect water samples in the IRL using a 1.7L horizontal Niskin bottle.

2.1.2 Sediment Sampling

Sediment samples were obtained using a 0.1 square meter (m^2) Ekman Grab that was lowered slowly from an anchored boat until it hit the bottom. This process has been observed by Self-Contained Underwater Breathing Apparatus (SCUBA) to verify collection of 10–15 centimeters (cm) of stratified sediment and overlying water (Figure 2-2). Any standing water was siphoned off prior to sample collection. An approximately 3 cm layer of surface sediments was subsampled from the grab using a clean spoon and placed in an approximately 55 milliliter (mL) polycarbonate vial that was then sealed with parafilm.

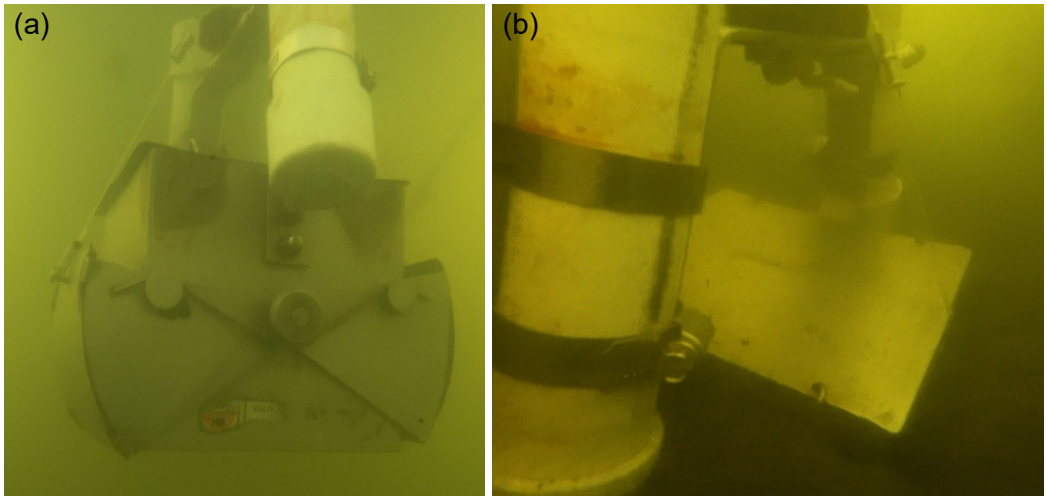

Figure 2-2. Ekman Grab photographed by scientist with SCUBA (a) descending through the water column and (b) settled in sediments with no visible disturbance to the sample.

2.1.3 Water Column Respiration, Sediment Oxygen Demand (SOD), and Nutrient Fluxes

Darkened, benthic (sediment) and "blank" chambers were used to determine fluxes of DO (SOD) and nutrients from sediments and from suspended particles (water column respiration). Methods used in this study were developed following guidelines in a synthesis of techniques by Boynton et al. (2018). Blank chambers containing HOBO U26 DO data loggers and mechanical stirrers were rinsed and then completely filled with bottom water (Figure 2-3a). Water samples were obtained and immediately filtered through Whatman 0.45 µm polypropylene syringe filters and stored on ice until return to the laboratory. The volume of water removed for samples was replaced with bottom water and chambers containing no air were sealed and incubated for 1.5 to 2 hours. Chambers were kept in the shade at a constant in-situ temperature for the duration of the incubation. Following the incubation period, chambers were opened, and a final water sample was extracted and immediately filtered and placed on ice for transport to the laboratory.

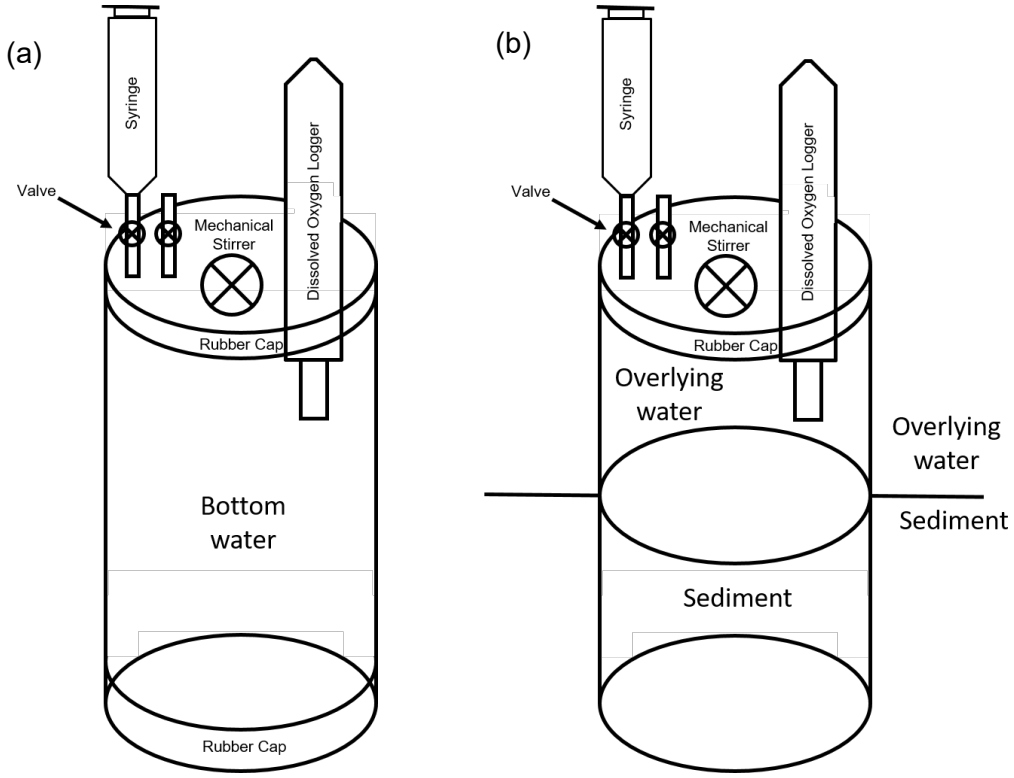

Figure 2-3. Schematic diagram of the (a) blank and (b) benthic chambers used to determine water column respiration, SOD, and nutrient fluxes. Chambers are darkened to prevent photosynthesis.

Benthic chambers were pushed vertically into sediments without side to side movement to avoid creating channels that would allow water exchanges. Chambers were pushed at least 10 cm into the sediments to prevent burrowing organisms from creating channels that would allow exchange of water with the outside environment. The height of each chamber was recorded to calculate the total volume of water in each chamber (e.g., Boynton et al. 2018). Once inserted, chambers were left open to the water column for 2–5 minutes to allow particles and sediments to settle and allow water to be exchanged with undisturbed bottom water. Before sealing each chamber, water samples were obtained from inside the chamber and immediately filtered using Whatman 0.45 µm polypropylene syringe filters. Chambers were then sealed with lids containing mechanical stirrers to keep the water well-mixed and to prevent buildup of a concentration gradient in a boundary layer at the sediment-water interface. Stirrers were designed and deployed to mix the overlying water without causing sediment resuspension. HOBO U26 DO data loggers were mounted through an airtight seal in the lid of each chamber (Figure 2-3b). The rate of decline of the DO within the chamber was then measured over a 1.5- to 2-hour period for sand and for 20 to 45 minutes for mud. At the end of each deployment, a syringe was attached to a valve on the top of the chamber and a 60 mL water sample for nutrient analysis was extracted and immediately filtered and stored on ice (Figure 2-4). At the end of each deployment, a sediment sample was obtained from inside the sediment chamber and placed in a polycarbonate vial (about 55 mL) for sediment analysis. At least 2 L of unfiltered bottom water was also collected for determination of turbidity and chlorophyll *a*.

Figure 2-4. Collecting water samples from a benthic chamber deployed in shallow water.

Sediment cores for laboratory incubation experiments were obtained by carefully pushing core barrels vertically into the sediments to avoid creating channels or resuspending/disturbing sediments. Cores were then capped to create a vacuum, extracted from the sediment, and a synthetic rubber stopper was immediately placed in the bottom of the core (Figure 2-5). Still underwater, caps were removed to prevent buildup of pressure as the synthetic rubber stopper was inserted fully. In addition to synthetic rubber stoppers, expansion plugs were inserted and expanded to prevent leaks. Caps were then replaced and the entire core, with no air, was placed in a cooler and transported to the laboratory. If any disturbance was noted throughout the collection process, the core was discarded, and a new core was obtained. Large (at least 2 L) unfiltered water samples were collected for replacement of the overlying water at the beginning of laboratory incubation experiments.

Figure 2-5. A student collects a sandy sediment core from shallow water for laboratory incubation (left). Dr. Austin Fox returns a sediment core from deeper water using SCUBA (right).

In March 2020, benthic chambers were retrofitted with collapsible external bladders to measure groundwater seepage into the IRL (Figure 2-6; e.g., Martin et al. 2007). Bladders from the mini-seepage meters were completely empty at the start of each deployment. At the end of each deployment, bladders were recovered and the volume of water was recorded. Seepage was calculated by dividing the volume of water in the bladder (mL = cubic cm) by the surface area of sediments in the chamber (square cm) by the length of deployment (days = hours/24) to yield seepage in cm/day, a unit consistent with values in the literature (e.g., Martin et al. 2007, Pandit et al. 2017).

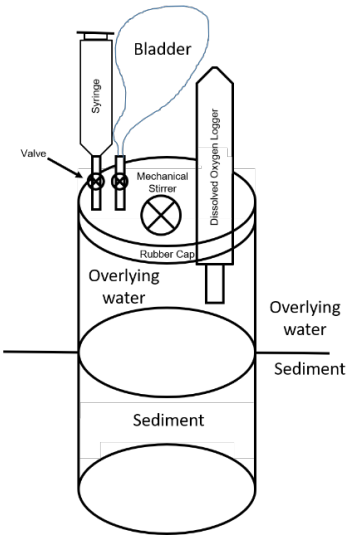

Figure 2-6. Schematic diagram of a benthic chamber modified to measure seepage.

2.2 Laboratory Analyses

2.2.1 Nutrient and Water Analyses

Concentrations of ammonium (NH_4), nitrate + nitrite (NOx), total dissolved nitrogen (TDN), ortho-phosphate (PO_4), total dissolved phosphorus (TDP), and SiO_2 were determined using a SEAL AA3 HR Continuous Segmented Flow Autoanalyzer following manufacturer's methods. The NIST-traceable Dionex 5-Anion Standard was analyzed as a reference standard with each batch of samples to ensure accuracy. Values are consistently within the 95% confidence interval for the prepared standard. Analytical precision (relative standard deviation) for lab duplicates was less than 3% for nutrient analyses.

pH was determined using Hach Sension1 pH meter and an Oakton field probe. The apparatus was calibrated using a 3-point calibration immediately prior to use. Initial calibration verification was checked using a pH 7 buffer and was always better than 1%.

Turbidity was determined on unfiltered samples using a Hach 2100 turbidimeter. The turbidimeter was calibrated prior to each use and checked periodically throughout the analyses.

Concentrations of chlorophyll *a* were determined by vacuum filtering approximately 50 mL of homogenized water through pre-combusted Whatman 0.7 µm pore size glass fiber filters. Filters were folded and placed in polypropylene centrifuge tubes and frozen overnight to lyse cell walls. Chlorophyll *a* was extracted from filters by placing them in a 90% acetone solution at 4 °C in the dark for at least 24 hours. Extracted chlorophyll *a* was analyzed using a Turner Designs 10-AU fluorometer (Turner Designs, San Jose, California) following methods by Welschmeyer (1994). The fluorometer was initially calibrated using a chlorophyll standard (Turner designs Part No. 10–850) and during sampling using a solid secondary standard (Turner Designs Part No. 10-AU-904).

Concentrations of chloride, sulfate and alkalinity were determined using a SEAL AQ400 discrete auto analyzer following manufacturer's methods.

2.2.2 Laboratory Incubation Experiments

Laboratory incubations were carried out in a manner consistent with previous studies (e.g., Cowan et al. 1996, Hammond et al. 2004, Boynton et al. 2018). Intact sediment cores were placed in temperature-controlled recirculating water baths set to approximate in-situ conditions (Figure 2-7). Incubations were set up by first removing caps used to transport cores and overlying water was siphoned off, leaving about 1 cm of overlying water to prevent disturbance of the sediment-water interface. Bottom water collected from the field site was then slowly pumped into the chamber using a floating diffuser to prevent disturbance of the sediment-water interface. Water was replaced before each incubation to ensure that water quality conditions at the start of the incubation were as close to in-situ conditions as possible and to remove any nutrient accumulation that had occurred between collection of each core and the beginning of the incubation. At the beginning of each incubation, water samples (T_0) were collected from each core. Water samples were immediately filtered using Whatman 0.45 µm polypropylene syringe filters and stored in a refrigerator until analysis. The volume of water removed for the initial sample was displaced by the HOBO U26 DO data logger and the mechanical stirrer that was attached to the lid. For laboratory incubations where salinity or temperature were manipulated, valves on each lid were open when the incubation cap was placed on the chamber to allow any air and excess water to leave the chamber. Chambers containing no air were then sealed and incubated for 1.5 to 2 hours. For experiments where DO was manipulated, mixed gases, air, and nitrogen (N_2) were bubbled into each chamber to maintain constant DO concentrations and valves in each lid were left open

to allow gases to escape. Following each incubation, chambers were opened and a final water sample (T_f) was extracted, immediately filtered and stored in the refrigerator at 4˚C until analysis.

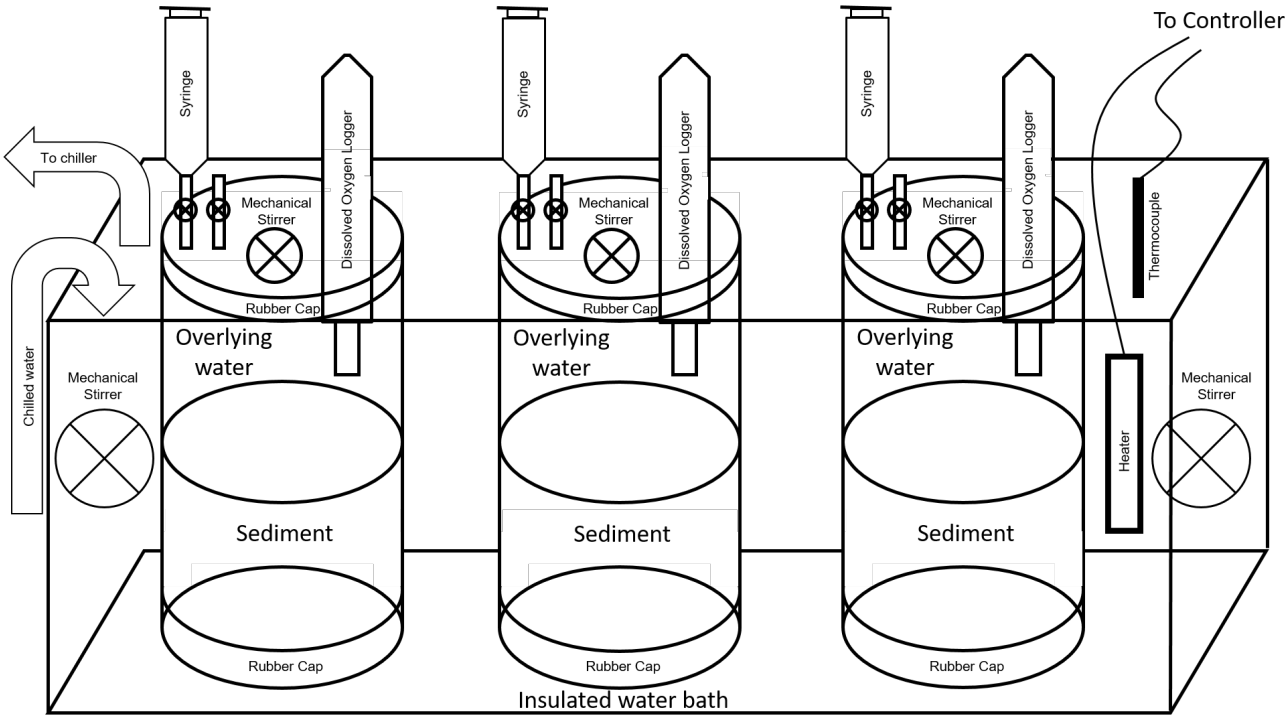

Figure 2-7. Schematic diagram of triplicate laboratory incubation chambers in an insulated, recirculating, temperature-controlled water bath.

2.2.3 Sediment Analyses

All sediment samples were weighed, freeze dried using a Labconco FreeZone 6 system, and reweighed to determine water content. Freeze dried samples were then powdered using a SPEX Model 8000 Mixer/Mill. Loss on Ignition (LOI) at 550˚C is determined following the method of Heiri et al. (2001). Values for LOI estimate the fraction of organic matter (OM) in the sample. Concentrations of calcium carbonate were determined by heating the sediment that had been treated for LOI at 550˚C to 950˚C following the method of Heiri et al. (2001). Average precisions for LOI and calcium carbonate (relative standard deviation) were, to date, 2.0% and 1.0%, respectively.

2.3 Data and Statistical Analyses

2.3.1 Data Processing

Data and graphical analyses were carried out using Systat 12, SigmaPlot 10 (Systat Software, Inc.), Excel 2016 (Microsoft), ArcGIS (Version 10.2.2.3552, Esri, Redlands, California) and HOBOware Pro 3.7.17. An alpha value to define statistical significance was set at 0.05 for statistical tests and regressions. Least squares linear regressions were calculated to determine relationships between individual pairs of parameters. Correlation coefficients (r) will be described on occasion using the following terms and intervals: very strong (greater than or equal to 0.90), strong (0.80–0.89), moderately strong (0.60–0.79), moderate (0.40–0.59), mild (0.2–0.39), and

weak (less than 0.2). All correlation coefficients are presented with a corresponding *p* value. Comparisons of two independent groups of data were carried out using two-tailed t-tests assuming equal variance unless otherwise noted. Independent groups of data with *p*-values >0.05 were considered not significantly different from one another.

2.3.2 Oxygen and Nutrient Flux Calculations

SOD was determined by subtracting the water column respiration (milligrams per liter [mg/L] per hour) values for "blank" chambers from values obtained from benthic chambers. The total rate of oxygen utilization by sediments, accounting for the volume in the benthic chamber (DO used by sediments [mg/L of O_2 per hour] times the volume of the benthic chamber [L], calculated using the height of the chamber above the sediments) was divided by the surface area of sediment to yield values for SOD. Values for SOD are reported in micromoles per square meter per hour (µmoles/m^2/hr).

Benthic nutrient fluxes were determined from benthic and blank chambers by subtracting initial nutrient concentrations (micromoles per liter [µM]) from final concentrations for both benthic and blank chambers. The changes in concentrations (µM) were then divided by the elapsed time (hours) of each incubation to yield rates in µM/hr. The rate of nutrient production/utilization in blank chambers was then subtracted from the rate calculated for benthic chambers, to determine the production/utilization by sediments and particles independently. The rate (µM/hr) for the benthic chamber was then multiplied by the volume of the chamber, calculated using the height of the chamber above the sediments, to yield the amount of nutrients produced / used by sediments in the chamber per hour (µmoles/hr). This value was divided by the surface area of sediments in the chamber to yield a flux in µmoles/m^2/hr consistent with units used in the literature (e.g., Boynton et al. 2018). A similar approach was used to determine nutrient fluxes from laboratory incubations. Nutrient fluxes were evaluated against the rate of oxygen utilization to ensure that linear nutrient production/utilization could be assumed. If the chamber went anaerobic during the deployment or oxygen utilization was non-linear, nutrient fluxes were flagged and not included in data interpretation.

3 Results and Discussion

3.1 Temperature, Salinity, and Density

Long-term datasets for lagoon and seawater temperature and salinity were obtained from the St. Johns River Water Management District (SJRWMD) and National Oceanic and Atmospheric Administration's National Data Buoy Center (Table 3-1). These datasets were used to complement discrete data obtained during this study. Overall, lagoon temperature followed seasonal patterns with a range of about 17°C from a minimum of approximately 15°C typically reported during February to maximum of approximately 32°C typically reported during August and September (Table 3-1). Overall, average annual temperatures were close to 25°C with small, yet significant differences among stations (Table 3-1; Figure 3-1). Vertical profiles for temperature typically showed an approximately 1˚C vertical temperature gradient in the lagoon, consistent with daytime heating and in most cases not restricted to a stratified surface layer (Figure 3-2).

Table 3-1. Temperature (°C) (average ± standard deviation) each month beginning January 2019

Location	Jan	Feb	Mar	Apr	May	Jun	Jul	Aug	Sept	Oct	Nov	Dec	Source
Sebastian	18.0 ± 4.2	18.8 ± 2.2	20.4 ± 2.1	23.4 ± 2.0	25.4 ± 1.3	26.1 ± 1.9	27.0 ± 1.8	27.0 ± 1.9	27.2 ± 1.4	26.3 ± 1.1	20.8 ± 3.7	20.2 ± 3.4	Ndbc.noaa.gov
Cape Canaveral Nearshore	19.9 ± 2.2	17.9 ± 1.5	20.1 ± 1.0	23.9 ± 1.3	26.2 ± 0.8	25.5 ± 1.1	27.5 ± 1.3	28.0 ± 1.0	28.2 ± 0.6	27.4 ± 0.3	23.5 ± 2.3	21.4 ± 1.0	Ndbc.noaa.gov
Trident Pier	20.1 ± 1.8	18.7 ± 1.5	20.2 ± 0.9	24.1 ± 1.6	27.2 ± 0.9	25.9 ± 1.3	28.0 ± 1.3	28.6 ± 0.8	28.6 ± 0.7	27.8 ± 0.4	24.1 ± 2.5	21.3 ± 0.6	Ndbc.noaa.gov
Fort Pierce	22.2 ± 1.6	19.8 ± 0.5	21.5 ± 1.2	24.0 ± 0.8	25.9 ± 0.7	27.0 ± 1.1	27.8 ± 1.0	28.6 ± 0.6	28.3 ± 0.4	28.0 ± 0.4	25.8 ± 1.5	23.9 ± 1.0	Ndbc.noaa.gov
Banana River	17.8 ± 2.9	20.7 ± 2.6	21.4 ± 1.9	24.8 ± 1.7	27.7 ± 1.0	29.5 ± 1.2	30.4 ± 1.0	29.8 ± 1.1	28.2 ± 1.4	27.3 ± 0.7	21.9 ± 3.2	19.8 ± 1.9	sjrwmd.com/data/water-quality/
Vero (Bethel)	19.4 ± 2.8	22.7 ± 2.5	23.1 ± 1.8	26.1 ± 1.5	28.8 ± 1.2	30.8 ± 1.4	31.8 ± 1.1	31.0 ± 1.1	28.9 ± 1.5	28.2 ± 0.7	23.2 ± 3.0	21.1 ± 1.6	sjrwmd.com/data/water-quality/

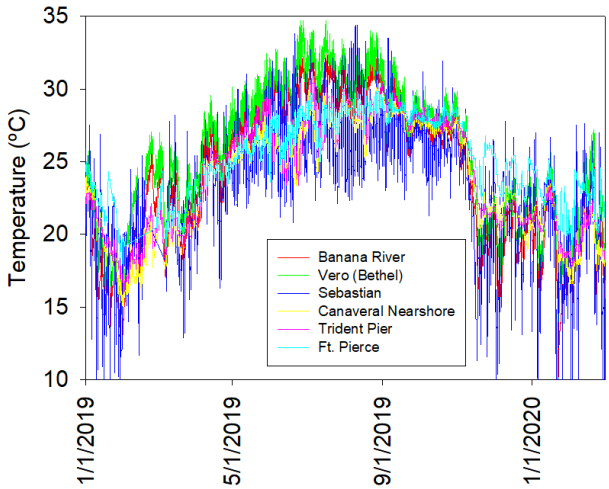

Figure 3-1. Temperature over time in BRL and Vero Beach near Bethel Creek.

Seawater temperature followed similar seasonal patterns; however, minimum temperatures during winter were higher and maximum temperatures during summer were lower compared to seawater for a smaller annual temperature range of approximately 16˚C from a minimum of approximately 16 typically reported during February to a maximum of approximately 31˚C typically reported during August and September (Table 3-1**;** Figure 3-1). In addition to a smaller annual temperature range, temperatures were more uniform across the study area from offshore at Vero Beach to Port Canaveral (Table 3-1). Vertical profiles for temperature along 10-m isobaths showed temperature stratification in the coastal ocean with distinct layers defined by an approximately 1˚C warmer surface layer (Figure 3-3). Horizontal transects from the surf zone to 10-m isobaths showed 1-2˚C warmer water in the surf zone compared to values further offshore (Figure 3-5). Water in Port Canaveral showed a gradient of water temperature with an up to 2˚C difference in surface versus bottom water temperature (Figure 3-4).

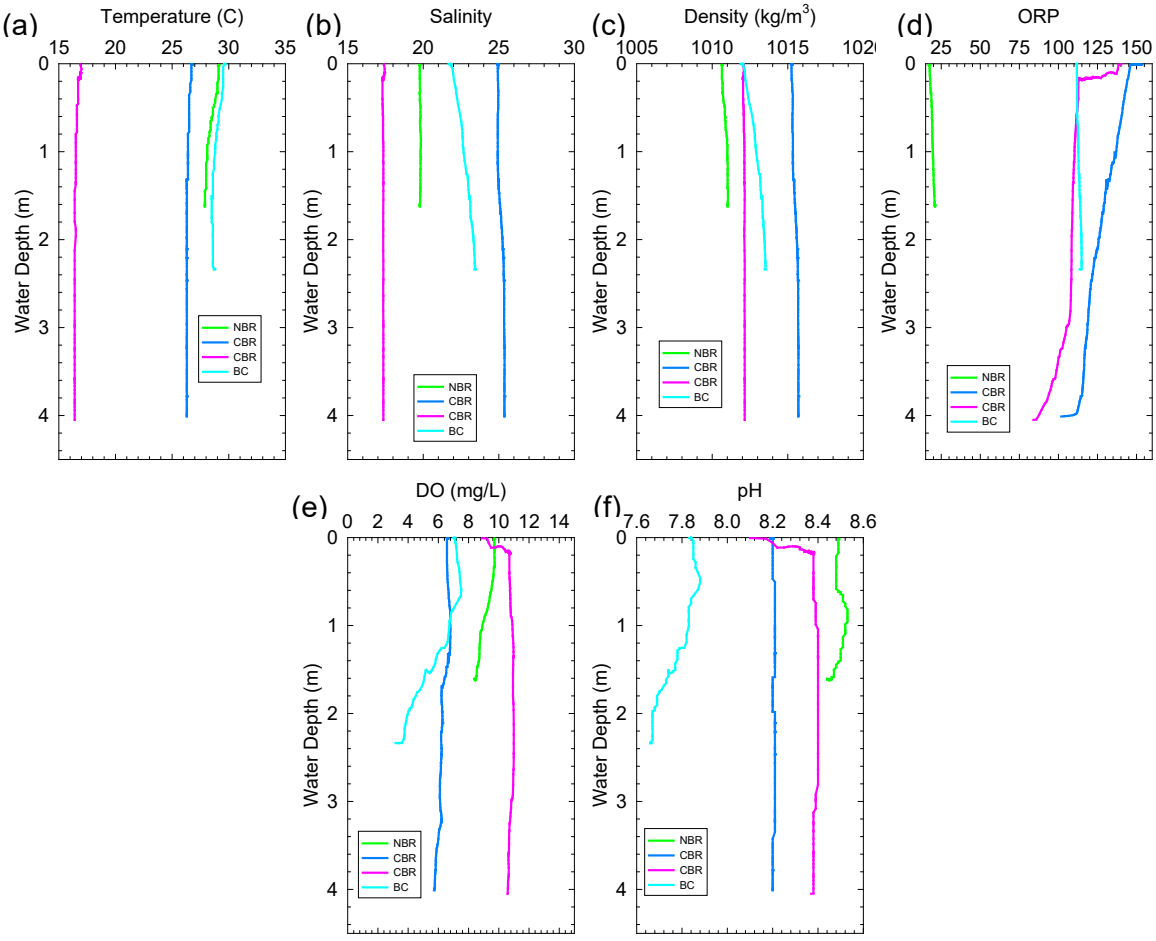

Figure 3-2. Vertical profiles for (a) temperature (ºC), (b) salinity, (c) density (kg/m^3), (d) ORP (mV), (e) DO (mg/L), and (f) pH in the Northern Banana River, Central Banana River, and Bethel Creek sites.

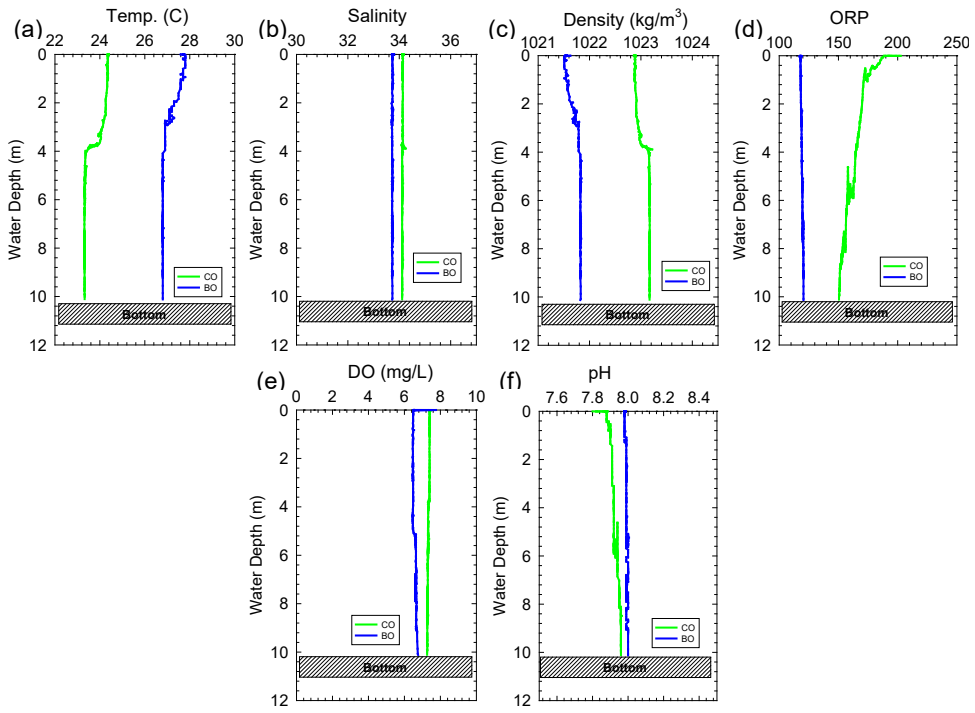

Figure 3-3. Vertical profiles for (a) temperature (ºC), (b) salinity, (c) density (kg/m^3), (d) ORP (mV), (e) DO (mg/L), and (f) pH in the Atlantic Ocean adjacent to the Central Banana River and Bethel Creek sites (Central Offshore and Bethel Offshore).

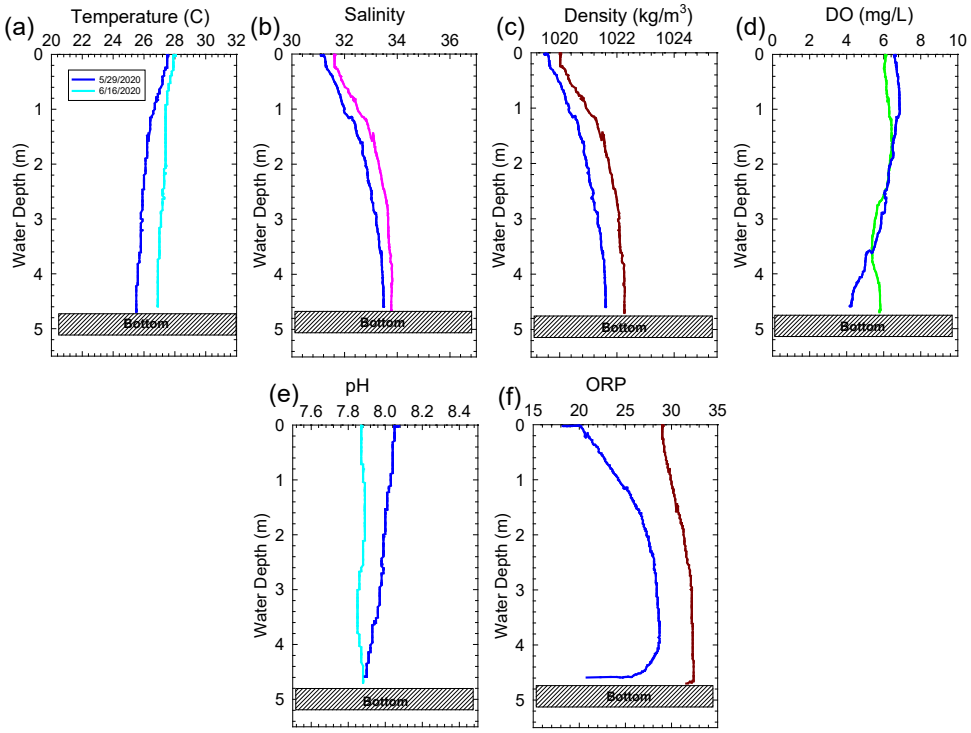

Figure 3-4. Vertical Profiles for (a) temperature (ºC), (b) salinity, (c) density (kg/m^3), (d) ORP (mV), (e) DO (mg/L) and (f) pH in Port Canaveral.

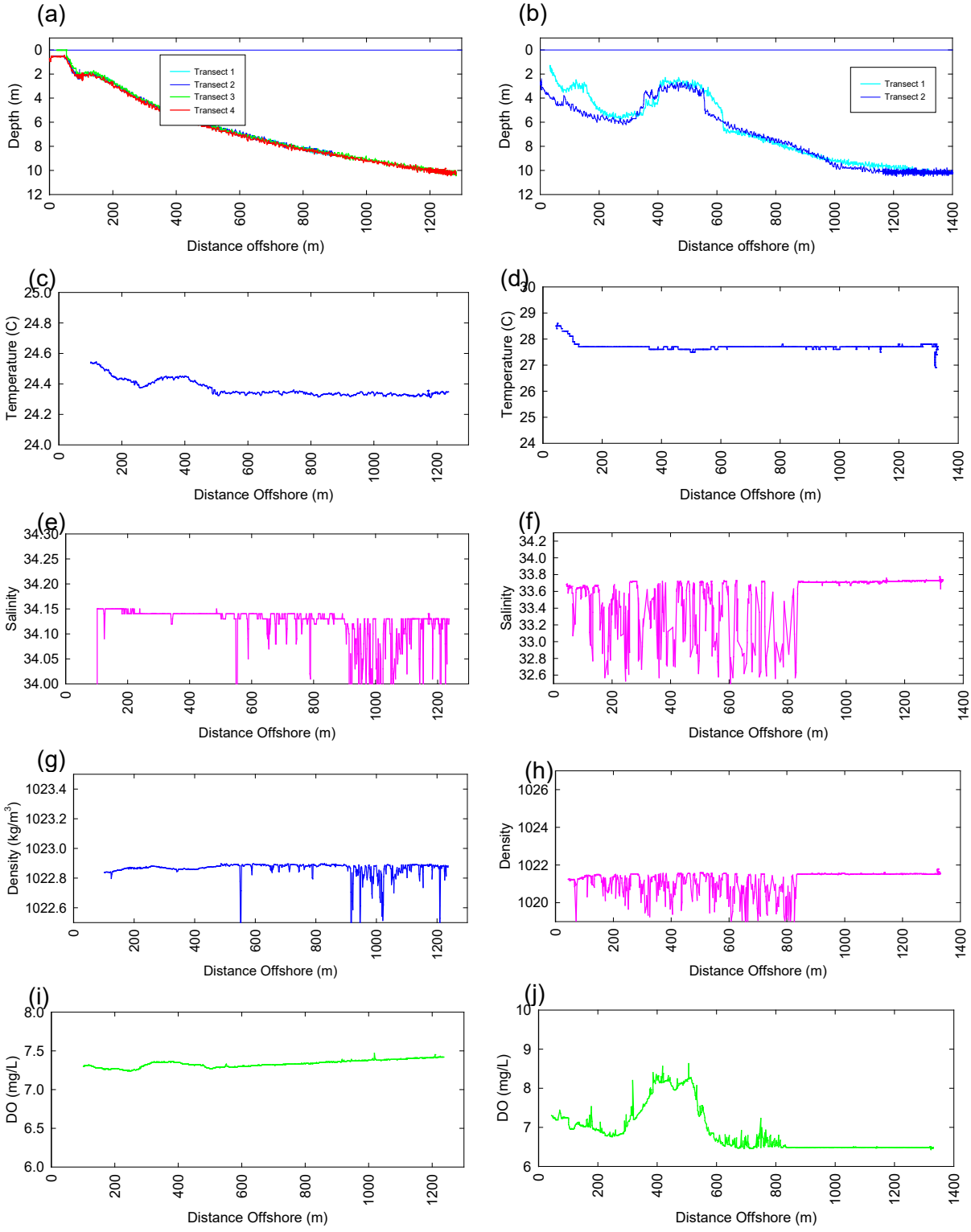
(a)
Depth (m)
Distance offshore (m)
Transect 1
Transect 2
Transect 3
Transect 4
(b)
Depth (m)
Distance offshore (m)
Transect 1
Transect 2
(c)
Temperature (C)
Distance Offshore (m)
(d)
Temperature (C)
Distance Offshore (m)
(e)
Salinity
Distance Offshore (m)
(f)
Salinity
Distance Offshore (m)
(g)
Density (kg/m3)
Distance Offshore (m)
(h)
Density
Distance Offshore (m)
(i)
DO (mg/L)
Distance Offshore (m)
(j)
DO (mg/L)
Distance Offshore (m)

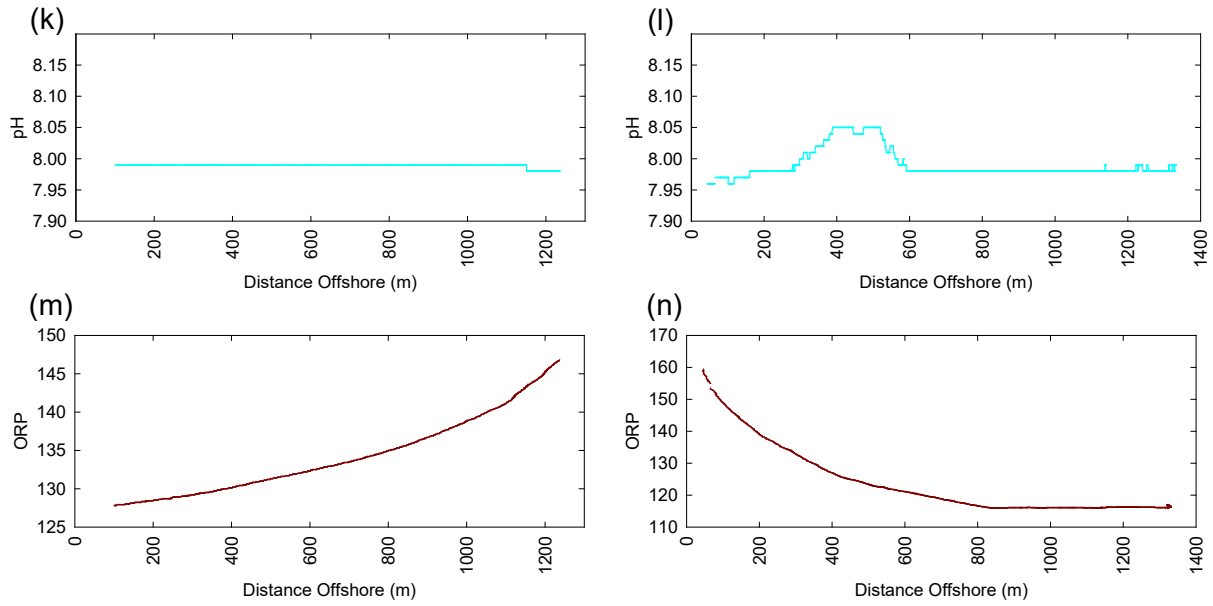

Figure 3-5. Transects from the surf zone to 10-m isobaths for (a, b) water depth (m), (c, d) temperature (°C), (e, f) salinity (PSU), (g, h) density (kg/m^3), (i, j) DO (mg/L), (k, l) pH, and (m, n) ORP (mV) in the Atlantic Ocean adjacent to the Central Banana River (left) and Bethel Creek (right) sites.

Overall, salinity was lower in the BRL compared to values for Vero Beach near Bethel Creek (Table 3-2 and temperature-salinity diagram Figure 3-6). For example, during 2019, salinity in Banana River ranged from 19.2–23.3 PSU relative to a range of 21.8–33.0 PSU in Vero Beach (Figure 3-6). As expected, these values were lower than the range of salinities obtained for the coastal Atlantic Ocean (33–35 PSU). Vertical profiles for seawater salinity offshore (10-m isobaths) from the three proposed inflow locations were well mixed with an average salinity for all sites during this study at 34.0 PSU. Horizontal transects from the surf zone to 10-m isobaths indicated that salinity was well mixed between the surf zone and 1–2 km offshore. Relative to samples collected offshore, seawater in Port Canaveral had lower salinity in surface water (31–32 PSU) increasing with depth to values consistent with values found offshore (33–35 PSU; Figure 3-4). These data are consistent with a source of lower salinity water, possibly related to the locks in Port Canaveral.

Table 3-2. Salinity (average ± standard deviation) for each month during 2019

Location	Jan	Feb	Mar	Apr	May	Jun	Jul	Aug	Sept	Oct	Nov	Dec	Source
Sebastian	-	-	-	-	-	-	-	-	-	-	-	-	Ndbc.noaa.gov
Cape Canaveral Nearshore	-	-	-	-	-	-	-	-	-	-	-	-	Ndbc.noaa.gov
Trident Pier	-	-	-	-	-	-	-	-	-	-	-	-	Ndbc.noaa.gov
Fort Pierce	-	-	-	-	-	-	-	-	-	-	-	-	Ndbc.noaa.gov
Banana River	21.9 ± 0.3	21.2 ± 0.3	22.1 ± 0.4	22.9 ± 0.5	23.3 ± 0.5	21.4 ± 1.4	21.7 ± 0.8	20.3 ± 0.6	20.1 ± 0.6	20.4 ± 0.3	19.2 ± 0.5	18.4 ± 0.5	sjrwmd.com/data/water-quality/
Vero (Bethel)	31.1 ± 1.2	26.9 ± 1.0	28.4 ± 1.3	29.9 ± 1.2	32.4 ± 1.1	33.1 ± 2.0	33.0 ± 1.8	21.8 ± 3.4	27.7 ± 2.8	27.8 ± 1.7	26.6 ± 1.2	23.5 ± 2.7	sjrwmd.com/data/water-quality/

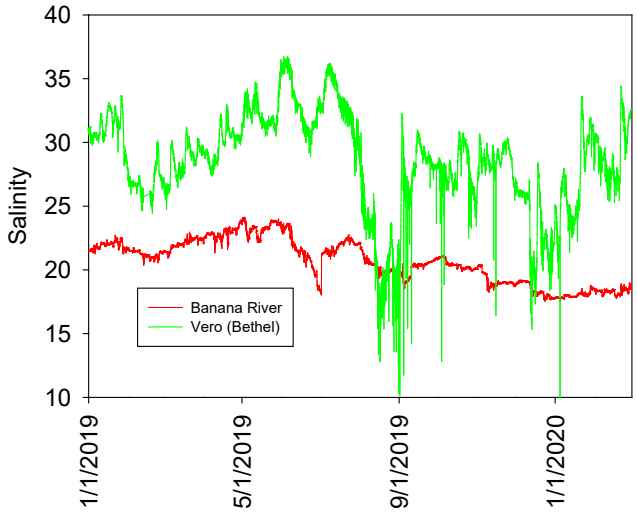

Figure 3-6. Salinity (PSU) over time in BRL and Vero Beach near Bethel Creek.

Using data for temperature and salinity, the density of each water mass was calculated as an indication of the likelihood of mixing or the degree of stratification that could occur if seawater were to be pumped into the system (Figure 3-7 and Figure 3-8). Overall, consistent with lower salinity, density was lower at the northern site in BRL with an average density during 2019 of 1,012 kg/m^3 relative to 1,018 kg/m^3 at the Bethel Creek site. These values were 1.3% and 1.7% less dense than typical seawater at 1,025 kg/m^3. This seemingly small difference in density is sufficient to maintain discrete stratified layers and is greater than differences in density identified among existing layers observed during this study. For example, during all offshore sampling events, discrete surface and bottom water layers were identified based on temperature alone with densities of 1,022.9 kg/m^3 and 1,023.2 kg/m^3 for surface and bottom water respectively (Figure 3-3), a difference of 0.03%.

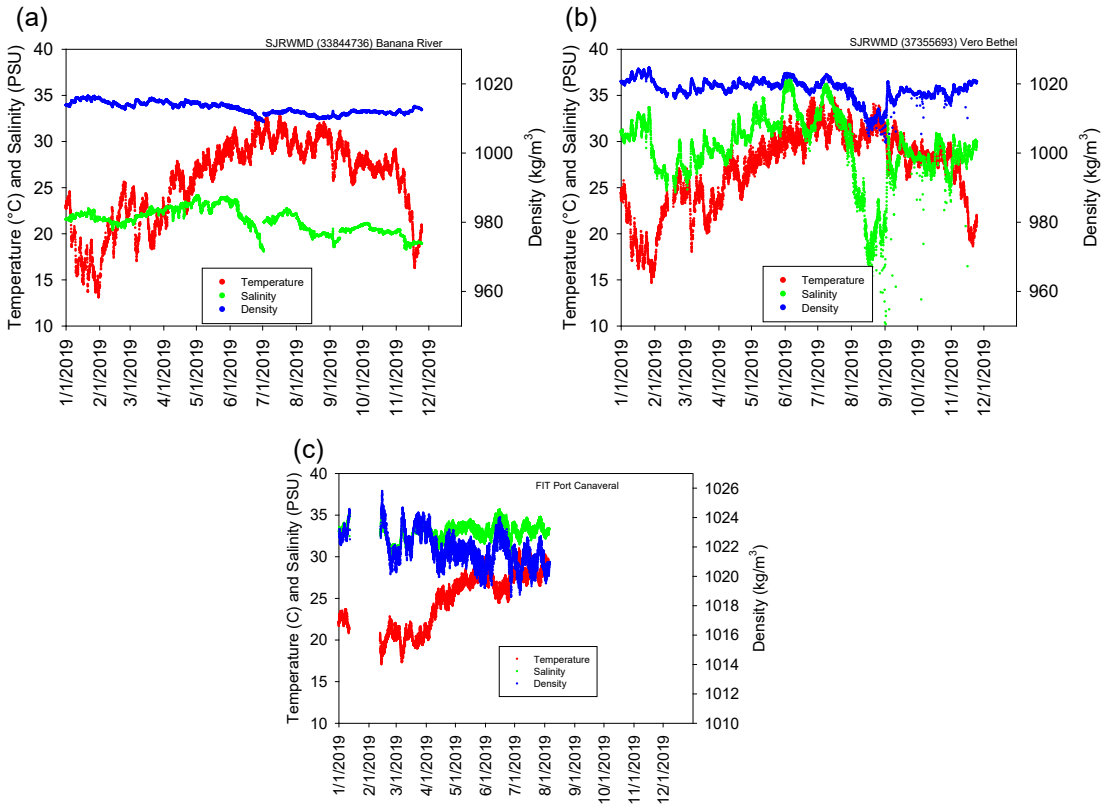

Figure 3-7. Temperature, salinity and density at sites in (a) BRL (b) Vero Beach near Bethel Creek, and (c) in Port Canaveral.

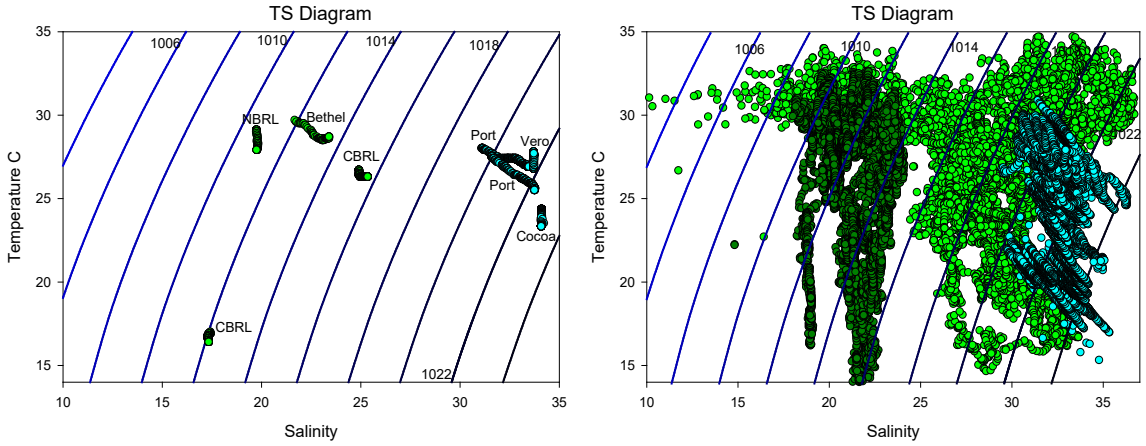

Figure 3-8. Temperature-salinity diagrams showing (a) data from discrete sampling events during this study and (b) long-term datasets for sites in Vero Beach (light green), Sebastian (dark green), and Port Canaveral (cyan).

With regards to potential inflow, two possible implications of density stratification are (1) pumping water from offshore would bring water from below the pycnocline into the lagoon versus a weir structure that would allow surface seawater to flow into the lagoon, and (2) seawater entering the lagoon could form a discrete higher density layer that flows along the bottom of the lagoon, depending on the method of seawater discharge into the IRL. The existence of such stratified

layers can be of importance towards controlling water quality. For example, stratified water columns within the IRL often result in lower bottom water DO concentrations that influence geochemical nutrient cycling, as discussed in Sections 3.3 and 3.4. Regardless the degree of mixing, inflow of seawater would stabilize temperature and salinity in the lagoon, producing cooler lagoon water during summer months and potentially warmer water during winter months. Salinity would likely increase in the area of inflow as discussed in the corresponding modeling section of the final report. The increase would likely be small, less than1 PSU; however, if stratification were to occur, sediments could experience salinities as high as 34–35 PSU and temperatures as much as a degree warmer or cooler depending on season and the degree of mixing that occurs at the proposed inflow location.

Trends for temperature and salinity represent what can be expected based on the conservative properties of seawater. Other variables that together with temperature and salinity collectively describe water quality would likely experience less predictable variations as a result of inflow. The following sections will discuss the approach to modeling how changes in the conservative properties of seawater could influence other variables. For example, a predictable quantity of nutrients (N and P) would be pumped into the lagoon via inflow and another quantity would be discharged through inlets into the coastal ocean. Simple calculations can describe this "conservative" approach to nutrients in the lagoon, and an estimate of the decrease in nutrient concentrations can be made. This approach fails to account for the non-conservative nature of nutrient geochemistry. For example, the standing stock of nutrients in the lagoon is based on an existing homeostasis between freshwater inputs including rainfall, tributaries, and groundwater plus in-situ N fixation and denitrification, evaporation, point sources, legacy loads, algal and bacterial biomass and cycling, existing water quality, as well as other processes. Changes to the system that could result from inflow would influence several of these confounding factors. For example, even though temperature and salinity were relatively uniform across sites in the open ocean, other water quality variable are subject to conditions offshore. For example, DO and pH were elevated (1–2 mg/L DO and 0.05 pH units) in a region between about 400–600 m offshore from the southern site in water overlying a rocky reef (Figure 3-5). In addition to variations among offshore locations, water quality (temperature, salinity, DO, pH, ORP) in Port Canaveral was quite different from water quality at offshore sites (e.g., Figure 3-3 versus Figure 3-4).

Changes to the system that could result from pumping would influence several of these confounding factors. To begin to address these issues, (Section 3.2) current nutrient loading from sandy and mucky sediments in the IRL/BRL and (Section 3.3) the potential impacts of changes to temperature, salinity, and DO concentrations on benthic fluxes of nutrients to the IRL were investigated.

3.2 Dissolved Nutrients

3.2.1 Concentrations and Speciation

Data obtained during this study complement long-term and existing datasets for nutrient concentrations in the IRL. Collectively, these data were used to evaluate potential direct impacts of inflow on nutrient concentrations in the IRL and to quantify nutrients that would likely be discharged through inlets to the coastal ocean if inflow were to occur. As discussed above, pumping water from offshore in the coastal ocean at the central and southern sites would bring cool seawater from below the thermocline into the lagoon versus a potential weir structure at the northern site that would supply warmer and less saline surface seawater from Port Canaveral. This subtle difference in seawater source would influence both direct nutrient exchanges and potential geochemical changes associated with different temperature, salinity, and DO.

During this study, seawater samples were collected from three distinct areas: (1) at 10-m isobaths located 1–2 km offshore, (2) in the surf zone (when weather prevented offshore sampling), and (3) in Port Canaveral. Overall, the lowest nutrient concentrations were obtained from offshore sites with average concentrations of TDN, TDP, and SiO_2 at 8.0 ± 2.4 µM TDN, 0.15 ± 0.05 µM TDP, and 3.3 ± 0.7 µM SiO_2, respectively, and no significant vertical trends were observed for TDN, TDP, SiO_2, or speciation (Figure 3-9). Offshore samples were also the most uniform spatially and temporally (e.g., Figure 3-9).

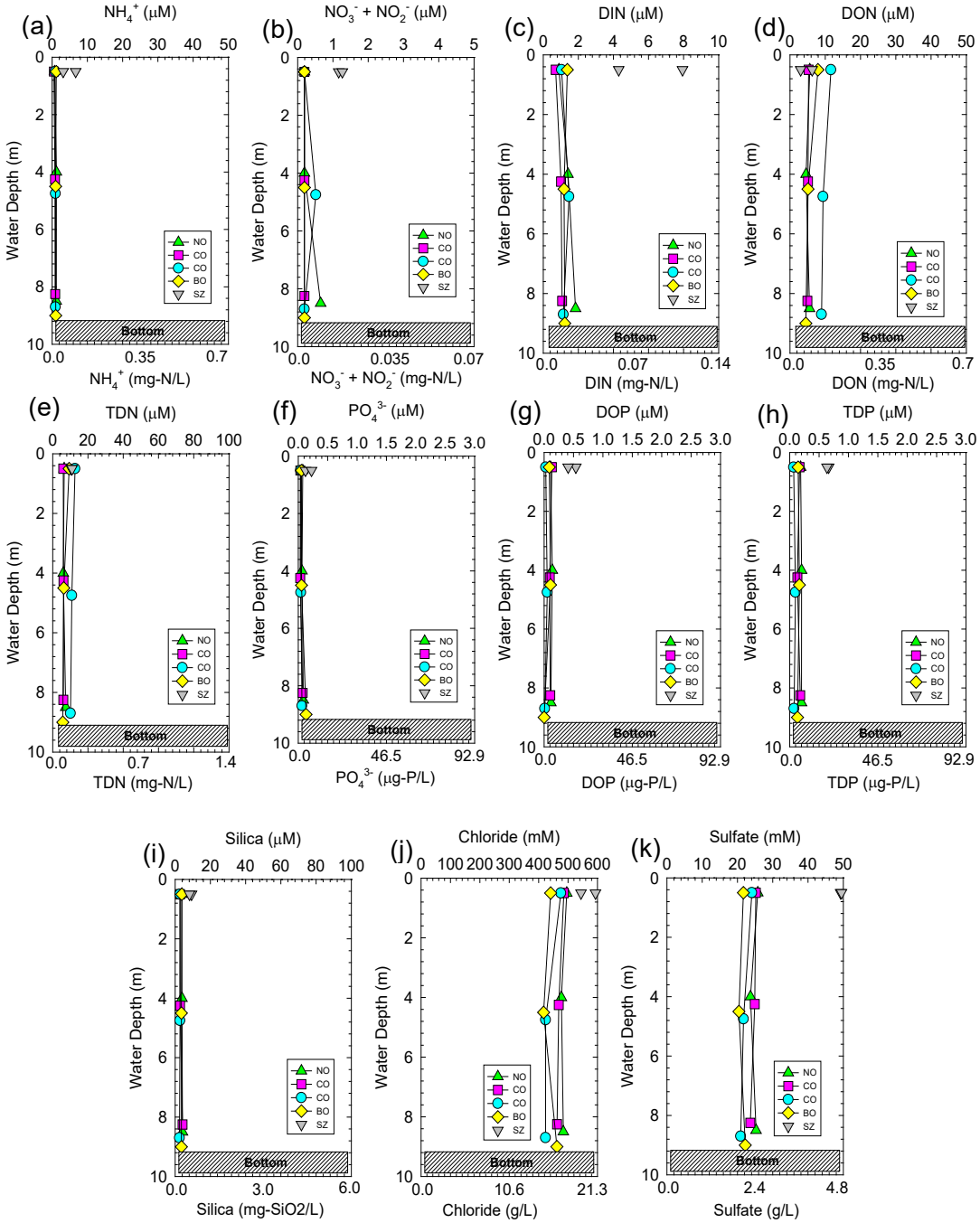

Figure 3-9. Vertical profiles for (a) NH_4, (b) NOx, (c) DIN, (d) DON, (e) TDN, (f) PO_4, (g) DOP, (h) TDP, (i) SiO_2, (j) chloride, and (k) sulfate in the coastal Atlantic Ocean (offshore) near the central BRL site.

Nutrient concentrations in Port Canaveral were variable with values fluctuating between those identified for offshore sites and lagoon water (discussed below), with average TDN, TDP, and SiO_2 at 24.4 ± 5.5 µM TDN, 0.44 ± 0.04 µM TDP, and 11 ± 2 µM SiO_2, respectively.

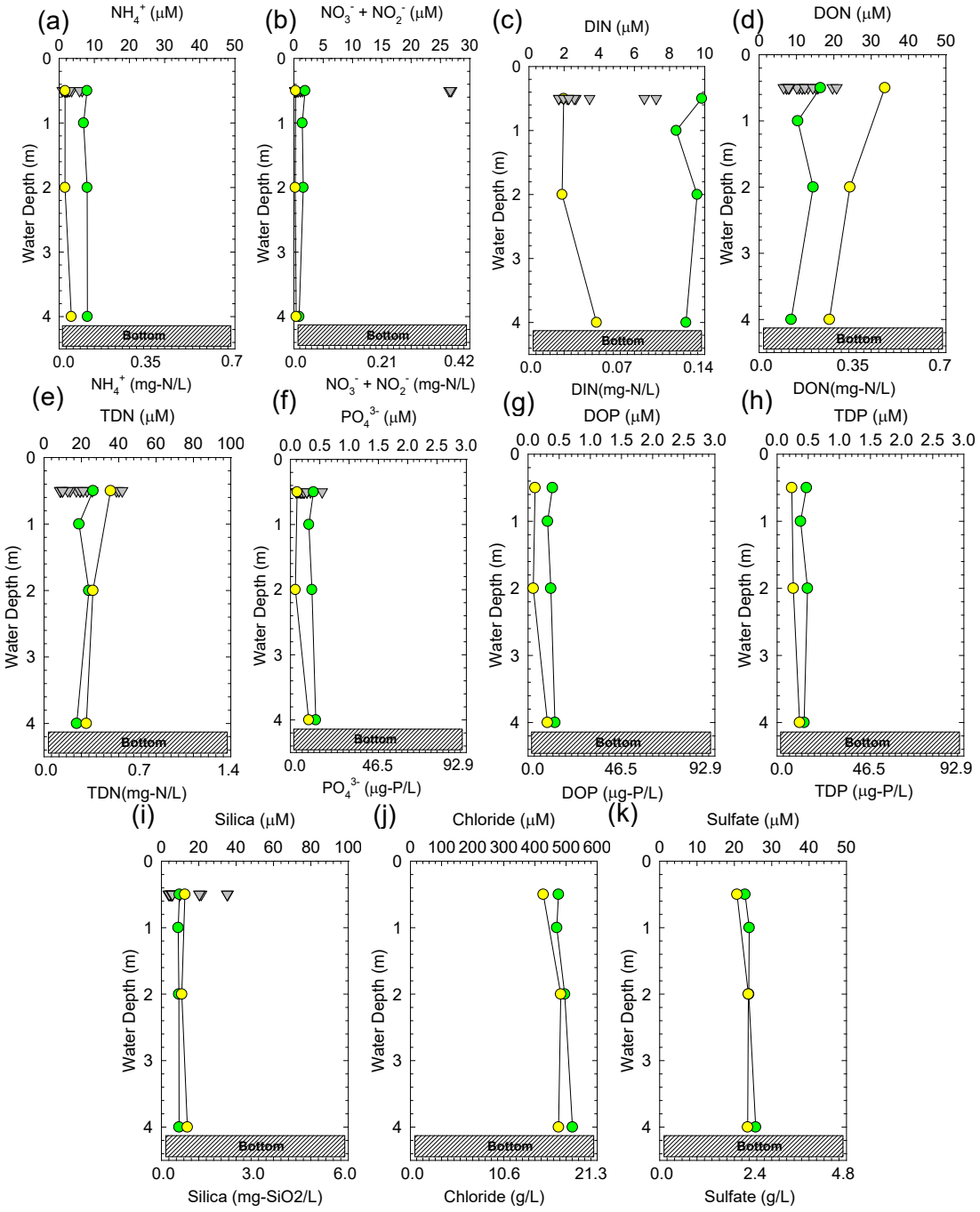

Figure 3-10. Vertical profiles for (a) dissolved NH_4, (b) dissolved NOx, (c) DIN, (d) DON, (e) TDN, (f) dissolved PO_4, (g) DOP, (h) TDP, (i) dissolved SiO_2, (j) chloride, and (k) sulfate in Port Canaveral.

Nutrient concentrations in the lagoon were more variable compared to values for seawater as shown using both discrete sampling events during this study and long-term datasets (e.g., Figure 3-11). Large differences were observed among samples from the open lagoon (northern and central sites) and in Bethel Creek (southern site). Overall, during this study, TDN, TDP, and SiO_2 at lagoon sites averaged 62.8 ± 24.3 µM TDN, 1.41 ± 0.72 µM TDP, and 51 ± 28 µM SiO_2, which are 7.9-fold, 9.4-fold, and 15.5-fold higher, respectively, than values for seawater. During this study, samples from the open lagoon averaged 72.1 ± 23.3 µM TDN, 1.38 ± 0.52 µM TDP, and 40 ± 13 µM SiO_2 versus 44.1 ± 12.7 µM TDN, 1.45 ± 0.91 µM TDP, and 71 ± 37 µM SiO_2 for samples from Bethel Creek. Lower concentrations of TDN and similar concentrations of TDP at the southern site (Bethel Creek), relative to values in the BRL (central and northern sites) during this study are consistent with trends observed from continuous monitoring (e.g., SJRWMD and Ocean Research and Conservation Association) and by Lapointe et al. (2020).

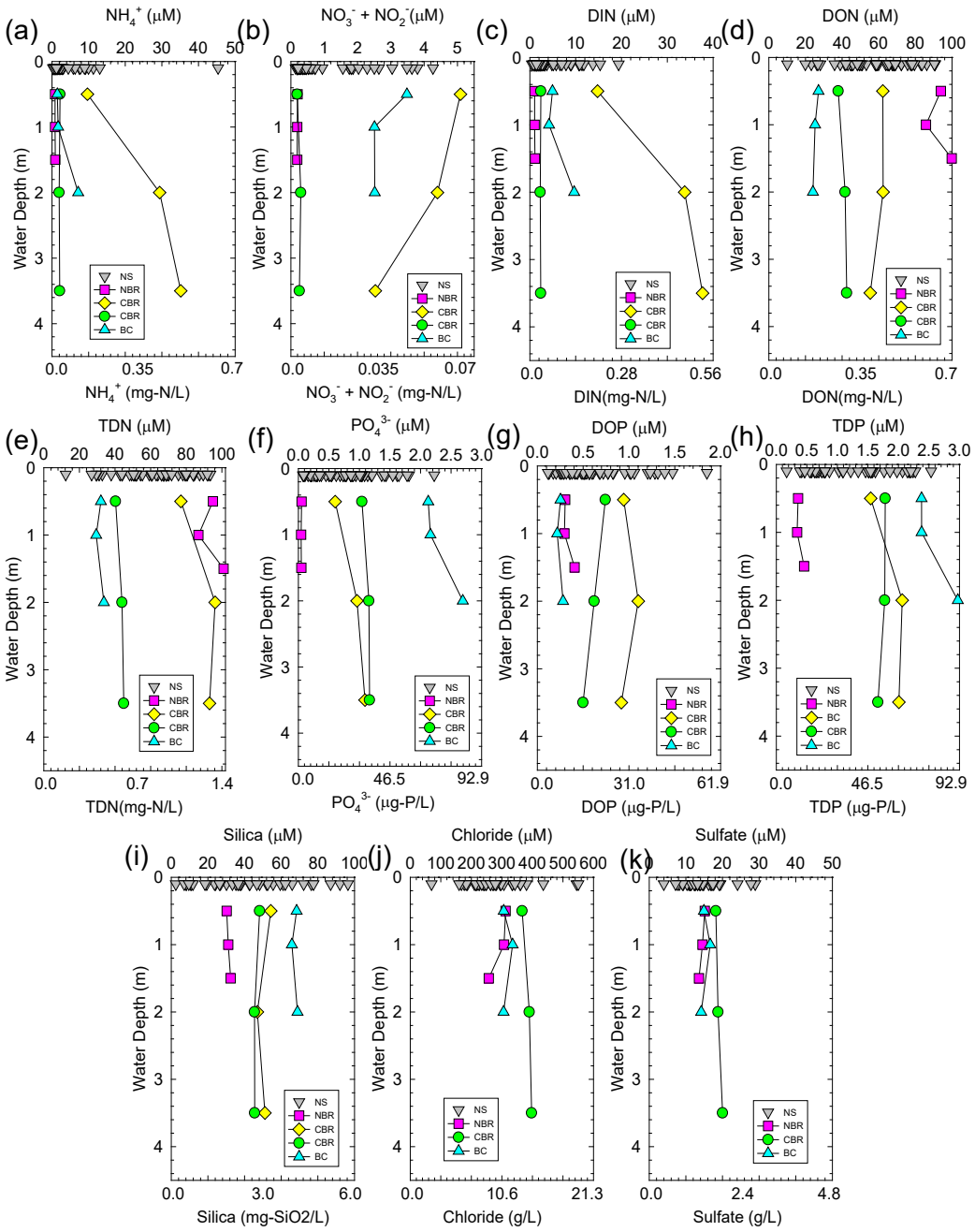

Figure 3-11. Vertical profiles for (a) dissolved NH_4, (b) dissolved NOx, (c) DIN, (d) DON, (e) TDN, (f) dissolved PO_4, (g) DOP, (h) TDP, (i) dissolved SiO_2, (j) chloride, and (k) sulfate from sites nearshore throughout the lagoon, in the north BRL, central BRL, and Bethel Creek.

Table 3-3. Average nutrient concentrations for samples from the (1) lagoon, (2) port, (3) surf zone, and (4) open ocean.

Site	NH_4 (µM)	NOx (µM)	TDN (µM)	DIN (µM)	DON (µM)	PO_4 (µM)	TDP (µM)	DOP (µM)	Silica (µM)	Cl (mM)	SO_4 (mM)	Alkalinity (mg Calcium Carbonate/ L)
Lagoon	3.5 ± 3	3.4 ± 4.7	62.8 ± 24.3	6.9 ± 7.1	37.4 ± 36.2	0.98 ± 0.63	1.41 ± 0.72	0.43 ± 0.24	51 ± 28	361 ± 95	19 ± 5	91 ± 8
Port	5.4 ± 2.8	1 ± 0.6	24.4 ± 5.5	6.3 ± 3.4	18.1 ± 8	0.38 ± 0.04	0.44 ± 0.04	0.04 ± 0.05	11 ± 2	490 ± 20	24 ± 1	73 ± 2
Surf Zone	2.6 ± 2.3	0.8 ± 0.4	9.2 ± 3.4	3.3 ± 2.6	5.9 ± 3.4	0.16 ± 0.09	0.42 ± 0.2	0.27 ± 0.18	6 ± 3	466 ± 105	34 ± 16	70 ± 5
Ocean	0.9 ± 0.2	0.3 ± 0.1	8 ± 2.4	1.2 ± 0.3	6.8 ± 2.4	0.06 ± 0.02	0.15 ± 0.05	0.09 ± 0.04	3 ± 1	466 ± 25	24 ± 2	69 ± 4

Large differences in TDN and TDP among sampling locations were accompanied by variations in nutrient speciation. For example, at offshore sites NH_4, NOx, and Org-N accounted for, on average, 15%, less than 4%, and 81% of the TDN, respectively, compared to 4%, less than 1%, and 95% respectively, at sites in the open lagoon; 11%, 20%, and 68% respectively, in Bethel Creek; and 25%, <4%, and 71%, respectively, in Port Canaveral. These data are consistent with trends observed for long-term datasets in the IRL (e.g., SJRWMD).

PO_4 and Org-P accounted for 38% and 62% of the TDP at offshore sites relative to 54% and 46% in the open lagoon, 82% and 18% in Bethel Creek, and 85% and 15% in Port Canaveral. Differences in speciation among locations influence bioavailability discussed below.

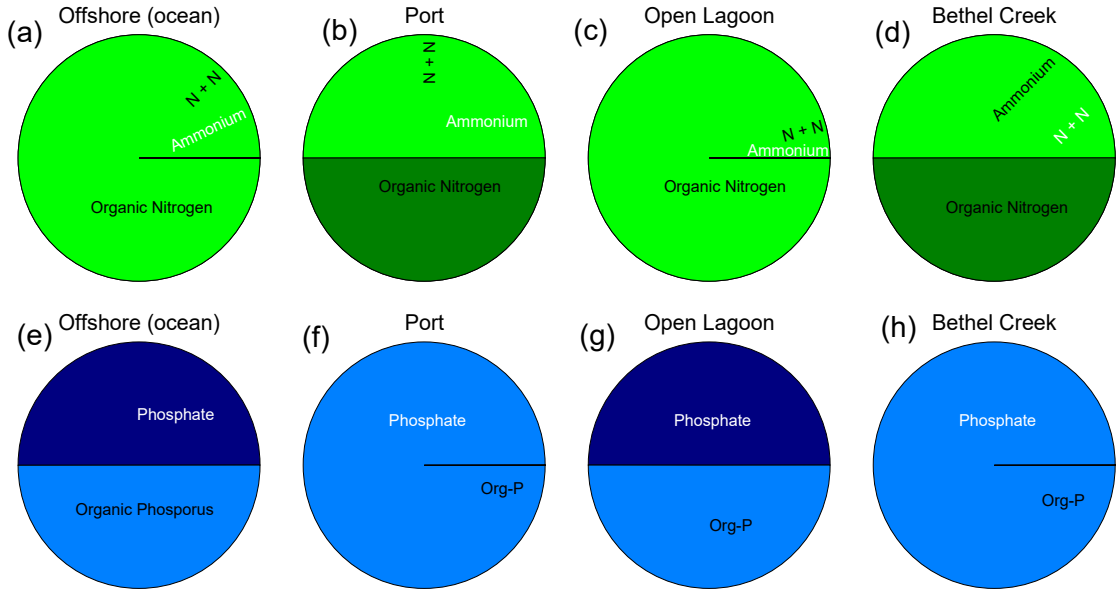

Figure 3-12. Pie diagrams showing (a, b, c, d) the percent NH_4, percent NOx, and percent Org-N, and (e, f, g, h) the percent PO_4 and percent Org-P in the water column.

3.2.2 DIN/DIP, TDN:TDP, N:P:SiO_2 Ratios (Current/Historical)

Although total nutrient concentrations are frequently used as an indicator of the eutrophic state of an estuary, speciation and the relative abundance of bioavailable species of N:P:SiO_2 have

consistently been shown to contribute to algal community composition whereby at the same total concentrations, shifts in speciation, and the relative abundance of N:P:SiO_2 can favor shifts from beneficial or less harmful photosynthesizers to harmful species or vice versa (e.g., Choudhury and Bhadury 2015). A basis for evaluating N:P ratios originated with Redfield in the 1930s (Redfield 1934) and this traditional N:P ratio at 16:1 has been utilized over decades and, in some cases, expanded to include other macro or micronutrients (e.g., Choudhury and Bhadury 2015). For example, many studies now include SiO_2 due to its importance for diatom growth. P is used as cellular energetic currency (adenosine triphosphate, adenosine diphosphate, and adenosine monophosphate) and N and SiO_2 are utilized as a structural components of hard (SiO_2 tests) and soft tissues (N for amino acids) whereby changes to N:P and N:SiO_2 ratios can promote one species versus another based on differences in metabolic and growth requirements (Harris 1986). Ratios have classically focused on nutrient species that are readily bioavailable, in other words: NH_4 + NOx versus PO_4 (DIN:SRP). More recently, several species of harmful algae, including *Aureoumbra Lagunensis,* the brown tide species in the IRL, have been identified to use Org-N and Org-P (Liu et al., 2001). In addition to the ability to use Org-N and Org-P, species such as *A. Lagunensis* are not able to use nitrate, complicating interpretations of water quality based on N:P. To provide a more complete picture, data are presented here for both DIN:SRP and TDN:TDP.

Overall, DIN:SRP ratios varied among sample locations; for example, DIN:SRP at offshore sites averaged 20, consistent with ratios previously identified for the coastal Atlantic Ocean (Kent et al. 2001, Martiny et al. 2014). This ratio was 5-fold higher than the DIN:SRP ratio of 3.9 for samples obtained during this study for the open lagoon and 2.4-fold higher than the DIN:SRP ratio of 8.4 in Bethel Creek. These values are consistent with median values less than the Redfield value at 16 (e.g., 10.0 at IRLI28 and 15.3 at IRLB) from long-term datasets (2010–2020 SJRWMD). At all sites, ocean and lagoon TDN:TDP ratios were greater than ratios of DIN:SRP (e.g., 53 ± 47 at IRLI28 and 74 ± 48). For example, based on all the data, offshore samples had median TDN:TDP at 37 ± 54 versus long term median values at >50 in the IRL.

These data show higher N:P ratios at northern sites in the IRL and Lapointe et al. (2020) showed a similar pattern for the N:P ratio in seagrasses *S. filiforme* at 19.4 ± 0.8 Central IRL, 21.2 ± 0.6 in the South IRL, and 30.2 ± 0.7 in the North IRL; *T. testudinum* at 26.6 ± 0.8 in the South IRL to 20.0 ± 0.4 in the Central IRL; and *H. wrightii* 33.6 ± 1.5 in the BRL, 29.4 ± 2.2 in the Mosquito Lagoon, and 28.4 ± 1.2 North IRL suggesting that some photosynthesizes adapt to varying abundances of N and P. Nevertheless, these seagrasses all fit in a relatively narrow range of N:P and large differences in N:P have been shown to drive change in species composition of photosynthesizes. Based on global trends plus data from this study and long term datasets, potential shift in N:P ratios (DIN:SRP and TDN:TDP and perhaps other N:P ratios) should be considered a major component of overall water quality.

3.2.3 Nutrients Exchanges Based on Standing Stocks Assuming Conservative Behavior (Direct Discharges)

Nutrient concentrations determined for the IRL/BRL during this study were not significantly different from long-term averages using data from SJRWMD. Nevertheless, to use the most robust dataset available, 5-year averages for nutrient concentrations at sites near each inlet (Figure 3-13) were used to calculated expected discharges (metric tons/year) based on various levels of pumping (Table 3-4, Table 3-5, and Table 3-6). Based on a proposed pumping rate of 5 m^3/sec at the central or southern site, 4.3 x 10^8 L of lagoon water are expected to be discharged through inlets per day or 1.6 x 10^{11} L per year (Table 3-4). Based on these data, annual discharges of nutrients through inlets to the coastal Atlantic Ocean associated with possible pumping (5 m^3/sec) are calculated at approximately 70 metric tons of N and 6.7 to 11 metric tons of P per

year (Table 3-5 and Table 3-6). The net direct discharge (5 m^3/sec) of dissolved nutrients is equal to about 5% and 5–8% of the annual total estimated inputs of N (1,400 tons/year) and P (140 tons/year) to IRL/BRL system, respectively (Tetra Tech 2020). Using average nutrient concentrations from Table 3-4 plus an average lagoon depth of 1.5 meters and a surface area for the BRL at 170 km^2 and 270 km^2 in the IRL, standing stocks of N and P are estimated at about 300 and about 30 metric tons, respectively. Overall, annual discharges would be equal to about 25% of the standing stock of N and P currently in the lagoon; however, due to rapid internal recycling, discharges are better viewed in the context of other inputs at 5 and 5–8% of total N and P inputs, respectively. Overall, the TDN discharged from either inlet would be about the same (70 tons/year); however, the speciation of the discharged nitrogen would differ among inlets. At Sebastian Inlet NH_4^+, NOx, and DON would account for about 4%, 2%, and 94% of the TDN, respectively, compared to approximately 9%, 5%, and 86%, respectively, at Fort Pierce Inlet. These data suggest that more readily bioavailable DIN (NH_4^+ and NO_x) would be preferentially discharged at the southern location. Estimated annual discharges of TDP were about 60% greater at Fort Pierce (11 tons/year) versus Sebastian (6.7 tons/year) Inlet, and the relative abundance of PO_4 to Org-P was higher at 50:50 relative to 30:70 at Sebastian inlet. Like N, discharges from the southern station would favor discharges of more readily bioavailable PO_4. Based on these data, molar ratios of DIN:DIP and TDN:TDP discharged from Sebastian Inlet would be 4.8 and 22, respectively, versus 3.8 and 14 if discharges were to occur from Vero Beach Inlet. Lower N:P values for water discharged from the lagoon versus water brought into the lagoon via inflow (DIN:SRP = 20 for ocean samples from this study) would promote an increase in lagoon N:P.

Table 3-4. Nutrient concentrations in µmoles/L (5-year running averages) at stations near Sebastian Inlet (IRLI28) and Fort Pierce Inlet (IRLIRJ08) plus data from this study.

Location	NH_4 (µM)	NOx (µM)	DIN (µM)	Org-N (µM)	TDN (µM)	PO_4 (µM)	TDP (µM)	DOP (µM)
Sebastian (IRLI28)	1.4	0.6	2.0	28.4	30.4	0.42	1.4	0.9
Fort Pierce (IRLIRJ08)	2.6	1.6	4.2	25.9	30.1	1.1	2.2	1.1
Open Lagoon (This Study)	3.5 ± 3	3.4 ± 4.7	6.9 ± 7.1	37.4 ± 36.2	62.8 ± 24.3	0.98 ± 0.63	1.41 ± 0.72	0.43 ± 0.24

Table 3-5. Tons of N and P that would be discharged to the coastal ocean per year from Sebastian Inlet, associated with various levels of inflow.

Pumping Rate	L/day	L/year	NH_4 (tons/yr)	NOx (tons/yr)	DIN (tons/yr)	Org-N (tons/yr)	TDN (tons/yr)	PO_4 (tons/yr)	TDP (tons/yr)	DOP (tons/yr)
2.5 m^3/sec	$2.2*10^8$	$7.9*10^{10}$	1.5	0.63	2.2	31	34	1.0	3.3	2.2
5 m^3/sec	$4.3*10^8$	$1.6*10^{11}$	3.0	1.3	4.5	64	68	2.1	6.7	4.5
10 m^3/sec	$8.6*10^8$	$3.2*10^{11}$	6.1	2.6	9.0	130	140	4.2	13	9.0
15 m^3/sec	$1.3*10^9$	$4.7*10^{11}$	8.9	3.8	13	190	200	6.1	20	13
20 m^3/sec	$1.7*10^9$	$6.3*10^{11}$	12	5.0	18	250	270	8.2	27	18

Table 3-6. Tons of N and P that would be discharged to the coastal ocean per year from Fort Pierce Inlet, associated with various levels of inflow.

Pumping Rate	L/day	L/year	NH_4 (tons/yr)	NOx (tons/yr)	DIN (tons/yr)	Org-N (tons/yr)	TDN (tons/yr)	PO_4 (tons/yr)	TDP (tons/yr)	DOP (tons/yr)
2.5 m^3/sec	$2.2*10^8$	$7.9*10^{10}$	2.9	1.7	4.7	29	33	2.7	5.3	2.6
5 m^3/sec	$4.3*10^8$	$1.6*10^{11}$	5.9	3.5	9.4	58	68	5.4	11	5.3
10 m^3/sec	$8.6*10^8$	$3.2*10^{11}$	11.8	7.0	19	120	140	11	21	11
15 m^3/sec	$1.3*10^9$	$4.7*10^{11}$	17.4	10	28	170	200	16	32	16
20 m^3/sec	$1.7*10^9$	$6.3*10^{11}$	23.3	14	37	230	270	21	42	21

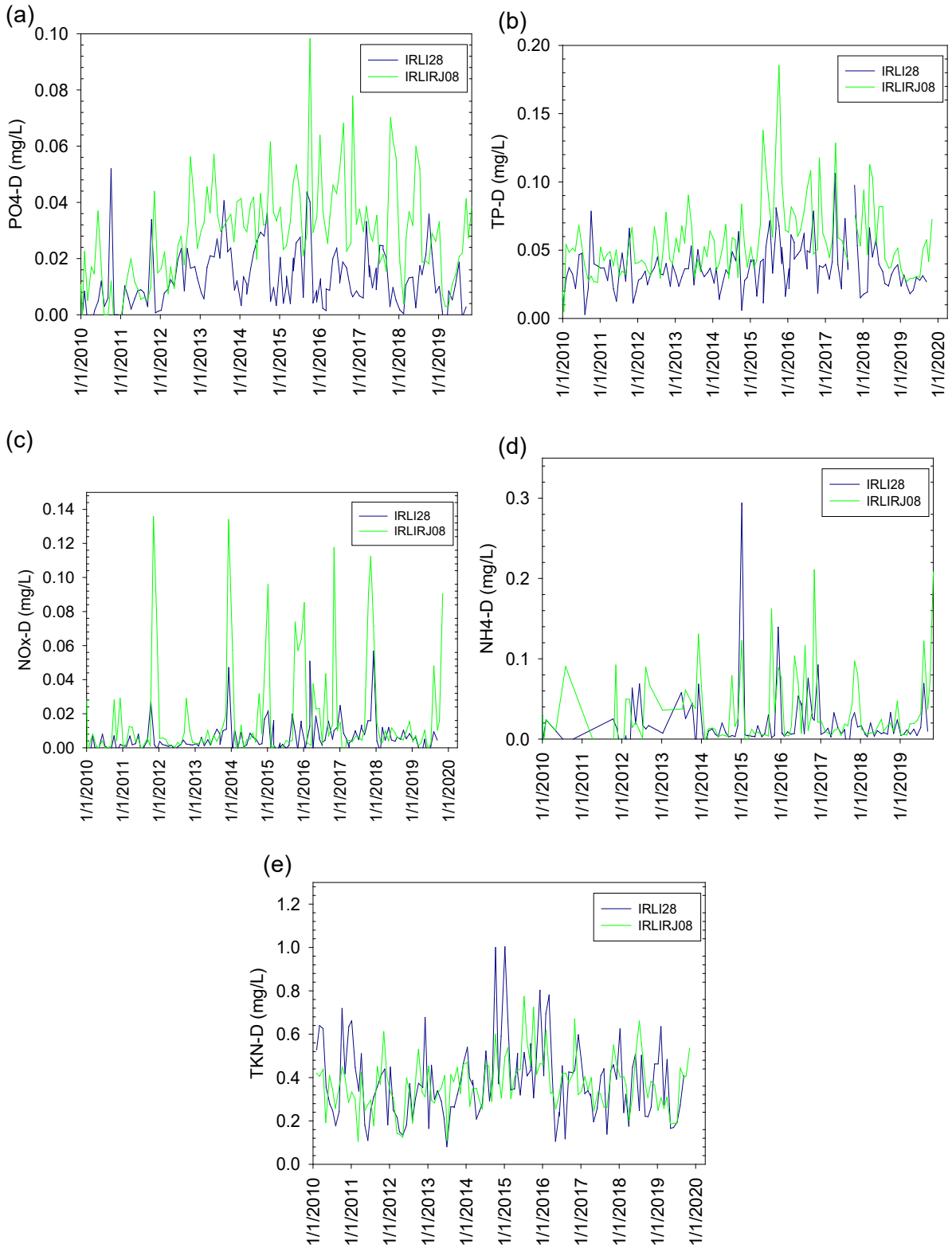

Figure 3-13. Concentrations of (a) dissolved PO_4, (b) TDP, (c) NH_4, (d) NOx, and (e) total Kjeldahl nitrogen at sites near Sebastian Inlet (IRLI28) and Fort Pierce Inlet (IRLIR08). Data obtained from SJRWMD.

Based on this preliminary dataset, incoming seawater pumped at 5 m^3/sec from offshore would bring approximately 18 metric tons of N and 0.7 metric tons of P into the lagoon per year from offshore (Table 3-8). Using these data, the net change in nutrients associated with pumping water from offshore (5 m^3/sec) into the lagoon is calculated at (out-in) an annual removal of in lagoon water are calculated at about 50 tons/year of N and between 6 and 10 metric tons/year of P.

A possible weir structure at the northern site would have a higher exchange rate for water with estimates ranging from an average of about 7 m^3/sec for a 50-m wide weir structure to about 20 m^3/sec for a 150-m wide weir structure. Based on these data, approximately 95 to 270 metric tons of N and about 9 to 27 metric tons of P are calculated to be discharged from inlets per year depending on the size of the weir structure (Table 3-5 and Table 3-6). Based on data obtained during this preliminary investigation, seawater overflowing a weir structure at 7 to 20 m^3/sec from Port Canaveral would bring 76 to 216 tons of N per year and 1.8 to 4.9 tons of P per year into the IRL from Port Canaveral (Table 3-9). These calculations are likely overestimates because as water entered the lagoon from Port Canaveral, water would be replaced from offshore leading to improved water quality within the port over time. Nevertheless, the net change to nutrients in the lagoon is an annual removal of 19 to 54 tons of N and 7 to 22 tons of P.

Table 3-7. Nutrient concentrations at offshore sites and in Port Canaveral (this study).

Location	NH_4 (µM)	NOx (µM)	DIN (µM)	Org-N (µM)	TDN (µM)	PO_4 (µM)	TDP (µM)	DOP (µM)
Offshore	0.9	0.3	1.2	4.8	8.0	0.06	0.15	0.09
Port Canaveral	5.4	1.0	6.4	18.1	24.4	0.22	0.26	0.04

Table 3-8. Tons of N and P that would be pumped into the lagoon associated with pumping seawater from offshore at various pumping rates.

Pumping Rate	L/day	L/year	NH_4 (tons/yr)	NOx (tons/yr)	DIN (tons/yr)	Org-N (tons/yr)	TDN (tons/yr)	PO_4 (tons/yr)	TDP (tons/yr)	DOP (tons/yr)
2.5 m^3/sec	$2.2*10^8$	$7.9*10^{10}$	1.0	0.3	1.3	5	9	0.1	0.4	0.2
5 m^3/sec	$4.3*10^8$	$1.6*10^{11}$	2.1	0.6	2.7	11	18	0.3	0.7	0.4
10 m^3/sec	$8.6*10^8$	$3.2*10^{11}$	4.2	1.2	5.4	21	36	0.6	1.4	0.9
15 m^3/sec	$1.3*10^9$	$4.7*10^{11}$	6.2	1.7	7.9	31	52	0.8	2.1	1.3
20 m^3/sec	$1.7*10^9$	$6.3*10^{11}$	8.3	2.3	10.6	42	70	1.1	2.8	1.8

Table 3-9. Tons of N and P that would flow into the lagoon from Port Canaveral associated with a weir structure.

Pumping Rate	L/day	L/year	NH_4 (tons/yr)	NOx (tons/yr)	DIN (tons/yr)	Org-N (tons/yr)	TDN (tons/yr)	PO_4 (tons/yr)	TDP (tons/yr)	DOP (tons/yr)
2.5 m^3/sec	$2.2*10^8$	$7.9*10^{10}$	6.0	1.1	7.0	20	27	0.5	0.6	0.1
5 m^3/sec	$4.3*10^8$	$1.6*10^{11}$	12	2.2	14	41	55	1.1	1.3	0.2
10 m^3/sec	$8.6*10^8$	$3.2*10^{11}$	24	4.3	28	81	110	2.1	2.5	0.4
15 m^3/sec	$1.3*10^9$	$4.7*10^{11}$	35	6.3	42	119	161	3.1	3.7	0.6
20 m^3/sec	$1.7*10^9$	$6.3*10^{11}$	48	8.5	56	160	216	4.2	4.9	0.8

Due to the non-conservative nature of nutrients and strong benthic-pelagic coupling in shallow estuarine systems, processes in sediments and on particles make it difficult to estimate how the combined inflow and discharges of nutrients from the lagoon would change concentrations and ratios of nutrients in lagoon water over time. To address these complex geochemical processes, nutrient and oxygen cycling were investigated in sediments throughout the lagoon and in laboratory experiments to investigate how changes to temperature, salinity, and DO might influence geochemical nutrient cycling. In other words, would changes to temperature, salinity, and DO, that would likely result from pumping promote geochemical processes, further decrease nutrient concentrations?

3.3 Geochemical Nutrient Cycling (In-situ)

Benthic fluxes of N and P from muck are estimated to contribute more than 40% of the annual N and P loading to the IRL (Tetra Tech 2020, Fox and Trefry 2018). These estimates are based only on fluxes from fine-grained, organic-rich sediments locally referred to as “muck.” Because sand covers at least 90% of the lagoon bottom, non-trivial fluxes from sand need to be considered when evaluating the importance of internal nutrient sources and geochemical nutrient cycling within the lagoon. During this investigation and with data from other lagoon projects, 34 in-situ flux chambers from sandy sites are discussed along with data from 7 new chambers deployed in muddy sediments. To evaluate the importance of these geochemical processes towards regulating nutrient concentrations in lagoon water, residence times for nutrients were calculated based on nutrient fluxes, long-term average nutrient concentrations in the lagoon (Table 3-4) water, and an average lagoon depth of 1.5 meters.

3.3.1 Benthic Fluxes

To date, no significant trends for benthic nutrient fluxes versus the composition of sandy sediments (e.g., sediment OM content) have been identified in the IRL. This pattern deviates from an established pattern where sediment water and OM content are strongly correlated with benthic fluxes from fine-grained, organic-rich sediments throughout the IRL (Fox and Trefry 2018). The absence of a trend for sandy sediments is likely at least partially due to groundwater seepage into the lagoon through water-permeable sandy sediments (Pandit, et al. 2017). Based on data from very simple mini-seepage meters deployed during this study, it is likely most benthic chambers were influenced to some extent by groundwater seepage with rates ranging from less than 1 up to about 30 cm/day (Bethel Creek) from sites within about 10 m of the shoreline. Where groundwater seepage occurs, fluxes are more likely the result of advective versus diffusive processes. Nevertheless, fluxes reported below represent either inputs (positive values) or removal (negative values) of nutrients or oxygen from the lagoon system. Preliminary results have begun to show significant correlations between nutrient fluxes and latitude (Figure 3-15).

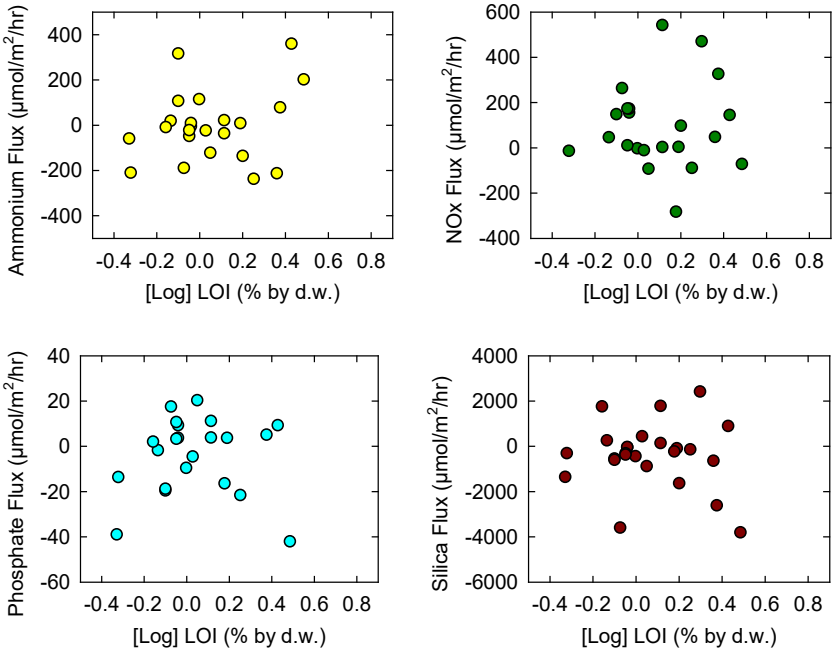

Figure 3-14. Fluxes of (a) NH_4, (b), NOx, (c) PO_4, and (d) SiO_2 versus OM content as log[LOI].

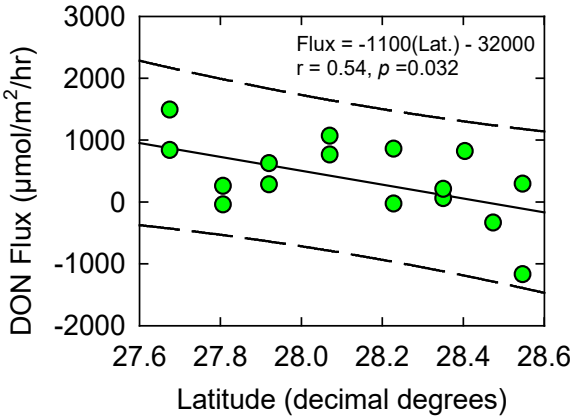

Figure 3-15. Benthic flux of DON versus latitude.

Median ± SE SOD (oxygen flux into sediments) for sandy sediments was -3,200 ± 900 µmoles $O_2/m^2/hr$. Values for sandy sediment in the IRL fit nicely within a range of values previously reported for estuaries around the world at 200 to 7,000 µmoles $O_2/m^2/hr$ (Boynton et al. 2018). SOD of muddy sediments were higher at -4,300 ± 2,500 µmoles $O_2/m^2/hr$; however, muddy sediments were investigated during November through February (cooler months) and fluxes from muddy sediments almost certainly underestimate annual average values.

Overall, median ± SE N fluxes varied among areas with sandy versus muddy sediments. At sandy sites DIN was released from sediments (median ± SE = 260 ± 170 µmoles/m^2/hr, 32 tons/km^2/year) primarily as NOx (63% of DIN, 150 ± 150 µmoles/m^2/hr, 20 tons N/km^2/year), and NH_4 accounted for 37% of the DIN efflux at 90 ± 60 µmoles/m^2/hr (11 tons N/km^2/year). At many sites, NH_4 fluxes were directed into sediments, possibly due to nitrification in aerobic surface sediments. Fluxes of DON were highly variable with median DON fluxes directed out of sediments for a median TDN flux from sandy sites at 290 ± 430 µmoles/m^2/hr (35 tons N/km^2/year).

At muddy sites (muck), fluxes of NOx were directed from the water into sediments (-180 ± 200 µmoles/m^2/hr; -22 tons N/km^2/year), consistent with the use of nitrate as an oxidizing agent for the decomposition of organic matter in suboxic/anaerobic sediments. Releases of DIN from muddy sediments were 100% ammonium at a median of 580 ± 460 µmoles/m^2/hr (71 tons N/km^2/year), 2.2-fold higher than DIN fluxes from sandy sediments. Fluxes of DON were highly variable and no consistent trend for DON was identified for muddy sediments.

At sandy sites, the median PO_4 flux was 4.1 ± 8.1 µmoles/m^2/hr (1.1 ton/km^2/year). This wide range of values was not unexpected because P fluxes vary as a result of bacterial decomposition and concentration gradients, but also due to changing redox conditions in sediments and overlying water. As sediments and water become aerobic, P is scavenged by oxidized iron and aluminum oxides; however, aerobic decomposition of sediment OM promotes the releases PO_4 from sediments. Under anaerobic conditions, bacterial metabolism of OM slows; however, P is released from reduced sediments temporarily increasing fluxes (Cowan and Boynton 1996, Boynton et al. 2018). The complex P chemistry is dependent on both changing redox conditions but also the length of time sediments have been oxic or anoxic. Overall, DOP flux was directed into sandy sediments at -4.7 ± 4.9 µmoles/m^2/hr consistent with mineralization of DOM and a concentration gradient driving fluxes into sediments. Based on these data, the net TDP flux was directed into sandy sediments from overlying water at -0.6 µmoles/m^2/hr (-0.2 tons/km^2/year).

At muddy sites, the median P flux was 34 ± 18 µmoles/m^2/hr (9.3 tons/km^2/year). Higher PO_4 fluxes in muddy/anaerobic sediments from the IRL are consistent with data previously reported for other estuaries (e.g., Cowan and Boynton 1996). Fluxes of DOP were also directed out of sediments at 13 ± 26 µmoles/m^2/hr (3.6 tons/km^2/year). Overall TDP fluxes were directed out muddy sediments and the net flux of P was large and positive, compared to a flux directed into sandy sediments (Table 3-10).

Table 3-10. Median ± SE for benthic fluxes from sandy and muddy sediments in µmoles/m^2/hour (2019–2020)

Sediment	Oxygen	NH_4	NOx	DIN	PO_4	TDP	DOP
Sand	-3200 ± 900	90 ± 60	150 ± 150	260 ± 170	4.1 ± 8.1	-0.6	-4.7 ± 4.9
Muck (winter)	-4300 ± 2500	580 ± 460	-180 ± 200	400	34 ± 18	47	13 ± 26

3.3.2 Benthic Flux O:N and N:P Ratios

Previous studies have used O:N (oxygen to NH_4) ratios to infer whether or not certain geochemical process are occurring in sediments (e.g., Cowan and Boynton 1996). For example, mineralization of phytoplankton derived organic matter yields stoichiometric ratios producing 16 atoms of N as nitrate (oxidized from NH_4), 1 atom of P as PO_4 for every 276 atoms of oxygen consumed (O:N = 17.25, O:P 276). If N is not oxidized and remains NH_4, the theoretical O:N ratio is 14.25. Certainly, other geochemical processes such as re-oxidation of reduced sediments can consume oxygen leading to higher ratios. It is also possible that the use of alternate oxidizing agents (e.g., NO_3, iron, manganese) under suboxic or anoxic conditions can lead to values lower than the Redfield ratio. Nevertheless, these ratios have been used to help describe sediment processes (e.g., Boynton et al. 2018). Based on data from this study, the median O:NH_4 for sandy sediments was 21.4 ± 34.2 versus 6.9 ± 6.8 for muddy sediments. These data suggest that coupled nitrification-denitrification may occur in sandy sediment (Nixon 1981) and also confirm the use of alternate oxidizing agents such as nitrate in muddy sediments. When O:DIN is considered, ratios for both sand and mud were 13, consistent with nitrification in sandy sediments and nitrate acting as an oxidizing agent under anaerobic conditions in muddy sediments.

Due to highly variable fluxes of both N and P, both into and out of sediments, it is difficult to identify a reliable molar N:P ratio for sandy or muddy sediments from this limited dataset. The wide range of N:P values identified during this study were consistent with wide ranges of values previously identified in the IRL, likely related to seasonal variations in temperature and DO (Fox and Trefry, 2018). The highly variable ratios can be rationalized based on geochemical processes known to occur in aerobic versus anaerobic sediments (e.g., Klump and Martens 1981). Sorption of P under aerobic conditions in sandy sediments can lead to a higher ratio of DIN:SRP and releases of P from inorganic iron or aluminum oxides under anaerobic conditions can contribute to elevated releases of P at muddy sites leading to lower ratios (Klump and Martens 1981, Cowan and Boynton 1996, Sundby et al. 1992, Harris et al. 2015). Other processes such as denitrification are known to decrease NOx (DIN) in many shallow coastal environments and can promote lower DIN:SRP ratios. Nevertheless, variable ratios were lowest under anaerobic conditions for muddy sediments (e.g., Cowan and Boynton, 1996).

3.3.3 Turnover Times

Benthic nutrient and oxygen fluxes plus existing nutrient concentrations in the IRL were used to estimate residence (turnover) times for nutrients in the IRL based on benthic-pelagic coupling alone. Residence times indicate the theoretical amount of time required for all of a nutrient in the water column to be either re-generated or consumed. If other nutrient sources were to be included

(e.g., tributaries), residence times for nutrients would decrease. Relatively short residence times for nutrients (e.g., hours to weeks) relative to water (months to years) indicate that benthic-pelagic coupling buffers nutrient concentrations against changes resulting from external sources, including a potential flushing project. Although existing conditions discussed in this section act to buffer against changes to nutrient concentrations, sediment process would respond to changes in water quality (e.g., temperature, salinity, and DO) of overlying water as discussed in Section 3.4.

Residence times based on fluxes alone were calculated using a 1 m^2 section of lagoon. Using an average lagoon depth of 1.5 m, each 1 m^2 section of lagoon contains 1.5 m^3 or 1,500 L of water (1 m_{Length} x 1 m_{width} x 1.5 m_{depth} = 1.5 m^3 = 1,500 L; Figure 3-16). Nutrient concentrations (µmoles/L from Table 3-4) times volume (1,500 L) yields the total quantity of nutrients (µmoles) in each 1 m^2 section of the lagoon. The total quantity of nutrients was then divided by fluxes (µmoles/m^2/hr) to yield residence times in hours or days.

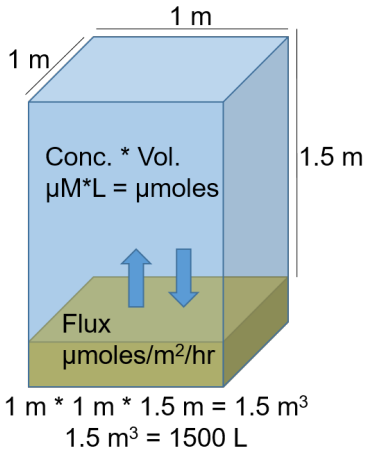

Figure 3-16. Conceptual diagram showing a 1 m^2 column of water and sediments from the IRL using an average depth of 1.5 m.

Turnover times for nutrients varied from hours to days. In sandy sediments, the residence time for ammonium ranged from 22 to 43 hours based on 5-year average NH_4 concentrations at Sebastian Inlet and Vero Beach (Table 3-4) (e.g., 1.4 µmoles/L near Sebastian Inlet times 1,500 L/m^2 of lagoon = 2,000 µmoles/m^2 divided by 90 µmoles/m^2/hr = 22 hours). Nitrate fluxes from sandy sediments were higher than NH_4 fluxes and concentrations in lagoon water were lower, for turnover times ranging from ~6 to 15 hours. Together, DIN fluxes could replace all dissolved nitrogen in the water column (TDN) in 190 hours or about 8 days. Turnover times for NH_4 and NOx from muck were 4–7 hours and 5–13 hours, respectively. Turnover times for nitrate were based on fluxes into sediments. Because nitrate fluxes into sediments are balanced by increased NH_4 fluxes from sediments, the NH_4 flux accounts for nitrate fluxes with regards to turnover of all the N in the water column. Based on these data, NH_4 could replace all the dissolved N in the water column overlying muck in approximately 80 hours or 3.3 days.

Turnover times for PO_4 from sandy sediments varied from 160–410 hours, 6.7–17 days compared to 18–48 hours, 0.75–2 days for areas with muck sediments. To cycle the complete pool of dissolved P, it would take 500–800 hours, 21–33 days for sandy sediments and 59–95 hours or 2.5–4.0 days for muck sediment.

Due to the large temporal and spatial variability in DO throughout the lagoon, turnover times for oxygen were highly variable. If the 5-year average DO concentration in the lagoon is used or 100% saturation at 20 PSU and 25˚C of 7.4 mg/L, turnover times based on SOD alone ranged from 110 hours for sandy sites to 80 hours for mucky sites (e.g., 7.4 mg/L / 32 mg/mmol * 1,000 µmol/mmol = 231 µmoles/L * 1,500L/m^2 of lagoon = 347,000 µmoles/m^2 divided by 3,200 µmoles/m^2/hr = 110 hours). Overall, water column respiration (dark conditions) was 0.2 ± 0.1 mg/L/hr (0.2 mg/L/hr / 32 mmol/mg * 1000 mmol/µmol = 6.3 µmol/l/hr). When water column respiration and SOD are considered together, turnover times based on a 1.5-m deep water column were 25–28 hours (6.3 µmol/l/hr * 1,500 L/m^2 = 9,400 µmol/m^2 of lagoon/hr). Based on these simple calculations, SOD accounted for 25% and 31% of the total oxygen demand for areas containing sand and muck, respectively. These short turnover times are relatively consistent with observed nighttime (dark) decreases in DO throughout the lagoon.

Table 3-11. Turnover times in hours calculated using benthic fluxes, nutrient concentration in the water column and an average depth of 1.5 m.

Sediment	Oxygen (hours)	NH_4 (hours)	NOx (hours)	DIN to replace TDN (hours)	PO_4 (hours)
Sand	110	22 to 43	6 to 15	190	160 to 410
Muck (winter)	80	4 to 7	5 to 13	80	18 to 48

Despite the importance of benthic-pelagic coupling and short residence times for nutrients in shallow coastal systems, improved water quality that could result from artificial inflow would likely modify geochemical processes, possibly increasing or decreasing benthic fluxes into overlying water and changing residence times for nutrients. To address some of these potential changes, laboratory incubation experiments were carried out to investigate how changes to temperature, salinity, and DO might influence nutrients in the lagoon.

3.4 Laboratory Experiments (Sandy Sediments)

Geochemical responses to changes in overlying water that could occur as a result of inflow were evaluated through a series of laboratory incubation experiments. These experiments were conducted to simulate changes in lagoon temperature, salinity, and DO. The most likely results of pumping would be a small decrease in lagoon temperature, an increase in salinity and more stable DO. To estimate how these possible changes may influence geochemical processes within the lagoon, laboratory experiments investigated fluxes from sandy sediments at temperatures ranging from 13˚C to 32˚C, salinities ranging from 0 to 34 PSU, and DO ranging from 0% (0 mg/L) to 100% (about 8 mg/L). Results from each set of experiments are presented here and considered separately. One possible next step would be to investigate the combined impacts of simultaneous changes to temperature and salinity plus DO.

3.4.1 Temperature

Temperature was adjusted between 13˚C and 32˚C using microcontroller controlled (±0.2˚C) recirculating water baths to simulate the maximum annual range of lagoon temperatures. Sediments cores from the IRL were slowly adjusted to the desired temperature within 1 hour of collection. After reaching the desired temperature, cores were allowed to equilibrate for at least 1 hour before overlying water was drained and replaced with new water from the collection site. Once temperature was stable for about 30 minutes, start samples (time 0) were collected and cores were sealed with DO loggers and mechanical stirrers. Stirrers were selected for their ability to prevent the buildup of concentration gradients at the sediment-water interface without causing resuspension. Overall, the lowest SODs were identified at 13˚C and 15˚C and the highest fluxes

were identified at 22˚C. Above 22˚C, SOD decreased as temperature increased towards 32˚C (Figure 3-17).

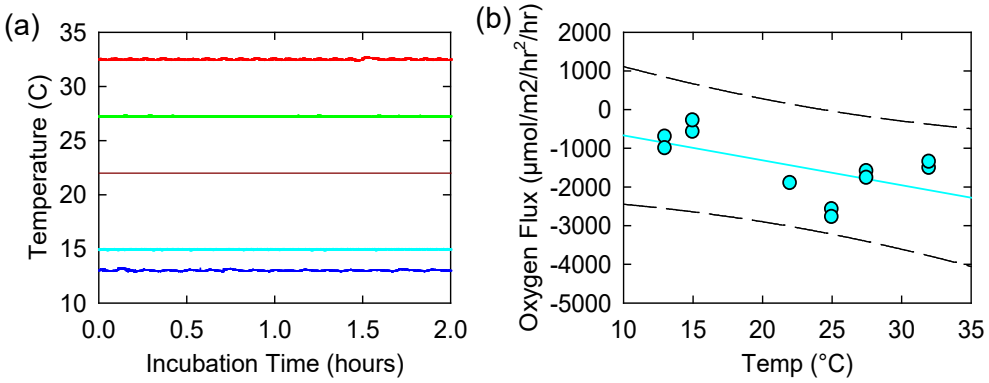

Figure 3-17. Data from laboratory experiments showing (a) laboratory-controlled sediment temperature over time and (b) oxygen flux (SOD) versus sediment temperature.

Nutrient fluxes responded to changes in temperature in different ways. No consistent temperature related trends were identified for fluxes of any N species from sandy sediments when temperatures ranged from 13˚C to 32˚C. NH_4 fluxes followed patterns for SOD (Figure 3-18); however, NH_4 accounted for a small fraction of the DIN and in many cases fluxes were directed into sediments. Fluxes of NOx were variable and positive in all but one core. These data suggest that some degree of nitrification (NH_4 converted to nitrate) occurred in sediments across the entire temperature range.

Fluxes of dissolved PO_4 from sandy sediments were positively correlated with temperature (PO_4 flux (µmol/m^2/hr) = 0.58 * [˚C] – 7.6, p = 0.04, r = 0.63) and increased from near 0 µmoles/m^2/hr at 13˚C to 5 to 10 µmol/m^2/hr at 32˚C. No consistent trends were identified for DOP or TDP (Figure 3-19). No significant correlation was identified for SiO_2 fluxes versus sediment temperature; however, a general trend (not-significant based on current data) for increasing SiO_2 with increasing sediment temperature was observed with a slope of 5.4 µmol/m^2/hr per ˚C.

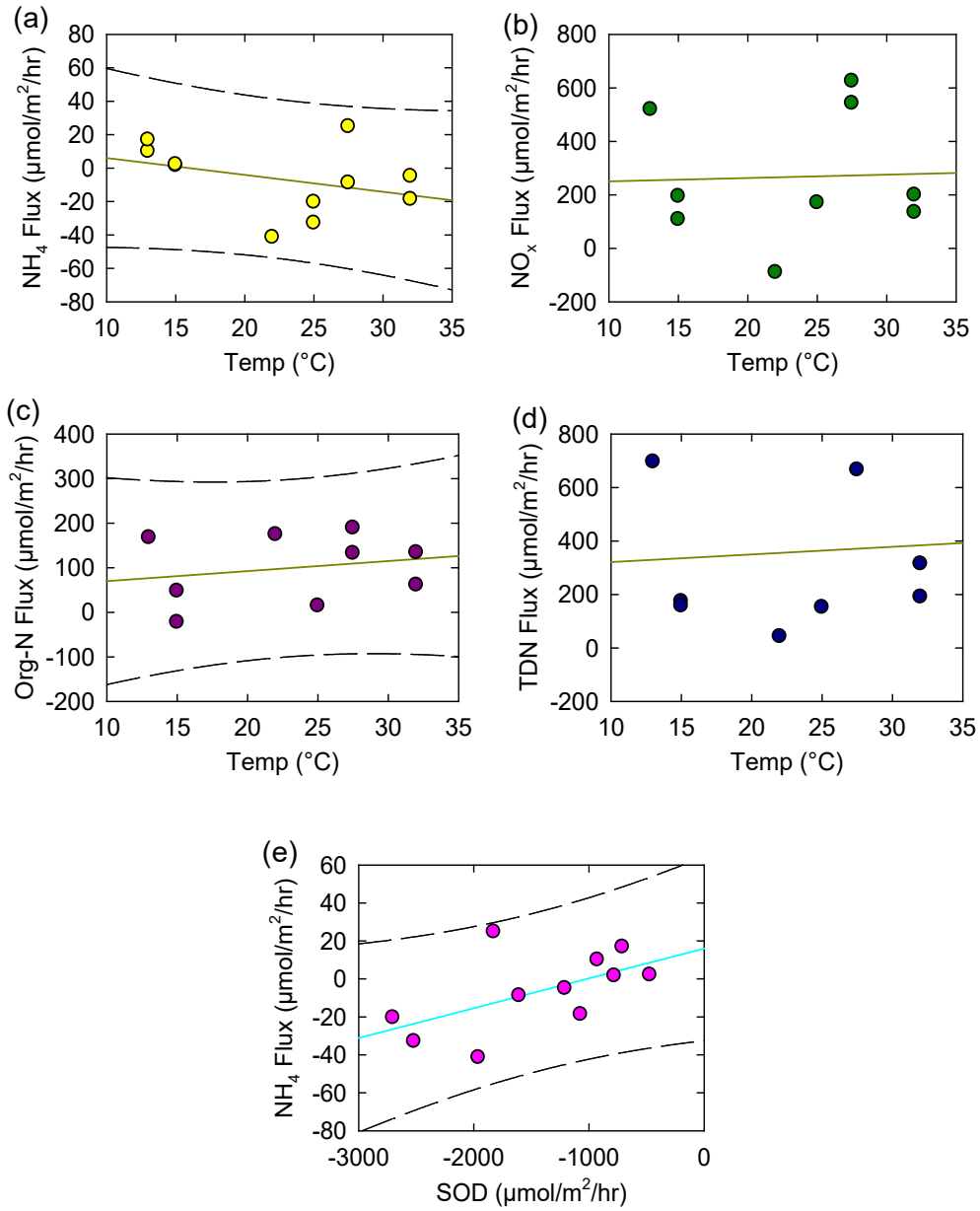

Figure 3-18. Results from laboratory incubation experiments showing fluxes in µmoles/m2/hour versus sediment temperature for (a) NH_4, (b) NOx, (c) Org-N, and (d) TDN plus (e) NH_4 flux versus SOD.

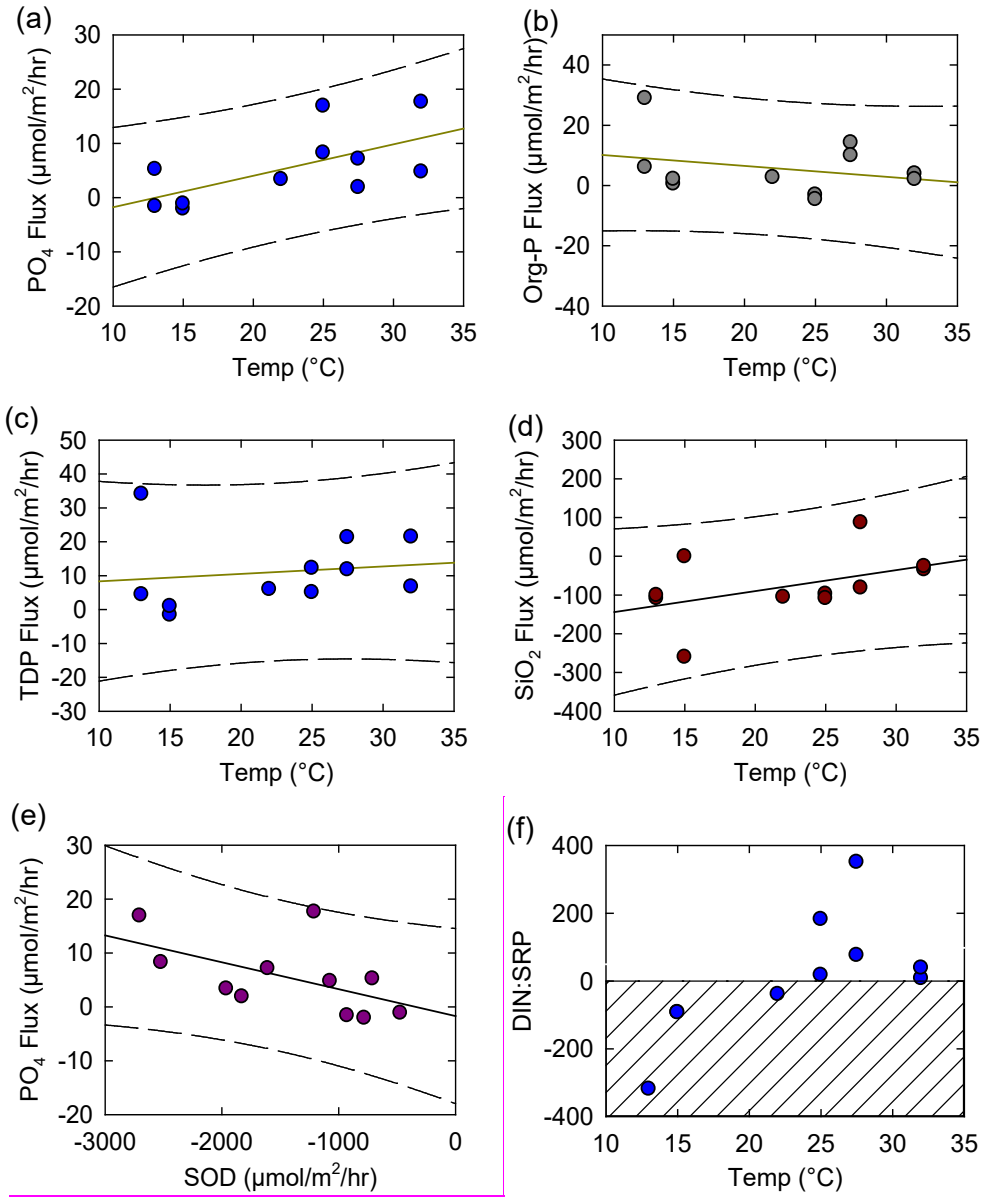

Figure 3-19. Results from laboratory incubation experiments showing fluxes in µmoles/m2/hour versus sediment temperature for (a) PO_4, (b) Org-P, (c) TDP, and (d) SiO_2 plus (e) PO_4 flux versus SOD and (f) molar ratios of DIN SRP versus sediment temperature. Hashed box shows DIN:SRP values below zero where either DIN or SRP were directed into sediments.

Because some fluxes were directed into sediments, it can be difficult to interpret molar N:P ratios with negative values plus no significant trend for N:P versus sediment temperature was identified during this study. Despite no significant trend for the molar N:P ratio, a positive correlation between PO_4 and temperature and no trend for N suggests that the N:P ratio may decrease with increasing temperature. This inference is consistent with the greater the SOD with increasing temperature and previously identified relationships between N:P and DO (e.g., Cowan and Boynton 1996).

Based on the significant positive correlation between sediment temperature and PO_4 flux, any decrease in water temperature associated with inflow would likely decrease PO_4 fluxes into the lagoon. Based on these data, a 1˚C decrease in lagoon temperature would decrease PO_4 fluxes from sandy sediments by about 0.16 tons/km^2/year (0.58 µmol/m^2/hr per ˚C) or about 15% from the current median at 4.1 µmol/m^2/hr (1.1 ton/km^2/year). Applied to the complete surface area of the lagoon, this potential decrease in phosphorus flux could be of more significance to PO_4 concentrations in the lagoon than decreases due to dilution by seawater.

3.4.2 Salinity

Laboratory experiments were carried out to evaluate potential uptake or releases of nutrients and oxygen consumption associated with changes to salinity in overlying water. These experiments were carried out in water baths at 22˚C (laboratory temperature). Before each experiment, overlying water was drained from cores and replaced with a mixture of either site water plus deionized water or with site water plus seawater. Once overlying water was exchanged, cores were allowed to equilibrate for at least 30 minutes before collecting start samples (time 0). Overall, no significant correlation was identified between SOD and the salinity of overlying water (Figure 3-20). Despite the absence of a trend across all salinities, SOD decreased with salinity for samples using a mixture of site water and deionized water. This decrease in SOD is not the result of lower water column respiration due to dilution of site water and water column processes were not likely the main driver of this trend.

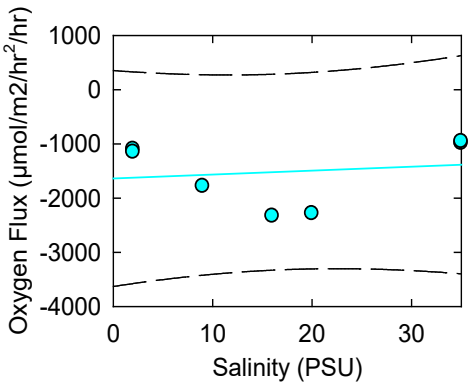

Figure 3-20. Results from laboratory incubation experiments showing oxygen flux (SOD) versus the salinity of overlying water.

All N species showed lower fluxes at higher salinities (Figure 3-21). Significant correlations were identified for NOx (flux (µmol/m^2/hr) = -4.7 * [PSU] + 180) with a decrease in NOx flux of 4.7 µmol/m^2/hr (about 0.6 tons/km^2/hr) per PSU or about 3% per PSU from the median of 150 µmol/m^2/hr (20 tons N/km^2/year) for sandy sites throughout the lagoon.

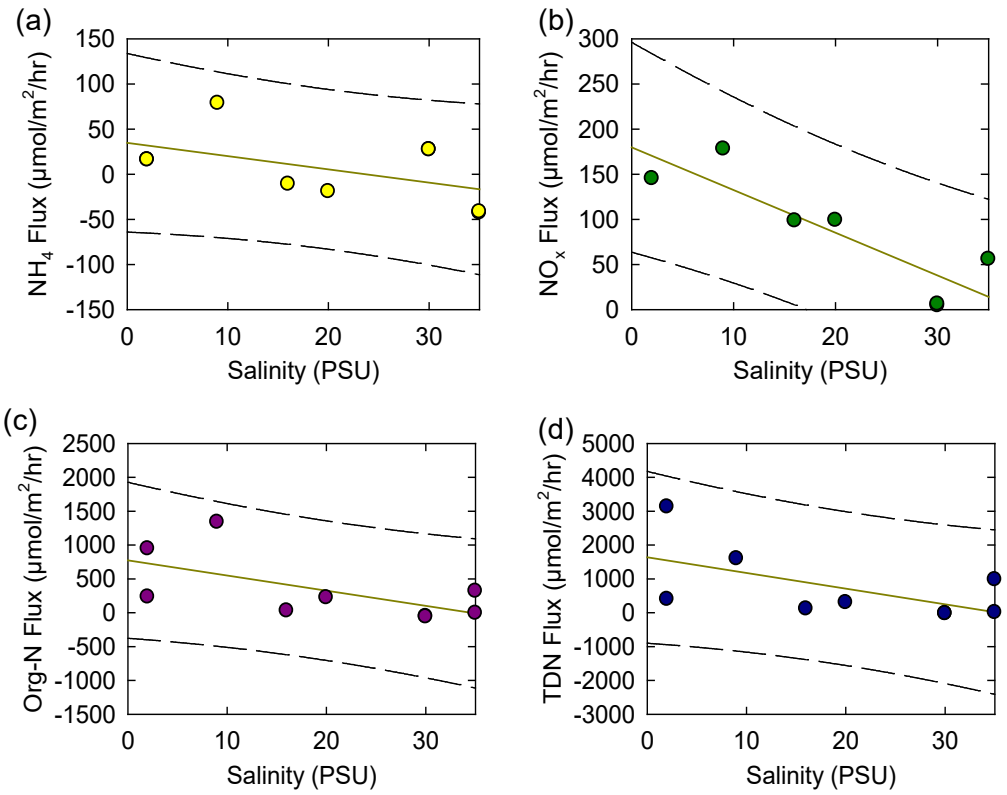

Figure 3-21. Results from laboratory incubation experiments showing fluxes in µmoles/m2/hour versus the salinity of overlying water for (a) NH_4, (b) NOx, (c) Org-N, and (d) TDN.

Fluxes of P and SiO_2 followed patterns observed for N with a general trend of lower fluxes at higher salinities; however, once salinity increased beyond about 20 PSU, fluxes of PO_4 once again increased, consistent with observations for oxygen (Figure 3-22). The absence of statistically significant trends is likely related to the relatively small sample size obtained during the first year of sampling. Both DIN and SRP fluxes decreased with increasing salinity, and based on these preliminary data, no shift in the ratio of DIN:SRP fluxes is currently expected base on a potential shift in lagoon salinity.

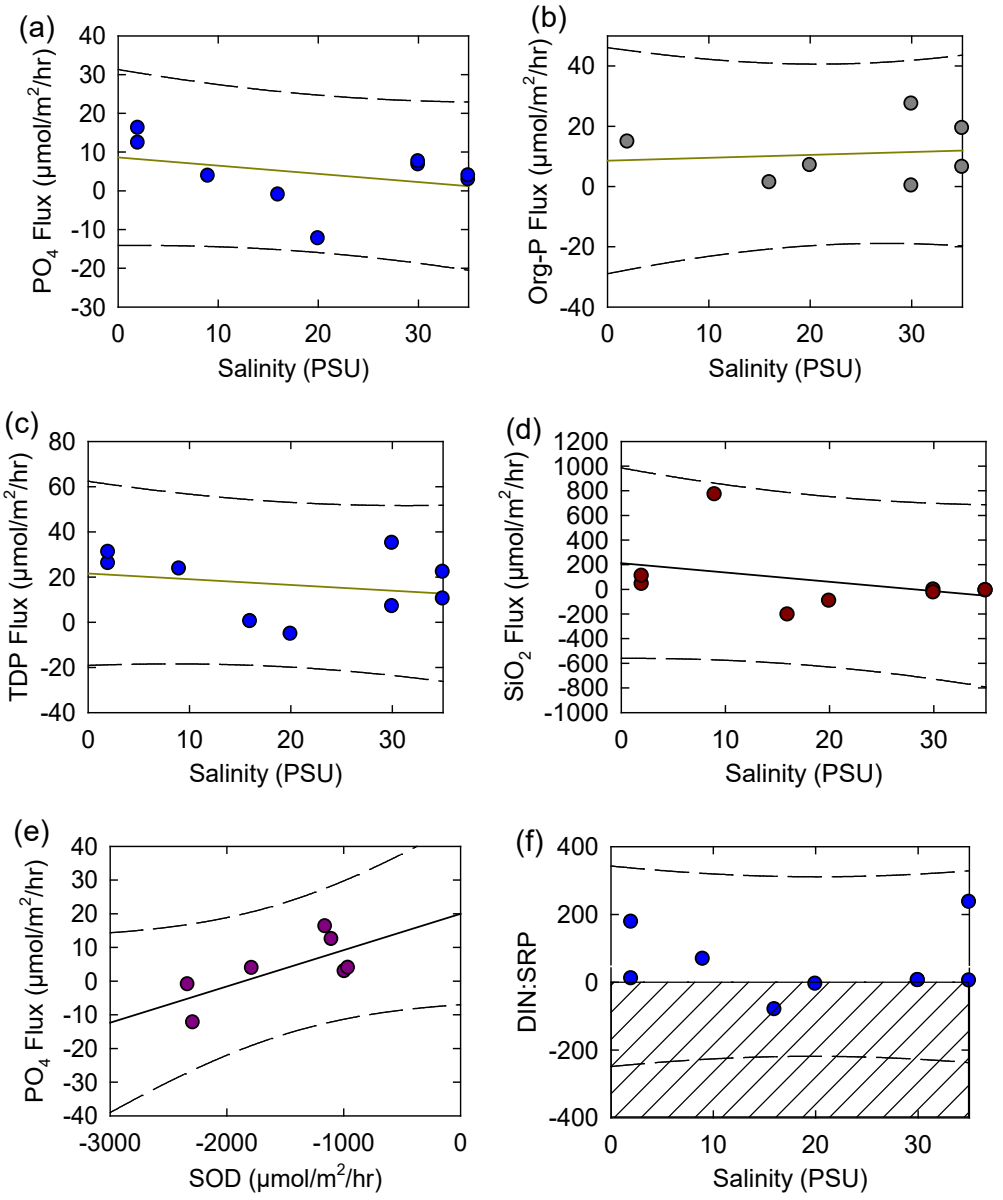

Figure 3-22. Results from laboratory incubation experiments showing fluxes in µmoles/m²/hour versus the salinity of overlying water for (a) PO_4, (b) Org-P, (c) TDP, and (d) SiO_2 plus (e) PO_4 flux versus SOD) during salinity experiments and (f) molar ratios of DIN to SRP versus sediment temperature. Hashed box shows DIN:SRP values below zero where either DIN or SRP were directed into sediments.

Decreased fluxes for effectively all nutrients and species with increasing salinity are consistent with a decrease in diffusion coefficients at higher salinities (Li and Gregory 1974, Trefry et al. 1992). These data are also consistent with lower fluxes identified for higher salinity areas within other estuaries (e.g., Cowan and Boynton 1996); however, most previous studies compare sites across up estuary salinity gradients where other confounding factors come into play. Many of these studies identify the highest fluxes at sites with moderate salinities, likely related to flocculation and enhanced OM deposition related to increasing ionic strength (salinity). Observations from this study are likely the result of changes to diffusion coefficients.

3.4.3 DO

Although DO is not a conservative property of seawater, it is one of the water quality variables likely to change if seawater were to flow into the lagoon by way of pumping or a weir structure. Changes to DO would likely result from (1) a change in solubility due to changing temperature and salinity, plus (2) inflow of lower turbidity seawater with lower respiration, and (3) higher density seawater and enhanced circulation that could disrupt areas currently subject to stagnation and low DO. To manipulate DO concentrations in the laboratory, cores were place in temperature stable water baths and continuously bubbled using mixed gases (air and nitrogen) to maintain DO concentrations between 0% (0 mg/L) and 100% saturation (7–8 mg/L). Because oxygen was controlled, no data for respiration or SOD were obtained for these experiments.

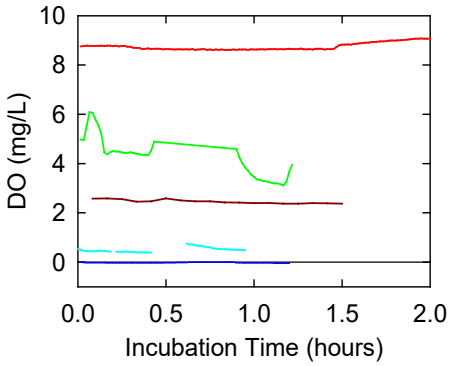

Figure 3-23. Data from laboratory experiments showing (a) laboratory controlled bottom water DO concentrations (mg/L) over time.

Overall, N fluxes were relatively low. Nevertheless, a significant positive correlation was identified between NH_4 fluxes and bottom water DO (NH_4 flux (µmol/m^2/hr) = 3.1 * DO[mg/L] + -0.22; p = 0.02, r = 0.64). No significant correlations were identified for other N species during this study. The significant trend for NH_4 fluxes versus DO was likely due to enhanced bacterial metabolism under aerobic versus anaerobic conditions.

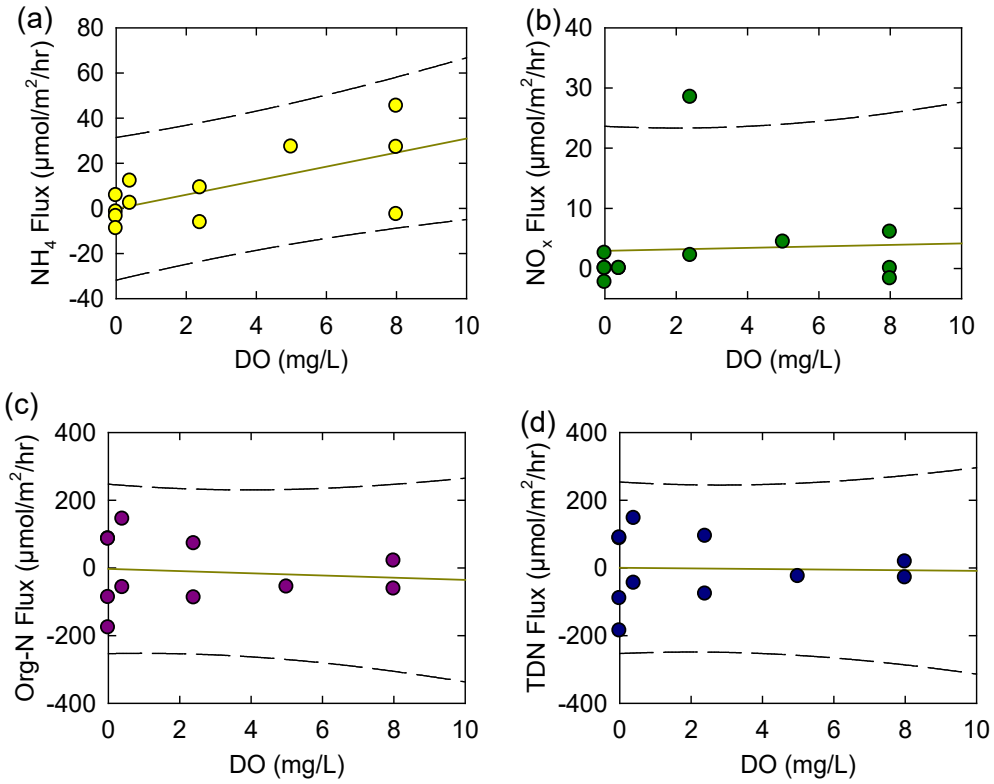

Figure 3-24. Results from laboratory incubation experiments showing fluxes in µmoles/m^2/hour versus bottom water DO concentrations (mg/L) for (a) NH_4, (b) NO_x, (c) Org-N, and (d) TDN versus the salinity of overlying water.

No significant correlations were identified for P fluxes versus bottom water DO; nevertheless, in anaerobic (0% DO) experiments PO_4 fluxes were always directed out of sediments (positive flux), consistent with the release of sorbed P from dissolution of iron oxy-hydroxides (Boynton et al. 2018, Foster and Fulweiler 2019). These data reinforce the recurring observation that releases of P relative to N are enhanced under low oxygen conditions and can support low molar N:P ratios in anaerobic environments (e.g., Boynton et al. 2018). A significant negative correlation was identified between SiO_2 and bottom water DO (SiO_2 flux [µmol/m^2/hr] = -19 * DO[mg/L] + -27; p = 0.02, r = 0.65).

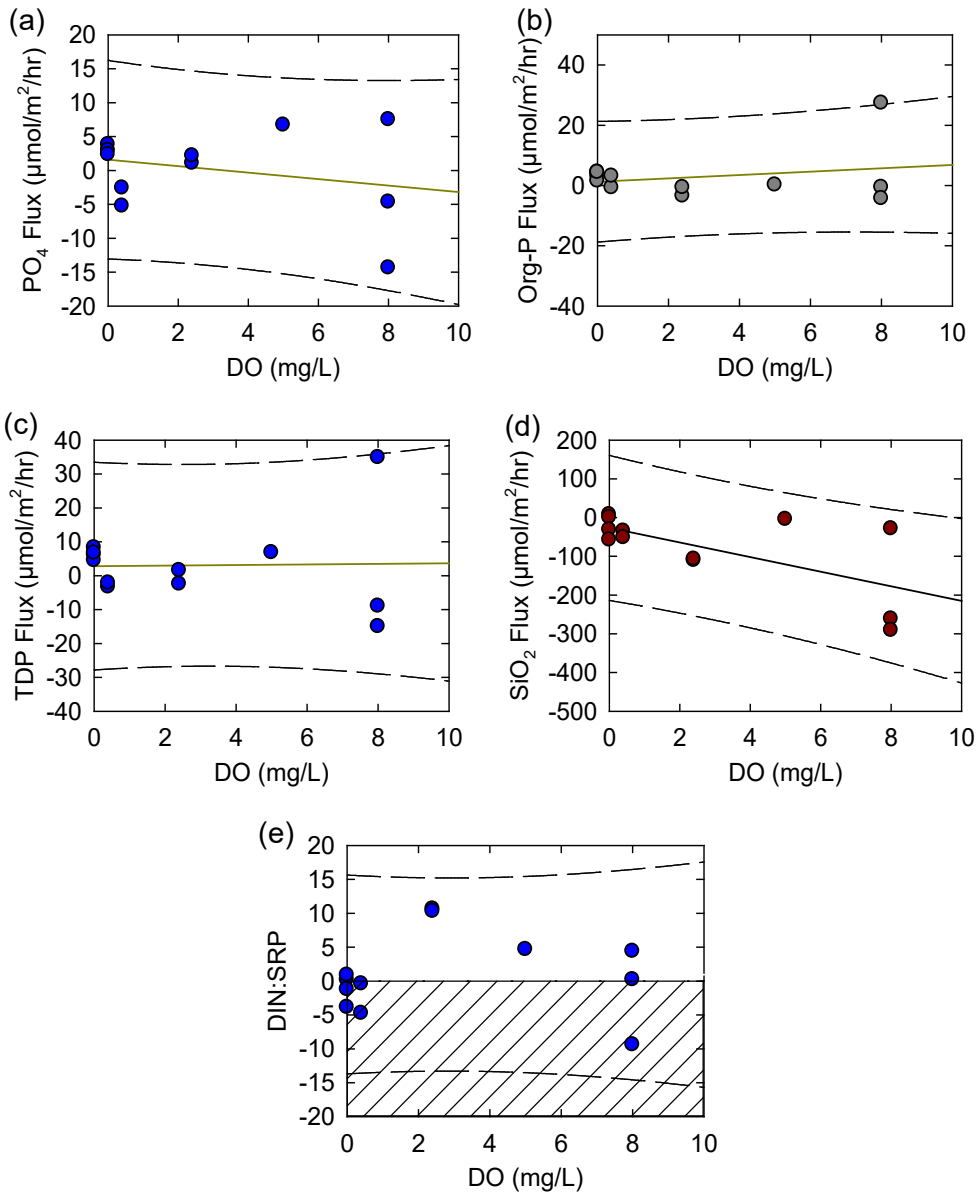

Figure 3-25. Results from laboratory incubation experiments showing fluxes in µmoles/m²/hour versus bottom water DO concentrations (mg/L) for (a) PO_4, (b) Org-P, (c) TDP, and (d) SiO_2 plus (e) molar ratios of DIN to SRP versus sediment temperature. Hashed box shows DIN:SRP values below zero where either DIN or SRP were directed into sediments.

Significant correlations were identified for NH_4 and SiO_2 fluxes versus bottom water DO. Nevertheless, complex biogeochemical responses to hypoxia make it difficult to extrapolate these data to estimate the potential impacts of possible inflow. Variable responses are consistently identified in the literature (e.g., Foster and Fulweiler 2019), mostly due to the complexities of the N and P cycles. For example, enhanced bacterial metabolism under aerobic conditions promotes decomposition of OM releasing NH_4 and P into porewater, hypothetically increasing fluxes. These same conditions promote nitrification and sorption of P to iron and aluminum oxy-hydroxides, processes that can decrease fluxes of NH_4 and P. As a result, fluxes of NH_4 and P vary based not only on DO concentrations but on the length of time sediments have been oxic or anoxic. To better

address these issues, future experiments should investigate fluxes for various DO concentrations over varying periods of time.

3.5 Bottom Water DO

Due to the dependence of biogeochemical nutrient cycling on DO, it is virtually impossible to appropriately model nutrient fluxes, turnover times or concentrations without a detailed picture of DO in the lagoon. To assist modeling efforts, long-term datasets for DO concentrations from the IRL and BRL were obtained for surface water from SJRWMD (Figure 3-26). Existing sensors record DO near the surface or at fixed depths and can miss events that are restricted to the near bottom. For example, sensors referenced in this study had averaged depths during 2019 of (about 0.5–1 m). Overall data for DO in surface water shows an annual trend that is relatively consistent with variations in DO solubility. For example, at a salinity of 25, a reasonable average for the IRL, DO solubility increases from 6.4 mg/L at 32°C to 8.7 mg/L at 15°C, an annual range of 2.3 mg/L (Figure 3-27). In addition to this expected range in DO (at 100%), values are often below saturation during summer with some instances of hypoxia (less than 2 mg/L) recorded in the surface water (e.g., values below the dashed line in Figure 3-26).

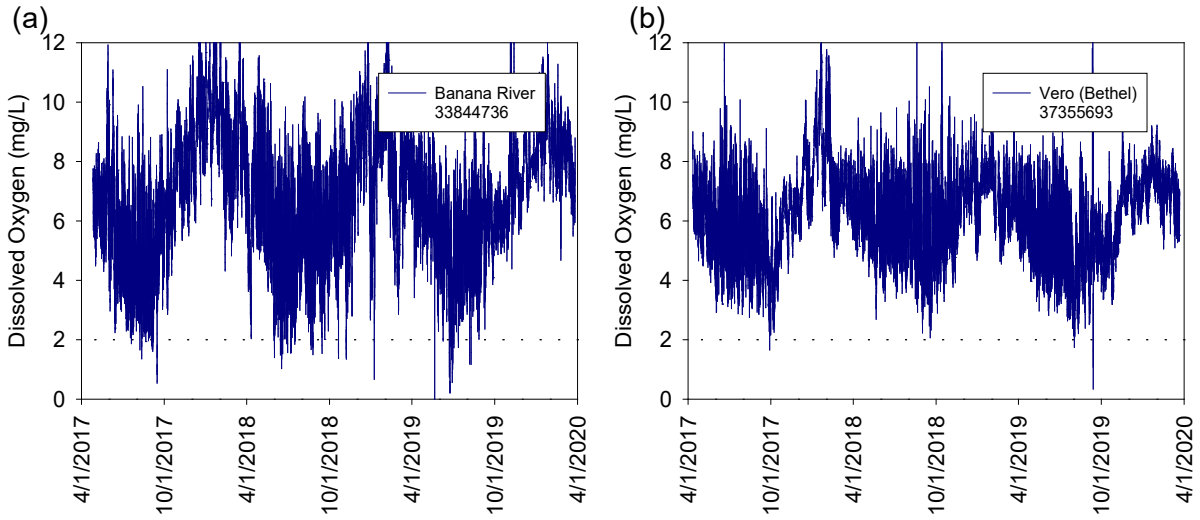

Figure 3-26. Concentrations of DO at fixed depths in (a) BRL and (b) Vero Beach near Bethel Creek.

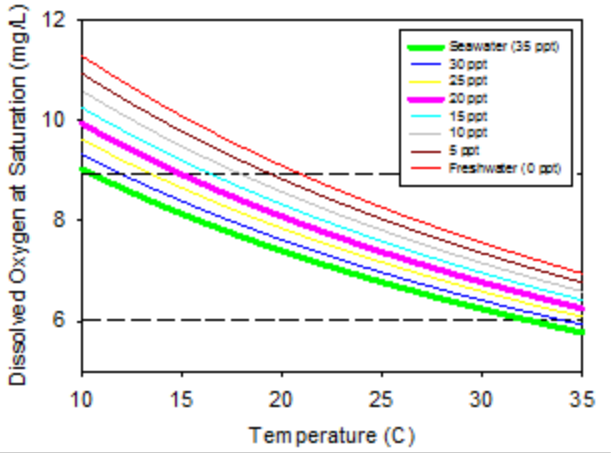

Figure 3-27. DO (mg/L) at saturation (100%) versus temperature for seawater at 35 PSU, freshwater at 0 PSU and at 5 PSU intervals.

Vertical profiles from this and other studies provide snapshots in time, sometimes showing stratification or gradients for DO in the water column (e.g., Figure 3-2). Data from vertical profiles suggest that long-term monitoring efforts focused on surface water or fixed depths may not adequately represent conditions in bottom water that are more closely linked to nutrient cycling in sediments. As discussed previously, SOD accounted for about 30% of the total respiration per m^2 of lagoon. Based on these observations, and due to exchanges with the atmosphere, large diurnal fluctuations in DO observed from near surface monitoring stations are buffered relative to fluctuations that occur in bottom water and at the sediment-water interface (e.g., Figure 3-28).

Temporal and spatial differences in bottom water DO can drive spatial and temporal changes where sediments alternate between sinks and sources of nutrients (Sections 3.3 and 3.4). Changes to DO in bottom water lead to changes in concentrations and the relative abundance of bioavailable nitrogen and phosphorus with implications to algal community composition and density.

Overall, DO in bottom water at sandy sites tracked values for surface water (Figure 3-28). In some cases, DO was much lower in bottom water, possibly related to fouling of the sensor by mud or smothering by drift algae as indicated in (Figure 3-28). To minimize the impacts of fouling and to provide adequate quality assurance and quality control for this data, two sensors were assigned to each station with one deployed and one returned for cleaning and calibration before redeployment on roughly 2-week cycles. Field calibration was verified by comparing data from sensors at the time of deployment and retrieval versus data from a sonde that was calibrated daily. Although the trend may be partially due to the presence of drift algae that restricted circulation with overlying water, DO in bottom water was close to values for surface water during cooler winter months. During April, a difference in DO began to develop between surface and bottom water and this difference has continued into summer months (Figure 3-28). Even if this trend is partially the result of a layer of drift algae, it still represents the conditions experienced in bottom water near the sediment-water interface that influence sediment processes. These data begin to establish a baseline for monitoring conditions near the sediment-water interface to better understand the relationship between DO in the water column and sedimentary processes.

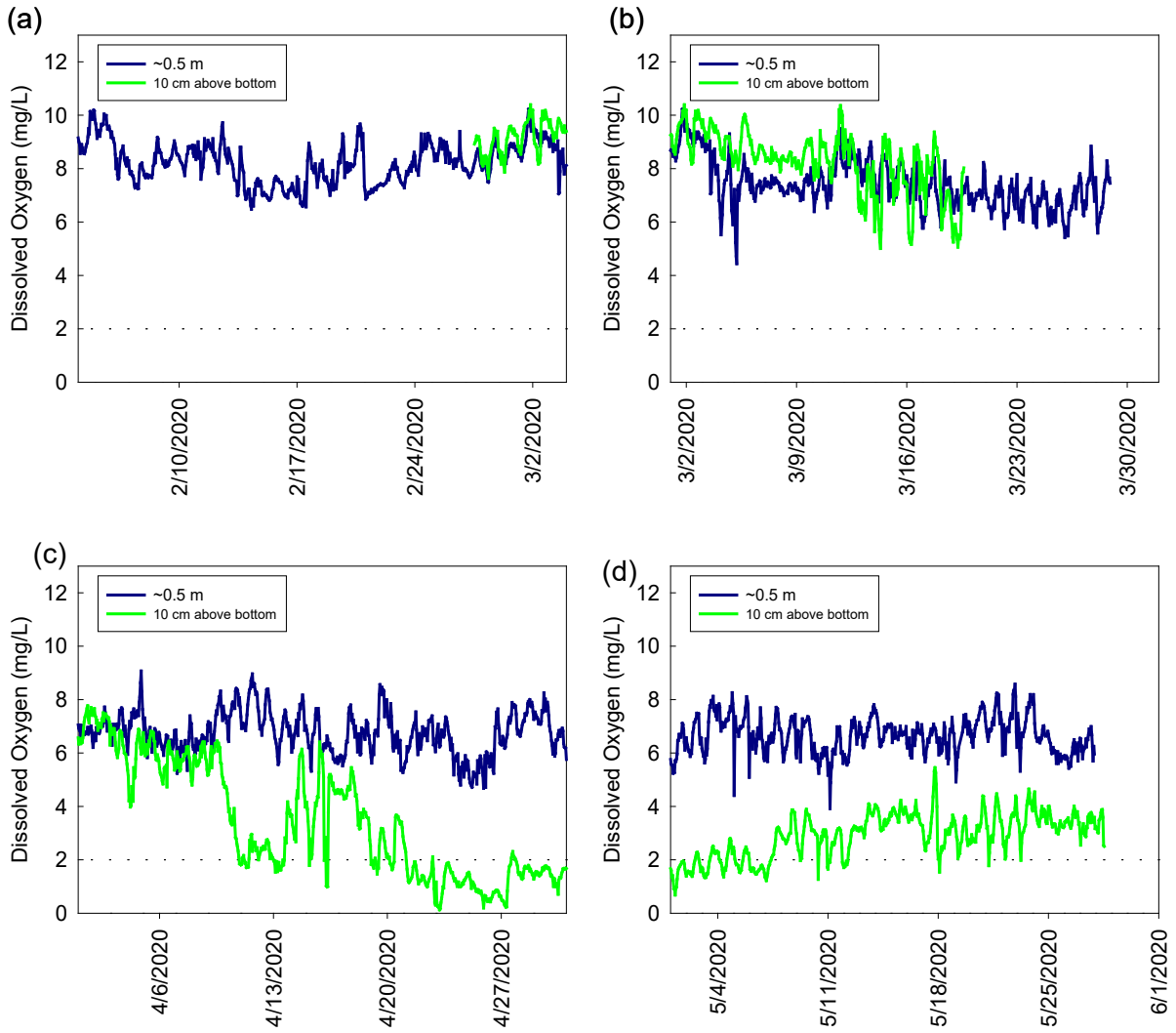

Figure 3-28. DO concentrations in bottom water (green line) and near the surface (blue line) in the IRL near the Eau Gallie Causeway during (a) February, (b) March 2020, (c) April, and (d) May 2020. Surface data obtained from SJRWMD.

Sensors deployed in BRL near the potential Central BRL pumping location show stark differences for bottom water overlying mud (muck) versus sand even though the sensors are only about 200-m apart (Figure 3-29). These data are consistent with differences in SOD among substrates from -3,200 µmoles/m2/hr for sandy sites (annual average) and -4,300 µmoles/m^2/hr for muddy sites (during winter months) and are consistent with the existence of a stratified water column at deeper sites where fine-grained sediments are more likely to accumulate. In addition to lower DO in bottom water overlying muddy sediments, DO concentrations were more variable with larger diurnal fluctuations in DO. These fluctuations were likely responsible for the large diurnal variability in DO overlying sandy sites adjacent to muck deposits (green line in Figure 3-29 versus green line in Figure 3-28). Bottom water in deeper areas overlying muddy deposits also experienced several extended periods of anoxia (Figure 3-29).

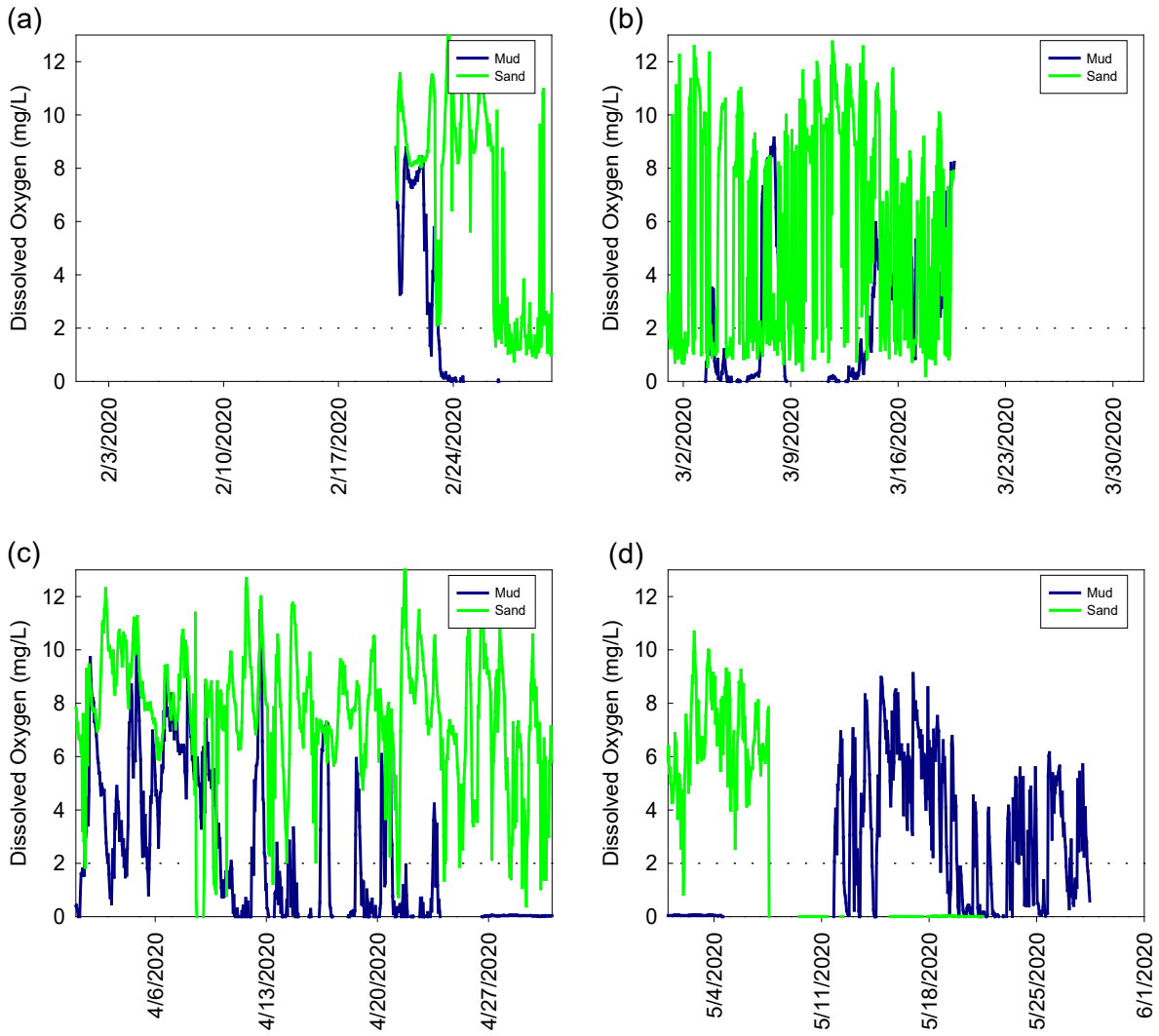

Figure 3-29. DO concentration in bottom water (less than 30 cm above the bottom) near the Central BRL location for an area with sandy sediments (green line) and muddy sediments (blue line) during (a) February, (b) March 2020, (c) April and, (d) May 2020. Sensors were only about 200 meters apart.

4 Summary/Conclusions

Enhanced inflow of seawater to the IRL system would drive corresponding discharges of lagoon water into the coastal ocean. These exchanges of water plus dissolved and particulate materials would lead to changes in water quality within the lagoon. These exchanges would have both direct impacts, such as conservative mixing of temperature and salinity, and indirect impacts, such as changes to geochemical nutrient cycling in response to changes to water quality. Based on a combination of data from this study plus long-term datasets, the coastal Atlantic Ocean is cooler than the lagoon by about 1°C during summer months and warmer than the lagoon during the winter. This subtle difference and potential buffering of temperature by inflow could mitigate extreme nutrient fluxes during hot summer months; but, it may also lead to small increases in flux during winter. Nevertheless, buffering against extreme cold in the lagoon may have some value based on observations leading up to the 2011 super bloom. Changes to both temperature and salinity would likely be small; however, the potential for stratification and the potential formation of a dense layer of seawater within the lagoon could be of significance at certain locations.

Nutrient concentrations in the coastal Atlantic Ocean were relatively uniform both spatially and temporally with average concentrations of TDN, TDP, and SiO_2 at 8.0 ± 2.4 µM, 0.15 ± 0.05 µM, and 3.3 ± 0.7 µM, respectively. Overall, lagoon samples averaged 62.8 ± 24.3 µM TDN, 1.41 ± 0.72 µM TDP, and 51 ± 28 µM SiO_2, which are 7.9-fold, 9.4-fold, and 15.5-fold higher than values for seawater.

Concentrations of dissolved nutrients in the IRL including Bethel Creek averaged 62.8 ± 24.3 µM TDN, 1.41 ± 0.72 µM TDP, and 51 ± 28 µM SiO_2, which are 7.9-fold, 9.4-fold, and 15.5-fold higher than values of 8.0 ± 2.4 µM TDN, 0.15 ± 0.05 µM TDP, and 3.3 ± 0.7 µM SiO_2 for seawater in the coastal Atlantic Ocean. In Port Canaveral, concentrations of nutrients varied between values identified for the lagoon and the coastal Atlantic. If inflow were to occur via pumping at 5 m^3/sec, direct exchanges of water would yield a net removal of about 50 tons of N and 6 to 10 tons of P per year from the lagoon. If inflow were to occur via a weir structure at 7– 20 m^3/sec, exchanges of water would yield a net removal of 19 to 54 tons of N and 7 to 22 tons of P per year from the lagoon.

Benthic nutrient fluxes from sandy sediments were higher than would be expected by extrapolating trends previously identified for muddy sediments in the IRL. These relatively high fluxes from sandy sediments located within 10 m of the shoreline in the IRL were likely related to groundwater seepage driving advective rather than diffusive fluxes. Regardless if fluxes were advective or diffusive, benthic fluxes would cycle nutrients in the lagoon in a matter of hours to days. Short residence times for nutrients versus water indicate that geochemical processes help to regulate concentrations of nutrients in the IRL and can buffer against changes that might result from external sources.

Laboratory experiments carried out to estimate the potential impacts of pumping on geochemical nutrient cycling showed that lower lagoon temperature and higher lagoon salinity both led to significant decreases in benthic fluxes for some nutrients, and trends, although not significant (likely due to the relatively small dataset obtained to date for other nutrients) for most nutrients in the lagoon. These observations suggest that geochemical responses to potential inflow would likely contribute to further decreasing nutrient concentrations within the IRL. Even seemingly small changes to benthic fluxes are large when applied to the entire surface area of sediments within the lagoon. Using changes to fluxes from this study, even a small decrease in lagoon temperature

(<1 ˚C) would likely prevent tons of phosphate from entering the lagoon from sandy sediments each year.

Concentrations of DO in bottom water followed patterns observed for surface water; however, often at lower concentrations. In some cases, lower concentrations near the bottom were likely related to the accumulation of drift algae that restricted circulation of water near the bottom. Nevertheless, DO near the sediments is most important towards geochemical cycling within the sediments. DO in bottom water overlying muck was lower than DO in bottom water overlying nearby sand, and in several cases, DO in water overlying muck remained anoxic for several days. Laboratory experiments showed that under anaerobic conditions PO_4 fluxes were directed out of sediments whereas under aerobic conditions sediments often were a sink for PO_4. Based on these data, enhanced circulation and increased bottom water DO would likely contribute decreasing PO_4 concentrations in lagoon water.

5 References

Azanza, R. V., Siringan, F. P., San Diego-Mcglone, M. L., Yniguez, A. T., Macalalad, N. H., Zamora, P. B., Agustin, M. B., Matsuoka, K. 2004. "Horizontal dinoflagellate cyst distribution, sediment characteristics and benthic flux in manila bay, philippines." *Phycological Research* 52(4):376-386.

Boynton, W.R., M.A.C. Ceballos, E.M. Bailey, C.L.S. Hodgkins, J.L. Humphrey, and J.M. Testa. 2018. "Oxygen and nutrient exchanges at the sediment-water interface: a global synthesis and critique of estuarine and coastal data." *Estuaries and Coasts* 41:301-333.

Brady, D.C., J.M. Testa, D.M. Di Toro, W.R. Boynton, and W.M. Kemp. 2013. "Sediment flux modeling: calibration and application for coastal systems." *Estuarine, Coastal and Shelf Science* 117:107-124.

Burkholder, J.M., D.A. Tomasko, and B.W. Touchette. 2007. "Seagrasses and Eutrophication." *Journal of Experimental Marine Biology and Ecology* 350:46-72.

Cavender-Bares, K.K., Karl, D.M., Chisholm, S.W. 2001. "Nutrient gradients in the western North Atlantic Ocean: Relationsips to microbial community structure and comparison to patterns in the Pacific Ocean." *Deep-Sea Research I* 2373-2395.

Choudhury, A.K., and P. Bhadury. 2015. "Relationship between N:P:Si ratio and phytoplankton community composition in a tropical estuarine mangrove ecosystem." *Biogeosciences Discussions* 12:2307-2355.

Cowan, J.L.W., and W.R. Boynton. 1996b. "Sediment-water oxygen and nutrient exchanges along the longitudinal axis of Chesapeake Bay: seasonal patterns, controlling factors and ecological significance." *Estuaries* 19:562-580.

Cowan, J.L.W., Pennock, J.R., and W.R. Boynton. 1996a. "Seasonal and interannual patterns of sediment-water nutrient and oxygen fluxes in Mobile Bay, Alabama (USA): regulating factors and ecological significance." *Marine Ecology Progress Series* 141:229-245.

Csanady, G.T. 1978. "The arrested topographic wave." *Journal of Physical Oceanography* 8:47-62.

Defne, Z, and Ganju, N.K. 2015. "Quantifying the residence time and flushing characteristics of a shallow, back-barrier estuary: application of hydrodynamic and particle tracking models." *Estuaries and Coasts* 38:1719-1734.

Diaz, R.J., and R. Rosenberg. 2008. "Spreading dead zones and consequences for marine ecosystems." *Science* 321:926-929.

DiDonato, G.T., E.M., Murrell, M.C. Lores, L.M. Smith, and J.M. Caffrey. 2006. "Benthic nutrient flux in a small estuary in northwest Florida (USA)." *Gulf and Caribbean Research* 18:15-26.

Foster, S.Q., and R.W. Fulweiler. 2019. "Estuarine sediments exhibit dynamic and variable biogeochemical responses to hypoxia." *Journal of Geophysical Research: Biogeosciences* 124:737-758.

Fox, A.L., and J.H. Trefry. 2018. "Environmental dredging to remove fine-grained, organic-rich sediments and reduce inputs of nitrogen and phosphorus to a subtropical estuary." *Marine Technology Society* 52: 42-57.

Hammond, D.E., K.M. Cummins, J. McManus, W.M. Berelson, G. Smith, and F. Spagnoli. 2004. "Methods for measuring benthic nutrient flux on the California margin: comparing shipboard core incubations to in situ lander results." *Limnology and Oceanography* 2:146.

Harris, G. P. 1986. *Phytoplankton ecology: Structure, function, and fluctuation.* London; New York: Chapman and Hall.

Harris, L.A., C.L.S. Hodgkins, M.C. Day, D. Austin, J.M. Testa, W. Boynton, L. Van Der Tak, and N.W. Chen. 2015. "Optimizing recovery of eutrophic estuaries: impact of destratification and re-aeration on nutrient and dissolved oxygen dynamics." *Ecological Engineering* 75:470-483.

Heiri, O., A.F. Lotter, and G. Lemcke. 2001. "Loss on ignition as a method for estimating organic and carbonate content in sediments: reproducibility and comparability of results." *Journal of Paleolimnology* 25:101-110.

J.B., Martin, J.E. Cable, C. Smith, M. Roy, and J. Cherrier. 2007. "Magnitudes of submarine groundwater discharge from marine and terrestrial sources: Indian River Lagoon, Florida." *Water Resources Research* 43:1-15.

Jassby, A.D., and E.E. Nieuwenhuyse. 2005. "Low dissolved oxygen in an estuarine channel (San Joaquin River, California): mechanisms and models based on long-term time series." *San Francisco Estuary and Watershed Science* 3(2).

Kemp, W.M., J.M. Testa, D.J. Conley, D. Gilbert, and J.D. Hagy. 2009. "Temporal responses of coastal hypoxia to nutrient loading and physical controls." *Biogeosciences* 6:2985-3008.

Kemp, W.M., P. Sampou, J. Caffrey, M. Mayer, K. Henriksen, and W.R. Boynton. 1990. "Ammonium recycling versus denitrification in Chesapeake Bay sediments." *Limnology and Oceanography* 35:1545-1563.

Klump, J.V., and C.S. Martens. 1981. "Biogeochemical cycling in an organic-rich coastal marine basin-2. Nutrient sediment-water exchange processes." *Geochimica Cosmochimica Acta* 45:101-121.

Lapointe, B.E., L.W. Herren, R.A. Brewton, and P.K. Alderman. 2020. "Nutrient over-enrichment and light limitation of seagrass communities in the Indian River Lagoon, an urbanized subtropical estuary." *Science of the Total Environment* 699:134068.

Li, H., and S. Gregory. 1974. "Diffusion of ions in sea water and in deep-sea sediments." *Geochemica Cosmochemica Acta* 88:703-714.

Liu, H., Laws, E. A., Villareal, T. A., Buskey, E. J. 2001. "(2001). nutrient-limited growth of aureoumbra lagunensis (pelagophyceae), with implications for its capability to outgrow other phytoplankton species in phosphate-limited environments." *Journal of Phycology* 37(4): 500-508.

Martiny, A,C., Vrugt, J.A., Lomas, M.W. 2014. "Concentrations and Ratios of Particulate organic carbon, nitrogen, and phosphorus in the Global Ocean." *Scientific Data* 140048(2014).

Nixon, S.W. 1981. "Remineralization and nutrient cycling in coastal marine ecosystems." In *Estuaries and Nutrients*, by B.J., Cronin, L.E.J. Ed. Nielson, 111-138. Clifton, New Jersey: Humana.

Pandit, A., H.H Heck, A. Berber, W. Al-Taliby, and K. Mamoua. 2017. *Sediment Survey and Fluxes of Nutrients from Sediments and Groundwater in the Northern Indian River Lagoon, Florida (Part III).* Annual report submitted to SJRWMD for Contract # 27815.

Pelegri, S.P., L.P. Nielsen, and T.H. Blackburn. 1994. "Denitrification in estuarine sediment stimulated by the irrigation activity of the amphipod Corophium volutator." *Marine Ecology Progress Series* 105:285-290.

Redfield, A. C. 1934. "On the proportions of organic derivations in sea water and their relation to the composition of plankton." In *James Johnstone Memorial Volume*, by Ed. R. J. Daniel, 177–192. Liverpool, UK: University Press of Liverpool.

Seitzinger, S.P. 1988. "Denitrification in freshwater and coastal marine ecosystems: ecological and geochemical significance." *Limnology and Oceanography* 33:702-724.

Seitzinger, S.P. 1991. "The effect of pH on the release of phosphorus from Potomac estuary sediments: implications for blue-green algal blooms." *Estuarine, Coastal and Shelf Science* 33:409-418.

Sigua, G.C., J.S. Steward, and W.A. Tweedale. 2000. "Water-Quality Monitoring and Biological Integrity Assessment in the Indian River Lagoon, Florida: Status, Trends, and Loadings (1988-1994)." *Environmental Management* 25:199-209.

Smith, N.P. 1993. "Tidal and nontidal flushing of Florida's Indian River Lagoon." *Estuaries* 16:739-746.

Smith, S.V. 1984. "Phosphorus versus nitrogen limitation in the marine environment." *Limnology and Oceanography* 29(6):1149-1160.

Sundby, B., C. Gobeil, and N. Silverberg. 1992. "The phosphorus cycle in coastal marine sediments." *Limnology and Oceanography* 37:1129-1145.

Tetra Tech. 2020. "Save our Indian River Lagoon Project Plan for Brevard County, Florida."

TEST1. 2002. "gdfgfdsg." *dadfdsf* 50-55.

Tweilley, R.R., J. Cowan, T. Miller-Way, P.A. Montagna, and B. Mortazavi. 1999. "Benthic Nutrient Fluxes in Selected Estuaries in the Gulf of Mexico." In *Biogeochemistry of Gulf of Mexico Estuaries*, by J.R. Pennock, R.R. Twilley Eds. T.S. Bibnchi, 163-209. John Wiley & Sons.

W.M., Kemp, Sampou P.A., Garber J., Tuttle J., and Boynton W.R. 1992. "Seasonal depletion of oxygen from bottom waters of Chesapeake Bay: relative roles of benthic and planktonic respiration and physical exchange processes." *Marine Ecology Progress Series* 85:137.

Welschmeyer, N.A. 1994. "Fluorometric analysis of chlorophyll a in the presence of chlorophyll b and phaeopigments." *Limnology and Oceanography* 39:1985-1992.